WESTFÄLISCHE
WILHELMS-UNIVERSITÄT
MÜNSTER

FROM DUST TO DUST

88. JAHRESTAGUNG

der Deutschen Mineralogischen Gesellschaft

DMG
Deutsche
Mineralogische
Gesellschaft

88th ANNUAL MEETING

of the German Mineralogical Society

19.–22. September 2010 • Münster

Abstracts

Table of Content

PLENARY TALKS

Mineralogical Evolution of Meteorites

Timothy J. McCoy (presenting author)[1]
[1]Dept. of Mineral Sciences, National Museum of Natural History, Smithsonian Institution, Washington, DC 20560-0119 USA.

In a provocative paper, Hazen et al. (2008) argued that the mineralogy of terrestrial planets evolves as a consequence of a range of physical, chemical and biological processes. From an initial inventory of approximately a dozen currently-known presolar minerals, processes including melting in the solar nebula, impact, melting and differentiation, plate tectonics, metamorphism, evaporation, atmospheric oxidation, and the rise of life produced the ~4300 mineral known today.   Examining mineralogy in the light of planetary evolution introduces geologic time to the study of, and teaching of, this fundamental geological discipline. In this abstract, I explore the earliest stages of such evolution, examining how the mineralogy recorded in meteorites tracks this diversification and questioning whether such a diversification is, in fact, linear.

The earliest mineral record dates from before the formation of our own Solar System. Presolar grains formed in a previous generation of stars seeded the solar nebula. First inferred from noble gas anomalies, acid dissolution and physical separation led to the identification of the carbon-bearing phases diamond, silicon carbide and graphite. In situ studies have subsequently identified nitrides, carbides, oxides and silicates. Among the most active areas of meteorite research, the inventory of minerals, including the identification of new minerals and the recognition of abundant amorphous materials, is likely to grow dramatically in the coming decade.

Condensation during cooling of the solar nebula produced the precursors of calcium-aluminum-inclusions (CAIs) and chondrules which were subsequently remelted by transient heating events. Composed of refractory oxides and silicates, the minerals found in CAI's sample all the crystal systems. Magnesian silicates dominate primitive, chondritic meteorites but are joined by a range of sulfides, oxides, carbides, silicides, and phosphides that reflect the oxygen fugacity under which the meteorites formed.

The accretion of chondritic components into km-sized asteroids initiated thermal and aqueous alteration, as well as leading to a dynamic impact environment. Within these asteroids, melting of ice produced phyllosilicates, oxides, carbonates, sulfates and halides. Thermal metamorphism produced albitic plagioclase and may have been responsible for the formation of phosphates, silica polymorphs, sinoite (Si_2N_2O), amphibole and others. Shock metamorphism transformed olivine into ringwoodite and wadsleyite, while pyroxene, ilmenite and SiO_2 all suffered similar fates.

The onset of melting first created additional diversity with S,C,P-rich metallic melts reacting to form Na-Ca-Mg phosphates and carbides. At this point, the seemingly unending increase in mineralogical diversity essentially reversed itself, as near-total melting produced a molten planet that may have only had olivine as a residual, solid mineral phase. However, separation into core, mantle and crust gave rise to a new set of minerals, with new silicates and oxides forming in the crust as a result of fractional crystallization and Fe,Ni, phosphide, nitride, sulfide and phosphate phases appearing in the core.

Absent from Earth, some meteoritic minerals were formed in environments that would never be repeated. A more remarkable feature is that many meteoritic minerals formed from processes – aqueous alteration, metamorphism, igneous differentiation – that formed and would continue to form many of the diverse minerals found on Earth.

Reference:
Hazen, R.M. et al. (2008) Mineral evolution. American Mineralogist 93, 1693-1720.

Oceanic floor basalts - a view of mantle processes and mantle history from the experimental study of phase relations and trace-element distributions

Hugh O'Neill[1], Xi Liu[2] and Frances Jenner[3]
[1]Research School of Earth, The Australian National University, Canberra ACT, Australia
[2]Now at: School of Earth and Space Sciences, Peking University, Beijing 100871, P. R. China
[3]Now at: Institute for Study of the Earth's Interior, Okayama University at Misasa, Yamada 827, Misasa, Tottori 682-0193, Japan.

The processes leading to the production of ocean-floor basalts (OFBs) by passive upwelling at mid-ocean ridges and other spreading centres are now considered to be reasonably well understood, but many interesting questions remain, such as what the variations in chemical composition of OFBs reveal about the physical conditions of melting, as opposed to chemical inhomogeneity in the mantle.

The phase equilibrium relations of partial melting of peridotitic mantle can be parameterized starting with a four-component system, the components being SiO_2, $AlO_{1.5}$, CaO and MO, where M stands for Mg and Fe^{2+}. Partial melting of upper mantle peridotite involves five phases, namely melt plus four solid phases: olivine, orthopyroxene, clinopyroxene, and an aluminous phase – plagioclase, spinel or garnet, depending on pressure. With five phases and four components, partial melting is thermodynamically univariant, so melt compositions and melting temperatures can be rigorously parameterized as a function of pressure without specifying the compositions of the solid phases. The isobaric invariance of the system is maintained if the concentration of each minor component added to the system is specified in just one phase. Hence the parameterization can be extended to natural composition using the concentrations of Na_2O, TiO_2, K_2O, P_2O_5, H_2O and CO_2 in the melt, all of which components are concentrated in the melt during partial melting. The effect of varying Mg/Fe^{2+} in the system can also be explicitly accounted for using this ratio in the melt; importantly, it has only a minor influence. The only significant compositional variable that cannot be accounted for adequately by its concentration in the melt is Cr, because of its highly compatible nature. Cr is important because Cr-Al solid solutions in the solid phases determine the activity of Al_2O_3 in the melt. The effect of Cr is parameterized using the molar Cr/(Al+Cr) (i.e., the Cr#) in spinel. Hence the parameterization is at present limited to melting in the spinel-lherzolite facies. Calibration of the parameterization utilizes the extensive experimental database in the literature on multiply saturated melting in both simple and complex ("natural") systems from 0 to 3.0 GPa. This database now comprises over 200 experiments.

We have applied the parameterization to analyses of mid-ocean ridge basaltic glasses from active spreading centres that are sufficiently primitive to have crystallized only olivine (± minor chromite) at low pressure, to infer for each glass: 1) its pressure of partial melting, assuming batch melting; 2) the Cr# of residual spinel; and 3) the extent of subsequent olivine fractionation. Unlike other petrologic methods aimed at obtaining the pressure of origin of oceanic basalts, no assumption needs to be made about the composition of the source mantle, nor does the calculated extent of olivine fractionation depend on assumptions about Mg-Fe partitioning. The calculated melting pressure of the glasses correlates well with the depth of water over the mid-ocean ridge from which it was sampled. However, variations in mantle potential temperatures are calculated to be small, suggesting that the variations in melting pressure may be due to cessation of melting due to heat loss by conduction to the surface.

The concentrations of 66 elements have been determined by electron microprobe and laser-ablation ICP-MS in 340 ocean floor basaltic glasses from the Smithsonian collection (Melson et al. 2002). The statistical distributions of K, P and Ti, three incompatible trace elements that are routinely determined by electron microprobe, are similar in our 340 glasses to their respective distributions in the full Smithsonian dataset (> 9000 samples), showing that our smaller dataset is representative. The distributions of all incompatible elements are approximately log-normal, with an interesting correlation of skewness and kurtosis with incompatibility. The smoothness of the distributions shows emphatically that there is no meaningful distinction between N-MORB and E-MORB; rather, OFBs sample a simple continuous spectrum of variably depleted or enriched mantle. There are no correlations between calculated partial melting conditions and incompatible trace-element chemistry, consistent with OFB-source mantle presently being sampled randomly at mid-ocean ridges. The OFB-source mantle appears to be the result of several cycles of melt extraction and refertilization during Earth's history, and is characterized by positive Eu and Sr anomalies, indicating that this history includes removal of plagioclase. This complex history is not consistent with the present day rate of production of oceanic crust (~ 20 km3 per year), which, if extrapolated back to the past, implies that less than one mass of the mantle should have been processed through the mid-ocean ridge system in the last 4.5 x109 years. The implication is that the production and recycling of oceanic crust must have been much more vigorous in the past.

Melson, W.G., O'Hearn, T. and Jarosewich, E., 2002. A data brief on the Smithsonian Abyssal Volcanic Glass Data File. Geochemistry Geophysics Geosystems, 3(4): 1-11.

Crystal Growth in Pores

George Scherer
Dept. Civil & Env. Eng./PRISM, Princeton University, Princeton, NJ 08544 USA

Crystallization of salt and ice in the pores of stone is a major contributor to the sculpting of landscapes and the destruction of monuments. This talk presents an overview of the thermodynamic and kinetic factors that control the magnitude of the stresses generated by growth of confined crystals. Sustained stress is made possible by the presence of a film of solution between the growing crystal and the confining surface. The forces responsible for the existence of the film, and recent attempts to characterize the film by direct measurement and numerical simulation, are discussed. Owing to the relatively large pore sizes in most rocks, the curvature of the crystal/liquid interface has no significant effect on solubility, so equilibrium thermodynamics predicts negligible stresses; however, destructive transient stresses are observed as equilibrium is approached. The factors affecting the magnitude and duration of the transients are reviewed. Given the stresses, the resulting strains can be predicted using composite theory or poromechanics, either of which gives satisfactory results when sufficient input data are available. To prevent damage to monuments by crystallization of ice and salt, it would be useful to reduce the repulsive (disjoining) forces that sustain the liquid film on the mineral surface. Some preliminary experiments suggest that this might be possible.

GOLDSCHMIDT LECTURE

Hf-W chronology and the accretion of inner solar system planets

Thorsten Kleine[1]
[1]Westfälische Wilhelms-Universität Münster, Institut für Planetologie, Wilhelm-Klemm-Str. 10, 48149 Münster, Germany (thorsten.kleine@uni-muenster.de)

The ^{182}Hf-^{182}W systematics of meteoritic and planetary samples provide firm constraints on the chronology of the accretion and earliest evolution of asteroids and terrestrial planets and lead to the following succession and duration of events in the earliest solar system. Formation of Ca,Al-rich inclusions (CAI) was followed by the accretion and differentiation of the parent bodies of some magmatic iron meteorites within less than ~1 Myr. Most chondrules formed more than ~2 Myr later than CAI, indicating that the chondrite parent bodies accreted later than those of the iron meteorites. Some magmatism on the parent bodies of basaltic achondrites started as soon as ~4 Myr after CAI formation and may have continued until ~10 Myr. A similar timescale is obtained for the high-temperature metamorphic evolution of chondrite parent bodies. Thermal modeling combined with these age constraints reveals that the different thermal histories of meteorite parent bodies primarily reflect their initial abundance of short-lived ^{26}Al, which is determined by their accretion age.

The strong fractionation of lithophile Hf from siderophile W during core formation makes the Hf-W system an ideal chronometer for this major differentiation event. In standard models for Earth's accretion and core formation the Hf-W timescale is always shorter than that obtained from U-Pb chronometry. This disparity in calculated accretion timescales most likely reflects disequilibrium during core formation as a result of incomplete re-equilibration of some impactor metal cores with Earth's mantle in large collisions during Earth's accretion. Assuming that only ~40% of Earth's core formed in equilibrium with the mantle brings the Hf-W and U-Pb of Earth's core into agreement, indicating that the formation of Earth's core terminated no earlier than ~50 Myr after solar system formation. This age constraint is consistent with Hf-W evidence that the Moon-forming giant impact and, hence, the final stage of Earth's core formation, occurred after extinction of ^{182}Hf .

The Hf-W chronology of the segregation of Earth's core and the formation of the Moon is difficult to reconcile with the preservation of ^{146}Sm-^{142}Nd evidence for an early (<30 Myr after CAI) differentiation of Earth's mantle because the Moon-forming giant impact most likely erased any evidence of a prior differentiation of Earth's mantle. The combined ^{182}W-^{142}Nd record of Earth's early differentiation therefore suggests that the Earth has superchondritic Sm/Nd and Hf/W ratios, probably as a result of collisional erosion of early-formed crust on Earth's precursor planetary bodies.

ORAL PRESENTATIONS

Section 01

———————

Early differentiation and core formation of the terrestrial planets

High pressure metal-silicate partitioning and the nature of the light component in the Earth's core

Highly siderophile elements in aubrites

David van Acken[1,2], Alan D. Brandon[1], Thomas J. Lapen[1]
[1]University of Houston, Department of Earth and Atmospheric Sciences, 312 Science & Research 1, Houston, TX 77204, USA
[2]NASA/Lyndon B. Johnson Space Center, 2101 NASA Parkway, MS KR, Houston, TX 77058, USA

Aubrites are achondrite meteorites that are mostly polymict breccias that consist mainly of Fe-free orthopyroxene, along with minor diopside, plagioclase, olivine, Fe-Ni metal and exotic sulfides such as oldhamite and daubreelite. Their extremely reduced oxidation state and oxygen isotope composition links them to enstatite chondrites. The exact nature of this link is unclear. Some studies suggest formation as cumulates during mantle differentiation of an enstatite chondrite-like parent body. Other studies interpret aubrites as restites from partial melting of enstatite chondrite lithologies. Most studies agree that aubrites originated on at least one parental body similar to, but different from both the EH and EL chondrite bodies.

Highly siderophile elements (HSE, Re, Os, Ir, Ru, Rh, Pt, Pd, and Au) have been shown to be useful tools to study planetary formation and differentiation history. Because the HSE display a wide range of both condensation temperature and compatibility during partial melting, they are especially suited to study the early stages of planetary formation and differentiation. In contrast to classical elemental tracers such as the rare earth elements, HSE are hosted in metal or sulfide phases. These phases may a) represent refractory material left from initial nebula condensation and thus record accretionary processes or b) have been formed during metal/sulfide segregation during planetary differentiation and thus record a different angle of planetary processing, especially in respect to formation of metal cores. In addition to their trace element properties, HSE include the long-lived Re-Os and Pt-Os isotope systems.

Concentrations of HSE in aubrites vary over several orders of magnitude. While the anomalous aubrites Shallowater and Mount Egerton show enstatite chondrite-like concentrations of several hundred ppb, HSE concentrations in Bishopville, Bustee, and Norton County are about three orders of magnitude lower. Many aubrites, including the paired Allan Hills aubrites, have intermediate HSE concentrations around $0.1 - 0.01$ times of CI chondrite values, with broadly chondritic inter-element HSE ratios and $^{187}Os/^{188}Os$ values around the enstatite chondrite value of 0.128. This is consistent with the interpretation that HSE in some aubrites may be dominated by chondritic inclusions, the HSE signature of which is 'diluted' by mixing with the extremely HSE-poor enstatite matrix of aubrites.

In contrast, HSE-poor aubrites show significant fractionation, especially enrichment of Pd and Re over more refractory/compatible HSE such as Os and Ir. Their low Os concentrations are coupled with radiogenic $^{187}Os/^{188}Os$ of up to 0.22, comparable to signatures found in terrestrial basalts. This may suggest a partial melting event on the parent body; and rules out an origin as nebular condensates for these samples, as suggested in earlier studies. While the bulk lithologies are orthopyroxenitic, these aubrites may yet constitute products of partial melting and melt/rock interaction on a reduced parent body. This is remarkable, as Rb-Sr and Ar-Ar dates of Norton County and Shallowater suggest formation of aubrites around 4.5 Ga. This implies planetary differentiation to be an active process on enstatite chondrite-like bodies even during the initial stages of the solar system. Bishopville, in contrast, has an age of $3.5 - 3.9$ Ga, consistent with late parent body processing.

In summary, aubrites can be clearly connected to enstatite chondrites. However, segregation of metal and sulfide on the parent body, partial melting, brecciation, and inclusion of chondritic material make for a complex history, which is recorded in HSE signatures and Os isotopic composition. While earlier studies suggested an origin as condensates, or simple mantle cumulates, HSE and Os isotopes reveal a more complex history.

The origin of the terrestrial noble gas signature

Hans Keppler, Svyatoslav S. Shcheka
Bayerisches Geoinstitut, Universität Bayreuth, 95440 Bayreuth, Germany

The relative abundance of noble gases on Earth is very different from the solar abundance pattern. Light noble gases are strongly depleted due to loss to space and even xenon isotopes show a fractionation pattern probably related to hydrodynamic escape from a primordial atmosphere. However, compared to argon and the abundance pattern found in chondrites, xenon appears to be particularly depleted on Earth. This cannot be due to hydrodynamic escape. Moreover, mass balance calculations suggest that only about 50 % of the ^{40}Ar produced by decay of ^{40}K over Earth´s history is in the atmosphere, suggesting that a large fraction of argon is hidden somewhere in Earth´s interior.

Noble gases are generally believed to be extremely incompatible in mantle minerals. However, while there are numerous studies on noble gas solubility and noble gas partitioning involving upper mantle minerals, the solubility of noble gases in $MgSiO_3$ perovskite, the main constituent of the lower mantle, has never been measured. We have therefore investigated the solubility of argon and xenon in both pure and Al-bearing magnesium silicate perovskite.

Glasses of appropriate composition were loaded together with 40 – 80 bars of argon or xenon into platinum capsules. These capsules were first run at 10 GPa and 1200 ˚C in a multi anvil press to convert the glass into dense crystalline phases. The capsules were then re-run at 24 GPa and 1800 ˚C for one hour to crystallize perovskite in the presence of excess noble gas. Run products were investigated by electron microprobe.

The run products contained large empty cavities demonstrating noble gas saturation during the experiment. Argon contents as measured by electron microprobe were found to be homogeneously distributed through the samples and reached up to 1.3 wt % (!). Bubble formation due to argon loss was observed when the samples were hit by the electron beam during analysis. Perovskite produced in the presence of excess xenon contained numerous cavities, sometimes still filled by high-density xenon after the experiment. However, microprobe analyses of the perovskite showed xenon contents close to detection limit (about 100 ppm). Xenon solubility therefore appears to be orders of magnitude lower than argon solubility in perovskite.

The high solubility of argon in perovskite is probably due to the presence of oxygen vacancies that are being filled by argon. The occurrence of oxygen vacancies in magnesium silicate perovskite is well documented. Microprobe analyses of our samples show a clear deficiency in Si, which for reasons of charge balance requires oxygen vacancies. The low solubility of xenon is probably related to its large atomic radius, which makes it unable to occupy the oxygen vacancies.

Our data suggest that the depletion of xenon relative to argon in the Earth is related to the preferred retention of argon in perovskite during the crystallization of a magma ocean. The primordial atmosphere was likely lost at some stage due to strong hydrodynamic escape and/or the effects of a giant impact. Mantle convection later released some of the argon, but very little xenon stored in the deep mantle.

New constraints on the age of the lunar Nectaris basin from Re-Os isotope systematics of Apollo 16 impact melt rocks

Mario Fischer-Gödde[1*], Harry Becker[1]
[1]Freie Universität Berlin, Institut für Geologische Wissenschaften, FR Geochemie, Berlin, Germany
(*mafische@zedat.fu-berlin.de).

The surface of the Moon is characterized by large impact basins, most of which are believed to have formed during a brief period of intense bombardment of the inner solar system. The majority of Ar-Ar ages obtained on impact melt rocks related to lunar basins fall within a restricted range from 3.75 to 3.95 Ga. The data may indicate that large impact basins on the Moon may have formed within a short period of ~60 Ma. The narrow time interval and the scarcity of ages older than 4.0 Ga, have been used to argue for a pronounced spike in the flux of large impacting bodies in the inner solar system around 3.9 Ga (Late Heavy Bombardment) [1,2]. In contrast, some studies interpret cratering record and age data to be consistent with a steady decline of impact rates with time and argue that the records of earlier impacts were erased by subsequent cratering [3].

Critical information on the impact flux rate to the Moon can be obtained from the age of the Nectaris basin, because the sharpness of the age spike in mass flux curves is largely anchored by the age of Nectaris. The preferred age of Nectaris is 3.92 Ga [1,2], but an age of ~4.1 Ga has also been discussed [4,5], and some contradicting data on Apollo 16 samples suggest that the exact age of the basin remains effectively unconstrained [6,7].

Here, we report the first precise Re-Os isochron age on a lunar impact melt rock from Apollo 16. Sample 67935 collected from Outhouse Rock on the rim of North Ray Crater was analyzed for Re and Os concentrations and $^{187}Os/^{188}Os$ isotopic compositions using isotope dilution, inductively coupled plasma mass spectrometry (ICP-MS) and negative thermal ionisation mass spectrometry (N-TIMS). Re-Os isotope data for subsample aliquots of Apollo 16 sample 67935 yield a well defined internal isochron corresponding to an age of 4.11 ± 0.12 Ga and initial $^{187}Os/^{188}Os$ of 0.099 ± 0.001 (MSWD = 0.93). In a plot of 1/Os vs. $^{187}Os/^{188}Os$ no systematic relationship between Os isotopic composition and Os concentration exists, thus eliminating mixing processes accounting for the variation.

The Re-Os isochron age obtained for 67935 most probably represents the age of the impact on the lunar surface. High abundances of Re and Os in ancient lunar impact melt rocks reflect addition of these elements by the meteoritic impactors. Fractionated Re/Os in 100 mg subsamples of 67935 can be explained by centimetre-scale partitioning between solid metal and C and S bearing metallic liquids during cooling of the impact melt sheets. Control by solid metal-liquid metal partitioning is consistent with observations of FeNi metal and troilite intergrowths in 67935. Many Apollo 16 impact melt rocks contain FeNi metal (up to 2wt.%), which is characterized by HSE relative abundances similar to the compositions of magmatic iron meteorite groups (e.g. low Ir/Au), suggesting an iron meteorite-like impactor [8].

The Re-Os age of 67935 is resolvably older than Ar-Ar ages obtained for the majority of Apollo 16 samples, which typically range from 3.75 – 3.96 Ga [9]. Sample 67935 was collected from a boulder (Outhouse Rock) which was apparently excavated ~50 Ma ago by the North Ray crater projectile. The boulder represents a part of the Descartes formation which most probably derives from the Nectaris impact [2]. Some of the Apollo 16 samples from the Descartes Formation show younger Ar-ages, consistent with an Imbrium provenance [7]. These ages may indicate a heterogeneous provenance of Descartes Formation, or, may reflect resetting of Ar ages by the Imbrium event. The Re-Os age of 4.11 ± 0.12 Ga obtained for 67935 in this study seems to be unaffected by subsequent cratering and bears evidence for large basin forming impact events, in the present case likely related to Nectaris, occurring significantly before 3.9 Ga. Assuming an age of 4.1 Ga for the Nectaris impact would extent the formation interval of the large lunar impact basins to ~300 Ma and weaken the hypothesis of a Late Heavy Bombardment at 3.92-3.80 Ga.

References:
[1] Ryder (2002), *J. Geophys. Res.* 107, 6-1-6-14. [2] Stöffler & Ryder (2001), *Space Sci. Rev.* 96, 9-54. [3] Hartmann (2003), *MAPS* 38, 579-593. [4] Korotev et al. (2002), *Lunar and Planetary Institute*, abstract #3029. [5] Warren (2003), In: Davis, M. (Ed.), *Meteorites, Comets, and planets*, Elsevier. [6] Maurer et al. (1978), *GCA* 42, 1687-1720. [7] Norman et al. (2010), *GCA* 74, 763-783. [8] Korotev (1987), *Proc. Lunar Planet. Sci. Conf.* 17, E491. [9] Norman et al. (2006), *GCA* 70, 6032-6049.

Formation of Metallic Iron in the Martian dunite NWA 2737

Ulrich Bläß[1], Catherine McCammon[2], Falko Langenhorst[2]
[1]Friedrich-Schiller-Universität Jena, Institute of Geosciences, Department Mineralogy, Jena, Germany
[2]Bayerisches Geoinstitut, Universität Bayreuth, Germany

Strong shock metamorphism appreciably alter mineral properties and may result in new phase assemblages. Recent investigations of Van de Moortèle et al. (2007) have shown that the shock induced staining of olivine could be related to the exsolution of metallic nanoparticles. It has been speculated whether such processes could influence the metal segregation during core formation since shock deformation of olivine frequently occurs during the accretion of planetesimals.

In order to elucidate the processes responsible for strong olivine staining after impact processes, we investigated the microstructural features of strongly stained olivines from the second known Martian chassignite NWA 2737. This meteorite shows several unique shock related characteristics like an intense brownish staining, the occurrence of perpendicular sets of bright lamellae and the exsolution of metallic nanoparticles, whereas its mineralogical composition is quite similar to Chassigny (Beck et al., 2006). Several authors have given various explanations for the formation of some of these features. Van de Moortèle et al. (2007) assumed a metastable transition of olivine to a new high pressure polymorph (-phase) to explain additional Raman bands and the occurrence of a few percent of trivalent iron. Treiman et al. (2007) inferred a second shock event and a intermittent low pressure deformation to explain the formation of the bright lamellae and therein comprised fractures, whereas Pieter et al. (2008) argued for a single shock event and assumed slightly lower local shock conditions for the bright lamellae. Here we present an alternative explanation, which does not only provide the first physical process responsible for the up to now unknown formation of metallic nanoparticles, but could also explain the formation of all observed microstructural features consistently.

Our results of detailed microstructural investigations using transmission electron microscopy (TEM), electron energy-loss spectroscopy (EELS) and Mössbauer milliprobe spectroscopy revealed that all strongly stained olivine regions are characterised by the occurrence of metallic iron nanoparticles and a fine mottled contrast in TEM bright field images, which is due to an extremely high density of polygonised dislocations with Burgers vector [001]. The quantification of EELS-spectra of these regions resulted locally in a high trivalent iron fraction of up to 16 %. In contrast, the bright lamellae contain nearly no metallic nanoparticles, a sufficiently lower trivalent iron fraction and at least one order of magnitude lower density of individual dislocations.

Model mass balance calculations suggest that the high content of trivalent iron can be incorporated as a laihunite-component into the dislocation core of polygonised dislocations and could therefore be responsible for the intense brown staining. Iron metallic nanoparticles would represent residual disproportionation products of originally divalent iron of olivine and darken the deformed olivine additionally. Expected UV-VIS spectra are consistent with spectroscopic observations described by Pieters et al. (2008). Since the polygonisation of dislocations and the exsolution of metallic iron are both diffusion controlled processes, the meteorite must have remained sufficient time at elevated temperatures. For typical diffusion length of < 10 nm in this meteorite we calculated an annealing time of several days at ~ 500°C or less than 1 h at 800°C.

The required time at elevated temperatures and the related formation of polygonised dislocations result in two important implications. First, individual dislocations occurring in the bright lamellae must be formed separately and indicate therefore a second shock event, whereas the bright lamellae itself likely recrystallised subsequently to the first shock event. Second, since the amount of metallic iron is related to the dislocation density in olivine, this process can only generate a metallic iron fractions on the sub-percent level and could therefore not contribute to early differentiation processes or core formation.

References:
Beck, P., Barrat, J.A., Gillet, P., Wadhwa, M., Franchi, I.A., Greenwood, R.C., Bohn, M., Cotten, J., van de Moortèle, B., Reynard, B.(2006), Geochim. Cosmochim. Acta 70, 2127-2139. Pieters, C.M., Klima, R.L., Hiroi, T., Dyar, M.D., Lane, M.D., Treiman, A.H., Noble, S.K., Sunshine, J.M., Bishop, J.L.(2008), J. Geophys. Res. 113, E06004; doi:10.1029/2007/JE002939. Treiman, A.H., Dyar, M.D., McCanta, M., Noble, S.K., Pieters, C.M.(2007), J. Geophys. Res. 112, E04002, doi:10.1029/2006JE002777. Van de Moortèle, B., Reynard, B., McMillan, P.F., Wilson, M., Beck, P., Gillet, P., Jahn, S.(2007a), Earth Planet. Sci. Lett. 261, 469-475. Van de Moortèle, B., Reynard, B., Rochette, P., Jackson, M., Beck, P., Gillet, P., McMillan, P.F., McCammon, C.A.(2007b), Earth Planet. Sci. Lett. 262, 37-49.

Determination of stable valence state of Ge oxide in silicate melts during core formation of the Earth.

Philip Kegler[1], Astrid Holzheid[1]
[1] Christian-Albrechts-Universität zu Kiel, Institut für Geowissenschaften, Experimentelle und Theoretische Petrologie, Kiel, Germany.

The abundance of Germanium in today's Earth mantle is caused by the conditions and processes during accretion of the Earth and the formation of its core. The knowledge of the geochemical behavior of Ge at core formation conditions (high pressure, high temperature, low oxygen fugacities) is crucial for the interpretation of the Ge abundances in regard to the accretion and core formation processes. But even the valence state of Ge under oxygen fugacities (fO_2) assumed at core formation of the Earth (about 2 log units below the iron-wuestite buffer i.e. IW -2) is still unclear. Schmitt et al (1989) determined GeO as stable species in the silicate melt (experimental conditions: 1 atm., 1300° C, fO_2 range: IW -0.5 to − 2.7) and Capobianco et al. (1999) GeO$_2$ (experimental conditions: 1 atm., 1260° C, fO_2, IW -1.3 to +3.8).

Therefore the metal-silicate partition coefficients of Germanium ($D^{met-sil}Ge$ = c Ge^{metal}/c Ge^{silicate}) in dependence on oxygen fugacity and melt composition at 0.5 GPa and 1350°C were experimentally determined. Piston cylinder press experiments were performed under effectively closed system conditions to avoid the loss of Germanium caused by its high volatility. Crucibles of the investigated Fe$_{97}$Ge$_3$ alloy were filled with silicate melts. Metal and silicate phases were equilibrated for at least 6 hours. The oxygen fugacity during the experiments was controlled by using synthetic "basaltic" silicate melts with different of FeO contents (0.15 wt. %, 7 wt. %, 10 wt. %, 15 wt. % and 20 wt. %). This approach leads to oxygen fugacities ranging from IW -0.9 to IW -2.7.

This method of varying the fO_2 causes a change of the melt composition (in the following expressed as NBO/T after Mysen, 1983). To determine the effect of melt composition on $D^{met-sil}Ge$ additional experiments with different melt compositions but constant FeO content (7 wt. %) were performed. NBO/T values of these experiments ranged from 0.75 to 1.73.

Major and trace element concentrations of all post run charges were analyzed using EMP (metal phase and silicate glass; Universität Kiel) and LA-ICP MS (Ge content in the silicate glass; Universität Münster).

In Fig. 1 the calculated log $D^{met-sil}Ge$ values are plotted as function of log fO_2 (rel. IW) and NBO/T. The regressed plain of the 3D plot is:

$$\log D^{met-sil}Ge = 3.32\ (\pm 0.07) - 0.50\ (\pm 0.03)*\log fO_2 - 0.29\ (\pm 0.04)*NBO/T \qquad (R^2 = 0.988).$$

The slope of the correlation between log $D^{met-sil}Ge$ and oxygen fugacity allows the NBO/T independent determination of the valence state of Ge in the silicate melt. Within the fO_2 range of the experiments the valence state of Ge is 1.98 (± 0.11), i.e. GeO is the stable species in the silicate melt. This is in good agreement with Schmitt et al. (1989) but disagrees with Capobianco et al. (1999). A change of the stable Ge oxide species (GeO, GeO$_2$) from reducing to oxidizing conditions might be possible within the overlapping fO_2 range of all three studies (see fig. 2).

To determine the dependence of $D^{met-sil}Ge$ on other important parameters like temperature and pressure the knowledge of valence state of Ge at reducing conditions allows a correction of these $D^{met-sil}Ge$ to core formation fO_2 conditions. The understanding of the metal-silicate partition behavior of Germanium allows, in

Fig. 1: 3 D plot of log $D^{met-sil}Ge$ as function of log fO_2 (rel. IW) and NBO/T.
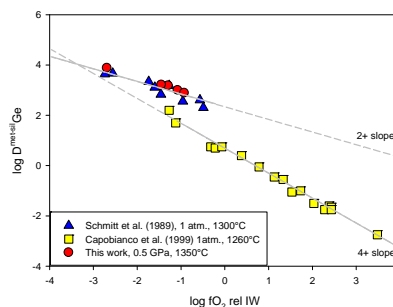
Fig. 2. Comparison of the experimental determined $D^{met-sil}Ge$ of Schmitt et al. (1989), Capobianco et al. (1999) and this work.

combination with other siderophile elements, a clearer view on the processes and conditions during core formation of the Earth and the other terrestrial planets.

Reference:

Capobianco, C. J., Drake, M. J., and de'Aro, J., 1999. Siderophile geochemistry of Ga, Ge, and Sn: Cationic oxidation states in silicate melts and the effect of composition in iron-nickel alloys. Geochim. Cosmochim. Acta, 63, 2667-2677.
Mysen, B. O., 1983. The structure of silicate melts. Ann. Rev. Earth Planet. Sci., 11, 75-97.
Schmitt, W., Palme, H., and Wänke, H., 1989. Experimental-determination of metal silicate partition coefficients for P, Co, Ni, Cu, Ga, Ge, Mo, and W and some implications for the early evolution of the Earth. Geochim. Cosmochim. Acta, 53, 173-185.

Si isotope fractionation in high-temperature metal-silicate systems of blast furnace simulation experiments - Implications for planetary core formation

Josepha Kempl[1], Elisa Bot[2], Pieter Vroon[1], Wim v. Westrenen[1]
[1]VU University Amsterdam, Faculty of Earth and Life Sciences, Department of Petrology, the Netherlands
[2]CORUS RD & T, IJmuiden Technology Centre, Department of Ironmaking, IJmuiden, the Netherlands

The largest differentiation event in the terrestrial planets was the process of early metal core segregation from a silicate mantle. Until a couple of years ago, the geochemical implications of this process were largely studied by linking trace element concentrations in planetary mantles with concentrations found in undifferentiated meteorites through trace element partitioning experiments. Recently, subtle differences in major element isotopic compositions have been used to further constrain core formation models (Poitrasson et al. 2004, 2009, Georg et al. 2007, Shahar et al. 2009, Fitoussi et al. 2009).

If Si is one of the light elements in the Earth's core, the distribution of stable Si isotopes between phases found in terrestrial and meteoritic material can be used to study terrestrial planetary core formation. In particular, the difference in Si isotope fractionation between meteorites and lunar and bulk silicate Earth (BSE) material led to the conclusion, that Si stable isotope fractionation between metal and silicate must have taken place at high-pressure, high-temperature conditions during core formation. In order to study Si isotope variations during early planetary metal core segregation, an experimental framework and systematic Si isotope measurements need to be developed.

In this study we present the results of Si isotope fractionation measurements in three ASAM (Advanced Softening And Melting rig) experiments, carried out at CORUS RD & T, IJTC, Department of Ironmaking, IJmuiden, NL. These experiments are used to study chemical reactions of steel producing metal liquids in blast furnaces and simulate the segregation of a metal alloy from ferrous silicate phases and iron-ores under reducing, high-temperature conditions. These experiments provide consequently a simplified model of terrestrial planetary core formation.

In the experiments 500 g of starting material, consisting of pellets of iron ore and iron silicates, iron bearing sinter material and partly ferrosilicic ore additives, was placed between coke layers under fixed temperature-gas atmosphere regimes in a carbon crucible. Temperature conditions were 1300 °C for one experiment and 1570 °C for two other ones, whereas atmospheric conditions were pre-reduced at 1000 °C to the Fe/FeO buffer before the experiment. In the course of each experiment the atmospheric conditions were further reduced to the Fe stability field. All runs were stopped with a cooling rate of ~ 400 °C/h after the final experiment temperature was reached.

Run products were composed of newly formed Si-bearing metal alloys, silicate slag of melilitic composition and few relicts of input material. All phases were analysed by electron microprobe. The Si isotope compositions of dissolved aliquots of each phase were measured by high-resolution multi-collector ICP-MS. All solutions have been dissolved using a NaOH alkaline digestion technique after van den Boorn et al. (2006).

With this work first Si isotope fractionation data determined from high-temperature experiments under reducing atmospheric conditions in metal-silicate systems will be presented.

References:
Boorn, v.d. S., Vroon, P.Z., Belle, v. C.C., Wagt, v.d. B., Schwieters, J., Bergen, M.J., Determination of silicon isotope ratios in silicate materials by high-resolution MC-ICP-MS using a sodium hydroxide sample digestion method, Journal of Analytical and Atomic Spectrometry, July 2006, 21

Fitoussi, C., Bourdon, B., Kleine, T., Oberli, F., Reynolds, B.C., Si isotope systematics of meteorites and terrestrial peridotites: implications for Mg/Si fractionation in the solar nebula and for Si in the Earth's Core, Earth and Planetary Science Letters, September 2009, 287

Georg, R.B., Halliday, A.N., Schauble, E.A., Reynolds, B.C., Silicon in the Earth's Core, Nature, June 2007, 447

Poitrasson F., Halliday A.N., Lee D.C., Levasseur S., Teutsch N., Iron isotope differences between Earth, Moon, Mars and Vesta as possible records of contrasted accretion mechanism, Earth and Planetary Science Letters, April 2004, 223

Poitrasson F., Roskosz M., Corgne A., No iron isotope fractionation between molten alloys and silicate melt to 2000 °C and 7.7 GPa: Experimental evidence and implications for planetary differentiation and accretion, Earth and Planetary Science Letters, February 2009, 278

Shahar, A., Ziegler, K., Young, E.D., Ricolleau, A., Schauble, E.A., Feu, Y., Experimentally determined Si isotope fractionation between silicate and Fe metal and implications for Earth's core formation, Earth and Planetary Science Letters, October 2009, 288

Rubidium isotopes constrain the origin of Earth's volatile elements and its Pb isotope evolution

Oliver Nebel[1,2], <u>Klaus Mezger</u>[2,3], Wim van Westrenen[4]
[1]The Australian National University, Research School of Earth Sciences, Canberra, Australia
[2]Westfälische Wilhelms-Universität Münster, Institut für Mineralogie, Münster, Germany
[3]Universität Bern, Institut für Geologische Wissenschaften, Bern, Switzerland
[4]FVU University Amsterdam, Faculty of Earth and Life Sciences, Amsterdam, The Netherlands

Relative to the composition of C1-meteorites the bulk silicate Earth (BSE) has a substantial deficit in volatile elements. This deficit is considered to be either due to incomplete condensation of these elements or volatile loss caused by heating during the early stages of the planet formation. This interpretation is predominantly based on observations of a first order progressive volatile depletion of the BSE relative to C1 chondrites that correlates roughly with the half-condensation temperatures of the elements. This general depletion trend for the volatile element abundances in BSE is complicated by the siderophile and/or chalcophile behavior of many moderately to strongly volatile elements during core formation processes. The combined cosmochemical and geochemical effects may be the cause for the irregularities observed in the depletion trend. In order to separate the different depletion processes that affected the final composition of BSE we compare the abundances of Rb and Pb and their isotope compositions in terrestrial samples and meteorites. Rubidium is a semi-volatile element and has a half condensation temperature that is close to that of Pb. Rubidium is strongly lithophile, thus its abundance is essentially only controlled by its volatility, whereas Pb can be chalcophile and possibly siderophile and may thus be even more depleted in BSE due to core formation.

Incomplete condensation and/or evaporation of a volatile element will result in stable isotope fractionation that should be measurable in meteorites and planetary materials and correlates with the element abundance. Thus if the depletion of the volatile elements on Earth is due to these processes BSE should have Rb that is enriched in the heavy isotope compared to primitive undepleted meteorites. In order to evaluate the variability of Rb isotopes in different solar system materials the Rb-isotope compositions of 17 primitive meteorites and terrestrial samples was analysed by MC-ICP-MS using Zr as an internal standard and standard-sample bracketing for mass bias correction. This technique results in a reproducibility of +/-0.2 ‰ on the ^{87}Rb/^{85}Rb.

The observed variation of the Rb-isotopes in all materials studied is less than 2 ‰. The variation does not correlate with the Rb elemental abundances relative to C1-chondrites. The unfractionated Rb-isotopes of the Earth imply that the volatile element depletion is not due to evaporation or incomplete condensation alone but requires at least a two step process. A more realistic model is that the Earth consists primarily of a large component of essentially volatile free material (Wänke & Dreibus, 1988) that was later mixed with a component that was not depleted in volatile elements. The extremely depleted component can have formed by incomplete condensation of the elements from the solar nebula or by evaporation due to impact processes that modified the first planetesimals which eventually formed the larger planets. In this model the Rb-isotope composition of the mixture is completely dominated by the isotope composition of the undepleted component. Mass balancing with a 90% depleted Proto-Earth and gain of 10% C1 material can account for the Rb isotope distribution and abundance in the present day BSE. If Pb behaved approximately like Rb, as is suggested by its similar half condensation temperature, BSE requires an additional Pb depletion event to account for its observed U/Pb and Pb-isotope systematics. However, the comparison of Rb abundances and isotopes with Pb abundances and isotopes implies that the Pb-depletion in the BSE was not solely due to core formation (Wood & Halliday, 2005, 2010) at ~110 Myrs after start of the solar system, but most of the Pb was already missing from the Earth prior to final core mantle equilibration.

References:
Wänke, H. and Dreibus, G. (1988), Philosophical Transactions of the Royal Society of London Series A-Mathematical Physical and Engineering Sciences 325, 545-557

Wood, B. J. and Halliday, A. N. (2005), Nature 437, 1345-1348

Wood, B. J. and Halliday, A. N. (2010), Nature 465, 767-770

Section 02

_____

Functional materials, Archaeometry

S02-T01

Crystal chemistry, structure and luminescence of hexaaluminates in the SrO-Al_2O_3-MnO_x-MgO system

<u>Andreas Richter</u>, Matthias Göbbels
University Erlangen- Nuremberg, GeoZentrum Nordbayern, Applied Mineralogy, Schlossgarten 5a, 91054 Erlangen, Germany

Luminescent materials are technologically used in energy-saving lamps, led's and laser applications. For the different applications materials with suitable excitation and emission spectra are necessary. The group of hexaaluminates is a group of materials with promising properties as host lattice for dopants generating luminescence. The Sr-hexaaluminate $SrAl_{12}O_{19}$ with magnetoplumbite structure type is known to generate luminescence with Mn^{2+} doping [1, 2]. In the ternary system SrO-Al_2O_3-MgO new types of hexaaluminates have been discovered [3]: SAM-II ($SrMgAl_{10}O_{17}$) belongs to the β-alumina structure type and SAM-I ($Sr_2MgAl_{22}O_{36}$) is a mixed layer structure built of magnetoplumbite and β-alumina units in 1:1 ratio [4]. Both are theoretically suitable to incorporate Mn as dopant to generate fluorescence. This leads to our interest in the pseudoquaternary system SrO-Al_2O_3-MnO_x-MgO to study the substitution mechanism, crystal chemistry and optical properties of SAM-I and SAM-II.

The ternary subsystems SrO-Al_2O_3-MgO [5] and SrO-Al_2O_3-MnO_x [6] are already known. For studying the phase diagram suitable samples were prepared by mixed oxide route and fired at 1700°C in air. The phase equilibria and crystal chemistry was determined by EPMA analyses. To study the optical properties and structure crystals were grown in an optical floating-zone furnace.

The Mn substitution in SAM-I and SAM-II was proven and calculations from EPMA data lead to Mn^{3+} substitution in both structures. The Al-rich part of the pseudoquaternary system will be presented and the substitution mechanism will be discussed.

The crystals were grown of stoichiometric ceramic precursors and an intermediate melting composition. The grown crystals are of good quality and show large single crystal areas but are crossed by cracks from cooling down. The process will be optimized.

Reference:

Kröger, F.A., *Some aspects of the luminescene of solids*. 1948: Elsevier.; Singh, V., et al., *Luminescence and EPR studies of Mn-activated SrAl12O19 phosphor prepared by facile combustion approach.* Physica B: Condensed Matter, 2008a. **403**(1): p. 120-125.; Iyi, N. and M. Göbbels, *Crystal Structure of the New Magnetoplumbite-Related Compound in the System SrO-Al₂O₃-MgO.* Journal of Solid State Chemistry, 1996. **122**(1): p. 46-52.; Göbbels, M. *Crystal Chemistry and Crystal Structures of Complex Hexa-aluminates and Hexa-ferrites.* in *Applied Mineralogy in Research, Economy, Technology, Ecology and Culture. Proc. ICAM (2004)*. 2004. Sao Paulo.; Göbbels, M., *Phasen der beta-Tonerd- und Magnetoplumbit- Familien mit 2-wertigen Kationen (Ca, Sr, Ba) - Phasenbeziehungen, Kristallchemie und Struktur*, in *Habilitationsschrift; Fakultät für Bergbau, Hüttenwesen und Geowissenschaften*. 1996, RWTH Aachen.; Richter, A. and M. Göbbels, *will be published.*

The impact of SO$_2$ polluted air on dolomitic lime mortar

Anja Diekamp[1], Jürgen Konzett[1], Peter W. Mirwald[1]
[1]University of Innsbruck, Institute for Mineralogy and Petrography, Innsbruck, Austria

The impact of SO$_2$-pollution on dolomitic lime mortars from a medieval church near Bolzano, Northern Italy (St. Martin/Kampill) was studied. The samples investigated are Romanesque to Baroque mortars from the façade and intonaco-plaster from Gothic interior frescos. Their binder essentially consists of calcite [CaCO$_3$], magnesite [MgCO$_3$] and hydromagnesite [4MgCO$_3 \cdot$ Mg(OH)$_2 \cdot$ 4H$_2$O]. SO$_2$-pollution from an adjacent industrial area and a freeway caused formation of gypsum and Mg-sulfate [hexahydrite MgSO$_4 \cdot$ 6H$_2$O], the latter restricted to areas under the shades of the eaves and as efflorescence on the frescoes.

Petrographic microscope and electron microprobe analysis of thin sections indicate that the Mg-phases of the binder are less prone to sulfation than calcite. Elemental mapping on a µm-scale shows the higher solubility of Mg-sulfate compared to gypsum.

In addition Mg-sulfate efflorescence experiments were conducted at different air humidities to study the deleterious hexahydrite-epsomite phase transition by micro-Raman spectroscopy. We find that hexahydrite persists for several weeks under air humidity levels where epsomite [MgSO$_4 \cdot$ 7H$_2$O] is thermodynamically stable. Thus the hexahydrite-epsomite phase transition may under certain circumstances be much more sluggish than previously assumed. These results are important for an assessment of damages and the development of restoration strategies for sulfate-contaminated mortars.

A new method for X-ray Investigation of Materials - Ranging from classical Bragg-Brentano type diffraction phase analysis to 3 dimensional CT microstructure analysis

Richard Wenda [1], Herbert Pöllmann[2], Roger Meier[3,] Gabriel Blaj[3], Uli Riedl[3], Thorbjoern Schoenbeck[4]
[1]Georg-Simon-Ohm-Hochschule, Fakultät für Werkstofftechnik, Nürnberg, Germany
[2]Martin-Luther-Universität, Institut für Geowissenschaften, FG Mineralogie/Geochemie, Halle, Germany
[3]PANalytical B.V., Application Competence Centre, Almelo, The Netherlands
[4]PANalytical GmbH, Kassel, Germany

X-ray diffraction is a widely-used technique in all fields of materials sciences. XRD can be used to identify and quantify phases, determine their crystallite size and particle size, derive the crystal structure or to measure texture of solid polycrystalline samples. In addition, several other x-ray characterization techniques exist apart from diffraction, such as x-ray absorption measurements or X-ray tomography (computer tomography, CT).

In this work we demonstrate the combination of multiple X-ray methods to investigate various ceramic and cementitious samples by a laboratory X-ray-system. We determined the x-ray density by absorption, phase assemblage, phase quantity and 3-dimensional texture of microstructured samples. Several detection modes are applied: Density (0D), Phase formation (1D), Phase distribution (2D), Microstructure (Fabric) and Pore Distribution (3D).

The figure shows the results for one of the analytical methods done on the laboratory system for μ-tomography. The pore size and pore orientation can easily be determined.
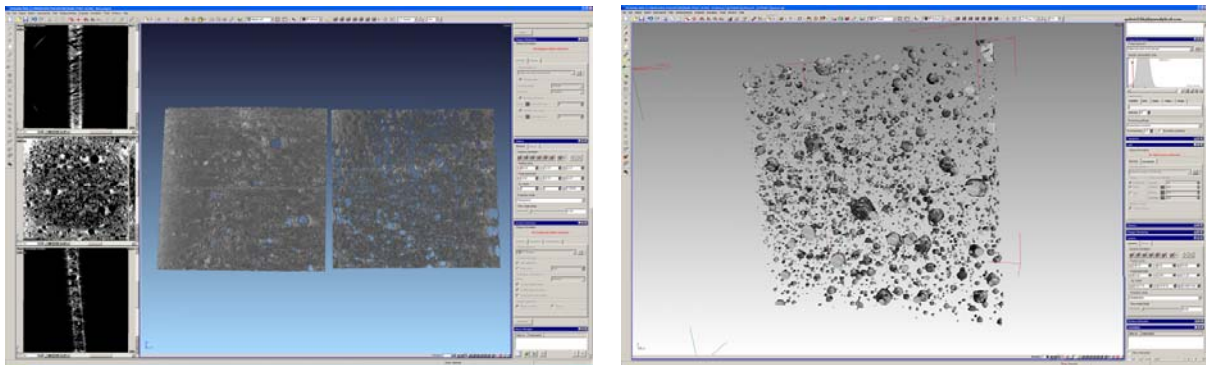

Fig.1: Left side: Comparision of voids in two different concrete samples. Right side: Visualization of pore size distribution.

In particular the CT results are well suited to correlate the microstructural features with macroscopic results such as the phase quantification and the pore size distribution. Furthermore it is a good basis for subsequent cutting/slicing of the samples and for SEM or electron microprobe analysis.

The impact of surface polishing in the susceptibility of stone to salt decay

Maja Urosevic[1], Eduardo Sebastián Pardo[1], Carolina Cardell[1],
[1] Department of Mineralogy and Petrology, Faculty of Science, University of Granada, Fuentenueva s/n, 18002 Granada, Spain.

Salt-induced deterioration of natural and artificial building materials (e.g. stones, mortars, bricks and ceramics) is drastically accelerated in coastal areas due to the action of marine aerosols, with significant cultural and economic implications (e.g. Mottershead et al., 2003; Cardell et al., 2003a,b, 2008). In fact, the sizeable investment to preserve the architectural heritage, as well as to repair damage due to salt weathering processes on ornamental and building materials used in modern constructions, makes necessary application of scientific knowledge. Despite the abundant literature concerning this topic, little attention has been paid to ascertain the effect of different stone surface finishing processes to mitigate stone decay caused by marine aerosols. In this study polished and rough travertine rock samples were subjected to a sea salt spray ageing test in controlled-atmosphere chamber to explore potentially contrasting stone decay behavior due to different surface finishing processes.

Travertine has been an important building material for monuments and civil constructions from Roman times until present throughout Europe and Near East (e.g. Török, 2006). It has been used as structural stone (ashlars and plane surfaces) and in ornamental elements as sculptures. In fact, travertine is one of the most frequently used stones in modern architecture worldwide. To reproduce more realistic conditions of building stone decay in marine environment, sea water was collected from the Mediterranean Sea at Granada coast (Salobreña, Southern Spain). The degree of salt damage was estimated by comparing changes in mineralogical and chemical composition, petrophysical characteristics and chromatic variations between freshly quarried samples and aged ones. The mineralogy of the samples was analyzed by X-ray powder diffraction, texture of the samples by polarized optical and environmental scanning electron microscope, and the travertine pore system by means of mercury intrusion porosimetry and gas sorption isotherms. Chromatic characteristics of rough and polished rock samples before and after the ageing test were determined by colorimetry.

Results have revealed that stone damage due to the impact of marine aerosols is strongly related to the stone surface finishing (i.e. rough or polished surface stone). In fact, the polished finishing – combined with a gypsum-based plaster and an epoxy silicone resin infilling – protects the travertine against marine salt corrosion. Moreover, the finishing process effectively blocks the pore system in the near-surface zone of the travertine, thus preventing penetration of the saline spray into the stone. By contrast, on the irregular rough travertine surface, salt crystallization is more abundant and induces larger open porosity and also higher surface fractal dimension than on the polished surface, which in turn make it more vulnerable to further salt spray attack. In terms of chromatic alteration, on rough surfaces chromatic changes are less intense than on polished rock surfaces.

This study emphasizes that prior to establishing conservation or maintenance practices, it is advisable to characterize the materials used in filled travertines (as well as in other stone types), since undesirable products such as gypsum salt can activate weathering mechanisms. Also, in coastal areas it is recommended to apply ad hoc, long-term salt-spray ageing tests on construction and decorative materials to optimize conservation interventions for buildings exposed to marine aerosols.

References:
Cardell, C., Delalieux, F., Roumpopoulos, K., Moropoulou, A., Auger, F., Van Grieken, R. (2003a), Salt-induced decay in calcareous stone monuments and buildings in a marine environment in SW France, Construction & Building Materials, 17, 165–179.
Cardell, C., Rivas, T., Mosquera, M.J., Birginie, J.M., Moropoulou, A., Prieto, B. (2003b), Patterns of damage in igneous and sedimentary stones under conditions simulating sea-salt weathering, Earth Surfaces Processes & Landforms, 28, 1–14.
Cardell, C., Benavente, D., Rodríguez Gordillo, J. (2008), Weathering of limestone building material by mixed sulfate solutions. Characterization of stone microstructure, reaction products and decay forms, Materials Characterization, 59(10), 1371–1385.
Mottershead, D., Gorbushina, A., Lucas, G., Wright, J. (2003), The influence of marine salts, aspect and microbes in the weathering of sandstone in two historic structures, Building & Environment, 38,1193–1204.
Török, Á. (2006), Influence of fabric on the physical properties of limestones, In: Kourkoulis, S.K. (Ed.), Fracture Failure of Natural Building Stones, Springer, 487–497.

Lithium isotopic self-diffusion in LiAlSi$_2$O$_4$ glasses

Anna-Maria Welsch[1], Sebastian Roß[1], Harald Behrens[1], Ingo Horn[1]
[1]Institut für Mineralogie, Leibniz Universität Hannover, Germany

The research focused on Li-diffusion in silicate systems is of great interest for geosciences and material sciences, particularly in relation to the technological applications for catalysts, sensors, adsorbents, advanced ceramics and especially solid state electrolytes for Li-ion batteries. Understanding the Li-isotopic fractionation kinetics which takes place between fluid, melt and solid phases leads to better defining geological processes in which lithium geochemistry plays an important role. This study focuses on the investigation of the Li isotopic effect in glasses of natural spodumene composition, LiAlSi$_2$O$_4$.

Lithium has two stable isotopes, ^{6}Li and ^{7}Li with the very uneven abundance, (7.42 % for ^{6}Li and 92.58 % for ^{7}Li) and the natural isotopic ratio ^{7}Li/^{6}Li = 12.48 according to the literature data. Due to the almost 17% differences in the masses the isotope-fractioning takes place during diffusive transport. In order to clarify the lithium self-diffusion isotopic effect we have treated the synthesized spodumene glasses with salt melts purely containing at different temperatures and exposure time, at the ambient pressure.

The glasses were made by melting the natural spodumene crystals of gem quality. In this manner the natural Li-isotope ratio was affected by the subsequent diffusion from the LiNO$_3$ salt melt distributed in the form of a thin film layer on the highly polished spodumene glass surface. Such treated samples were exposed to high temperature for different periods of time and later on cut perpendicularly to the treated surface. The change in the natural ^{7}Li/^{6}Li ratio was tested by the UV femtosecond laser ablation ICP-MS as the function of the penetration depth. The ICP-MS combined with the UV femtosecond laser ablation as the highly precise method which does not lead to additional recombination of the isotopic ratio and is particularly applicable for the investigation of light element isotopic fractionation.

Additionally to this method, we have tested the change in the conductivity of the treated samples by impedance spectroscopy, in the range between 1 Hz to 1 MHz. We present the results of our investigations on Li-isotopic self-diffusion in the spodumene crystals obtained by these experimental approaches which unequivocally indicate to the scale of the isotopic exchange at different temperatures and its effect on the ionic conductivity.

Magnesium Phosphate Acid-Base Cement

Katrin Schollbach (presenting author)[1], Herbert Pöllmann (co-author)[1]
[1]Martin-Luther-Universität Halle-Wittenberg, Institute of Geosciences, Halle, Germany

One of the oldest known systems of acid-base cements are Sorel cements, which are formed by the reaction of magnesium oxide with a magnesium chloride solution, reacting to $5Mg(OH)_2 \cdot MgCl_2 \cdot 8H_2O$ and $3Mg(OH)_2 \cdot MgCl_2 \cdot 8H_2O$. This cement is fast setting, resistant to acid and salt attacks, has a high early strength and can be produced with lower CO_2 emissions compared to ordinary Portland cement (OPC). But its low resistance to water has prevented a more widespread use of this material. Today it is mostly used in seals for deep geological repositories and tiles or cast floors. One possible way of solving this problem is the use of phosphates, particularly magnesium phosphates to improve water resistance.

Magnesium phosphates can be obtained by mixing magnesium oxide or magnesium hydroxide with phosphoric acid to form acid-base cement. According to Kingery (1950) and Finch & Sharp (1989) the main reaction product is Newberyite $MgHPO_4 x 3H_2O$ along with amorphous phases, however the reaction was not studied in detail as a function of age or chemical starting composition. To gain an overview MgO and $Mg(OH)_2$ was mixed with phosphoric acid and water, with the composition varying between 10-30 wt% $MgO/Mg(OH)_2$, 20-85 wt% H_3PO_4 and 15-60 wt% H_2O. The MgO used was burned at 1100°C for 2h to slow down the strong exothermic reaction between MgO and the phosphoric acid.

Investigations with X-Ray diffraction show that in most cases Newberyite is present, along with unreacted MgO or $Mg(OH)_2$ and a broad amorphous hump between 18 and 33° 2Theta (Cu Kα). However $Mg(H_2PO_4)_2$ and $Mg(H_2PO_4)_2 x 2H_2O$ have also been observed, along with some unidentified peak marked Y in Figure 1. $Mg(H_2PO_4)_2$ is marked with X.

This shows that the reaction is occurring as reported in literature, and that some yet unknown phases exist in the $MgO/Mg(OH)_2$-H_3PO_4-H_2O system. Further research is necessary to investigate how Phosphate changes the reaction products and properties when introduced different Sorel system.
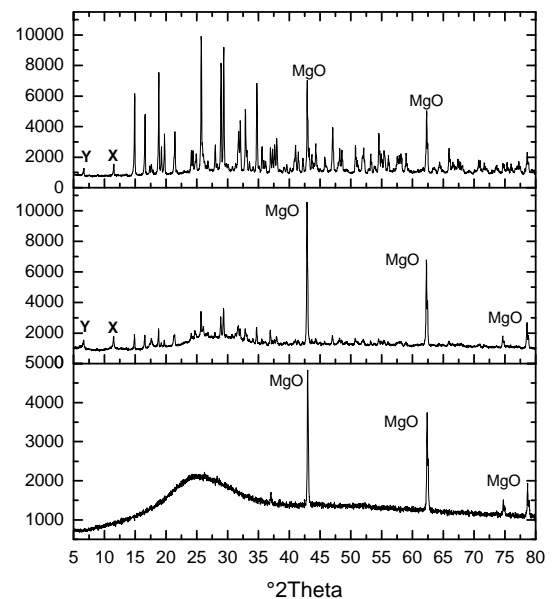

Figure 1) X-ray diffractogramms taken from a sample with 20wt% MgO, 15wt% H_2O and 65wt% H_3PO_4 after 4h, 4d and 19d. The peaks marked X belong to $Mg(H_2PO_4)_2$. The unidentified peak is marked Y. Unmarked Peaks belong to Newberyite

Reference:
Kingery, W.D. (1950), Fundamental Study of Phosphate Bonding in Refractories I-III, Journal of the American Ceramic Society, Aug. 1 1950, 239
Finch, T. & Sharp J.H. (1989), Chemical Reactions between magnesia and aluminium orthophosphate to form magnesia-phosphate cements, Journal of Materials Science, 24, 1989, 4379

Structural point defects in CuInS$_2$: a neutron powder diffraction study

Susan Schorr[1], Christiane Stephan[2], Michael Tovar[3], Hans-Werner Schock[2]
[1]Freie University Berlin, Institute of Geological Sciences, Berlin, Germany
[2]Helmholtz Zentrum Berlin für Materialien und Energie, Department of Solar Energy Research, Berlin, Germany
[3]Helmholtz Zentrum Berlin für Materialien und Energie, Department of Structural Research, Berlin, Germany

Roquesite (CuInS$_2$) is not only a well known ore mineral, it is also a compound suitable for applications in thin film photovoltaics. Thin film solar cells with a CuInS$_2$ absorber layer reach efficiencies up to 12%.

CuInS$_2$ is one of the I-III-VI$_2$ compounds crystallizing in chalcopyrite type crystal structure (space group $I\overline{4}2d$). Both cations are tetrahedrally coordinated by the anions and vice versa. The Cu$^+$ cations are situated on a 4a (0 0 0), the In^{3+} cations on a 4b (0 0 ½) and selenium on a 8d position (x ¼ ½).

In general these compounds have a non-stoichiometric composition which can be expressed by the general formula Cu$_{1-y}$In$_y$S$_{1/2+y}$ with y≠0.5. At y=0.5 the stoichiometric compound CuInS$_2$ is observed. With deviation of stoichiometry the chalcopyrite type structure still consists, but structural parameters are changing.

In general 12 intrinsic point defects can exist in the chalcopyrite type structure (vacancies, interstitials and anti-site defects). A number of successful studies have been made concerning the characterisation of electronic defect levels, especially in CuInSe$_2$, by absorption and photoluminescence techniques, but very little is known about the structural origin of defects.

In this study a systematic investigation on non-stoichiometric (copper-poor, copper-rich) CuInS$_2$ powder samples is presented, to get a basic knowledge about the dominant intrinsic point defects existing in off-stoichiometric CuInS$_2$. Neutron powder diffraction with subsequent Rietveld analysis is a suitable method to determine the cation distribution within the crystal structure.

Powder samples of Cu$_{1-y}$In$_y$Se$_{1/2+y}$ with various Cu/In ratios (0.99 - 0.80) have been prepared by solid state reaction of the pure elements (99.9999 % purity) in sealed, evacuated silica tubes at T=850°C. This procedure has been repeated three times, with homogenizing the samples in between by grinding them in an agate mortar. To observe the chemical composition of the powder samples, wavelength dispersive X-ray analysis (WDX) was applied using a JEOL-JXA 8200 electron microprobe system. In order to obtain reliable results from the WDX measurements, the system was calibrated using standards. The neutron powder diffraction data were collected at the Berlin Research Reactor BERII at the fine resolution powder diffractometer using a wavelength of λ=1.79776 Å. Data treatment was done by full pattern Rietveld-Refinement (Rietveld 1969) using the FullProf Suite software package (Rodriguez-Carvajal 2001) .

To figure out the type of intrinsic point defects in non-stoichiometric Cu$_{1-y}$In$_y$S$_{1/2+y}$ the method of average neutron scattering length was applied. The values of the experimentally determined average neutron scattering length of the 4a site ($\overline{b}_{4a}^{\,exp}$), where normally Cu is situated, decrease with ongoing copper deficiency and in return the values of $\overline{b}_{4b}$ are increasing. This decrease of $\overline{b}_{4a}^{\,exp}$ can be caused by the formation of copper vacancies (V$_{Cu}$) and/or an In$_{Cu}$ anti-site defect. On the other hand, the simultaneous increase of the average neutron scattering length of the 4b site ($\overline{b}_{4b}^{\,exp}$) can only be caused by the formation of a Cu$_{In}$ anti-site defect, because $b_{Cu} > b_{In}$. Taking into account the chemical composition, the cation-vacancy distribution can be derived by a successive approximation of experimentally determined and calculated average neutron scattering lengths of the cation sites, the latter are derived using a certain cation-vacancy distribution model.

These investigations have shown, that with decreasing Cu/In ratio the concentration of copper vacancies is increasing accompanied by a slight formation of Cu$_{In}$ anti site defects. If the vacancy concentration reaches a limit level, the vacancy compound CuIn$_5$S$_8$ is formed by clustering of the defects.

This work has shown that neutron powder diffraction is a well suitable method for studying the intrinsic point defects in off stoichiometric copper chalcopyrites.

Reference:
Rietveld, H. M. (1969), A Profile Refinement Method for Nuclear and Magnetic Structures, Journal of Applied Crystallography 2, 65

Rodriguez-Carvajal, J. (2001), Recent Developments of the Program FULLPROF, Commission on Powder Diffraction (IUCr). Newsletter 26, 12-19

Die Helix-CT: eine neue Methode in der archäometrischen Forschung

Alexandra Franz [1], Klaus Bente[1], Randolph Hanke[2]
[1] Universität Leipzig, Institut für Mineralogie, Kristallographie und Materialwissenschaft, D-04275 Leipzig
[2] Entwicklungszentrum Röntgentechnik, gemeinsame Abt. des IZfP Saarbrücken u. IIS Erlangen, D-90762 Fürth

Die Untersuchung mittels 3D-Röntgencomputertomographie ist eine sich mittlerweile etablierende Methode zur Analyse von archäologischen sowie kunst- und kulturhistorischen Objekten. Die Methode ist zerstörungsfrei sowie berührungslos und erlaubt sowohl die dreidimensionale Darstellung nicht zugänglicher Geometrien im Inneren von Untersuchungsobjekten.

Computertomographie basiert auf der Abschwächung polychromatischer Röntgenstrahlung bei Durchdringung eines Objektes. Bestimmt wird der lineare Schwächungskoeffizient μ, der sich als Funktion der Position im Raum, der Dichte und der verwendeten Röntgenenergie darstellt. Das Prinzip besteht darin, das zu untersuchende Objekt in Schichten aufzuteilen und für jede Schicht eine Vielzahl von Projektionen unter verschiedenen Winkeln aufzunehmen. Aus diesen Projektionen kann durch Rücktransformation ein virtuelles Volumenbild rekonstruiert werden. Die Rekonstruktion des dreidimensionalen Datensatzes mittels des Kegelstrahl-Rekonstruktionsalgorithmus nach Feldkamp et al. basiert auf einer reinen Kreisbahn des Fokus um das Objekt(siehe Abb. 1).
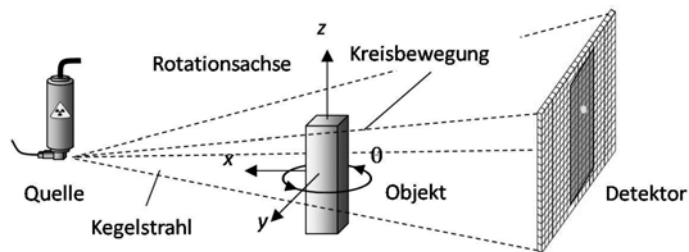

Abbildung 1 prinzipielle Funktionsweise der 3D μ-CT

Diese wie auch andere abbildende Methoden, die auf Strahlung basieren, erzeugen Artefakte die zusammen dem real gemessenen Objekt in den Messdaten dargestellt werden.

Es gibt mehrere Typen von Artefakten, die die Messdaten negativ beeinflussen. Dies sind zum Beispiel Artefakte, die aufgrund der polychromatischen Strahlung auftreten (Strahlaufhärtungsartefakte) oder die in mehrphasigen Proben mit unterschiedlich starker Schwächung zu sogenannten „Absorptionsschatten" und damit zu Informationsverlusten führen.

Bei großen Öffnungswinkeln des Kegelstrahls kann es zu hütchenartigen Abbildungsfehlern, den „Feldkamp-Artefakten" kommen, die vor allem im Bereich abseits der mittleren Ebene des Röntgenstrahls auftreten und die Bildqualität in eben diesen nicht zentralen Schichten deutlich verringern.

Um diese Mängel zu beheben wurde eine spiralförmige Aufnahmegeometrie realisiert -die Helix-CT.

Hier wird nicht, wie bei der konventionellen Computertomographie eine kreisförmige Bahn zum Scannen des Objekts beschrieben, sondern das Messobjekt von Projektion zu Projektion gedreht und gleichzeitig in Richtung der Drehachse verschoben(siehe Abb. 2). Der Rekonstruktionsalgorithmus ist eine Erweiterung des Feldkamp-Algorithmus in Anlehnung an die Arbeit von K. Sourbelle und W.A. Kalender.

Die Helix-CT hat mehrere Vorteile. Zum einen werden die Feldkamp-Artefakte vollständig vermieden, zum anderen wird dadurch, dass sich das jede Schicht des Messobjekts einmal im zentralen Teil des Kegelstrahls befindet die Bildqualität deutlich erhöht. Durch die spiralförmige Schraubung wird die Messbereichshöhe nur durch die maximal verfahrbare Wegstrecke entlang der Drehachse beschränkt. Somit können auch lange Objekte mit einer Messung vollständig erfasst werden.

Diese Methode wird derzeit am Institut für Mineralogie, Kristallographie und Materialwissenschaft auf ihre Anwendbarkeit in der Archäometrie getestet, vor allem in
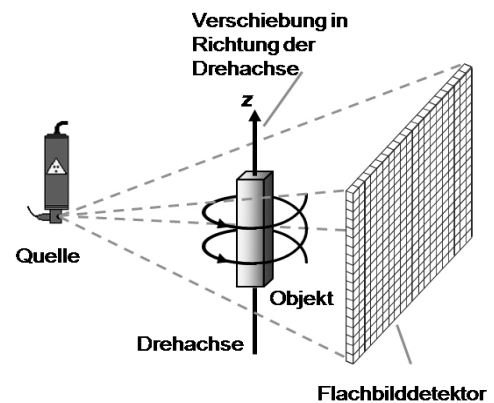

Abbildung 2: prinzipielle Funktionsweise der Helix-CT

Hinblick auf die Verbesserung der Datenqualität für weitergehende Analysen.

Reference:

R. Hanke, Vortrag zur DGZfP Jahrestagung, Erfurt 2010
W.A. Kalender, Computertomographie. Grundlagen, Gerätetechnologie, Bildqualität, Anwendungen. 2. überarb.
Und erw. Auflage. Publicis Corporate Publishing, Erlangen 2006

Section 03

———————

Metamorphic processes

From mineral transformations to plate dynamics: the contribution of the metamorphic petrology

Romain Bousquet[1], Roland Oberhänsli[1], Diane Arcay[2]
[1] Institute of Earth and Environmental Sciences, University of Potsdam, Potsdam, Germany
[2] Géosciences Montpellier, UMR 5243 - CC 60, Université Montpellier 2, Montpellier, France

Many large-scale dynamic processes, from continental rifting to plate subduction, are intimately linked to metamorphic reactions. During rifting, phase transformations in the rising lithospheric mantle cause uplift. At convergent margins metamorphic reactions help make plate subduction self-sustained and may also facilitate plate bending and trigger intra-slab earthquakes. Consequences of metamorphic reactions on geodynamic processes are, in spite of appearances, yet poorly understood. For example few attention has been paid to important aspects of the metamorphic processes: consequences of mineral transformations on rocks physical properties.

We propose first to explore how constrain and model the evolution of physical parameters as density or seismic velocities in dynamic systems and then we will discuss the possible implications:

- on the dynamic of the subduction and associated reactions. We will show that some subduction preserved OH-minerals then are more propitious to exhume (U)HP rocks and to obstruct the subduction dynamic. Other subduction are more propitious to dehydrate and to produce heavier rocks and self-sustained subduction.

- on the dynamic of the mantle wedge, where the upper plate dynamic seems to be influenced by the dehydration reactions. We test the role of bulk composition variation of the lithosphere on the back-arc dynamic. Preliminary results suggest that chemistry favoring appearance of OH-minerals induce local convection and formation of back-arc basin while other chemistry will enhance the stability of mobile belts.

- on orogenic plateau for which the lithospheric mantle is supposed to be delamined. We propose alternatively a thinning process of the lithosphere by the formation of hydroxylated minerals inside the hydrated lithosphere to explain plateau uplift as well the seismic anomaly.

We will show that mineral transformations associated to the metamorphism can be an alternative to changes attributed solely to thermal and compositional differences.

S03-T02

New insights into the Early Paleozoic history of the multistage Qinling orogen (East central China)

<u>Thomas Bader</u>[1], Leander Franz[1], Christian de Capitani[1], Lothar Ratschbacher[2], Bradley R. Hacker[3], Carsten Weise[2], Maria Wiesinger[2], Michael Popp[2]

[1]Mineralogisch-Petrographisches Institut, Universität Basel, CH-4056 Basel
[2]Institut für Geologie, Technische Universität Bergakademie Freiberg, D-09599 Freiberg
[3]Geological Sciences, University of California, Santa Barbara, CA-93106

The multistage Qinling orogen was formed during several subduction-accretion events, which occurred between the Neoproterozoic and the Triassic. A Cambrian orogeny manifests itself by the formation and exhumation of rare ultra-high pressure (UHP) metamorphic eclogites enclosed in widespread paragneisses at the northern margin of the Qinling Group that is interpreted as microcontinent; the UHP metamorphism is proven by diamond inclusions in ~507 Ma old metamorphic zircons (Yang et al., 2003). Southerly abutting Upper Proterozoic felsic gneisses and intercalated metabasites of the Qinling Group underwent ultra-metamorphism and where intruded by numerous granitoid intrusions when a Devonian continental arc built up above a north-dipping subduction zone (see Ratschbacher et al., 2003 for review).

Here, we present new petrologic data derived by equilibrium assemblage calculations using the Domino-Theriak (de Capitani & Petrakakis, 2010) and the TWQ (Berman, 1991) programs as well as conventional geothermobarometry that were combined with $^{40}Ar/^{39}Ar$ and U/Th/Pb geochronology.

Along the northern margin of the Qinling Group, fine to medium-grained, weakly foliated eclogites occur as lenses in garnet bearing phengite gneisses. Texturally, our samples give indications for the UHP event by numerous radial cracks around quartz inclusions in garnet pointing to former coesite. Based on the assemblage garnet (core) – omphacite – coesite – kyanite, we calculated 570 °C at 2.8 GPa, conditions at the coesite – quartz transition. The phengite bearing eclogite sample 811081A reveals quartz-eclogite facies conditions of ~ 600 °C at 1.8-2.2 GPa, representing an early exhumation stage. The exhumation history of the eclogitic rocks is further constrained by the amphibolite facies mineral assemblage garnet (rim) – amphibole – plagioclase – quartz – ilmenite pointing to 650 °C at 1.0-1.4 GPa. The garnet bearing gneisses 75223A and 75214D recrystallized at similar conditions of 630 °C at 1.5 GPa and 630-660°C at 1.0 GPa, respectively. The central and southern sections of the Qinling Group in part reveal ultra-metamorphic PT conditions as evidenced by migmatisation of felsic gneisses. Peak metamorphic assemblages comprise garnet – plagioclase – K feldspar – quartz – sillimanite – ilmenite or garnet – hornblende – plagioclase – quartz – ilmenite in metabasites. PT estimates using the DOMINO program and conventional geothermobarometry point to 680-770 °C at 0.5-0.8 GPa. The lower temperatures are interpreted to reflect retrograde equilibration. Gneisses as well as metabasites do not show indications of eclogite facies conditions. However, the discovery of a small body of strongly overprinted spinel peridotite in the southwestern part of the Qinling Group, which had re-equilibrated to 630-670 °C (i.e. identical temperatures to the surrounding gneisses and amphibolites), points to a probable early HP event.

$^{40}Ar/^{39}Ar$ dating of phengites from the eclogite bearing unit along the northern margin of the Qinling Group yielded 470 ± 1 Ma. Significantly younger ages were obtained from the central and southern Qinling Group. $^{40}Ar/^{39}Ar$ dating of metamorphic hornblende yields 373-395 Ma while biotite yields 330-390 Ma. Th/Pb ion-probe monazite ages of granitoids (~393 Ma) and ultra-metamorphic gneisses (~397 Ma and ~381 Ma) substantiate the Devonian continental arc. Remarkably, four out of five monazite samples contain grains reflecting a ~352 Ma growth event.

During their exhumation, the UHP metamorphic rocks underwent two major recrystallization stages, one at 600°C and 1.8-2.2 GPa and the other at 630-660°C and 1.0-1.5 GPa. The exhumation from the diamond stability field to the lower crust occurred within ~37 Ma. Arc magmatism started significantly later in the Early Devonian and might display two peak activities at ~380-395 Ma and ~352 Ma.

References:
Berman, R.G. (1991), Thermobarometry using multi-equilibrium calculations: a new technique, with petrological applications, Canadian Mineralogist, 29, 833–855
De Capitani, C. & Petrakakis, K. (2010), The computation of equilibrium assemblage diagrams with Theriak/Domino software, American Mineralogist, in press
Ratschbacher, L., Hacker, B.R., Calvert, A., Webb, L.E., Grimmer, J.C., McWilliams, M., Ireland, T., Dong, S. & Hu, J. (2003), Tectonics of the Qinling Belt (Central China): Tectonostratigraphy, geochronology, and

deformation history, Tectonophysics, 366, 1-53

Yang, J., Xu, Z., Dobrzhinetskaya, L. F., Green II, H. W., Pei, X., Shi, R., Wu, C., Wooden, J. L., Zhang, J., Wan, Y., Li, H. (2003), Discovery of metamorphic diamonds in central China: an indication of a > 4000-km-long zone of deep subduction resulting from multiple continental collisions, Terra Nova, 15, 370-379

Pan-African re-working of late Archean-early Paleoproterozoic crust in the Madurai Block of South India, and implications for Gondwana reconstructions

Situated in a central position in most Gondwana reconstructions, the Southern Granulite Terrane (SGT) of Peninsular India is a key area for studying the formation of the supercontinent during the Pan-African orogeny in the late Neoproterozoic. However, the precise geotectonic position of the SGT in Gondwana and its link with other supercontinent fragments are controversial (e.g. Gosh et al., 2004; Collins et al. 2007) as the geodynamic evolution of the SGT is poorly understood.

We have reconstructed the metamorphic evolution of metapelitic Grt-Crd migmatites from the northern Palni Hills, situated in the central part of the Madurai Block, the largest but at the same time least understood crustal domain of the SGT, by integrating petrological with geochronological data. The Grt-Crd migmatites occur in a paragneiss sequence, which also comprises Grt-Opx-bearing metaquartzites and metagreywackes and was intruded by the precursors of charno-enderbitic orthogneisses.

We have constrained a clockwise P-T evolution for the Grt-Crd migmatites by integrating calculated pseudosections in the NCKFMASHT system with thermobarometric data: The peak-assemblage garnet-sillimanite-mesoperthite-rutile-quartz formed through progress of biotite-dehydration-melting reactions during heating up to ultrahigh-temperature (UHT) conditions of ca. 1000°C/12.5 kbar. During subsequent high-temperature decompression to ca. 7.5 kbar the peak-assemblage was extensively replaced by cordierite, which occurs in several post-peak reaction textures (in monomineralic coronas around garnet as well as in symplectites with orthopyroxene or spinel). Back-reactions with melt led to the re-growth of biotite during post-decompressional cooling.

LA–ICPMS U-Pb zircon dating combined with in-situ U-Th-total Pb electron microprobe dating of monazite provides strong evidence for two metamorphic events: Detrital zircon cores with $^{207}Pb/^{206}Pb$ ages between 3.3-2.5 Ga are rimmed by broad oszillatory-zoned overgrowths yielding an upper-intercept age of ca. 2480 Ma. The overgrowths are interpreted to have formed during early Paleoproterozoic partial melting, which is corroborated by isochron ages of ca. 2450 Ma of rare monazite cores. The majority of the monazite grains yields early Paleozoic ages of 520 Ma, indicating a strong Pan-African overprint, which is also recorded by late Neoproterozoic lower-intercept ages of rare and narrow zircon rims around the early Paleoproterozoic overgrowths.

The geochronological data demonstrate that early Paleoproterozoic high-grade metamorphism affected the major part of the Madurai Block. High-temperature metamorphism is presumably related to the voluminous emplacement of the precursors of the charno-enderbitic orthogneisses, which has been dated at ca. 2530 Ma (Brandt et al., under review). During the Pan-African orogeny the rocks were reworked, and the UHT metamorphism and clockwise P-T path are attributed to collisional tectonics during the final assembly of Gondwana in the late Neoproterozoic. Uplift of the rocks may reflect extension of the overthickened crust. The new data show that late Archean to early Paleoproterozoic crust south of the Dharwar Craton extends much further south of the Palghat Cauvery shearzone than previously assumed and therefore question the significance of the shearzone, which has been interpreted as a major Pan-African collisional zone (e.g. Collins et al., 2007).

References:
Brandt, S., Schenk, V., Raith, M.M., Gerdes, A. & Srikantappa, C. (under review). Late Neoproterozoic P-T evolution of HP-UHT granulites from the Palni Hills (South India): new constraints from phase diagram modelling, LA-ICP-MS zircon dating and in-situ EMP monazite dating. (Journal of Petrology, under review)
Collins, A. S., Clark, C., Sajeev, K., Santosh, M., Kelsey, D. E. & Hand, M. (2007). Passage through India: the Mozambique Ocean suture, high-pressure granulites and the Palghat–Cauvery shear zone system. Terra Nova 19, 141–147.
Ghosh, J. G., deWit, M. J. & Zartman, R. E. (2004). Age and tectonic evolution of Neoproterozoic ductile shear zones in the Southern Granulite Terrain of India, with implications for Gondwana studies. Tectonics, 23 (TC3006). doi:10.1029/2002TC001444. (TC3006). doi:10.1029/2002TC001444.

The exotic provenance and two-stage exhumation of eclogite-facies rocks from SW Norway: a U-Pb and Rb-Sr study

Matthijs A. Smit[1], Michael Bröcker[1], Ellen Kooijman[1], Erik E. Scherer[1]
[1]Westfälische Wilhelms-Universität Münster, Institut für Mineralogie, Münster, Germany

During Scandian times (430-395 Ma), the proto-continent Baltica collided with Laurentia and parts of it were subducted to depths beyond 200 km. This process and subsequent exhumation tectonics produced the majority of the large-scale deformational and metamorphic features in the Scandinavian Caledonides. In spite of pervasive regional overprinting, several meta-crustal rock fragments in the thrust belt retain a geochronological record of short-lived subduction-exhumation cycles that predate the continental collision stage. These provide insight into the evolution of the contracting basin and show that both proto-continents had a plate-destructive margin that episodically recycled crustal material (e.g., Brueckner & van Roermund, 2004). An example of such recycled crust is the eclogite-gneiss association of the Jæren nappe, SW Norway. The eclogites were dated at 471 ± 1 Ma (2σ) by Lu-Hf garnet geochronology (Smit et al., 2010). To constrain provenance and the exhumation history of these rocks, we have performed U-Pb analysis on detrital zircon and Rb-Sr dating of mica from paragneisses that host the eclogites.

Four samples were selected for U-Pb zircon dating. In all samples, a few zircon analyses provided concordant or slightly discordant Caledonian ages, yielding a weighted mean $^{206}Pb/^{238}Pb$ age of 469 ± 6 Ma (2σ). This result is identical to the HP age provided by garnet dating (Smit et al., 2010), indicating that the eclogite-gneiss association formed already a coherent unit during the HP stage. Detrital age populations cluster at ca. 0.61, 0.92, 1.0-1.4 and 1.6-1.9 Ga. In addition, some zircon in 3 of the samples yielded Archaean ages. Such grains are large (up to 500 μm) and show a euhedral acicular morphology, and contain significant U (> 200 ppm), indicating that they were most likely metamict prior to Caledonian overprinting. These aspects suggest that their sedimentary transport pathway was short, thereby excluding the distal Archaean terranes of Baltica as a plausible source area. Instead, a Laurentic source is inferred, which reveals the exotic nature of the eclogites in relation to their current Baltica-proximal setting.

For 5 out of the 7 samples that were subjected to Rb-Sr dating yielded phengite ages that are identical within error (weighted mean age = 424.4 ± 1.5 Ma, 95% confidence limits; c.l.). For biotite, the Rb-Sr ages were nearly identical for 5 samples, providing a weighted mean age of 413.9 ± 2.7 Ma. These apparent ages are interpreted to date cooling through the closure temperatures for Sr diffusion in either mica and imply that cooling along the inferred Barrovian geotherm (ca. 30 °C/km) occurred at an average rate of ca. 10-20 °C/Myr. Cooling followed a first stage of near-isothermal exhumation through the subduction channel and the incorporation of the rocks into a composite nappe pile that unroofed along the western edge of Baltica during orogenesis. A single Rb-Sr age of 319.8 ± 2.2 Ma (95% c.l.) that was provided by statically-crystallized biotite records local heating during the post-orogenic rifting, presumably by circulation of hydrothermal fluids.

The results of this study provide new insight into the complex history of the Jæren nappe and of the Caledonides in general, and demonstrate the need to reassess existing models on the geodynamic evolution of the region.

References:
Brueckner, H. & van Roermund, H.L.M. (2004), Dunk tectonics: A multiple subduction/eduction model for the evolution of the Scandinavian Caledonides, Tectonics, TC2004, 1-20.
Smit, M.A., Scherer, E.E., Bröcker, M., van Roermund, H.L.M. (2010), Timing of eclogite facies metamorphism in the southernmost Scandinavian Caledonides by Lu-Hf and Sm-Nd geochronology, Contributions to Mineralogy and Petrology, 159, 521-539.

Ultrahigh pressure metamorphism in the Bohemian Massif: more widespread than previously thought?

Patrick J. O'Brien[1], Jana Kotkova[2] & Martin A. Ziemann[1]
[1]Institut für Erd- und Umweltwissenschaften, Universität Potsdam, Karl-Liebknecht-Str. 24-25, 14476 Potsdam-Golm, Germany
[2]Czech Geological Survey, Klárov 3, 118 21 Praha1, Czech Republic

Ultrahigh pressure metamorphism (UHPM), a special extension of the eclogite facies requiring pressures expected only at mantle depths of at least 90 km, was once a rarity but is becoming increasingly recognised in collisional belts worldwide (Liou et al., 2009 and refs therein). The high-pressure polymorphs of carbon (i.e. diamond) and SiO_2 (i.e. coesite or stishovite) are unequivocal indicators of UHPM, whereas other features such as K in clinopyroxene, exsolved majorite component in garnet or PbO_2 -structure in TiO_2 are not easy to identify or interpret. Locations where diamond has been positively identified in continental crust rather than mantle rocks are scant namely: Kokchetav (Kazakhstan), Saidenbachtal (Erzgebirge), Rhodope (Greece) and Qinling (China). Microdiamond in Norwegian HP rocks, sampled by rock dissolution, has not been found *in situ* in quartzofeldspathic gneisses although it has been identified *in situ* in mantle rocks from the same area.

The Bohemian Massif, as elsewhere in the Variscides, is unusual in that there are two different eclogite-bearing associations (Massonne & O'Brien 2003 and refs therein). An early, pre-Upper Devonian (older than 380 Ma), subduction stage is recorded in medium-temperature eclogites and blueschists derived from low-pressure basaltic and gabbroic protoliths now found as minor relics in amphibolite facies meta-ophiolite or gneiss-metabasite nappe complexes. A second subduction and exhumation event produced further complexes containing different types of mantle peridotites, along with their enclosed pyroxenites and high-temperature eclogites, associated with large volumes of high-temperature–high-pressure felsic granulites. The association of felsic granulite and garnet peridotite is an oddity of the European Variscides that needs to be explained. The most obvious solution is to have subducted continental crust deep into the mantle and thus allow tectonic incorporation of garnet peridotite (formed at 3 to 5 GPa!). At these great depths coesite or even diamond would have been stable in the subducted continental crust: is there any evidence of this?

Diamonds were first identified in Variscan units of the Central Erzgebirge, Germany, at the Saidenbachtal reservoir but the host garnet-phengite gneiss is a very unusual and rare rock type that has even been given the special name Saidenbachite. Coesite is also known from Saidenbachtal but only in rare eclogites. In the rest of the Bohemian Massif, apart from in the Saidenbachtal eclogites, only polycrystalline quartz aggregates proposed to be pseudomorphing former coesite have so far been reported. UHP conditions have also been proposed for unusual grossular-rich garnet-bearing gneisses in Poland and Mg-rich garnet+orthopyroxene rocks from Moravia but again these are exotic rocks of very minor extent.

The dominant high pressure series of the Bohemian Massif, cropping out over tens of square kilometers, are granulites of felsic (Grt-Ky-mesoperthite-quartz) and intermediate (Grt-Cpx-Pl-Qtz) composition. These have been shown to be in fact eclogite facies rocks transformed during exhumation still at high temperature. We will present data from newly discovered microdiamond- and coesite- bearing samples of such 'normal' granulites and outline characteristic features that may be used as indicators of UHPM to unearth suspected UHPM in such bulk compositions elsewhere.

References:
Liou J.G., Ernst W.G., Zhang R.Y., Tsujimori T. & Jahn B.M. (2009): Ultrahigh-pressure minerals and metamorphic terranes – The view from China. J Asian Earth Sci 35, 199-31 and refs therein.
Massonne H.-J. & O´Brien P.J. (2003): The Bohemian Massif and the NW Himalaya. In: D.A. Carswell & R. Compagnoni (eds.), Ultrahigh-pressure metamorphism. EMU notes in Mineralogy 5, Mineralogical Society of America, 145-187 and refs therein.

The garnet-bearing serpentinite of Zöblitz (Erzgebirge) – attempts of a reconstruction of the retrograde part of the story

Axel D. Renno[1], Susan Duhra[1]
[1]TU Bergakademie Freiberg, Institute of Mineralogy, Freiberg, Germany

The garnet bearing serpentinite of Zöblitz is the largest ultramafic body in the Gneiss-Eclogite-Unit of the Erzgebirge. Its prograde metamorphic evolution was described in detail by several authors, e.g. Schmädicke & Evans (1997), and Massonne & Neuser (2005), but information about the retrograde evolution of this body is scarce.

We tried such a reconstruction and a parallelizing with local and regional events. We combined the information about several types of metamorphic microstructures of the serpentinites with information about the mineralogical and chemical composition and geothermobarometric assessments.

The serpentinites are characterized by the common occurrence of features typical for pseudomorphic and non-pseudomorphic microstructures cut by paragranular and transgranular serpentinite veins.

Nearly all garnets show a kelyphite-like rim, most of the garnets are completely chloritized. The chlorite pseudomorphs and the kelyphitic rims are cut by the serpentinite veins too.

Using several optical microscopic methods, like polarization microscopy, phase contrast microscopy, and differential interference contrast microscopy in combination with Raman spectroscopic measurements and electron microprobe analysis of the chemical composition of the single minerals, we were able to differentiate the mineralogical composition of the single microstructural features. The meshes and bastitic pseudomorphs are comprised of lizardite. Recrystallized non-pseudomorphic structures are composed of antigorite, while the veins are filled with chrysotile and antigorite. The chlorites are without exception klinochlore with differing Al content.

The retrograde metamorphic evolution of the garnet peridotite started with the formation of the kelyphitic rims and the formation of the chlorite pseudomorphs after garnet (T > 460°C) , followed by the beginning of the first step of serpentinization (lizardite meshes).

This pseudomorphic microstructure starts to recrystallize and the newly formed non-pseudomorphic features occur together with klinochlore (T ≈ 200°C). The next step is a second serpentinization, mostly related to para- and transgranular veins and the formation of antigorite. This metamorphic phase is characterized by higher temperatures (340 – 390°C), higher activities of CO_2 and SiO_2, and lower oxygen fugacity.

Reference:
Massonne, H.-J. & Neuser, R. (2005), Ilmenite exsolution in olivine from the serpentinite body at Zöblitz, Saxonian Erzgebirge, Mineral. Mag., 69, 119-124.
Schmädicke, E. & Evans, B.W. (1997), Garnet-bearing ultramafic rocks from the Erzgebirge, and their relation to other settings in the Bohemian Massif, Contrib. Mineral. Petrol., 127, 57-74.

Implications of CO_2 inclusions in Jack Hills zircons for Early Earth Environment

Martina Menneken[1], Thorsten Geisler[1,2], Alexander Nemchin[3]
[1]Westfälische Wilhelms-Universität Münster, Institute for Mineralogy, Münster, Germany
[2]Universität Hamburg, Institute for Mineralogy and Petrography, Hamburg, Germany
[3]Curtin University of Technology, Western Australian School of Mines, Perth, Australia

The interpretation of origin of detrital zircon grains from Jack Hills, Western Australia, has been an intensely debated issue for a few decades, especially after the discovery of heavy oxygen compositions in some of these grains in 2001 (e.g., Wilde et al. 2001; Mojzsis et al., 2001). Compelling evidence for the existence of stable felsic continental crust, sedimentation, oceans and plate tectonics on the Hadean Earth have been brought forward by the studies of oxygen isotopes (Wilde et al. 2001; Mojzsis et al., 2001), REE patterns (Wilde et al. 2001), Hf isotope compositions (Harrison et. al. 2005), Ti in-zircon temperature estimates (Watson & Harrison, 2005) and analysis of mineral inclusions (Hopkins et al. 2008) in Jack Hills zircons. However, there are also equally strong arguments that all morphological, chemical and isotopic features of these zircons can be explained by their formation in mafic rocks without involvement of processes characteristic of evolution of modern continental crust and in the absence of significant volumes of water or plate tectonics (e.g., Kamber et al., 2005, Coogan & Hinton, 2006).

Here we report the discovery of CO_2 inclusions in seven zircon grains from Jack Hills. Their $^{207}Pb/^{206}Pb$ ages, obtained by SHRIMP, range from 3.35 to 4.13 Ga with four zircon grains that yielded ages between 3.35 to 3.45 Ga. The densities of the inclusions, obtained by Raman spectroscopy, vary from 0.15 g/cm³ to high densities of up to 1.08 g/cm³. Two grains, one with single spot $^{207}Pb/^{206}Pb$ ages ranging from 3.51 ± 10 to 3.80 ± 24 Ga (W74-9-9) and one with ages ranging from 3.78 ± 41 to 4.13 ± 11 Ga (JH1-42), contain a large number of CO_2 inclusions. Their densities vary from 0.36 to 1.08 g/cm³ and from 0.17 to 0.95 g/cm³. More importantly, however, is the observed internal distribution of CO_2 densities. Whereas the densities of the CO_2 inclusions in grain W74-9-9 define two maxima at 0.6 and 0.8 g/cm³, the CO_2 densities in grain JH1-42 define a lognormal distribution with a single maximum at about 0.8 g/cm³ and a tail towards decreasing densities. Such a distribution indicates the postformation re-equilibration of the CO_2 inclusions and can be interpreted in the following way: The maximum, defined by most CO_2 inclusions, represents a prolonged time of re-equilibration or possibly, if there is no tail to higher values, the pressure of entrapment (Hansteen & Klügel, 2008). The temperature of formation for the zircon grains was estimated to be 678 ± 18 °C (JH1-42) and 682 ± 17 °C (W74-9-9) using the Ti-in-zircon thermometer (Ferry & Watson, 2007). We assume that the maximum CO_2 density of 1.08 g/cm³ reflects the entrapment pressure. At a crystallisation temperature of 680 °C this density translates to an entrapment pressure of about 6.7 kbar when using the equation of state for pure CO_2 given by Span and Wagner (1996). Depending on the density of the overlying rock this pressure corresponds to a depth of about 19 to 22 km. Such P-T estimate agrees well with those obtained by thermobarometric analyses of 4.02–4.19-Gyr-old inclusion-bearing zircons made by Hopkins et al. (2008). The overall distribution of CO_2 densities in the investigated zircon grains indicates that they remained at this depth for a prolonged period of time between at least 4.13 to 3.35 Ga. This indicates that relatively stable blocks (with the thickness of at least 20 km), that have been isolated from the mantle convection and reworking, have existed on Earth as early as 4.13 Ga.

Reference:
Coogan L. A. & Hinton R. W. (2006) Do the trace element compositions of detrital zircons require Hadean continental crust?, Geology, Vol. 34 pp. 633-636
Ferry, J.M. & Watson E.B. (2007), New thermodynamic models and revised calibrations for the Ti-in-zircon and Zr-in-rutile thermometers, Contrib Mineral Petrol., Vol. 154, pp. 429–437
Hansteen, T.H. & Klügel, A. (2008), Fluid Inclusion thermobarometry as a tracer for Magmatic Processes, Reviews in Mineralogy & Geochemistry, Vol. 69 pp. 143-177
Harrison, T.M. et al. (2005), Hadean Hafnium: Evidence of Continental Crust at 4.4 to 4.5 Ga
Hopkins, M., Harrison, T.M., Manning, C.E., (2008) Low heat flow inferred from >4 Gyr zircons suggests Hadean plate boundary interactions, Nature, Vol. 456, pp. 493-496
Kamber B. S. Whitehouse M. J. Bolhar R. and Moorbath S. (2005), Volcanic resurfacing and the early terrestrial crust: Zircon U-Pb and REE constraints from the Isua Greenstone Belt southern West Greenland: Earth and Planetary Science Letters Vol. 240 pp. 276-290
Mojzsis, S.J., Harrison, T.M., Pidgeon, R.T. (2001) Oxygen-isotope evidence from ancient zircons for liquid water at the Earth's surface 4300 Ma ago, Nature Vol. 409 pp. 178–181
Span &Wagner, (1996), A New Equation of State for Carbon Dioxide Covering the Fluid Region from the Triple-Point Temperature to 1100 K at Pressures up to 800 MPa, J. Phys. Chem. Ref. Data 25, 6, (1996),

pp.1509-1597.

Watson, E.B. & Harrison, T.M. (2005), New geothermometer reveals minimum melting conditions on earliest Earth, Science Vol. 308 pp. 841–844

Wilde, S.A., Valley, J.W., Peck, W.H., Graham, C.M. (2001) Evidence from detrital zircons for the existence of continental crust and oceans on the Earth 4.4 Gyr ago, Nature Vol. 409, pp. 175–177

Section 04

_____

CO_2 sequestration into geological reservoirs and laboratory analogues

CO$_2$-sequestration: Permeability variations of the Buntsandstein sandstone under the influence of supercritical carbon dioxide

Nils Gafert-Kalaitzidis[1], Jutta von der Gönna[1], Jens Köster[2],Ulrike Hilse[2], Reinhard Gaupp[2], Georg Nover[1]
[1]Rheinische Friedrich-Wilhelms-Universität Bonn, Steinmann Institut, Endogene Prozesse, Bonn, Germany
[2]Friedrich-Schiller-Universität Jena, Institute of Earth Science, Jena, Germany

Deep saline aquifers are considered to be suitable sites for long term geological storage of CO$_2$ in the underground. To evaluate the potential of such sites for injection of large amounts of CO$_2$, it is essential to study the interaction host rock - supercritical CO$_2$ (scCO$_2$) - brine under conditions comparable to the aquifer conditions. Changes in petrophysical rock properties, in particular permeability and porosity, due to dissolution/precipitation of mineral phases are of great importance for both: injection and migration of CO$_2$ inside the aquifer.

 In this study plugs from two different locations of the Buntsandstein of N-Hesse and S-Thuringia were studied as a natural analogue for the industrial CO$_2$-sequestration to determine the influence of CO$_2$ – brine interaction on porosity and permability under supercritical conditions. The arkosic to subarkosic medium to very fine grained sandstones are texturally and structurally mature. Generally two phenotypes (i) unbleached and (ii) bleached can be distinguished. Both types show quartz, feldspar, illite, smectite, chlorite, hematite, calcite and dolomite cements. Not all authigenic phases are present in all samples. The comparison of the two phenotypes revealed elevated contents of illite and calcite cements in the bleached samples. Authigenic phases caused reduction of primary porosity while on the other hand dissolution of feldspar and volcanic/magmatic clasts resulted in extended secondary porosity. Porosities of the untreated samples range from 15-17 %, permeability is in the order of $10^{-15} – 10^{-17}$ m.

In two different experimental setups (i) saturated plugs in a brine-saturated CO$_2$-fluid and (ii) saturated plug in a CO$_2$-saturated brine) the Buntsandstein samples were exposed to scCO$_2$ (p = 120-160 bar and T = 120-140 °C, 7 – 40 d).
Mineralogical composition of the samples was determined before and after the experiments using qualitative and quantitative X-ray powder diffraction techniques, XRF measurements were used to check for alteration the chemical composition. Structural changes were studied using optical microscopy and Scanning Electron Microscopy.

All Samples from brine-saturated CO$_2$-fluid experiments show a distinct, time-dependant increase in permeability while porosity was not affected over the time. These findings are supported by XRF data, which showed a significant decrease in CaO-content. A similar trend was described by Rimmelé et al. (2009).

Reference:
Rimmelé, F., Barlet-Gouédart, V., Renard, F. (2009), Evolution of the petrophysical and mineralogical
properties of two reservoir rocksunder thermodynamic conditions relevant for CO2 storage at 3 km depth: Oil & Gas Science and technology Ref.IFP (2010)

Estimated and „true" geometric surfaces and their possible impact on experimentally and thermodynamically derived mineral dissolution and precipitation rates in CO2-brine-mineral reactions

Wolf-Achim Kahl, Astrid Holzheid
Christian-Albrechts-Universität zu Kiel, Institut für Geowissenschaften, Kiel, Germany

Sandstone aquifers are considered to be potential reservoirs for the geological sequestration of industrial carbon dioxide. The efficiency and time required to store CO2 by hydrodynamic trapping, solubility trapping and mineral trapping is under research in field and laboratory related studies as well as in numerical simulation scenarios. In both approaches, i.e., field/laboratory studies and numerical simulations, the estimation of effective reactive surfaces of minerals are of crucial importance for the determination of mineral dissolution and precipitation rates in CO2-brine-mineral reactions.

The effective reactive surface depends only on those fractions of mineral surfaces that are in contact with the formation fluids. The effective reactive surface combines the geometric surface area with the surface roughness. The geometric surface area can be easily overestimated: (a) Pore space cementation in sandstones occurs in many cases as domains of completely clogged pores (Pape et al., 2005), because carbonate or anhydrite cementations share surface contacts mostly to neighbouring mineral grains (see highlighted area I in Figure 1; the cementation in this example is calcite). The remaining open porosity has therefore a disproportional large contact to the grain matrix, i.e. quartz, (see highlighted area II in Figure 1), resulting in an overestimated geometric surface of the phases of cementation. (b) The approach to estimate geometric surfaces based on spherical grain geometries of the matrix phases - assuming average grain diameters of the matrix phases and using the weight percentages of the matrix and cementation phases to calculate the reactive surfaces of the matrix and cementation phases - would also result in an overestimation of the geometric surface of the phases of cementation as the assumption of 'smooth' spherical matrix grains underestimates the true 'uneven' surfaces of the matrix grains. At present, we quantify the difference between the estimated and the „true" geometric surfaces in cemented sandstones. A sandstone sample with carbonate cementation (Solling Formation, Bunter Sandstone) was chosen as an example. A micro plug (Ø 10 mm) was scanned using the X-ray computed microtomograph Skyscan 1172 (μ-CT) with a beam energy of 100 kV, a flux of 100 μA and a resolution of 2.7 μm per cubic voxel. The volume percentages of matrix quartz and calcite cement can be derived by quantitative image analysis of the μ-CT measurements. Stereological image analysis of the segmented microstructural elements provides the average grain sizes of matrix quartz and calcite cement. The estimated surface areas based on spherical grain geometries (using the information of volume percentages and average grain sizes), are 97 cm²/g (quartz) and 238 cm²/g (calcite). The „true" surface areas are calculated using the fractions of the mutually shared object surfaces of the pore space, quartz and calcite phases. The mutually shared object surfaces are derived from quantitative 3D image analysis. The ratio of (contact surface calcite to pore space) to (contact surface quartz to pore space) is smaller compared to the ratio based on the estimated surface areas. In addition, first results of the „true" surface areas show smaller absolute surface areas of calcite and quartz compared to estimated surface areas of calcite and quartz based on spherical grain geometries.

As mentioned above, surface areas are needed to calculate experimentally derived dissolution and precipitation rates of minerals involved in CO2-brine-mineral reactions. Experimentally derived reaction rate values are sometimes several orders of magnitude greater than natural reaction rate values of weathering measured in the field (Lasaga, 1995). The differences between the estimated and the „true" geometric surfaces could – among others - explain the discrepancy between experimentally derived and natural reaction rates. Furthermore, incorrect reactive surfaces using spherical grain geometries (as applied by e.g., Zerai et al., 2006, for calculation of reactive surfaces) might have a significant impact on calculated reaction rates based on kinetic modeling.
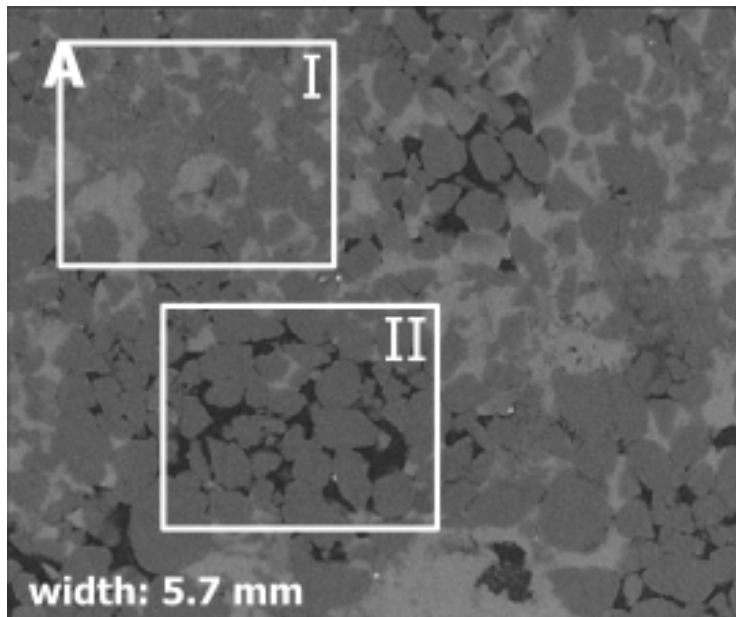
Figure 1: μ-CT image of a carbonate cemented Bunter Sandstone
(see text for more details on highlighted areas I and II).

References:

Lasaga, A.C., 1995. Fundamental approaches in describing mineral dissolution and precipitation rates. In: White, A.F., Brantley, S.L. (Eds.), Chemical Weathering Rates of Silicate Minerals, Reviews in Mineralogy, 31, 23–86.
Pape, H., Clauser, C., Iffland, J., Krug, R., Wagner, R., 2005. Anhydrite cementation and compaction in geothermal reservoirs:
Interaction of pore-space structure with flow, transport, P–T conditions, and chemical reactions. Int. J. Rock Mech. and Mining Sci., 42, 1056-1069.
Zerai, B., Saylor, B.Z., Matisoff, G., 2006. Computer simulation of CO2 trapped through mineral precipitation in the Rose Run Sandstone, Ohio. Appl. Geochem. 21, 223–240.

Geological storage of CO2 - Different approaches to monitor CCS

The development of strategies for sustainable and secure technologies to reduce substantially emission of greenhouse gases to the atmosphere is one of the major challenges of the next decades. Geological CO2 storage is a promising technology to reduce effectively anthropogenic greenhouse gas emissions to the atmosphere. Different storage technologies are under development and are tested at large scale experiments with different focuses. As part of the Norwegian Sleipner project, off-shore storage of CO2 in a saline aquifer with high permeability is conducted at an industrial scale and primarily monitored by 4D seismic and gravity measurements. The use of enhanced oil and gas recovery as a storage technology for CO2 is currently being tested at the Weyburn and the K12B field sites. Improving monitoring and verification, and the efficiency of storage operations in saline aquifers is the main issue of the on-shore projects in USA (Frio), Australia (Otway), Japan (Nagaoka), and Algeria (In Salah). In Europe, the CO2SINK (**CO2 S**torage by **I**njection into a **N**atural Saline Aquifer at **K**etzin) project is the first pilot project for on-shore geological CO2 storage into a saline aquifer. The main focus of this project is the development, testing and benchmarking of monitoring techniques, using a broad range of geophysical, geochemical and microbiological methods. Monitoring and verification technologies are tested to observe the CO2 plume in different subsurface geological environments. At present, the highest injection rate is applied at the Sleipner project with approximately 1 Mt CO2/year. If carbon capture and storage (CCS) is intended to be an effective option for decreasing greenhouse gas emissions, more demonstration projects are required to verify monitoring and safety technologies before the storage technology will be ready for implementation and commercial use with the public acceptance necessary.

Within the development of storage technologies the following issues are of particular interest:
- Monitoring migration of CO2 within the reservoir
- Rate at which CO2 dissolves in brine or reacts with reservoir minerals
- Assessing storage capacity and quality of the seals
- Predicting and monitoring of upward migration of CO2
  - Leakage to the shallow subsurface through faults and fractures
  - Leakage along artificial pathways (casing and cementation of injection/ observation boreholes)

The presentation will give an overview of the existing pilot studies and will present some detailed results from the CO2SINK project.

Geochemical investigations of interactions between CO_2 and CO_2-SO_2, formation fluids and rock forming minerals under in-situ conditions of potential storage horizons (COSONOStRA)

Franziska Wilke[1,2], Thomas Wiersberg[1], Jörg Erzinger[1] and the COSNOStRA-Team[1,2]
[1]Helmholtz-Centre Potsdam, German Research Centre for Geosciences, Section 4.2 Inorganic and Isotope Geochemistry, Potsdam, Germany
[2]University of Potsdam, Institute for Earth- and Environmental Sciences, Potsdam, Germany

The storage of CO_2 in the deep underground is one possibility to reduce the release of anthropogenic CO_2 in the atmosphere. Gas–fluid–rock interactions are assumed to be a crucial factor to control dissolution or precipitation of minerals in the CO_2 storage horizons. Under this aspect, a number of experimental studies are ongoing in Germany and worldwide. COSONOStRA (CO_2-SO_2-NO_x Stimulated Rock Alteration) aims to investigate chemical corrosion of rocks and rock-forming minerals with impure supercritical CO_2 ($scCO_2$) at possible storage conditions of >73.7 bar and >31°C. The mixture of gases used for the experiments is chosen with respect to the composition of CO_2 captured from coal-fired power plants using the Oxyfuel technology. The resulting data build a base for the long-term prediction of the behavior of CO_2 storage reservoirs.

Experiments up to 1000h have been performed with 3n NaCl solution, 12 discrete mineral phases and pure $scCO_2$ or $scCO_2$+SO_2 (99.5+0.5vol-%; "impure $scCO_2$") gas mixture. The brine composition reflects the average composition of deep formation waters of the North German Basin. To increase the reaction rates all minerals were crushed and ground and the reagents agitated either by stirring or shaking in 1L-reaction autoclaves. The autoclaves consist of Hastelloy™ or ferromagnetic stainless steel fully coated with PTFE to avoid contact between metal and reaction agents. Before, during and after the experiments reaction fluids were sampled and analyzed by ICP-MS and IC. Solid phases were characterized by ICP-MS, EMPA and XRF before and after the experiment and pH, pressure and temperature are monitored.

Interactions with pure $scCO_2$ show slight changes in the mineral compositions of anhydrite, albite and microcline at a min. pH of 4. RFA analyses of albite after the experiment show a significant increase of a carbonate phase that might point to the formation of dawsonite. Experiments with pure $scCO_2$ reveal generally a higher pH compared to experiments with $scCO_2$+SO_2 at which experiments with silicate phases show a lower pH than experiments with carbonates. Latter is probably due to partial dissolution and buffering followed by precipitation reactions. This can also be seen by an increasing Mg content in the fluid during the experiments of dolomite with pure, but also impure $scCO_2$.

EMPA analyses are in progress to identify possible element mobilization in the mineral phases whereas Raman microprobe spectroscopy is planed to resolute finest phase transitions at the mineral surface.

The influence of trace gases in the CO_2 stream on the sequestration in deep saline aquifers – an experimental and modeling approach

Andreas Riße[1], Katja Heeschen[1] and Christian Ostertag-Henning[1]
[1]Bundesanstalt für Geowissenschaften und Rohstoffe, Hannover, Germany

The separation of CO_2 from flue gas streams of anthropogenic point sources and its injection into geological formations, e.g. deep saline aquifers is one favored technical option for reducing the global emission of carbon dioxide. The basis for operation of underground storage sites over a long period is the exact understanding of the fate of the injected CO_2, including the gas-fluid-rock interactions at in situ pressures and temperatures, and thus, the possibility to model these processes with adequate accuracy. Despite a rapidly growing knowledge about the occurring chemical reactions, present databases are not sufficient to model the CO_2 + trace gas solubility in brine, thermodynamic properties and kinetic rates. Furthermore, most studies focus on pure CO_2. However, depending on the capture process the waste gas stream contains up to a few vol. % of co-injected gases (e.g. O_2; SO_2; CO; NO; H_2; H_2S…) with variable potential to modify the geochemical environment at depth. Major gaps still exist in our knowledge about the behavior and chemical reactions of these trace gases. To overcome these gaps precise lab experiments at in situ conditions are required using well described mineral phases, analog fluids and gas compositions expected from the capture methods.

The project COORAL -"CO_2 Purity for Separation and Capture"- is investigating the influence of these accessory gases in the CO_2 stream on the capture, transport, injection and storage processes. The presented subproject studies gas-fluid-mineral/rock interactions at elevated, in situ temperature (≤ 200 °C) and pressure (≤ 400 bar) to identify changes of gas and fluid compositions, mineral alterations as well as dissolution, precipitation or redox reactions and to generate kinetic data for numerical simulations.

The focus is placed on experiments using well characterized natural minerals typical for potential storage sites in Germany, artificial brines with salt load of 150-300 g/l and binary gas mixtures. A chemically inert and flexible reaction cell made of a thin gold foil with a titanium outlet allows sampling of fluid and gas during the experiments. The reaction cell is pressurized and heated within a stainless steel batch reactor filled with water (Seyfried et al., 1978). The newly formed solids and the altered minerals will be studied with EPMA, REM EDX, XRD, XRF and wet chemistry, changes in the fluid chemistry with ICP-/IC-methods. Isotopic measurements will be applied to verify data of conventional methods and to quantify reaction rates of less reactive silicates that show very slow dissolution, precipitation and replacement reactions under the given conditions. Thus, part of the experiments will be performed with isotopically-labelled fluids and gases (e.g. ^{13}C; ^{18}O). The incorporation of isotopic material into newly formed precipitates or reaction rims will be analyzed with ToF-SIMS (Time-of-Flight Secondary Ion Mass Spectrometry) in cooperation with the University of Münster. This method is suited for simultaneous mapping of elements, isotopes and molecules with high spatial resolution and for depth profiling with step sizes in the range of single atomic layers.

In quite a few investigations the effect of CO_2 on given minerals are not clearly distinguishable from effects caused by disequilibrium between the minerals and the primary brine. Therefore, preliminary experiments were performed to study dissolution equilibriums of minerals and deionised water. Mineral powders (feldspars, phyllosilicates and carbonates) and pure water (18.2 MΩ*cm) were enclosed in small gold capsules using predefined solid-fluid ratios (1:1; 1:2 and 1:4) and heated to 200 °C at 100 bar for more than 1700 h. After the experiments were ceased the remaining fluids (100-200 µl) and solids (50-100 mg) were analyzed with ICP-OES/MS. First results indicate for lattice elements Mg and K in illite and Mg in chlorite a stoichiometrical solution behavior. Such cation concentrations in the fluids were interpreted as snapshots of the dissolution process far from equilibrium.

Reference:
Seyfried, W.E., Gordon, P.C. and Dickson, F.W. (1979), A new reaction cell for hydrothermal solution equipment, American Mineralogist, 64, p. 646-649

Experimental approach to study geomechanical and geochemical rock behaviour during the storage of impure CO$_2$: first results of COORAL[1] project

Herwig Marbler, Michael Schmidt, Kirsten Erickson, Christof Lempp, and Herbert Pöllmann
Martin-Luther-Universität Halle Wittenberg, Geowissenschaften, Von Seckendorff Platz 3, 06120 Halle/Saale

The storage of CO$_2$ with inherent impurities, such as SO$_X$, NO$_X$, O$_2$, CO, etc. affects fluid-fluid-rock interactions in deep geological formations. These include mineral alteration processes as well as pore space evolution and changes in rock strength and formation stability. The knowledge of these dynamic processes both in geochemical/mineralogical and geomechanical terms is of great importance to allow for long-term safety predictions over timescales of up to thousands of years.

For this purpose a combination of long-term geochemical/mineralogical experiments and geomechanical tests on various types of potential reservoir rocks are carried out with supercritical (sc) CO$_2$ containing variable degrees of impurities in autoclave systems and in triaxial pressure cells.

Mineralogical and geochemical laboratory experiments are executed in autoclave systems under simulated in-situ temperature conditions. In these autoclave systems rock samples of different silicate and carbonate bearing sandstones are allowed to react with artificial formation fluids and well-defined compositions of impure scCO$_2$ to study geochemical alteration effects in the mineralogical assembly of different sandstones such as dissolution and mineral transformation. These investigations are carried out to optimize real-time alteration scenarios in the reservoir rocks during the CO$_2$ storage.

Geomechanical investigations are carried out under lithostatic pressure conditions to determine parameters like rock deformability and strength, and effects of pore fluid pressure of the reservoir rocks. The first results show that increasing scCO$_2$ pore fluid pressure has strong effects on the elastic behaviour and strength of the host rock. CO$_2$ in the supercritical form is able to infiltrate small pore space in the reservoir rock, displace water or dissolve into the formation waters. This so called capillary trapping plays an important role for long term storage of CO$_2$ in deep underground formations. However, scCO$_2$ in sandstone samples induces fine fractures especially in inhomogeneities within the rocks which may result in a decrease of fracture strength of the reservoir rocks, especially under enhanced injection pressure over a period of several years. Therefore, evolution of the pore space, formation of cracks and fractures and additional alteration effects under interacting CO$_2$ may influence the storage capacity and long-term safety of the storage formation.

S04-T07

Microbial monitoring during CO2 storage in deep subsurface saline aquifers in Ketz in Germany

Hilke Würdemann, Daria Morozova, Maren Wandrey, Sebastian Fischer, Kornelia Zemke,

Investigations on subsurface saline aquifers has shown an active biosphere composed of diverse groups of microorganisms in the subsurface. Since microorganisms represent very effective geochemical catalysts, they may influence the process of CO2 storage significantly. In the frames of the EU Project CO2SINK a field laboratory to study CO2 storage into saline aquifer was operated. Our studies aim at monitoring of biological and biogeochemical processes and their impact on the technical effectiveness of CO2 storage technique. The interactions between microorganisms and the minerals of both the reservoir and the cap rock may cause changes to the structure and chemical composition of the rock formations, which may influence the reservoir permeability locally. In addition, precipitation and corrosion may be induced around the well affecting the casing and the casing cement. Therefore, analyses of the composition of microbial communities and its changes should contribute to an evaluation of the effectiveness and reliability of the long-term CO2 storage technique.

In order to investigate processes in the deep biosphere caused by the injection of supercritical CO2, genetic fingerprinting (PCR SSCP Single-Strand-Conformation Polymorphism) and FISH (Fluorescence in situ Hybridisation) were used for identification and quantification of microorganisms. Although saline aquifers could be characterised as an extreme habitat for microorganisms due to reduced conditions, high pressure and salinity, a high number of diverse groups of microorganisms were detected with downhole sampling in the injection and observation wells at a depth of about 650m depth. Of great importance was the identification of the sulphate reducing bacteria, which are known to be involved in corrosion processes. Microbial monitoring during CO2 injection has shown that both quantity and diversity of microbial communities were strongly influenced by the CO2 injection. In addition, the indigenous microbial communities revealed a high adaptability to the changed environments after CO2 injection.

In order to investigate processes in the rock substrate long term CO2 exposure experiments on freshly drilled, pristine Ketzin reservoir core samples were accomplished for 24 months using sterile synthetic brine under in situ pressure and temperature conditions. The composition of the microbial community dominated by chemoorganotrophic bacteria and hydrogen oxidizing bacteria changed slightly under CO2 exposure. In addition, changes in porosities were observed with time. During the experiments porosity first increased due to mineral dissolution but then tend to decrease due to mineral precipitation. These mineralogical changes are consistent with changes in fluid composition during the course of the experiments that indicate notably increased K^+, Ca^{2+}, Mg^{2+}, and SO_4^{2-} concentrations. K^+, Ca^{2+}, Mg^{2+} concentrations exceeded the reservoir brine composition significantly and can be attributed to the CO2 exposure.

Dissolution rates of calcite in CO2-bearing brines – a comparison of experimental and literature data

Katja Beier, Wolf-Achim Kahl, Astrid Holzheid
Christian-Albrecht-University, Institute for Geosciences, Experimental & Theoretical Petrology, Kiel, Germany

As one part of the joint project CO2-MoPa* chemical interaction processes between carbonates, highly mineralized synthetic model brines and dense CO2 were accomplished on laboratory experiments with closed teflon autoclaves to determine kinetic data like the dissolution rate, the rate constant or the activation energy. The experimental conditions were: calcite grains (Cc) of different size fractions (< 63 μ / 63 – 160 μm / 160 – 250 μm / 250 – 500 μm) as solid starting material; a synthetic model brine (TDS: ~ 156 g/L) based on a natural formation water of a Lower Cretaceous sandstone; temperatures of 100°C and 150°C; total pressure of 85 bars (induced by dry ice); run durations between 1 and 30 days. The chemical changes of the fluid composition during the experiments were monitored by ICP-OES measurements of the initial and the post-run fluids (inorganic chemistry lab, D. Garbe-Schönberg, IfG, CAU Kiel).

The changes of the Ca-concentration in the fluid phases were used to derive the dissolution rates (R) of calcite. As Result of the derivation the following observations could be made: (1) during the first 10 days all accomplished experiments have not achieved an equilibrium state. Between 10 and 20 days the dissolution rate values of all experiments converge. The equilibrium state was achieved after 20 days. (2) smaller grain size fractions, by definition, result in a larger reactive surface. Therefore the dissolution rate of the smaller grain size fraction should be higher. In contrast our experiments show, that the largest grain size fraction (250 – 500 μm) compared to the smaller grain size fraction (< 63 μm) exhibits higher dissolution rates by a factor of 23. One possible reason for this observation was proved by the help of Micro-Computer-Tomography (μ-CT) analyses. These analyses show that two different grain size fractions exhibit nearly the same volumes of the grain phase (160 – 250 μm: 66% / 250 – 500 μm: 63%) and the pore space (160 – 250 μm: 34% / 250 – 500 μm: 37%). The analyses also show, that the pore thickness distribution varied between these two grain size fractions: while the smaller grain size fraction is dominated by smaller pores, pores with a larger diameter dominate the larger grain size fraction. As result of that the permeability decrease and cause a smaller dissolution rate for samples with the smaller grain size fraction.

A comparison between experimental and literature data of the dissolution rate of Cc show a wide range of these R-values. These variations could be for example caused by different reactor types: experiments in mixed-flow reactors result in permanent disequilibrium states due to continuous feeding of fresh material, while experiments in batch reactors induce equilibrium after defined run durations, resulting in lower dissolution rates in our study. Furthermore the choice of complex model brines causes a larger number of chemical interactions which might also result in lower dissolution rates for high mineralized fluids. To conclude: caused by the high diversity of scientific questions, the choices of the proper starting material or the reactor type are not the only important variables to determine kinetic data. Many more parameters like the permeability, the fluid flow or the effective reactive surface have to be considered attentively when experimentally derived kinetic data were compared.

At present, experiments with orthoclase and anorthite (as representatives of the feldspar series) are under progress. Experimental techniques and conditions as well as evaluation processes are identical to the calcite experiments. Caused by the composition of these two minerals the Ca-component of the anorthite respectively the K-component of the orthoclase could be providers for long-term carbonate like mineral trapping during the CO2-sequestration process. First results of these experiments will be presented at the DMG meeting.

**Experimentelle Daten zur Ozeanversauerung durch anthropogenes CO$_2$**

Fabian Matthias Gäb[1], Chris Ballhaus[1], Henrik Blanchard[1]
[1]Rheinische Friedrich-Wilhelms Universität Bonn, Steinmann Institut, Bereich Endogene Prozesse

Die Diskussion über die Auswirkungen gestiegener CO$_2$-Partialdrücke in der Erdatmosphäre durch Nutzung fossiler Brennstoffe ist zur Zeit sehr präsent. Neben globaler Erwärmung wurde in den letzten Jahren verstärkt auch über die Auswirkungen steigender CO$_2$-Gehalte in der Atmosphäre auf die Ozeanchemie diskutiert (vgl. Caldeira et al. 2003 & Riebesell et al. 2007), denn steigender pCO$_2$ führt zur einer Absenkung des pH des Meerwassers (ocean acidification). Niedrige pH-Werte gefährden die Existenz aller mariner Taxa, die CaCO$_3$-Schalen aufbauen, denn mit steigendem pCO$_2$ der Atmosphäre (fallendem pH im Wasser) nimmt der Grad an Aragonit- und Calcitübersättigung im Meerwasser ab. Die meisten Modellierungen künftiger pH-Entwicklungen beruhen allerdings auf thermodynamischen Daten, die in Randsystemen mit künstlichen Meerwasserproxies generiert wurden. Systematische experimentelle Untersuchungen mit natürlichem Meerwasser über weite pCO2 liegen nicht vor.

Als Beitrag zum Thema wurde Ägäis-Meerwasser mit einer Ionenstärke von 0.72 bei 25°C und Raumdruck mit synthetischen Atmosphären verschiedener CO$_2$-Gehalte equilibriert. Die verwendeten Atmosphären waren N$_2$:O$_2$ (5:1) Gemische mit 10, 200, 1000, 2000, 5000, 20000 und 100000 ppmv CO$_2$ sowie reines CO$_2$. Die pH-Entwicklung wurde in-situ mit einer pH-Elektrode gemessen. Nach Einstellung von Gleichgewicht mit der Atmosphäre wurde das Meerwasser in-situ mit 0.1 n HCl-Maßlösung titriert und die Carbonat-Alkalinität ermittelt. Die Ergebnisse zeigen eine stark nicht-lineare Abhängigkeit des pH-Wertes von der CO$_2$-Konzentration der Atmosphäre. Im pH-Bereich, der durch Atmosphären mit 10^2 bis 10^3 ppmv CO$_2$ erreicht wird, ist Meerwasser schlecht gepuffert, während oberhalb von $5*10^3$ ppmv CO$_2$ die Pufferungskapazität deutlich zunimmt. Die Carbonat-Alkalinität ist erwartungsgemäß nahezu unabhängig von pCO2, da mit CO$_2$ eine elektrisch neutrale Spezies im Meerwasser gelöst wird. Oberhalb eines CO$_2$-Gehaltes von etwa 10 Vol.% geht die Carbonat-Alkalinität deutlich zurück. Hier ist der pH-Wert so niedrig, dass HCO$_3^-$ zunehmend zu CO$_2^{\circ}$ (aq) reagiert und in die Gasphase übergeht oder nur noch physikalisch gelöst ist, damit also in die Carbonat-Alkalinität nicht mehr eingeht. Bei sehr niedrigen pCO$_2$, entsprechend einem pH > 9, beobachten wir dagegen eine spontane Fällung von Aragonit durch Verschiebung des Carbonatgleichgewichtes zu höheren CO$_3^{2-}$-Konzentrationen.

Der CO$_2$-Partialdruck der Atmosphäre bestimmt die Konzentrationsverhältnisse von HCO$_3^-$ und CO$_3^{2-}$ sowie den pH-Wert des Meerwassers. Die Carbonat-Alkalinität misst die absoluten Konzentrationen an Carbonat und Hydrogencarbonat. Carbonat-Alkalinität des Wassers und der pCO$_2$ der Atmosphäre sind weitgehend entkoppelt, allerdings nur kurzfristig; langfristig wird eine Erhöhung des CO$_2$-Partialdrucks die terrestrische Verwitterungsrate und damit den Eintrag von Carbonat und Hydrogencarbonat über Verwitterungslösungen in das Meer erhöhen. Die Experimente zeigen, dass der Grad an CaCO$_3$-Sättigung im Meerwasser damit nicht nur von pCO2 (Orr et al. 2005), sondern auch von der Carbonat-Alkalinität abhängig. Im Umkehrschluss ist es nicht möglich, aus Alkalinitäten CO$_2$-Partialdrücke vergangener Epochen abzuleiten.
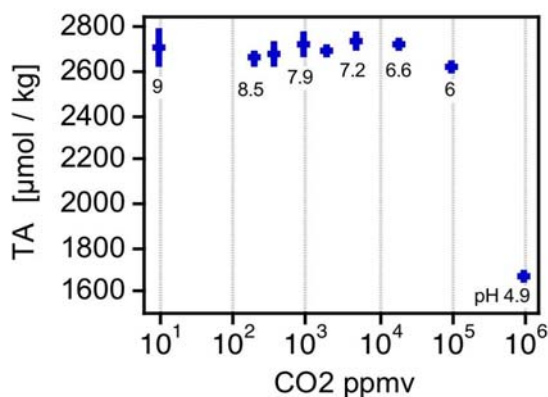
(Abb. 1: Gesamt-Alkalinität (TA) gegen pCO$_2$)   (Abb. 2: pH gegen pCO$_2$)
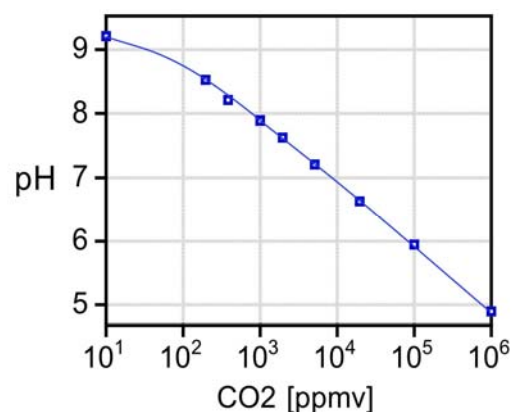
Reference:

Caldeira, K. & Wickett, M.E. (2003), Anthropogenic carbon and ocean pH, Nature, Vol 425. 2003, 325

Orr, J.C. (2005), Anthropogenic ocean acidification over the twenty-first century and its impact on calcifying organisms, Nature, Vol 437. 2005, 681 – 686

Riebesell, U. Schulz, K.G. Bellerby, R.G.J. Botros, M. Fritsche, P. Meyerhöfer, M. Neill, C. Nondal, G. Oschlies, A. Wohlers, J. & Zöllner, E. (2007), Enhanced biological carbon consumption in a high CO_2 ocean, Nature, Vol. 450, 2007, 545 – 547

Schneider, A. Wallace D.W.R. & Körtzinger, A. (2007), Alkalinity of the Mediterranean Sea, Geophysical Research Letters, Vol.34, 2007,

Section 05

Early solar system

The thermal evolution of the L chondrite parent body – a ^{182}Hf-^{182}W and ^{207}Pb-^{206}Pb perspective

Peter Sprung[1], Christa Göpel[2], Thorsten Kleine[3], James A. van Orman[4], Bernard Bourdon[1]
[1] ETH Zürich, Institut für Geochemie und Petrologie, Clausiusstrasse 25, 8092 Zürich, Switzerland
[2] Institut de Physique du Globe de Paris, 4, place Jussieu, 75252 Paris, France
[3] WWU Münster, Institut für Planetologie, Wilhelm-Klemm-Str. 10, 48149 Münster, Germany
[4] Department of Geological Sciences, Case Western Reserve University, 10900 Euclid Ave, Cleveland, Ohio 44106-7216, United States

Knowledge of the earliest evolution of planetesimals and small planetary objects is key to understanding the evolution of the early solar system and the formation of the terrestrial planets. Constraining the thermal evolution of a parent body by analyzing multiple meteorites of various petrologic types provides information on the internal structure, size and growth rate of the planetary object. Recently, the synthesis of several chronometers whose closure temperatures range over ~800 °C yielded a well-constrained thermal history for the H chondrite parent body that is consistent with a concentrically layered internal structure (Trieloff et al. 2003; Kleine et al., 2008). Given that its closure temperature approximates peak metamorphic temperatures, the short-lived ^{182}Hf-^{182}W-system (t$_{1/2}$ = [8.90 ±0.09]×10^6 yr) is ideally suited to constrain the high-temperature evolution of a planetary body (Kleine et al., 2008). Combined with ^{207}Pb-^{206}Pb phosphate age data for the same meteorites, the high-temperature cooling history (i.e., from peak metamorphic temperatures down to ~400-500 °C) can thus be dated. Previous Pb-Pb phosphate age data indicate a more complex thermal history of the L compared to the H chondrite parent body, possibly as a result of impact disruption of the L chondrite parent body (Göpel et al., 1994). However, relatively little is known about the high-temperature evolution and cooling history of this body. Here we apply the Hf-W system to equilibrated L chondrites (Saratov, Elenovka, Bruderheim) that exhibit the entire range of metamorphic conditions from type 4 to 6.

Following removal of any saw marks using abrasive paper, all samples were ultrasonicated in deionized water. Gentle crushing in an agate mortar and sieving preceded metal separation using a hand magnet. Grinding under ethanol, repeatedly washing off the silicate dust and leaching with HF produced highly pure metal (M) fractions. Non-magnetic (NM, i.e., silicate) fractions were further purified from remaining metal grains and divided into fractions of differing magnetic susceptibility using a Frantz magnetic separator. Digestion, Hf and W concentration determination by isotope dilution, and ion exchange chromatography followed standard procedures. All analyses were conducted on a *Nu Plasma* MC-ICPMS at ETH Zürich. Reported ^{182}W/^{184}W isotope compositions of samples are given as ε-unit deviation (i.e., parts per 10 000 deviation) from the terrestrial value.

All metal separates yielded ^{180}Hf/^{184}W below 0.004 underlining their high level of purity. As illustrated by high ^{180}Hf/^{184}W of up to ~115 and ε^{182}W of up to ~63 that are observed for some NM fractions, the applied separation technique provides silicate fractions of high purity. The high ^{180}Hf/^{184}W and radiogenic ε^{182}W values in the NM fractions enable us to determine precise age data with uncertainties below ±1 Myr in most cases. The Hf-W age data (Δt_{CAI}) for L chondrites that were obtained in this study increase with increasing metamorphic grade and range from 3.12±0.97 Myr for Saratov (L4) to 10.01±0.75 Myr for Bruderheim (L6).

Increasing Δt_{CAI} for Hf-W closure with increasing petrologic type as indicated by our new data match the systematic displayed by H chondrites (Kleine et al., 2008). In conjunction with Pb-Pb age data for phosphate fractions from Bruderheim (4514.58 ±0.54 Ma, Sprung et al., 2010) and Elenovka (4535 ±1 Ma, Amelin 2000), the new Hf-W closure age data imply that the high-temperature thermal histories and the initial internal structures of the L and H chondrite parent bodies were very similar: ~200 km wide, concentrically layered bodies that were internally heated by the decay of ^{26}Al.

The initial ε^{182}W of Saratov, Elenovka, and Bruderheim in conjunction with their initial ^{182}Hf/^{180}Hf indicates a bulk Hf/W of the L chondrite parent body indistinguishable from that of carbonaceous chondrites (1.23 ±0.15; Kleine et al., 2009) but exceeding that of the H chondrite parent body (Kleine et al., 2008). Metal-silicate fractionation by nebular processes is the most likely cause for the distinct Hf/W ratios of the different chondrite parent bodies.

References:
Göpel et al. (1994) EPSL, 121, 153-171
Kleine et al. (2008) EPSL, 270, 106-118
Kleine et al. (2009) GCA, 73, 5150-5188

Trieloff et al. (2003) Nature 422, 502-506
Sprung et al. (2010) 41st Lunar Planet. Sci. Conf., abstract #1921

S05-T02

^{182}Hf-^{182}W chronometry on weakly irradiated iron meteorites: Differentiation within <1 Myr after formation of Ca,Al-rich inclusions

Thomas Kruijer[1], Peter Sprung[1], Thorsten Kleine[2], Ingo Leya[3], Rainer Wieler[1]
[1]ETH Zürich, Institute of Geochemistry and Petrology, Zürich, Switzerland
[2]WWU Münster, Institut für Planetologie, Münster, Germany
[3]University of Bern, Space Research & Planetary Sciences, Bern, Switzerland

Introduction:
Preceding Hf-W studies showed some iron meteorites to be as old as Ca,Al-rich inclusions, the oldest known objects in the solar system (Kleine et al., 2005; Scherstén et al., 2006; Markowski et al., 2006a). However, minor cosmic-ray induced tungsten isotope variations (Leya et al., 2000, 2003) may at least in part be responsible for the old apparent ages of some iron meteorites (Kleine et al., 2005; Scherstén et al., 2006; Markowski et al., 2006a, 2006b; Burkhardt et al., 2008; Kleine et al., 2009). Accordingly, determining accurate Hf-W ages for iron meteorites requires a quantification of cosmic-ray induced effects on W isotopes or preferably the identification of samples that have been effectively shielded from any cosmic-ray induced nuclear reactions. Cosmic-ray produced noble gas abundances may provide an appropriate monitor for the degree of cosmic-ray exposure and shielding conditions (Wieler et al., 2002; Markowski et al., 2006b). We here report data of a combined Hf-W and noble gas isotope study that seeks to better constrain the pristine Hf-W systematics and the differentiation ages of magmatic iron meteorites.

Methods:
After careful cleaning and leaching of iron meteorite samples, tungsten was separated using conventional anion exchange chromatography. Tungsten isotope compositions were measured using a Nu Plasma MC-ICPMS at ETH Zurich following previously published procedures (Kleine et al., 2005). The ^{182}W/^{184}W compositions of the iron meteorites are reported as ε-unit deviations (i.e. parts per 10 000 deviation) relative to a terrestrial W standard that was measured bracketing the sample analyses. Reported are average ε^{182}W values of multiple solution replicates (n=5-8) at an external reproducibility of <0.2 ε-units (95% conf.). Cosmogenic noble gas (^{3,4}He, ^{21,22}Ne and ^{38}Ar) abundances of the same iron meteorite specimens were determined at the University of Bern.

Results:
Cosmogenic noble gas concentrations in the analyzed samples were found to be at the lowest end of the range previously observed in iron meteorites; ^{3}He abundances range from 0 to 133, ^{21}Ne from 0 to 2.61, and ^{38}Ar from 0.002 to 14.5 [all in 10^{-8} cm^{3}STP/g]. We determined W isotope compositions for the four samples having the lowest abundances of cosmogenic noble gases [Cape York (IIIAB), Gibeon (IVA), Muonionalusta (IVA), Edmonton (IIAB)]. These samples have ε^{182}W values ranging from -3.3 to -3.2, indistinguishable from the CAI initial of -3.28±0.12 (Burkhardt et al., 2008).

Conclusions:
The lack of W isotope compositions that are significantly less radiogenic than the initial W isotope composition of CAIs underlines the power of our combined approach and connotes that any ε^{182}W values lower than the CAI initial result from the interaction with cosmic rays. The W isotope results are compatible with iron meteorite parent bodies having differentiated within <1 Myr after CAI formation (Kleine et al., 2005; Burkhardt et al., 2008; Kleine et al., 2009), hence predating the formation of both chondrules and chondritic meteorites (Amelin et al., 2002; Kunihiro et al., 2004; Rudraswami & Goswami et al., 2007).

References:
Amelin, Y. et al., (2002). Science 297: 1678-1683.
Burkhardt, C. et al. (2008). Geochimica et Cosmochimica Acta 72: 6177-6197.
Kleine, T. et al. (2005). Geochimica et Cosmochimica Acta 69: 5805–5818.
Kleine, T. et al. (2009). Geochimica et Cosmochimica Acta 73: 5150-5188.
Kunihiro, T., et al. (2004). Geochimica et Cosmochimica Acta 68: 2947-2957.
Leya, I. et al. (2000). Earth and Planetary Science Letters 175: 1-12.
Leya, I. et al. (2003). Geochimica et Cosmochimica Acta 67: 529-541.
Markowski, A. et al. (2006a). Earth and Planetary Science Letters 242: 1-15.
Markowski, A. et al. (2006b). Earth and Planetary Science Letters 250: 104-115.
Rudraswami, N.G. & Goswami J.N. (2007). Earth and Planetary Science Letters: 257, 231-244.

Scherstén, A. et al. (2006). Earth and Planetary Science Letters 241: 530-241.
Wieler, R. et al. (2002). Reviews in Mineralogy and Geochemistry 47: 125-170.

Inefficient mixing of the solar nebula: Evidence from p-process ^{180}W heterogeneity in iron meteorites

T. Schulz[1,2] and C. Münker[1,2].

[1]Institut für Geologie und Mineralogie, Zülpicher-Str. 49b, 50674 Köln, Germany;

[2]Steinmann Institut für Endogene Prozesse, Poppelsdorfer Schloss, 53115 Bonn, Germany. E-mail: toni.schulz@arcor.de

Introduction: An efficient homogenization of materials in the protoplanetary disk seems to be reflected by uniform abundances of non-radiogenic isotopes (in particular r- and s-process isotopes) in early solar system materials. Notably, however, several recent high-precision studies have revealed that a small number of elements display distinct anomalies, interpreted as being nucleosynthetic [e.g. 1,2]. As a consequence of their low abundances, only few studies so far have measured abundances of the neutron-deficient p-process isotopes [e.g. 3]. Their low abundances reflect the particular formation conditions of p-process isotopes that most likely originate from Ne/O layers in type II supernovae [e.g. 4]. The p-nuclei are synthesized by photodisintegration of s-nuclei during helium burning in the progenitor. Here we present the first high-precision measurements of the heavy p-process nuclide ^{180}W in iron meteorites from different groups.

Samples and analytical techniques: In our study, several groups of magmatic and non-magmatic iron meteorites with W contents of up to 5 ppm were analyzed. Metal from a reduced terrestrial basalt (Dzheltul`skii massive) was also examined. Separation of W was performed by anion exchange techniques using AG 1x8 resin, following a modified elution procedure from [5]. Isotope compositions were measured using the Neptune multicollector ICP-MS at Universität Bonn that is equipped with high sensitivity 10^{12} Ohm amplifiers for measuring ^{180}W and the ^{180}Hf interference monitor. For multiple measurements of AMES W standard solutions we obtained external reproducibilities of ca. ±80 ppm (2σ r.s.d.) for ca. 200ng of W. Ratios of ^{178}Hf/^{183}W of the meteorite samples were typically below 10^{-5}, an order of magnitude lower than required for accurate ^{180}Hf interference corrections.

Results and Discussion: Except for the terrestrial metal, most samples display clearly resolvable positive anomalies in ε^{180}W from the terrestrial standard value. Notably, significant and systematic abundance variations exist between different groups of iron meteorites, ranging to values as high as +7 ε-units for magmatic iron meteorites. Conversely, non-magmatic IAB iron meteorites display only barely resolvable ε^{180}W anomalies of ~ +1 ε-unit. Cosmogenic effects due to burnout of ^{180}W (σ_{th}=22.6±1.7 barn [7]) would shift the measured anomalies to the terrestrial value (and below) and were observed for the meteorites with the longest exposure ages (e.g. Ainsworth). Hence, the observed systematics suggest inefficient mixing of ^{180}W in the earliest stages of solar system evolution, at least in the inner solar system region, where iron meteorites are thought to have formed [6]. Our first data appear to indicate that the increasing homogenization of the early solar system is mirrored by increasingly lower ^{180}W anomalies in younger iron meteorite groups, suggesting mixing-timescales in the order of several million years.

References: [1] Andreasen R. and Sharma M. (2006) Science 314, 806-809; [2] Trinquier A. et al. (2007) ApJ 655, 1179-1185; [3] Fehr M.A. et al. (2005) 69, 5099-51112; [4] Woosley S.E. and Howard W.M. (1978) ApJS, 36, 285; [5] Horan M.F. et al. (1998) GCA 62, 545-554; [6] Bottke W.F. et al. (2006) Nature 439, 821-824; [7] Kang et al. (2007) PhR C 76.

Nucleosynthetic Mo Isotope Anomalies in Planetary Materials as Tracers of Mixing, Fractionation and Accretion in the Circumstellar Disk.

Christoph Burkhardt[1], Thorsten Kleine[2], Felix Oberli[1], Andreas Pack[3], Bernard Bourdon[1], Rainer Wieler[1]
[1]ETH Zürich, Institute of Geochemistry and Petrology, Zürich, Switzerland
[2]Westfälische Wilhelms-Universität Münster, Institute of Planetology, Münster, Germany
[3]Georg-August-Universität Göttingen, Geowissenschaftliches Zentrum, Göttingen, Germany

Introduction: Stars and their accompanying planets are formed by the collapse of molecular cloud cores. Thereby mass and angular momentum is transported through an accretion disk. Modern disk models are able to explain spectroscopic observations of young stars with accretion disks but come with a large set of free parameters, thus leaving pathways, mixing and thermal processing of material within the disks poorly constrained. Meteorites probe the physico-chemical conditions of the disk at various evolutionary stages. Therefore the recently discovered nucleosynthetic anomalies in bulk meteorites and their components might serve as an important tool to better constrain mixing, fractionation and accretion within the disk and thereby test and refine disk models. Nucleosynthetic Mo isotope anomalies are here of particular interest because Mo is a refractory and moderately siderophile element (and therefore is fairly abundant in all meteorite classes) and its 7 isotopes of roughly equal abundance are produced by different nucleosynthetic processes. However, the extent to which Mo isotope variations exist among bulk meteorites is currently unclear as previous studies reported discordant results (Dauphas et al. 2002; Yin et al. 2002; Becker and Walker, 2003). Here we present new Mo isotopic data on a comprehensive set of chondrites, CAIs and iron meteorites that were acquired using improved digestion and mass spectrometric techniques.

Samples and analytical techniques: We processed samples from all major iron meteorite groups, two pallasites, chondrites from the CI, CM, CO, CV, CR, CB, H and L clans and the Allende CAI A-ZH-1 to A-ZH-5 (Burkhardt et al. 2008). To assess potential artifacts due to incomplete digestion of refractory materials the chondrite samples were fused at both reducing and oxidizing conditions with a CO_2 laser at Göttingen before being digested in Teflon beakers in a HF-HNO_3-$HClO_4$ mixture. Some samples were digested without previous fusion. The iron meteorites were dissolved in HCl. To obtain sufficiently pure Mo cuts the solutions were processed through a three column ion exchange chromatography before the Mo isotopic composition was measured using the Nu Plasma 1700 MC-ICP-MS at ETH. Instrumental and natural mass-dependent isotope fractionation was corrected relative to $^{98}Mo/^{96}Mo = 1.453174$. Internal normalization to other isotope pairs yields an internally consistent dataset, indicating that analytical artifacts are absent. The data is reported in ε-units as deviation from the terrestrial standard value in parts per 10 000. The reproducibility and accuracy of our method was monitored by analyses of a range of standard materials all of which yielded the terrestrial Mo isotopic composition.

Results: With the notable exception of the late-formed non-magmatic IAB and IIICD irons all iron meteorites exhibit Mo isotopic compositions different from that of the Earth. These Mo isotopic anomalies are consistent with a variable deficit in s-process Mo relative to the Earth. The largest anomalies of up to 2 ε-units for ^{92}Mo are found in the IVB irons. Except for ordinary and CI chondrites, whose anomalies are at the limit of our analytical resolution, all chondrites show well-resolved anomalies, the largest of which were found in the CM chondrite Murchison (~6.3 $ε^{92}Mo$). Laser-fused and acid-digested samples do not show significant differences in their Mo isotopic compositions, indicating that undigested refractory minerals are not the cause for the measured Mo isotopic anomalies in chondrites. The CAIs A-ZH-1 to A-ZH-4 show anomalies consistent with an excess in r-process Mo relative to the Earth, whereas the large anomalies of A-ZH-5 (up to 22 $ε^{92}Mo$) are more readily explained by an s-process deficit.

Discussion: Our results reveal nucleosynthetic Mo isotope anomalies on a planetary scale which requires the existence of nebular regions with a variable mix of nucleosynthetic components. This may reflect an initial heterogeneous distribution of nucleosynthetic components in the solar nebula or physico-chemical processes that enriched some components over others within an initially homogeneous nebula. Whatever the exact cause, the nucleosynthetic anomalies enable the use of Mo isotopes as a tracer of mixing, fractionation and accretion processes in the solar proto-planetary disk. All the anomalies can be described by a three component mixture between terrestrial Mo, an s-deficit and an r-excess component. Of note no bulk planetary object with a negative Mo isotopic anomaly relative to Earth has been found so far. The Mo isotopic data hint towards an increasing homogenization of the solar nebula, as the old and highly volatile depleted IVB irons show the largest anomalies of all iron meteorites whereas the rather young IAB-IIICD irons exhibit a terrestrial Mo isotopic composition.

References:
Becker H. and Walker R.J., (2003): Efficient mixing of the solar nebula from uniform Mo isotopic composition of meteorites. Nature, 425, 152-154.
Burkhardt et al. (2008): Hf-W mineral isochron for Ca,Al-rich inclusions: Age of the solar system and the timing of core formation in planetesimals. Geochimica et Cosmochimica Acta 72, 6177-6197.
Dauphas N et al. (2002): Molybdenum evidence for inherited planetary scale isotope heterogeneity of the protosolar nebula. The Astrophysical Journal, 565, 640-644.
Yin et al., (2002): Diverse supernova sources of pre-solar material inferred from molybdenum isotopes in meteorites. Nature, 415, 881-883

Ba isotope composition of equilibrated meteorites and Allende CAI

Katherine Bermingham[1], Klaus Mezger[2]
[1]Westfälische Wilhelms-Universität Münster, Institut für Mineralogie, Münster, Germany
[2]Universität Bern, Institut für Geologie, Bern, Switzerland

The extent of isotopic heterogeneity in the Solar System on the bulk sample scale is a key parameter constraining its early environment and dynamic evolution. It also indicates if regional isochrons need to be developed due to isotopic heterogeneity on the bulk scale throughout the Solar System. Nucleosynthetic isotopic anomalies have been reported at both the grain scale and bulk sample scale. Anomalous isotopic systems on the bulk sample scale include Ti (Trinquier et al., 2009), Ni (Regelous et al., 2008), Ba (Hidaka et al., 2003; Andreasen and Sharma, 2007; Carlson et al., 2007), Sm and Nd (Andreasen and Sharma, 2007; Carlson et al., 2007).

Barium has seven stable isotopes (^{130,132,134,135,136,137,138}Ba) which sample three nucleosynthetic processes that may have contributed to the Solar System's composition. These nucleosynthetic processes are the s-process (^{134,135,136,137,138}Ba), the r-process (^{135,137,138}Ba), and the p-process (^{130,132}Ba). Additionally, direct evidence for live ^{135}Cs can be observed in the Ba isotope system as the decay of ^{135}Cs to ^{135}Ba, $t_{1/2} \sim 2.3$ Myr (Hidaka et al., 2001), contributed to the ^{135}Ba abundance. These features make the Ba isotope system particularly useful when investigating the question of isotopic heterogeneity in the Solar System.

We undertook a study of eleven bulk samples to determine if the phases bearing large isotope anomalies were homogeneously distributed in the early Solar System. Here we report Ba isotope data for four equilibrated ordinary chondrites (Oesede H5, Pultusk H5, Butsura H6, Tugalin-Bulen H6), two non-cumulate eucrites (Juvinas and Stannern), one diogenite (Johnstown), and four CAI from CV3 chondrite Allende. Equilibrated samples were selected to avoid as much as possible the potential problem of not dissolving refractory presolar grains with potentially large anomalies.

The mass fractionation corrected Ba isotope data obtained indicate that the bulk meteorite samples measured are isotopically indistinguishable from terrestrial standards. Three of the measured Allende CAI possess an excess in ^{135}Ba of $\sim$ ½ ε unit, however, no anomalies are resolvable for the other stable Ba isotopes. A sole positive ^{135}Ba anomaly suggests that this excess is due to decay of short-lived radioisotope ^{135}Cs, thus signifying radiogenic-growth of ^{135}Ba as the source of the isotopic anomaly. This is in contrast to a heterogeneous distribution of isotopically anomalous bearing phases, such as presolar grains. Except for the in-growth of ^{135}Ba from the decay of ^{135}Cs, all Allende CAI studied have identical Ba isotopic composition as terrestrial standards.

The terrestrial isotope composition of the studied samples indicate that isotopically anomalous bearing phases were homogeneously distributed throughout the feeding zones of common Allende CAI, Earth, the HED parent body and the parent bodies of the equilibrated ordinary chondrites. This signifies thorough mixing of the solar nebula prior to onset of condensation. It also implies a homogeneous distribution of short-lived isotopes (e.g. ^{26}Al). As a consequence, the short-lived isotopes used for constraining the chronology of key processes in the early Solar System or for heating of planetesimals, are universally applicable to date processes in the early Solar System.

References:
Andreasen R. & Sharma M. (2007), Mixing and homogenization in the early solar system: Clues from Sr, Ba, Nd, and Sm isotopes in meteorites, Astrophysical Journal, 665, 874-883
Carlson R.W., Boyet M. & Horan M. (2007), Chondrite barium, neodymium, and samarium isotopic heterogeneity and early earth differentiation, Science, 316, 1175-1178
Hidaka H., Ohta Y., Yoneda S. & DeLaeter J.R. (2001), Isotopic search for live Cs-135 in the early solar system and possibility of ^{135}Cs-^{135}Ba chronometer, Earth Planet Science Letters, 193, 459-466
Hidaka H., Ohta Y. & Yoneda S. (2003), Nucleosynthetic components of the early solar system inferred from Ba isotopic compositions in carbonaceous chondrites, Earth Planet Science Letters, 214, 455-466
Regelous M., Elliott T. & Coath C.D. (2008), Nickel isotope heterogeneity in the early Solar System, Earth Planet Science Letters, 272, 330-338
Trinquier A., Elliott T., Ulfbeck D., Coath C., Krot A.N. & Bizzarro M. (2009), Origin of nucleosynthetic isotope heterogeneity in the solar protoplanetary disk, Science, 324, 374-376

Fe-isotope composition of meteorite fusion crust as analogues for evaporation and re-condensation processes in the early solar nebula.

Dominik C. Hezel[1], Graeme Poole[1], Caroline Smith[1], Jack Hoyes[1] and Mark Rehkämper[2]
[1]Natural History Museum, Department of Mineralogy, Cromwell Road, SW7 5BD, London, UK
[2]Department of Earth Science and Engineering, Imperial College, London, SW7 2AZ, UK

Meteorites hit the Earth with up to a couple of tens of km/s and are completely decelerated during atmospheric entry caused by friction of the meteorite surface with air. The friction heats, melts and ablates the outermost layer of the meteorite for seconds to minutes. This produces a black fusion crust of solidified melt, usually around a millimetre thick. This brief heating might serve as an analogue process for possible evaporative fractionation processes during chondrule formation, which is as well a brief high-temperature event.

Bulk chondrules have only minor Fe isotope fractionations (Mullane et al., 2005; Needham et al., 2009; Hezel et al., 2010) that are at least partially the result of evaporation and re-condensation processes during chondrule formation in the solar nebula (Hezel et al., 2010). Stable isotope studies of cosmic spherules, sub-mm sized glassy micro-meteorites that have been completely melted during atmospheric entry, have an enrichment of 56Fe of up to several tens of per mil, close to what is expected from Rayleigh fractionation (Alexander et al., 2002). There is no comparable study of Fe isotopes in meteorite fusion crusts, however, the melting of the meteorite surface is possibly also accompanied by evaporation and fractionation of chemical elements such as Fe. If this is the case, the light isotopes of Fe (54Fe) will be preferentially lost by evaporation and, hence, the fusion crust should be enriched in the heavy isotopes (56Fe, 57Fe). There are so far only few data that have been obtained as part of other Fe isotope studies (Needham, pers. comm.). These, however, show only minor Fe isotope fractionations. In addition, there are a few Si- and K-isotope data of meteorite fusion crusts (Molini-Velsko et al., 1986; Humayun and Clayton, 1995) that also show only minor fractionation. There are only few studies of meteorite fusion crusts (e.g. Genge and Grady, 1999; Thaisen and Taylor, 2009) and to our knowledge no dedicated isotope study. We selected equal amounts of H, L and LL ordinary chondrites from 10 finds and 10 falls, spanning the entire range of petrologic types. The terrestrial age of most finds is unknown, but these meteorites were presumably exposed to the atmosphere and weathering for thousands of years. From the falls we selected those with the most pristine fusion crust. Criteria were (i) an as small as possible time interval between fall and recovery of the meteorite, (ii) macroscopically unaltered fusion crust, i.e. the blacker and more shiny the better, and (iii) large samples, as fusion crust not in direct contact and not lose to soil will presumably be less affected by weathering. The Fe isotope composition of the fusion crusts and bulk meteorites, as well as bulk chemical compo sitions of the meteorites are currently measured at the Natural History Museum and the MAGIC laboratories at Imperial College. The measurements are complemented by petrologic studies of the meteorites and their fusion crusts.

The results will be presented at the meeting and the relevance of fusion crust as analogue material for early solar system processes discussed.

Reference:
Alexander, C. M. O'D, Taylor, S., Delaney, J. S., Ma, P., and Herzog, G. F. (2002) Mass-dependent fractionation of Mg, Si, and Fe isotopes in five stony cosmic spherules. Geochimica et Cosmochimica Acta 66, 173.
Genge, M. J. and Grady, M. M. (1999). The fusion crusts of stony meteorites: Implications for the atmospheric reprocessing of extraterrestrial materials. Meteoritics and Planetary Sciences 34, 341.
Hezel, D. C., Needham, A. W., Armytage, R., Georg, B., Abel, R., Kurahashi, E., Coles, B.J., Rehkämper, M. and Russell, S. S. (2010) A nebula setting as the origin for bulk chondrule Fe isotope variations in CV chondrites.
Earth & Planetary Science Letters (in press) [doi: 10.1016/j.epsl.2010.05.029].
Humayun, M. and Clayton, R. N. (1995) Potassium isotope cosmochemistry: Genetic implications of volatile element depletion. Geochimica et Cosmochimica Acta 59, 2131.
Molini-Velsko, C., Mayeda, T. K., and Clayton, R. N. (1986) Isotopic composition of silicon in meteorites. Geochimica et Cosmochimica Acta 50, 2719.
Mullane, E., Russell, S. S., and Gounelle, M. (2005) Nebular and asteroidal modification of the iron isotope composition of chondritic components. Earth & Planetary Science Letters 239, 203-218.
Needham, A. W., Porcelli, D., and Russell, S. S. (2009) An Fe isotope study of ordinary chondrites. Geochimica et Cosmochimica Acta 73, 7399-7413.Thaisen, K. G. and Taylor L. A. (2009) Meteorite fusion crust variability. Meteoritics and Planetary Sciences 44, 871.

Mass-Independent Cadmium Isotope Fractionation during Evaporation
Frank Wombacher (presenting author)[1]
[1] Universität zu Köln, Institut für Geologie und Mineralogie, 50674 Köln, Germany

Isotope cosmochemistry deals with a multitude of isotope effects, including radiogenic ingrowth, nucleosynthetic anomalies, irradiation effects, mass-dependent and mass-independent (MIF) stable isotope fractionation. Here, we investigate mass-independent Cd isotope fractionations that result from evaporation in an experimental setup, where liquid Cd was evaporated into vacuum at an estimated temperature of about 180°C. Analyses of three residues from evaporation (samples C, D, E) by MC-ICP-MS revealed large mass-dependent Cd isotope fractionations with 1000ln α ranging from -23.2 to -48.3 ‰ for $^{110}Cd/^{114}Cd$ relative to the starting material (A) (Wombacher et al. 2004). Because of this large isotope fractionation, the mass-scaling for the evaporation process could be quantified precisely using the generalized power law (GPL) of Marèchal et al. (1999). The observed GPL exponent q = -0.34 ±0.05 for sample E was significantly different from the mass-scaling expected for kinetic (q -> 0) and equilibrium isotope fractionations (q = -1) (Young et al. 2002; Wombacher et al. 2004).

The residual Cd samples were now reanalyzed at high precision using a Neptune MC-ICP-MS, with ion beam intensities typically larger than 20V for ^{114}Cd and analysis times of about 30 minutes. Each sample was measured at least twice using an Aridus membrane desolvator and once more using a glass spray chamber and different collector settings. The three samples C, D and E reveal a slightly different mass-scaling with GPL exponents q between -0.25 to -0.35 for different residues. Accurate correction of the mass-dependent isotope fractionation using the GPL and normalization to the $^{110}Cd/^{114}Cd$ ratio of the starting material resolves small deficits for ratios involving odd isotopes ($^{111}Cd/^{114}Cd$: -28 ±5, -26 ±5, -12 ±6 ppm; $^{113}Cd/^{114}Cd$: -22 ±7, -19 ±5, -9 ±3 ppm) and the even isotope ^{116}Cd ($^{116}Cd/^{114}Cd$: -16 ±11, -10 ±3, -8 ±5 ppm) in samples C, D and E respectively. For comparison, $^{112}Cd/^{114}Cd$ (4 ±5, 2 ±4, 1 ±2 ppm) does not display resolvable deviations (all uncertainties are 2sd; n = 3 or 4). Sample D, which displays only ~50% MIF also displays only about the half the mass-dependent fractionation.

MIF for ^{111}Cd, ^{113}Cd and ^{116}Cd is consistent with the comparatively smaller mean-squared nuclear charge radii for these isotopes (Angeli, 2004) and is therefore most probably the result from nuclear volume effects (NVE) (Bigeleisen 1996; Schauble et al. 2007). Moreover the observed relative MIF for ^{111}Cd, ^{113}Cd and ^{116}Cd is most similar to that observed for Cd isotopes during isotope exchange reactions on crown ether (Fujii et al. 2009). Also, Estrade et al. (2009) observed similar odd isotope deficits for the experimental evaporation of Hg. Both studies suggested that NVE were responsible (for most) of the mass-independent fractionation. Evaporation of Cd into vacuum is expected to be a kinetic process (Wombacher et al. 2008), but NVE are expected to result from equilibrium isotope partitioning. Therefore, the mass-independent NVE and part of the mass-dependent isotope fractionation probably result from partial re-equilibration between Cd vapor and liquid.

Reference:
Angeli, I (2004), A consistent set of nuclear rms charge radii: properties of the radius surface R (N, Z). At. Data. Nucl. Data Tables, 87, 185-206.
Bigeleisen, J (1996), Nuclear size and shape effects in chemical reactions. Isotope chemistry of the heavy elements, J. Am. Chem. Soc, 118, 3676-3680.
Estrade N, Carignan J, Sonke J E & Donard O F X (2009), Mercury isotope fractionation during liquid-vapor evaporation experiments, Geochim. Cosmochim. Acta, 73, 2693-2711.
Fujii T, Moynier F, Telouk P & Albarède F (2009), Nuclear field shift effect in the isotope exchange reaction of cadmium using a crown ether, Chem. Geol., 267, 157-163.
Maréchal C N, Télouk P & Albarède F (1999), Precise analysis of copper and zinc isotopic compositions by plasma-source mass spectrometry, Chem. Geol., 156, 251-273.
Schauble, E A (2007), Role of nuclear volume in driving equilibrium stable isotope fractionation of mercury, thallium, and other heavy elements, Geochim. Cosmochim. Acta, 71, 2170-2189.

Wombacher F, Rehkämper M & Mezger K (2004), The mass-dependence of cadmium isotope fractionation during evaporation, Geochim. Cosmochim. Acta, 68, 2349-2357.
Wombacher F, Rehkämper M, Mezger K, Bischoff A & Münker C (2008) Cadmium stable isotope cosmochemistry, Geochim. Cosmochim. Acta, 72, 646-667.
Young E D, Galy A & Nagahara H (2002), Kinetic and equilibrium mass-dependent isotope fractionation laws in nature and their geochemical and cosmochemical significance, Geochim. Cosmochim. Acta, 66, 1095-1104.

Evaporation of Na and other volatiles from Na bearing minerals and silicate melts

Marko Gellissen [1,2], Astrid Holzheid[1], Philip Kegler[1], Ralf Dohmen[3], Sumit Chakraborty[3], Herbert Palme[2]
[1]Universität Kiel, Institut für Geowissenschaften, Kiel
[2]Forschungsinstitut und Naturmuseum Senckenberg, Sektion Meteoritenforschung, Frankfurt/Main
[3]Universität Bochum, Institut für Geologie, Mineralogie und Geophysik, Bochum

The depletion of the volatile lithophile elements, e.g., F, Na, Mn, K, Rb, or Zn, when compared with solar abundances or CI-abundances is a distinctive chemical signature of the Earth's mantle and all solid inner solar system materials. Particularly striking is the similar depletion of the geochemically very different elements Na and Mn. We want to find out if this depletion is the result of heating processes in the late history of the Earth or Earth forming embryos, or if it is a result of incomplete condensation at the beginning of the solar system. In a series of experiments with varying oxygen fugacities, temperatures, and mineral compositions we will quantify the evaporative losses of Na, Mn, and other volatiles from their host minerals and/or from melts, to better understand the behavior of the two elements during heating. Here we report the first results.

Minerals: Heating experiments with albite, oligoclase, nepheline, and sodalite were performed at various oxygen fugacities (ranging from air to below the iron-wuestite buffer), temperatures from 1000 to 1400°C, and run durations of up to 3 hours. In some of the experiments the run temperatures were above the liquidus temperature. We find that heating of pure albite, oligoclase, and nepheline crystals does not produce any loss of Na, independent of oxygen fugacity. Even melts of these minerals do not loose Na. Sodalite looses Cl quantitatively and about 20% of the Na after 100 minutes of heating at 1200°C. Further heating for 3 hours has no additional effect on evaporation. Experiments at oxygen fugacities of one atmosphere and 10^{-13} atm gave similar results.

Melts: An anhydrous CI-chondritic starting composition (about 180 mg) was heated in Pt-containers (length/width/height: 4/4/4 mm) to 1500°C at an oxygen fugacity of log fO_2 = -10.6 (ca. 1.8 log units below the iron-wuestite (IW) buffer). Time series from a few minutes to two hours were performed. Experimental post-run charges were analyzed by electron microprobe and XRF techniques. Losses of Na were observed after one hour. After 2 hours 24 % of the Na was lost. Manganese losses are not observed at these conditions. Experiments by Tsuchiyama et al. (1981), who heated their charges (about 40 mg) in wire loops (wire diameter: 0.1 mm; loop diameter: 3.2 mm), showed much more rapid losses at conditions comparable to those used in our experiments reflecting the higher surface to volume ratio in the wire loop experiments (surface to volume ratios [mm^2/mm^3]: ~1.8 (wire loop filled with spheroidal shaped silicate melt) and ~0.5 (container half-full with silicate melt)).

In addition to the heating experiments with the CI-chondritic starting composition, wire loop experiments with Fe-pre-saturated Pt-loops (wire diameter: 0.35 mm; loop diameter: 2 mm; about 3 mg sample inside the loop) were performed with melts of roughly andesitic composition with high Al_2O_3 resembling the continental crust and with an Al_2O_3-free, alkali-rich silicate melt. Time series experiments at constant temperature (1300°C) and log fO_2 of IW-1 as well as experiments at oxygen fugacities of IW+2 to IW-1.5 were performed in 1-atm gas mixing furnaces to determine the effects of silicate composition and oxygen fugacity on evaporation of Na, K, and Mn. The chemical compositions of the post run charges were determined by electron microprobe analyses. In the Al_2O_3-free, alkali-rich silicate melt, losses of 86% Na and 57% K, and no loss of Mn (all abundances normalized to Ti) were observed after 240 minutes and at 1300°C. The experiments with variable oxygen fugacity showed an increase of Na and K losses with decreasing oxygen fugacity, i.e., at more reducing conditions. This trend is also found by Tsuchiyama et al. (1981) and in the experiments of Wulf et al. (1995). The K and Na losses in the crustal composition silicates were much lower. It thus appears that Al_2O_3 might have an important influence on the volatilisation of alkalis, presumably through the formation of albite like species in the melt. Further experiments using synthetic albitic melt will be done for confirmation.

In summary, these data demonstrate that Na- and also K-losses are extremely variable and depend on bulk composition, oxygen fugacity, and on the geometry of the charges (loop vs. container). The latter point has not been sufficiently appreciated in the literature and an experimentally based systematic investigation of that influence is in progress.

Reference:
Suchiyama, A., Nagahara, H. & Kushiro, I. (1981), Volatilization of sodium from silicate melts spheres and its application to the formation of chondrules, Geochim. Cosmochim. Acta, 45, 1357-1367

Wulf, A.V., Palme, H. & Jochum, K.P. (1995), Fractionation of volatile elements in the early solar system: Evidence from heating experiments on primitive meteorites, Planet. Space Sci., 43, 451-468

Refractory element fractionation in the Allende meteorite

Andreas Stracke[1], Herbert Palme[2,5], Marko Gellissen[2], Thorsten Kleine[1,3], Karin Birbaum[4], Detlef Günther[4], Bernard Bourdon[1], and Jutta Zipfel[5]
[1]Institute of Geochemistry and Petrology, ETH Zürich, Switzerland.
[2]Institute of Geology and Mineralogy, Univeristy of Cologne, Germany.
[3]Westfälische Wilhelms-Universität Münster, Institute for Planetology, Münster, Germany.
[4]Laboratory of Inorganic Chemistry, ETH Zürich, Switzerland.
[5]Senckenberg Forschungsinstitut und Naturmuseum Frankfurt, Germany.

Chondrites are mixtures of components of different origin and with very different compositions, e.g. chondrules, matrix, metal, and rare Ca, Al-rich inclusions (CAI). Bulk analyses of different aliquots of a single meteorite thus depend on the size and distribution of these constituents. A certain sample size is required to avoid compositional bias due to sample heterogeneity, and to assure a truly representative bulk composition.

Here, we investigate the effect of sample heterogeneity on the major and trace element composition of the CV3 chondrite Allende using a single 30 g slice, which is 22.5 cm^2 in dimension and 4 mm thick. Thirty-nine equally sized pieces (about 7 x 7 x 4 mm) with an average sample weight of 0.6 g were individually powdered and aliquots of 0.12 g and 0.02-0.03 g were analyzed by XRF [1] and ICP-MS [2, 3] for major and trace elements, respectively. Two samples, one dominated by a large CAI and the other by a dark inclusion, were excluded.

In the remaining thirty-seven samples Mg, Si, and Fe concentrations are surprisingly uniform (S.D. 0.9, 1.3 and 2.6%, respectively) on the mm scale [4]. This is also true for the other non-refractory trace elements Ni, Co, Cr, Mn, P and Zn. In contrast, refractory elements are much more variable in absolute concentrations and in element ratios, probably produced by the admixture of refractory inclusions (CAI, [4]), many of them with strongly fractionated group II CI-normalized rare earth element (REE) patterns [5] and corresponding fractionations in other refractory elements, with enrichment of the more volatile refractory elements (Ta, U, Nb, Sr, Tm, Nd) over the strongly refractory elements (Lu, Zr, Hf). With increasing bulk Al and Ca concentrations group II-type REE patterns become more pronounced, but also more variable, as both the absolute and relative abundance of the refractory trace elements vary about twofold. Thus the composition of the refractory component of Allende is not uniform. The average of all thirty-seven samples shows a distinctive group II REE pattern, with Nb and U being 30% more enriched than Er and Lu when normalized to CI [6]. A fractionated group II REE pattern for bulk Allende has been inferred earlier by Fegley and Kornacki [7].

If the fractionated refractory element pattern of our 30 g Allende sample is representative of its parent body, bulk planetary bodies may also have refractory element ratios different from CI chondrites. In the case of Allende this requires large-scale removal of a super-refractory component in the solar nebula. Hence on the basis of our data, planetary-forming bodies may not be strictly chondritic in their refractory element patterns.

References:
[1] Wolf, D. & Palme, H., 2001. Earth Planet. Sci. Lett. 36, 559-571. [2] Willbold, M. and Jochum, K. P., 2005. Geostandard Newslett. 29, 63-82. [3] Stracke, A. et al., 2009. Geochim.. Cosmochim. Acta, 73, A1281. [4] Gellissen, M., et al., 2008. Meteoritics Plan. Sci. Suppl. 43, 5306. [5] Mason, B. & Taylor, S.R., 1982. Smithonian Contrib. Earth Sci. 25, 1-30. [6] Palme, H. & Jones A., 2005. Treatise in Geochemistry, 1, 41-61. [7] Fegley B., & Kornacki A. S., 1984. Lunar Plan. Sci. Conf. XV, 262-263.

Rare Earth Element abundances in bulk chondrites and Earth

Verena Bendel[1], Andrea Patzer[1], Andreas Pack[1], Charlotte Allen[2], Carsten Münker[3]
[1]Georg-August-Universität Göttingen, Institute Geosciences, Department Isotope Geology, Göttingen, Germany
[2]Research School of Earth Sciences, The Australian National University, Canberra, Australia
[3]Universität zu Köln, Institute for Geology and Mineralogy, Köln, Germany

Rare earth elements (REE) are important indicators for fractional condensation and evaporation processes in the early solar system. Fractionation occurs due to differences in condensation temperature among REEs (Boynton, 1975). Here we examine REE patterns in a large set of bulk chondrites in order to identify volatility-controlled fractionations on the asteroidal scale. As reference material we use the Orgueil (CI1) meteorite, which is taken as the solar system reference (Lodders, 2003). Selected terrestrial samples were also analyzed along with meteorites in order to identify volatility-controlled fractionation of REEs in the bulk Earth.

We analyzed the REE contents by means of laser ablation inductively coupled plasma mass spectrometry (LA-ICPMS) at the Australian National University (Canberra) employing a Lambda Physique excimer laser, in-house constructed ablation cell, and Agillent 7500S ICP-MS. Bulk rock samples were homogenized and prepared for LA-ICPMS analysis following the method described by Pack et al. (2010) and applied by Pack et al. (2007) and Patzer et al. (2010). Samples were ground to powder in an agate mortar. Metal bearing meteorite samples were oxidized in a muffle furnace before grinding. The powder was briefly fused with a 50 W CO_2 laser in a reducing atmosphere of a mixture of Ar and H_2 (7 vol.%). The spheres were then put on top of a vertical gas stream, briefly fused for 2 or 3 times and homogenized. The samples were quenched by switching off the laser. The spheres were embedded in resin and polished for EPMA and LA-ICPMS. The concentrations of REEs were calculated using NIST SRM 612 (concentration values from Pearce et al., 1997) and other reference materials as external standards. Calcium was used for internal normalization. The Ca concentrations were measured by electron microprobe analysis (EPMA). The precision of our LA-ICPMS measurements of REEs is usually better than ±5% (1σ, SD). With LA-ICPMS it is possible to measure all REEs, including the monoisotopic elements Pr, Tb, Ho and Tm, which are important to identify volatility-controlled fractionation. These elements are not accessible by isotope dilution mass spectrometry.

All samples are normalized to the mean value of 12 measurements of Orgueil. The precision of this mean value is, except for Ce, better than ±3%. Our results show that chondrites usually do not have chondritic (i.e. flat) REE patterns. The relative REE fractionations are, with Orgueil as a reference, about ±10%. The reproducibility of REE in different spheres of the same sample is usually better than ±5%. The analyzed carbonaceous chondrites have distinct REE patterns. Murchison (CM2) shows a slight fractionation with an enrichment of heavy REE (HREE) over light REE (LREE). This is typical for ultrarefractory condensates. Two carbonaceous chondrites of the CV3 group (Allende and Mokoia) show highly fractionated REEs with a strong enrichment of LREE over HREE and a strong positive anomaly in Tm. Such patterns are typical for group-II calcium aluminium inclusions (CAI), which are present in both, Allende and Mokoia. We analyzed different aliquots (200 to 300 mg) of Allende. Aliquots with a large amount of CAI material show more pronounced REE fractionations. The amount of CAI material is reflected in the Ca/Si and Al/Si concentration ratios. Several ordinary chondrites were analyzed. Many of them show a slight fractionation with enriched HREE. The REE patterns cannot easily be explained by fractional condensation. Two enstatite chondrites show very similar patterns with HREE over LREE enrichment and a strong depletion in Eu. The terrestrial samples, which are normalized to Orgueil, show very smooth REE patterns.

Most chondrites have fractionated REE relative to CI1. CI1 resembles the composition of the sun and has REEs that are likely representative of the bulk solar system. The very smooth REE patterns in our terrestrial samples (normalized to our measurements on Orgueil) support that Orgueil and the bulk Earth have unfractionated REEs, with respect to the bulk solar system. The fractionated patterns of most chondrites support that fractional condensation controlled the refractory element inventory of solar system bodies on the asteroidal scale.

References:
Boynton, W.V. (1975), Fractionation in the solar nebular: condensation of yttrium and the rare earth elements, *Geochim. Cosmochim. Acta*, **39**, 569-584.
Lodders, K. (2003), Solar system abundances and condensation temperatures of the elements, *The Astrophysical Journal*, **591**, 1220-1247.
Pack, A., Russell, S.S., Shelley, J.M.G. and van Zuilen, M. (2007), Geo- and cosmochemistry of the twin elements yttrium and holmium, *Geochim. Cosmochim. Acta*, **71**, 4592-4608.

Pack, A., Kremer, K., Albrecht, N., Simon, K. and Kronz, A. (2010), Description of an aerodynamic levitation apparatus with applications in Earth sciences, *Geochem. Transact.*, in revision.

Patzer, A., Pack, A. and Gerdes, A. (2010), Zirconium and hafnium in meteorites, *Meteorit. Planet. Sci* ,in revision.

Pearce, N.J.G., Perkins, W.T., Westgate, J.A., Gorton, M.P., Jackson, S.E., Neal, C.R. and Chenery, S.P. (1997), A compilation of new and published major and trace element data for NIST SRM 610 and NIST SRM 612 glass reference materials, *Geostandards Newsletter*, **21**, 115-144.

A new Model for Early Lunar Differentiation from High Precision Measurements of High Field Strength Elements in Lunar Rocks

Carsten Münker
Universität zu Köln, Institut für Geologie und Mineralogie, Köln, Germany

The compositional spectrum of lunar rocks is commonly explained by melting of fossil cumulate layers that formed during crystallisation of a lunar magma ocean (LMO). Lunar mare basalts are inferred to tap trace element depleted, olivine and orthopyroxene-rich cumulate layers formed at the base of the LMO. The petrogenesis of high-Ti mare basalt group, however, is explained by direct melting of or, alternatively, by assimilation of late stage ilmenite-rich cumulate layers. Trace element enriched KREEP rocks tap mantle layers representing the final stages of LMO crystallisation. Based on measurements of ^{182}W (Touboul et al. 2007) and ^{142}Nd compositions of lunar samples (e.g., Boyet & Carlson 2007), it has been proposed that crystallisation of the LMO did not occur until 60 Ma after solar system formation and possibly lasted until 250 Ma. High precision isotope dilution measurements of HFS elements (W-Nb-Ta-Zr-Hf) and REE (Sm-Nd-Lu) on a representative suite of lunar rocks can now cast ne light on the processes active during the petrogenesis of lunar rocks. In addition, the new trace element data can also improve our understanding of the significance of lunar ^{182}Hf-^{182}W and ^{146}Sm-^{142}Nd data.

As expected from previous models, KREEP-rich and mare basalts display complementary Sm/Nd, Nb/Ta and Zr/Hf ratios, therefore confirming the presence of complementary enriched and depleted reservoirs in the lunar mantle. Compositions of high-Ti mare basalts, however, are not consistent with a simple two component model. These rock types display the lowest Nb/Ta and Zr/Hf of all lunar rocks analysed, although hig-Ti basalts tend to exhibit higher concentrations of many incompatible trace elements. Moreover, the high-Ti mare basalts analysed also exhibit tightly correlated Ta/W and Hf/W (up to values of 23 and 136, respectively), unlike any known terrestrial MORBs that typically exhibit more or les uniform Ta/W.

Trace element modelling can show that the strong (and coupled) increase of Ta/W, Hf/W and Sm/Nd in the high-Ti basalts can be best explained via assimilation of up to ca. 20% of ilmenite- and clinopyroxene-rich LMO cumulates by more depleted melts from the lower lunar mantle. During cumulate assimilation, the ^{182}W and ^{142}Nd isotope signatures of the hybrid magmas get decoupled from the ambient Hf/W and Sm/Nd ratios, because Hf and Sm are much more enriched relative to W and Nd, respectively. These observations require a different view on the interpretation of Sm-Nd and Hf-W systematics in lunar rocks. The co-variations of lunar samples in ^{182}W vs. Hf/W and ^{142}Nd vs. Sm/Nd spaces, previously been interpreted as isochrons with an age significance, might rather constitute mixing lines. Employing combined trace element and isotope modelling, the lunar Hf-W and Sm-Nd data would then be fully consistent with an "early" crystallisation age of the LMO (as early as 50 Myrs after solar system formation when the Moon is likely to have formed.

The new high precision HFSE data also permit to re-evaluate the timescales for formation of the Earth-Moon system as inferred from Hf-W chronometry. Together with a compilation of existing W/Th data for lunar rocks, the new Hf/W and Ta/W data indicate that the terrestrial and lunar mantles are indistinguishable in their Hf/W. Nearly similar Hf/W in the silicate Earth and the silicate portion of the Moon may explain the similar ^{182}W abundance in both bodies and also suggest for a strong temporal link between the final core-mantle equilibration on Earth and the Moon forming giant impact event.

References:
Boyet, M & Carlson, R.W. (2007), A highly depleted moon or a non-magma ocean origin for the lunar crust? Earth and Planetary Science Letters 262, 505-516.
Touboul, M., et al. (2007), Late formation and prolonged differentiation of the Moon inferred from W isotopes in lunar metals, Nature 450, 1206-1209.

Dating volatile depletion of basaltic achondrite parent bodies

Ulrik Hans[1], Thorsten Kleine[2], Bernard Bourdon[1]
[1]ETH Zürich, Institute of Geochemistry and Petrology, Zürich, Switzerland
[2]Westfälische Willhelms-Universität Münster, Institut für Planetologie, Wilhelm-Klemm-Str. 10, 48149 Münster, Germany

Many planetary objects are depleted in moderately volatile elements but the exact mechanisms involved remain unclear. ^{87}Rb-^{87}Sr chronometry provides a powerful tool for determining the timing of volatile depletion, which is key for understanding its causes. To better constrain the timing of volatile depletion in early protoplanets we obtained high-precision Sr isotopic data for angrites and eucrites.

Sr isotopic measurements were performed in dynamic mode using the Thermo TRITON at ETH Zurich. The external reproducibility for the ^{87}Sr/^{86}Sr ratio was estimated from repeated measurements of the NBS987 standard and is ±5 ppm (2 SD). Basaltic and cumulates eucrites plot on a single isochron, whose initial ^{87}Sr/^{86}Sr is consistent with previously reported values for BABI [Papanastassiou D. A. and Wasserburg G. J.]. Several mineral separates from angrites D'Orbigny and Angra dos Reis have indistinguishable ^{87}Sr/^{86}Sr but variable ^{87}Rb/^{86}Sr ratios, indicating a recent addition of Rb to these angrites. Thus, using the measured ^{87}Rb/^{86}Sr to correct for ^{87}Rb-decay results in spuriously low initial ^{87}Sr/^{86}Sr for angrites. The initial ^{87}Sr/^{86}Sr determined in this study is thus higher than those obtained in previous studies [Lugmair and Galer] and is indistinguishable from that of eucrites.

Both angrites and eucrites have initial ^{87}Sr/^{86}Sr ratios that are higher than that of Ca-Al rich inclusions (CAI) [Podosek et al.]. This difference may be used to determine the timing of volatile loss from the angrite and eucrite parent bodies. This requires assumptions regarding the Rb/Sr ratio of the material from which the parent bodies of basaltic achondrites accreted. If this material had a solar Rb/Sr then Rb-loss occurred at 3 ± 1 Myr after CAI formation. (relative to CAI 3529-Z [Podosek F. A. et al.]). However, if the parent material of the angrite and eucrite parent bodies had a lower-than-solar Rb/Sr, then volatile loss occurred later. For instance, for CI-chondritic Rb/Sr the model age of Rb-loss is ~4 Myr after CAI formation. The latest possible time of volatile depletion is given by the ~4 Myr crystallization age of D'Orbigny, about similar to the Rb model age for a CI-chondritic Rb/Sr. Thus, the basaltic achondrite parent bodies must have accreted from material that had Rb/Sr ratios at least as high as CI chondrites. The basaltic achondrite parent bodies may thus represent volatile-rich planetesimals that accreted early and lost their volatiles late by energetic impacts [Halliday and Porcelli 2001]. Alternatively, the basaltic achondrites derive from bodies that accreted late from incompletely condensed material. As early planetesimals are thought to be volatile-poor bodies (because volatiles have not yet condensed) the second possibility is more likely.

Yet another interpretation of the elevated initial ^{87}Sr/^{86}Sr ratios of angrites/eucrites compared to CAIs is that the Sr isotopic composition of CAIs is not representative of the initial ^{87}Sr/^{86}Sr in the angrite-forming region. This may be the case if CAIs carry nucleosynthetic Sr isotope anomalies or if their Sr isotopic composition was modified by stable Sr isotope fractionation [Patchett P. J.]. Clearly, high-precision Sr isotope data for CAIs are required to address this question.

Reference:
Papanastassiou D. A. and Wasserburg G. J. (1969), Initial strontium isotopic abundances and the resolution of small time differences in the formation of planetary objects, EPSL 5:361–376; Podosek F. A. et al. (1991), Correlated study of initial ^{87}Sr/^{86}Sr and Al-Mg isotopic systematics and petrological properties in a suite of refractory inclusions from the Allende meteorite, GCA 55:1083-1110; Lugmair G. W. and Galer S. J. G. (1992), Age and isotopic relationships among the angrites Lewis Cliff 86010 and Angra dos Reis, GCA 56:1673-1694; Halliday A. N. and Porcelli D. (2001), In search of lost planets – the paleocosmochemistry of the inner solar system, EPSL 192:545-559: Patchett P. J. (1980), Sr isotopic fractionation in Allende chondrules: a reflection of solar nebular process, EPSL 50:181-188

S05-T13

Ureilitic and chondritic lithologies in the Almahata Sitta meteorite breccia and implications for the evolution of asteroid 2008 TC$_3$

Marian Horstmann[1], Addi Bischoff [1]
[1]Westfälische Wilhelms-Universität Münster, Institut für Planetologie, Münster, Germany

On October 7, 2008, the asteroid 2008 TC$_3$ detected and investigated in space impacted the Earth in the Nubian Desert, northern Sudan. Subsequent field campaigns revealed more than 200 meteorite fragments and these were named collectively as the Almahata Sitta meteorite. Based on one studied fragment, Jenniskens et al. (2009) classified Almahata Sitta as an anomalous polymict ureilite.

40 meteorite fragments (2.6-50g) collected in the asteroid´s strewn field in July and October 2009 were investigated by Bischoff et al. (2010) and Horstmann et al. (2010). The mineralogy and textures of the samples were studied by optical and electron optical microscopy. Semiqantitative and quantitative analyses were performed using a JEOL 6610-LV electron microscope (EDS, Oxford Instruments) and a JEOL JXA 8900 electron microprobe, respectively. Short- to medium short-lived cosmogenic radionuclides were measure at the Laboratori Nationali del Gran Sasso, Italy (Bischoff et al., 2010; Horstmann et al., 2010).

Among the analyzed, mainly monolithic samples 23 achondritic (ureilitic) and 17 chondritic rocks were identified. These belong to a large number of at least 20 different lithologies (Bischoff et al., 2010). The ~10 different ureilitic lithologies are fine- or coarse-grained rocks (grain sizes: <20-30μm and 100μm- >1mm, respectively) with variable mineral chemistry (Fa$_{0-21}$, Fs$_{0-18}$Wo$_{1-12}$ and Fa$_{2-22}$, Fs$_{0.5-22}$Wo$_{1-11.5}$, respectively). Similar ureilitic lithologies in Almahata Sitta have been described by e.g. Jenniskens et al. (2009). Two unique samples show sulfide-metal assemblages with silicate (ureilite) material attached. The chondritic samples comprise two H chondrites (H5, H5/6) and 14 enstatite chondrites (EH3, EL3/4, EL6, EL breccias, several different types of EL and EH impact melt rocks and impact melt breccias (some shock-darkened)) that belong to at least 7 different lithologies (Bischoff et al., 2010). Additionally, one "unique" chondrite was found (Horstmann et al., 2010). The detection of short-lived cosmogenic radionuclides (^{46}Sc, ^{54}Mn, ^{57}Co) in two chondritic samples (Bischoff et al., 2010) is consistent with the Almahata Sitta event. In combination with fall statistics, this gives strong evidence that a large number, if not all fragments belong to this fall. These aspects point towards Almahata Sitta being a complex polymict breccia.

Goodrich et al. (2004) proposed a model for the ureilite parent body and its evolution. Based on the ureilite collection available, they suggest that the ureilite parent body was stratified in pyroxene-type and chemistry with increasing Mg-number and decreasing depth/pressure as a result of smelting (pressure-dependent carbon redox control). This body was catastrophically disrupted due to an impact that delivered ureilitic material from all depths to space. The debris reassembled into one or several "ureilite second-generation" asteroids. According to Goodrich et al. (2004) these are the source bodies for the present ureilite collection on Earth. We adopted this model and additionally suggested that there is strong evidence that all the different types of chondritic material found in our study were mixed with the ureilitic material before it reaccreted into the second generation asteroid. Asteroid 2008 TC$_3$ parental to Almahata Sitta was presumably a highly unconsolidated fragment of one second generation asteroid. While flying through the Earth´s atmosphere the asteroid disintegrated into mainly monolithic fragments that were later found in the Nubian Desert (Horstmann & Bischoff, 2010).

Thus, Almahata Sitta provides an important sample for future studies on the composition and evolution of asteroidal (ureilitic) bodies as the existence and abundance of foreign and exotic fragments in meteorites gives some measure of the degree of mixing among asteroids in the asteroid belt (Bischoff et al., 2010).

Reference:
Bischoff, A., Horstmann, M., Pack, A., Laubenstein, M. & Haberer, S. (2010), Asteroid 2008 TC$_3$ – Almahata Sitta: A spectacular breccia containing many different ureilitic and chondritic lithologies, Meteoritics & Planetary Science 45 (submitted).
Goodrich, C. A., Scott, E. R. D. & Fioretti, A. M. (2004), Ureilitic breccias: clues to the petrologic structure and impact disruption of the ureilite parent asteroid, Chemie der Erde – Geochemistry 64, 283-327.
Horstmann, M. & Bischoff, A. (2010), Formation and evolution of the highly unconsolidated asteroid 2008 TC$_3$, Meteoritics & Planetary Science 45 (in press).
Horstmann, M., Bischoff, A., Pack, A. & Laubenstein, M. (2010), Almahata Sitta – fragment MS-CH: Characterization of a new chondrite type, Meteoritics & Planetary Science 45 (submitted).
Jenniskens, P., Shaddad, M. H. & co-authors (2009), The impact and recovery of asteroid 2008 TC$_3$, Nature 458, 485-488.

Northwest Africa (NWA) 5073: The coarsest-grained eucrite and its complex postcrystallization history

Julia Roszjar[1], Addi Bischoff[1], Erik E. Scherer[2], and Knut Metzler[1]
[1]Westfälische Wilhelms-Universität Münster, Institut für Planetologie, Münster, Germany
[2]Westfälische Wilhelms-Universität Münster, Institut für Mineralogie, Münster, Germany

Northwest Africa (NWA) 5073 is a basaltic eucrite with the coarsest texture ever found among samples of the so-called HEDO suite (howardites, eucrites, diogenites, olivine diogenites) of achondrites (Roszjar et al., 2009a). This meteorite is a desert find with a total mass of 185 g. It is unequilibrated, non-brecciated, moderately weathered (W2-3) and very weakly shocked (S2). NWA 5073 is mainly composed of zoned pyroxene and plagioclase laths ($An_{76-92}Ab_{8-22}Or_{0-3}$) up to 1.2 cm and 0.3 cm in length, respectively, with minor amounts of mesostasis. The latter mainly consists of ilmenite, Fe-metal, chromite, apatite, silica, and anorthite ($\sim An_{95}$). Euhedral to anhedral silica grains (tridymite) with up to 1 mm were restricted to the mesostasis. Zircon and baddeleyite grains with diameters 1 to 25 μm occur in the mesostasis (Roszjar et al., 2009a). The presence of skeletal plagioclase, unequilibrated pyroxene, and rather narrow (<1μm) exsolution lamellae in some pyroxene grains indicate that this meteorite cooled rapidly. Raman spectroscopic data on selected zircon grains (Roszjar et al, 2009b) indicate that the latter underwent some thermal annealing, perhaps as a result of a thermal metamorphic event that occurred after crystallization. Effects of thermal metamorphism are also visible in the silicates (e.g Fe-Mg-exchange in pyroxene, formation of Fa-rich olivine veins in large pyroxene laths).

Additionally, Lu-Hf isotopic analyses of this sample were performed using multi collector-inductively coupled mass spectrometry (MC-ICPMS) and a total sample mass of 2.2 g, comprising ten mineral separates and one whole rock sample. Pyroxene and plagioclase were concentrated using magnetic separation and heavy liquids. The whole rock fraction was digested with $HF-HNO_3$ at 180°C in a steel-jacketed Teflon bomb, whereas mineral concentrates were digested in Teflon vials on a hotplate using alternating $HF-HNO_3-HClO_4$ and HCl. The latter procedure was used to digest the bulk of the sample while leaving any zircon grains largely intact. Thus, zircon, which may predate the last equilibration event, is essentially excluded from the analysis. For chemical separation and isotopic analysis we followed the procedures given by Münker et al. (2001) and Scherer et al. (2001). The accuracy and 2 s.d. external precision of Hf isotope analyses as a function of Hf concentration were evaluated by repeated measurement of standard solutions at different intensities (Bizzarro et al., 2003). Ages were calculated using a decay constant of 1.867×10^{-11} yr^{-1} for ^{176}Lu (e.g., Scherer et al., 2001, Söderlund et al., 2004).

The Lu-Hf data for the whole rock, a hand magnet fraction, and mixed fractions ranging from mostly pyroxene to mostly plagioclase do not define a simple isochron (Roszjar and Scherer, 2010). The three highest Lu/Hf fractions (mostly pyroxene) trend toward the whole rock, yielding an apparent age of 4.68 ± 0.14 Ga and ^{176}Hf/^{177}Hf$_i$ = 0.27976± 13(2σ). The whole rock analysis lies on the "isochron" defined by all published whole rock data for eucrites, and the ^{176}Hf/^{177}Hf$_i$ is similar to estimates for eucrites. In contrast, all mineral fractions excluding the whole rock yield 4.31 ± 0.14 Ga and a higher ^{176}Hf/^{177}Hf$_i$ of 0.28020 ± 8(2σ). The whole rock lies below this trend, suggesting the presence of a relatively unradiogenic, low-Lu/Hf phase such as zircon in the bomb-digested whole rock. The lower Lu/Hf mineral fractions digested on a hotplate lack this component, giving a younger age and a higher-than-expected ^{176}Hf/^{177}Hf$_i$. This is consistent with a late partial re-equilibration of Lu-Hf among major silicate minerals, but with zircon remaining an essentially closed system during this event. Such a scenario is consistent with our observation that NWA 5073 is petrographically complex due to thermal- and shock metamorphism (Roszjar et al., 2009a).

References:
Bizzarro, M. Baker J. A., Haack H., Ulfbeck D., Rosing M. (2003) Early history of Earth's crust-mantle system inferred from hafnium isotopes in chondrites, Nature 421, 931-933.
Münker C., Weyer S., Scherer E. E., Mezger K. (2001) Separation of high field strength elements (Nb, Ta, Zr, Hf) and Lu from rock samples for MC-ICPMS measurements, G-cubed 2, 10.1029/2001GC000183.
Roszjar J., Metzler K., Bischoff A., Greenwood R. C., Franchi I. A (2009a) Northwest Africa (NWA5073) - An eucritic basalt with cm-sized pyroxenes, Meteoritics & Planetary Science 44, A178.
Roszjar J., Geisler T., Scherer E. E., Bischoff A. (2009b) The thermal history of zircon from the NWA 5073 eucrite as revealed by Raman spectroscopy, Meteoritics & Planetary Science 44, A187.
Roszjar J. & Scherer E. E. (2010) Lu-Hf systematics of the NWA 5073 eucrite reflect a complex thermal history, Meteoritics & Planetary Science 45 (in press).
Scherer E. E., Münker C., Mezger K. (2001) Calibration of the lutetium-hafnium clock, Science 293, 683-686.
Söderlund U. Patchett P. J., Vervoort J. D., Isachsen C. E. (2004) The ^{176}Lu decay constant determined by Lu-Hf

and U-Pb isotope systematics of precambrian mafic intrusions, *Earth* and *Planetary Science Letters* 219, 311-324.

Section 6

_____

Experimental and theoretical petrology

Hydrogen incorporation in rutile – evidence from hydrothermal experiments on synthetic single-crystal rutile

Friedrich Lucassen [1,2], Monika Koch-Müller[2], Michail Taran[3], Gerhard Franz[1]
[1]Technische Universität Berlin, Fachgebiet Petrologie. Berlin, Germany
[2]Deutsches Geoforschungszentrum; Potsdam, Germany
[3]National Academy of Sciences of Ukraine; Kyiv, Ukraine

The incorporation of H in natural rutile has long been recognized (Hammer and Beran, 1991). The link between H incorporation and substitution of Ti^{4+} by lower valence cations has been studied by synthesis of trace element–doped rutile under high P and T under water saturated conditions (Bromiley and Hilairet, 2005). In our experimental approach we use synthetic rutile of considerable size (2000 μm x 1000 μm x 1000 μm) grown by flame fusion as nearly pure TiO_2 single-crystals starting material. The crystals were then hydrated with distilled water at 400 MPa and 600°C, in arc welded Au capsules, using conventional cold seal hydrothermal autoclaves. Oxygen fugacity was externally controlled near the Ni-NiO buffer. After 14 days run-time the autoclaves were cooled to ambient temperature within 5 minutes. Possible dissolution of rutile as controlled by SEM is negligible. Polarized FTIR spectra were measured in the OH stretching region. Hydrogen contents reported as total wt. ppm H_2O were quantified using the absorption coefficient for rutile by Maldener et al. (2001). In addition polarized optical absorption spectra in the UV/VIS range were studied to get insight into the valence state of Ti.

In the synthetic rutile, the well-orientated {110} faces allow precise adjustment of the sample with respect to crystallographic *c*-axis. The OH-absorption bands in the polarized FTIR measurements are strongest perpendicular and near zero parallel to *c*. Molecular H_2O was not detected. The H_2O equivalent in the untreated material is quantified as ~ 3 ppm. The H_2O equivalent after hydration ranges between ~ 310 to 430 ppm, with most measurements between ~330 to 370 ppm. No systematic spatial distribution between core and rim regions of the crystals was observed. In the visible spectra a strong change of colour occurs from colourless or reddish (caused by traces of ~ 1 ppm Fe in one crystal) before to deep blue after the treatment. No optical zoning is observed. Absorbance of untreated and treated rutile is strong at the UV edge of the visible spectrum. The colourless Fe-free untreated rutile shows no other absorption bands, whereas the Fe bearing rutile shows a broad absorption band with maximum at ~20850 cm^{-1} and of a half width of ~5300 cm^{-1}. This is due to intervalence charge transfer of the type $Fe^{2+} + Ti^{4+}$ to $Fe^{3+} + Ti^{3+}$, but the effect is at least one order of magnitude smaller than in the hydrated blue rutile: strong absorption (parallel *c* > perpendicular *c*) occurs with a maximum at ~6400 cm^{-1}, that indicates the presence of Ti^{3+} (Khomenko et al., 1998). Considering the prominent increase in H from untreated to the blue rutile the mechanism could be described by $Ti^{4+} + O^{2-} = Ti^{3+} + OH^-$. Hydrogen is introduced by diffusion and the uniform H content of the rutile indicates equilibrium. No indication for H-loss during quenching of the experiment was found. Experiments evaluating the influence of the trace elements Nb, Cr and V on the H-incorporation in synthetic rutile are in progress.

References:
Bromiley GDB, Hilairet Nh (2005) Hydrogen and minor element incorporation in synthetic rutile. Mineralogical Magazine 69:345-358
Hammer VMF, Beran A (1991) Variations in the OH concentration of rutiles from different geological environments Mineralogy and Petrology 45:1-9
Khomenko V, Langer K, Rager H, Fett A (1998) Electronic absorption by Ti^{3+} ions and electron delocalization in synthetic blue rutile. Physics and Chemistry of Minerals 25:338-346
Maldener J, Rauch F, Gavranic M, Beran A (1998) OH absorption coefficients of rutile and cassiterite deduced from nuclear reaction analysis and FTIR spectroscopy. Mineralogy and Petrology 71:21-29

Solubility of Al, Cr and Si in TiO2-rutile at high pressure and high temperature. A comparative study.
Alberto Escudero, Falko Langenhorst. Bayerisches Geoinstitut, Universität Bayreuth, D-95440 Bayreuth, Germany. Alberto.Escudero@uni-bayreuth.de

Titanium dioxide (TiO2) has been intensively studied for a few decades due to both basic and applied interests in material science and geosciences. On one hand, TiO2 is widely used, due to its photoconductive and catalyst characteristics, in both research and industrial applications. On the other hand, rutile is a common accessory mineral in metamorphic and plutonic igneous rocks. The trace element geochemistry of rutile provides useful information on provenance [Zack 2004], temperature and pressure [Tomkins 2007], and ages [Mezger 1989]. The are several indications that the solubility of certain tri- and quadrivalent cations increases with pressure. For instance, exsolutions of corundum and spinel have been reported in rutile from kimberlites and diamondiferous eclogites from South Africa [Sobolev 2000] and natural SiO2 rich rutile has been found in nature, as well [Yang 2003]. In this experimental study we have tested on whether the solubility of Al, Cr, and Si in rutile could be useful as potential geobarometer.

To study the aluminium, chromium and silicon solubilities in rutile we have performed high pressure-high temperature multi-anvil experiments at the Bayerisches Geoinstitut, Bayreuth from 0.5 to 3 GPa and 1300ºC in a piston cylinder and from 5 to 20 GPa and 1300ºC in a 1200 tonne MA8 Kawai-type multi-anvil press. The samples have been characterised by XRD, 27Al MAS-NMR, 29Si MAS-NMR, SEM and EDX-TEM. The behaviour of the systems with trivalent cations is completely different than the one of the Si-doped TiO2. In general, the solubility of all dopants in rutile increases with pressure. However the incorporation of the trivalent cations into TiO2 is much more effecient than the uptake observed in the Si-doped system. XRD and NMR data indicate two different mechanisms for Al3+ incorporation in rutile that have also been observed at atmospheric pressure [Stebbins 2007]. The main mechanism of solubility is the substitution of Ti4+ by Al3+ on normal octahedral sites (substitutional), compensating the lower charge by the formation of oxygen vacancies [Slepetys 1969]. At higher pressures, Al3+ is also incorporated into octahedral interstices of the rutile structure, although this mechanism is much less important. The incorporation of Al3+ into these interstices at pressures > 2.5 GPa reduces the rutile symmetry, which transforms from tetragonal into orthorhombic, giving rise to a microstructure consisting of [110] twins. High-pressure enhances drastically the Al2O3 solubility in TiO2. Rutile is able to accommodate up to 8.8 % weight Al2O3 at 6 GPa and 1300ºC, to be compared to compared to 1.22 % weight at atmospheric pressure. A similar behaviour has been observed for Cr-doped rutile.

On contrary, the behaviour of the Si-TiO2 system is completely different. There are neither appreciable changes in the unit cell parameters nor in the symmetry of Si-doped rutile with pressure up to 7 GPa. Both NMR and EDX data indicate that the solubility of Si in rutile at high pressure and 1300ºC is extremely low, compared to the trivalent cation systems. Less than 1% weight SiO2 incorporates into rutile even a 7 GPa.

Both the solubility of trivalent cations such as Al3+ and Cr3+ and the microstructure of the doped rutile grains have been shown to be highly pressure dependent. These observations suggest that both the incorporation of Al3+ and Cr3+ into rutile could constitute potential geobarometers. The SiO2 solubility in rutile also increases with pressure, but is not sensitive enough to act as a useful pressure calibrant.

References:
Zack, T.; Moraes, R.; Kronz, A. (2004), Temperature dependence of Zr in rutile: empirical calibration of a rutile thermometer. Contributions to Mineralogy and Petrology 2004, 148, (4), 471-488a
Tomkins, H. S.; Powell, R.; Ellis, D. J. (2007), The pressure dependence of the zirconium-in-rutile thermometer. Journal of Metamorphic Geology 2007, 25, (6), 703-713
Mezger, K.; Hanson, G. N.; Bohlen, S. R. (1989), High precision U-Pb ages of metamorphic rutile. Application to the cooling history of high grade terranes. Earth and Planetary Science Letters 1989, 96, (1-2), 106-118.
Sobolev, N. V.; Yefimova, E. S. (2000), Composition and petrogenesis of Ti-oxides associated with diamonds. International Geology Review 2000, 42, (8), 758-767
Yang, J. S.; Bai, W. J.; Fang, Q. S.; Yan, B. G.; Shi, N. C.; Ma, Z. S.; Dai, M. Q.; Xiong, M. (2003), Silicon-rutile - an ultra-high pressure (UHP) mineral from an ophiolite. Progress in Natural Science 2003, 13, (7), 528-531.
Stebbins, J. F. (2007), Aluminum substitution in rutile titanium dioxide: New constraints from high-resolution Al-27 NMR. Chemistry of Materials 2007, 19, (7), 1862-1869.
Slepetys, R. A.; Vaughan, P. A. (1969), Solid solution of aluminum oxide in rutile titanium oxide. Journal of Physical Chemistry 1969, 73, (7), 2157-2162.

The new high pressure Phase HAPy

Johannes Fischer[1], Mauro Gemmi[1], Marco Merlini[1], Patrizia Fumagalli[1], Stefano Poli[1]
[1]Università degli Studi di Milano, Dipartimento di Scienze della Terra, Milan, Italy

Studying hydrous minerals with different chemical compositions and PT conditions in the $MgO-Al_2O_3-SiO_2-H_2O$ (MASH) system, a new hydrous aluminum rich silicate occured.

The first indication of Phase HAPy was found in cr-chlorite synthesis experiments with a cr-clinochlore bulk of $Mg_5Al_{0,85}Cr_{0,15}(Si_3Al)O_{10}(OH)_8$. Microprobe analysis show results close to Mg:Al:Si 2:2:1 for the new Phase. To proof the existence of a new phase a gel with this bulk was produced and run successfully. Runproducts are up to 80 wt.% Phase HAPy, coexisting with ~10 wt.% forsterite, max. 20 wt.% pyrope and little amounts of spinel and diaspore, around 0.5 wt.%. At 6.0 GPa; 800°C Phase HAPy was not observed, phases present at this PT conditions are forsterite, pyrope and spinel. More experiments are in progress.

The experiments were fluid saturated, performed in a walker-type multi anvil apparatus and analyzed by EMPA as well as XRPD, synchrotron diffraction (with Rietvelt refinement) and conventional electron diffration using TEM. Furthermore the automated electron diffraction tomography technique (ADT) was used to solve the structure. This new technique allows a single crystal electron diffraction experiment on crystals of less than 1 μm. It is the first high pressure phase solved in this way.

The new Phase HAPy with a composition of $Mg_{2.1}Al_{1.8}Si_{1.1}O_6(OH)_2$ is stable between 5.2 GPa, 700°C and 5.4 GPa, 720°C and contains around 6 wt.% water; its monoclinic with space group C 2/c and shows unit cell parameters with a=9.882 Å, b=11.623 Å , c=5.081 Å and β =111.1°.

Phase Hapy has a pyroxene-like structure, but with 3 cations instead of 2 in the octahedral layer, which forces the tetrahedral chains to be more separate. The two anion sites of the extra octahedral cation, that are not shared with any tetrahedra, are occupied by an hydroxyl.

The results obtained by a combination of the described analytical methods are consistent and additionally confirmed by image simulation of high resolution electron microscopy images.

Reference:
Grove, T.L. et al. (2006): "The influence of H_2O on mantle wedge melting"; Earth and Planetary Science Letters 249, 74-89
Mugnaioli, E., Gorelik, T., Kolb, U. (2009):"'Ab initio' structure solution from electron diffraction data obtained by a combination of automated diffraction tomography and precession technique"; Ultramicroscopy 109, 758-768

The effect of fS_2 on PGE solubility in silicate melts – Implications for ore forming processes

Vera Laurenz[1], Chris Ballhaus[1], Raùl O.C. Fonseca[1], Klaus Peter Jochum[2], Paul J. Sylvester[3]
[1]Rheinische Friedrich-Wilhelms Universität Bonn, Steinmann Institut, Bonn, Germany
[2]Max Planck Institut für Chemie, Abteilung Biogeochemie, Mainz, Germany
[3]Department of Earth Sciences, Memorial University of Newfoundland, St. John's, Newfoundland, Canada

Platinum-group elements (PGE) are characterized by being both highly siderophile and chalcophile. Mostly due to their chalcophile nature, the PGE budget of the Earth's mantle is thought to be controlled by sulfides. Moreover, most of the known PGE enrichments in the crust are associated with sulfides (primary or otherwise) found in mafic layered intrusions (e.g. Merensky Reef, Bushveld Complex; JM Reef, Stillwater Complex). Despite the obvious importance of sulfur on PGE geochemistry, there is ongoing debate on the processes that allow sulfides, in a sulfide-melt/silicate-melt system, to produce such high enrichments in PGE. In particular, little is known about the possible effect of sulfur fugacity (fS_2) on the solubility of PGE in silicate melts, namely the role of S^{2-} as possible ligand for the PGE. Moreover, the known experimental PGE solubilities in silicate melts measured in S-free systems, are over an order of magnitude too low to explain the purported PGE abundances in some magmas associated with PGE deposits for the same T and fO_2 conditions (e.g. ~18 ppb Pt for the parental magma of the Merensky Reef - Davies and Tredoux 1985).

In order to experimentally investigate the effect of S^{2-} on the solubility of PGE in silicate melts, a natural picrite was equilibrated with Pd or Ru metal at 1300°C in a 1 atm vertical gas mixing furnace under controlled fS_2 and fO_2. Sulfur fugacity was held below sulfide saturation. Run products are quenched in air to silicate glass, which were subsequently analyzed for major elements and dissolved S by EMP. Pd or Ru were analyzed by LA-ICP-MS to allow for the detection of heterogeneities such as discrete nanonuggets of Pd or Ru metal.

Results show that Pd metal is unstable at fS_2 as low as 0.0001 bar and readily reacts with the continuously supplied SO_2 of the gas mixture to form an immiscible Fe-Pd-sulfide melt. As a result, Pd solubilities in the coexisting silicate melt decrease with increasing fS_2 but constant fO_2.

In contrast, Ru metal was previously shown to be stable also at high fS_2 (Bockrath et al. 2004). Experiments at the same temperature and fO_2 show that the solubility of Ru in silicate melt is enhanced up to a factor of 10 in sulfur-bearing systems when compared to S-free melts. Our results appear to indicate that Ru preferentially bonds with S^{2-} anions in much greater proportion than with O^{2-} anions. Hence, the proportion of Ru associated with the S^{2-} ligand will be extracted straight into an exsolving sulfide melt, once sulfide saturation is reached. If the other PGE show a similar behavior it will have profound implications to our current models for PGE enrichment processes in sulfide bearing mafic layered intrusions.

References:
Bockrath C., Ballhaus C. and Holzheid A. (2004) Stabilities of laurite RuS_2 and monosulfide liquid solution at magmatic temperature. Chemical Geology Vol. 208, 265-271.
Davies G. and Tredoux M. (1985) The platinum-group element and gold contents of the marginal rocks and sills of the Bushveld Complex. Economic Geology Vol. 80, 838-848.

Fe^{3+}/Fe_{tot} ratios in clinopyroxene and garnet as a function of temperature

Horst Purwin[1], Stefan Lauterbach[1], Hans-Joachim Kleebe[1], Gerhard P. Brey[2], Alan B. Woodland[2]
[1] Technische Universität Darmstadt, Institut für Angewandte Geowissenschaften, Darmstadt, Germany
[2] J. W. Goethe-Universität Frankfurt, Institut für Geowissenschaften, Frankfurt am Main, Germany

The garnet-clinopyroxene geothermometer is one of the most widely applied methods for obtaining formation temperatures of eclogites and other (ultra)basic metamorphic rocks containing garnet and clinopyroxene. It is based on a Fe-Mg exchange reaction between these two minerals. In former studies, only the total iron content of the samples, determined by electronprobe-microanalysis (EPMA), was considered for the calibration of this geothermometer (e.g., Ellis & Green, 1979; Krogh, 1988; Ai, 1994), since it was assumed that the ferric iron content in the experiments was negligible. Due to recent studies, the calibration experiments must have produced garnets and clinopyroxenes with substantial Fe^{3+} contents, and the reason for the unreliability of Fe-Mg exchange geothermometry is deduced to uncertainties of the Fe^{3+} content in natural phases and phases generated in the experiments from which the thermometer formulations were calibrated (Canil & O'Neill, 1996). As a step forward to improve the garnet-clinopyroxene geothermometer we investigate the Fe^{3+} content in synthetic clinopyroxene and garnet as a function of temperature in this study.

Synthetic eclogite of the system $CaO-FeO-Fe_2O_3-MgO-Al_2O_3-SiO_2$ was produced in graphite/Pt capsules at a fixed pressure of 30 kbar and temperatures ranging from 1000°C-1300°C using a Belt apparatus. The oxidation state (expressed as Fe^{3+}/Fe_{tot} ratio) of clinopyroxene and garnet was investigated by electron energy-loss spectroscopy (EELS) on a transmission electron microscope (TEM). EPMA was performed to obtain the total iron content. The combination of EELS and EPMA allowed for a quantification of Fe^{2+} and Fe^{3+}.

First results show significant Fe^{3+}/Fe_{tot} ratios in both, clinopyroxene and garnet. However, the differences are rather small between distribution coefficients considering Fe^{2+} and distributions coefficients which are based on total iron. A possible reason for the experimental result is seen in a solubility limit of Fe^{3+} in the crystal lattice, which is also affected by the intrinsic Al-content, as will be discussed in the presentation.

References:
Ai, Y. (1994), A revision of the garnet-clinopyroxene Fe^{2+}-Mg exchange geothermometer, Contrib. Mineral. Petrol., 115, 467-473
Canil, D. & O'Neill, H.St.C. (1996), Distribution of ferric iron in some upper-mantle assemblages, J. Petrology, 37, 609-635
Ellis, D.J. & Green, D.H. (1979), An experimental study of the effect of Ca upon garnet-clinopyroxene Fe-Mg exchange equilibia, Contrib. Mineral. Petrol., 71, 13-22
Krogh, E.J. (1988), The garnet-clinopyroxene Fe-Mg geothermometer – a reinterpretation of existing experimental data, Contrib. Mineral. Petrol., 99, 44-48

The role of crystal fractionation in the genesis of island-arc tholeiites: experimentally determined phase relations in parental magma of Mutnovsky volcano, Kamchatka

<u>Tatiana Shishkina</u>[1], Renat Almeev[1], Roman Botcharnikov[1], Francois Holtz[1]
[1]Leibniz Universität Hannover, Institut for Mineralogy, Hannover, Germany

Mutnovsky volcano is located in the southern part of the Eastern Volcanic Front of Kamchatka peninsula (Russia). The volcano is a complex multi-stage structure with four stratocones of different ages, composed of a wide spectrum of volcanic rocks, ranging from basalts to rhyolites. Basalts, which are typical island arc high-Al, low-K tholeiites, are the most abundant rocks on Mutnovsky volcano (Melekestsev, 1987; Selyangin, 1993). Mutnovsky is the object of the proposed ICDP drilling project focused on the investigation of the connection and interaction between magmatic and adjacent hydrothermal systems. Identification of magma storage conditions (depths of magma chamber, regime of volatiles, redox conditions etc.) is crucial to understand the role of magmatic component in the magmatic-hydrothermal system of Mutnovsky volcano. In addition, this information can be also used to constrain a general genetic model of the formation of island arc tholeiitic series.

Mineral associations and their compositions have been studied in natural basaltic lavas from Mutnovsky volcano. Three major types of basalts can be distinguished: Ol-Plag-, CPx-Ol-Plag- and rare OPx-CPx-Plag-bearing rocks. Phenocrysts vary in composition from sample to sample and in general are in the range from Fo_{75} to Fo_{83} in olivine, from An_{85} to An_{92} in plagioclase, from $Mg\#_{73}$ to $Mg\#_{80}$ in high-Ca pyroxene and from $Mg\#_{71}$ to $Mg\#_{73}$ in low-Ca pyroxene. No hydrous phases have been observed in basalts and more evolved andesites. The character of natural mineral assemblages in Mutnovsky basalts suggest that parental melts probably evolved along Ol+Pl and Ol+Pl+Cpx low-pressure cotectics, similar to MORB-type magmas. However in contrast to MORBs, Mutnovsky volcanics exhibit pronounced FeO and TiO_2 depletion and weak SiO_2 enrichment, suggesting earlier Fe-Ti-oxide onset crystallization, which, in turn, can be achieved only in the presence of significant amounts of water at more oxidized conditions (Sisson & Grove, 1993).

To simulate magma differentiation processes in magma chamber beneath Mutnovsky volcano, we performed a set of crystallization experiments using the most magnesian basaltic sample. This sample N72 was previously investigated for H_2O-CO_2 solubilities in the range of pressures from 50 to 900 MPa (Shishkina et al., 2010 a, b). Crystallization experiments were conducted at 300 MPa in temperature range 950-1250°C in internally heated pressure vessels (IHPV) at intrinsic redox conditions, corresponding to the values NNO+2.6 (NNO - nickel-nickel oxide oxygen buffer) at water-saturated conditions, and to (NNO-0.7) at nominally anhydrous conditions.

At 1200°C Mutnovsky basalt was above the liquidus for the whole range of investigated water activities (aH_2O). At 1150°C all runs with high aH_2O demonstrated crystallization of magnetite (Mt), whereas at low aH_2O (<0.35) crystallization of plagioclase (Pl) was also observed. In general, with decreasing temperature, the crystallization sequence was as follows: Mt → Mt + Pl → Mt + Pl + Ol → Mt + Pl + Ol + Cpx → Mt + Pl + Cpx + Opx, where Cpx and Opx are high and low-Ca pyroxene respectively. At higher water activities this crystallization sequence was complicated by the stabilization of amphibole (Hbl). In the presence of Hbl, Cpx and Opx did not crystallize simultaneously. Crystallization of olivine (Ol) was observed only in runs at 1050-1150°C at $aH_2O < 0.5$ (< 4wt.% H_2O in the residual melt). The mineral compositions in these runs (Ol (Fo_{71-83}) − Pl (An_{69-83}) − Cpx ($Mg\#_{72-80}$, $Fs_{12-18}En_{45-50}Wol_{30-42}$)) were close to those observed in natural basalts. However experimental plagioclase in association with olivine is less calcic, than in natural Ol-Plag associations. High-Ca Plag (An_{83-88}) similar in composition to natural plagioclases was found only in Ol-free H_2O-rich runs.

The experimental glass compositions at 300 MPa reproduce the Mutnovsky liquid lines of descent, indicating a genetic link between parental basaltic and more evolved compositions. Our new crystallization experiments show that crystal fractionation might be, in principal, the major process controlling the magma evolution in Mutnovsky conduit. However the final conclusion can be made after the study of melt inclusions with respect to undegassed volatile concentrations in Mutnovsky magmas. These data will provide us independent information on the depth of magma reservoir and water activities which could be directly compared with our experimental data, obtained at different pressures (experiments at 100 MPa are in progress).

References:
Melekestsevet al. (1987) Volcanology and Seismology. P. 3-18
Selyangin (1993). Volcanology and Seismology. Vol. 1. P. 17-35
Shishkina et al. (2010a) EMPG Conference Abstract

Shishkina et al. (2010b) Chemical Geology (submitted)

Sisson & Grove (1993). Contributions to Mineralogy and Petrology. Vol. 113. P. 143-166.

Experimental investigations on vesiculation and crystallization processes during Unzen's 1991-1995 magma ascent

Sarah B. Cichy[1], Francois Holtz[1], Roman E. Botcharnikov[1], Harald Behrens[1]
[1]Leibniz Universität Hannover, Institut für Mineralogie, Hannover, Germany

Our goal is to simulate experimentally the 1991-1995 Unzen magma ascent from ca. 10 to 1.5 km depth (below ICDP target) as well as to the surface. Two main experimental approaches have been used: (i) crystallization experiments in a broad range of temperatures (800-1000°C) and pressures (50-300 MPa) to reproduce the equilibrium phase relations in rhyodacitic magmas at different activity of water, varying from ~ 0.1 to 1.0; (ii) isothermal decompression experiments conducted at different temperatures (850°C and 930°C) and decompression rates to investigate kinetic processes of magma degassing and crystallization. Our experimental results are used to interpret textural features of natural samples from surface and depth which were analysed for the distribution of microlites and bubbles. The quantitative interpretation provides constraints on magma ascent processes during Unzen eruption.

The occurrence of the mineral phases, especially amphibole (Amph) and plagioclase (Plag), is very sensitive to the activity of water in the system ($aH_2O \sim X_{H2O}^{fluid}$) at these conditions. Our data illustrate that the mineral assemblage of Plag+Amph+Opx in rhyodacitic magma is only stable at temperatures $\leq 850°C$ and in the systems with water activity close to 0.9-1.0. As pressure decreases, the stability field of Amph shifts to lower temperatures and to a wider range of X_{H2O} (> 0.5). At water-saturated conditions ($X_{H2O} = 1.0$), Plag starts to crystallize close to or below 200 MPa. As water activity decreases in the fluid-saturated system, Plag becomes stable at higher pressures and temperatures.

In decompression experiments, simulating magma ascent from depths with pressure of 300 MPa to those with pressure of 50 MPa at 850°C (set-I), equilibrium concentrations of water in the residual glasses are reached at decompression rates ≤ 1 MPa/s for the H_2O+CO_2-bearing system and ≤ 0.1 MPa/s for the H_2O-bearing system. The bubble number density (BND) values range from $10^{10.5}$ m^{-3} to $10^{11.4}$ m^{-3} in both the H_2O-bearing and the H_2O+CO_2-bearing systems. In the H_2O-bearing system, the nucleation and growth of Plag is accompanied by an increase of BND.

The onset of crystallization, observed from changes in the chemical composition of the residual melt, occurs at decompression rates < 0.1 MPa/s. At the lowest decompression rate (0.0002 MPa/s), the chemical composition of the residual melt in the H_2O+CO_2-bearing system becomes similar to the natural matrix glass composition. There is no significant variation of the microlite number density (MND) value as a function of the decompression rate. The MND values range from $10^{2.4}$ mm^{-3} to $10^{3.0}$ mm^{-3} and are at least two order of magnitude lower than those from natural samples (10^5-10^6 mm^{-3}), implying major microlite nucleation events until surface pressures.

In this set of decompression experiments Plag microlites only nucleated and grew in experiments of the H_2O-bearing system with the two lowest conducted decompression rates (0.0005 and 0.0002 MPa/s). The length of those plagioclases reaches up to 200-250 μm which is consistent with the size of Plag microlites in natural samples. Plagioclase microlites in the H_2O+CO_2-bearing system were already present in the starting assemblage at 300 MPa and grew to a maximum size of ~80 μm during decompression. The size and shape of microlites nucleating and crystallizing during decompression are useful to constrain ascent rates at the onset of the crystallization of the corresponding phaseand indicate magma ascent rates of ~ 30-50 m/h (average velocity estimated for the pressure range 200 to 50 MPa).

BND values of water-saturated experiments simulating the magma ascent until surface pressures (starting from either 200 MPa, set-II, or from 50 MPa, set-III, to final 0.1 MPa) are higher ($10^{19.6}$ to $10^{19.8}$ m^{-3}) than in decompression experiments of set-I, implying major bubble nucleation during the final stage of magma ascent. Significant changes in the chemical composition of the residual melts can only be observed in set-II at decompression rates < 0.1 MPa/s, becoming similar to natural glass composition following the trends of set-I (H_2O-bearing). Hence, further crystallization processes during the ascent to surface pressures are indicated, which could lead to the above mentioned major increase in MND values. In contrast, the residual melts of set-III-samples are in the range of natural dome rocks at all conducted decompression rates, showing nearly no changes with decreasing decompression rates.

Finally, several decompression experiment sets have been analyzed by synchrotron-based X-ray tomographic microscopy. This non-destructive technique allows 3D visualization of textural characteristics with high resolution (about 0.3 μm voxel size). The significant difference in density between silicate glass and fluid bubbles provides excellent opportunity to reconstruct 3D textures of vesiculated samples. This method will be used to determine exact bubble volume and distribution within the sample.

Section 07

_____

General and applied crystallography

Modelling and calculation of FCC structures and principles of the algorithm structure Si

Kulpash Iskakova[1], Rif Achmaltdinov[2]
Kazakh National Pedagogical University by Abay, Almaty, Dostyk str. 13, Kazakhstan,

The analysis of the results on the study of the processes of defect formation in single-crystal silicon. Shown defect in different areas of interaction of atoms in the formation of the lattice. Such defects lead to the restriction of the boundary conditions until the next break. The main condition for calculating the band structures - is the presence of lattice points of discontinuity. Points of discontinuity occur at certain distances. Computer modeling of Si shows: how many periodically arranged atoms included in the group divide. The mechanisms of formation of the semiplatonic and Archimedean figures taking into account gaps and structure of these figures.

Crystallographic structure of Si is FCC addiction bars [1]. Modeling the spatial arrangement of atoms Si showed that compared with the fcc-Si lattice is aperiodic repetition of aperiodic groups. Regarding the origin aperiodic group distances is the set $\{3, 1, 4\}$. Violation of the frequency of FCC-Si lattice occurs when moving from node to node number 168 number 169. There must be change in the distance at half the lattice constant $a_0/2$, but it equals $\sqrt{5}$ $a_0/2$ [2]. The next such violation occurs between the nodes number 530 and number 531. The set of distances $\{3, 5\}$ appears at intervals through 422 knots.

The source of difficulty in the calculation of band spectra is a priori is laid in these calculations the translational invariance, which involves the study does not end, real crystals, and the infinite, ideal. Manipulations with infinite objects are allowed in the initial stages of the abstraction of subject area (in our case, solid bodies), but they become simply mathematical trick when trying to obtain information about the physical properties of such complex objects as solid bodies. Solid body, as really existing system, and not a mathematical trick, requires a different approach than adopted for the simple monatomic isolated objects.

One of the advantages described technique - applicable to the systems with neighbor order, where Bloch's theorem is not applicable as the initial conditions, since the translational invariance in the real space and in the quasi-momentum space is not the necessary condition for the determination of the crystalline potential, the wave functions of the energy values in the space of wave vectors.

Atomic nodes of the third sphere are away from the second sphere is within residue the scope of a0/2. The three groups of the atomic skeletons of a building are equal to the distance between the nodes 3, 1, 4. These groups are limited to ten sphere structure. In this sequence radius R11 of the 11th sphere should be changed to a0/2, but there comes a gap of this sequence. There are the following differences of the radii:

R12–R11 = R22–R21 = R33–R32 = R43–R42 = R53–R52 = R65–R64 = R76–R75 = = R86–R85 = R97–R96 = R108–R107 = R119–R118 = R129–R128 = R140–R139 = = R161–R160 = R171–R170 = $\sqrt{5}$ a0/2;

R39–R38 = R82–R81 = R125–R124 = R167–R166 = $\sqrt{7}$ a0/2;

R151–R150 = $\sqrt{2}$ a0.

We can develop an algorithm for constructing the structure of compound semiconductor-type A3B5, based on this principle. For example, to the type of A3B5 of semiconductor compounds include compound GaAs. Its crystal lattice-two face-centered cubic lattices shifted relative to each other at ¼ spatial diagonal. Each Ga atom has four nearest neighbors located at the tops of a tetrahedron. Each ion is surrounded by four nearest neighboring ions of opposite sign. There are four ions with qi qj=-1 at a distance $a_0 \frac{\sqrt{2}}{2}$, eight ions of opposite sign of qi qj=+1 at the distance $a_0 \sqrt{2}$. The system of links of the GaAs structure establish the order of the atomic body along tetrahedral combinations /2, 3/. For such compounds of the tetrahedral group of atoms is one-eighth of the basic lattice, so it is convenient to consider as a superstructure. The cell of the GaAs lattice consists of four tetrahedral sublattices.

Reference:
[1] http://elib.nlr.ru/ru/search/catlist/189/?p=35

[2] Iskakova K.A., Starostenkov M.D., Kuketaev T.A. Computer simulation and calculation of the structure of GaAs abstracts of the 7th International Seminar. Barnaul, Russia, 2003, p. 76-77.
[3] Iskakova K.A., Achmaltdinov R., Kuketaev T.A. Possibilities of the modifications of the method of calculation of wave function and zonal spectrum of crystal structure. PCI-2010 «12th International Conference on the Physics and Chemistry of Ice». Japan

The surface energy of fcc and bcc metals calculated by the bond-deficiency model.

Andreas Mutter[1], Lars Peters[2], W. Depmeier[1]
[1] University of Kiel, Institute of Geoscience, Germany
[2] RWTH Aachen University, Institute of Crystallography, Germany

The surface energy is an important physical property of crystalline solids, due to its high impact on many surface phenomena. A number of physical and chemical processes in solids, such as adsorption, growth, oxidation, catalysis, reconstruction, crystal morphology, *etc*., are closely related to the surface energy and, hence, to the crystal structure. As a consequence, the determination of surface energies of various materials is vital for obtaining the ability to control these surface processes. Many theoretical and experimental attempts were made to derive values for the surface free energy of, *e.g.*, various metals. Even though the results of such investigations are of vital importance, only few experimental data exist on surface energies.

Here, we present an alternative method to obtain realistic estimates for surface free energies of crystalline metals. This method is closely related to the well established broken-bond-model (Mackenzie et al., 1962) and bond-valence deficiency model (*Mutter, 2007*). Our approach is based on the assumptions that *i*) the bond strength and the atomic coordination in the crystal structure are constant for a given metal and *ii*) a simple relationship exists between the surface energy, the *d-* spacings and the standard enthalpy of formation ΔH_f. Even though these assumptions may be considered oversimplified, the method is shown to give fairly realistic estimates for the surface energies of various surfaces. Furthermore, the results are obtained in very short time compared to established, more sophisticated methods.

The surface energies for 10 surfaces of fcc metals Cu, Ni, Ag, Al, Au, Pd, Pt, Rh, Ir and 6 bcc metals Mo, W, V, α-Fe, Nb and Ta have been calculated using the bond-deficiency model. By introduction of a proportionality factor P, derived from the bond-deficiency of the crystal surfaces, we deduce a linear relationship between the lattice spacing and the surface energy of the bulk-termination. This relationship is linked to the standard enthalpy of formation ΔH_f . Thus the surface energy of a given crystal face of a fcc or bcc metal can be estimated by easy and very fast calculations. The results agree well with other established models. The range of error of our calculations is determined by the accuracy of the lattice parameters and the standard enthalpy of formation ΔH_f . The derived method can be used to estimate the relative surface energies of fcc and bcc metals, from which the equilibrium shape of crystals can be obtained.

(1) J.K. Mackenzie, A.J.W. Moore and J.F. Nicholas (1962) Bonds broken at atomically flat crystal surfaces I: Face-centered and body-centered cubic crystals. J. Phys. Chem. Solids 23 (1962) 185.

(2) Mutter, A. (2007): The bond-valence deficiency model: A new application to describe mineral surface reactions. URN: urn:nbn:de:hbz: 6-98539587759. (Thesis).

EBSD measurements on surfaces prepared by FIB: a case study on an experimentally grown reaction rim

Gregor Neusser[1], Bastian Joachim[1], Emmanuel Gardés[2]
[1] Inst. Für Geologische Wissenschaften, Freie Universität Berlin, Germany
[2] Helmoltz Zentrum Potsdam, Germany

Reaction rims between adjacent incompatible mineral phases are quite common in nature and contain a lot of information about the history of a rock. Because the progress of these reactions depends strongly on the mass flux through the growing rim it is crucial to investigate possible pathways like grain boundaries for the diffusing species. These pathways depend on the grain shape, grain size and the orientation of the grains relative to each other. This information can be obtained in-situ by investigations with electron backscatter diffraction (EBSD).

EBSD is a surface sensitive method where the signal comes out of the first $10 - 20$ nm of the specimen only. It is important to achieve an extremely well polished sample surface, which is normally done by an additional chemo – mechanical polishing step with a basic colloidal suspension. The final polish has the characteristic to amplify contrasts in the relief of the surface. In the case of reaction rims of 10 to 30 µm in thickness the rim is often deeply excavated compared to the adjacent phases. An EBSD measurement of this region is impossible because the rim area is shadowed after tilting the sample to 70°. Therefore the aim of this study is to find an alternative way of polishing a sample area for EBSD measurements on an experimental reaction rim made of forsterite and enstatite between quartz and MgO single crystals.

This study was done on a Quanta 3D FEG microscope from FEI equipped with two columns, a field emission gun (FEG) as an electron source and a focused ion beam (FIB) using a gallium source. It has the possibilities to deposit platinum on the specimen via a gas injection system (GIS) and in-situ lift out of parts cut free by FIB with an Omniprobe manipulator needle. The microscope is equipped with an EBSD system from EDAX – TSL.

We used two approaches:

- EBSD measurements on a tiny foil cut and polished by FIB

After the deposition of a platinum protection layer a foil of 15 x 10 µm is cut by two parallel trenches. The roughness of the foil surface is cleaned by successively thinning with reduced ion beam currents. The foil is lifted out with the help of a manipulator needle and welded on a small copper grid. The copper grid was glued on the edge of a stub in order to achieve the correct geometry for EBSD measurement. It is important to weld the foil on the very edge of the copper grid to avoid shadows on the EBSD camera although the copper grid is only a ~ 20 µm thick.

- Direct polish of a small part of the specimen surface.

The specimen is placed on a pre – tilted stub to achieve the correct geometry for a sliding polish with the FIB. First two trenches are cut in front and behind the region of interest to avoid shaded areas on the CCD camera. Then the specimen is tilted towards the FIB with an angle of $5 - 7$ ° for low kV cleaning of the surface. About 300 nm are removed that way.

Two EBSD maps were produced: one parallel (foil) and one perpendicular to the reaction front (polished specimen surface). Inverse pole figure (IPF) maps show, that the grains are columns with an isometric profile and an elongation perpendicular to the reaction interface. No preferred orientation of the grains was observed. The misorientation between neighboring grains is usually high with values around 50 to 80°. These high angle grain boundaries provided fast pathways for mass transport.

It is demonstrated that EBSD mappings are possible on silicate surfaces prepared by FIB. These methods provide the opportunity of 3D information in order to avoid misinterpretation of datasets due to cut effects.

Translation interface modulation in pyrrhotite: Structural self-organisation observed by transmission electron microscopy

<u>Dennis Harries</u>, Kilian Pollok, Falko Langenhorst
Bayerisches Geoinstitut, Universität Bayreuth, D-95440 Bayreuth, Germany

Pyrrhotite is a layered iron sulfide of the general non-stoichiometric composition $Fe_{1-x}S$ ($x < 0.125$) and is one of the most abundant iron sulfides in the Earth's crust. Due to variable Fe deficiency large numbers of possible structural variants arise from the ordering of Fe vacancies within the NiAs-based structure. The resulting superstructures show very different physicochemical and magnetic properties bearing on pyrrhotite's contribution to rock magnetisation and the paleomagnetic record, as well as on many issues in geochemistry, petrology, and technical mineral processing.

In ferrimagnetic monoclinic 4C-pyrrhotite ($Fe_{0.875}S$) vacancies are ordered into every second Fe layer of the NiAs substructure, alternating along the c-axis with fully occupied Fe layers. In (pseudo-)hexagonal NC-pyrrhotites ($Fe_{0.875}S$ to ~$Fe_{0.92}S$) Fe deficiency and ordering sequences of vacant and filled Fe layers are different and commonly lead to vanishing net magnetic moments at ambient temperatures. Selected area electron diffraction within the transmission electron microscope (TEM-SAED) frequently shows them to be of a structure variant in which the superstructure periodicity relates in a non-integral manner to the substructure periodicity. Because NC-pyrrhotites are generally richer in Fe compared to the 4C variety, structural models suggest that Fe enrichment is accomplished by insertion of additional fully occupied Fe layers, forming double layers in which all lattice positions are filled by Fe. We suggest that the variably ordered periodic or aperiodic arrangements of such double layers, being equivalent to non-conservative anti-phase domain boundaries of the 4C Fe sublattice, result in translation interface modulated structures.
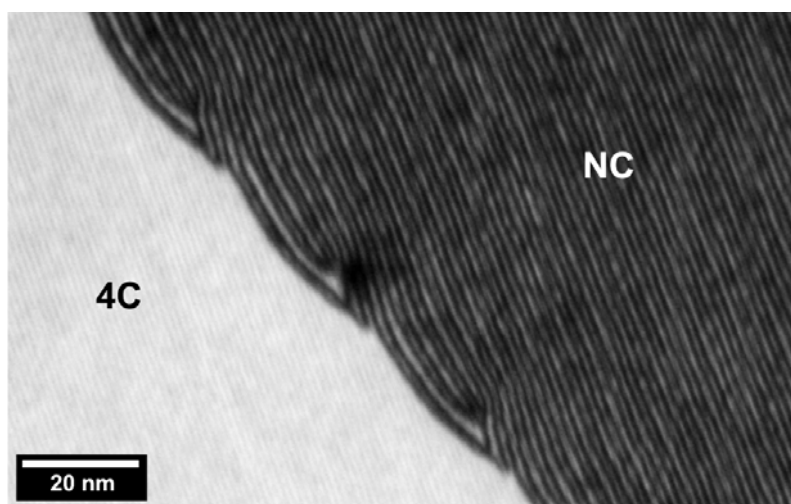
Fig. 1: TEM-SDF image of the interface between 4C- and NC-pyrrhotite.

We illustrate the usefulness of TEM to decipher structural complexity in pyrrhotite by obtaining dark field images from superstructure reflections (TEM-SDF). This imaging technique allows direct observation of double Fe layers and their complex behaviours at internal phase boundaries formed from exsolution of 4C-pyrrhotite lamellae in the host NC-pyrrhotite. In different samples from various geological settings we found large (tens of nm) and very similar node structures in which double layers annihilate (Fig. 1) – these observations point to a common mechanism of self-organisation. The driving forces of such structure formation and the consequences for physicochemical and magnetic properties are matter of current research and may have important implications for the geophysical and geochemical understanding of pyrrhotite in nature.

S07-T05

Die effizienteste Methode um Turmaline zu charakterisieren: Röntgenographische Einkristalluntersuchungen

Andreas Ertl[1], Ekkehart Tillmanns[1]
[1]Universität Wien, Institut für Mineralogie und Kristallographie, Althanstrasse 14, 1090 Wien, Österreich, andreas.ertl@a1.net, ekkehart.tillmanns@univie.ac.at

Jahrzehntelange Erfahrungen mit der Untersuchung von Turmalinen haben gezeigt, dass die röntgenographische Einkristalluntersuchung zweifelsohne die effizienteste und schnellste Methode ist, um Turmaline zu charakterisieren. Anhand von Strukturverfeinerungen und interatomaren Abständen lassen sich sehr gute Ergebnisse bei der Bestimmung der Besetzung der Atompositionen erzielen. Interessanterweise sind dazu chemische Analysen nicht unbedingt erforderlich.

Die Al-Mg-Unordnung zwischen den [6]-koordinierten Atompositionen, welche in Mg-reichen Turmalinen mehr oder weniger stark ausgeprägt auftritt, lässt sich in der Tat nur röntgenographisch durch die unterschiedlichen mittleren (Al,Mg)-O Abstände bestimmen. Auch die Besetzung der Tetraederposition, welche von Si, Al, und/oder B besetzt sein kann, lässt sich durch Einkristallstrukturdaten relativ gut bestimmen.

Sogar die Na- und Ca-Anteile der Kali-/Alkaliposition lassen sich recht gut mittels Strukturdaten abschätzen. K tritt in praktisch allen Turmalinen nur sehr untergeordnet auf. Diese Abschätzung beruht einerseits auf der deutlich unterschiedlichen Anzahl der Elektronen, sowie auch auf den interatomaren Abständen.

Da an der planar koordinierten Bor-Position bis jetzt keine Leerstellen nachgewiesen werden konnten und B aber auch im Tetraeder eingebaut werden kann, muss B ≥ 3 Atome pro Formeleinheit (apfu) sein.

Der Li-Anteil im Turmalin kann theoretisch in Li-reichen Pegmatiten bis zu 2 apfu betragen. Da aber in solchen Turmalinen, die meistens auch Al-reich sind, Leerstellen an der Li-Position nachgewiesen werden konnten, kann davon ausgegangen werden, dass eine Li-Bestimmung mittels Al-Li-Verfeinerung eine geringe Überbestimmung des Li-Anteils mit sich bringen wird.

Trotz der sehr vielfältigen Turmalin-Mischkristallreihen, lassen sich auch ohne Vorliegen von chemischen Analysen, die mengenmäßig am stärksten vertretenen Atomsorten der jeweiligen Positionen, recht gut bestimmen. Nur Cr, V, Mn, Ti und Cu, welche auch nur relativ selten in größeren Anteilen im Turmalin eingebaut werden, lassen sich ohne chemische Analyse nicht verifizieren. Ein großer Vorteil der Einkristallstrukturanalyse ist unter anderem die relativ rasche Verfügbarkeit der Daten. Es sei hier noch darauf hingewiesen, dass fast jeder Turmalinkristall für eine Röntgen-Strukturanalyse verwendet werden kann, da Turmalin meistens sehr gut kristallisiert ist und keine Verzwillingung auftritt.

Compositional dependence of elastic, piezoelectric and dielectric properties of tourmalines

Chandra Shekhar Pandey, Jürgen Schreuer
Ruhr-Universität Bochum, Institute for Geology, Mineralogy and Geophysics, Bochum, Germany

Tourmaline is a complex ring silicate with boron and aluminum, containing varying amounts of iron, lithium, sodium, magnesium, manganese, calcium, potassium, hydroxyl and fluorine and is a promising piezoelectric material for acoustic-electronic application devices. Because of its variability in chemical composition the compositional dependence as well as the temperature dependence of the relevant electromechanical properties has not yet been studied in detail. In contrast to α-quartz, $LiNbO_3$ and $Ca_3Ga_2Ge_4O_{14}$-type crystals, the application of tourmaline at temperatures up to about 1000 K is not limited by phase transitions, electrical conductivity or strong ultrasound dissipation effects.

In this research, the full sets of elastic, piezoelectric, dielectric constants and coefficients of thermal expansion of five natural single crystal tourmalines of gem quality have been determined between 100 K and 903 K. The different chemical compositions of the investigated crystals allow for a systematic study of the main influence of Li and Fe on elastic and piezoelectric properties of tourmalines. To this end we employed a combination of different experimental techniques including the well-known substitution method [1], high-resolution dilatometry and the innovative method of resonant ultrasound spectroscopy (RUS) [2].

An unexpected irreversible softening of all resonance frequencies was observed during first heating on four of five investigated samples. The anomalies are most probably due to an increase of configurational entropy caused by order/disorder processes on certain cation sites. The onset temperature of the softening depends on chemical composition. The well reproducible spectra collected in the second and subsequent heating/cooling cycles were used for the calculation of elastic and piezoelectric constants and of their temperature derivatives. At high temperatures the evolution of the elastic properties is quite normal, i.e. all temperature derivatives are negative. The piezoelectric constants behave almost linearly in the investigated temperature interval and, except e_{22}; the piezoelectric properties are almost independent of the lithium or iron content.

Our research shows that the electromechanical properties of elbaite and schörl tourmalines are nearly independent from their chemical composition. Further, a correlation between the dielectric constants k_{11} and k_{33} as well as between k_{11} and the chemical composition of tourmalines could be derived.

References:
[1] Andeen, C., Fontanella, J. and Schuele, D.: Accurate determination of the dielectric constant by the method of substitution, Rev. of Sci. Inst. **41** (1970) 1573-1576.
[2] Schreuer, J.: Elastic and Piezoelectric properties of $La_3Ga_5SiO_{14}$ and $La_3Ga_{5.5}Ta_{0.5}O_{14}$: An application of resonant ultrasound spectroscopy, IEEE Trans. on Ultrasonics, Ferroel. and Freq. Control **49** (2002) 1474- 1479.

Elastic properties of Eifel sanidines as function of temperature and composition

Peter Sondergeld, Jürgen Schreuer, Pia Schröer
Ruhr-Universität Bochum, Institut für Geologie, Mineralogie and Geophysik, Bochum, Germany

Sanidine megacrystals from the Eifel, Germany, are well known for fast irreversible changes of their optical properties at moderately high annealing temperatures (starting from about 750°C), which have been interpreted as changes in the Al,Si order within the tetrahedral framework (Zeipert and Wondratschek, 1981). However, our recent results based on X-ray diffraction and NMR studies draw a more complex picture. In order to get additional insight into the behaviour of the crystal's bonding system at high temperatures we studied the elastic properties of single crystal sanidines from various eruptive centres of the Eifel and from Madagascar (served as a reference) between room temperature and 1100°C using resonant ultrasound spectroscopy. The major advantage of RUS is the possibility to obtain all independent elastic constants of a crystal (13 in the case of monoclinic sanidine) from a single sample with high internal consistency. Since no medium is required for transducer – sample coupling, RUS can easily be applied in a broad temperature range. Unfortunately, no analytical solution exists for the direct calculation of elastic constants from resonance frequencies. The elastic constants have to be evaluated by a non-linear least-squares procedure, the convergence of which depends critically on the proper choice of initial values and the correct assignment of calculated to observed modes. In the case of alkali feldspars the latter task is particularly demanding because the structural instability driving the ferroelastic phase transition due to framework shearing leads to complex patterns of acoustic eigenmode variations as a function of temperature. Therefore, we developed a graphical software tool to navigate easily within an experimental resonance spectrum as well as across different temperatures. The visualisation of experimental versus calculated resonance lines and of the extrapolation of temperature induced frequency shifts help to easily spot and correct errors in the identification of resonances.

The elastic properties of our Madagascar sanidine agree well with literature values obtained by the plateresonance technique close to room temperature (Haussühl, 1993). The temperature evolution of the elastic constants is fully reversible without any discontinuity. Remarkable is the positive temperature coefficient of the shear stiffness c_{44} which is a consequence of the ferroelastic instability. Additionally, a small ultrasound dissipation peak appears at about 890°C. On the other hand, sanidines from the Eifel show a reversible exponential increase of ultrasound dissipation above 800°C, followed by rapid irreversible softening of all resonance frequencies by about 8 % above 970°C. The latter phenomenon is most likely related to the development and propagation of micro-cracks in the sample. Both effects are probably caused by the increasing mobility and eventually the loss of water dissolved in the crystal structure of these nominally anhydrous minerals. In contrast to the low-sanidines from Madagascar (~ 1 wt-ppm) Eifel sanidines contain a relatively high amount of H_2O (~ 200 wt-ppm) (Beran, 1986, Johnson and Rossman, 2004).

References:
C. Zeipert, W. Wondratschek: Ein ungewöhnliches Temperverhalten bei Sanidinen von Volkesfeld / Eifel. N. Jb. Min. Monat. **9** (1981) 407-411.
A. Beran: A model of water allocation in alkali feldspar, derived from infrared-spectroscopic investigations. Phys. Chem. Min. **13** (5) (1986) 306-310.
E. A. Johnson, G. R. Rossman: A survey of hydrous species and concentrations in igneous feldspars. Am. Min. **89** (4) (2004) 586-600.
S. Haussühl: Thermoelastic properties of beryl, topaz, diaspore, sanidine and periclase. Z. Krist. **204** (1993) 67-76.

In-situ dehydration studies on bentonite bonded moulding sands with neutron radiography

Constanze Eulenkamp[1], Mohammed Nurul Islam[1], Guntram Jordan[1], Wolfgang Schmahl[1], Elbio Calzada[2], Burhkard Schillinger[2],

[1]LMU München, Department für Geo- und Umweltwissenschaften, Sektion Kristallographie, Germany
[2]Technische Universität München, Forschungsreaktor FRM II, Neutronentomographie ANTARES, Germany

Natural bentonites are an important material in the casting industry. Smectite clay minerals as their main component plasticize and stabilize quartz sand moulds for cast metals. Depending on the time-temperature history during the casting, the initially moist smectites become partially or completely dehydrated. Although rehydration of the smectites should be a reversible process per se, the industrial dehydrated smectites lose their capability to reabsorb water. This limits the number of possible process cycles of the mould material.

The dehydration process of the moulding sand is not completely understood yet. Pore water as well as interlayer water within the smectites are lost as a function of time, location and temperature. As the reusability of the moulding sand is critically related to the hydration and dehydration of smectites, we designed a special casting simulation experiment to investigate the dehydration kinetics in-situ with neutron radiography (ANTARES at FRM II, Germany). Due to the sensitivity of the neutrons towards water, neutron radiography is the only method to visualize the dehydration process in-situ.
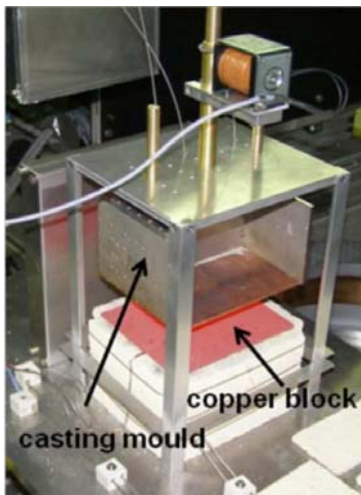
Fig.1. Experimental set up of the casting experiment.

The experiment consists of a casting mould filled with moulding sand (12% bentonite) which is dropped on a hot copper block (figure 1). The design ensured an ideal heat transfer corresponding to the thermal shock-like heat induction during the real casting process. With this experimental set up, we were successful to visualize water fluxes during the dehydration process within the moulding sand quantitatively with high temporal and spatial resolution. Thermocouples placed within the moulding sand simultaneously provided information on the temporal temperature gradients. The hydrated- and dehydrated moulding sands were also investigated with neutron diffractometry to determine the different hydration states of the smectites.

The radiographs (Fig. 2) show the removal of water from the mould. The process initiates at the heat source on the bottom. The grey scale depends on the water amount in the moulding sand. The dehydrated material appears light-gray while the hydrated material is dark-gray. The vertical dark stripes are thermocouples. The experiments revealed a progressive movement of water in the sand and resolved a broad transitional zone from the pristine hydration state of the sand to a fully dehydrated state. At this transitional zone positions can be determined which on one hand relate to the onset of pore water dehydration and on the other hand relate to the completion of interlayer dehydration. Thus, the experiments allowed us to successfully simulate the shock-heating of the mould material in an industrial casting process. The consequence of the shock-heating is a strongly non-linear temperature-time-position relation convoluted with the diffusion processes. A quantitative evaluation of the simulation data will be presented.
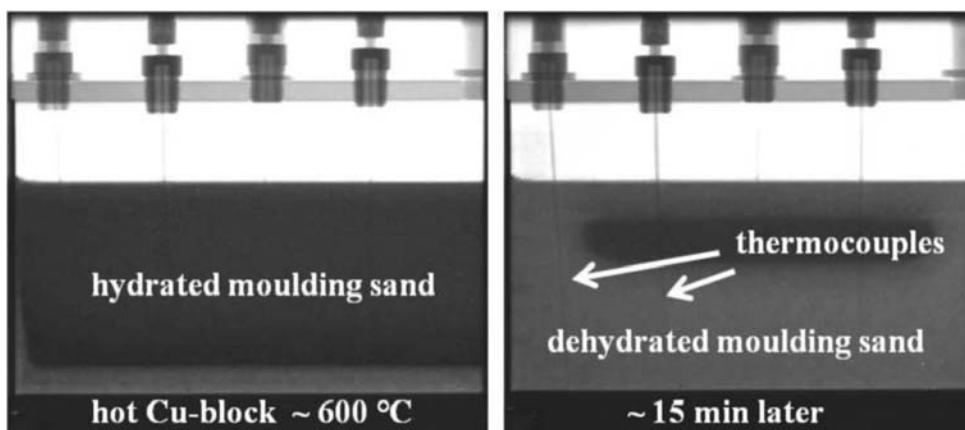

Fig.2. Two neutron radiographs showing the dehydration of the moulding sand. The width of the container is 14 cm. The process initiates at the hot bottom. The transitional zone between the pristine hydration state (top) and the fully dehydrated state (bottom) can be seen.

In-situ investigations of hydration processes and spatial phase analysis of cement and concrete by X-ray diffraction methods

Moritz-C. Schlegel[1], Urs Mueller[2], Ulrich Panne[1], Franziska Emmerling[1]
[1]BAM, Federal Institute of Material Research and Testing, Berlin, Germany

Cementitious building materials are a substantial part of our built environment. Due to the nature of the cementitious binder those materials can be described as multi component nano composite materials. However, analyzing their microstructure and the phase composition of the hydration products is a difficult task due to their nano size and poor crystallinity. Furthermore, for studying degradation mechanisms spatial chemical or phase analytical data are needed, which can be linked to the microstructure of the cementitious paste. In recent years new possibilities have been established in order to investigate these complex materials by means of analysis with synchrotron radiation. The objectives of this work are the observation of the early hydration of cement and the analysis of the phase assemblage of chemical attacked mortar and concrete including synchrotron methods. The latter one is performed spatially and in conjunction with chemical data in form of elemental maps and spectroscopic methods.

The hydration processes were examined by diffraction with synchrotron radiation in transmission geometry (λ=1.0656 Å) at the μ-spot beamline at BESSY II (HZB, Berlin). An ultrasonic trap provided the contact free analysis of a sample and ensures a constant water cement ratio within the sample holder. This is a tremendous improvement since former studies using capillaries coupled with water injection system could not guarantee a homogeneous dispersion of water within the cement suspension. The integration time for a single diffraction pattern was about 30 sec due to the high photon flux of the synchrotron facility and allowed a detailed view into the dynamics of the hydration processes at early stages. The results were completed by long-time studies on common cement (PZ) and pure cement clinker phases (C_3S, C_2S, C_3A) over 28 days using the X-ray diffractometer D5000 (Bruker AXS, Karlsruhe) with $Cu_{K\alpha}$-X-Ray source and Bragg-Brentano geometry.

Fig. 1. The high photon flux of synchrotron radiation allows a spatial [...]

The spatial phase analysis was performed on cement paste and mortar specimens, which were exposed to sulphate and chloride solutions over different time periods. The reaction fronts of sulphur and chloride were localised by elemental mapping with a micro X-ray fluorescence analysis. Synchrotron X-ray diffraction was used in-situ for the identification of the phase composition. The primary focussing optics established a spatial resolution of 10 μm for thick film section samples with a thickness of ca. 200 μm. These thick film sections were glued to an acrylic substrate and can be utilized for further analysis, e.g. by a SEM. That means phase analysis can be performed in-situ with a high local resolution and within the microstructure of the sample (s. Fig. 1). Common preparation techniques (e.g. grinding) are not necessary and the sample specimens can be investigated without destroying their microstructure. First results show patterns with a good peak to background ratio. The measurement of sulphate exposed cement paste samples reveal a phase composition, determined by synchrotron XRD which corresponds well to the chemical profile measured by micro XRF. The penetration depth of the reaction fronts and changes of the phase assemblage induced by the chemical attack due to the sulphate solution are also approved by micro RAMAN spectroscopy.
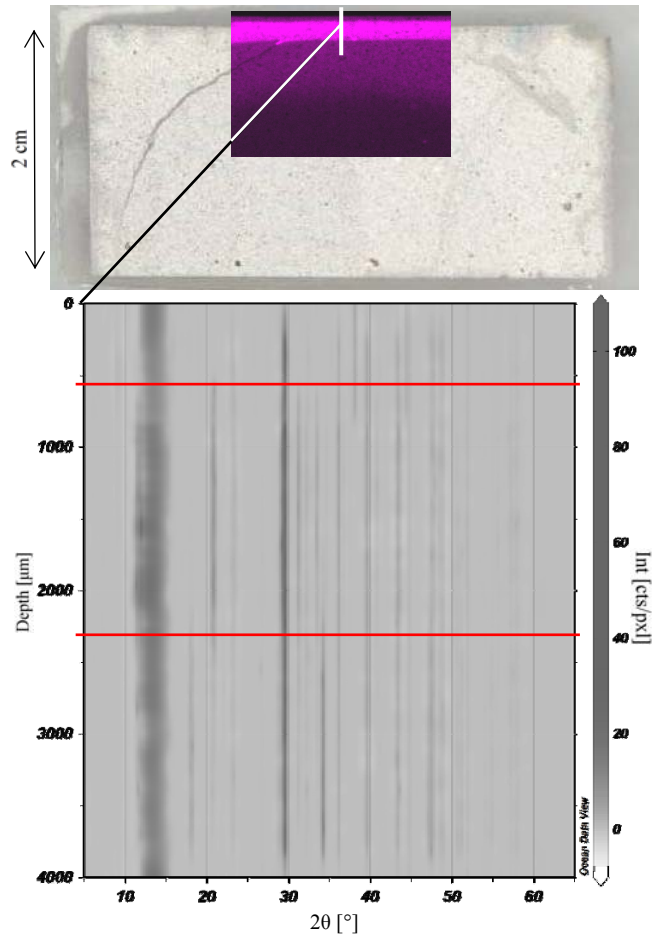
Sulfur speciation in sodalite as a redox proxy

Kai Hettmann[1], Thomas Wenzel[1], Insa Derrey[1], Florian Thaler[1], Michael Marks[1], Gregor Markl[1]
[1]Eberhard-Karls-Universität Tübingen, Institute for Geoscience, Tübingen, Germany

Sodalite ($Na_8Al_6Si_6O_{24}Cl_2$) is a common zeolite-like mineral in alkaline magmatites. Its structural cavity is mainly occupied by chlorine and sulfur. Sulfur-species determined in sodalite include sulfate (SO_4^{2-}), sulfide (S^{2-}) and different polysulfides (S_n^{2-}) (e.g. Fleet 2005, Lede et al. 2007). X-ray absorption near edge structure (XANES) studies have shown that sulfate and sulfide are the major species in natural sodalite, and that polysulfides, although responsible for the typical blue color, are only minor components (Fleet 2005). However the speciation of sulfur in sodalite is redox-dependent and can therefore be used as a redox proxy.

The analysis of sulfur speciation in sodalite is non-trivial, since no pure sulfide endmembers have been found in nature. To overcome the problem that synthetic sulfide-bearing sodalites (which contain very high amounts of polysulfides) have been shown to differ from natural ones, we used density functional theory (DFT) to predict its Raman-, IR- and X-ray emission spectroscopic (XES) properties. Raman spectroscopy can be used to study the sulfur speciation of sulfur-rich sodalites, such as nosean ($Na_8Al_6Si_6O_{24}SO_4$) and lazurite ($Na_8Al_6Si_6O_{24}[SO_4,S]$). Sulfate and sulfide peaks separate well in the Raman spectra and peak height-ratios can be used as a semi-quantitative estimate. However many natural sodalites only contain minor amounts of sulfur, and Raman spectroscopy is not applicable to them. On the other hand XES is an ideal tool to study these samples and can be applied in-situ using an electron microprobe analyzer (EMPA). This technique has been used to study the sulfur speciation of basaltic glasses (Carrol & Rutherford 1988) and we show that it is sensitive down to concentrations as low as 0.1 wt% sulfur in sodalite.

We applied this technique to sodalite-group minerals from several localities including nosean and hauyn ($Na_6Ca_2Al_6Si_6O_{24}[SO_4]_2$) from the Laacher See volcanics, West Germany, sodalite and helvite ($Mn_8Be_6Si_6O_{24}S_2$) from the Ilímaussaq intrusion, South-West Greenland, and sodalite from the Mont Saint-Hilare complex, Canada. The results show differences in the sulfur speciation ranging from sulfate-dominated to approximately equal amounts of sulfate and sulfide (and pure sulfide for helvite, see Fig. 1), and can qualitatively be correlated to differences in the previously determined oxidation states (deduced by phase petrology) of the magmatic host rocks.
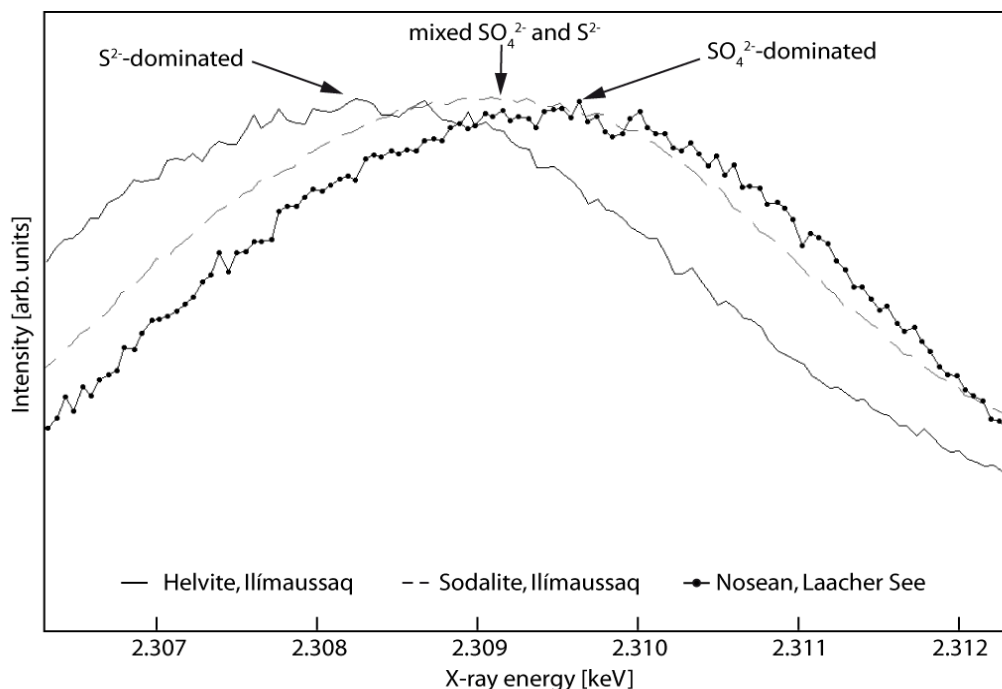

Figure 1: Sulfur Kα-Peaks of sodalites differing in their sulfur speciation

References:

Carrol, M.R. & Rutherford, M.J. (1988), Sulfur speciation in hydrous experimental glasses of varying oxidation states: Results from measured wavelength shifts of sulfur x-rays, American Mineralogist, 73, 845-849

Fleet, M.E. (2005), XANES spectroscopy of sulfur in earth material, The Canadian Mineralogist, 43, 1811-1838

Lede, B., Demortier, A., Gobeltz-Hautecœur, N., Lelieur, J.-P., Picquenard, E. & Duhayen, C. (2007) Observation of the ν_3 Raman band of S_3^{2-} inserted into sodalite cages, Journal of Raman Spectroscopy, 38, 1461-1468

Single-crystal structure refinement of hydrated zeolite A based on synchrotron data.

Reinhard X. Fischer[1], Thorsten M. Gesing[1], Carsten Paulmann[2]
[1]Universität Bremen, FB05 Kristallographie, Klagenfurter Straße, 28359 Bremen, Germany
[2]Universität Hamburg, Mineralogisch-Petrographisches Institut, 20146 Hamburg, Germany

Zeolite A, with idealized composition $Na_{12}Al_{12}Si_{12}O_{48} \cdot 27\ H_2O$, is one of the most prominent zeolites due to its outstanding ion-exchange properties mainly used for the softening of water by exchanging Ca and Mg ions by Na. The annual production of zeolite A just for household detergents exceeds one million metric tons. Its crystal structure was solved by Reed and Breck (1956) in space group $Pm3m$ with $a = 12.3$ Å, but later on it has been shown that the compound is better described in space group $Fm3c$ with $a = 24.6$ Å. The face-centered unit cell permits the ordering of Si and Al atoms which usually are in a ratio approximating 1 : 1. Gramlich and Meier (1971) refined the crystal structure in the subgroup but constrained the nonframework atoms to the symmetry of the supergroup. The crystal structure can be described as being built from *toc* ($4^6 6^8$) units (formerly called sodalite cages) linked by *cub* (4^6) units via common 4-rings enclosing the big *grc* ($4^{12} 6^8 8^6$) cavities (Fig. 1, also called -cages). Eight of the assemblages form the superstructure in the F-centered unit cell. However, despite its enormous importance, there do not exist complete structure refinements of the superstructure due to the pseudosymmetry closely resembling $Pm3m$ with a random distribution of Si and Al. Further descriptions of its properties and crystal structures are given by Fischer and Baur (2006) with many references therein. Here we present crystal-structure refinements based on synchrotron radiation data. The experiments have been carried out at the HASYLAB facility (DESY, Hamburg) using the Kappa-diffractometer at beamline F1 equipped with a SMART CCD system.

The crystal with dimensions of 0.08 x 0.08 x 0.08 mm^3 was grown by the method after Charnell (1971) having a chemical composition with slight access of Si. Data collection between $-51 \leq h \leq 57$, $-55 \leq k \leq 57$, $-52 \leq l \leq 42$

up to 2 = 71.29° (= 0.50 Å) at room temperature yielded 1,082,264 reflections, merged to 4271 unique reflections after data reduction. The internal R-value is 9.05%. The crystal structure was refined in space group $Fm3c$ resulting in residuals of R1 = 7.08% for 2837 reflections with Fo > 4sig(Fo) and 10.29% for all 4271 data. The characteristic feature of the crystal structure is the cluster of H_2O molecules enclosed in the *grc* unit forming a sodalite-like *toc* cage as shown in Fig. 1. Additional, randomly distributed water molecules are bonded to this cluster. Further molecules are present in the *toc* units. Si-O distances in the aluminosilicate framework range from 1.598(1) to 1.610(1) Å, Al-O distances from 1.719(1) to 1.736(1) Å. The Na atoms reside close to the 8-ring window of the *grc* unit and to the 6-ring opening of the *toc* unit.
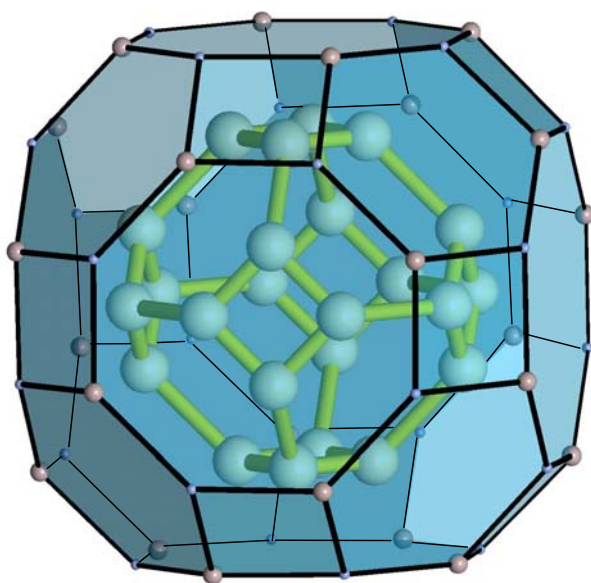
Fig. 1. Cluster of H_2O molecules within the *grc* unit of zeolite A.

References:
Charnell, J.F.: Gel growth of large crystals of sodium A and sodium X zeolites. Journal of Crystal Growth 8 (1971) 291-294.
Fischer, R.X., Baur, W.H.: Microporous and other framework materials with zeolite-type structures. New Series Landolt Börnstein IV Vol. 14D. Springer, pp 454.
Gramlich, V., Meier, W.M.: The crystal structure of hydrated NaA: A detailed refinement of a pseudosymmetric zeolite structure. Zeitschrift für Kristallographie 133 (1971) 134-149.
Reed, T.B., Breck, D.W.: Crystalline Zeolites. II. Crystal structure of synthetic zeolite, type A. Journal of the American Chemical Society 78 (1956) 5972-5977.

Boron incorporation into mullite

Hanna Lührs[1], Reinhard X. Fischer[1], Hartmut Schneider[2]
[1]Universität Bremen, Fachbereich Geowissenschaften, Bremen, Germany
[2]Universität Köln, Institut für Kristallographie, Köln, Germany

The aluminosilicate mullite is one of the most prominent ceramic materials. Its composition can be described as a solid solution series $Al_2(Al_{2+2x}Si_{2-2x})O_{10-x}$ with $0.18 \leq x \leq 0.88$ (Fischer et al., 1996). The crystal structure of mullite can incorporate a large variety of ions (Schneider and Komarneni, 2005). The incorporation of boron is highly interesting because for boron-doped mullites favorable properties as very low thermal expansion, high thermal shock resistance, and resistance against boron glass attack are expected. Dietzel and Scholze (1955) assumed a solid-solution series between mullite and $Al_{18}B_4O_{33}$. In contrast, Griesser et al. (2008) showed that only up to 20 mole % boron can be incorporated into mullite. However, their syntheses did not correspond to a 1:1 isomorphous substitution of silicon by boron and thus does not represent the desired solid solution.

Our approach is to use starting compositions where boron replaces silicon in equal amounts. Powdered samples of boron-doped mullite were prepared by heating sol-gel-derived precursor materials, following the synthesis route of Griesser et al. (2008). Synthesis temperatures varied between 950 and 1400°C in order to find the best temperature for producing mullite powders of high crystallinity. X-ray powder diffraction techniques were applied for all samples including Rietveld refinements in space group *Pbam*. All initial refinements focused on the determination of lattice parameters *a*, *b* and *c*. As no chemical analyses were performed so far, all given compositions correspond to the initial weights of the gel.

Comparing the powder patterns of samples containing 0 to 25 mole % B_2O_3 the major changes affect the diffracted intensities of the mullite peaks including gradual peak shifts. Heat treatment of the precursor materials below 1100°C results in poorly crystalline mullite powders whereas treatment at 1200°C yields well crystallized mullite. A better resolution due to narrower diffraction peaks was achieved by further heat treatment at 1300 and 1400°C. Though crystallinity can be improved by higher temperatures, our data indicate the development of alumina as an impurity phase at higher temperatures. For phase identification, characteristic peaks for five phases were evaluated. Below ~10 mole % B_2O_3, mullite is the only phase, with increasing boron content more and more alumina is present. For the synthesis at 1200°C an alumina phase not yet identified occurs with its characteristic peak at 45.3°2θ. Only the sample with the highest boron content (23 mole %) contains the aluminium borate $Al_{18}B_4O_{33}$, in addition to the nonidentified alumina phase and corundum. Heat treatment of the samples at 1300°C (5h) causes transformation of the alumina phase to θ-alumina which partially transforms to α-alumina after heating to 1400°C for 5 hours. For the 1300° and 1400°C treated samples, $Al_{18}B_4O_{33}$ is observed already for the specimen containing 17.5 mole % B_2O_3. The powders were pressed to pellets and heated at 1400°C for a period of 90 hours. Subsequent phase analysis yielded mullite and α-alumina for all samples containing more than 3 mole % B_2O_3. The amount of alumina increases with the boron content whereas mullite decreases.

Rietveld refinements using the structural model of mullite succeeded for samples containing a maximum of about 10 mole % B_2O_3. Using a model-free approach, refinements in space group *Pbam* were possible up to 17 mole % B_2O_3. Considering the lattice parameters obtained by the model-free refinements, variation with increasing boron content and increasing temperature was observed. For lattice parameter *a,* the variation is rather small. Lattice parameter *b* clearly decreases with increasing boron content and becomes somewhat larger for higher temperatures. The most distinct changes can be observed looking at lattice parameter *c*. It significantly decreases with increasing boron content. For higher temperatures, *c* becomes larger again, especially for samples with high boron contents. For *b* and especially for *c,* the observed changes exceed the expected variation due to changing Al_2O_3 content in mullite (Fischer et al., 1996); for *a*, changes are within this range.

Changes of lattice parameters and diffracted intensities indicate that a high amount of boron can be incorporated into the mullite structure. The presence of an excess of alumina for samples with high boron content indicates that there is no complete solid solution between mullite and aluminum borate.

References:
Dietzel, A. & Scholze, H. (1955), Untersuchungen im System B_2O_3-Al_2O_3-SiO_2, Glastechn. Ber. **28**, 47-51
Fischer, R.X., Schneider, H., Voll, D (1996), Formation of aluminium rich 9:1 mullite and its transformation to low alumina mullite upon heating, Journal of the European Ceramic Society **16**(2), 109-113
Griesser, K. J., Beran, A. et al. (2008), Boron incorporation into mullite, Mineralogy and Petrology **92**(3-4), 309-

320
Schneider, H. & Komarneni, S. (2005), Mullite, Weinheim, wiley-VCH Verlag

Orientation of magnetite and ilmenite inclusions in plagioclase

Hans-Rudolf Wenk[1], Kai Chen and Rebecca Smith[1]
[1]Department of Earth and Planetary Science, University of California at Berkeley, USA

It is well known that oriented iron and titanium oxide inclusions occur in pyroxenes and plagioclase of anorthosites and granulites and are attributed to exsolution at subsolidus conditions. The exsolved oxides occur as needles or platelets. In this study we determine, for the first time, the morphology of oxide needles as well as their orientation in plagioclase (An 30-35) for an anorthositic gneiss from the Adirondack mountains. The investigation was done with electron backscatter diffraction (EBSD) in a scanning microscope as well as Laue diffraction with a microfocus synchrotron X-ray beam at the Advanced Light Source in Berkeley. It was observed that the needle direction is [110] in magnetite and [10-10] in ilmenite. The needle direction is consistently parallel to [001] of plagioclase. Furthermore, (111) of magnetite and (0001) of ilmenite are parallel approximately, but again consistently, sub-parallel to (120) and (-120) of plagioclase.

We note that for directions [110] in the magnetite structure and [10-10] in ilmenite, oxygens are close-packed, and (111) and (0001) are close-packed planes, correspondingly. In plagioclase [001] is a direction with open channels as well as approximate alignment of Si tetrahedral edges, thus providing nucleation sites with a coincidence lattice relationship. (120) and (-120) in this triclinic mineral are planes with approximate tetrahedral sides so that the relationship is structurally plausible. From Laue diffraction we can determine that the magnetite needle axis is subject to an extensional stress, most likely attained during cooling of the inclusions within the plagioclase host.

Section 08

The composition and buoyancy of hydrous partial melt at conditions of the 410 km seismic discontinuity

S08-T01

Mineral Physics of Chemically Homogeneous Spin Transition Zone in Earth's Lower Mantle

L. Dubrovinsky[1], O. Narygina[1], C. McCammon[1], K. Glazyrin[1], S. Pascarelli[2], M. Hanfland[2], I. Kantor[2,3], V. Prakapenka[3]
[1]BGI, Bayreuth University, Germany
[2]ESRF, France
[2]GSECARS, USA

The effect of spin crossover in lower mantle silicate perovskite (Pv) and ferropericlase (Fp) on the iron-partitioning between these two phases remains uncertain, mainly due to the lack of *in situ* experiments under the relevant pressure and temperature conditions. Combining *in situ* synchrotron X-ray absorption and diffraction measurements of natural $(Mg_{0.88}Fe_{0.12})_2SiO_4$ San Carlos olivine and synthetic ringwoodite at pressures between 22 GPa and 115 GPa treated at temperatures 1950 K to 2300 K, we found that temperature promotes iron partitioning into silicate perovskite, while pressure acts oppositely. There is a limited but clear effect of spin crossover in co-existing Pv and Fp on iron partitioning which, in turn, promotes chemical homogeneity within the Earth's spin transition zone.

S08-T02

The composition and buoyancy of hydrous partial melt at conditions of the 410 km seismic discontinuity

Daniel J. Frost (presenting author)[1], Mainak Mookherjee (co-author)[1]
[1] Bayerisches Geoinstitut, Universität Bayreuth, Germany

Seismic observations of low S-wave velocities at 410 km depth have been interpreted as evidence for the presence of silicate melt on top of the Earth's transition zone. The difference in the water storage capacity of upper mantle versus transition zone minerals may cause dehydration melting as material up-wells across the 410. It has been proposed that hydrous partial melts may be neutrally buoyant in the mantle at these conditions. In order to assess these possibilities it is important to determine the likely composition of small degree hydrous melts at these conditions and to measure the H2O contents of mantle minerals coexisting with this melt phase.

The composition of a hydrous melt in equilibrium with a mantle peridotite composition has been determined at conditions equivalent to the top of the 410 km seismic discontinuity i.e. 13 GPa and 1550°C. Sandwich experiments were performed in the Fe-free CMASH system where an "initial-guess" hydrous melt composition was equilibrated with 50% anhydrous peridotite. Fe-free compositions ensured that H_2O was not lost during the experiments as H_2, because H_2O contents must be determined through mass balance using the starting bulk composition. The resulting melt composition was used to assemble a further melt, which was then equilibrated in the same way. After several iterations it was possible to derive a melt composition, which was in equilibrium with a mineral assemblage identical to that observed for an anhydrous peridotite composition at the same conditions. In addition we performed further experiments to assess the Fe-Mg partitioning between hydrous silicate melt and mineral phases at the same conditions. With these partition coefficients the composition of the melt phase could be calculated. We found the equilibrium melt to contain 7 wt % H_2O but to have a lower FeO content then previously predicted. The results of melt density calculations indicate that this melt would not be neutrally buoyant at conditions compatible with the base of the upper mantle.

Fe L$_{2,3}$-edge energy-loss near-edge structure of high pressure minerals in a K-bearing MORB

Nobuyoshi Miyajima[1], Falko Langenhorst[1]
[1]Bayerisches Geoinstitut, Universität Bayreuth, Bayreuth, Germany

Ferric iron contents in high pressure minerals are under the spotlight on discussions of oxygen fugacity and transport properties in the Earth's deep mantle. We have determined the $Fe^{3+}/\Sigma Fe$ ratio of Al-bearing $(Mg,Fe)SiO_3$ perovskite (MgPv), calcium ferrite-structured aluminous phase (CF), and hexagonal aluminous phase (NAL), synthesized in a K-bearing mid-oceanic ridge basalt (MORB) at 27 GPa and 2473 K (a courtesy sample of Hirose et al. 1999), by the electron energy-loss near-edge structure (ELNES) spectroscopy.

The results (Figure 1 & 2) demonstrate that the NAL phase, which is the second Fe rich phase in a subducting MORB crust, is enriched in Fe^{3+} rather than Fe^{2+} with $Fe^{3+}/\Sigma Fe$ ratios of 0.70(3). In contrast, the CF-phase and the MgPv-phase are substantially lower than that of the NAL phase, with $Fe^{3+}/\Sigma Fe$ ratio of 0.38(5) and 0.43(4), respectively. We conclude that the higher affinity of Fe^{3+} for the NAL phase, rather than for the other Fe-bearing silicates phases, is related strongly to the substitution mechanism of trivalent cations. The mechanism is described as $Fe^{3+} + Al^{3+} = Mg^{2+} + Si^{4+}$ in an octahedral site of the structure formula, $[^{IX}(M^+,Ca)_1 {}^{VI}(Mg,Fe^{2+})_2]\ _3{}^{VI}(Mg,Al,Fe^{3+},Si)_{5.5-6.0}O_{12}$ (where $M = Na^+, K^+$) of the NAL phase (Miyajima et al. 2001). The both Al-rich phases in a MORB composition likely contain a considerable amount of ferric iron, which affects various physical properties in the uppermost of the lower mantle corresponding to post-garnet transformations. Fe^{3+} and Al solubility in MgPv can be complementary influenced by phase stability of these aluminous phases.
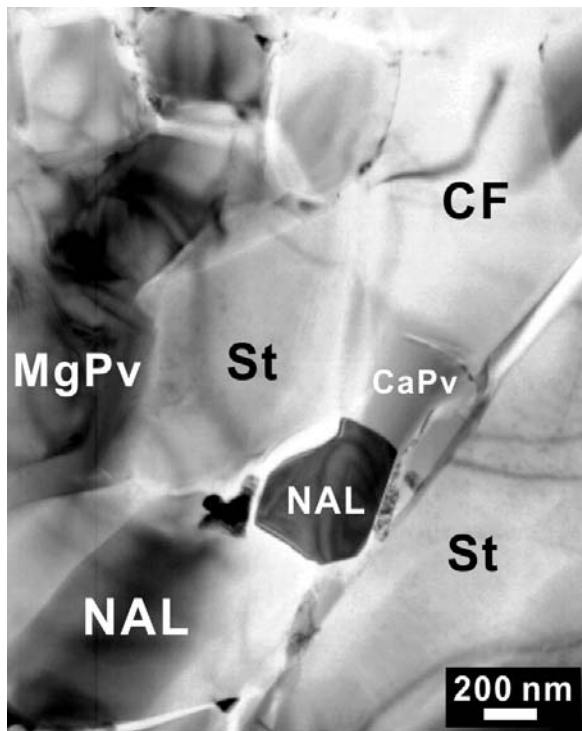
Figure 1. Bright-field TEM image of the NAL phase in a K-bearing MORB. MgPv: magnesium perovskite, CaPv: calcium perovskite, NAL: hexagonal aluminous phase, CF: calcium ferrite phase, St: stishovite.
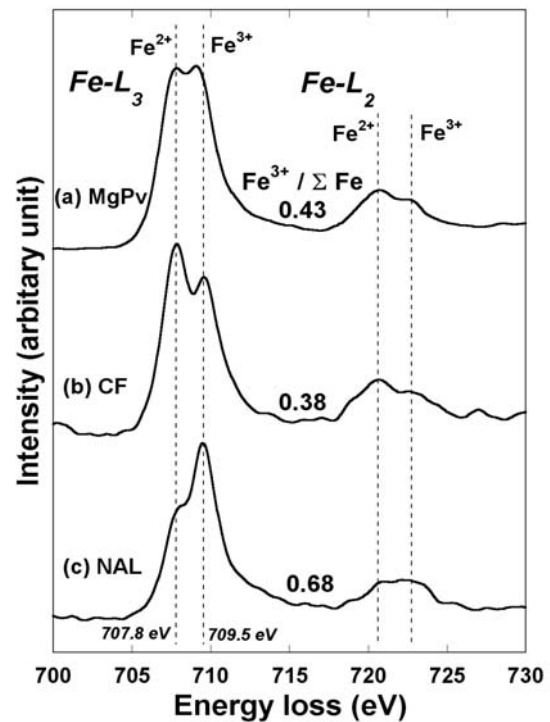

Figure 2. Fe-L$_{2,3}$ edge ELNES of coexisting Fe-bearing silicate phases in a K-bearing MORB.

Reference:

Hirose, K., Fei,Y., Ma, Y., & Mao, H.K. (1999), The fate of subducted basaltic crust in the Earth's lower mantle. Nature, 397, 53-56

Miyajima, N., Yagi, T., Hirose, K., Kondo, T., Fujino, K. & Miura, H. (2001), Potential host phase of aluminium and potassium in the Earth's lower mantle. American Mineralogist, 86, 740-746

In Situ Determination of Textures at Simultaneous High-Pressure and –Temperature by Means of the Resistive Heated Radial X-ray Diffraction Diamond Anvil Cell (RH-RXD-DAC)

Hanns-Peter Liermann[1], Sebastien Merkel[2], Lowell Miyagi[3], Jane Kanitpanyacharoen[4], Pamela Kaercher[4], Carole Nisr[2], Sylvain Petitgirard[1], Sergio Speziale[5], Hans-Rudolf Wenk[4]

[1] Deutsches Elektronen Synchrotron (DESY), Hamburg, Germany
[2] Université des Sciences et Technologies de Lille, Laboratoire de Structure et Propriétés de l'Etat Solide, UMR CNRS 8008 - Bat C6, 59655 Villeneuve d'Ascq Cedex, France
[3] Yale University, Department of Geology and Geophysics, Kline Geology Laboratory, New Haven, CT 06511, USA
[4] University of California, Berkeley, Department of Earth and Planetary Science, Berkeley CA, USA
[5] Deutsches GeoForschungsZentrum (GFZ), Potsdam, Germany

Radial diffraction in the Diamond Anvil Cell (DAC) has long been used to determine the stress state and the strength of materials under non-hydrostatic compression. This technique is also a major tool to investigate textures and infer deformation mechanisms in the earth's mantle and core. However, until now most of these experiments have been conducted at ambient temperatures and therefore the results require difficult extrapolation to the deep earth conditions.

We have further improved the Resistive Heated – Radial Diffraction – Diamond Anvil Cell (RH-RD-DAC, Liermann et al. 2009). The new design considerably extends the range of pressure-temperature conditions at which texture measurements can be performed. Here we present texture data collected at simultaneous high-pressure and temperature collected at HPCAT sector 16 of the Advanced Photon Source (Argonne National Laboratory, Chicago) on the plastic deformation of iron as well as $(Mg,Fe)_2SiO_4$ up to 40 GPa and ~ 1550 K.

Our results indicate that bcc-iron develops a mixed {100} and {111} texture that remains active during heating. This is compatible with previous observations on bcc-iron and interpreted as slip on {110}<111>. Textures obtained after transformation of fcc-iron at simultaneous high-pressure and temperatures show a pronounced maximum at {110} with minima at {100} and {111}. This texture is typical for fcc metals in compression with slip on {111}<110>.

Recently, we deformed samples of polycrystalline $(Mg,Fe)_2SiO_4$ in the RH-RD-DAC at constant temperature of 1200 K and pressures of up to 34 GPa. During the experiment we first synthesized ringwoodite and increased temperature to 1561 K at 24 GPa to convert ringwoodite to perovskite and MgO. During the experiment we studied the development of stress and texture as the sample is compressed between ambient and high pressures (up to 40 GPa). In all cases, we collected diffraction data in a radial diffraction geometry that will be used to extract lattice strains and Lattice Preferred Orientation (LPO) in the sample. Details of the experiments along with initial results of the LPO measured will be presented.

References:
Liermann, H.-P., Merkel S., Miyagi L., Wenk H.-R., Shen G., Cynn H. & Evans W. J. (2009), Experimental method for *in situ* determination of material textures at simultaneous high pressure and high temperature by means of radial diffraction in the diamond anvil cell, Review of Scientific Instrumentation, 80, 104501.

D" beneath Bering Sea and Alaska – transition from low to medium velocity region

Stefanie Hempel[1], Christine Thomas[1]
[1]Institute for Geophysics, University of Münster, Münster, Germany

Seismic array data are used to study a region of approximately 15x15 degrees beneath the eastern Bering Sea. We use P and S wave reflections off the core-mantle-boundary (CMB) and the D" reflector with source-receiver combinations from 60 to 85 degrees distances. Twenty Japanese and east Russian earthquakes of magnitudes from 5.7 to 7.3 were recorded by several seismic networks and arrays in western Canada and the western United States: Caltech Regional Seismic Network, Cascade Chain Volcano Monitoring network, Intermountain West Seismic Network, POLARIS, and some of the temporary stations of earthscope (US-Array).

Array methods such as vespagrams or slowness-backazimuth analysis are used to determine travel time differences, slowness and backazimuth of P, PdP, PcP, S, SdS and ScS. Applying filters and comparing amplitudes, waveforms and polarities of reflected observed signals with synthetic seismograms, we aim to determine the thickness of the reflector and the impedance contrast between lower mantle and D" layer.

In our dataset we find events without D" reflections, others show clear D" reflection and some possibly exhibit one or two not clearly determinable PdP or SdS reflection off D". These observations indicate a very heterogeneous lowermost mantle in the transition from a region of lower to a region of slightly higher than average D" seismic velocity. The western part of the low velocity region beneath the Bering Sea shows a clearer existence of the D" reflector, forming an edge of comparably lower velocity material in the lowermost mantle with steep sides and a velocity gradient of about 90km. Towards a zone of slightly higher than average velocity east of that region the topography of D" might be too strong on scales lower than seismically possible resolution, therefore annihilating reflected signals. Different models exist to explain these phenomena: an upwelling of warm material above the CMB, transition from an upwelling to a downwelling, or an accumulation of old subducted MORB material, in combination with a phase transition from perovskite to post-perovskite or a chemically isolated amount of material with different iron content than the average mantle. With our dataset we are testing those hypothesis to find the best fitting model.

Section 09

———————

Subduction zone processes

Compositions and Nature of Melts, supercritical Fluids and Liquids liberated by Dehydration of subducted oceanic Lithosphere: Experimental Constraints and Consequences for Subduction Zone Metasomatism

Peter Ulmer[1], Ronit Kessel[2], Max W. Schmidt[1]
[1]ETH Zürich, Institute of Geochemistry and Petrology, Zürich, Switzerland
[2]The Hebrew University, Institute of Earth Sciences, Jerusalem, Israel

At crustal pressures, phase relations in natural rock-H_2O systems involve low density aqueous fluids (supercritical with respect to the endpoint of the H_2O liquid-vapor curve) and/or high density hydrous melts. The wide miscibility gap between these two liquid phases leads to a dichotomy of mobile phases with quite distinct major element solubilities and trace element geochemical signatures. As pressure increases, the fluid-melt miscibility gap closes at ever lower temperatures, until the crest of the miscibility gap intersects the fluid-saturated solidus at its endpoint, leaving a single liquid that has chemical and physical properties continuously evolving with temperature, and which is supercritical with respect to the endpoint of the fluid-saturated solidus. The question is then, at what conditions would the endpoint of the solidus be relevant for natural rock compositions. We have experimentally determined these endpoints in a variety of systems ranging from K-free MOR basalt, to pelitic systems and to the simplified mantle systems $MgO-(Al_2O_3)-SiO_2-H_2O$ (M(A)SH) using different experimental techniques in the P-T range from 3.0 GPa/700°C to 13.5 GPa, 1300°C. Supercriticality occurs over a wide range of pressure – temperature conditions ranging from as low as 1 GPa/1100°C for the SiO_2-H_2O system to 12-13 GPa in the SiO_2-poor to undersaturated part of the MSH system.

In the K-free MORB system, representing potentially subducting hydrated oceanic crust, major element compositions of the fluid/melt phase evolve at pressures of 4 – 6 GPa from peralkaline, H_2O-rich, 'granitic' compositions to metaluminous, 'andesitic' to basaltic compositions with increasing temperature. The endpoint of the fluid-saturated solidus occurs between 5 and 6 GPa, and just above 1000 °C indicating that at higher pressures, the dichotomy of fluid versus melt ceases to exist in the oceanic crust. Similar conditions were determined for pelitic and greywacke systems representing deep-sea sediments subducted together with basaltic oceanic lithologies. In the mantle-like system M(A)SH measured and extrapolated critical endpoints for the fluid/melt solvus along the inferred mantle solidus are located between 12 and 13.5 GPa around 1100°C. Whereas melt compositions buffered by olivine and opx remain enstatite – olivine normative below the critical endpoint, fluids below the endpoint become progressively enriched in MgO and are enstatite undersaturated (Mg/Si ratios > 2) at pressures exceeding about 6 GPa. The P-T evolution of fluids and liquids in the MSH system allows drawing some first order conclusions regarding the effects of Mg-Si metasomatism in the overlying mantle wedge of a subduction system leading to regions with silica enrichment or depletion.

The consequences of the solidus' endpoint on the trace element characteristics of the metasomatizing agents emanating from the subducted oceanic crust produced by the breakdown of hydrous phases or by fluxing with H_2O-rich fluids originating from dehydration of the underlying serpentinites were investigated in the K-free MORB system represented by rutile and partly epidote saturated eclogitic assemblages. The trace element partitioning between garnet, cpx and aqueous fluid, hydrous melt, or a supercritical liquid were investigated at 4-6 GPa and 700 – 1200°C. Hydrous melts and supercritical liquids are almost indistinguishable in their trace element pattern, the mobility of Th and Be is even increased in the supercritical liquid. Modeling of trace element signatures of fluids and supercritical liquids generated from dehydration of serpentine (the most effective H_2O reservoir in deeply subducted oceanic lithosphere), passing through eclogitic crustal lithologies during their ascent into the overlying mantle wedge indicate that (at least) two additional factors control their trace element geochemistry: (1) The mode of fluid advection – porous flow resulting in low fluid to rock ratios or – focused fluid flow in narrow conduits leading to high fluid to rock ratios – produces rather contrasting trace element signatures and (2) the presence or absence of accessory phases such as epidote (allanite, e.g. Klimm et al., 2008) or rutile controls to a large extent the concentrations of high field strength elements, Th, U and light REE elements. Thus, inversion of geochemical compositions of igneous products in supra-subduction settings to constrain the nature (fluid or melt) and composition of metasomatizing agents released from hydrated, subducted oceanic lithosphere is definitely not straightforward and it is unlikely that an unequivocal solution is obtained. Therefore, caution in the interpretation of such data is advised.

Reference:
Klimm, K., Blundy, J.D. & Green, T.H. (2008) Trace element partitioning and accessory phases saturation during H_2O-saturated melting of basalt with implications for subduction zone chemical fluxes, Journal of Petrology, 49, 523-553.

Combining thermodynamic and trace element modeling to quantify fluid-rock interaction in subduction zones

Matthias Konrad-Schmolke[1], Thomas Zack[2]
[1]Universität Potsdam, Department for Earth- and Environmental Sciences, Potsdam, Germany
[2]Johannes Gutenberg Universität Mainz, Department of Geosciences, Mainz, Germany

Understanding fluid migration above a subducted oceanic slab and the resulting fluid-rock interaction is a key to interpret trace element and isotopic signatures in terms of deep seated subduction zone processes. We present samples from high pressure rocks that record fluid-rock interaction directly on top of a downgoing oceanic slab and allow quantification of trace element budgets during fluid flux and associated mineral reactions. The Western Alpine Sesia-Lanzo Zone (SLZ) is a sliver of eclogite-facies continental crust that got exhumed from mantle depth in the hanging wall of the subducted Piemont oceanic plate. It was subjected to the influx of fluids originating from devolatilisation reactions in the subducted slab beneath it. Prior to the retrograde fluid influx the SLZ rocks were affected by multiple dehydration reactions during Alpine high-pressure (HP) overprint.

Weakly deformed samples preserve relict eclogite-facies mineral assemblages that show fluid-induced compositional re-equilibration along grain boundaries, brittle fractures and other fluid pathways. Multiple fluid influx stages are indicated by retrogression of primary omphacite forming phengite, albite and epidote as well as by a characteristic partial compositional replacement and/or overgrowth zoning in phengite and sodic amphibole producing step-like compositional zoning patterns with respect to major and trace elements. Step-like major element zoning in phengite and sodic amphibole is characterised mainly by a drastic Fe-Mg exchange with significantly lower X_{Mg} values in the overprinted areas that are well-visible in back scattered electron images. The concentrations of fluid mobile trace elements, such as Li, Be, B, Sr and Pb are different in the cores of phengite and amphibole from different samples and are much lower and tend towards a common value in the affected areas of both minerals. In contrast, mylonitic samples from a major blueschist-facies shear zone have well-equilibrated textures with respect to their major- and trace element mineral compositions and phengite as well as sodic amphibole have much lower trace element contents than the rims of the weakly-deformed grains.

Thermodynamic forward modelling indicates a minimum reactive fluid influx of 0.1 to 0.5 wt% in weakly-retrogressed samples and 1 to 3 wt% in strongly-retrogressed mylonitic samples. Combining thermodynamic and mass-balanced trace element distribution models, incorporating the effect of fluid influx and fluid liberation, enables quantification of fluid amounts, fluid trace element compositions as well as the distinction between reaction- and fluid-controlled trace element distributions. Our results show that retrograde epidote growth in the SLZ rocks largely controls the budget of Sr and Pb concentrations in the fluid and the wall rock phases. Therefore, it is not possible in this case to calculate fluid compositions for these elements. In contrast, concentrations of Li, Be and B in phengite and sodic amphibole are largely controlled by the composition of the infiltrating fluid thus being excellent tracers of the fluid-rock interaction. Best fit models show that concentrations in the infiltrating fluid were ca 3, 20, and 250 µg/g for Be, B and Li respectively and that the fluid/rock ratio during infiltration was between 0.05 and 0.1. Fluid-rock interaction and mineral reactions in the wall rock can lead to significant enrichment of Li up to concentrations of 650 µg/g, but has little effect on the concentrations of Be and B, in the fluid. These results suggest a significant fluid-triggered mobilisation of B and Li in subduction zones at blueschist-facies conditions.

Record of high permeability channelways for overpressured fluilds during high pressure antigorite dehydration

Padrón-Navarta J. A.[1], Tommasi A.[2], Garrido C.J.[3], López Sánchez-Vizcaíno V[4]., Gómez-Pugnaire M. T.[1,3], Jabaloy A.[4], and Vauchez A[2].

[1]Dep. Mineralogía y Petrología, Universidad de Granada, Facultad de Ciencias, 18002 Granada, Spain
[2]Géosciences Montpellier, CNRS & Université Montpellier 2, F-34095 Montpellier cedex5, France
[3]Instituto Andaluz de Ciencias de la Tierra (IACT), CSIC & UGR, Facultad de Ciencias. 18002 Granada, Spain
[4]Dep. Geología, Universidad de Jaén, Escuela Pol. Sup., Alfonso X, 23700, Linares, Spain
[5]Departamento de Geodinámica, Universidad de Granada, 18002 Granada

Transfer of fluids from the subducting slab to the mantle wedge is an essential process in subduction dynamics, as it controls the onset of the partial melting process and, hence, the location and the chemical characteristics of the arc magmatism. The mechanisms allowing the extraction of aqueous fluids from the slab and cold supra-slab mantle, where devolatilization reactions take place, are however still a matter of debate. The dehydration of serpentinite (hydrated ultramafic rocks) through a series of discontinuous reactions is the process that potentially produces the largest amounts of fluids at high pressure conditions, that is, below the magmatic arc (e.g. Poli and Schmidt 2002).

Before attaining the mantle wedge, where they trigger partial melting, volatiles released from dehydration reactions in the slab have to migrate across a relatively cold (<750ºC), peridotite layer above the incoming slab. In order to unravel the mechanisms allowing for this initial stage of fluid transport, we performed a detailed field and microstructural study of prograde peridotites in the Cerro del Almirez ultramafic massif, where evidences of one of the most important dehydration reactions in subduction zones, the high pressure antigorite breakdown (P = 1.6-1.9 GPa and T ≈ 680ºC), can be mapped in the field (Trommsdorff et al. 1998, Padrón-Navarta et al. 2010). The Cerro del Almirez ultramafic massif is the largest (~2.3 km^2) of several small and discontinuous ultramafic bodies intercalated in the upper part of the Nevado-Filábride Complex, the lowermost unit of the Internal Zones of the Betic Cordillera (Southern Spain). The antigorite breakdown led to arborescent growth of centimeter-size olivine and orthopyroxene, producing a chlorite-harzburgite with a spinifex-like texture. Microstructural observations and crystal preferred orientations (CPO) mapping show no evidences of solid-state deformation during the prograde growth of olivine and orthopyroxene at the expenses of antigorite

However, a few tens to a hundred meters away from the reaction front, the metamorphic texture is partially obliterated by grain-size reduction in roughly planar conjugate zones, a few mm to meters wide (Padrón-Navarta et al., in press). Grain size reduction zones (GSRZ) are characterized by (1) sharp contacts with undeformed spinifex-like texture domains, (2) important reduction of the olivine grain size (60-250 μm), (3) olivine color change from brownish to colorless, (4) decrease in the modal amount of orthopyroxene, and (5) at the mm- to cm-scale, irregular shapes and abrupt terminations. Field and microstructural observations exclude that relative displacement took place across these GSRZ. Analysis of olivine crystal-preferred orientations (CPO) in GSRZ shows patterns similar, but more dispersed than those in neighboring spinifex-like domains. It also reveals mm- to cm-scale discrete domains with rather homogeneous crystallographic orientations suggesting inheritance from the preexisting spinifex-like olivines in the host peridotite. We propose that GSRZ record brittle deformation (microcraking) of the spinifex-like chlorite-harzburgite, probably induced by hydrofracturing at high pressure and relative low temperature conditions (680-710ºC). Microcraking may allow the formation of high permeability channelways for overpressured fluids in an otherwise almost impermeable and cold peridotite. High-pressure hydrofracturing may be an essential mechanism in the first stages of fluid flow through the coldest parts of top-slab mantle in subduction zones. The near-lithostatic pressures associated with this process will produce transient low seismic velocities, high Poisson ratios, and high attenuation zones, similar to those associated with episodic tremor and slip attenuation zones.

References:
Padrón-Navarta J. A., Hermann J., Garrido C., López Sánchez-Vizcaíno V., and Gómez-Pugnaire M. T. (2010) An experimental investigation of antigorite dehydration in natural silica-enriched serpentinite. Contributions to Mineralogy and Petrology 159(1), 25-42.
Padrón-Navarta J. A., Tommasi A., Garrido C., López Sánchez-Vizcaíno V., Gómez-Pugnaire M. T., Jabaloy A., and Vauchez A. (in press) Fluid transfer into the wedge controlled by high-pressure hydrofracturing in the cold top-slab mantle. Earth and Planetary Science Letters.
Poli S. and Schmidt M. W. (2002) Petrology of subducted slabs. Annual Review of Earth and Planetary Sciences 30(1), 207-235.

Trommsdorff V., López Sánchez-Vizcaíno V. L., Gomez-Pugnaire M. T., and Müntener O. (1998) High pressure breakdown of antigorite to spinifex-textured olivine and orthopyroxene, SE Spain. Contributions to Mineralogy and Petrology 132(2), 139-148.

Formation of amphibole and epidote during exhumation of eclogite in a subduction channel: Examples from the Erzgebirge (Germany) and the Dabie Shan (China)

Hans-Joachim Massonne[1]
[1]Universität Stuttgart, Institut für Mineralogie und Kristallchemie, Stuttgart, Germany

Eclogites from the Dabie Shan in eastern China, occurring northwest of the town of Taihu, and those with MORB signature from the western Erzgebirge often contain porphyroblasts of amphibole and epidote. Occasionally, these late eclogitic phases also occur as fine-grained oriented minerals due to a deformation event at high pressures. One sample from each locality was studied in detail with the aid of the electron microprobe and subsequently evaluated by geothermobarometric methods especially by constructing P-T pseudosections for the corresponding bulk-rock compositions. These pseudosections for the P-T range 1-4 GPa and 400-800°C in the system Si-Ti-Al-Fe-Mn-Mg-Ca-Na-K-O-H were also contoured by various parameters such as modal contents and chemical compositions of minerals as well as contents of water bonded to minerals.

The selected eclogite from the Variscan Erzgebirge contains mm-large idiomorphic garnet grains which show a concentrical chemical zonation with highest and lowest Mn contents in the core and in the outermost rim, respectively. Mg contents, being as high as $XMg = Mg/(Mg+Fe^{2+}+Mn+Ca) = 0.32$, behave opposite. Ca contents vary only between $XCa = 0.21$ and 0.24. In preserved portions of the studied eclogite mm-sized omphacite occurs whereas in other portions of this rock omphacite is widely replaced by oriented, relatively fine-grained epidote and amphibole of barroisitic composition. Coarser-grained amphibole and phengite with Si contents up to 3.47 per formula unit (pfu) appear in the widely preserved portions. The P-T path, deduced from the above characteristics, begins at about 2.7 GPa and 500°C and shows a nearly isothermal heating to 680°C. The subsequent exhumation through P-T conditions of about 1.5 GPa and 550°C resulted in formation of epidote and amphibole for which an addition of somewhat more than 1 wt.% $H2O$ is required.

The studied eclogite from the Dabie Shan is characterized by up to cm-sized epidote as well as porphyroblasts of amphibole with barroisite-like composition. In addition, relatively large gedritic amphibole and talc grains occur as late stage phases as well. Garnet and some preserved omphacite grains are usually smaller than 0.2 mm. Garnet grains with Mn contents continuously below $XMn = 0.03$ show variable non-concentrical zonations. Nevertheless, it can be recognized that early garnet is compositionally characterized by $XMg > 0.4$ and XCa around 0.12. Late garnet shows XMg as low as 0.33 and XCa around 0.17. Rare phengite contains Si contents between 3.4 and 3.5 pfu. On the basis of garnet core compositions early P-T conditions were very likely those of the high-pressure granulite facies ($P \geq 1.5$ GPa, $T > 800$°C). Subsequently, the studied rock significantly cooled down during a burial event. Corresponding peak pressure conditions could not be precisely determined but were above 3 GPa, consistent with coesite found in adjacent eclogites, and probably below 4 GPa. Temperatures at this stage were only somewhat above 600°C. After an isothermal exhumation event hydrous phases such as Si-rich phengite started to form, for instance, at 2.7 GPa. Further exhumation accompanied by slight cooling led to a continuous replacement of omphacite mainly by amphibole and epidote at eclogite facies conditions. The latter mineral reached a modal content of about 25 vol.% by this process. Altogether, ca. 1 wt.% of $H2O$ is required to result in the observed replacement of dry phases by hydrous minerals. More water would have been necessary for the chloritization of garnet at pressures ≤ 2 GPa and temperatures ≤ 580°C, but this process did not take place.

Although both studied eclogites experienced different P-T evolutions, the major metamorphic events affecting these rocks occurred in a subduction-channel environment. The rock from the Erzgebirge represents oceanic crust subducted to depths of 80 km where this crustal material was partially involved in an upwards-directed forced flow starting with the approach to the boundary to the hot overlying mantle at such depths. The rock from the Dabie Shan was probably part of the lower crust after crustal thickening. Afterwards, it was involved in Triassic subduction to great depths by tectonic erosion before becoming part of the upwards-directed forced flow in the subduction channel similar to the rock of the Erzgebirge. The hydration event at an early stage of exhumation is typical for both studied rocks and many other eclogites in their vicinity. This event is explained by dehydration of the downgoing subducting slab close to the ascending rocks. At depths of 70-80 km, these downgoing rocks are, in fact, only as hot as 400-500°C but hot enough for the formation of garnet + $H2O$ from hydrous minerals.

The metamorphic evolution of jadeite-bearing metatrachytes within a Variscan collision zone (Kaczawa Mountains; SW Poland)

R. Kryza[1], A.P. Willner[2,3], H.-J. Massonne[2], A. Muszyński[4], H.-P. Schertl[3]
[1]Wroclaw University, Institute of Geological Sciences, 50-205 Wroclaw, Poland
[2]Universität Stuttgart, Institute for Mineralogy and Crystal chemistry, 70174 Stuttgart, Germany
[3]Ruhruniversität Bochum, Institute for Geology, Mineralogy and Geophysics, 44780 Bochum, Germany
[4]Adam Mickiewicz University, Institute of Geology, 60-665 Poznan, Poland

The Kaczawa Mountains in the West Sudetes (NE Bohemian Massif) are composed of Cambrian to Lower Carboniferous metasedimentary and metavolcanic rocks (slates, minor limestones, bimodal metavolcanics, pillowed metabasalts and mélange) that originated during early- to mid-Palaeozoic rifting and separation of the peri-Gondwanan terranes. All rocks show a low grade metamorphic overprint that is related to Late Palaeozoic (Variscan) collision. The Lubrza metatrachyte (486 Ma, U/Pb zircon; Kryza et al. 2007) occurs within the Kaczawa metavolcanic succession and is characterized by relics of sodic pyroxene. Pyroxene composition ranges from nearly pure jadeite ($Jd_{0.98}Ae_{0.02}$) in corroded grains of albite phenocrysts, to aegirine-rich compositions ($Jd_{0.15}Ae_{0.85}$) in tiny prisms of the matrix. Relict jadeite, glaucophane, phengite (with up to 3.8 Si atoms per fomula unit) and titanite belong to the peak pressure assemblage of an early HP-LT metamorphic event. Most rocks are intensely overprinted by a later greenschist facies metamorphism of Variscan age represented by epidote, chlorite, low-Si potassic white mica and actinolite (replacing the pre-existing glaucophane).

We calculated PT-pseudosections in the range 250°-650°C, 5-20 kbar to evaluate the conditions of formation of jadeite in the metatrachytes and to derive a pressure-temperature path. Nearly pure jadeite forms at conditions exceeding 8 kbar at 300°C and 12 kbar at 500°C. Considering the PT position of varied prograde, peak and retrograde metamorphic assemblages and respective mineral compositions such as that of phengite the following equilibration stages were derived: 10.5±1 kbar, 330°±30°C (stage I), 9±0.5 kbar, 390°±20°C (stage II); 320°±20°C, 6±1 kbar (stage III) and <5 kbar, <300°C (stage IV). These data are consistent with the evolution of neighboring blueschist of the same succession that was studied earlier (Kryza et al. 1990)

The metamorphic gradient for the peak pressure is estimated at ca. 10°C/km, which is typical of a subduction setting involving downgoing continental crust, in particular of a exhumation channel system within a collision zone of a microplate. Based on earlier structural observations, the ESE oriented subduction in the NE Bohemian Massif was confined with WNW thrusting and followed by extension and ESE backward normal faulting. Most probably these processes took place during Early Carboniferous times (Kryza et al. 1990, 2007).

Reference:
Kryza R, Muszynski A (1990) Glaucophane-bearing assemblage overprinted by greenschist-facies metamorphism in the Variscan Kaczawa complex, Sudetes, Poland. J. metamorphic Geol. **8,** 345-355
Kryza R, Zalasiewicz JA, Mazur S, Aleksandrowski P, Sergeev S, Presnyakov S (2007) Early Palaeozoic initial-rift volcanism in the Central European Variscides (the Kaczawa Mountains, Sudetes, SW Poland): evidence from SIMS dating of zircons. J. Geol. Soc. London **164**, 1207-1215

Geochemistry of jadeitites and jadeite-lawsonite rocks from the Rio San Juan Complex (northern Dominican Republic): Interaction between jadeitite-forming fluids and metamorphic rocks within a subduction channel

Rauno Baese[1], Walter Maresch[2], Volker Schenk[1], Hans-Peter Schertl[2]
[1]Christian-Albrechts-University Kiel, SFB 574: Volatiles and fluids in subduction zones, Kiel, Germany
[2]Ruhr-University Bochum, Institute for Geology, Mineralogy and Geophysics, Bochum, Germany

Jadeitites occur in different subduction-channel-related mélanges worldwide and came into the focus of many recent studies as they are interpreted to precipitate from subduction-zone-related fluids (Harlow and Sorensen 2005). In most localities, jadeitites are found as lenses or blocks within a serpentinite matrix. The distinct feature of the Rio San Juan Complex (RSJC) that is not observed at other jadeitite localities is the occurrence of jadeitite veins within lawsonite-blueschist blocks entrained in a serpentinite mélange (Schertl et al. 2007). The jadeitite and jadeite-lawsonite rocks can be subdivided on the basis of their microstructure:

1. Foliated type: occurs as blocks; textural relics indicate a granitic gneiss as protolith.

2. Massive type: occurs as blocks and also as veins in blueschists; growth texture of jadeite crystals indicates precipitation from a fluid.

These two types differ in their REE patterns: the foliatedtype is enriched in LREE and the normalied ratios decrease towards the HREE. This pattern is similar to that of granitic gneisses found within the same mélange. The massive-type samples show REE patterns which are slightly U-shaped with a pronounced positive Eu-anomaly. The shape of the REE patterns is similar to that of jadeitites known from other localities worldwide (Japan: Morishita et al. 2007; Myanmar: Shi et al. 2008; Guatemala: Yui et al. 2010). However, the Dominican samples have up to ten times higher normlied ratios.

To get a better understanding of the vein-forming process, trace-element concentrations of whole-rock slices were analyzed along a traverse from the adjoining blueschist into the vein center (massive type). A depletion of the MREE and HREE towards the vein is obvious within the blueschist. Moreover, compared with the rim, the vein center is depleted in MREE and HREE, but enriched in LREE.

Samples of the foliated type have $\delta^{18}O$ values between 11.0‰ and 12.4‰, which are only slightly lower than those of the massive-type samples with 11.3‰ to 13.0‰. In a diagram showing $\delta^{18}O$ values against the Garlick index (1), all massive-type samples plot near the same $\delta^{18}O$ isopleth (13.5‰) calculated for a fluid in isotopic equilibrium with the rock at the metamorphic temperature of 400°C. In the same diagram, the position of the different rock types indicates that the foliated jadeitites can be explained by a metasomatic influence of that calculated fluid on the gneisses within the same mélange.

$$(1)\ \text{Garlick index} = \frac{\left(\text{Si} + 0.58\text{Al}\right)\ \text{equivalents}}{\text{total cation equivalents}}$$

In summary, it is a remarkable feature that the RSJC contains two different types of jadeitites and jadeite-lawsonite rocks. The massive type forming veins in blueschists precipitated from a fluid characterized by high crustal $\delta^{18}O$ values between 13‰ and 14‰ and by REE patterns similar to those known from other jadeitite localities. The vein-forming fluid may also have reacted with the gneisses that occur in the same mélange and may in this way have produced the intermediate $\delta^{18}O$ values of the second, foliated type of jadeitites and jadeite-lawsonite rocks. The increasing depletion of REE in blueschists towards the adjoining jadeitite veins can be explained by a leaching process caused by the penetrating fluid.

Reference:
Harlow, G.E. & Sorensen, S.S. (2005) Jade (nephrite and jadeite) and serpentinite: metasomatic connections, International Geology Review, 113-146, 47
Morishita, T., Arai, S., Ishida, Y. (2007) Trace element compositions of jadeite (+omphacite) in jadeitites from the Itoigawa-Ohmi district, Japan: Implications for fluid processes in subduction zones, Island Arc, 40-56, 16
Schertl, H.-P., Krebs, M., Maresch, W.V., Draper, G. (2007) Jadeitite from Hispaniola: a link between Guatemala and Antigua? 20th Colloquium on Latin American Earth Sciences, Kiel, Germany, Abstract Volume 167-168

Shi, G., Cui, W., Cao, S., Jiang, N., Jian, P., Liu, D., Miao, L., Chu, B. (2008) Ion microprobe zircon U-Pb age and geochemistry of the Myanmar jadeitite, Journal of the Geological Society, London, 221-234, 165

Yui, T.-F., Maki, K., Usuki, T., Lan, C.-Y., Martens, U., Wu, C.-M., Wu, T.-W., Liou, J.G. (2010) Genesis of Guatemala jadeitite and related fluid characteristics: Insights from zircon, Chemical Geology, 45-55, 270

Northwestern Central American Volcanic Arc: Increased contribution of enriched lithosphere to lavas along the volcanic front from Nicaragua to Guatemala and behind the volcanic front

Ken Heydolph[1], Kaj Hoernle[1,2], Paul v.d. Bogaard[1,2], Folkmar Hauff[1]
[1]Leibniz-Institut für Meereswissenschaften IFM-GEOMAR, Wischhofstr. 1-3, D-24148 Kiel, Germany
[2]Sonderforschungsbereich 574, Wischhofstr. 1-3, D-24148 Kiel, Germany

The Central American Volcanic Arc (CAVA) has been subject of intensive research over the past decades, leading to a large variety of different models for the origin of CAVA lavas with various source components. Based on a comprehensive new geochemical data set (i.e. major and trace elements and Sr-Nd-Pb-Hf-O isotope ratios) of mafic volcanic front (VF), behind the volcanic front (BVF) and back-arc (BA) lava and tephra samples from NW CAVA (Nicaragua to Guatemala), we present a new model for the NW Central American Volcanic Arc volcanism. Additional potential source component sample data from subducting Cocos Plate sediments, igneous oceanic crust and Guatemalan granitic and metamorphic continental basement further contributes to our new model.

We find systematically increasing Pb isotope ratios and decreasing Nd and Hf isotope ratios along the arc from NW Nicaragua to Guatemala. BVF lavas generally have more radiogenic Pb and less radiogenic Nd and Hf isotopic compositions than related VF lavas, similar to what is observed for trace element ratios going northwards along the VF. Combined isotope and trace element data indicate the presence of three endmembers for the volcanism in NW Central America: (1) NW Nicaraguan VF samples with very high Ba/(La, Th) and U/Th, low La/Yb, relatively radiogenic Sr, Nd and Hf but unradiogenic Pb, (2) NW Guatemalan VF and Guatemalan and Honduran BVF samples with low Ba/(La, Th) and U/Th, high La/Yb, radiogenic Sr and Pb but unradiogenic Nd and Hf, and elevated d18O, and (3) Honduran and Nicaraguan BVF samples with low Ba/(La, Th) and U/Th, high La/Yb, unradiogenic Sr but radiogenic Nd, Hf and Pb. We interpret the NW Nicaragua VF endmember to be dominated by a largely serpentinite-derived fluid flux from the subducting slab, possibly with small amounts (<1 wt. %) of sediment melts, to a depleted N-MORB type of mantle wedge, resulting in large degrees of melting of primarily peridotitic material. Based on combined Hf and Nd and Hf and Pb isotope systematics, the isotopically enriched Guatemala VF and BVF endmember cannot be explained by the addition of subducted pelagic sediments to the source. Instead this endmember could be derived from pyroxenitic cumulates in the lithospheric mantle (and possibly lower crust) that were derived from parental magmas for plutonic rocks in NW Central America, which were melted during the Quaternary subduction-related volcanism. The isotopically depleted Honduras and Caribbean BA endmember could be derived from melting of young, recycled, oceanic crust in the asthenosphere upwelling in the back-arc, based on the OIB-like major and trace element but relatively depleted isotopic compositions of these samples. Mixing between these three endmember types of magmas can explain the observed systematic geochemical variations along and across the NW Central American Arc.

Along- and Across-Arc Variations in the Southern Volcanic Zone, Chile

Guillaume Jacques[1], Kaj Hoernle[1], Heidi Wehrmann[1], Dieter Garbe-Schönberg[2], Paul van den Bogaard[1], Folkmar Hauff[3], Luis Lara[4]
[1] Sonderforschungbereich 574,IFM-GEOMAR, Kiel, Germany
[2] Institute of Geosciences of the University of Kiel, Kiel, Germany
[3] IFM-GEOMAR, Kiel, Germany
[4] Servicio Nacional de Geología y Minería, Santiago, Chile

Within Collaborative Research Center (SFB574), we are studying the changes in the chemistry of olivine-bearing volcanic rocks along the volcanic front of the Southern Volcanic Zone (SVZ) in Chile and in the rear and backarc in Argentina.

Samples from the volcanic front (VF) have typical trace element signatures of subduction zone volcanic rocks, characterized, for example, by negative Nb and Ta anomalies and positive Pb, Sr, Cs, Rb, Ba, Th and U anomalies on incompatible element (spider) diagrams. Samples from Longavi in the forearc are distinct in having lower abundances of the HREE's, high Sr/Y and geochemical signatures characteristic of adakitic rocks believed to be derived through melting of the subducting slab. The northern Southern Volcanic Zone (NSVZ) samples from Tupungatito and San José have the most enriched highly to moderately incompatible element ratios, high Rb/Ba and low La/Ta and Ba/La, suggesting involvement of lower crust in the petrogenesis of these rocks. We observe systematic variations in Sr and Nd isotopic compositions along the arc, with Sr isotopes showing a dramatic increase and Nd isotopes showing a dramatic decrease in the NSVZ, which is where the crust begins to thicken significantly. The increase in Sr and decrease in Nd in the VF is coupled with an increase in the degree of differentiation of the Tupungatito and San José ($SiO2 > 58\%$, MgO = 2-4%) volcanoes. On the Pb isotope diagrams, the VF rocks trend from MORB-like compositions to the field for pelagic sediments, consistent with involvement of subducted sediments in generating the VF rocks. Interestingly, samples from the NSVZ form the lower end of the VF array (have the least radiogenic Pb isotopic compositions) on the uranogenic Pb isotope diagram, but extend to the left of the rest of the VF array on the thorogenic Pb isotope diagram, showing evidence of at least a second enriched component. The presence of the second enriched component could reflect assimilation of lower crust or addition of lower crust through subduction erosion into the manlte wedge.

Quaternary backarc samples in Argentina also show subduction signatures in their incompatible elements but generally show lower fluid signatures than the VF samples. Although the Pb isotopic compositions of backarc rocks are similar to MORB, the low Nd isotopic compositions indicate the presence of enriched material within the backarc. Although no systematic variation is seen in Sr and Nd isotopic composition from north to souths, the Pb isotope ratios show systematic spatial variations with the northern samples having the most enriched Pb isotope ratios. The lower fluid signatures in the backarc volcanoes, coupled with less radiogenic Pb isotopic compositions are consistent with a decreasing influence of the subduction signature into the backarc. With the addition of Hf and O isotope data we should be able to better constrain the different reservoirs involved in generating the diverse geochemical compositions of the SVZ volcanic rocks.

Ignimbrite generation in the Central Andes during crustal thickening characterized by O and Sr isotope compositions of phenocrysts

Heye Freymuth[1,2], Gerhard Wörner[1]
[1]Georg-August-Universität Göttingen, Abteilung Geochemie, Göttingen, Germany
[2]University of Bristol, Bristol Isotope Group, Bristol, UK

Numerous ignimbrites of variable volumes and compositions erupted in the Central Andean subduction zone throughout the Neogene. However, little is still known about the processes that generate these large amounts of melts. The most voluminous ignimbrites with individual flows reaching >1.000 km³ are monotonous crystal-rich dacites-rhyodacites with dominantly crustal sources. Ignimbrites with small to intermediate volumes (10s to 100s of km³) are generally crystal-poor and compositionally less homogeneous rhyolites with lower proportions of crustal melts.

We analyzed O and Sr isotopes of phenocrysts from ignimbrites that erupted in two different crustal domains at the northern end (Paracas domain) and in the central part (Arequipa domain) of the Central Andes. Calculated $\delta^{18}O_{melt}$ and $^{87}Sr/^{86}Sr$ ratios of all intermediate-volume rhyolitic ignimbrites and of the large-volume dacitic-rhyolitic Oxaya ignimbrites were found to be indistinguishable from spatially and temporally associated stratovolcanoes and suggest that crustal assimilation did not exceed 20-30 %. Major and trace element compositions of these ignimbrites are consistent with a derivation from sources similar to those of strato-volcanoes.

The large-volume Oxaya ignimbrites erupted at 19 to 20 Ma, a time when the Central Andean crust had been uplifted and thickened. However, these magmas formed prior to the youngest phase of thickening (< 10 Ma to recent) during which the crustal thickness reached its present value of 70 km. We propose that a hot crustal root formed by massive intrusion of magmas from the mantle wedge. This hot zone comprised of mantle magmas, solidified intrusions and partially molten crustal rocks then convected upward and (re-)melted to form a crustal melt zone from which these ignimbrites erupted. The lower volume and younger rhyolitic ignimbrites show a stronger involvement of deep crustal melting in the garnet-stability zone at a time when the crust thickened further to its present 70 km, followed by shallow evolution to rhyolites in the cold upper crust.

Section 10
_____

Environmental mineralogy and geochemistry

Computer simulations of CaCO3-MgCO3-CdCO3 system and calculations of solid solution - aqueous solution equilibria

Victor L. Vinograd[1], Dmitrii Kulik[2], Paolo Raiteri[3], Julian D. Gale[3], Bjoern Winkler[1]

[1]University of Frankfurt, Institute of Geosciences, Frankfurt a.M., D-60438, Germany

[2]Paul Scherrer Institute, Nuclear Energy and Safety Research Department, Villigen, CH-5232, Switzerland

[3]Nanochemistry Research Institute, Department of Chemistry, Curtin University, Perth,   WA 6845, Australia

Atomistic simulations of the thermodynamic of mixing functions were performed using an expansion method (Vinograd et al. 2009, 2010), which considers composition dependent pairwise Ca-Mg, Ca-Cd and Cd-Mg interactions at 11 distances within a 3x3x1 supercell of calcite. The calculations were performed using a set of empirical interatomic potentials (J.D. Gale et al, to be published), which predicts excess energies of a number of intermediate compounds in $CaCO_3$-$MgCO_3$ and $CdCO_3$-$MgCO_3$ systems in good agreement with *ab initio* calculations of Burton and van de Walle (2003). The simulations quantitatively reproduced experimental phase relations in the binaries $CaCO_3$-$MgCO_3$ and $CdCO_3$-$MgCO_3$ and made it possible to predict phase relations in the ternary. The activity-compositions relations along the binaries $CaCO_3$-$CdCO_3$ and $CaMg(CO_3)_2$ - $CdMg(CO_3)_2$ were further used to calculate Lippmann diagrams. The effectiveness of the incorporation of Cd^{2+} in lattices of calcite and dolomite is discussed.

References:

Vinograd, V.L., Sluiter, M.H. & Winkler, B. (2009), Subsolidus phase relations in the $CaCO_3$– $MgCO_3$ system predicted from the excess enthalpies of supercell structures with single and double defects. Phys. Rev. B 79, 104201.

Vinograd, V.L., Paulsen, N. van de Walle, A. & Winkler, B. (2010), Thermodynamics of mixing in the ternary rhombohedral carbonate solid solution, $(Ca_xMg_yMn_{1-x-y})CO_3$, from atomistic simulations. CALPHAD, 34, 113.

Burton, B.P. & van de Walle, A. (2003), First-principles-based calculations of the $CaCO_3$-$MgCO_3$ and $CdCO_3$-$MgCO_3$ subsolidus phase diagrams, Phys. Chem. Minerals, 30, 88.

The enthalpy of formation of KH_2PO_4 and KH_2AsO_4

Klaus-Dieter Grevel[1,2], Juraj Majzlan[1], Bernd Marler[2], Pia Tewes[2]
[1]Friedrich-Schiller-Universität Jena, Institute of Geosciences, Burgweg 11, D-07749 Jena, Germany
[2]Ruhr-Universität Bochum, Institute for Geology, Mineralogy and Geophysics, D-44780 Bochum, Germany

Within a frame of a larger project on the arsenic and phosphorus environmental contamination, we are currently investigating the chemical and physical properties of selected arsenates and phosphates. In this study, we report the enthalpy of formation of KH_2AsO_4 and KH_2PO_4; the latter phase is often utilized as fertilizer and thus abundantly present in agricultural soils.

For this purpose, single crystals of KH_2PO_4 and KH_2AsO_4 were grown from aqueous solution by slow evaporation of the solvent and identified by X-ray diffraction. The enthalpy of dissolution of both phases in sodium molybdate ($3Na_2O \cdot 4MoO_3$) at $T = 700\ °C$ was obtained by high temperature oxide melt solution calorimetry . The calorimeter was calibrated by dropping ~15 mg pellets of corundum into an empty crucible and relating the integrated signal to the known heat content (Ditmars $et\ al.$, 1982). The performance of the calorimeter was tested by checking the heat of dissolution of hematite (-Fe$_2$O$_3$, Majzlan $et\ al.$, 2002). Then aliquots of KH_2PO_4 or respectively KH_2AsO_4 crystals were ground, pressed into pellets of ~15 mg and dropped into the calorimetric solvent. From the resulting enthalpy of dissolution values, the enthalpies of formation of the two title compounds were now obtained.

Table 1: Enthalpies of KH_2PO_4 and KH_2AsO_4 and its forming compounds

Phase	ΔH_{dsol} [kJ mol^{-1}]	No. of experiments	Reference
KH_2PO_4	191.35 ± 2.45	7	This study
KH_2AsO_4	207.40 ± 0.98	6	This study
K_2CO_3	108.87 ± 1.02	10	Majzlan $et\ al.$ (2002)
P_2O_5	-164.6 ± 0.85	12	Ushakov $et\ al.$ (2001)
As_2O_5	76.7 ± 0.80		Forray & Navrotsky (pers. comm.)
H_2O	68.93	heat content calculated	Robie & Hemingway (1995)
CO_2	31.95	heat content calculated	Robie & Hemingway (1995)
Phase	$\Delta_f H^0_{298}$ [kJ mol^{-1}]	Note	Reference
K_2CO_3	-1150.18 ± 2.1		Chase (1998)
P_2O_5	-1504.95 ± 4.45		Chase (1998)
As_2O_5	-917.59	± 4 (estimated)	Nordstrom & Archer (2003)
H_2O	-285.80 ± 0.10		Robie & Hemingway (1995)
CO_2	-393.51 ± 0.13		Robie & Hemingway (1995)
KH_2PO_4	-1582.87 ± 3.54		This study
KH_2AsO_4	-1184.59 ± 2.55		This study

References:

Chase, M.W. (1998), NIST-JANAF Thermochemical Tables, 4th ed., J. Phys. Chem. Ref. Data, Monograph Series, No. **9** by M.W. Chase (Editor), Am. Chem. Soc., Am. Inst. Phys., 1951 p.

Ditmars, D.A., Ishihara, S., Chang, S.S., Bernstein, G., West, E.D. (1982), Enthalpy and heat-capacity standard reference material: synthetic sapphire (α-Al_2O_3) from 10 to 2250 K: J. Res. Nat. Bur. Stand., **87**, 159–163.

Majzlan, J., Navrotsky, A., Neil, J.M. (2002), Energetics of anhydrite, barite, celestine, and anglesite: A high-temperature and differential scanning calorimetry study: Geochim. Cosmochim. Acta, **66**, 1839–1850.

Nordstrom, D.K. & Archer D.G. (2003), Arsenic thermodynamic data and environmental geochemistry, in: Welch, A.H. & Stollenwerk, K.G., eds., Arsenic in ground water, geochemistry and occurrence: Boston, Kluwer Academic Publishers, 1–26.

Robie, R.A. & Hemingway, B.S. (1995), Thermodynamic properties of minerals and related substances at 298.15 K and 1 bar (105 Pascals) and at higher temperatures. U.S. Geol. Surv. Bull. **2131**, IV + 461 p.

Ushakov, S.V., Helean, K.B., Navrotsky, A., Boatner, L.A. (2001), Thermochemistry of rare-earth orthophosphates. J. Mater. Res. **16**(9), 2623–2633.

The X-ray Beamline of the Synchrotron Radiation Laboratory for Environmental Studies at ANKA

Jörg Göttlicher[1], Ralph Steininger[1]
[1]Karlsruhe Institute of Technology, Institute for Synchrotron Radiation, Eggenstein-Leopoldshafen, Germany

Samples required to solve environmental questions are often complex (e.g., contaminated soils, lake and dump sediments). They consist of mixtures of mineral phases (often with small particle sizes), microbes, and living tissues. Elemental distribution, spatially resolved chemical speciation and mineral phase identification are helpful to uncover relationships between mineral phases, main and trace elements and finally to comprehensively understand anthropogenic affected systems. Such problems can be addressed by a combination of microfocused synchrotron X-ray techniques as they have been setup with the Synchrotron Radiation Laboratory for Environmental Studies (SUL) at the synchrotron radiation facility ANKA. The lab consists of a microfocus X-ray beamline (SUL-X) that enable elemental mapping using X-ray fluorescence analysis (XRF), chemical speciation with X-ray absorption spectroscopy (XAS) and mineral phase determination by X-ray diffraction (XRD), successively at the same sample position. Moreover, the laboratory is supplemented with an infrared microscope (SUL-IR) at an IR beamline. The experimental station of SUL-X is equipped with various detectors for different X-ray techniques: Ionization chambers, 7 element solid state detector for XAS and XRF-spectroscopy; a CCD detector for X-ray diffraction and a light microscope in transmission and reflection for adjusting sample positions. Research fields comprise for example speciation of As and Sb from mining activities, incorporation of Pb in the human body, and mineral precipitations in polar regions. SUL-X is operating in the energy range from 2.1 to 20 keV covering absorption edges from P (K-edge) to Nb (K-edge) and U (L(III)-edge). Because of the low energy option the experimental station can be operated under vacuum.

Speciation of Copper and Arsenic enriched in Agricultural Lime

Michael Kersten[1], Tatjana Y. Reich[1], Gerald Schmidt[1], Ka H. Lui[1], Damdinsuren Zuzaan[1], Jörg Göttlicher[2]
[1] Johannes Gutenberg-University, Geosciences Institute, Mainz, Germany; kersten@uni-mainz.de
[2] ANKA Institute for Synchrotron Radiation, Karlsruhe Institute of Technology (KIT), Eggenstein-Leopoldshafen, Germany

Agricultural liming materials are used to correct soil acidity and to improve microbial functionality and plant growth. A brownish colored agricultural lime was found to contain up to 180 mg/kg copper and 125 mg/kg arsenic which is well above any fertilizing materials code threshold (Schmidt et al., 2009; Kersten et al., 2010). The dark color of the milled material is due to ample black and brown dendrites decorating the limestone plates. X-ray diffraction analyses revealed the black dendrites to consist of the tectomanganate mineral romanechite, while the brown dendrites consist of a mixture of the two nano-crystalline Fe-oxides ferrihydrite and goethite. A four-step sequential extraction analysis of the lime powder was not sufficient to differentiate clearly whether the As and Cu load is hosted by the carbonate matrix or the oxide dendrites, or in case of the latter which of the three oxide phases. Microprobe analyses confirm that the dendrites rather than the carbonate matrix are responsible for elevated Cu and As concentrations in the limestone, where the Cu is bound by the Mn oxide and the As by the Fe oxide dendrite phases. X-ray absorption spectroscopy (XAS) at all relevant element K-edges (Fe, Mn, and Ba as the matrix elements, As and Cu as trace pollutants) was used for a less ambiguous solid-state micro-spectroscopic speciation analysis approach. The XAS spectra were measured at the SUL and XAS beamlines of the ANKA synchrotron facility. Deconvolution and fitting of the spectra were performed by using the Artemis and FEFF codes. The fitting results indicated that the octahedral coordinated Jahn-Teller cation Cu^{+2} is bound predominantly into lattice sites of the tectomanganate phase, with both Mn-Cu and Cu-Mn distances indicating a substitution of Mn^{3+} tectomanganate tunnel edge sites by the Cu^{2+} cations. This structural intercalation of the Cu is clearly more stable than if bound as surface adsorbate complexes. On the other hand, XAS results at the As K-edge revealed the As to be bound as pentavalent arsenate surface adsorbate, with As-Fe distance and coordination indicating a strong bidentate inner-spheric complex formation onto goethite particle surfaces. In conclusion, both the Cu and As are more or less strongly bound and not likely to be mobilized or bioavailable under ambient physicochemical soil conditions, and the agricultural lime may therefore pose little threat to soils.

References:
Schmidt, G.T., Lui, K.H. & Kersten, M. (2009), Speciation and mobility of arsenic in agricultural lime. J. Environ. Qual. 38, 2058-2069.
Kersten, M., Reich, T.Y., Zuzaan, D., Lui, K.H., Schmidt, G. & Göttlicher, J. & (2010), Speciation of copper enriched in agricultural lime. Soil Sci. Soc. Am. J. (in press).

Biogenic sulfide formation in sediments from an abandoned copper mine: An example for the importance of nanoparticles to assess element mobility

Kilian Pollok[1], Kevin B. Hallberg[2]
[1]Universität Bayreuth, Bayerisches Geoinstitut, Bayreuth, Germany
[2]School of Biological Sciences, Bangor University, Bangor, UK

Abandoned mine sites are well known to cause short- and long-term effects on the environment. One aspect is the microbial catalyzed weathering of sulfides which produces acidic sulfate-rich surface waters and mobilizes toxic metals. The transport properties of these metals (e.g. Cu, Zn, Pb) depend highly on whether they are bound by adsorption (e.g. on iron oxides or clays) or as colloidal particle (with a certain size distribution) and how this binding reacts to varying biogeochemical conditions. For example, biofilm communities in stream sediments can facilitate the microbial reduction of sulfate by sulfate-reducing bacteria (SRB) which leads to the precipitation of metal sulfides and thus to a natural retention of toxic metals.

Here, we present first results on such a biogenic sulfide formation in sediments close to an adit of an abandoned copper mine in Mynydd Parys, Wales, for which operation ended about 100 years ago. The acid mine drainage stream itself is about 0.5 m wide by about 30 cm deep, and flows out of the adit at a rate of about 0.5 m^3/min. The water have a pH of 2.4 and contain about 65 mg/L Zn, 40 mg/L Cu, 19 mg/L Mn, and 600 mg/L Fe. The sample was taken from the sediment of the stream, approximately 2 cm below the surface, and consists of mainly ochrous material and some biofilm.

Powder XRD indicates the presence of mackinawite and potentially sphalerite but the patterns is dominated by quartz and kaolinite peaks. Analytical transmission electron microscopy (TEM) was used to further identify the mineral phases and to document their morphological characteristics. Abundant shaggy aggregates with a size of 100-300 nm consist of nanocrystalline mackinawite. The individual crystals are in the range of 5-10 nm as revealed by HRTEM. However, other morphologies of mackinawite (round and platy aggregates) which in part cover the microorganisms have been observed as well. A second nanocrystalline phase is sphalerite which occurs as round aggregates with a wide size distribution from a few hundred nm down to a few nm. Surprisingly, ZnS significantly binds As as determined by STEM-EDX maps. Furthermore, an amorphous phase with elevated contents of Cu, Pb, and As but with no Zn was found. Beside some phyllosilicates some carbonate is also present and shows elevated Mn contents.

In general, nanocrystalline phases are considerably more reactive than larger crystals of the same minerals and also potentially bio-available. Mackinawite is well known to be very reactive even in anoxic environments and may transform to pyrite over time. However, sphalerite with its size distribution at nanoscale and its elevated As contents is a very critical phase but data on its transport properties and stability are largely missing. These results reemphasize the importance research on nanoparticles in the field of environmental mineralogy to assess the condition at which they form, how long they persist and how they interact with natural waters and sediments.

How surface roughness governs colloidal retention in the environment

Cornelius Fischer[1,2], Gopala K. Darbha[1], Alex Michler[1], Thorsten Schäfer[3,] Andreas Lüttge[2]
[1]GZG, Georg-August-Universität Göttingen, Germany,
[2]Rice University, Houston, TX 77005, USA,
[3]Inst. f. Nukleare Entsorgung, KIT, Karlsruhe, Germany

The retention of small mineral particles (colloids) at mineral surfaces is an important environmental process. Mineral surfaces in contact with aqueous solutions have a point of zero charge (pH_{pzc}). At this pH value the surface is electrically neutral. Above the pH_{pzc}, the surface is negatively charged. Around neutral pH, most minerals have a negatively charged surface. Under these conditions, the adsorption of mineral colloids at mineral surfaces is electrostatically unfavorable. Theoretical approaches predicted that the DLVO interaction energy between surfaces is significantly influenced by surface roughness (e.g. Bhattacharjee et al., 1998) and, as a consequence, the retention of particles is increased, also under electrostatically unfavorable conditions. The DLVO approach combines both electrostatic and van der Waals interaction forces.

Here we present experimental results about the enhancement of colloidal retention at mineral surfaces due to surface roughness under electrostatically unfavorable conditions. The flow-through chamber experiments include three major parts: (i) the evaluation of particle attachment and detachment at surfaces as a function of hydrodynamics at well-defined, artificial, machined structured surfaces, (ii) the evaluation of the impact of roughness variation on particle retention at natural mineral surfaces under well-defined hydrodynamic conditions, and, (iii) the evaluation of particle retention at rock surfaces with surface topography and roughness variations that are typical for the environment. Negatively charged latex particles were applied as an analog to natural colloids. Spherical particles were used to prevent any influence on particle deposition due to particle shape variations.

Particle deposition density at pitted surfaces is a function of pit diameter, pit distance, particle diameter, particle polydispersity, particle concentration, and fluid velocity. For a given particle size distribution, the number of adsorbed particles correlates well with amplitude variations of the surface topography, expressed by the parameter *root mean square roughness* (*Rq*). The correlation between the number of particles deposited as a function of total surface area of rough mineral surfaces is however weak in comparison with *Rq*. This was evaluated using calcite surface topography variations in the nanometer scale (Darbha et al., 2010).

Porous mineral aggregates with rough surfaces show a remarkable high efficiency in the retention of particles. A calcite micrite sample with micron to submicron surface topography variations was investigated. Applied particle diameter was 428 nm and 1000 nm. Generally, preferred sites for adsorption are pore walls and edges of mineral aggregates. Compared to pitted calcite crystal surfaces, the amount of adsorbed particles indicates higher retention efficiency of rough micrite surfaces. This combination of results from experiments using different types of surfaces allows for a quantitative approach to the prediction of particle retention in the environment.

References:
Bhattacharjee, S., Ko, C.H. and Elimelech, M., 1998. DLVO interaction between rough surfaces. Langmuir, 14(12): 3365-3375.
Darbha, G.K., Schäfer, T., Heberling, F., Lüttge, A. and Fischer, C., 2010. Retention of Latex Colloids on Calcite as a Function of Surface Roughness and Topography. Langmuir, 26(7): 4743-4752.

Section 11

_____

Fluid-rock and fluid-mineral interaction

δ^{56}Fe variations in Fe-Ti oxides and sulphides in hydrothermally altered rocks from the oceanic crust

Wanja Dziony[1], Ingo Horn[1], Jürgen Koepke[1], François Holtz[1]
[1]Leibniz Universität Hannover, Institute for Mineralogy, Hannover, Germany

The formation of the oceanic crust is one of the main fundamental processes building our planet. Representing the first completely drilled section of the upper oceanic crust the basalts and gabbros recovered from IODP Hole 1256D (Eastern Pacific) provides us with the good opportunity to improve our understanding of the formation and evolution of the crust.

Currently Fe isotope ratios are investigated in oxides and sulphides from basalts and gabbros of IODP Hole 1256D in order to gain basic knowledge of the Fe isotope cycle in the ocean crust. The open question is whether these isotopic signatures can be used as a proxy of hydrothermal alteration.

In this approach a deep UV-femtosecond laser ablation system coupled to a MC-ICP-MS is used. This method allows us to determine iron isotope ratios *in-situ* at high spatial resolution with a precision of ±0.1‰ (2σ) for the δ^{56}Fe ratio (δ^{56}Fe = (^{56}Fe/^{54}Fe$_{sample}$/^{56}Fe/^{54}Fe$_{IRMM-14}$-1)*1000). Additionally it has been shown that a high degree of matrix-independency has been reached using this technique allowing a single metallic standard to be used for the analysis of a large variety of matrices (Horn et al., 2006)

Although igneous rocks show little variations in their whole rock δ^{56}Fe values (e.g. Beard et al, 2003), within the investigated samples large variations in δ^{56}Fe are observed on the micron scale for both, magnetite and ilmenite. Δ^{56}Fe$_{magnetite-ilmenite}$ values (δ^{56}Fe$_{magnetite}$ - δ^{56}Fe$_{ilmenite}$) of coexisting pairs of magnetite and ilmenite are in agreement with the general trend of temperature-dependent fractionation. However, a shift towards higher Δ^{56}Fe values compared to the predicted values implies that isotopic equilibrium has not been reached. These observations can be explained by the influence of hydrothermal alteration, since all investigated samples show petrographic evidence typically for hydrothermal alteration. It has been shown that Cl-bearing supercritical fluids can contain considerably amounts of bi-valent iron (Chou & Eugster, 1977). Such solutions of Fe^{2+} tend to favor mobilization of isotopically light iron. Assuming that magnetite is more sensitive to exsolution of iron than ilmenite in the presence of a Cl-bearing fluids, an increase in the δ^{56}Fe value of magnetite is observed which in turn also increases the Δ^{56}Fe magnetite-ilmentite. Variations of up to 0.4‰ in δ^{56}Fe within a single grain of magnetite illustrates that isotopic alteration can be extremely localized. The analysis of pyrites shows two populations with a large gap in the δ^{56}Fe between them. In the lowermost part of the sheeted dike complex we found a δ^{56}Fe of +0.4‰ to +0.6‰ , whereas in all other investigated samples the δ^{56}Fe of pyrite lies between -1.1‰ and -0.6‰ , identifying them as precipitations from a low-T fluid.

References:

Horn, I., von Blanckenburg, F., Schoenberg, R., Steinhoefel, G., Markl, G., 2006. In situ iron isotope ratio determination using UV-femtosecond laser ablation with application to hydrothermal ore formation processes. Geochim. Cosmochim. Acta 70, 3677–3688.

Beard B. L., Johnson C. M., Skulan J. L., Nealson K. H., Cox L. and Sun H. (2003a) Application of Fe isotopes to tracing the geochemical and biological cycling of Fe. Chem. Geol. 195, 87–117.

Chou I.-M. and Eugster H. P. (1977) Solubility of magnetite in supercritical chloride solutions. Am. J. Sci. 277, 1296–1314.

S11-T02

Mantle xenoliths from Lower Carboniferous volcaniclastic rocks of the Dill-syncline, Rhenish Massif

Christian Hansen[1], Andres Höweling[1], Wolfgang Bach[1], Niels Jöns[1]
[1]Universität Bremen, Fachbereich Geowissenschaften, Germany

Mantle xenoliths occur in Palaeozoic basanitic and alkalibasaltic pyroclastic rocks from the Dill-syncline and provide insights into mantle provenance and melting processes. They are heavily altered, with a strong imprint of both silicification and carbonatization. Rocks were collected from outcrops described in Nesbor (2003) and examined by thin section microscopy and electron microprobe analyses within the framework of two Bachelor Thesis projects.

The precursor rock of the strongly altered samples was a spinel lherzolite (ca. 60 vol.% olivine, 15 vol.% clinopyroxene, 20 vol.% orthopyroxene, 5 vol.% spinel). Samples show a protogranular texture with spinel occurring in symplectitic intergrowth with pyroxene. Amongst the primary mineral phases, spinel is commonly preserved. It is homogeneous in composition with Mg/(Mg+Fe)= 0.72-0.79 and Cr/(Cr+Al)= 0.15-0.23. TiO_2 contents range from 0.03 to 0.09 wt.% and small amounts of ZnO are present (<0.3 wt.%). Although typically completely hydrated, primary clinopyroxene might be present. It is classified as diopside (X_{En}= 0.48-0.50 , X_{Fs}= 0.05-0.06, X_{Wol}= 0.44-0.47), but contains significant amounts of Na (up to 0.1 p.f.u., based on 6 O) and some TiO_2 (0.11-0.25 wt.%).

All primary silicate minerals show intense to complete replacement by secondary mineral phases. Although no fresh olivine is present, its former presence can be deduced from mesh textures. These meshes consist of trails of hematite, and mesh centers are filled with either quartz or calcite or a mixture of both. Occasionally, Ni-bearing talc (Mg/[Mg+Fe]= 0.77-0.85; NiO= 1-8 wt.%) is also present as mesh filling. Orthopyroxene is completely replaced by chlorite (Mg/[Mg+Fe]= 0.60-0.85), which contains significant amounts of Ni (up to 1.8 wt.% NiO). In addition, thick lamellae of calcite form parallel to the cleavage planes of chlorite. Pseudomorphic replacement textures after clinopyroxene consist of slightly less magnesian chlorite (Mg/[Mg+Fe]= 0.55-0.65) and quartz, but locally calcite seems to overprint the chlorite+quartz assemblage. Where spinel-bearing symplectites break down, Cr-bearing chlorite (Mg/[Mg+Fe]= 0.55-0.65, Cr/[Cr+Al]= 0.2-0.4) and small amounts of anatase are among the alteration products. Furthermore, accessory sulfide minerals (e.g., millerite, chalcopyrite, and bornite) are present.

The compositions of primary clinopyroxene (high Na, high Al, low Ti) and spinel (high X_{Mg}, low X_{Cr}) point to low extents of melting of a very fertile mantle that had been sampled by the volcanic rocks of the Dill-syncline. The mineral compositions are most compatible with deep melting in a geotectonic regime of overall low magma flux, most likely continental rifting. We therefore propose that the examined mantle xenoliths represent remnants of the subcontinental mantle and are not derived from an oceanic spreading setting.

Intense metasomatic overprinting of the primary mineralogy took place during the Variscan orogeny. The texture and phase assemblage indicate an evolution of peridotite-fluid reactions, including early serpentinization, subsequent steatitization and finally silicification and carbonation of former olivine. The same fluids also caused chloritization of both massive orthopyroxene and orthopyroxene lamellae in clinopyroxene. The distinct textures associated with pyroxene replacement indicate early reaction of orthopyroxene to chlorite and late formation of chlorite + calcite after clinopyroxene.

The secondary phase relations suggest that external buffering of intergranular fluid compositions by interaction with mafic volcanics surrounding the peridotite nodules plays a critical role in the silicification of the latter. Specifically the pronounced gradients in SiO_2 activity between the two rock types facilitated the silicification of the nodules. Moreover, the fact that carbonation reactions appear late in the metasomatic history may indicate an increase in fluid X_{CO2} as fluid-rock interactions progressed.

References:
Nesbor, H.-D. (2003) Geol. Jb. Hessen 131: 145-182

Remobilization processes in hydrothermal veins in the Schwarzwald, SW Germany Susanne Göb[1], Anselm Loges[1], Thomas Wenzel[1], Michael Bau[2], Matthias Barth[3], Gregor Markl[1]
[1]Eberhard Karls Universität Tübingen, Institut für Geowissenschaften, Tübingen, Germany
[2]Jacobs University Bremen, Earth and Space Sciences, Bremen, Germany
[3]Johannes Gutenberg-Universität Mainz, Institute of Geosciences, Mainz, Germany

The Schwarzwald ore district in SW Germany hosts more than 1000 hydrothermal vein-type deposits which cut the crystalline basement as well as parts of the discordantly overlying sediments. These veins are fluorite-barite±quartz±carbonate veins that contain various mineralization assemblages of Cu-Pb, Pb-Zn, Fe-Mn or Co-Bi-Ni-U-Ag. Both gangue and ore minerals have been remobilized several times and the formation of secondary minerals still continues today.

To characterize remobilization processes, primary and secondary minerals from the veins were analyzed with respect to Rare Earth Elements (REE) and other trace elements. Secondary minerals include supergene minerals probably formed since the Tertiary as well as (sub-)recent sinters. In addition, water samples taken from mines have been analyzed to characterize the modern remobilizing fluid(s). The combination of mineral and water data allows a better understanding of dissolution, transport and reprecipitation processes in the near-surface environment.

The chemistry of the mine waters is influenced by the host rock, the veins and the surface, as shown by REE patterns of waters from the host rock and the vein and by comparison with vein minerals. Calcite and fluorite precipitating from these waters show similar REE patterns as the waters, suggesting only minor fractionation during incorporation of REE into Ca minerals. In marked contrast, minerals that incorporate REE as major elements or Mn-oxides that scavenge REE via surface-compelxation do fractionate the REE (e.g., Mn oxides produce Ce anomalies). Co-genetic minerals influence each other with respect to their REE incorporation. Mn-oxides that fractionate Cerium can lead to a negative Ce-anomaly in co-genetic REE minerals, whereas REE minerals that fractionate REE can cause a change of REE incorporation into co-genetic minerals, as for example calcite.

Obviously, the mobilizing fluid has changed from primary mineralization over remobilization in the past until recent reprecipitation. This is e.g. recorded by calcites of different generations. Whereas the primary and an older secondary calcite show different REE patterns with respect to the waters, the youngest sinter has a REE pattern that resembles that of the recent water. Therefore, primary and older secondary calcite must have been precipitated from different fluids which both differed from recent waters.

From these results we can show that REE are a powerful tool to decipher the complex remobilization processes in hydrothermal vein-type deposits. They reach from small-scale processes between co-genetic minerals to processes that involve both vein and host rock.

**Hafnium isotope homogenization in amphibolite-facies rocks <630°C:
consequences for zircon solubility and Zr-Hf mobility in aqueous solutions**

Armin Zeh[1], Axel Gerdes[1]

[1]Institute of Geosciences, University of Frankfurt, Altenhöferallee 1, D-60438 Frankfurt am Main, Germany

Zircon occurs in nearly all silici-clastic sedimentary rocks worldwide in form of detrital grains. Due to their high mechanical and chemical stability during weathering, transportation, re-sedimentation and metamorphic processes, these detrital grains can gain important information about the provenance of metasedimentary rocks, in particular for vanished Hadean terranes. However, several experiments and field-based studies have shown that primary (magmatic-detrital) zircons can loose their information (partially or totally) by several processes, which can occur under very low-grade to high-grade metamorphic conditions (for summary see Lenting et al., 2010; Zeh et al., 2010). Such processes commonly led to the formation of metamorphic zircon domains or grains, which generally look different in cathodoluminescence (CL) images and have lower U-Pb ages and Th/U ratios than the primary zircons. At this point, however, it is important to note that metamorphic zircon domains (e.g. rims around detrital magmatic grains) can be formed by at least two very different processes: (i) by *in-situ* pseudomorphic alteration of primarily detrital grains (PZ – pseudomorphic zircon), and (ii) by new grew from a fluid phase (NZ – new zircon). While PZ formation can take place under low- to high-grade metamorphic conditions (by different mechanisms), NZ formation is most effective in high-grade rocks in the presence of a melt phase. Under such conditions detrital grains are effectively dissolved, and the hafnium isotope system can homogenize prior to new zircon precipitation, causing that all metamorphic zircon domains show identical or very similar ^{176}Hf/^{177}Hf on hand specimen scale or even beyond (e.g., Gerdes & Zeh, 2009). In contrast, hafnium isotope homogenization (on hand specimen scale) is not expected to occur under sub-solidus conditions in (detrital zircon bearing) metapelitic rocks, due to the very low solubility of zircon and the limited mobility of zirconium und hafnium in silica-saturated aqueous solutions (e.g., Schmidt et al., 2006; Kovalenko & Ryzhenko, 2009). This conclusion, however, is refuted by new results obtained from combined CL imaging and U-Pb-Lu-Hf isotope analyses carried out on amphibolite-facies metapelitic rocks (550-630°C) from the Shackleton Range (Antarctica) and the Limpopo Belt (South Africa). More than 50 randomly selected metamorphic zircons from two Shackleton Range rocks (600-630°C) yielded within error identical ^{176}Hf/^{177}Hf of 0.28160 ± 0.00003 and 0.28142 ± 0.00003, respectively (less than ±1.2 epsilon units variations), providing evidence for effective hafnium isotope homogenization during metamorphic zircon growth. Total Hf-isotope homogenization in rocks from the Limpopo Belt (c. 550°C) is constrained by a precise six point Lu-Hf isochrone age of 2040 ± 3 Ma, comprising ID-measurements of garnet and whole rock, and LA-ICP-MS data from metamorphic zircons analysed in thin sections.

Reference

Lenting, C., Geisler, T., Gerdes, A., Kooijman, E., Scherer, E. and Zeh, A. (2010). The stability of the Hf isotope system in metamict zircons: hydrothermal experiments. Am. Mineral., in press.

Gerdes A. and Zeh A. (2009) Zircon formation versus zircon alteration – new insights from combined U-Pb and Lu-Hf in-situ LA-ICP-MS analyses, and consequences for the interpretation of Archean zircon from the Central Zone of the Limpopo Belt. Chem. Geol. 261, 230-243.

Kovalenko, N. I. and Ryzhenko, B. N. (2009). Comparative study of the solubility of zircon and baddeleyite. Geochem. Internat. 27, 405-413.

Schmidt, C., Rickers, K., Wirth, R., Nasdala, L. and Hanchar, J. M. (2006) Low-temperature Zr mobility: An in situ synchrotron-radiation XRF study of the effect of radiation damage in zircon on the element release in H_2O + HCl ± SiO_2 fluids, *Am. Mineral.* 91, 1211-1215.

Zeh, A., Gerdes, A., Will, T. M. & Frimmel, H. E. (2010). Hafnium isotope homogenization during metamorphic zircon growth in amphibolite-facies rocks, examples from the Shackleton Range (Antarctica). Geochim. Cosmochim. Acta, in press.

S11-T05

Effects of variable input of magmatic volatiles on the modes of alteration and mineralization in felsic-hosted hydrothermal systems in the Eastern Manus Basin, Papua New Guinea

Dominik Niedermeier[1]*, Wolfgang Bach[1], Eoghan Reeves[1], Jeffrey Seewald[2], Jörg Erzinger[3]
[1]Universität Bremen, Geoscience Department, Bremen, Germany (*dniedermeier@uni-bremen.de)
[2]Woods Hole Oceanographic Institution, Woods Hole, USA
[3]GeoForschungsZentrum Potsdam, Germany

The eastern Manus Basin (EMB) features seafloor hydrothermal systems with compositionally diverse vent fluids, issuing from a range of volcanic host rocks. The great diversity in fluid and basement compositions is reflected in a large range of types of rock alteration and mineralization observed at the seafloor. These systems facilitate a direct examination of the effect of host rock composition and magma degassing on mass transport in hydrothermal systems.

During an RV *Melville* cruise in 2006, we collected rock and fluid samples from the PACMANUS, Desmos and North Su sites using the ROV *Jason II*. Fresh rocks show a compositional range from basaltic andesite to rhyodacite. Hydrothermal fluids are variably enriched in sulfuric acid, carbonic acid and have variable salt and metal contents. Hydrothermal alteration of basement in the EMB includes propyllitic (talc-chlorite-abite), sericitic to argillic (illite-pyrophyllite/kaolinite-quartz), and advanced argillic (alunite-cristobalite-sulfur) alteration types in the immediate vicinity of the fluid discharge. The fluids sampled from hydrothermal systems in the EMB exhibit substantially lower pH and greater compositional variability than basalt-hosted hydrothermal systems at mid-ocean ridges. Fluid pH at the PACMANUS venting sites is generally between 2.3 and 2.8, irrespective of the concentrations of dissolved gases and metals. The extreme acidity (pH=0.9-1.5) of acid-sulfate fluids venting at the Desmos and North Su vent sites is due to magmatic contribution of SO_2, which disproportionates to sulfuric acid and H_2S as well as native sulfur upon cooling.

The following modes of alteration and mineralization have been observed in the EMB:

(1) In the PACMANUS area, two sites of high-temperature fluid discharge -Satanic Mills (288°C) and Fenway (356°C) and one low-temperature site -Snowcap (151°C) show contrasting styles of mineralization.

At Satanic Mills the assemblage of kaolinite-barite-anhydrite-sulfides (sphalerite, pyrite, chalcopyrite, tennantite-tetrahedrite) is representative for the subseafloor stockwork zone of black-smoker-type hydrothermal systems. Mostly aphyric dacite fragments, forming volcaniclastic breccias at Fenway, are intensely altered along perlitic cracks. Only the cores of propyllitically altered domains show relicts of plagioclase. The main alteration assemblage is quartz-illite/smectite-anhydrite. Sparsely microphyric dacite from Snowcap shows alteration textures similar to the Fenway dacite, but the dominant alteration assemblage here is pyrophyllite-quartz-alunite.

(2) Basaltic andesite at Desmos is aphyric to plagioclase- and clinopyroxene-phyric and highly vesicular. Rocks from the vicinity of acid-sulfate fluid vents show distinct outward zoning patterns from fresh to propyllitic (talc–biotite–feldspar) to argillic (pyrophyllite–cristobalite–pyrite) to advanced argillic (Na-alunite–sulfur–cristobalite) alteration.

(3) Andesite at North Su is highly porphyritic and undergoes advanced argillic alteration. Altered rocks that have been sampled show pyrophyllite/beidellite-cristobalite-Na-alunite parageneses. Various sulfate phases are present at North Su, including jarosite, K-alunite and anhydrite.

Fresh rock compositions, alteration mineral assemblages, and fluid geochemistry were used in geochemical reaction path modelling to determine the changes in phase relations during progressive host rock alteration.

These models suggest that the zoning patterns observed in the rocks can be reproduced in a simple reaction path, in which the hydrothermal fluid is titrated with fresh rock at the temperature of fluid venting.

Changes in fluid chemistry during hydrothermal activity can be deduced from alteration mineral assemblages at Snowcap, where the pyrophyllite-quartz-alunite assemblage indicates former acid-sulfate alteration, similar to that observed at Desmos and North Su.

Acid-sulfate fluid venting at Desmos and North Su represents a natural experiment that provides insights into the development of alteration types and patterns known from epithermal high-sulfidation systems.

Silicate weathering and Si isotope fractionation in a glacial, granitic catchment

Ben Reynolds[1], Emmanuel Lemarchand[1], Ruth Hindshaw[1], Ed Tipper[2], Bernard Bourdon[1]
[1]ETH Zürich, Institute für Geochemie und Petrologie, Zürich, Switzerland
[2]Department of Earth Sciences, University of Cambridge, Cambridge, UK

Chemical weathering of silicate rocks consumes CO_2, affecting climate on geological timescales, and it releases dissolved cations and silicon (Si). Stable isotope variations of such elements can now be used to investigate the processes controlling chemical weathering and subsequent cycling within ecosystems. Here we utilize the potential of stable Si isotopes, alongside investigations of stable cation isotopes, to characterize the release of ions and silicic acid from granitic rocks under glacial conditions in a small mountainous catchment, where biological influence is at a minimum.

The Damma glacier in the central Swiss Alps erodes the Central Aar Granite massif, and the glacial retreat is known over the last 150 years, providing a chronosequence of soil development and vegetation growth. The soil and water chemistry has been extensively studied as part of a large multi-disciplinary investigation of the chronosequence (BigLink - http://www.cces.ethz.ch/projects/clench/BigLink). Soil samples collected along the chronosequence gradient have similar chemical compositions to the underlying lithology as little chemical weathering has occurred, despite the build-up of organic carbon. The waters in the main streams draining the catchment were sampled biweekly during the snow-free summer months, and over one 24-hour cycle. The chemistry of these waters varied considerably, and they are distinct from the underlying lithology. Depositional inputs from snow and rain are generally low for most elements, even though the waters have very dilute concentrations of dissolved solids.

Streamwater Si isotope compositions were analyzed using a MC-ICPMS (Nu Plasma 1700), after removal of the cation matrix via cation exchange chromatography. The dissolved stable Si isotope compositions were much heavier ($> 0.3‰$ ^{30}Si; relative variations in the ^{30}Si/^{28}Si ratio in part per thousand) at all times of the year compared to the source rocks and soils, which have a relatively uniform Si isotope composition. The dissolved Si isotope compositions slightly varied over the year, with heaviest Si during autumn and winter, when flow was severely limited and Si concentrations were highest. These variations are in stark contrast compared to the dissolved divalent cations of Ca and Sr (Hindshaw et al. in review, de Souza et al. 2010), for which no significant stable isotope variations were observed, with values which were close to those of the source rocks. However, Li and Mg isotopes of the dissolved load in the streams do show large stable isotope variations over the season, like Si isotopes, especially in the waters flowing out from beneath the melting glacier and dead-ice. These sub-glacial environments are, excluding microbial actions, free of significant biological processes.

Significant Si, Mg and Li isotope fractionation into the dissolved phase within the sub-glacial environment is clearly evident, even though the waters are undersaturated with respect to secondary clay minerals. For Si isotopes, these results are in agreement with similar results from rivers draining basaltic lithologies, and with the hypothesis that the main causes of fractionation must be the formation of secondary clays during mineral dissolution, or adsorption onto iron oxides. These processes appear to occur without fractionation of Ca and Sr isotopes, which are more sensitive to biological uptake and fractionation. The exact mechanism of stable Si isotope fractionation operating at the mineral surfaces needs to be addressed in future laboratory studies.

Reference:
de Souza, G. F., Reynolds, B.C., Kiczka, M. & Bourdon, B. (2010), Strontium stable isotope fractionation in a glaciated granitic watershed, Geochimica et Cosmochimica Acta, 74 (9) p2596-2614, 2010.
Hindshaw, R.S., Reynolds, B.C., Wiederhold, J.G., Bourdon, B. & Kretzschmar, R. (in review), Calcium isotopes in a proglacial weathering environment: Damma glacier, Switzerland.

Hydrogeochemische Prozesse im geothermischen System:
SiO$_2$(aq)-Konzentrationen im Löslichkeitsgleichgewicht mit Quarz

Elke Bozau, Wolfgang van Berk
TU Clausthal, Hydrogeologie, Leibnizstraße 10, 38678 Clausthal-Zellerfeld

Lange Verweilzeiten und hohe Temperaturen der Formationswässer in tiefen Aquiferen begünstigen die Einstellung von Löslichkeitsgleichgewichten zwischen gelösten Spezies und mineralischen Feststoffphasen. Quarz wird als die Feststoffphase angesehen, welche die Konzentration der aquatischen Si-Spezies im Löslichkeitsgleichgewicht bestimmt.

Deshalb werden im Rahmen des Forschungsverbundes „Geothermie und Hochleistungsbohrtechnik" (gefördert durch das Niedersächsische Ministerium für Wissenschaft und Kultur und von Baker Hughes Industries) chemisch-thermodynamische Gleichgewichtsberechnungen mit dem Programm PHREEQC durchgeführt, um Gleichgewichtskonzentrationen von SiO$_2$(aq) im Löslichkeitsgleichgewicht mit Quarz in geothermisch nutzbaren Gesteinshorizonten in Abhängigkeit von der chemischen Zusammensetzung der Formationswässer unter den entsprechenden Temperatur- und Druckbedingungen bestimmen zu können.

Bedingt durch die hohen Ionenstärken der Formationswässer (Total Dissolved Solids: 100 bis 300 g l^{-1}) sind für die chemisch-thermodynamischen Gleichgewichtsberechnungen die Pitzer-Parameter zur Berechnung der Aktivitätskoeffizienten (ionenspezifische Korrekturfaktoren zur Beschreibung der Wechselwirkung geladener und ungeladener aquatischer Spezies) zu verwenden. Der mit dem PHREEQC-Rechenprogramm bereitgestellte thermodynamische Pitzer-Datensatz muss um die Spezies SiO$_2$(aq) und die Festphase Quarz mit den entsprechenden Gleichgewichtskonstanten für die zugehörigen Massenwirkungsgesetze sowie um den Pitzer-Parameter λ für die Wechselwirkung des Komplexes SiO$_2$(aq) mit den Hauptan- und -kationen erweitert werden, so dass die Gleichgewichtseinstellung in reiner NaCl-Lösung berechnet werden kann.

Da die Formationswässer neben Na$^+$- auch hohe Ca^{++}-Konzentrationen aufweisen, muss der thermodynamische Datensatz zur korrekten Berechnung um weitere aquatische Komplexe ergänzt werden. Zudem wird die Gleichgewichtskonstante für Quarz mit Hilfe des Programmes SUPCRT92 auf die in Formationswässern angetroffenen Temperatur- und Druckbedingungen umgerechnet.

Mit dem so erweiterten Datensatz können zum Beispiel die in den geothermisch genutzten Wässern der Bohrungen Horstberg und Bruchsal gemessenen Konzentrationen an SiO$_2$(aq) als Konzentrationen im Löslichkeitsgleichgewicht mit Quarz modellierend nachvollzogen werden.

Im weiteren Verlauf des Projektes ist vorgesehen, an die jeweilige Problemstellung angepasste chemisch-thermodynamische Datensätze zu erstellen, mit denen die geothermisch genutzten Formationswässer hinreichend beschrieben werden können und eine Prognose ihrer chemischen Entwicklung im Rahmen der geothermischen Erschließung und Nutzung möglich ist.

Water-rock-interaction in submarine hydrothermal systems and their influence on fluid chemistry: an experimental approach

Christof Kusebauch, Dieter Garbe-Schönberg, Astrid Holzheid
Christian-Albrechts-Universität zu Kiel, Institut für Geowissenschaften, Kiel

Some of the recently discovered vent fluids at 5°S on the Mid Atlantic Ridge (MAR) are characterized by extreme temperatures, very high element concentrations (Koschinsky et al., 2008) and a unique rare earth element (REE) pattern with a depletion of light and heavy REE and no positive europium anomaly (Schmidt et al., 2010; these fluids are labeled 'special' in Figure 1). Phase separation, up-welling and final venting most likely occur under 'supercritical' pressure and temperature conditions. The REE patterns of these 'special' fluids are in contrast to more 'typical' REE patterns of hydrothermal fluids that are also present at the 5°S MAR field. These 'typical' REE patterns exhibit a continuous increase of REE concentrations towards La and a positive Eu anomaly (see 'typical' fluids in Figure 1). To shed some light on the water-rock interactions that produce the 'special' fluids at the 5°S MAR field, an experimental study was performed to investigate the processes leading to the special element characteristics of the 5°S MAR fluids and their dependencies on pressure, temperature and water-to-rock ratio (w/r). All experimental pressure (p) and temperature (T) conditions mimicked natural p-T-conditions of the reaction zone of the 5°S MAR field.

Experimental and analytical methodology: Cold-seal-pressure-vessel experiments were performed using original unaltered MORB-glass and Atlantic bottom seawater from 5°S MAR as starting materials. The p-T-conditions covered by the experiments range from 400-4000 bar and 350°-500°C. Post-run solid phases (altered MORB-glass and secondary minerals) were analyzed by EMP (major and minor elements) and LA-ICP-MS (trace elements). Post-run fluid phases were analyzed by ICP-OES (major and minor elements) and ICP-MS (trace elements).

Results and interpretation: The partitioning behavior of transition metals between coexisting basaltic glass and seawater depends mainly on temperature and pressure and, to a lesser extent, on the water-to-rock ratio. Most of the transition metals are considerably enriched in post-run fluids of high temperature - low pressure experiments. These compositional trends are in good agreement with other experimental studies (e.g., Hemley et al., 1986). All REEs are strongly enriched in the experimental fluids. The REE concentrations seem to be controlled by w/r ratio only, the dependency on T and p is negligible. The REE patterns are characterized by slight depletion of light and heavy REEs and an absence of an europium anomaly (see 'exp. fluid' in Figure 1). The REE patterns of the post-run fluids mimic the REE pattern of the silicate starting material (MORB glass). This led to the conclusion, that the post-run fluids are 'primary' fluids directly produced by interaction between seawater and rock, i.e., the 'special' pattern of 5°S MAR fluids might represent a fluid originating close to the reaction zone of the entire hydrothermal system.
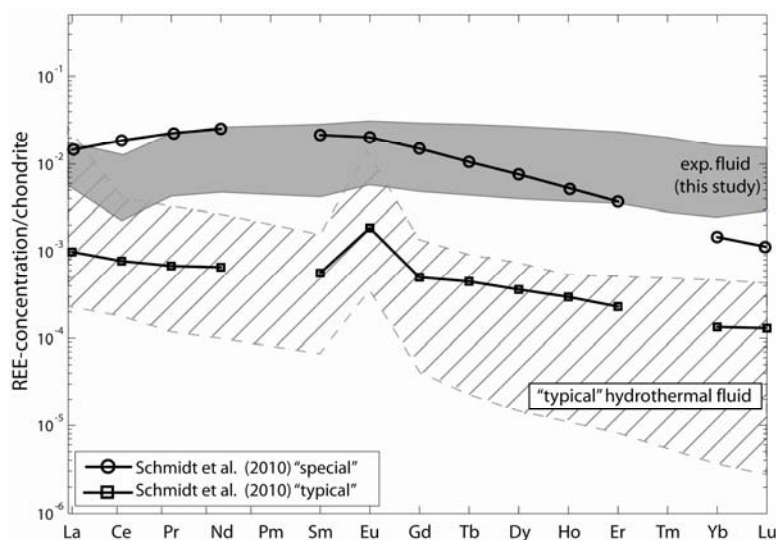
Figure 1:

Chondrite-normalized rare earth element concentrations of 2 different black smoker fluids from 5°S MAR in comparison to our experimental fluids. Note that these high-temperature experimental fluids display a flat REE-pattern and no positive Eu-anomaly. A more "typical", subcritical hydrothermal fluid REE pattern exhibits a positive Eu anomaly and a continuous increase of REE concentrations towards La. The experimental fluids differ strongly from this more "typical" type.

Reference:
Hemley, J.J. et al. (1986) Geology, 14, 377-379

Koschinsky, A. et al (2008) Geology, 36, 615–618
Schmidt, K. et al. (2010) Geochim. Cosmochim. Acta, 74, 4058-4077

S11-T09

Li isotope fractionation between fluids and minerals: Insights from experiments and simulations
Sandro Jahn, Piotr Kowalski, Bernd Wunder
Deutsches GeoForschungsZentrum GFZ, Sektion 3.3, Telegrafenberg, 14473 Potsdam, Germany

Stable isotopes are widely used as tracers of geochemical processes such as weathering, magma differentiation or element cycling. A reliable interpretation of isotopic signatures requires an understanding of the geochemical mechanisms that lead to isotopic fractionation. Since two different isotopes of an element are expected to have almost identical electronic structures in the same chemical environment, the main driving force for isotopic fractionation are the differences in isotope mass. Thermodynamically, different particle masses lead to changes in the vibrational frequencies, which change the vibrational entropy contribution to the free energy. Our goal is to understand and eventually predict the mass-dependent equilibrium isotope fractionation between minerals and fluids using both experimental and first principles modeling techniques.

In this study, we focus on Li isotope fractionation between Li-bearing silicates and aqueous fluids at high pressures and temperatures. According to a simple coordination rule, the heavy isotope ($7Li$) fractionates preferentially into the phase with the more strongly bonded Li site. This rule is qualitatively confirmed by experimental data (summarized in Wunder *et al*., 2010). Negative $\Delta 7Li$(solid-fluid) values are observed for silicates that have Li in octahedral coordination. *Ab initio* molecular dynamics simulations (Jahn & Wunder, 2009) predict a considerably lower Li coordination between 4.0 and 5.0 (and hence stronger bonding) in the fluid at pressures between about 1 and 6 GPa at a temperature of 1000 K. On the contrary, the tetrahedral Li coordination in staurolite results in a positive $\Delta 7Li$(staurolite-fluid). However, the coordination rule alone is not sensitive enough to differentiate between more or less distorted cation coordination polyhedra of the same kind, i.e. to predict the experimentally observed change in solid-fluid fractionation between different silicates with octahedral Li.

Apparently, a more systematic approach to establish the link between local atomic structure and isotopic fractionation is needed. Qualitatively, the coordination rule may be improved by relating the observed fractionation to the mean Li-O bond lengths. Stronger bonds lead to shorter bond distances and simultaneously to an increasing incorporation of the heavy isotope. We show that the bond valence model (Brown, 2009) may provide a suitable theoretical framework for this relation (see also Wunder et al., 2010). Finally, we present first results of a new fully predictive method to calculate solid-fluid isotope fractionation based on density functional theory. Our preliminary data suggest an almost quantitative agreement between calculations and experiment.

References:
Brown, I.D. (2009), Recent developments in the methods and applications of the bond valence model, Chemical Reviews 109, 6858-6919
Jahn, S. & Wunder, B. (2009), Lithium speciation in aqueous fluids at high P and T studied by ab initio molecular dynamics and consequences for Li-isotope fractionation between minerals and fluids, Geochimica et Cosmochimica Acta 73, 5428-5434
Wunder, B., Meixner, A., Romer, R.L. & Jahn, S. (2010), Li isotope fractionation between silicates and fluids: pressure dependence and influence of the bonding environment, submitted to European Journal of Mineralogy

The effect of water on component mobilities in bimineralic diopside-merwinite reaction rims

Bastian Joachim[1,2] Emmanuel Gardés[1], Rainer Abart[3], Wilhelm Heinrich[1]
[1]HelmholtzZentrum Potsdam, Deutsches GeoForschungsZentrum GFZ, Sektion 3.3, Telegrafenberg, 14473 Potsdam
[2]Freie Universität Berlin, Institut für Geologische Wissenschaften, Malteserstraße 74-100, 12249 Berlin
[3]Universität Wien, Department of Lithospheric Research, Althanstraße 14, A-1090 Wien

We synthesized bimineralic merwinite + diopside reaction rims along the interfaces of cylindrically shaped single crystals of monticellite and wollastonite at 900°C and 12 kbar and different run durations. The corresponding reaction reads:

2 monticellite ($CaMgSiO_4$) + 2 wollastonite ($CaSiO_3$) → 1 merwinite ($Ca_3MgSi_2O_8$) + 1 diopside ($CaMgSi_2O_6$)
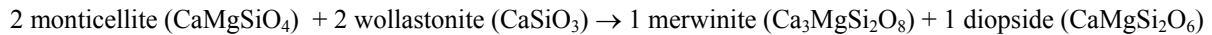
Periclase│ wollastonite│ monticellite - sandwiches were loaded into a platinum capsule and brought into a piston cylinder apparatus at 900 °C and 1.2 GPa for 5 to 65 hours. SEM analyses of the synthesized microstructures reveal that the initial monticellite-wollastonite interface is always located in the centre of the merwinite + diopside reaction rim.
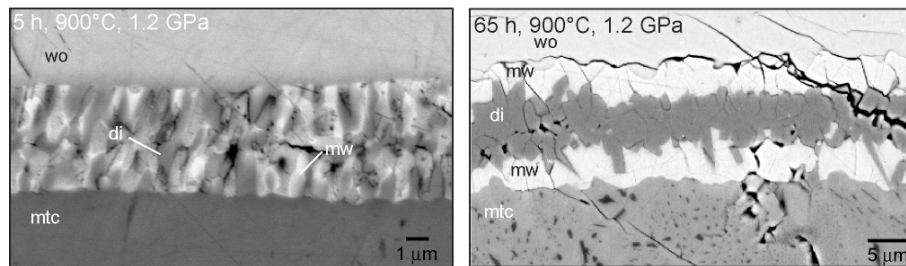
Fig.1: Bimineralic diopside-merwinite reaction rims, growing between wollastonite and monticellite single crystals. After 5 h at almost dry conditions (left), a palisade structure with alternating mw-di slats developed. After 65 (right), a three-plied rim with the layer sequence mw-di-mw has formed.

This implies that rim growth primarily occurred by transfer of the mobile MgO component from the interface between rim and monticellite towards the opposite interface between rim and wollastonite. Rim growth rates were determined from measured rim thicknesses. Applying the model of Abart et al. (2009), the effective diffusion coefficient D_{MgO}^{eff} at 900°C is estimated at $1.99 \cdot 10^{-16} \pm 3.42 *10^{-17}$ m²/s.

IR-spectra of periclase at the alternate side of the sandwich, which was not involved in this reaction, shows incorporation of OH-defects after the experiment that were not initially present. H_2O, released by natural, water-containing CaF_2 used as solid pressure medium, must have diffused into the Pt-capsule during the rim growth experiment. The amount of water in the capsule increased with increasing run duration. This, however, did not affect the overall rim growth rate.

During the first stage of rim growth, merwinite and diopside develop a palisade microstructure with long axes of the grains normal to the original monticellite-wollastonite interface (Fig. 1, left). Here, both product phases are homogeneously distributed within the rim. At longer run durations, when more water becomes available by diffusion from outside into the capsule, diopside and merwenite start to segregate into layers with diopside accumulating in the centre and merwinite at both sides of the reaction rim. After 65 h, segregation of the product phases is almost complete and a triple layer rim with the sequence mtc│mw│di│mw│wo has been produced (Fig. 1, right).

Grain boundaries are energetically more favorable than phase boundaries and it might well be that this is the driving force for segregation of the product phases into three distinct mineral layers. This segregation is, however, only possible, when CaO + SiO_2 become relatively mobile compared to MgO. This suggests that the

ingress of water into the capsule during the experiment increases the relative mobility of CaO + SiO_2 compared to the MgO-mobility. Mobility of MgO is still controlling overall rim growth. Consequently, small amounts of water may significantly change internal rim organization even if overall rim growth kinetics remains unaffected.

Reference:
Abart R., Petrishcheva E., Fischer F.D., Svoboda J. (2009), Thermodynamic model for diffusion controlled reaction rim growth in a binary system: application to the forsterite-enstatite-quartz system, American Journal of Science, Vol. 309, pp. 114-131

Olivine reaction with acidic solutions: Implications of oscillatory textures

Helen E. King1, Thorsten Geisler2 and Andrew Putnis1 1Westfälische Wilhelms-Universität Münster, Institute for Mineralogy, Münster, Germany. 2Universität Hamburg, Mineralogisch-Petrographisches Institut, Hamburg, Germany,

The interaction of silicate minerals with acidic fluids to produce amorphous silica in volcanic environments is proposed to occur via a leaching mechanism (Africano & Bernard, 2000). In this mechanism cations are preferentially removed leaving the rest of the mineral structure intact. For our experimental study we have chosen olivine because its structure consists of isolated silica tetrahedra connected by cations, thus the formation of an amorphous silica layer must occur as a separate step during the reaction. The experiments were carried out with olivine single crystals in Teflon-lined steel autoclaves at 90 °C and concentrations of sulfuric acid between 0.1 to 3.6 mol/L. One oxygen isotope tracer experiment was performed with a 3.6 mol/L sulfuric acid solution that was enriched with 18O. The reaction products were examined by scanning electron microscopy, electron microprobe, and Raman spectroscopy. We show experimentally that an oscillatory texture in amorphous silica replacing olivine, similar to that observed for pyroxene silicification in fumarolic environments, can be generated via an interface-coupled dissolution-reprecipitation mechanism.

At high acidities the reaction of olivine with sulfuric acid produced nano-porous, amorphous silica pseudomorphs of the original olivine grain, as revealed by Raman spectroscopy. Decreasing the concentration of sulfuric acid increases the fragility of the silica layer until at 0.1 M sulfuric acid no pseudomorph formed and hematite was also produced. Back-scattered images from cross-sections of the pseudomorphs showed that the replacement rim had an oscillatory texture with layers of amorphous silica. The silica formed in the 18O-enriched solution also shows a strong enrichment of 18O, as measured by Raman spectroscopy. Mg, Fe, and Ni occurred only in trace concentrations in the silica product. The dissolution of olivine in acidic solutions is usually thought to proceed via the exchange of Mg with H+ ions from the solution leaving isolated silica tetrahedra at the surface which then condense to form a silica enriched layer (Pokrovsky et al., 2000). However, the fast exchange of H+ and slow formation of siloxane bonds (Si-O-Si) in acidic solutions (Iler, 1979) suggests that condensation of isolated silica tetrahedra at the reacting olivine surface is unlikely. The release of silica into solution can explain the pseudomorphic tendencies and layering at high acid concentrations because the gel time, i.e., the time needed for a silica gel to solidify, is dependent on the concentration of silica in solution. As the silica concentration increases due to the fast dissolution of olivine the gel time decreases, hence a solid gel layer is quickly formed creating a pseudomorph. The formation of oscillating patterns in experimental systems has been associated with fluctuations in the supersaturation of different phases resulting from depletion of a slowly diffusing ion (Sherif et al. 2002). Therefore, in our system the restriction of the H+ diffusion through the amorphous silica layer, due to its catalytic role in the formation of siloxane bonds within the solidified gel, could cause the oscillatory textures. The formation of highly polymerized, porous silica that pseudomorphically replaces olivine along with the incorporation of 18O into the silica structure is consistent with an interface-coupled dissolution-reprecipitation reaction as proposed by Putnis and Putnis (2007).

Reference:

Africano, F. & Bernard, A. (2000) Acid alteration in the fumarolic environment of Usu volcano, Hokkaido, Japan. Journal of Volcanology and Geothermal Research, 97, 475-495.

Iler, R.K. (1979) The chemistry of silica: solubility, polymerization, colloid and surface properties, and biochemistry: Wiley-Interscience, New York.

Pokrovsky, O.S. & Schott J. (2000) Kinetics and mechanism of forsterite dissolution at 25°C and pH from 1 to 12. Geochimica et Cosmochimica Acta, 64, 3313-3325.

Putnis, A. & Putnis C. (2007) The mechanism of reequilibration of solids in the presence of a fluid phase. Journal of Solid State Chemistry, 180, 1783-1786.

Sherif Z., Al-Ghoul M. & Sultan R. (2002) Effect of competitive complex formation on patterning and front propagation in periodic precipitation. ChemPhysChem, 3, 592-598.

Mechanism and crystallographic control in portlandite carbonation reaction

Encarnación Ruiz-Agudo[1], Christine V. Putnis[1], Carlos Rodriguez-Navarro[2], Andrew Putnis[1]
[1]Westfälische Wilhelms-Universität Münster, Institute for Mineralogy, Münster, Germany
[2]University of Granada, Department of Mineralogy and Petrology, Granada, Spain

Traditional lime mortars set and harden following carbonation of $Ca(OH)_2$, resulting in the precipitation of $CaCO_3$. Dissolution/precipitation could be responsible for the setting of lime mortars, as there is evidence that carbonation of lime mortars only occurs in the presence of humidity (Moorehead, 1986). It is unclear, however, if the carbonation of $Ca(OH)_2$ results from a topotactic replacement reaction. Besides the relevance for the design of conservation mortars, improving our understanding of the mechanisms of portlandite carbonation has other technological implications. Geological storage of CO_2 is a potentially interesting technique to help mitigate greenhouse gas emissions to the atmosphere. To be effective, long-term storage is required. Wells in storage formations are possible weak points in the storage. Cement is the main component of the wells, and it is known to react strongly with CO_2-rich fluids, changing its mineralogy. It is vital to understand whether these carbonation reactions alter the long-term storage capacity of cement wells (Regnault et al., 2009). Portlandite is one of the main crystalline phases composing cements and is responsible for their hydraulic and mechanical properties. Hence, an accurate description of portlandite carbonation, is a key preliminary step to broaden our understanding of the various geochemical phenomena occurring during cement contact with CO_2-rich fluids or during the setting of lime mortars, in order to design appropriate conservation treatments based on the use of traditional lime mortars.

In this research we have obtained mm-sized portlandite crystals by homogeneous synthesis through counter-diffusion of $CaCl_2$ and NaOH solutions. Subsequently, in situ Atomic Force Microscopy (AFM) carbonation experiments were performed. Precipitation of calcium carbonate was observed upon contact of portlandite {0001} faces with carbonate-bearing solutions. Dissolution of portlandite releases calcium to the solution, leading to the formation of the observed thick, three dimensional islands of calcium carbonate. These islands appeared oriented on the portlandite substrate, thus indicating that their precipitation is crystallographically controlled. Our observations point to a Volmer-Weber mechanism of epitaxial growth of calcium carbonate onto portlandite {0001} surfaces.

References:
[1] Moorehead, D.R. (1986) Cementation by the carbonation of hydrated lime, *Cement and Concrete Research*, 16, 700; [2] Regnault, O.; Lagneaus, V. & Schneider, H. (2009) Experimental measurement of portlandite arbonation kinetics with supercritical CO_2, *Chemical Geology* 265, 113

Crystal growth from undersaturated solutions: the role of the boundary fluid/mineral interface

Christine V. Putnis[1], Encarnacion Ruiz-Agudo[1], Andrew Putnis[1]
[1]Institut für Mineralogie, Westfälische Wilhelms-Universität, Münster

Crystal growth takes place from solutions supersaturated with respect to the precipitating phase. However, atomic force microscopy (AFM) experiments have shown that growth on mineral surfaces can occur from solutions when the bulk composition is undersaturated with respect to the precipitating phase. The implication therefore is that the composition of the solution in the fluid boundary layer in contact with the mineral surface must become supersaturated with the new phase growing at that surface. This has been observed in a number of systems, including the growth of new phases on calcite cleavage surfaces, such as Ca phosphonates [1] and on gypsum surfaces, such as Ca phosphates [2], where the partial dissolution of the substrate provides ions included in the new phase. The precipitation of calcite from pure water flowing over a stressed calcite surface is a clear example of a boundary layer becoming supersaturated with the precipitating phase when the bulk fluid contains no ions included in the new phase. This can be explained in terms of the increased solubility of stressed calcite allowing the boundary layer to become supersaturated with an unstressed calcite phase which then precipitates. The thickness of the boundary layer can be deduced from the solution composition and the reacting surface area.

The concept of a boundary layer becoming supersaturated with respect to another phase, which then precipitates, is essential to the understanding of coupled dissolution-precipitation as a mechanism of mineral replacement [3]. Real-time phase-shift interferometry has been used to show the steep compositional gradient at the surface of a crystal of KBr being pseudomorphically replaced by KCl [4] and this has been used as a model system for more complex Earth systems during such processes as metasomatism, metamorphism and weathering.

References:
[1] Ruiz-Agudo E. et al. (2010) *Crystal Growth and Design*, [2] Pinto A. et al. (2010) *American Mineralogist*, [3] Putnis A. and Putnis C.V. (2007) *Journal of Solid State Chemistry*, [4] Putnis C.V., et al. (2005) *American Mineralogist*.

3D-view of a reaction front for a dissolution-precipitation reaction – the rutile-titanite reaction

Friedrich Lucassen[1,2], Gerhard Franz[1], Richard Wirth[2]
[1]Technische Universität Berlin, Fachgebiet Petrologie. Berlin, Germany
[2]Deutsches Geoforschungszentrum; Potsdam, Germany

Titanite growth on rutile was studied experimentally in the systems TiO_2-SiO_2-CaO-NaCl-H_2O and TiO_2-SiO_2-Al_2O_3-CaO-NaCl-H_2O ($\pm CaF_2$) at 600°C and 0.4 GPa and variable run duration (1, 3, 7, 14, 30, 60, and 107 days). Natural rutile crystals in a perforated Pt-tube were placed into an Au-capsule containing natural wollastonite crystals, -Al_2O_3, optional powdered CaF_2, and a mixture of NaCl and H_2O 1:1 by weight. Elements between the Ca, Si (and Al) sources and the Ti source are transported by the NaCl-brine. The formation of titanite results in the formation of a reaction rim on the rutile crystal; it restricts to the location of the Ti-source, i.e. the rutile and Ti is immobile compared with Ca, Si, and Al (for details: Lucassen et al. 2010). After the run, the titanite was removed by dissolution in HF, which does not attack the virtually insoluble rutile. The titanite overgrowth leaves an impressive imprint on the rutile surface, allowing to view the reaction front between the two minerals.

Growth patterns of titanite on the rutile surface are very different in the two systems. In the Al-free system, the rutile is completely overgrown by titanite already after 1 day. The small lozenge shaped crystals are commonly arranged in floral textures. With longer run times the number of titanite crystals per unit area decreases sharply, i.e. the size of the crystals increases. The arrangement of the crystals is increasingly dominated by prismatic habits with euhedral crystal faces at the fluid-titanite interface. Titanite growth on titanite is locally present but no continuous second layer of titanite crystals grew. The rutile shows commonly crystal faces (110; 100) parallel to *c* whereas other faces (101; 011) are less common. The trace of the titanite overgrowth on the rutile is independent of the rutiles' crystallographic orientations and dominated by the changing arrangement of the titanite crystals. Dissolution of the rutile is large in the vicinity of titanite-titanite grain boundaries and diminishes towards the centre of the titanite crystals. This results in a 'hump-and-valley' morphology on the rutile. After longer run-times flat-bottomed holes with stepped walls occur in the surface of the rutile,. The holes possibly mark locations with stable grain boundaries in the titanite overgrowth. Sub-µm large etch-pits restrict to flat bottoms and terraces in the walls of such holes. The dissolved rutile at the titanite-rutile interface is replaced by titanite. The titanite forming reaction includes a volume increase by factor of ~3 compared with the volume of dissolved rutile; the stress during growth enhances the solubility. Ti that is not consumed by new titanite at the titanite-rutile interface is transported along titanite-titanite grain boundaries through the reaction rim to the titanite-fluid interface and reacts to titanite.

In the Al-system, solitary euhedral titanites grow and the interface rutile-fluid (free rutile surface) persists in all runs. The prismatic crystals have a length up to 100 µm already after 1 day. With longer run-times the size of titanites increases and groups of coarse grained titanites form. The rutile becomes partially overgrown by titanite. Growth of large euhedral titanite into the fluid is common. On the rutile surface, three areas are distinguished, the free rutile surface, rutile beneath solitary titanite crystals and beneath polycrystalline titanite overgrowths. Dissolution at the free rutile surface is uniform and pronounces features like *c*-axis parallel striation and steps that are already present in the unreacted rutile. Solitary titanites rest on humps and overgrow the slope that evolves successively with the lowering free rutile surface. Rutile surfaces beneath connected titanite overgrowth show a very pronounced 'hump-and-valley' morphology following the outline of the grain boundaries between the titanites.

Dissolution textures in the rutile beneath the titanite grain boundaries indicate strong material transport for very mobile Ca, Si and Al, but on the µm-scale also for immobile Ti. Dissolution of rutile is strongly connected to the growth of titanite.

References:
Lucassen F, Franz G, Rhede D, Wirth R (2010) Ti-Al zoning of experimentally grown titanite in the system CaO-Al2O3-TiO2-SiO2-NaCl-H2O-(F) - evidence for small scale fluid heterogeneity. American Mineralogist in press

Segmentation of Epitaxial Magnesian Calcite Thin Films Induced by Interfacial Strain

Ingo Sethmann[1], Jianwei Wang[2], Udo Becker[2], Andrew Putnis[3]
[1] Technische Universität Darmstadt, Institute of Applied Geosciences, FG Geomaterial Science, Darmstadt, Germany
[2] University of Michigan, Department of Geological Sciences, Ann Arbor, MI, U.S.A.
[3] Westfälische Wilhelms-Universität Münster, Institute for Mineralogy, Münster, Germany

During heteroepitaxial growth of thin films lattice mismatch may induce elastic strain in the lattice of the film. The strain energy increases with every monolayer added to the thickness of the precipitating crystal. Accumulated strain energy may be reduced by relaxation through a change in the growth pattern from a layer-by-layer mode towards the growth of multilayer islands, as in the Stranski-Krastanow growth mode (SK) (Seifert et al. 1996). The multilayer islands produced by the SK provide an increased surface area enabling lateral strain relaxation. In the related Asaro-Tiller-Grinfeld instability (ATG), the strain is relaxed by corrugation of the surface, followed by diffusion of lattice ions from the troughs to the bulges, where the growth of multilayer islands provides additional surface area to laterally relax elastic strain (Spencer et al. 1993). These growth and relaxation patterns are known mainly from semiconductor systems that are hardly accessible for detailed in-situ observations.

We present direct observations of heteroepitaxial growth of Mg-calcite thin films on pure calcite substrates by scanning the crystal surfaces in the growth solutions using atomic force microscopy. Aqueous solutions with Mg^{2+}/Ca^{2+} concentration ratios in the range between 2 and 6.4 were used in order to precipitate a calcite-magnesite solid solution with significant amounts of $MgCO_3$ incorporated. High supersaturation in the aqueous solution enhanced the incorporation of Mg into the calcite to increase the lattice mismatch at the calcite Mg-calcite interface, resulting in elastic lattice strain.

After fast thin film growth to a critical thickness of about 40 monolayers (~12 nm) by spreading of monolayer islands on calcite cleavage faces, intriguing structural rearrangements took place within the precipitated Mg-calcite. Linear ridges with about 1 nm in height appeared at the crystal surface. These ridges did not grow on the surface, but formed by bulging of the precipitated Mg-calcite layers.
Formation of a ridge started at one point and proceeded in one of three crystallographically defined directions, $[\bar{4}41]$, $[48\bar{1}]$, $[2\bar{2}1]$, until it connected to another ridge. Progressive development of new ridges led to a segmentation of the growing crystal, similar to a micro-mosaic. Spreading monolayers stopped at the ridges and formed stationary multilayer steps resulting in separate and individually growing crystal segments that gave the impression of a mosaic.
As an approach to explaining the formation of ridges, molecular dynamics simulations were performed. These suggested elastic interfacial strain due to lattice mismatch between the calcite substrate and the grown Mg-calcite. Equilibration of the strain energy led to semi-epitaxial contact at the interface and to linear disordered zones perpendicular to the surface of the thin film, resulting in ridges similar the ones observed in the experiments.

Some aspects of the observed growth and deformation pattern remind of the SK growth mode and the ATG: In our observations, the formation ridges at the Mg-calcite surface resembles the corrugation described for the ATG. The bulging of the ridges and the formation of disordered zones underneath, as suggested by molecular dynamics modeling, have the function of relaxation of lateral compressive strain by squeezing out lattice ions in the directions of least resistance. The cracks that finally form between the mosaic blocks enable additional lateral strain relaxation, comparable to the island in the SK and ATG. However, in the experimentally observed system, surface diffusion, as in the ATG, does not seem to play a role in the formation of mosaic blocks and the spreading of monolayers is primarily limited by the disordered zones of the ridges and not by the elastic strain in the Mg-calcite as in the SK.

References:
Seifert, W., Carlsson, N., Miller, M., Pistol, M.-E., Samuelson, L. & Wallenberg, L.R. (1996), Prog. Crystal Growth Charact., 33, 423-471.
Spencer, B.J., Voorhees, P.W. & Davis, S.H. (1993), J. Appl. Phys. 73, 4955-4970.

Section 12

_____

*Geochemical signatures in environmental archives:
Formation, preservation and application*

S12-T01

FINGERPRINTS FROM DUST – Die Bedeutung mineralogischer Eigenschaften von Staubkörner für chemische Herkunftsanalysen zugehöriger Komponenten

Gerd Weckwerth

Institut für Geologie und Mineralogie der Universität zu Köln, Zülpicher Str. 49b, 50674 Köln

Wenn etwas zu Staub zerfällt, verbleiben gewisse physikalische und chemische Restinformationen, die Rückverfolgung und Herkunftsanalysen ermöglichen. Zugehörige Fingerprints verdankt der Staub meist der unversehrten Mineralogie, die deutlich mehr Herkunftsspuren besitzt als Bulkgehalte, z.B. nach einer Hochtemperaturdurchmischung von Gasen. Diese Spuren können sich sehr lokal in Einzelkörnern zeigen, oft mit Problemen Anteil und globale Bedeutung beurteilen zu können. Besser gelingt das, wenn man mineralogisch fixierte Eigenschaften wie Farbe, Form oder Korngröße zur Vorselektion von Proben nutzen kann, speziell wenn damit bereits bestimmte Herkunftsmerkmale verbunden sind.

Beispiele für einen Informationsverlust liefert der Sternenstaub präsolarer Komponenten, von denen nach Aufheizung und Durchmischung des solaren Nebels kaum mehr zu unterscheidende Beiträge zu Bulkkonzentrationen übrig bleiben. In differenzierten Meteoriten kam es dann zu einem planetenspezifischen Staub, der heute durch geeignet gewählte Elementverhältnisse eine chemische Herkunftsanalyse z.B. von Mond und Mars erlaubt [1]. Schwieriger wird es schon geeignete Proben von zurückliegenden Ereignissen auf der Oberfläche von Planeten zu finden. Aber selbst von einem vor 3 Milliarden Jahren möglicherweise ausgestorbenen Leben auf dem Mars könnten Restinformationen erhalten sein, die z.B. ermöglichen, organisch von anorganisch entstandenem Kalziumphosphat zu unterscheiden [2].

Besonders komplex werden solche chemischen Herkunftsanalysen auf der stark differenzierten Erdoberfläche. Schwierig ist es vor allem Fingerprints einzelner Herkunftskomponenten nach einer vollständigen Durchmischung von Stäuben im Gesamtschwebstaub wieder herauszufiltern, wenn mögliche Leitkonzentrationen durch andere Komponenten überlagert werden. Wie eine mineralogisch basierte Vorselektion solche Überlagerungen wieder beseitigen kann, lässt sich am Beispiel von metallischen Abrieben aus Bremsen und Schienen erkennen. Solche durch physikalische Niedertemperatur-Prozesse (Abriebe, Erosion) entstehende, eher grobkörnigen Stäube lassen sich von denen aus Hochtemperaturprozessen mit primär gasförmigen Emissionen (Sulfate, Ruß) anhand der Korngröße unterscheiden, da deren Kondensate selten zu festen Körnern >1 μm anwachsen. Ihre aus Verbrennung S-haltiger Matrialien stammende hohe Anreicherung chalkophilen Metalle (Se, Sb, Mo, As, Cu) führt zur Überlagerung der Leitelemente aus Verkehrsabrieben. Sie lässt sich durch die in vielen Staubsammlern mögliche Korngrößentrennung in > und < 2.5μm weitgehend beseitigen.

Am besten gelingt das trotz weiter Variation heutiger Bremsbeläge beim Bremsstaub [3], der einen weltweit ähnlich Verlauf bestimmter Elementverhältnisse in mittleren Gehalten von Abrieben aufweist. Während das am höchsten angereicherte Sb bei etwa der Hälfte aller heutigen Bremsen in Form von Trisulfid als Feinschmiermittel eingesetzt wird, dient 5-20% Cu neben Fe dem Grundaufbau von Bremsbelägen. Nimmt man Orte mit nahen Cu-Emissionen z.B. durch Abrieb von Oberleitungen von Zügen aus, lassen sich die für Bremsbeläge typischen Verhältnisse von Sb zu Cu und Mo in Proben des gesammelten grobkörnigen Schwebstaubs wieder finden. Da sie sich deutlich von den sonst vorhandenen Verhältnissen des Bodenstaubs unterscheiden, impliziert das eine Dominanz der Bremstaubkomponente von dem zwar nur ~20% des Fe, aber meist deutlich über 90% des Cu und über 99% des Sb dem Bremsabrieb zuzuschreiben sind. Wie eine aktuelle Publikation [4] zeigt, gilt das auch für die im Bahnverkehr benutzten Bremsbeläge. Deren typischen Elementverhältnisse korrelieren mit dem Abstand zu Bahntrassen auch mit As, das zusammen mit dem rötlichem Rost von Schienen emittiert wird. in denen bis zu 300 ppm an As enthalten sind.

Sb und As sind in den auftretenden Verbindungen toxisch, zum Teil sogar karzinogen und damit in Abrieben ein bisher wenig beachtetes Umweltrisiko. Für die ursprünglich in Bremsen eingebackenen Sb_2S_3-Stäube hat sich beim Versuch Umwandlungsraten in krebsverdächtiges Sb_2O_3 zu messen ein unerwartetes Auffindungsproblem unter der Mikrosonde ergeben. Möglicher Grund könnte eine kurze Gas- oder Schmelzphase der Sb-Verbindung z.B. bei erhitzten Bremsen sein, der zur breiteren Verteilung und Reduzierung von Sb-Spitzen auf deutlich unter 1% führt. Im Gegensatz zum Dieselruß müsste die Korngröße aber weitgehend >2.5μm bleiben. Letztlich symbolisiert diese Hypothese ein Problem des Informationsverlusts bei möglichen Phasenumwandlungen.

Literatur:
[1] Palme,H., Spettel,B., Weckwerth,G., Wänke H (1983): Antarctic meteorite ALHA 81005, a piece from the

ancient lunar crust, *Geophysical Research Letters* Vol. 10 No.9, 817f
[2] Weckwerth, G., Schidlowski, M. (1995): Phosphorus as a potential guide in the search for extinct life on mars,
   Advances in Space Research Vol 15, No.3, p185-191
[3] Weckwerth G. (2005) Das weiterhin bestehende Krebsrisiko von Bremsbelägen *Immissionsschutz* 1, S.15-20
[4] Weckwerth G. (2010) Origin of fine dust in urban environmental zones in print by *Applied Radiation and Isotopes*

The oxygen isotope exchange between $(CO_3^{2-})_{aq}$ and water: An *in situ* Raman spectroscopic study

Thorsten Geisler[1], Argyrios Kasioptas, Christina Perdikouri[2]
[1]Westfälische Wilhelms-Universität Münster, Institute for Mineralogy, Münster, Germany

Studies on the mechanism and kinetics of the oxygen isotope exchange reaction between H_2O and aqueous oxo-anions are important for the interpretation of natural variations in the oxygen isotope composition of minerals precipitated from solution and the utilization of their oxygen isotope composition as a geochemical indicator. The kinetics of the oxygen isotope exchange between aqueous oxo-anions and water as well as the isotope fractionation associated with this process is usually studied by isothermal time-series experiments where the solution is quenched to room after certain reaction times and the respective oxo-anion is precipitated as a solid (e.g., as $BaCO_3$ in the case of aqueous carbonate species) which is then analyzed by mass spectrometric techniques for its oxygen isotope composition. When using this method, it is assumed that the isotopic composition of rapidly precipitated minerals records the value of the dissolved oxo-anion in the system.

Using the carbonate-water system as an example, we demonstrate in this contribution that *in situ* Raman spectroscopy is a valuable tool to directly monitor the oxygen isotope exchange between distinct aqueous oxo-anion species and water without the need to quench the system. The *in situ* oxygen isotope exchange experiments between aqueous CO_3^{2-} and water were carried out an in-house-made Teflon-based fluid cell using a $1M$ Na_2CO_3 solution at 45, 60, 75, and 100°C. The carbonate solution was prepared with H_2O enriched with 97 at.% ^{18}O. Speciation calculations show that at all four temperatures CO_3^{2-} is the main aqueous carbonate species (>99% CO_3^{2-}), which is confirmed by Raman spectroscopy. At the beginning of the reaction at the experimental temperatures the Raman spectrum of the carbonate solution shows an intense band near 1067 cm^{-1} that can be assigned to the $\nu_1(CO_3)$ symmetric stretching vibration of the CO_3^{2-} molecule. With increasing reaction time three well-separated bands successively appear in the $\nu_1(CO_3)$ frequency region. These bands result from mass-related (isotopic) splitting of the $\nu_1(CO_3)$ mode and reflect the symmetric stretching vibration of the oxygen-related isotopologue species (n = 1, 2, and 3). The relative integrated intensity ratios of these bands are related to the number of ^{18}O atoms in the aqueous CO_3^{2-} molecule, which allowed monitoring the time-dependent distribution of the four isotopologues. The observed distributions of the four isotopologues with increasing reaction time agree well with those modeled on the basis of the consecutive reactions:

$$C^{18}O_n^{16}O_{3-n}^{2-} + H_2^{18}O \rightleftharpoons C^{18}O_{n+1}^{16}O_{3-n+1}^{2-} + H_2^{16}O \quad (n = 0, 1, \text{and } 2).$$
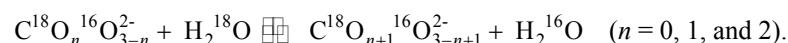
The four measured overall exchange rates define a linear trend in the Arrhenius diagram with a slope that yields an apparent activation energy of 119 ± 2 kJ/mol for the oxygen transfer between CO_3^{2-} and water. This activation energy is quite high for aqueous reactions. However, it agrees within the errors with an activation energy of 99 ± 18 kJ/mol that was conventionally determined by Beck (2004) from three time-series experiments at 15, 25, and 40°C. Future experiments will be designed to also investigate the dependence of the oxygen exchange kinetics between aqueous carbonate and water on the pH conditions and the carbonate concentration.

Reference:

Beck, W.C. (2004) Experimental studies of oxygen isotope fractionation in the carbonic acid system at 15°C, 25°C, and 40°C. Unpubl. M.Sc. thesis, Texas A&M University, College Station, Texas.

From stratosphere to rodent teeth – isotopically anomalous oxygen in fossil bioapatite as paleo-CO_2 proxy

Andreas Pack[1], Alexander Gehler[1]
[1]Georg-August-Universität, Geowissenschaftliches Zentrum, Abteilung Isotopengeologie, Goldschmidtstrasse 1, 37077 Göttingen

The coupling between mean global temperature and atmospheric p_{CO2} is well documented for the last 800,000 a from ice cores. Beyond the 800,000 a time limit, p_{CO2} has to be determined using proxies from the rock record. We have developed a new high-resolution proxy for p_{CO2} from high-precision triple oxygen isotope analyses of mammalian teeth.

Oxygen has 3 stable isotopes. During mass-dependent fractionation (MF) processes, variations in $^{18}O/^{16}O$ and $^{17}O/^{16}O$ are closely coupled with $\alpha^{17/16} = (\alpha^{18/16})^{\beta}$. The β value is the triple isotope fractionation exponent and, for oxygen, can vary between 0.50 and 0.53. For equilibrium processes values between 0.523 and 0.529 have been observed. Mass independent fractionation (MIF) processes are characterized by $\alpha^{17/16} \neq (\alpha^{18/16})^{\beta}$. On Earth, MIF is known for many atmospheric reactions. As result of MIF during stratospheric ozone formation, tropospheric molecular O_2 has a small triple isotope anomaly. The size of the anomaly is function of global bioproduction rate and atmospheric p_{CO2}.

The magnitude of the isotope anomaly of tropospheric O_2 can be determined on base of isotope analyses of fossil teeth. The anomaly is transferred from inhaled air to body water, from where it is transferred to skeletal apatite. Small mammals are characterized by high specific metabolic rates (i.e. high specific O_2 consumption). We demonstrate on measurements of a large set of recent mammals that about 40% of the oxygen in the bodies of small mammals source from inhaled air O_2. This means that apatite of small mammals inherit ~40% of the oxygen triple isotope anomaly of inhaled air. The quantitative relation between the anomaly of apatite and inhaled air O_2 is calibrated using recent mammals and a detailed mass balance calculation.

The uncertainty in predicted p_{CO2} is in the range of only ±200 ppmv and covers a wide range of p_{CO2}.

We apply mass balance model to analyses of fossil bioapatite with ages between 0.12 and 153 Ma. The calculated p_{CO2} confirm the decrease in p_{CO2} throughout the Cenozoic. A datum for the Late Jurassic suggests low p_{CO2}. The low p_{CO2} coincides with an ice age during the otherwise greenhouse world of the Mesozoic.

Calcium isotopes of fossil bones and teeth – biogenic versus diagenetic origin

Alexander Heuser[1], Thomas Tütken[1], Nikolaus Gussone[2], Stephen J.G. Galer[3]
[3]Rheinische Friedrich-Wilhelms-Universität Bonn, Steinmann-Institut, Abteilung Endogene Prozesse, Bonn, Germany
[2]Westfälische Wilhelms-Universität Münster, Institute for Mineralogy, Münster, Germany
[3]Max-Planck-Institut für Chemie, Department Biogeochemistry, Mainz, Germany

We present Ca isotope ($^{44/40}$Ca) data of Late Triassic to Late Cretaceous dinosaur bones and teeth from different sympatric sauropods and theropods as well as from the embedding sediments. The Ca isotopic composition of fossil skeletal tissues can be used to reconstruct ancient food chains and/or type of food ingested by the animal. To study the potential influence of diagenetic alteration processes on the original Ca isotopic composition we also analyzed skeletal tissues from extant reptiles and mammals.

$^{44/40}$Ca values of fossil tooth enamel range from –1.6 to +0.5‰ (relative to SRM 915a) while most corresponding dentin values are enriched in "heavy" Ca by about 0.2 to 0.5‰ compared to enamel. There are two possible explanations for this difference in $^{44/40}$Ca between dentin and enamel ($_{dentin-enamel}$): (1) it reflects the original in vivo difference between enamel and dentin caused by different biomineralization processes during dental tissue formation which are preserved; (2) it is caused by chemical changes during fossilisation. Dentin is known to be more susceptible for diagenetic changes than enamel and thus the increase of dentin $^{44/40}$Ca values relative to enamel could indicate a diagenetic alteration. However, as Ca is a major element in apatite (~40wt.%), such an alteration would imply a significant post mortem Ca exchange with the environment. Because similar $_{dentin-enamel}$ values were found in extant and fossil reptile teeth a preservation of original biogenic values seems likely. Thus the $_{dentin-enamel}$ of fossil teeth may be used as an indicator for diagenetic alteration of the Ca isotopic composition.

No systematic differences of $^{44/40}$Ca values of bone apatite do exist between herbivorous and carnivorous dinosaurs as would be expected due the trophic level difference (Skulan and DePaolo, 1999). As no Ca isotope fractionation between diet and soft tissue occurs, the lack of a trophic level offset between herbivores and carnivores can be explained if the investigated carnivorous dinosaurs only fed on soft tissue from herbivores. This would result in very similar $^{44/40}$Ca of the diet of herbivores and non-bone-ingesting carnivores and thus in very similar $^{44/40}$Ca ratios of the mineralized tissues.

In contrast, the $^{44/40}$Ca of a T-Rex enamel sample is ~1‰ lower than those of all other herbivorous and carnivorous dinosaurs analyzed. As T-Rex was capable to crush and ingest bone (Chin et al., 1998) we hypothesize that T-Rex ingested significant amounts of bone tissue with low $^{44/40}$Ca values. This would explain the lower $^{44/40}$Ca value than for presumably non-bone-ingesting carnivorous dinosaurs.

References:
Skulan J & DePaolo D (1999) Calcium isotope fractionation between soft and mineralized tissues as a monitor of calcium use in vertebrates. Proc. Nat. Acad. Sci. 96, 13709–13713.
Chin K, Tokaryk TT, Erickson M & Calk LC (1998) A king-sized theropod coprolite. Nature 393, 680–682.

Kinetic cation stable isotope fractionation during CaCO$_3$ precipitation

Frank Wombacher (presenting author)[1], Anton Eisenhauer[2], Florian Böhm[2], Nikolaus Gussone[3]
[1] Universität zu Köln, Institut für Geologie und Mineralogie, 50674 Köln, Germany
[2] IFM-GEOMAR Leibniz-Institut für Meereswissenschaften, Wischhofstr. 1-3, D-24148 Kiel, Germany
[3] Institut für Mineralogie, Universität Münster, Corrensstr. 24, D-48149 Münster, Germany

Applications of cation/Ca and cation stable isotope ratios in biogenic CaCO$_3$ as proxies in Earth sciences call for a proper understanding of cation partitioning and isotope fractionation effects during CaCO$_3$ crystal formation. Here, we evaluate cation isotope fractionation during CaCO$_3$ precipitation based on Li, Mg and Ca isotope data (e.g. Galy et al. 2002; Marriott et al. 2004; Gussone et al. 2005; Hippler et al. 2009; this study).

Cations like Li, Mg and Ca display light isotope enrichments in biogenic and experimentally precipitated carbonate minerals relative to hydrated cations in solution. The light isotope enrichment in CaCO$_3$ led Gussone et al. (2003) to propose a kinetic transport model that involved the diffusion of Ca^{2+}-aquocomplexes. In contrast, several arguments suggest equilibrium isotope partitioning of cations between the CaCO$_3$ lattice and solution, including a) fairly constant fractionation factors for many inorganic and biogenic aragonite or calcite samples b) observed mass-dependencies in Mg three isotope plots and 3) temperature dependencies that often appear to be in accord with equilibrium isotope partitioning. Equilibrium isotope partitioning is also consistent with the stronger light Li and Ca isotope enrichments in aragonite (9-fold coordinated) relative to calcite (6-fold coordinated). In regard of this mineralogical control, the possible role of the Ca-O bond length and strength has been stressed for Ca isotopes by Gussone et al. (2005), Griffith et al. (2008) and Huang et al. (2010). This observation, however, does not seem to fit with the smaller Mg isotope fractionation in aragonite compared to calcite.

Is isotopic equilibration between CaCO$_3$ crystal lattices and solution at low temperatures realistic? CaCO$_3$ precipitation is surface controlled, where net precipitation commonly overrides dissolution by far. Thus, equilibrium partitioning between crystal lattice bond and hydrated cations is implausible. Alternatively, equilibration may occur between dissolved cations and those adsorbed at the crystal surface. However, cations are only partially dehydrated and weakly bond at the crystal surface and Ca ions may not absorb at all (Raiteri et al. 2010). Finally, Fantle and DePaolo (2007) observed no measurable Ca isotope fractionation between calcite and dissolved Ca^{2+} in a marine sedimentary section where equilibrium is to be expected. They proposed a kinetic model where the balance of attachment and detachment fluxes controls the Ca isotope fractionation.

Based on the available data, we propose that the light cation isotope enrichment during CaCO$_3$ precipitation results from a chemical kinetic process, i.e. the kinetic incorporation of cations at kink sites that does not involve kinetic transport processes. Constant kinetic fractionation factors relate to the activation energy required for cation incorporation, which is probably set by cation and surface dehydration and bond formation at the incorporation site, whereby the crystal surface properties apparently define the observed mineralogical control (aragonite vs. calcite) on cation isotope fractionation.

Reference:
Fantle M S & DePaolo D J (2007), Ca isotopes in carbonate sediment and pore fluid from ODP Site 807A: The Ca^{2+}(aq)-calcite equilibrium fractionation factor and calcite recrystallization rates in Pleistocene sediments, GCA 71, 2524-2546.
Galy A, Bar-Matthews M, Halicz L & O´Nions R K (2002), Mg isotopic composition of carbonate: insight from spelothem formation, EPSL, 201, 105-115.
Griffith E M, Schauble E A, Bullen T D & Paytan A. (2008) Characterization of calcium isotopes in natural and synthetic barite, GCA, 72, 5641-5658.
Gussone, N., Eisenhauer, A., Heuser, A., Dietzel, M., Bock, B., Böhm, F., Spero, H. J., Lea, D., Bijma, J., and Nägler, T. F., 2003. Model for kinetic effects on Ca isotope fractionation (d44Ca) in inorganic aragonite and cultured planktonic foraminifera. GCA 67, 1375-1382.
Gussone N, Böhm F, Eisenhauer A, Dietzel M, Heuser A, Teichert B M A, Reitner J, Wörheide G & Dullo W-C (2005), Calcium isotope fractionation in calcite and aragonite, GCA, 69, 4485-4494.
Hippler D, Buhl D, Witbaard R, Richter D K & Immenhauser A (2009), Towards a better understanding of magnesium-isotope ratios from marine skeletal carbonates, GCA 73, 6134-6146.
Huang S, Farkas J & Jacobsen S B. (2010) Calcium isotopic fractionation between clinopyroxene and orthopyroxene from mantle peridotites. EPSL 292, 337-344.
Marriott C S, Henderson G M, Crompton R, Staubwasser M & Shaw S (2004) Effect of mineralogy, salinety,

and temperature on Li/Ca and Li isotope composition of calcium carbonate, Chem. Geol. 212, 5-15.
Raiteri P, Gale J D, Quigley D & Rodger P M (2010) Derivation of an Accurate Force-Field for Simulating the Growth of Calcium Carbonate from Aqueous Solution: A New Model for the Calcite−Water Interface, J. Phys. Chem. C.

Ca-isotope systematics in marine porewaters during early diagenesis

Charlotte Ockert[1], Barbara M.A. Teichert[2], Stephan Kaufhold[3], Laura M. Wehrmann[4], Timothy G. Ferdelman[4], Nikolaus Gussone[1]

[1]Westfälische Wilhelms-Universität Münster, Institute für Mineralogie, Münster, Germany

[2]Westfälische Wilhelms-Universität Münster, Institut für Geologie und Paläontologie, Münster, Germany

[3]Bundesanstalt für Geowissenschaften und Rohstoffe, Hannover, Germany

[4]Max-Planck-Institut für Marine Mikrobiologie, Bremen, Germany

Diagenetic and synsedimentary processes that take place within marine porewaters involving the element calcium (Ca) are not yet fully understood. Since Ca-isotope ratios of organic and inorganic mineral precipitates from marine sediments have been used as a proxy for monitoring the oceanic Ca-budget or recording changes in paleo-temperature, it is of great importance to find out how diagenetic processes, like Ca-carbonate dissolution or cation exchange reactions with clay minerals, have the potential to alter the proxy archives.

Porewater analyses of three sites in the North Atlantic (IODP Expedition 303; this study) and from the East Pacific (ODP Leg 204; Teichert et al., 2009), which all exhibit different dominating lithologies, showed different Ca-concentration developments with depth and revealed a relationship of ammonium-concentration and Ca-isotope ratios. Interestingly, this correlation could not be found for NH_4^+-concentration and Ca-concentration. The coefficient of determination of the ammonium-$\delta^{44/40}Ca$ (SRM 915a) correlation can be directly related to the presence of clay minerals in the lithology, displaying a better fit when clay minerals occur. Consequently, we propose that during Ca-adsorption and -desorption onto clay minerals in marine sediments isotope fractionation occurs, explaining light Ca-isotope ratios in porewaters which cannot be attributed to Ca-carbonate dissolution.

In order to find out more about the adsorption and desorption interaction between calcium and marine sediments or clay minerals, a radiotracer technique employing ^{45}Ca was carried out. This method also made it possible to determine the ammonium-Ca interaction of the different exchangers in an artificial seawater matrix.

The different materials, in particular pure clay mineral separates and IODP sediments from Site U1306 (Expedition 303), revealed different calcium exchange capacities in a seawater matrix. When clays were equilibrated in Ca-free artificial seawater, initial Ca-adsorption (by cation exchange) was slower than Ca-Ca exchange, which started immediately after introducing the Ca-tracer. The addition of ammonium into the artificial seawater and clay mineral slurry resulted in desorption of Ca.

The results from the deep sea drillings show that the release of light Ca into the porewater might be a general diagenetic process in siliciclastic, organic bearing sediments and that Ca-ammonium exchange might be an important process to understand porewater Ca-isotope depth profiles. Further laboratory experiments which focus on the Ca-isotope fractionation during adsorption and desorption onto clay minerals in a seawater environment are in progress.

Reference:
Teichert, B.M.A., Gussone, N., Torres, M.E. (2009), Controls on calcium isotope fractionation in sedimentary porewaters. Earth and Planetary Science Letters, 279, 373-382.

Calcium carbonate veins in oceanic crust – Recorders of seawater-crust exchange and past seawater composition

Svenja Rausch[1]*, Wolfgang Bach[1], Andreas Klügel[1], Florian Böhm[2], Anton Eisenhauer[2]
[1]Universität Bremen, Geoscience Department, Bremen, Germany (*srausch@uni-bremen.de)
[2]IFM-GEOMAR, Kiel, Germany

Calcium carbonate veins in drill cores from upper oceanic basement provide an archive of 180 Myrs of seawater circulation within the ocean crust. The chemical compositions of these veins reflect both past seawater composition and interaction of seawater with the basaltic crust. Veins formed at ambient deep-sea temperatures are unaffected by exchange between seawater and basalt and constitute faithful recorders of past seawater composition. Those that formed at elevated temperatures reveal changes in composition the magnitude of which correlates with temperature. We have examined calcium carbonate veins from twenty-three drill sites sampled by the Deep Sea Drilling Project and the Ocean Drilling Program in the past 40 years for chemical and isotopic compositions. The sites represent slow spread crust from age 2 to 130 Myrs old and intermediate to fast spread crust from age 2 to 180 Myrs old and buried by pelagic sediments of variable thickness (30 to 500 m). Our analyses include chemical (Ca, Mg, Sr) analyses and isotopic (Sr, Ca, O, C) of bulk separates as well as spot LA-ICP-MS analyses of trace elements and Sr isotopes.

It was recently demonstrated that calcite veins from the ocean crust record changes in Mg/Ca ratios of seawater at least as well as fossils and fluid inclusions in halite (Coggon et al., 2010). These authors also proposed that calcium carbonate veins truthfully record changes in Sr/Ca of seawater in the past 180 Myrs. Coggon et al. (2010) present data indicating that both Mg/Ca and Sr/Ca were constant between 24 Myrs and 180 Myrs at values that are lower by a factor of 2.5-3 (Mg/Ca) and 4-5 (Sr/Ca) relative to modern seawater. These authors postulate an increase in both ratios in the past 24 Myrs, which may be related to waning hydrothermal exchange fluxes following a post-Cretaceous slow-down of crustal production rates. The <24 Myrs old drill sites Coggon et al. (2010) examined comprise the <3.5 Myrs old Juan de Fuca ridge flank, which gives values similar to modern seawater, and the 15 Ma site 1256 in the eastern equatorial Pacific, which is buried under 251 m of sediment and features carbonates formed at temperatures between 20 and 31 °C. The existing record of the crucial interval of seawater compositional changes is hence strongly controlled by a site for which past seawater reconstruction is made difficult by extensive seawater-basalt interaction.

We have focused our work on sampling drill sites (332, 335, 395, 396, 407, 409) in the slow spread North Atlantic crust between 4 and 35 Myrs old and find carbonate vein Sr isotope ages that provide good coverage of the critical interval of seawater change since the early Miocene. Our data show temporal changes of Mg/Ca very similar to the trend in Coggon et al (2010). But the increase in Sr/Ca is much more subdued (factor of 2 to 2.5 increase) in our data. Apparently, for veins of similar age, the aragonite-based Sr/Ca of past seawater are systematically higher that calculated for calcite.

Investigating veins from a large number of sites covering the critical time interval of seawater compositional change allowed us to validate and better constrain the increases in Mg/Ca and Sr/Ca in the past 25 Myrs. Hydrothermal processes constitute a sink for Mg and a source of Ca to the oceans, while Sr is essentially unaffected. Hydrothermally driven changes should hence affect Mg/Ca of seawater more than they affect Sr/Ca. Our data indicate a lower magnitude of change for Sr/Ca so are more in line with the idea that hydrothermal waning causes the increases in Mg/Ca and Sr/Ca. Still, the essentially constant Mg/Sr of seawater in the past 180 Myrs is unexpected if the driver of change is hydrothermal. The case may not be closed yet. In addition, our data show considerable scatter within single sites, suggesting that the geochemical signature recorded in the carbonate veins is not merely a function of seawater composition.

To examine the nature of this variability, we measured trace element concentrations across carbonate veins by LA-ICP-MS. The data show that some veins are uniform in composition, but others are strongly variable. One type shows growth zones with Ca/Sr and Ca/Mg ratios up to 6 times lower than the expected values, while another type shows domains unusually rich in Sr. Differences of even greater magnitude can be detected in the REE+Y systematics, with many veins showing contrasting patterns with respect to the development of Y and Ce anomalies. The range in Sr isotope ages indicates that some of these veins apparently were conduits for seawater flow for extended periods of time and record shifting fluid compositions (from fluid- to rock-dominated; e.g., dropping Y/Ho, disappearing Ce anomalies). The drop in Ca/Sr and Mg/Ca may relate to the fact that the rates of growth of the carbonate veins in ocean crust is probably orders of magnitude slower that growth rates during the experimental calibration of Sr and Mg partitioning.

Reference:

Coggon, R. M., D. A. H. Teagle, et al. (2010), Reconstructing Past Seawater Mg/Ca and Sr/Ca from Mid-Ocean Ridge Flank Calcium Carbonate Veins. Science: science.1182252, Feb. 2010.

Constraints on the global cycle of ^{238}U/^{235}U

Janine Noordmann[1], Stefan Weyer[2], Mukul Sharma[3], R. Bastian Georg[4], S. Rausch[5], W. Bach[5]
[1]Institute of Geosciences, University of Frankfurt, Germany
[2]Institute of Mineralogy, University of Hannover, Germany
[3]Department of Earth Sciences, Dartmouth Collage, New Hampshire, USA
[4]Department of Earth Sciences, University of Oxford, UK
[5]Geosciences Department, University of Bremen, Germany

Recent studies observed ^{238}U/^{235}U isotope fractionation between oxic and anoxic oceanic environments, which may be used to constrain the oceanic U mass balance. However, U isotope fractionation during continental weathering and transport to the oceans, as well as during hydrothermal alteration (the second most important sink for U) is yet unknown (Stirling et al., 2007; Weyer et al., 2008). Previous mass balance considerations assumed only minor U isotope fractionation between the continental crust and rivers (the major U source to the ocean) and during hydrothermal alteration.

In this study, we have been analyzing water samples from rivers of different climatic conditions, e.g. Venezuela, India, Pakistan, Germany and three different rivers from Switzerland (grant 2000 20/101 780) to constrain the range of U isotope compositions of rivers. Additionally, we analyzed five different hydrothermal fluids from the Juan de Fuca Ridge (i.e. low-temperature and high-temperature fluids) and altered oceanic crust from the Bermuda Rise, Reykjanes Ridge and Pigafetta Basin to give a first estimate for the hydrothermal sink. Furthermore, ^{238}U has been measured for granites of different localities and ages to expand the very limited data set for samples from the continental crust.

The major rivers display in average a ^{238}U of -0.24 ‰ (against CRM-112A) which is very similar to the average value of the granites (^{238}U= -0.30 ‰) and to that of basalts (^{238}U= -0.28 ‰), indicating that in average only minor U isotope fractionation occurs during weathering and transport. This limited fractionation may be explained by an essentially quantitative transfer of the well soluble Uranyl complex during oxidative weathering from the eroded continental crust to the rivers. The hydrothermal waters display a tight range of ^{238}U (-0.32 and -0.54 ‰) around the seawater value of ^{238}U= -0.41 ‰ (Weyer et al., 2008), however, at much lower U concentration levels (0.08 to 0.24 ppb) compared to that of seawater (3.3 ppb, after Weyer et al., 2008). Also most of the analysed altered basalts have ^{238}U similar to that of fresh basalts (^{238}U= -0.42 to -0.23 ‰, with two exceptions: 0.18 and 0.31 ‰). Accordingly, removal of U from the ocean water during hydrothermal alteration of the oceanic crust appears not to result in significant U isotope fractionation in most cases.

References:
Weyer, S., Anbar, A. D., Gerdes, A., Gordon G., Algeo T., Boyle E. (2008) Natural fractionation of ^{238}U/^{235}U, *GCA*, **72**, 345-359
Stirling, C. H., Andersen, M. B., Potter, E.-K., Halliday, A. N. (2007) Low-temperature isotopic fractionation of uranium, *EPSL*, **264**, 208-225

Seawater derived REE+Y and HFSE systematics of Archean Banded Iron Formation (BIFs)

Sebastian Viehmann[1], J. Elis Hoffmann[1,2], Carsten Münker[2], Brian Alexander[3], Michael Bau[3]
[1] Universität Bonn, Steinmann Institut, Abt. Endogene Dynamik, Bonn, Germany (fumi@uni-bonn.de)
[2] Universität zu Köln, Geologisch-Mineralogisches Institut, Köln, Germany
[3] Jacobs Universität Bremen, School of Engineering & Science, Bremen, Germany

The trace element and isotope signatures of Banded Iron Formations (BIFs) can be used to place constraints on the Archean seawater composition [e.g., 1]. To evaluate the REE-Y and HFSE budget of early and late Archean seawater, we measured HFSE, Lu-Hf and Sm-Nd isotope compositions together with concentrations of other trace elements in ca. 3.7 Ga old BIFs from the Isua Greenstone Belt (SW Greenland) and ca. 2.7 Ga old BIFs from the Temagami Formation (Superior Province, Canada).

Chert and magnetite layers were separated and digested in Parr® bombs with HF-HNO_3-$HClO_4$ acid mixtures and Lu, Hf, Sm, Nd, Zr-Nb and Ta were separated by ion exchange column chemistry [2]. The HFSE were measured on a Finnigan Neptune MC-ICP-MS at the University of Bonn through applying isotope dilution techniques [2]. Due to the very low amounts of Lu and Hf in the splits from chert layers (Lu= 3-28 ng, Hf= 0.36-1.6 ng), sample-blank ratios were between 10 and 100. Typical amounts of Lu and Hf in magnetite layers were 5 to 22 ng Lu and 5 to 10 ng Hf, generally yielding sample blank ratios >100. Blank uncertainties were always included in error calculations. Aliquots of the same digestions were analysed by Quadrupole ICP-MS at Bremen for other trace elements.

Both the ca. 3.7 Ga Isua BIFs and the ca. 2.7 Ga Temagami BIFs exhibit typical seawater-like REE+Y patterns, consistent with previous studies [1,3]. The compositions indicate no or only minor contributions from crustal sources to the REE+Y budget. REE+Y patterns from both localities are similar in shape and total abundance. The PAAS normalized REE+Y concentrations in chert bands are generally one order of magnitude lower than in magnetite-rich layers (e.g., La_N for cherts $0.01 - 0.1$, for magnetite $0.04 - 0.7$). In contrast to modern seawater REE+Y patterns, the patterns exhibit no significant Ce-anomalies. The local Archean seawater must therefore have been at rather reduced conditions [1]. However, strongly positive Eu, Y, Gd anomalies are compareable to modern seawater.

In contrast to the REE+Y patterns, there are marked differences in HFSE systematics between the two Archean localities. The early Archean Isua BIFs are characterized by variable Zr (0.099 – 13.3 ppm), Hf (2.49 - 230 ppb), Nb (18.6- 210 ppb), and Ta concentrations(0.656 - 4.71 ppb). The late Archean Temagami BIFs generally show higher concentrations with strong vartiations in Zr (1.34 - 21.9 ppm), Hf (70.9 - 360 ppb), Nb (101 - 900 ppb), and Ta (9.97 - 52.3 ppb). As for REE+Y, concentrations of HFSE in chert-rich layers are in general one magnitude lower than in the magnetite-rich layers.

Ratios of Hf/Ta (1.93 - 94.8) and Nb/Ta (18.7 - 59.2) in early Archean Isua BIFs show a wider range in comparision to Hf/Ta (4.53 - 28.6) and Nb/Ta ratios (14.1 – 27.0) in the late Archean Temagami BIFs. The chert Isua BIF bands exhibit near chondritic to superchondritic Zr/Hf (31.3 - 58.0) ratios while magnetite-rich bands display all over superchrondritic Zr/Hf (44.9 – 53.8) ratios. Ratios of Zr/Hf in Temagami chert layers extend towards lower, subchondritic values (Zr/Hf=18.9 - 28.5) while magnetite bands display superchondritic ratios (Zr/Hf= 38.1 - 47.1). These patterns point towards a different behaviour of the HFSE in early Archean seawater if compared to late Archean seawater compositions.

^{176}Lu/^{176}Hf and ^{147}Sm/^{143}Nd isotope systematics indicate a disturbance of the Isua BIFs during amphibolite facies metamorphic events, resulting in extremely variable intial Hf(t) = -1242 to +905.4 and Nd(t) = -74.1 to +39.7 values at 3.71 Ga. In contrast, the less disturbed Temagami BIFs define an ^{176}Lu-^{176}Hf errorchron corresponding to an age of 2760±120 Ma (MSWD 0.49) and a ^{147}Sm-^{143}Nd isochron corresponding to an age of 2605 ± 140 (MSWD 2.1), both in agreement with the previously published age of 2736±3 Ma [4]. Initial Hf(t) and Nd(t) values for Temagami BIFs range from Hf(t) = +6.5 to +23.9 and from Nd(t) = +0.3 to +3.7, arguing for a decoupling of both isotope systems in the Archean seawater. In comparison with recent pacific seawater [e.g., 5], which shows Hf= +3.5 to +8.6 and Nd= -5.6 to -2.8 [5], we find a similar decoupling, but much less radiogenic values for Hf and Nd. The generally positive initial Hf(t) and Nd(t) compositions for Temagami confirm that there is little crustal contribution to the trace element composition of these BIFs. Altogether, the results of this study indicate there are differences between early and late Archean seawater composition in the HFSE inventory while the seawater-like REE+Y patterns for both localities are similar.

References:

[1] Bau M., Alexander B., 2009: *Distribution of high field strength elements (Y, Zr, REE, Hf, Ta, Th, U) in adjacent magnetite and chert bands and in reference standards FeR-3 and FeR-4 from the Temagami iron-formation, Canada, and the redox level of the Neoarchean ocean*. Precambrian Research 174, 337-346.

[2] Münker C., Weyer S., Scherer E., Mezger K., 2001: *Separation of high field strength elements (Nb, Ta, Zr, Hf): and Lu from rock samples for MC-ICPMS measurements.* Geochemistry Geophysics Geosystems 2

[3] Friend C.R.L., Nutman A.P., Bennett V.C., Norman M.D., 2007: *Seawater-like trace element signatures (REE+Y) of Eoarchaean chemical sedimentary rocks from southern West Greenland, and their corruption during high-grade metamorphism*. Contrib. Mineral Petrol, 229- 246

[4] Bowins R.J., Heaman L.M., 1991: *Age and timing of igneous activity in the Temagami greenstone belt, Ontario: a preliminary report*. Can. J. Earth Sci. 28, 1873–1876.

[5] Zimmermann B., Porcelli D., Frank M., Rickli J., Lee D.-C., Halliday A.N., 2008: *The hafnium isotope composition of Pacific Ocean water*. Geochim. et Cosmochim. Acta 73, 91-101

Section 13

———

Ion Microprobe characterization of geo-materials

Novel and unique applications of large-geometry secondary ionization mass spectrometry (SIMS)

Martin J. Whitehouse[1]
[1]Swedish Museum of Natural History, Stockholm, Sweden

The present generation of large-geometry secondary ionization mass spectrometers (or ion microprobes) remain unrivalled tools in high-spatial resolution, high sensitivity isotope and trace element analysis of geological material. This keynote address will highlight a number of technical innovations implemented on the recently upgraded IMS1280 (formerly IMS1270) instrument at the Nordsim facility in Stockholm as a means of demonstrating what can now be achieved with a state-of-the-art SIMS instrument.

High-precision (e.g. to <0.2 ‰, 1SD) stable isotope ratio measurement (e.g. C, O, S) has been routine for several years since the advent of multicollector (multiple Faraday cup) capability. Addition of a nuclear magnetic resonance field regulator effectively "locks" the magnetic field in static multicollector measurements, permitting use of much narrower peak flats which allows a wider entrance slit and hence higher transmission. The most obvious benefits of this are higher count rates from a similarly sized analytical volume or similar count rates from a smaller spot. Applied to sulphur isotopes, the least abundant ^{36}S isotope which, like ^{33}S, is subject to mass independent fractionation may be analysed at high count rate in an electron multiplier simultaneously with ^{32}S, ^{33}S and ^{34}S in Faraday detectors.

Scanning ion imaging has been a unique feature of the Cameca instruments for many years. Recently implemented multicollector ion imaging better utilises the duty cycle of the instrument compared to peak-hopping mode into a single detector and can yield isotope ratio information at comparable precision to spot analysis on a user-defined area. Examples using both Pb and Hf isotopes in zircon will be presented that highlight this technique. Additionally, applications that utilize the three low-mass detectors in tandem with the axial direct (micro-channel plate) imaging system in order to locate targets in a complex matrix such as lunar regolith will be presented.

The unique capability of SIMS for light stable isotopes together with its low depth penetration (essential "micro-destructive") mean that the new SIMS instruments will continue to be essential in situ high spatial resolution geoscience applications long into the future.

Model compounds of artificial soils characterized by NanoSIMS 50L

Carmen Höschen[1], Galina Moutchnik[1], Carsten W. Mueller[1], Katja Heister[1], Ingrid Kögel-Knabner[1]
[1]Lehrstuhl für Bodenkunde, Department für Ökologie und Ökosystemmanagement, TU München, Freising-Weihenstephan, Germany

Clay minerals, iron and aluminium (hydr)oxides are considered as major components controlling the formation of soil interfaces and aggregates which are relevant for the sorption of organic matter. These functions of soils are intimately linked to the heterogeneous three-dimensional structure and its unique and specific properties. In this context the formation and dynamics of microaggregates (<250μm) play a crucial role. Due to their small size, the characterization of the architecture and the investigation of the functions of microaggregates are limited by the availability of techniques operative at the microscale and progressively smaller scales. The fact that many processes playing a significant role in soils are happening at low spatial scales and concentrations requires a proper technique which allows answers to the still outstanding questions.

The, in terms of soil science, revolutionary nano-scaled secondary ion mass spectrometer NanoSIMS 50L which enables multi-isotopic investigations (up to seven ion species simultaneously) at high spatial resolution and high sensitivity seems to provide the technique of choice. As own previous studies showed, by the use of the NanoSIMS 50 we were able to study important soil functions and in situ spatial organo-mineral assemblages at a submicron scale, which were never resolved before in soil science (Mueller C. W. et al.).

The formation of microaggregates structures was studied using artificial soils differing in amounts of organic matter, clay minerals and pedogenic oxides.

We present the potentials of this new technique for the study of model compounds (clay minerals, iron and aluminium (hydr)oxides) representing main constituents of the artificial soils.

We discuss some of the most recent results obtained with the NanoSIMS 50L instrument at the Lehrstuhl für Bodenkunde, TU München, Freising-Weihenstephan during the first months of operation.

Reference:
Mueller, C. W. et al., Submicron scale imaging of soil organic matter dynamics using NanoSIMS-from single particles to intact aggregates, Organic Geochemistry, 2010, under review

Trace element and isotopic zoning patterns in phengite and sodic amphibole from blueschist-facies rocks as tracers for fluid-rock interactions in subduction zones

Matthias Konrad-Schmolke[1], Thomas Zack[2], Horst Marschall[3] and Michael Wiedenbeck[4]
[1]Universität Potsdam
[2]Universität Mainz
[3]University of Bristol
[4]GeoForschungsZentrum Potsdam

Phengite and sodic amphibole grains in weakly deformed felsic and basic high-pressure rocks throughout the internal Sesia-Lanzo Zone (SLZ; Western Alps) have pronounced compositional zonations with respect to major and trace elements. Amphibole and phengite grains show a distinct increase in Fe^{2+} content associated with a Mg decrease. Chemical modification of the mineral grains is visible in high contrast back scattered electron images, occurs along grain boundaries, fractures and other fluid pathways and is often restricted to clearly separated narrow zones with step-like compositional gradients towards the pristine cores of the grains. In contrast, analogous mylonitic samples of the same rock types show compositionally homogeneous phases and well-equilibrated textures. Thermodynamic forward models show that the observed compositional trends in amphibole and phengite are the result of influx of a hydrous fluid phase at around 1.3 GPa during the exhumation of the SLZ on top of a subducted oceanic slab. Compositional and textural differences between weakly deformed and mylonitic samples are the result of different fluid flux intensities within and around a large-scale blueschist-facies shear zone.

The trace element zoning patterns differ between phengite and amphiboles in the weakly deformed samples. Whereas phengite rims have lower concentrations of B, Pb, Sr, Li, and Be with respect to the cores, sodic amphiboles show lower B, Pb and Sr, but higher Li and Be concentrations in the rims than in the cores. Again, thermodynamic and trace element forward models indicate that differences in Li, Be and B trends can be explained by differences in fluid influx intensity, whereas Pb and Sr concentrations are controlled by the retrograde formation of epidote in our samples. Increasing Li and Be concentrations in sodic amphibole rims are the result of a rehydration-induced internal redistribution of these elements between consumed omphacite and newly precipitated sodic amphibole overgrowth zones. In contrast, decreasing concentrations of Li, Be and B in phengite rims can only be modeled assuming a significant leaching effect by a free fluid phase percolating through the rock volume. Interestingly, amphibole as well as phengite in the mylonitic samples do not show core-rim differences with respect to the investigated trace elements and have much lower trace element contents compared to the weakly deformed samples supporting the interpretation of a fluid-induced trace element leaching during large-scale shearing.

Ion microprobe measurements of $\delta^{11}B$ values in the compositionally zoned phengites from weakly deformed samples yielded a consistent pattern with lower core values between -20 and -10 ‰ and higher rim values between -10 and 0 ‰ consistent with the assumption of equilibration with an externally derived fluid. Corroborating this interpretation is the observation that phengites in the mylonitic samples are unzoned with respect to the B isotopic composition with $\delta^{11}B$ values between 0 and +5 ‰. Overprinted areas of phengite and sodic amphibole also yielded consistently lower δD values than the relic cores, further supporting an influx of external fluid.

All of the above observations demonstrate that in-situ measurements of Li, Be and B concentrations as well as B and H isotopes in metamorphic minerals are excellently suited for tracing fluid-rock interaction and, if combined with thermodynamic and trace element forward models, yield detailed quantitative insight into the trace element redistribution during metamorphic and metasomatic events.

The contamination of mid-ocean ridge basalts – processes and timing as deduced from δ^{11}B

Nicole A. Stroncik[1], Marc-Sebastian Krienitz and Michael Wiedenbeck[1]
[1]Helmholtz-Zentrum Potsdam Deutsches GeoForschungsZentrum-GFZ, Potsdam, Germany

Mid-ocean ridges are one of the key features responsible for mass and thermal fluxing between the Earth's interior and its surface. Some 20 km^3 of oceanic crust, average 6 km in thickness, are generated annually from the 60,000 km long global mid-ocean ridge network. Magmatic processes operating at mid-ocean ridges are important both for crustal accretion and in supplying heat to drive hydrothermal circulation. These two factors are key features in geochemical dynamics, as the composition of oceanic crust is determined not only by mantle melting and fractional crystallisation but also by magma contamination processes.

The nature, location and origin of these contamination processes continue to be debated. Contaminations with a brine phase or seawater during magma ascent or the assimilation of altered oceanic crust at shallow levels have both been proposed as possible mechanisms. To elucidate this phenomenon we have used SIMS to determine δ11B values, in conjunction with Ne and Ar isotopes and Cl and K concentrations, of fresh, basaltic glasses from the Pacific-Antarctic Rise between 37 and 42°S. Very high Cl/K ratios (up to 1.87) of the analysed glasses show that magmatic contamination along the PAR is the rule rather than the exception. The δ^{11}B signature of these glasses ranges between 1.3 (± 0.9; 1s; n=3) and -13.4 (± 0.2; 1s; n=2), indicating that contamination must have taken place at variable, relatively deep depth levels, as otherwise such glasses should be more enriched in ^{11}B from seawater and oceanic crust affected by low temperature alteration characterised by high δ^{11}B values. Further support for this conclusion is the high isotopic ^{20}Ne/^{22}Ne and ^{40}Ar/^{36}Ar ratios as compared to air demonstrating that neither seawater nor a brine phase could have served as the contaminant for the investigated magmas.

SIMS Analyses of Carbon Isotopes in Moissanite (SiC) from Ophiolites: A Light Carbon Reservoir in the Earth's Lower Mantle?

Robert B. Trumbull[1], Jing-Sui Yang[2], Paul T. Robinson[1,3], Michael Wiedenbeck[1]

[1] Deutches GeoforschungsZentrum GFZ, Potsdam, Germany

[2] Key Laboratory for Continental Dynamics, Institute of Geology, Chinese Academy of Sciences, Beijing, China

[3] Department of Earth Sciences, Dalhousie University, Halifax, Nova Scotia, Canada

Moissanite (natural SiC) is a widespread accessory mineral in diamondiferous kimberlites and it has now also been discovered in chromitites from several ophiolite complexes worldwide, including Luobusa and Donqiao in Tibet, Semail in Oman, and Ray-Iz in the Polar Urals (Trumbull et al., 2009). The occurrence of moissanite in the earth's mantle implies at least locally extremely low redox conditions, which is supported by the common inclusions of native Si and Fe-Si alloys ($FeSi_2$, Fe_3Si_7) in the moissanite grains. To better understand the origin of SiC in the mantle we have analyzed the carbon isotope composition of grains from the above-mentioned ophiolite complexes at the Potsdam SIMS laboratory.

The SIMS analyses of single grains and grain fragments of ophiolite-hosted moissanite revealed ubiquitous and distinctive ^{13}C-depleted isotopic composition (^{13}C from -18 to -35 ‰, n= 36), which is much lighter than the main carbon reservoir in the upper mantle (^{13}C near -5‰) and agrees with published data from moisssanite of the kimberlite association. isotopic composition . The implication is that either moissanite formation involves a rather uniform, isotopically light carbon reservoir in the mantle or formation involved strong isotopic fractionation from "normal" mantle carbon. However, the magnitude of fractionation needed to explain the moissanite compositions appears prohibitively large considering the high temperatures involved. Subducted biogenic carbon has been suggested as a source (Mathez et al., 1995) and this scenario might also satisfy the unusual low redox constraints on moissanite formation. This material would need to stay chemically isolated from the upper mantle until it reached the high-T stability field of moissanite, which would seem a difficult condition to meet and perhaps unlikely.

The origin of moissanite in the mantle is still unsolved and more than one mode of formation is possible. All evidence from upper mantle materials and relevant experimental studies indicates that SiC cannot have formed there, barring special and local redox conditions. We suggest that the widespread occurrence of moissanite argues against special and local processes. Instead, the SiC may have formed in the lower mantle, tapping an indigenous reservoir of ^{13}C-depleted carbon that may be of primordial origin. Support for the existence of such a reservoir comes from the prevalence of light carbon in the solar system (Grady et al., 2004; Hashizume et al., 2004)

References:

Grady, M.M. et al. (2004) Magmatic carbon in Martian meteorites: attempts to constrain the carbon cycle on Mars, International Journal of Astrobiology, 3, 117-124.

Hashizume et al. (2004) Protosolar carbon isotopic composition: implications for the origin of meteoritic organics, The Astrophysical Journal, 600, 480-484.

Mathez, E.A. et al., (1995) Carbon isotope composition and origin of SiC from kimberlites of Yakutia, Russia, Geochimica et Cosmochimica Acta 59, 781-791.

Trumbull, R.B. et al. (2009) The carbon isotope composition of natural SiC (moissanite) from the Earth's mantle. New discoveries from ophiolites, Lithos, 113, 612-620.

IMS 1280-HR, an improved model of ultra high sensitive and precise SIMS

H.-U. Ehrke[1], P. Peres[2], F. Fernandes[2], E. De Chambost[2], P. Saliot[2] and M.Schuhmacher[2]
[1]Cameca GmbH, Carl-von-Linde-Str. 42, 85716 Unterschleissheim, Germany
[2]Cameca SA, 29 Quai des Gresillons, 92622 Gennevilliers, France

Secondary Ion Mass Spectrometry (SIMS) technique provides direct *in situ* measurement of elemental and isotopic composition in selected μm-size areas of the sample. The CAMECA IMS 1280 is an ultra high sensitivity ion microprobe that delivers unequalled analytical performance for a wide range of SIMS applications: isotope ratio measurements [1], geochronology applications like U-Pb dating in Zircon [2] and trace element analyses [3]. In order to optimize the performance at high mass resolution conditions, both in monocollection and multicollection modes, a new model of the CAMECA IMS 1280 is introduced: the IMS 1280-HR.

Main targeted applications are the K/Ca and Rb/Sr dating, in monocollection mode at Mass Resolving Power (MRP) > 20,000, as well as Mg and metal isotope analysis in multicollection mode at MRP > 5,000.

The IMS 1280-HR combines the well-proven features of the standard IMS 1280 with new developments oriented towards high mass resolution / high transmission capabilities:

1) Redesign of the coupling section, implementation of a new hexapole that completely cancels second order aberrations, which are known to limit the MRP capabilities

2) Modification of the magnet pole piece boundary in order to minimize the off-axis aberrations and improve the peak shape in multicollection mode

3) Low noise electronics, new Hall probe and associated pre-amplifiers for an improved magnetic field stability

4) Magnet flight tube with new baking system for a better abundance sensitivity.

Data obtained on a prototype will be presented. Transmission tests performed for the 40K in Adularia sample showed a transmission of > 100 cps/ppm/nA at a MRP (10%) of 34,000 in monocollection mode.

In multicollection mode, a reproducibility of < 0.3‰ (1σ) could be obtained for the 25Mg and 26Mg ratios measured at MRP (10%) > 6, 800 in Olivine San Carlos.

References:
[1] F.Z. Page *et al*. (2007), *Ame. Min.* **92**, 1772.
[2] G. Srinivasan *et al*. (2007), *Science* **317**, 345.
[3] T. M. Harrison *et al*. (2007), *EPSL* **261**, 9

Section 14

_____

Magmatic processes

Tracing core material and recycled oceanic crust in the La Palma mantle source using combined radiogenic W isotope and stable Mo isotope data

<u>Matthias Willbold</u>[1], Tim Elliott[1], Corey Archer[1]
[1]University of Bristol, Department of Earth Sciences, Bristol, United Kingdom

Deep recycling and long-term storage of oceanic and continental lithosphere through the mantle has long been sought to reconcile the fate of subducting plates and the compositional variations seen in plume-related ocean island basalts. Radiogenic isotopes have so far been the prime geochemical tools to investigate this question. However, neither the age nor the location of parent-daughter fractionation is known making these systems severely model dependent. More recently, trace elemental constraints in ocean island basalts have been utilized to better constrain the mantle additives involved in the formation of enriched mantle (EM) basalts. In particular, it has been shown that combined trace element and radiogenic isotope data have great potential in characterising the presence of different amounts of recycled upper and lower continental crust in some of the EM-type sources (Willbold & Stracke, 2010). However, while these results, in conjunction with many previous studies (e.g. Marcantonio et al., 1995; Stracke et al., 2003), imply that recycled oceanic crust must be present in the mantle sources of ocean island basalts direct evidence is missing. In fact, the role of recycled oceanic crust in the formation of oceanic basalts has been questioned (Niu & O'Hara, 2003).

In addition to invoking surficial materials recycled back into the mantle, enrichment of ^{187}Os and ^{186}Os in some plume-related ocean island basalts have been interpreted in terms of chemical interaction between the Earth's core and mantle (Walker et al., 1997). Yet, radiogenic Os isotopes can also be produced by the recycling and long-term storage of Fe-Mn crusts (Scherstén et al., 2004). These seawater precipitates are highly enriched in platinum-group elements compared to the mantle and would thus dominate the Os isotopes in the sources of oceanic basalts. In this study we used radiogenic ^{182}W (expressed as ε^{182}W) and stable Mo (expressed as δ^{98}Mo) isotope measurements on a series of basalts from La Palma to further explore the role of core contribution and recycling of oceanic crust in the formation of ocean island basalts. Owing to the short half-life of the parent nuclide ^{182}Hf (ca. 9 Ma) significant differences in ε^{182}W are only expected to exist between the Earth's core and bulk silicate Earth making this isotope system ideal to investigate core-mantle interaction (Scherstén et al., 2004). Similarly, stable Mo isotopes are only fractionated in low-temperature environments such as during seawater alteration of oceanic crust or precipitation of Mn-Fe crusts (Anbar, 2004) and thus will provide important clues about the presence of these components in ocean island basalts.

Despite having very radiogenic Os isotopes (Marcantonio et al., 1995), the average ε^{182}W value of the La Palma basalts (0.06 ± 0.08; 2σ; N = 4) is indistinguishable from that of bulk silicate Earth in keeping with measurements from Hawaii (Scherstén et al., 2004). Our data therefore preclude a core contribution to the La Palma mantle source. However, the samples show negative δ^{98}Mo values (-0.01 to -0.35‰) well beyond the reproducibility of our method (0.07‰; 2σ). Such negative values are unlike those found in other oceanic basalts with unradiogenic Os isotope ratios (δ^{98}Mo > 0‰). This suggests that a striking low-δ^{98}Mo component must be present in the mantle source of La Palma. So far, negative δ^{98}Mo values have only been identified in Fe-Mn crusts and associated pelagic sediments (δ^{98}Mo < -0.25‰; Anbar, 2004). We therefore suggest that the low δ^{98}Mo values and the radiogenic Os isotopes in the La Palma samples were caused by recycling and long-term storage of oceanic crust that was impregnated by Fe-Mn precipitates during seawater alteration on the seafloor.

References:
Anbar, A.D. (2004), Molybdenum stable isotopes: observations, interpretations and directions. Reviews in Mineralogy and Geochemistry 55, 429-454.
Marcantonio, F., Zindler, A., Elliott, T. & Staudigel, H. (1995), Os isotope systematics of La Palma, Canary Islands: Evidence for recycled crust in the mantle source of HIMU ocean islands. Earth and Planetary Science Letters 133, 397-410.
Niu, Y. & O'Hara, M.J. (2003), Origin of ocean island basalts: A new perspective from petrology, geochemistry, and mineral physics consideration. Journal of Geophysical Research 108, Paper number 2002JB002048.
Scherstén, A., Elliott, T., Hawkesworth, C. & Norman, M. (2004), Tungsten isotopic evidence that mantle plumes contain no contributions from the Earth's core. Nature 427, 234-237.
Stracke, A., Bizimis, M. & Salters, V.J.M. (2003), Recycling oceanic crust: Quantitative constraints. Geochemistry Geophysics Geosystems 4, Paper number 2001GC000223.
Walker, R.J., Morgan, J.W., Beary, E.S., Smoliar, M.I., Czamanske, G.K. & Horan, M.F. (1997), Applications of the ^{190}Pt-^{186}Os isotope system to geochemistry and cosmochemistry. Geochimica et Cosmochimica Acta 61, 4799-4807.

Willbold, M. & Stracke, A. (2010), Formation of enriched mantle components by recycling of upper and lower continental crust. Chemical Geology, in press.

Partitioning of Ba, La, and Y between haplogranitic melts and aqueous fluids: in-situ vs. ex-situ analysis

Manuela Borchert (presenting author)[1], Max Wilke[2], Christian Schmidt[2], Jean Cauzid[3]
[1]Hamburger Synchrotronstrahlungslabor HASYLAB at Deutsches Elektronen-Synchrotron DESY, Hamburg, Germany
[2]Helmholtzzentrum Potsdam Deutsches GeoForschungsZentrum (GFZ), Telegrafenberg, Potsdam, Germany
[3]G2R, Nancy-Université, CNRS, BP 70239, 54506 Vandœuvre-lés-Nancy, France

The present knowledge on fluid-melt partitioning of barium, lanthanum, and yttrium is only fragmentary, and available data are inconsistent. For example, experimental studies suggest a preference of the REE and particularly yttrium for the fluid at high salinities, but available results from natural cogenetic fluid and melt inclusions in granites show partition coefficient ($D^{f/m}$) distinctly smaller than one.

Here, we performed partitioning experiments between fluid-saturated haplogranitic melts and aqueous solutions at 750 to 950°C and 0.2 to 1 GPa to investigate the effects of melt and fluid composition, pressure and temperature. Partition coefficients of Ba, La, and Y were determined using different experimental and analytical approaches to evaluate if the 'quench effect' can explain the inconsistency of available data. On the one hand conventional quenched experiments were performed, and on the other hand, trace element contents in the aqueous fluid were determined directly at elevated temperatures and pressures using a hydrothermal diamond-anvil cell and synchrotron radiation X-ray fluorescence microanalysis of K-lines. The latter required a high excitation energy of 50 keV due to the high energies necessary to excite K-lines of these elements. Furthermore, a small spot size is of advantage to avoid mixed analyses of fluid and melt. Both, a high excitation energy and a small beam size, were achieved for the first time via application of a new Kirkpatrick-Baez mirror at beamline ID 22 (ESRF, France).

For barium, fluid-melt partition coefficients from quenched and in-situ experiments are in good agreement for experiments with peraluminous melts and chloridic solutions. If water was used as starting fluid, partitioning data from quenched experiments are one to two orders of magnitude lower than comparable in-situ results. For metaluminous compositions, quenched experiments show up to one magnitude higher $D^{f/m}_{Ba}$ than comparable in-situ runs with similar fluid salinities and pressures Altogether, the data for Ba from both techniques show qualitative agreement, i.e., melt compatible behavior (D<1) for all melt and fluid compositions, even at high fluid salinities.

For lanthanum and yttrium, the concentrations in the quenched solutions after the run were below detection limit in experiments using H_2O as starting fluid. Therefore, no partition coefficients could be obtained that could be compared to in-situ data. For chloridic fluids, La partition coefficients from both techniques are in relatively good agreement and show a melt compatible behavior at all studied fluid salinities. The observed maximum fluid-melt partition coefficient of La is associated with high salinities, high pressures, or both, and scatters around 0.1. Results for metaluminous and peraluminous melts are similar for in-situ experiments, but quite different for quenched experiments. For yttrium, the in-situ data represent maximum partition coefficients, and are also associated with a substantial error due to Y contents in the fluid that are close to detection limit. Therefore, it remains unclear if there is a quench effect. Nevertheless, in-situ and quenched data are roughly similar, and show always a preference for the melt.

In summary, the comparison of partitioning data determined with in-situ analysis of trace element contents in fluids at elevated PT conditions to those from quenched experiments proves that the fluids change their trace element signature upon cooling ('quench effect'). We suggest that the observed quench effect is most likely due to back reactions between fluid and melt during cooling rather than precipitation of phases during the quench because the latter was not observed in our experiments.

Reference:
Borchert et al. (accepted): Partitioning of Ba, La, Yb, and Y between haplogranitic melts and aqueous solutions: an experimental study. Chemical Geology

Archean TTG formation and early intracrustal differentiation inferred from HFSE systematics

J. Elis Hoffmann[1,2], Carsten Münker[2], Tomas Næraa[3,4], Minik T. Rosing[3], Adam A. Garde[4], Dieter Garbe-Schönberg[5]

[1] Universität Bonn, Steimann Institut, Abt. Endogene Prozesse, Bonn, Germany (hoffjoel@uni-bonn.de)
[2] Universität zu Köln, Geologisch-Mineralogisches Institut, Köln, Germany
[3] Nordic Center for Earth Evolution, Natural History Museum of Denmark, Copenhagen, Denmark
[4] Geological Survey of Denmark and Greenland, Copenhagen, Denmark
[5] Universität Kiel, Institut für Geowissenschaften, Kiel, Germany

The geodynamic setting as well as the melting depths of the Archean tonalite-trondhjemite-granodiorite (TTG) suite are still subject of controversial debates (Foley et al., 2002; Rapp et al., 2003). Most studies conclude that TTGs formed by partial melting of hydrous mafic crust, either as slab-melts in a subduction environment or by melting of thickened mafic crust. Moreover, it is debated, if melting occurred in the stability field of rutile-eclogite, garnet-amphibolite or amphibolite (Foley et al., 2002; Rapp et al., 2003). High-field-strength-element (HFSE) and other trace element ratios of TTGs can be applied to distinguish between these source mineralogies because of their different partitioning behaviour into residual mineral phases such as Ti-phases (e.g. rutile, ilmenite), garnet, amphibole and clinopyroxene. Whereas the presence of residual rutile increases Nb/Ta ratios, the presence of amphibole lowers this ratio.

Following this approach, we measured concentrations of HFSE (Nb, Ta, Zr, Hf), Sm, Nd and Lu in 2.80 to 3.85 Ga old TTGs and related crustal rocks from SW-Greenland, Canada and India by MC-ICP-MS, applying isotope dilution (Münker et al., 2001). In combination, we also measured concentrations of major and other trace elements by XRF and quadrole ICP-MS. For the purpose of distinguishing truly juvenile TTGs from intra-crustal differentiates, the isotope compositions of Hf and Nd were also measured.

The TTGs have low Ni (2-9 ppm) and Cr concentrations (7-16 ppm) and low Mg# (35-49). Intial Hf(t) values for the pristine early Archean TTGs range from near to chondritic to +2.3 and for the meso to late Archean TTGs up to +4.5. Initial Nd$_{(t)}$ values for the pristine early Archean TTGs range from -0.9 to +4.0 and for the meso to late Archean TTGs from +0.1 to +2.5. Pristine, juvenile TTGs with Hf$_{(t)}$ and Nd$_{(t)}$ values >0 exhibit Nb/Ta ranging from 7 to 27. Even higher Nb/Ta (up to 42) were obtained for migmatitic TTGs and intra-crustal differentiates. For the pristine TTGs, positive correlations between Nb/Ta and La/Yb, Gd/Yb, Zr/Sm, Zr/Nb and Sr/Y are observed. For the pristine early Archean TTGs Nb/Ta are correlated with intial Hf(t) values. For the meso to late Archean samples, however, this co-variation between Nb/Ta and Hf(t) is not observed.

To illustrate the influence of variable source compositions at different P/T conditions on the trace element inventory of TTGs, trace element compositions of melts from three residual mineralogies (rutile-eclogite, garnet-amphibolite, amphibolite) were modeled, employing batch-melting calculations on a representative early Archean tholeite. Non of the modeled partial melting trends can explain the whole observed compositional variability in HFSE and REE ratios of the TTGs. However, the observed variability can be explained by mixing of melts generated at different depths, including both the stability field of garnet-amphibolite and rutile-eclogite. In addition to this observation, a successful petrogenetic model also has to account for the co-occurrence of high- and low Nb/Ta TTGs within the same geologic terrane and for the systematic co-variation between Nb/Ta and Hf$_{(t)}$ values in early Archean TTGs. Altogether these features are best explained by a model where TTG melting occured at progressively increasing pressures in a tectonically thickening mafic crust. Such a model is also supported by low Ni and Cr concentrations and low Mg# indicating a lack of interaction with mantle wedge peridotite. The high Nb/Ta obtained for the migmatitic TTGs and for the intra-crustal differentiates are best explained by further fractionation of Nb from Ta during fluid infiltration, partial melting and migmatisation.

References:
Foley S., Tiepolo M. and Vanucci R. (2002), Growth of early continental crust controlled by melting of amphibolite in subduction zones. Nature 417, 837-840
Münker C., Weyer S., Scherer E., and Mezger K. (2001), Separation of high field strength elements (Nb, Ta, Zr, Hf): and Lu from rock samples for MC-ICPMS measurements. Geochem. Geophys. Geosys. 2 (G3) paper number 10.1029/2001GC000183
Rapp R.P., Shimizu N. and Norman M.D. (2003), Growth of early continental crust by partial melting of eclogite. Nature 425, 605-609

Thermobarometric investigations of lavas from the Quaternary Emmelberg volcano (West Eifel)

Matthias Gothieu[1], Andreas Klügel[1]
[1]Universität Bremen, Fachbereich Geowissenschaften, Bremen, Germany

The well exposed scoria cone of Emmelberg volcano near Üdersdorf (West Eifel) features a pyroclastic sequence consisting of a basal phreatomagmatic unit and different magmatic units capped by welded bombs and agglutinates. The deposits are associated with two or three eruptive centers, where agglutinate beds marking former crater walls indicate a syn-eruptive northward migration of the main vent. The erupted lavas are olivine nephelinites (9.2-11.1 wt% MgO, 124-175 ppm Ni, 359-455 ppm Cr) with olivine (7-10 %) and clinopyroxene (3-5 %) phenocrysts; reversely zoned olivines and green-core clinopyroxenes are common. There are no systematic compositional changes across the entire eruptive sequence exposed; the geochemical variations appear rather random and largely reflect mildly varying amounts of phenocrysts.

In order to infer the pressures of crystal fractionation before eruption, we have applied the clinopyroxene-melt thermobarometer of Putirka et al. (2003) to clinopyroxene rim and matrix compositions. Because even quenched samples show abundant late-grown microlites, no glass representing the intratelluric melts was available for analysis. We thus calculated the melt composition by a least-squares approach combining (1) subtraction of phenocryts compositions from whole-rock analyses and (2) addition of microlite compositions to matrix glass analyses. Following the saturation surface model of Putirka (1999), the calculated melt is in fair chemical equilibrium with the analyzed clinopyroxenes. Curiously, the analyzed matrix glass appears to be closer to equilibrium with the clinopyroxene rims than does the calculated melt, even though this is petrologically not resonable. This discrepancy may reflect the highly undersaturated olivine nephelinites being not well represented by the calibration data for the Putirka (1999) model.

Calculated pressures for 29 phenocrysts range from 630 to 830 MPa (average 720 MPa), and temperatures from 1155 to 1195 °C (average 1180 °C), which we interpret as P-T conditions of magma storage prior to eruption. If the analyzed matrix glass rather than the calculated melt composition is used, the pressure range shifts to 430-680 MPa (average 560 MPa). This difference is significant but is within the standard error of estimate (170 MPa) for the thermobarometer. The calculated pressures overlap remarkably well with pressure estimates of 600-700 MPa for CO_2-rich fluid inclusions in crustal xenoliths in lavas from Kempenich (East Eifel) that were interpreted to reflect the presence of magma reservoirs at 22-25 km depth, in the lower crust near the Conrad discontinuity (Sachs and Hansteen, 2000). Our data also agree with pressure estimates for the nearby Gemündener Maar (Shaw, 2004) and with a generalized model for the evolution of olivine nephelinites from the West Eifel (Duda and Schmincke, 1985).

We conclude that final storage and crystal fractionation of the Emmelberg lavas took place in a magma reservoir near the Conrad discontinuity, which is consistent with their relatively evolved character compared to other olivine nephelinites and basanites from the West Eifel (ONB suite; Mertes and Schmincke, 1985) and with the complete lack of peridotite xenoliths from the upper mantle. Reverse phenocryst zonations indicate a late magma mixing event that may have triggered the eruption.

References:
Duda, A. & Schmincke, H.U. (1985), Polybaric differentiation of alkali basalt magmas: evidence from green-core clinopyroxenes (Eifel, FRG), Contrib. Mineral. Petrol. 91, 340-353
Mertes, H. & Schmincke, H.U. (1985), Mafic potassic lavas of the Quaternary West Eifel volcanic field, Contrib. Mineral. Petrol. 89, 330-345
Putirka, K. (1999), Clinopyroxene + liquid equilibria to 100 kbar and 2450 K, Contrib. Mineral. Petrol. 135, 151-163
Putirka, K.D., Mikaelian, H., Ryerson, F. & Shaw, H. (2003), New clinopyroxene-liquid thermobarometers for mafic, evolved, and volatile-bearing lava compositions, with applications to lavas from Tibet and the Snake River Plain, Idaho, Am. Mineral. 88, 1542-1554
Sachs, P.M. & Hansteen, T.H. (2000), Pleistocene underplating and metasomatism of the lower continental crust: a xenolith study, J. Petrol. 41, 331-356
Shaw, C.S.J. (2004), The temporal evolution of three magmatic systems in the West Eifel volcanic field, Germany, J. Volcanol. Geotherm. Res. 131, 213-240

Off-axis seamounts along the East Pacific Rise – inferences on melt extraction and source heterogeneities in the upper mantle

Philipp Brandl[1], Christoph Beier[1], Marcel Regelous[1], Karsten M. Haase[1], Wafa Abouchami[2], and C.-Dieter Garbe-Schönberg[3]

[1]GeoZentrum Nordbayern, Friedrich-Alexander-Universität Erlangen-Nürnberg, Erlangen, Germany
[2]Max-Planck-Insitut für Chemie, Mainz, Germany
[3]Christian-Albrechts-Universität Kiel, Institut für Geowissenschaften, Kiel, Germany

Seismic studies have shown that beneath the fast-spreading East Pacific Rise (EPR), melt is produced over a wide region of the mantle, yet most flows are apparently emplaced within a few km of the ridge axis. Magma mixing during melt migration and focussing within the mantle and crust homogenise melt compositions, with the result that it is difficult to infer melting processes and the role of mantle heterogeneity from geochemical studies of axial lavas alone. Lavas emplaced on off-axis seamounts, away from the main magma plumbing system, typically have more variable compositions, and provide a clearer picture of the scale and origin of mantle heterogeneity.

Seamount 6 is a small volcano (~60 km^3) located about 180 km east of the EPR at 12° 45' N. The seamount erupted on crust younger than 1 Ma and therefore within 45 km distance from the ridge axis, but outside the neovolcanic zone as indicated by paleomagnetic data (Honda *et al.*, 1987). Previous geochemical studies (e.g. Batiza & Vanko, 1984, Zindler *et al.*, 1984) have shown that lavas from this seamount have variable chemical and isotopic compositions.

We present new major and trace element analyses and high-precision radiogenic isotope data for Seamount 6 lavas, which confirm their extreme variability. Lavas range from MOR-like tholeiites to OIB-like alkalibasalts. The large range in incompatible trace element concentrations (e.g. Nb 6 to 56 ppm) and ratios (e.g. Nb/Zr 0.08 to 0.18) with a limited range in Mg# from 71 to 50 cannot be generated by fractional crystallisation or partial melting processes from a single source composition. This is confirmed by isotope data; for example, the range in $^{206}Pb/^{204}Pb$ is greater than observed in axial lavas from the entire northern EPR. Most samples have enriched trace element and isotope compositions relative to average MORB from the adjacent EPR, indicating that these seamount lavas cannot simply represent near-instantaneous melts which aggregated to form average axial lavas. Instead, the seamount lavas likely result from small degrees of melting beneath the ridge flanks, which preferential samples an enriched, relatively fertile mantle component.

Correlations between Sr-Nd-Pb isotope ratios, incompatible trace element ratios and major and trace element concentrations indicate that magma mixing, between an enriched endmember with high La/Sm, Nb/Zr, $^{87}Sr/^{86}Sr$, low $^{143}Nd/^{144}Nd$, and a depleted endmember with a composition similar to N-MORB, must have occurred shortly before eruption. We show that mixing of melts derived by variable degrees of dynamic melting of an incompatible element depleted peridotite and an enriched, garnet-bearing pyroxenite can explain the large chemical and isotopic variation within lavas from Seamount 6. Our data highlight the range in compositions that must exist on the <10 km scale in the upper mantle even far from active hotspots, and which is not evident in lavas from the adjacent ridge axis where more extensive mixing within the magma plumbing system homogenises melt compositions to a much greater degree. An important implication of our results is that melting models which attempt to constrain the depth and degree of melting beneath mid-ocean ridges based on trace element variations in MORB (e.g. Salters, 1996, Shen & Forsyth, 1995) may need to be reconsidered.

References:
Batiza, R. & Vanko, D. (1984), Petrology of Young Pacific Seamounts. J. geophys. Res. 89, 11235-11260
Honda, M., Bernatowicz, T., Podosek, F., Batiza, R. & Taylor, P. (1987). Age determinations of eastern Pacific seamounts (Henderson, 6 and 7) - Implications for near-ridge and intraplate volcanism. Marine geology 74, 79-84
Salters, V. (1996), The generation of mid-ocean ridge basalts from the Hf and Nd isotope perspective. Earth and Planetary Science Letters 141, 109-123
Shen, Y. & Forsyth, D. (1995), Geochemical constraints on initial and final depths of melting beneath mid-ocean ridges. J. geophys. Res 100, 2211-2237
Zindler, A., Staudigel, H. & Batiza, R. (1984), Isotope and trace element geochemistry of young Pacific seamounts: implications for the scale of upper mantle heterogeneity. Earth and Planetary Science Letters 70, 175-195

S14-T06

A revised W budget of the bulk silicate Earth with implications for the timing of core formation

S. König[1], C. Münker[2], S. Hohl[1], H. Paulick[1], A. Köhler[1], J. Pfänder[3], A. Büchl[4]

[1] Universität Bonn, Steinmann Institut für Geologie, Mineralogie und Paläontologie, Poppelsdorfer Schloss, 53115 Bonn, Germany

[2] Universität zu Köln, Institut für Geologie und Mineralogie, Albertus-Magnus-Platz, 50674 Köln, Germany

[3] Technische Universität Bergakademie Freiberg, Institut für Geologie, Bernhard-von-Cotta Str. 2, 09599 Freiberg, Germany

[4] Max-Planck-Institut für Chemie, Abteilung Geochemie, Postfach 3060, 55020 Mainz, Germany

In the past years, new high-precision W concentration data have revealed strong fractionations of W from other highly incompatible lithophile elements (e.g., W, U, Ta) in arc rocks [3], in contrast to the traditional view [1;2] arguing for near constant W/U and W/Th ratios in most silicate reservoirs on Earth due to a similar incompatibility of these elements. The observed trace element fractionations reflect a selective enrichment of W in the sub-arc mantle via fluid-like subduction components [3]. Here we present further high-precision HFSE data for rocks from other tectonic settings (MORB, OIB), revealing a selective depletion of W in OIBs and MORBs relative to immobile HFSE (e.g., high Ta/W). The W budget in MORBs reflects cpx-controlled partial melting and cannot be explained by residual W-rich phases as claimed elsewhere [4]. Rather, the W depletion in MORBs and OIBs (high Ta/W) is complementary to the enrichment observed in arc rocks (low Ta/W). Together with estimated compositions of the continental crust, our data therefore permit an independent estimate of the Ta/W ratio of the Earth's primitive mantle. The abundance of W relative to other incompatible elements (i.e Ta/W, W/Th) in the depleted mantle is therefore not representative of the primitive mantle. According to our mass balance calculations, the W abundance of the Earth's primitive mantle is significantly lower (11 ppb) and the Hf-W ratio of the BSE is higher (ca. 27.6) than previously estimated (13-16 ppb and 17.6 [1;2]). This results in a younger core formation age that is typically inferred from [182]W abundance and the Hf/W of the silicate Earth.

Reference:

[1] Newsom et al. (1996) *GCA* 60, 1155-1169. [2] Arevalo & McDonough (2008) *EPSL* 272, 656-665. [3] König et al. (2008) *EPSL* 274, 82-92. [4] Babechuk et al. (2010) GCA 74, 1448-1470.

A new evolutionary model for the Paleo-Tethys and platinum potential of SW Yunnan, China

Daniel Hennig[1], Bernd Lehmann[1], Dirk Frei[2], Boris Belyatski[3], Ray Burgess[4]
[1]Clausthal University of Technology, Mineral Resources, Clausthal-Zellerfeld, Germany
[2]Stellenbosch University, Earth Sciences, Private Bag X1, 7602 Matieland, South Africa
[3]Institute of Precambrian Geology and Geochronology, Makarova 2, 199034 St Petersburg, Russia
[4]University of Manchester, Earth, Atmospheric and Environmental Sciences, Manchester M13 9PL, UK

Southwestern Yunnan is a key region for the understanding of the complex geological evolution of the Paleo-Tethys at the end of the Paleozoic and the formation of the 260 Ma-old Emeishan Large Igneous Province (ELIP), which hosts several important magmatic ore deposits. The same region is also intensively affected by Himalayan escape tectonics, with large-scale strike-slip movements. The most prominent Cenozoic fault zone in SW China is the NW–SE trending Red River-Ailaoshan Shearzone (RRASSZ) with left-lateral displacement of at least 300 km. The RRASSZ is generally believed to represent the southern boundary of the ELIP.

We investigate the possible continuation of the ELIP south of the RRASSZ, and estimate the platinum potential of mafic to ultramafic rock complexes along the Lancang River (further south known as Mekong). From north to south the target areas comprise the Banpo complex about 80 km NW of Simao, the Nanlianshan and Huijingfang complexes at Jinghong, and the Paleng complex close to the border with Laos. Lithogeochemical and geochronological data of these volcano-plutonic complexes are compared with PGE-bearing mafic to ultramafic intrusions associated with the ELIP and elsewhere. In addition, small granodiorite intrusions and a dacite belt were sampled at Jinghong, and the Lincang granite batholith was sampled close to Fengqing. The Lincang granite is part of a Triassic granite belt extending from Tibet to Indonesia and marks the final closure of the Paleo-Tethys.

The MORB-like basaltic andesite to microgabbro of the Nanlianshan complex has a U–Pb zircon age of 292 ± 1 Ma and indicates Early Permian sea-floor spreading (Hennig et al. 2009). The calc-alkaline, mafic to ultramafic Banpo intrusion hosts arc-related harzburgites and gabbros with a U–Pb zircon age of 286 ± 2 Ma (Jian et al. 2009). The granodiorite intrusions have U–Pb zircon ages of 284 ± 1 Ma to 282 ± 2 Ma. Their geochemical signatures attest to an arc setting. The mafic to ultramafic Paleng complex at the border to Laos is similar in composition to the Banpo complex and hosts amphibole gabbro cumulates with arc signature. U–Pb zircon ages for this complex are 262 ± 3 to 258 ± 2 Ma, and Ar–Ar ages on hornblende are 259 ± 1 and 259 ± 2 Ma. The amphibole gabbro is associated with arc-type basaltic andesite and within-plate basalt of 262 ± 2 Ma (U–Pb on zircon) which resembles in major and trace element characteristics the lavas of the ELIP. The data from the Paleng complex suggest a relationship of the Paleo-Tethyan arc magmatism and the ELIP magmatism at ca. 260 Ma, and it appears likely, that the ridge-trench collision scenario of Anderson (1994) applies to the situation in SW China. Subduction of the Paleo-Tethys, at least beneath Simao, went on until 239 ± 1 Ma as attested by the Lincang granite (U–Pb zircon age), which has a geochemical signature typical of syn- to postcollisional granites, and as attested by the arc-related Jinghong dacite (249 ± 3 Ma; U–Pb on zircon). Postorogenic rifting is indicated by rift-basalts of the Huijingfang complex, which have an Early Jurassic U–Pb zircon age of 194 ± 2 Ma.

Chalcophile trace elements and platinum-group elements of the Banpo and Paleng complexes depict drastic depletion, which is in the range of the sulfide-saturated Nadezhdinsky Formation of the Siberian Trap (host to the Noril`sk Ni–PGE deposit), of the sulfide-depleted northern Deccan Trap, and of the ELIP. The 286 ± 2 Ma-old Banpo gabbro shares geologic and geochemical similarities with the host rocks of a number of ELIP-associated ore deposits, such as Yangliuping and Jinbaoshan (PGE), and Hongge and Baimazhai (Fe–Ti–V oxide) in SW China, as well with Ban Phuc (Ni–PGE) in Vietnam. The Paleng cumulate sequence shows similarities to the Panzhihua and Baimazhai Fe–Ti–V deposits. Both the Banpo and Paleng mafic-ultramafic intrusive complexes have high platinum potential which needs testing by detailed exploration.

References:
Anderson, D. (1994). The sublithospheric mantle as the source of continental flood basalts; the case against the continental lithosphere and plume head reservoirs. Earth and Planetary Science Letters 123, 269-280.
Hennig, D., Lehmann, B., Frei, D., Belyatski, B., Zhao, X.F., Cabral, A.R., Zheng, P., Zhou, M.F., Schmidt, K. (2009). Early Permian seafloor to continental-arc magmatism in the eastern Paleo-Tethys: U–Pb age and Nd–Sr isotope data from the southern Lancangjiang zone, Yunnan, China. Lithos 113, 408-422.
Jian, P., Liu, D., Kröner, A., Zhang, Q., Wang, Y., Sun, X. & Zhang, W. (2009). Devonian to Permian plate

tectonic cycle of the Paleo-Tethys Orogen in southwest China: Geochemistry of ophiolites, arc/back-arc assemblages and within-plate igneous rocks. Lithos 113, 748-766.

Geochemical evolution of lavas of the Rabaul caldera, Papua New Guinea - Implications for the fractionation of Fe isotopes and HFSE ratios during fractional crystallization

Simon Hohl[1], Stephan König [1,2], Carsten Münker[1,2], Stephan Schuth[1,3], Jonathan Kuduon[4]
[1]Steinmann Institut, Rheinische Friedrich-Willhelms Universität Bonn, Germany
[2]Institut für Geologie und Mineralogie, Universität zu Köln, Germany
[3]Institut für Geographie, Universität zu Köln, Germany
[4]Rabaul Volcanological Observatory, Rabaul, Papua New Guinea.

The Rabaul area, Papua New Guinea, is among the few examples worldwide, where the magmatic evolution of a single, still active system can be examined *in situ*. Our work focusses on the geochemical evolution of the Rabaul caldera system, and on differences between the two major volcanic cycles found at Rabaul. For this purpose, representative volcanic units of Rabaul Caldera have been analyzed for their major and trace element concentrations and Sr-Nd-Hf isotope compositions. Additionally, Fe stable isotope compositions were analysed to determine the impact of crystal fractionation and to verify previous models [e.g. Schuessler *et al*., 2009] for high temperature fractionation of iron isotopes within a magmatic system.

The Rabaul volcanic complex is located at the north-eastern tip of the New Britain arc. It is related to the subduction of the Solomon plate beneath the Bismarck plate. Rabaul is dominated by a large caldera structure (9x14km in diameter). Two collaps events within the last 3500 years divide Rabaul into an older outer caldera complex and a younger (<640 A.D.) intra-caldera complex. Compositions vary from mafic lavas in the outer caldera cones to dacitic and even rhyolitic lavas within the caldera.

Harker-diagram variations of the two major volcanic suites reveal crystal fractionation of olivine, pyroxene and plagioclase as the most important process controlling the long-term magmatic evolution, confirming previous models of Wood *et al*. (1995). For the inner caldera complex, the abscence of systematic variations in Sr-Nd-Hf isotope compositions with MgO or SiO_2 suggests that the volcanic system has been in steady state or even behaved as closed system, indicating that isotopically different materials such as crustal rocks or older basement have not been assimilated to a significant extent. Within the analytical error of ±0.4 ϭ-units, most Fe isotope compositions of inner caldera lavas (ϭ ^{56}Fe from 0.01 to 0.14 ‰) overlap with the mafic samples and compositions of terrestrial basalts. Only some felsic samples show slightly lower values indicating possible fractionation of magnetite (Shahar et al., 2008).

Trace element compositions of Rabaul lavas indicate that slab derived fluids control the subarc enrichment of the mantle wedge. Low Sr isotope values ($^{87}Sr/^{86}Sr$ from 0.703605 to 0.703928) rule out a possible influence of subducted continental material. Coupled Hf-Nd isotope compositions (εHf from +13.9 to +15.4 and εNd from +6.4 to +8.1) reveal the presence of the Indian-Australian mantle domain beneath Rabaul. High-precision HFSE data obtained by isotope dilution reveal subchondritic Nb/Ta ratios (15.5 to 18) and near chondritic Zr/Hf (40-44). Ratios of Nb/Ta tend to decrease with increasing degree of differentiation, consistent with amphibole fractionation. Likewise, a distinct increase of Zr/Hf ratios from the basaltic lavas (40) to the dacitic lavas (43-44) can be explained by fractionation of clinopyroxene or amphibole. Increasing W/Th (0.27-0.42) and decreasing Ta/W (0.73-0.49) ratios with increasing degree of differentiation indicate a higher incompatibility of W relative to Th and Ta. The overall low Ta/w and high W/Th in Rabaul lavas support previous models [e.g. König *et al*., 2008] arguing for a high mobility of W in fluid-dominated subduction systems.

References:
Wood, C.P.; Nairn, I.A.; McKee, C.O. & Talai, B. (1995): Petrology of the Rabaul Caldera area, papua Papua New Guinea. Journal of Volcanology and Geothermal Research **69** 285-302.
Shahar, A.; Young, E. and Manning, C.E. (2008): Equilibrium high-tempertaure Fe isotope fractionation between fayalite and magnetite: An experimental calibration. Earth and Planetary Science Letters **268**, 330-338.
König, S.; Münker, C.; Schuth, S. & Dieter Garbe-Schoenberg (2008): Mobility of tungsten in subduction zones. Earth and Planetary Science Letters **274** 82- 92.

PGE-enrichment and redistribution in sulfide mineralization hosted by quartz-diorite dikes of the Sudbury Impact Structure (Canada)

Lutz Hecht[1,2], Susann Siegert[2], Marion Tichomirowa[3]
[1]Museum für Naturkunde, Leibniz-Institut für Evolution und Biodiversitätsforschung an der Humboldt-Universität zu Berlin, Germany
[2]Institut für Geologische Wissenschaften, Freie Universität Berlin, Germany
[3]Institut für Mineralogie, TU Bergakademie Freiberg, Germany,

World-class Ni-Cu-PGE-deposits are associated with the Sudbury impact melt system. The most prominent deposits are associated with the differentiated impact melt sheet, called the Sudbury Igneous Complex (SIC). However, approximately 40% of the resources are spatially associated with so-called Offset dikes (Farrow and Lightfoot 2002) that are radially and concentrically arranged quartz-diorite dikes, which are interpreted as part of the impact melt system (e.g. Deutsch et al. 1995). In comparison to the typical Contact and Footwall deposits at the base of the SIC mineralization in Offset Dikes are relatively PGE-rich (Farrow and Lightfoot 2002). Models of PGE-enrichment in the Sudbury Ni-Cu-PGE mineralization include early sulfide/silicate melt unmixing, sulfide melt fractionation and hydrothermal alteration (Farrow and Lightfoot 2002 and ref. therein). However, only little detailed studies have yet been published on the Offset dike ores (e.g. Rickard and Watkinson 2001, Huminicki et al. 2005). To test the models of PGE-enrichment a petrographic, whole rock and mineral chemical study of PGE-rich sulfide mineralization of three Offset Dikes (Trill, Parkin and Worthington) has been performed.

Locally PGE have definitely been redistributed to some extent during secondary processes as indicated by PGE-bearing metamorphic pyrite porphyroblasts or vug-filling michenerite for example. Sulfur isotope data show no involvement of external fluids of different isotope composition. No or very low fractionation of S-isotopes between coexisting pyrrhotite and chalcopyrite either indicate sulfide mineralization under rather high temperatures or S-isotope redistribution from primary sulfides (e.g. pyrrhotite and pentlandite) to secondary chalcopyrite. The latter is supported by the textures with chalcopyrite commonly replacing other base metal sulfides. However, comparison of whole rock and mineral PGE analyses suggests that the high PGE contents of the Offset dikes are primary and not preferentially a result of secondary remobilization and redistribution processes.

The lack of correlation (at least for the Parkin and Trill dike mineralization) of whole rock PGE contents with fractionation indicators for sulfide melts, like Cu/Ni, suggest, that other mechanism than crystal fractionation of magmatic sulfides are responsible for the relative PGE- rich composition of these dike-related ores in comparison to the Contact and Footwall deposits. Most likely Offset dike mineralization have a relatively large component of sulfide melt that separated early from the cooling impact melt system. During segregation of the sulfide melt from the silicate melt the highly siderophile elements should be most enriched in the early formed sulfide melts (at high R-Factors). Compositional differences between samples with only spotted mineralization (sulfide droplets) and samples with more massive sulfide mineralization of the Offset dikes most likely also reflect this continuous process of sulfide melt segregation and successive accumulation. Later accumulation of successive sulfide segregates to larger sulfide pods and veins would have most likely reduced or even completely homogenized such time-dependent isotopic and chemical variations within more massive sulfide mineralization.

References:
Deutsch, A., Grieve, R. A. F., Avermann, M., Bischoff, L., Brockmeyer, P., Buhl, D., Lakomy, R., Müller-Mohr, V., Ostermann, M. and Stöffler D. (1995), The Sudbury Structure (Ontario, Canada): A tectonically deformed multi-ring impact basin; Geologische Rundschau, 84, p. 697-709.
Farrow, C.E.G. and Lightfoot, PC. (2002), Sudbury PGE revisited: Toward an intergrated model. In Cabri, L.J. (ed.): The geology, geochemistry, mineralogy and mineral benefication of platinum-group elements. CIM Special Volume 54: 273-297.
Huminicki, M.A.E., Sylvester, P.J., Cabri, L.J., Lesher, C.M. and Tubrett, M. (2005), Quantitative mass balance of platinum group elements in the Kelly Lake Ni-Cu-PGE deposit, Copper Cliff Offset, Sudbury; Economic Geology, 100, p. 1631-1646.
Rickard, J.H. and Watkinson, D.H. (2001), Cu-Ni-PGE Mineralization within the Copper Cliff Offset Dike, Copper Cliff North Mine, Sudbury, Ontario: Evidence for Multiple Stages of Emplacement; Explor. Mining Geol., 10, Nos. 1 and 2, p. 111–124.

Formation of silicic magmas in the oceanic crust by assimilation-crystal fractionation processes – a geochemical and isotopic investigation of lavas from the Pacific-Antarctic-Rise

Sarah Freund[1], Karsten M. Haase[1], Christoph Beier[1]
[1]GeoZentrum Nordbayern, Friedrich-Alexander-Universität Erlangen-Nürnberg, Erlangen, Germany

The oceanic crust typically consists of mafic rocks but there are many regions of the Earth's spreading axes where more evolved rocks occur. However, the formation of the evolved magmas is debated and end-member models are that they either form by fractional crystallization of basaltic liquids or by partial melting of the oceanic crust. Glassy lavas from the Pacific Antarctic Rise (PAR) close to the Foundation intraplate volcanoes in the SE Pacific show an unusual abundance of lavas with evolved compositions.

The glass data from the PAR show variable SiO_2 contents between 49 and 68 wt.% and range from basalts, basaltic andesites, andesites to dacites. The trace element compositions range from depleted to slightly enriched mid-ocean ridge basalts (MORB) for the basalts whereas the andesites are much more enriched in most incomatible elements but show negative anomalies of Ba, Nb, Pb, Sr and Ti and positive anomalies in Rb, U, Zr and Hf compared with the basalts. Whereas the basalts display a small increase in K_2O with decreasing MgO, the andesites exhibit a strong negative correlation (increasing K_2O with decreasing MgO). In terms of major elements the basalts, andesites and dacites lie on typical tholeiitic fractionation trends. The incompatible element ratios like the Nb/Zr ratio of the data vary and indicate two potential liquid lines of descent between basalts and evolved lavas which is in general agreement with Sr-Nd-Pb isotope data. Thus, most of the chemical variation between basalts and dacites is due to crystal fractionation processes. Inverse zoning of clinopyroxenes in an andesitic sample suggests at least one recharge of the magma chamber by a more primitive magma. Magma mixing is also indicated by the major and trace element compositions of several lavas.

However, the evolved magmas lie on similar trends as the basalts in Nd and Pb isotopes spaces while there is a strong deviation towards higher Sr isotope ratios at a given Nd or Pb isotope ratio. The increased Sr isotope ratios likely reflect assimilation of hydrothermally altered crustal rock portions. The basaltic glasses have typical $\delta^{18}O$ values of around 5.6 commonly found in MORB. However, the andesitic and dacitic glasses have lower $\delta^{18}O$ values and correlate with increasing Cl/K ratios. The negative correlation of oxygen isotopes and Cl/K implies significant assimilation of hydrothermally altered upper oceanic crust. Because light $\delta^{18}O$ values occur only in the lower part of the oceanic crust (> 1 km depth) the assimilation and fractional crystallization (AFC) processes probably occur at the lower boundary of the sheeted dikes. The hypothetic assimilant is most likely an amphibolite formed by hydrothermal alteration of the oceanic crust. The petrogenesis of the evolved magmas will be modeled quantitatively using MELTS (Ghiorso, 1995) and EC-RAFC (energy-constrained recharge, assimilation and fractional crystallization) (Bohrson & Spera, 2003, 2007). We conclude that AFC processes lead to the formation of evolved magmas in the oceanic crust indicating substantial similarities to magma evolution in the continental crust.

Reference:
Bohrson, W.A. & Spera, F.J. (2003), Energy-constrained open-system magmatic processes IV: Geochemical, thermal and mass consequences of energy-constrained recharge, assimilation and fractional crystallization (EC-RFAC), Geochemistry Geophysics Geosystems, Vol. 4, Article
Bohrson, W.A. & Spera, F.J. (2007), Energy-Constrained Recharge, Assimilation, and Fractional Crystallization (EC-RAXFC): A Visual basic computer code for calculating trace element and isotope variations of open-system magmatic systems, Geochemistry Geophysics Geosystems, Vol. 8, Technical Brief
Ghiorso, S. & Sack, R.O. (1995), Chemical mass transfer in magmatic processes IV. A revised and internally consistent thermodynamic model for the interpolation and extrapolation of liquid-solid equilibria in magmatic systems at elevated temperatures and pressures, Contrib Mineral Petrol, (1995) 119:197-212

Osmium isotopes and highly siderophile element fractionation in the massif-type anorthosites of the Mesoproterozoic Kunene Intrusive Complex, NW Namibia

Philipp Gleißner[1], Kirsten Drüppel[1], Harry Becker[2]
[1]Technische Universität Berlin, Institut für Angewandte Geowissenschaften, Berlin, Germany
[2]Freie Universität Berlin, Institut für Geologische Wissenschaften, Berlin, Germany

Massif-type anorthosite complexes, that commonly form huge intrusions composed of plagioclase cumulate rocks, are characteristic features of the Proterozoic crust. Despite extensive investigation, no general agreement has been reached on the origin and evolution of their parental melt. The formation of anorthosites is discussed in terms of fractional crystallization from high-Al basaltic mantle-derived parental melts (e.g. Ashwal, 1993) and contrastingly the crystallization from ferrodioritic lower crustal melts (e.g. Duchesne et al., 1999).

The anorthosites of the 1.38 Ga Kunene Intrusive Complex (Angola/Namibia) experienced no metamorphic overprint after emplacement and hence allow a direct study of the magmatic processes active during their formation (Drüppel et al., 2007). New Os isotope and highly siderophile element data of anorthosites and mineral separates of the Kunene Intrusive Complex provide insights into highly siderophile element fractionation during fractional crystallization of mafic melts and hence into the petrogenesis of massif-type anorthosites.

The bulk anorthosites and separated magnetite and ilmenite are characterized by low Os (2-7 ppt), Ir, Ru and Rh concentrations. Higher absolute and relative concentrations were measured for Pt (30-130 ppt), Pd, Re and Au. The strongly fractionated chondrite-normalized highly siderophile element patterns indicate their origin from highly fractionated magmas. Previous fractional crystallization of olivine, chromite and possibly magmatic sulphides may have effectively fractionated Os, Ir and Ru from mafic melt precursors (e.g. Puchtel & Humayun, 2001) and could be responsible for the observed patterns. This interpretation is in accordance with a mantle origin of the anorthosites. Such an early fractionation of olivine and chromite could additionally explain generally intermediate magnesium numbers and low chromium contents of the anorthosites, which are also reported for other massif-type anorthosites (e.g. Ashwal, 1993). The overall abundance of Re in the bulk rocks varies by one order of magnitude (17-560 ppt) and is correlated with the iron content, which in turn reflects the modal proportion of oxides. This behavior suggests compatibility of Re in fractionating Fe-Ti oxides like titanomagnetite during anorthosite formation.

The initial Os isotope composition of the bulk anorthosites ranges from near-mantle values in the most primitive leucotroctolites ($^{187}Os/^{188}Os$ 0.2±0.1) to highly radiogenic values in more evolved leucogabbronorite ($^{187}Os/^{188}Os$ 5±2). Together with the results from recent trace element and O-Sr-Nd isotopic studies (Drüppel et al., 2007; Gleißner et al., 2010) these data are consistent with the formation of the massif-type anorthosites from a mantle-derived but variably crustally contaminated parental magma via assimilation and fractional crystallization processes.

References:
Ashwal, L.D. (1993). Anorthosites. Minerals and Rocks Series 21. Springer-Verlag, Berlin.
Drüppel, K., Littmann, S., Romer, R.L. & Okrusch, M. (2007). Petrology and isotope geochemistry of the Mesoproterozoic anorthosite and related rocks of the Kunene Intrusive Complex, NW Namibia. Precambrian Research 156, 1-31.
Duchesne, J.C., Liégois, J.P.,Vander Auwera, J. & Longhi, J. (1999). The crustal tongue melting model and the origin of massive anorthosites.Terra Nova 11, 100-105.
Gleißner, P., Drüppel, K. & Taubald, H. (2010). Magmatic evolution of anorthosites of the Kunene Intrusive Complex, NW Namibia: Evidence from oxygen isotope data and trace element zoning. Journal of Petrology 51, 897-919.
Puchtel, I. & Humayun, M. (2001). Platinum group element fractionation in a komatiitic basalt lava lake. Geochimica et Cosmochimica Acta 65, 2979-2993.

Compositional evolution of mafic alkaline lavas at the Rockeskyllerkopf volcanic complex, West Eifel, Germany

Alan B. Woodland [1], Cliff S.J. Shaw [2]
[1] Institut für Geowissenschaften, Universität Frankfurt, Altenhöferallee 1, Frankfurt, Germany
[2] Department of Geology, University of New Brunswick, Fredericton, NB, Canada

Intraplate mafic volcanism provides an important window into the nature of the sub-continental mantle. Not only does such volcanic activity frequently transport mantle xenoliths to the surface, but the lava compositions themselves give us insights into the melting process and the presence of metasomatic domains in the mantle. The West Eifel volcanic field is a classic example of continental intraplate volcanism and has been the subject of a number of studies over the years. Mertes & Schmincke (1985) and Schmincke (2007) identified two major regional groupings of primitive mafic lavas based on petrographic and geochemical characteristics: 1) Foidite Suite (leucitite, nephelinite, ± melilite ±olivine ± sodalite foidites), which is the most voluminous and 2) the ONB Suite (olivine nephelinite, basanite), which are generally younger lavas. Instead of investigating regional variations in lava composition, we have focussed on a single volcanic complex in order to determine the temporal evolution of the magmatic system, which may reflect changes in source composition, fractionation and assimilation processes. We chose the Rockeskyllerkopf volcanic complex since it is one of the best exposed complexes and the volcanic stratigraphy is well constrained (Shaw et al. 2010).

The complex comprises three geochemically distinct overlapping monogenetic volcanic centers: 1) Southeast Lammersdorf (SEL), 2) Mäuseberg (M) and 3) Rockeskyllerkopf (RKK) that erupted ~470 ka ago (Shaw et al. 2010). The SEL center is a phreatomagmatic tuff ring composed of lithic-rich fall and surge deposits. The lavas are olivine and clinopyroxene (cpx) phyric basanites. The crater wall and first series of crater fill deposits are primitive (mg# 63 to 70) with higher Ni and Cr and lower incompatible element concentrations than the lower mg# lavas of the youngest SEL deposits. La_N/Yb_N in these lavas range from 25 to 33. Chemical trends, together with the presence of olivine and cpx point to the evolution of a single magma batch by fractional crystallization. The Mäuseberg center is predominantly magmatic in character and comprises olivine phyric basanites. The M lavas have a narrow range of mg# (61 to 66) and are compositionally distinct from the older SEL lavas as they have higher REE concentrations and La_N/Yb_N of 37 to 45. The youngest center, RKK, comprises a well-developed proximal crater wall sequence that passes upward into a crater fill sequence. The final eruptions were massive lava flows that ponded within the RKK crater. The RKK lavas are cpx to olivine-cpx phyric basanites with higher Al_2O_3 than those of the older centers for the same mg# (62 to 65). La_N/Yb_N is similar to that of the SEL lavas. The lava flows at the top of the sequence have the highest Na_2O and among the highest K_2O of all the lavas in the complex. We find no evidence for significant fractional crystallization in the magma that formed the M and RKK centers.

Variations in lava composition from the three centers cover virtually the entire range observed for the Foidite Suite lavas in the West Eifel (Mertes & Schmincke 1985). A number of samples, particularly from the RKK center have low Ce/Pb ratios, indicative of lower crustal assimilation (Haase et al. 2004). Other samples are uncontaminated and have primitive magma compositions consistent with selective reaction of asthenosphere-derived magma with LREE-rich clinopyroxene and phlogopite in a metasomatised lithosphere. The enriched geochemical signature of the M lavas requires assimilation of an additional phase, probably apatite, which could reside either in the metasomatised lithosphere or in high-pressure cumulates formed by fractional crystallisation of the earlier SEL magma.

References:
Haase KM, Goldschmidt B, Garbe-Schönberg C-D (2004) Petrogenesis of Tertiary continental intra-plate lavas from the Westerwald region, Germany. J Petrol 45, 883–905
Mertes H, Schmincke H-U (1985) Mafic potassic lavas of the Quaternary West Eifel volcanic field. Contrib Mineral Petrol, 89, 330–345
Schmincke H-U (2007) The Quaternary Volcanic Fields of the East and West Eifel (Germany) In: Ritter JRR, & Christensen UR (eds) Mantle Plumes, Springer, Berlin, 241–322
Shaw CSJ, Alan B. Woodland AB, Hopp J, Trenholm ND (2010) Structure and evolution of the Rockeskyllerkopf Volcanic Complex, West Eifel Volcanic Field, Germany. Bull Volcanol, in press.

S14-T13

Experimental investigation of the differentiation of iron-rich peralkaline magma

Christopher Giehl, Philipp Bellucci, Huy-Tung Nguyen, Michael Marks, Marcus Nowak
Eberhard-Karls-Universität Tübingen, Institut für Geowissenschaften, Tübingen, Germany

In this study we investigate the magmatic differentiation of peralkaline Fe-rich phonolitic melts. These are highly evolved compositions with an alkalinity index ((Na+K)/Al ratio >1) and are believed to be differentiated from mantle-derived alkali basaltic sources. The studied composition (FeO$_{tot}$ = 11.6 wt%, #Fe = 0.98, (Na+K)/Al = 1.46) resembles a dyke rock, which is a potential source composition for the Ilímaussaq peralkaline nepheline syenite complex embedded in the Mid-Proterozoic Gardar rift province, South Greenland (Marks & Markl, 2003).

Recent experimental work showed that the crystallization behavior of alkali basalt strongly depends on oxygen fugacity (Freise et al., 2009). Relatively oxidizing conditions cause early crystallization of magnetite leading to strong iron depletion in the residual melts (calcalkaline trend). In contrast, reducing conditions favor olivine precipitation resulting in significant iron enrichment (tholeiitic trend).

Early magmatic phases of the studied dyke rock are ulvøspinel-rich magnetite (sp), hedenbergite-rich clinopyroxene (cpx), fayalitic olivine (ol), alkalifeldspar (afs) and nepheline (ne). As indicated by phase equilibria this dyke rock crystallized during unusually reduced conditions (log fO_2 ~ ΔFMQ -1.5 to -3). This is consistent with CH$_4$-dominated fluid inclusions found in the associated peralkaline nepheline syenites (Konnerup-Madsen, 2001). The groundmass consists of extremely Na-rich minerals like aegirine-rich cpx, sodic amphibole and aenigmatite (aen, Na$_2$Fe$_5$TiSi$_6$O$_{20}$). These mineral assemblages might indicate an unusually large temperature interval of crystallization from about 900 to 450°C (Marks & Markl, 2003).

However, the liquid line of decent of such Fe-rich phonolitic compositions is not well understood because of a lack of experimental data. Therefore, we performed H$_2$O-saturated crystallization experiments with synthetic glass starting material in gold capsules at 1 kbar and 950 to 750°C with 4 h run time. We used hydrothermal rapid quench vessels with an intrinsic oxygen fugacity of NiNiO (log fO_2 ~ ΔFMQ +1). Additional experiments at equivalent P-T conditions were carried out with graphite-lined gold capsules. The reaction of H$_2$O with graphite at the applied conditions is expected to form a CH$_4$-bearing C-O-H fluid (e.g. Huizenga, 2001), which was calculated to lower the redox state to log fO_2 ~ ΔFMQ -1.5. Further reduction in both gold and gold-graphite capsules is achieved by H$_2$O-undersaturation. For our nominally anhydrous experiments, run times of 3 weeks were necessary to achieve near-equilibrium conditions.

H$_2$O-saturated experiments reproduce only parts of the observed early magmatic phases of the dyke rock (sp + cpx). In contrast, under nominally anhydrous and therefore even more reducing conditions, the complete early magmatic phase assemblage of the dyke rock (sp, cpx, ol, afs, ne) and an alkali-rich residual melt ((Na+K)/Al = 1.51) was successfully reproduced at 750°C. Spinel is identified as liquidus phase at 950°C, followed by cpx and afs at 850°C. The latest crystallizing phases are ne, ol and occasionally aen (850 to 750°C). Extensive afs crystallization is a prerequisite for increasing the alkalinity of the residual melt, which is essential for aen crystallization observed in residual melt pockets in some of the experiments performed at 750°C. This study will elucidate the complex differentiation process due to the unusually large temperature interval of crystallization suggested for such magma compositions.

References:
Freise, M., Holtz, F., Nowak, M., Scoates, J.S. & Strauss, H. (2009), Differentiation and crystallization conditions of basalts from the Kerguelen large igneous province: An experimental study, CMP 158, 505-527.
Huizenga, J.M. (2001), Thermodynamic modelling of C-O-H fluids, Lithos 55, 101-114.
Konnerup-Madsen, J. (2001), A review of the composition and evolution of hydrocarbon gases during solidification of the Ilímaussaq alkaline complex, South Greenland, Geol. Greenl. Surv. Bull. 190, 159-166.
Marks, M. & Markl, G. (2003), Ilímaussaq 'en miniature': closed-system fractionation in an agpaitic dyke rock from the Gardar Province, South Greenland, Min Mag 67, 893-919.

Geochemical Investigation of Mantle Xenoliths from the Central Rio Grande Rift and Colorado Plateau Margin, New Mexico, USA: Constraints on Lithosphere Delamination Associated with Continental Rifting

John C. Lassiter[1], Benjamin Byerly[1]
[1]Geological Sciences Department, University of Texas at Austin, Austin, TX, USA

Removal of continental lithosphere through stretching, delamination, or convective erosion plays a critical role in the development of continental rift systems, and the decrease of lithosphere thickness in response to continental extension is a controlling variable on the volume and composition of magmatic products associated with rifting. Tomographic models of the central Rio Grande Rift (RGR) and adjacent Colorado Plateau (CP) in the southwestern United States reveal anomalously low V_s and V_P velocities beneath the central rift extending up to the MOHO, suggesting that the original Proterozoic lithospheric mantle has been thinned to a thickness of <40 km and replaced by hot, upwelling asthenosphere (c.f., Gao et al., 2004). However, assuming an initial lithosphere thickness of >120 km (based on lithosphere thickness beneath the adjacent CP and Great Plains regions), the degree of inferred thinning is inconsistent with passive extension alone given the estimated total crustal extension of only ~25%. Instead, several studies have suggested that lithosphere delamination or edge-driven convection along the CP margin has resulted in active removal and replacement of lithospheric mantle beneath the RGR (Gao et al., 2004; Van Wijk et al., 2010). Similar processes have been proposed for other active and passive continental rifts, including the Rhine Graben and the East African Rift. We have examined major and trace element and Os-isotope variations in two suites of spinel peridotite xenoliths and constituent phases from the central RGR (Elephant Butte) and adjacent CP margin (Cerro Chato) to constrain the thickness of Proterozoic lithosphere beneath the central rift and test recently proposed lithosphere delamination models.

Spinel peridotites from Cerro Chato (CP margin) are moderately refractory, with bulk Al_2O_3 ranging from 0.8 to 3.1 wt.%, similar to other Proterozoic lithospheric mantle xenoliths from the CP interior and worldwide. Correlations between bulk major elements, spinel Cr#, and clinopyroxene (cpx) Y and Yb contents reflect variable previous melt depletion. However, bulk xenoliths and cpx display variable LREE enrichment, reflecting metasomatic overprinting subsequent to melt depletion. The combination of melt depletion and metasomatic enrichment signatures is ubiquitous in continental lithospheric mantle samples, and the Cerro Chato xenoliths most likely sample intact Proterozoic lithosphere, indicating that the lithosphere beneath the CP margin is intact to depths of ~60 km.

In contrast to the Cerro Chato xenoliths, spinel peridotites from Elephant Butte (central RGR) on average are more fertile (bulk Al_2O_3 from 1.2 to 4.6 wt.%), and most bulk xenoliths and cpx display moderately LREE-depleted patterns, and are compositionally similar to abyssal peridotites. However, a small subset of Elephant Butte xenoliths are refractory and display LREE-enriched patterns similar to those found in Cerro Chato xenoliths. The similarity of the majority of Elephant Butte xenoliths to abyssal peridotites suggests that these xenoliths derive from asthenospheric mantle that recently replaced the pre-existing Proterozoic lithosphere beneath the central RGR, with only small remnants of this original lithosphere still surviving.

$^{187}Os/^{188}Os$ values in the Cerro Chato and Elephant Butte xenoliths range from ~0.120 to 0.133. Os-isotopes are correlated with proxies for degree of melt depletion (e.g., spinel Cr#, bulk Al_2O_3), with the most refractory samples defining Re-depletion model ages of ~1.4 Ga, similar to the inferred age of the original lithospheric basement (~1.6-1.65 Ga). In detail, the "fertile" Elephant Butte samples have Os-isotopes similar to those found in abyssal peridotites ($^{187}Os/^{188}Os > 0.125$), whereas "refractory" Elephant Butte and Cerro Chato xenoliths have less radiogenic Os-isotopes, reflecting long-term Re depletion as a result of prior melt extraction.

Two-pyroxene equilibration temperatures for both suites range from ~900-1100^{0}C. Based on regional heat flow, these temperatures correspond to depths ranging from ~40 km (Elephant Butte) up to ~60 km (Cerro Chato). The "asthenosphere-like" compositions of most Elephant Butte xenoliths therefore indicate the original lithosphere beneath the central rift has been thinned to <~40 km thickness. Although the Cerro Chato xenoliths provide only a minimum estimate of lithosphere thickness beneath the CP margin, host lavas from Cerro Chato have "asthenosphere-like" compositions, and SiO_2-in-melt thermobarometry suggests these lavas formed at ~70-80 km depth, suggesting a lithosphere thickness of 60-80 km. These results confirm substantial thinning of the lithosphere beneath the central RGR and support the suggestion that "active" processes of lithosphere removal (e.g., delamination or convective erosion) play an important role in continental rift development.

References:

Gao, W, Grand, SP, Baldridge, WS, et al., Upper mantle convection beneath the central Rio Grande rift imaged by P and S wave tomography, J. Geophys. Res. 109, Art. # B03305, 2004.

Van Wijk, JW, Baldridge, WS, van Hunen, J, et al., Small-scale convection at the edge of the Colorado Plateau: Implications for topography, magmatism, and evolution of Proterozoic lithosphere, Geology, 38, 611-614, 2010.

Compositional variations of Parinacota and Taapaca volcanic rocks, Central Andes: Experimental constraints on the role of differentiation vs. magma mixing.

André Stechern[1], Roman E. Botcharnikov[1], François Holtz[1], Magdalena Banaszak[2], Gerhard Wörner[2]
[1]Institute for Mineralogy, Leibniz University of Hannover, Germany
[2]Abteilung Geochemie, Geowissenschaftliches Zentrum der Universität Göttingen, Germany

The volcanism in the Central Volcanic Zone (CVZ) in northern Chile is induced by the subduction of the Nazca plate beneath the South American plate. Parinacota and Taapace volcanoes are located close together but the chemistry of lavas differ strongly although the source rocks may be similar. Parinacota volcano is a 6.348 m high strato-volcano. The eruptive history lasts over 163.000 years with eruptive rates of about 0.5-1 km^3/ka. Taapaca volcano (5.860 m) lies about 35 km westwards and is part of a volcanic complex with a long eruptive history (over 1.270.000 years) and relatively low eruptive rates of about 0.024 km^3/ka.

The erupted lavas from Parinacota volcano have a wide variety in compositions and range from basaltic andesites to rhyolites, but without any sign of a continuous evolution with age (Wörner et al., 1988, Clavero et al. 2004 and Hora et al. 2007). The major element compositions of the lavas produce continuous trends as a function of MgO and K_2O, which are typically used as differentiation index, indicating that magmas could be generated by differentiation. In contrast Taapaca volcano shows almost no variation in chemistry. All erupted lavas have a dacitic composition. In this study, phase equilibria were determined experimentally for both volcanic systems to clarify the differentiation and magmatic processes leading to the formation of these two fundamentally different suites.

Parinacota: Starting material for Parinacota phase equilibria experiments was a natural basaltic andesite, representing the most primitive composition found at this volcano with ~54wt% SiO_2 and ~5wt% MgO. Water activity in the system was varied using different proportions of H_2O and CO_2 in the coexisting fluid phase (X_{H2O} = 1 - 0.3). Experiments were performed at 300 MPa in internally heated pressure-vessels (IHPV) with controlled fO_2. Experimental temperatures ranged from 1050 to 900 °C. Redox conditions were between NNO and NNO+1. A second set of experiments was conducted under more oxidizing conditions (NNO+3) in the same temperature range and at 100 and 300 MPa to investigate the influence of oxygen fugacity.

The phases observed in the experimental products at redox conditions corresponding to the NNO buffer were: Ol, Cpx, Mt, Ap, Hbl and Pl (order of crystallization with decreasing temperature). The results of the experiments show that the liquid lines of descent in magmas undergoing close-system differentiation are significantly different from the natural trends. In particular, the SiO_2 vs. MgO trend has a well-developed concave shape for the experimental residual liquids whereas bulk rock compositions of Parinacota lie along an almost linear trend. The results of thermodynamic calculations performed for the experimental conditions (including fH_2O, fO_2) using the MELTS program (Ghiorso and Sack, 1995) confirm the concave shape of liquid line of descent. The discrepancy between experimental melt compositions and natural products can only be interpreted by assuming that magma-mixing processes controlling the geochemical features of the erupted magmas.

Taapaca: The composition of Taapaca samples is very homogeneous (dacite) and the rocks show two important features: a frequent occurrence of large, zoned sanidine phenocysts (length up to 10 cm) and mafic inclusions hosted in the dacites. The latter observation leads to the hypothesis that Taapaca rocks might be generated by magma mixing processes.

In order to determine the temperature and volatile contents of the magmas contributing to a possible magma mixing processes, crystallization experiments with a Taapaca composition (69wt% SiO_2 and 2.0wt% MgO) and a slightly more evolved composition (69wt% SiO_2 and 0.5wt% MgO), which may represent the low temperature end-member, where conducted. Particular attention was given to determine the stability field and composition of sanidine, which is one of the main phases present as phenocrysts in the investigated natural samples.

Experiments show that sanidine can only be generated from the more evolved composition at very low temperatures around 700°C. The influence of fO_2 is still under investigation.

Although Taapaca volcanic rocks are extremely homogeneous in time and space, our preliminary results show that magma mixing plays an important role. In contrast to Parinacota, the end- members for Taapaca mixing processes cannot be found in the field. However, our experimental approach, combined with geochemical investigations and with observations from Parinacota, is useful to identify the composition of possible end-members. We conclude that large magma chambers, "buffering" the chemical composition, may exist beneath dacitic volcanic systems such as Taapaca. Experimental results will be used to get constraints on the depth at which mixing occurred and, therefore, on the depth of possible magma chambers.

Reference:
Clavero, J.E. et al. (2004) _Revista Geologica de Chile_, 31, 317–347.

Ghiorso, M.S., and Sack, R.O. (1995) *Contributions to Mineralogy and Petrology.* 119, 197-21.
Hora J.M. et al. (2007) *GSA Bulletin*, 119, 343-362.
Wörner et al. (1988) *Bulletin of Volcanology*, 50, 287–303.

Source composition and melting temperatures of late-orogenic granodiorites (Damara orogen, Namibia): a comparison with experimental studies

Lennart Osterhus (presenting author), Stefan Jung (co-author)
Mineralogisch-Petrographisches Institut, Universität Hamburg, Grindelallee 48, 20146 Hamburg, Germany

Exposed cross-sections of the lower crust, observed directly (e.g., Percival et. al., 1992), or through study of xenoliths from the lower crust (e.g., Rudnick & Taylor, 1987) have demonstrated that underplating of basaltic magmas is an important element of crustal growth and thickening (Voshage et al., 1990), and that in general the lower crust is mafic in composition (Dawson et al., 1986). Melting experiments are an important approach to draw conclusions on the origin of mafic to intermediate magmatic rocks. For this study, data from the granodioritic late-orogenic Gawib pluton (Namibia) consisting of A-type and I-type subtypes, are compared with data from melting experiments by Rapp & Watson (1995) and Patiño Douce & Beard (1995). The granodiorites have SiO_2 concentrations ranging from 63.2–68.0 wt.% and are metaluminous (molar A/CNK: Al_2O_3/ $(CaO+Na_2O+K_2O)$) < 1. TiO_2, MgO, CaO, Al_2O_3 and P_2O_5 decrease with increasing SiO_2, indicating processes linked to fractional crystallization of amphibole, Ti-magnetite, plagioclase and apatite. Trace element abundances of Zr and Y decrease also with increasing SiO_2. The chondrite-normalized REE patterns show high REE abundances with LREE enrichment and HREE depletion and feldspar-related Eu-anomalies. Both, HREE and LREE are higher in the A-type granodiorites than in the I-type granodiorites. The similar SiO_2, but variable TiO_2, Zr, Y and REE contents indicate that the Gawib granodiorites represent melt fractions derived from (at least) two different meta-basaltic sources. Isotope data (unradiogenic $^{87}Sr/^{86}Sr$; low Nd values (Nd: c. -12), old Nd model ages between 2.0 and 2.5 Ga, unradiogenic $^{206}Pb/^{204}Pb$ with significant variation in $^{207}Pb/^{204}Pb$ indicate derivation of the granodiorites from meta-basaltic lower crustal rocks. Temperature estimates using Al_2O_3/TiO_2 systematics (Jung & Pfänder, 2007) and application of apatite saturation thermometry indicate higher temperatures for the A-type granodiorites (ca. 980°C) than for the I-type granodiorites (ca. 920°C). Melting experiments using metabasaltic material show that intermediate liquids can only be produced by high T (> 1050°C) and high P (16-32 kbar; Rapp and Watson, 1995) melting whereas melting experiments using quartz amphibolites at lower P (3-15 kbar) and T (< 1000°C) produce felsic liquids with SiO_2 > 70 wt. %. Hence, the generation of granodioritic melts require protoliths more mafic than metasedimentary rocks, quartz amphibolites or pre-existing felsic sources. Partial melting of an alkali-rich basalt produces liquids that have lower CaO and Na_2O but higher TiO_2 than the Gawib samples. MgO and FeO abundances fit the compositions observed in the Gawib granodiorites. Liquids produced by melting of a low-K basalt have too high CaO and Na_2O but similar contents of TiO_2, MgO and FeO and melting of an Archaean low-K greenstone yields liquids with higher CaO, Na_2O and TiO_2 but similar MgO and FeO relative to the Gawib granodiorites. The best match is observed considering a low-K/high-Al basalt as the source which produces CaO, TiO_2, MgO, FeO and Na_2O concentrations similar to those observed in the Gawib samples. These melts represent 20-40 % melting and coexist with a granulite residuum consisting of garnet+clinopyroxene+orthopyroxene±plagioclase. An apparent feature of the Gawib suite is the decrease of Al_2O_3, CaO and Na_2O which is explained by plagioclase fractionation. Hence, the apparently too low CaO and Na_2O abundances in the Gawib samples relative to the experiments using a low K basalt or greenstone may in fact be related to fractionation processes and cannot be used to rule out low-K sources. Overall, alkali-rich sources can be excluded and the source of the Gawib granodiorite may be an Archaean to Proterozoic low-K/high-Al mafic granulite (meta-basalt) in the lower crust.

References:
Dawson, J. B., Carswell, D. A., Hall, J. & Wedepohl, K. H. (eds) (1986), *The Nature of the Lower Continental Crust*. Geological Society Special Publication 24, 363-374.
Percival, J. A., Fountain, D. M. & Salisbury, M. H. (1992), Exposed crustal cross sections as windows on the lower crust. In: Fountain, D. M., Arculus, R. J. & Kay, R. W. (eds) *The Continental Lower Crust.* Amsterdam: Elsevier, 269—316
Patiño Douce, A. & Beard, J. S. (1995), Dehydration-melting of Biotite Gneiss and Quartz Amphibolite from 3 to 15 kbar. J. Petrol., 36, 707-738.
Rapp, R. P. & Watson, E.B. (1995), Dehydration melting of metabasalt at 8–32 kbar: implications for continental growth and crust mantle recycling. J. Petrol., 36, 891–932.
Rudnick, R. L. & Taylor, S. R. (1987), The composition and petrogenesis of the lower crust: a xenolith study. Jour. Geophys. Res. 92, 13981-14005.
Voshage, H., Hofmann, A. W., Mazzucchelli, M., Rivalenti, G., Sinigoi, S., Raczek, I. & Demarchi, G. (1990), Isotopic evidence from the Ivrea Zone for a hybrid lower crust formed by magmatic underplating. Nature 347, 731-736.
Jung, S. & Pfänder, J. A. (2007), Source composition and melting temperatures of orogenic granitoids:

constraints from CaO/Na$_2$O, Al$_2$O$_3$/TiO$_2$ and accessory mineral saturation thermometry. Eur. J. Min., 19, 859-870.

Initial results for the composition of the igneous basement of the Bowers and Shirshov Ridges (Bering Sea, NW Pacific)

Maren Wanke[1,2], Maxim Portnyagin[1], Reinhard Werner[1], Folkmar Hauff[1], Kaj Hoernle[1]
[1]IFM-GEOMAR, Leibniz Institute of Marine Sciences, Wischhofstraße 1-3, 24148 Kiel, Germany
[2]Christian-Albrechts-University of Kiel, Christian-Albrechts-Platz 4, 24118 Kiel, Germany

The Bowers and Shirshov Ridges (hereafter BR and SR, respectively) are two prominent submarine structures of unknown age and provenance in the Bering Sea. So far only a few geochemical data exist on the composition of basement rocks from the SR (Silantyev et al., 1985) and none for the BR. Age and geochemical data are crucial to evaluate if the ridges represent remnant island arcs (Cooper et al. 1981, Scholl 2007), former pieces of Kamchatka rifted away through seafloor spreading (SR: Baranov et al. 1991) or parts of the Mesozoic Hawaiian hot-spot (Steinberger & Gaina, 2007).

Here we report the first geochemical data on the composition of the basement rocks from the BR and SR, recovered during KALMAR R/V SONNE cruise 201 (Legs 1b and 2) in 2009. Fresh to moderately altered volcanic rocks were dredged from the northern slope of the BR, from seamounts on the western extension of the BR and from the western slope of the central part of the SR. We studied the petrography of the samples and carried out geochemical analyses of major and trace elements by XRF and ICPMS at ACME Lab (Vancouver, Canada) and CAU (Kiel).

The rocks from the northwestern slope of the BR are clinopyroxene (cpx)-phyric basalts with minor amounts of olivine (ol) and plagioclase (plag) microphenocrysts, as well as hbl-plag-cpx-bearing basaltic andesites and trachyandesites. The rocks are strongly enriched in LREE (La_N/Yb_N = 3.2 – 8.5, N indicates normalization to primitive mantle), fluid-mobile elements (Ba, U, K) relative to NMORB and exhibit clear negative anomalies of HFSE (Nb, Ta and Ti) in primitive mantle-normalized incompatible element diagrams. The BR rocks also have a moderate adakitic signature, as indicated by elevated Sr_N/Y_N ratios (6.9 – 12.9). Hbl-cpx-plag trachybasalts from the SR have similar major and trace element compositions (La_N/Yb_N = 2.1 – 4.9) to the BR rocks. The other magmatic series from the SR comprises massive trachyandesites, trachytes and dacites with rare phenocrysts of plag and cpx. These rocks also have island-arc type incompatible element patterns and are distinct from other rock types from the BR and SR with less LREE enriched patterns (La_N/Yb_N ~ 1.8) and a strong negative Eu anomaly (Eu/Eu* = 0.74).

Rocks dredged from a seamount on the western extension of the BR have very distinctive petrographic and geochemical characteristics. These are ol-phyric pillow basalts with minor (less than 5%) amounts of plag and cpx. The freshest whole rocks and pillow-rim glasses have relatively smooth patterns of incompatible trace elements, akin to intraplate oceanic basalts and in some characteristic incompatible element ratios (e.g. Th_N/Ba_N = 0.6, Sr_N/Ce_N = 1.2, La_N/Yb_N = 3.3) are similar to Hawaiian hotspot tholeiites.

In summary, petrography and preliminary geochemical results indicate an island-arc origin for major parts of the BR and SR. The discovery of intraplate basalts suggests that fragments of the Emperor Seamount Chain could also be preserved in the Bering Sea (Steinberger & Gaina 2007) as seamounts and in the BR and SR basement. Our further studies will be focused on obtaining absolute age data for the studied rocks, which will allow combining the petrologic data with tectonic and geodynamic models for the NW Pacific.

Petrographic and microanalytical evidence for a dynamic Axial Magma Chamber (AMC) under fast-spreading ocean ridges in the Wadi Gideah (Oman Ophiolite; Wadi Tayin Massif)

Marcel Dietrich[1], Ute Bauer[1], Eric Wolff[1], Jürgen Koepke[1], Dieter Garbe-Schönberg[2]
[1] Institut für Mineralogie, Leibniz Universität Hannover, Callinstr. 3, 30167 Hannover, Germany
[2] Institut für Geowissenschaften, Universität Kiel, Ludewig-Meyn-Straße 10, 24118 Kiel, Germany

The formation and evolution of the oceanic lithosphere at mid-ocean ridges is the dominant process in the chemical differentiation and physical evolution of our planet. The ~60.000 km long mountain chains of ocean ridges beyond the oceans bears 90% of the Earth volcanism and produces ~25 % of heat release of the Earth, thus exerting the primary control on mass and heat transfer between the Earth's interior and hydrosphere. Models on the geodynamics of oceanic spreading centers imply that axial magma chambers (AMC) under fast-spreading ridges are transient phenomena, moving up and down in distinct time scales. The transition between the small melt lens observed on top of the AMC and the overlying sheeted dike complex marks the interface between the magmatic and the hydrothermal convective system. It is therefore critical to our understanding of fast spreading ridge accretion processes. During upward moving of an AMC into previously hydrothermalized dikes, vast reactions are ongoing causing assimilation and stoping of the altered dikes. Upward migrations are also responsible for a granoblastic overprint of the root of the dikes which documents to reheating of previously hydrothermally altered lithologies which can even trigger hydrous partial melting due to the lowering of the solidus of mafic lithologies by the presence of a water activity. This is identified as one possible process to produce oceanic plagiogranites. Downward migrations of the the AMC result in the freezing of the melt lens to the so-called varitextured gabbros at its roof, which represent the partly fossilized melt lens. Melt lens fossilization eventually occurs when magma supply is stopped or at the melt lens margins where the thermal conditions become cooler. Petrological and geochemical evidence for the processes outlined above are provided from only two locations word-wide, due to the very limited access to deeper parts of fast-spreading oceanic crust: IODP (Integrated Ocean Drilling Program) drilling at Site 1256, (15 Ma old crust formed at the East Pacific Rise), and from the Oman ophiolite, the best proxy for fast-spreading oceanic crust on land (Koepke et al., 2008, France et al., 2009, 2010).

During a mapping project in the Oman ophiolite during January/February 2010 we discovered in the Southern end of Wadi Gidea in the Ibra area (Wadi-Tayin-Massif) an outcrop which perfectly shows the record of those magmatic and metamorphic processes ongoing during the interaction between primary MORB magma, previously hydrated sheeted dikes, plagiogranitic melt formed by partial melting of altered dikes, and involved water-rich fluids probably formed by dehydration of hydroxyl-bearing minerals within altered dikes. This study presents the petrographical and mineral-chemical result of a detailed outcrop mapping and the corresponding interpretations of the processes behind. We identified following lithological/structural components:

(1) Varitextured gabbro with a marked patchiness and spotty appearances composed of gabbros differing in texture (subophitic and granular) and mineralogy (clinopyroxene- and hornblende-dominated), interpreted as the fossilized record of intermingled/mixed mushes within the axial melt lens; (2) late plagiogranite with numerous xenoliths of altered sheeted dikes interpreted as melts generated by hydrous partial melting of altered dike rocks triggered by water-rich fluids; (3) granoblastic dikes in a high level above the gabbro intrusion interpreted as metamorphosed product of previously altered dike rocks due to the thermal imprint of the gabbroic intrusion below; (4) late basaltic dikes cutting all other lithologies; (5) very late zones of low-temperature shearing coupled with pathways for hydrothermal alteration. Based on the mineral-analytical results, geothermometry, and petrographic investigations we present a model of a very dynamic AMC active in the Oman paleoridge 90 Ma ago.

Reference:
France, L., Ildefonse, B. & Koepke, J. (2009): Interactions between magma and the hydrothermal system in the Oman ophiolite and in IODP hole 1256D: fossilisation of a dynamic melt lens at fast spreading ridges. Geochem. Geophys. Geosyst.: 10, doi:10.1029/2009GC002652.
France, L., Koepke, J., Ildefonse, B., Cichy, S. & Deschamps, F. (2010), Hydrous partial melting in the sheeted dike complex at fast spreading ridges: experimental and natural observations. Contrib Mineral Petrol: 159, doi: 10.1007/s00410-010-0502-6.
Koepke, J., Christie, D.M., Dziony, W., Holtz, F., Lattard, D., Maclennan, J., Park, S., Scheibner, B., Yamasaki, T. & Yamasaki, S. (2008), Petrography of the Dike/Gabbro Transition at IODP Site 1256D (Equatorial Pacific): The evolution of the Granoblastic Dikes, Geochem. Geophys. Geosyst.: 9, doi:10.1029/2008GC001939

Atomistic simulation approach to trace element partitioning between silicate melts

Volker Haigis[1], Sandro Jahn[1]
[1]GFZ German Research Center for Geosciences, Potsdam, Germany

Element partitioning, i.e. the preferred incorporation of certain cations into a given chemical environment rather than into other coexisting phases, plays a fundamental role in processes such as crystallization of silicate magmas or planetary differentiation. The lattice strain model proposed by Blundy & Wood (1994) attempts to explain the observed partitioning of trace elements between coexisting minerals and melts entirely in terms of the strain induced in the host crystal lattice by the size misfit of the incorporated cation: the closer the cation's ionic radius to the ideal ionic radius in the host lattice, the more easily it enters the mineral, otherwise it is enriched in the melt. The influence of the melt structure on the partitioning, on the other hand, is neglected by the lattice strain model.

However, recent experiments by Prowatke & Klemme (2005) challenge this view: they show that, for a given silicate crystal structure, the partitioning of many trace element cations (e.g. Y) depends strongly on the composition of a coexisting silicate melt, in particular on the ratio of the Al to alkali and alkaline earth contents. It was suggested that this ratio influences the framework structure of the melt and hence also the local environment of incorporated ions, which in turn determines the thermodynamics of partitioning. A detailed understanding of atomic-scale structures in melts leading to the observed behavior is still missing.

Atomistic simulation is a valuable tool to investigate the local environment of ions in melts. It provides a direct link between the atomic-scale structure and thermodynamic properties of matter, supports the interpretation of experimental results and allows predictions about systems that are not accessible to experiments. First-principles simulations based on quantum theory, e.g. density functional theory (DFT), have proven to be highly accurate, but are very demanding in terms of computation time. On the other hand, simulations based on classical atomic interaction potentials are computationally much cheaper but potentially less accurate and hence have to be tested carefully before being used as a predictive tool.

Here, we present a combined DFT and classical potential approach to trace element partitioning in silicate melts, taking Y as a trace element. First, a classical ionic interaction potential, including ionic polarization terms, is established for the system Y_2O_3 - CaO - Al_2O_3 - SiO_2. Its parameters are obtained by fitting ionic forces, dipoles and stresses to those calculated with DFT. The resulting potential is tested by comparing its predictions for thermal expansivities of crystals and for neutron structure factors of oxide melts to experimental data and DFT calculations.

Then the potential is used in atomistic simulations to investigate the coordination environment of Y in silicate melts of different compositions. As compositional variable the ratio Al_2O_3/CaO is chosen, which is expected to drive the observed variation of the partition coefficient. We explore the relation between melt composition and the local melt structure around Y, and discuss qualitatively its relation to the partitioning behavior of Y. This constitutes the initial step towards a quantitative atomic-scale understanding of trace element partitioning.

References:
Blundy, J. & Wood, B. (1994), Prediction of crystal-melt partition coefficients from elastic moduli, Nature 372, 452
Prowatke, S. & Klemme, S. (2005), Effect of melt composition on the partitioning of trace elements between titanite and silicate melt, Geochim. Cosmochim. Acta 69, 695

Towards a reference profile for fast–spreading oceanic crust: Petrology and geochemistry of the "Wadi Gideah" cross section in the Southern Oman ophiolite.

Paul Eric Wolff[1], J. Koepke[1], H. Straus[2], D. Garbe–Schönberg[3], M. Dietrich1, M. Oeser[2]
[1]Leibniz University Hannover, Institut für Mineralogy, Hannover, Germany
[2]Westfälische Wilhelms–Universität Münster, Institut für Geologie und Paläontologie, Münster, Germany
[3]Christian–Albrecht–Universität zu Kiel, Institut für Geologie und marine Klimaforschung, Kiel, Germany

The formation and evolution of the oceanic lithosphere at mid–ocean ridges is one of the major geodynamic processes on Earth. Ocean crust accretion by seafloor spreading has been operating for at least 3.8 billion years, and more than 60% of the Earth's surface today was formed in this way. Plate tectonic processes completely repave the ocean basins every 100–200 million years. From its formation until its return to the mantle by subduction, the evolving oceanic lithosphere interacts with seawater, sequesters water and other materials, and ultimately recycles them back into the mantle.

Structure, architecture, properties, accretion, cooling and alteration is fundamentally differing between fast/intermediate–spreading and slow–spreading systems. Ocean crust formed at fast–spreading rates exhibits a relatively uniform seismic stratigraphy and is regarded as layered and relatively homogeneous (Dick, 2006), in contrast to oceanic crust generated at slow–spreading ridges. Importantly, theoretical models on magmatic accretion of the oceanic crust, thermal models, mass balance calculations for the whole ocean crust, or general alteration models only exist for fast–spreading systems. For slow–spreading systems corresponding models and calculations are either not available, or not of general character. This is due to the considerable heterogeneity of slow–spreading ocean crust, where crustal accretion is dominated by tectonic processes instead of pure magmatic. However, due to the lack of exposures and drilled sections of the deep basement of fast–spread crust, most models for fast–spread crust are not tested up to date by using natural samples. Therefore, it is necessary to perform complementary studies of ophiolites, in particular the Oman ophiolite, which is regarded to present the best example of fast–spreading oceanic crust on land, and which played a vital role in developing crucial paradigms for understanding sea floor spreading (Nicolas, 2000).

During February 2010 we undertook a detailed field campaign on the Wadi Gideah which is located in the Wadi–Tayin Massif in the Southern part of the Oman Ophiolithe in order to sample a complete section through fast-spreading-oceanic crust. The Southern massifs of the Oman ophiolite, especially the Wadi-Tayin massif, is regarded as the best area for studying primary "normal" fast-spreading ridge processes, where subduction-zone related magmatism triggered by intraoceanic slicing (beginning of obduction) is widely absent. Up to now, our profile contains ~100 samples from mantle peridotites, gabbros to dikes and lavas. This profile is representative for fast–spread oceanic crust both in terms of completeness of the crust–forming structural components and in coherence of geochemical and petrological data to be obtained, thus well–suited for shedding light on crustal accretion processes and the evolution of primary and secondary geochemical cycles of fast–spreading oceanic crust. In order to obtain data sets as coherent as possible (major and trace elements, isotopes, and microanalytical results), we will follow a modern concept to perform all analytical investigations on the same samples. Our study follows an approach of an US working group in the late 1970s to obtain a complete profile through the Oman ophiolite (Pallister & Hopson, 1981). Today, 30 years later after tremendous increase of knowledge on the geodynamics of ocean ridges especially due to ship–based science and due to continuous research on the Oman ophiolite, many of the paradigms valid at that time changed making it necessary to resample/reinterpret the Wadi-Gideah profile.

In this study we present our first data obtained, in order to present geochemical and petrological profiles of the Wadi-Gideah section. Main interest in this stage of the project is to focus on the mineral chemical evolution (Mg# of mafic phases, Anorthite content of plagioclase) as well as the bulk major/trace element compositional evolution. Far-reaching goals are to elaborate the complete evolution of the hydrothermal alteration cycles (by using Sr, O, S, and other suitable isotopes) and a "modern" mass balance considering the state of the art knowledge (e.g., excluding all members of the so-called "late-stage" magmatism, which were included in old mass balcance calculations)

References:
Dick, H. et al. (2006), Past and Future: Impact of Deep Drilling in the Oceanic Crust and Mantle. Oceanography, 19, 72–80.
Nicolas, A. et al. (2000), Accretion of Oman and United Arab Emirates ophiolite – Discussion of a new structural map. Marine Geophysical Researches, 21, 147–179.

Pallister, J. S. & Hopson, C. A. (1981), Samail ophiolite plutonic suite: field relations, phase variation, cryptic variation and layering, and a model of a spreading ridge magma chamber. Journal of Geophysical Research, 86 (B4), 2593–2644

Lu-Hf and Re-Os isotopic systematics in highly metasomatised mantle: a case study in Letlhakane peridotite xenoliths, Botswana

M. Behrens[1*], A. Luguet [1], D. Herwartz [1], D.G. Pearson[2]
[1] Rheinische Friedrich-Wilhelms-Universität Bonn, Steinmann Institut, Endogene Prozesse, Bonn, Germany (*correspondence: melanie@behrens-haslach.de)
[2] University of Durham, Department of Earth Sciences, Northern Centre for Isotopic and Elemental Tracing, Durham, UK

The diamondiferous Letlhakane kimberlite is intruded into the early Proterozoic Magondi mobile Belt, which lies at the NW margin of the Zimbabwe Craton. Given the general association of diamond deposits with Archean cratons, the setting of Letlhakane kimberlite is somewhat anomalous. We have conducted a petrological and geochemical study of peridotite xenoliths erupted by the Letlhakane kimberlite in order to better understand lithosphere evolution in relation to the surrounding Kalahari craton. Eleven garnet and spinel facies peridotites, ranging in depletion from lherzolites to harzburgites were analysed for whole-rock major and trace elements, whole-rock, garnet and clinopyroxene Lu-Hf isotopic systematics and whole-rock Re-Os isotopic systematics.

Letlhakane peridotites have low Al_2O_3 (0.28-1.66 wt%), low CaO (0.42-1.60 wt%) and high MgO contents typical of mantle residues generated by high degree of partial melting. They also have experienced metasomatism, manifest in the presence of phlogopite and in their significant enrichment in incompatible trace elements.

Os isotope analyses show a range of Re depletion ages ranging from 2.2 to 2.8 Ga, clearly indicating the presence of Archean mantle beneath this area, but with significant Palaeo-Proterozoic modification (this study & Carlson et al., 1999). Whole-rock Lu and Hf concentrations in Letlhakane peridotite xenoliths range from 0.00276 to 0.0220 ppm and 0.0139 to 0.565 ppm, respectively, with $^{176}Hf/^{177}Hf$ ratios ranging from non-radiogenic to radiogenic values of ε_{Hf} = –6.8 to +29.4. The samples show significant scatter in $^{176}Hf/^{177}Hf$ vs. $^{176}Lu/^{177}Hf$ space. However, three samples show a positively sloped correlation, yielding an errorchron age of approximately 2.1 Ga (MSWD = 4.8) with an initial $^{176}Hf/^{177}Hf$ ratio of 0.28225 ± 49 (ε_{Hf} = -18.5). A clinopyroxene-garnet internal isochron (sample MB1) defines a two point isochron age of 132 ± 38 Ma which is within error of the eruption age of the Orapa kimberlite (i.e 93 Ma, Davis, 1977), located in the same mobile belt and assumed to be erupted in the same phase of magmatic activity as the Letlhakane kimberlite (Stiefenhofer et al., 1997).

None of the Lu-Hf isotope systematics are consistent with the Archean depletion event indicated by the Re-Os isotope system. The Lu-Hf isotopic systematics have been highly disturbed by the petrological modifications experienced by the lithospheric mantle under Letlhakane and thus challenge the robustness of the Lu-Hf isotopic systematics in highly metasomatised peridotites for dating depletion age and formation of the mantle root.

References:

Carlson, R. W., Pearson, D. G., Boyd, F. R., Shirey, S. B., Irvine, G., Menzies, A. H., Gurney, J. J. (1999), Re-Os systematics of lithospheric peridotites: Implications for lithosphere formation and preservation: Proc. 7th Int. Kimb. Conf., Eds J.J. Gurney, J.L. Gurney, M.D. Pascoe & S.H. Richardson, National Book Printers, Goodwood, S. Africa, pp 99-108.
Davis, G.L. (1977), The ages and uranium contents of zircons from kimberlites and associated rocks, extended abstract, Second Int Kimberlite Conf (unpaginated).
Stiefenhofer, J., Viljoen, K.S., Marsh, J.S. (1997), Petrology and geochemistry of peridotite xenoliths from the Letlhakane kimberlites, Botswana, Contrib Mineral Petrol 127:147-158.

Cenozoic melilite-bearing igneous rocks at the western end of the Eger (Ohře) Rift in Saxony and western Bohemia

Michael Abratis[1], Lothar Viereck-Götte[1], Dirk Munsel[2], Jaromir Ulrych[3]
[1]Friedrich-Schiller-Universität Jena, Institute of Geoscience, Jena, Germany
[2]Karlsruher Institut für Technologie, Institute for Mineralogy and Geochemistry, Karlsruhe, Germany
[3]Academy of Sciences of the Czech Republic, Institute of Geology, Praha, Czech Republic

Late Cretaceous to Cenozoic alkaline intraplate igneous rocks in the Bohemian Massif are spatially associated with the Eger (Ohře) Rift. Their compositions comprise the entire range of mafic alkaline silica-undersaturated igneous rocks (melilitites, nephelinites, basanites, tephrites, alkali basalts) (Ulrych et al. 1999, Haase & Renno 2008). Melilite-bearing igneous rocks are especially known from the area where the Eger (Ohře) Rift is intersected by the Labe (Elbe) Zone (Ulrych et al. 2008). However, these strongly silica-undersaturated rocks are also abundant at the western end of the rift where it is intersected by the Mariánské Lázně Fault Zone, especially in the Saxonian Vogtland (Abratis et al. 2009).

Numerous volcanic plugs, dikes and diatremes of Tertiary (or Upper Cretaceous?) age are present within the small volcanic field of the Vogtland in SW Saxony, north of the Eger (Ohře) Rift, within the trace of the Mariánské Lázně fault zone. The outcropping igneous rocks – olivine melilitites, melilite bearing and melilite free olivine nephelinites, melanephelinites and a few tephrites – are strongly silica undersaturated and characterized by the appropriate mineralogy showing abundant nepheline and melilite as the silica-depleted substitutes for feldspars and pyroxenes. Other mineral phases are perovskite, haüyne/nosean, phlogopite/ biotite and apatite besides diopsidic and aegirine-augitic pyroxene, forsteritic olivine and titanian magnetite. Furthermore, carbonate globules – possibly derived from carbonate-silicate melt unmixing – occur within some of the rocks. Most minerals indicate that the rocks are generated from melts which were highly enriched in incompatible elements and volatiles. Mineralogy and geochemistry suggest that melting occurred at rather deep levels >80 km and very low degrees of melting within a strongly metasomatized, CO_2-rich mantle. Ponding of melts at the mantle-crust boundary is evidenced by the occurrence of green-core pyroxenes in some of the rocks. Rapid ascent of the mantle melts through the crust is suggested by the association with the deep fault systems characterizing the region and by the presence of mantle-derived xenocrysts in the volcanics. Secondary minerals such as zeolites, analcite, apophyllite and some of the carbonate document late and post-magmatic hydrothermal activity within an area which is still affected by intense intracrustal magmatic fluid migration as indicated by abundant mofettes and frequent earthquake swarms within the Vogtland (Saxony, Germany) and western Bohemia (Czech Republic).

References:
Abratis, M., Munsel, D. & Viereck-Goette, L. (2009), Melilithite und Melilith-führende Magmatite des sächsischen Vogtlands: Petrographie und Mineralchemie: Zeitschrift geologischer Wissenschaften 37, 41-79.
Haase, K. & Renno, A. (2008), Variation of magma generation and mantle sources during continental rifting observed in Cenozoic lavas from the Eger Rift, Central Europe: Chemical Geology 257, 192-292.
Ulrych, J., Pivec, E., Lang, M., Balogh, K. & Kropáček, V. (1999), Cenozoic intraplate-volcanic rock series of the Bohemian Massif: a review: Geolines 9, 123-129.
Ulrych, J., Dostal, J., Hegner, E., Balogh, K. & Ackerman, L. (2008), Late Cretaceous to Paleocene melilitic rocks of the Ohře/Eger Rift in northern Bohemia, Czech Republic: Insights into the initial stages of continental rifting: Lithos 101, 141-161.

Volatiles in Ferrar LIP, North Victoria Land, Antarctica; Implications of age, water- and sulfur-contents, speciation and isotopic ratios of sulphur.

Bernhard Mayer[1], Lothar Viereck-Götte[2], Michael Abratis[2]
[1]Universität Hamburg, Mineralogisches-Petrographisches Institut, Hamburg, Germany
[2]Friedrich-Schiller-Universität Jena, Institute for Geosciences, Department Mineralogy, Jena, Germany

The Ferrar Large Igneous Province was sampled during the German expedition GANOVEX IX in austral summer 2005 in North Victoria Land. In the Deep Freeze Range fresh isotropic glasses from chilled margins of shallow (< 300m) sill intrusions and rims of pillows were found. While the sills are of andesitic composition the younger pillow lavas are less differentiated basaltic andesites.

The isotropic glasses were analysed for their contents of volatiles (H, C, O, F, and S by the DEGAS method: high-vacuum-hot-extraction combined with a quadrupol mass spectrometer), their S-isotopes (by MC-MS after precipitation as AgS), as well as the speciation of S in mineral inclusions (by micro-Raman spectroscopy).

Analysis of their 40Ar/39Ar ages exhibit a variable range of the ages with 10-30 Ma lower than the formation age of about 184 Ma due to a well known Cretaceous hydrothermal event. However, primary informations were preserved: andesitic sill "glasses" contain more sulphur and water than the basaltic andesite pillow rims, the their closing temperatures are lower by 200°C (~900°C compared to ~1100°C). Isotope analyses helped to identify samples with original primary condition, that still exhibit a primary isotopy of sulphur.

Based on the measured TiO_2/FeO ratio of the samples as well as sulphur contents of around 200ppm in the margins of sills and 500 ppm in the glassy rims of pillowed lavas a magmatic sulphur content about ~1000 ppm is deduced for melt inclusions. Verification by analyses of inclusions using EPMA are still ahead. A comparatively small leakage of around 2 x 1015 g of SO2 is assumed during the emplacement of the Ferrar LIP, cf. to 65 x 1015 g for the Deccan Traps).

S14-T24

Petrology of upper cretaceous igneous rocks in Javaherdeh area by the specific attention on volcanic rocks in Laj syncline

M.Sc. Seyedeh Roghayeh Mousavi, Dr. Mohammad Hashem Emami, Dr. Monireh Kheirkhah
Geological Science Research Center of geological survey of Iran

Igneous rocks of Cretaceous in Iran distribute in rifting structure zone around of center Iran Block and in Alborz mountain range, that Javaherdeh volcanic rocks on center of Alborz mountain range provide especial relative unweathered outcrops of volcanic rocks that can be study in Laj synclinal by some section that lie south of the area but the most part of volcanic rocks area in north covered by forest and vegetation however in some place can be seen uncovered outcropped.

The geological units of Precambrian, Paleozoic, Mesozoic, Cenozoic, quaternary have been exposed in the Javaherdeh area that majority of these exposures are related to the volcanic rocks of Mesozoic. Igneous rocks of upper cretaceous have been spread in northern and central parts of Javaherdeh area that research on petrology of the volcanic rocks and relationship with geodynamic of area is the main object.

Existence of igneous rocks in this area depends on the major changes in the earth crust of Iran and fission of different parts of it in the different times. The magmatism type is mainly volcanic rocks with composition of basic to intermediate such as basalt, andesite and spilitic basalt some times can see a few oltramaphic and maphic intrusive rocks.

The volcanic rocks of upper cretaceous of the area have been exposed in two series include of Aptian-Turonian stage (under part of upper cretaceous) and Maastrichtian stage (upper part of upper cretaceous). The under series often is seen in central and east of study area; in the folding crest. These rocks have been studied in Laj syncline in east of Javaherdeh area in three surveys from border toward center.

In first stage Laj synclinal have been surveyed in three section so for microscopic study 67 sample have been taken, in second stage have been done surveying from north to south of area with 9 sample taking; 3 sample from lower part of upper cretaceous, 5 sample from upper and lower part of lower cretaceous volcanic rocks, also 1 sample from a dike in javaherde sedimentary formation have been tacken. The samples are mainly from volcanic rocks but there are three samples from adjacent volcanic rocks to sedimentary rocks. 24 samples from upper cretaceous and 5 samples from lower cretaceous have been chosen for XRF analysis.

The rocks of lower series have been composed in a submarine environment in form of volcanic lavas and explosive, falling, hyaloclastites and pyroclastics. These lavas have been poured into soft sediments and have made peperite.

The volcanic rocks of upper series have been spread in north of the area. These lavas exposed in form of sheet flow, pillow lava and pyroclastic rocks in submarine environments and some area associated with oltramaphic and maphic intrusive rocks.

The lavas have been formed of alkali-olivin basalt in lower series that some times are seen intermediate rocks too in them. The pyroclastic rocks are separated in autoclastic and hydroclastite facies and falling pyroclastic sediments such as: tophite and aglomera in this series. Spilitization is a phenomenon that influences on the zone rocks and are observed secondary minerals resulted by this phenomenon in rocks very much. The lavas of northern Rahimabad and western Garmabdasht have been formed of pyroxin-olivin basalt. The stones of low series of Upper Cretaceous generally locate in basalt limit but some times have been entered to trackit-basalt limit considering geochemical diagrams. Some samples distinguished by trackit-andesite basalt composition in microscopic studies, have been entered to the areas of andesite, trackit-andesite, andesitic basalt in these diagrams. Basalt rocks of the zone are the same to MORB, E type and ocean crust in spider diagrams that are enriched in comparison to elements of Rb, K, Ba and are depleted in comparison to Nb elements that reveal crust contamination. Increasing La element in the zone can be related to crust contamination too. The incontinental basalts with MORB origin often have been showed by separating diagrams of tectonic environments.

In the geochemistry diagrams for basalts of the study area indicate some times alkaline, subalkaline and toleite composition that can be in transitional series same as Wilson definition from transitional series.

Mineralogy of the study area gives information that origin of basalt and trackit-basalt can be peridotite spinel, moreover enriched lerzolite can produce basalt-alkaline in 50-70 km depths too, another origin for the basalt in this area can be pyrolite with 20% partial melting on pressure of 1.35-1.8 Gpa.

The geochemistry, petrography and fielding studies indicate rifting geodynamic; basalts of this area have been generated in the margins of rifts in an extensional environment. Also existence of sedimentary-pyroclastic units under volcanic layers shows that faulty valleys caused by rift and the environment have been suitable for sedimentation of limestone units by progressive sea can seen in the study area.

Refrence:
S.R. Mousavi, Dr M. Emami (2003), Petrology of upper cretaceous igneous rocks in Javaherdeh sheet by the specific attention on volcanic rocks in Laj syncline, MSC thesis, Geological Science Research Center of geological survey of Iran

Section 15

_____

Time constraints on geological processes

Age constraints for events during the Archaean-Palaeoproterozoic transition: U-Pb geochronology on detrital zircons from FAR-DEEP drill cores, Fennoscandian Shield

Claudia Gärtner[1], Heinrich Bahlburg[1], Victor A. Melezhik[2,3], Aivo Lepland[2], Jasper Berndt[4], Ellen Kooijman[4] and the FAR-DEEP scientists
[1]Westfälische Wilhelms-Universität Münster, Institute for Geology and Palaeontology, Münster, Germany
[2]Geological Survey of Norway, Trondheim, Norway
[3]Centre for Geobiology, University of Bergen, Norway
[4]Westfälische Wilhelms-Universität Münster, Institute for Mineralogy, Münster, Germany

During the Archaean-Palaeoproterozoic transition many significant changes occurred in the Earth's environmental system. At the same time plate tectonic reorganisations like the break-up of the supercontinent Kenorland took place. Some of the changes are the Huronian glaciation, the Lomagundi-Jatuli positive excursion of $\delta^{13}C$ in sedimentary carbonates, and the Shunga event of enhanced accumulation of the organic matter, all occuring between 2.5 and 2.0 Ga. The Huronian glaciation (named after the Huronian Supergroup in Canada) was the first known glacial event with presumably global extensions. Palaeoproterozoic glacial deposits have also been reported from Africa and the Fennoscandian Shield. Three subevents of the Huronian glaciation have been recognized in Canada, and available geochronological data suggest the duration of the glaciation from around 2.45 Ga to 2.3 Ga or 2.22 Ga. The Huronian glaciation was followed by the Lomagundi-Jatuli Event that is characterized by ^{13}C-rich sedimentary carbonates, reported from all continents. The end of the glaciation at 2.3 Ga points to a beginning of the Lomagundi-Jatuli Event at this time. It continued until 2.06 Ga and was followed by the Shunga Event.

Although all events listet above are global in nature, and have been reported from different continents, age constraints for most of them are rather poor. Only the Huronian glaciation has been investigated geochronologically, but especially on the Fennoscandian Shield reliable data are rare. We applied LA-ICP MS U-Pb geochronology on detrital zircons from siliciclastic sedimentary rocks, which were drilled during the Fennoscandian Arctic Russia – Drilling Early Earth Project (FAR-DEEP) to improve age constraints for these three hallmark events. The FAR-DEEP aims at the Archaean-Palaeoproterozoic transition and provided a nearly complete record of the time interval from 2.5 to 2.0 Ga. The analysed samples derive from drill cores taken from five formations in the Pechenga and Imandra-Varzuga Greenstone Belts in the Kola province on the Fennoscandian Shield. Results of U-Pb geochronology on detrital zircons have provided one prominent age group of 2.9-2.6 Ga in all but two samples. This age group is related to the formation of the Fennoscandian Shield. The youngest ages in individual samples vary depending on their stratigraphic position and range up to 1.85 Ga. They give maximum depositional ages for the sampled formations. The results from the Seidorechka Sedimentary Formation and the Polisarka and Neverskrukk formations constrain the accumulation of glacial diamictites into the time interval from 2.43 Ga to 2.2 Ga. Similar ages have been reported for the glacial deposits in the Huronian Supergroup, Canada and the Pretoria Group, South Africa, consistent with a global glaciation at that time.

Maximum depositional ages from the Kuetsjärvi and Kolasjoki Sedimentary Formations indicate a duration of the Lomagundi-Jatuli event and the accompanying $\delta^{13}C$ excursion from at least 2.3 Ga to 2.06 Ga, in agreement with previous ages from these formations. For the Shunga event, no reliable geochronological data are available. Based on the suggestion that the Shunga event directly followed the Lomagundi-Jatuli event, we assume that it has started at 2.06 Ga. The youngest zircons from the Kolasjoki Sedimentary Formation show similar ages up to 2.0 Ga. Considering the analytical error, these zircon ages confine the transition from the Lomagundi-Jatuli event to the Shunga event to 2.06-2.0 Ga. Eventually the interval of the transition might be widened, when zircon ages of 2.0-1.85 Ga are verified by ID-TIMS analysis.

Does the global U-Pb age and Hf isotope record of detrital zircons reflect supercontinent cycles or is biased in favour of collisional orogens? A test considering Paleozoic sedimentary rocks of the proto-Andean accretionary orogen, Ecuador to Patagonia

Heinrich Bahlburg
Westfälische Wilhelms-Universität Münster, Institute für Geologie und Paläontologie, Münster, Germany;
Hbahlburg@uni-muenster.de

The global record of detrital zircon ages is frequently interpreted as reflecting cycles of supercontinent assembly and dispersal. When peaks in zircon age distributions are combined with data on the relative production of juvenile crust through time, a coincidence between the data sets is discernible for events mainly in the Archean and Paleoproterozoic. Hawkesworth et al. (2009) recently concluded that peaks in U-Pb detrital ages (n=7000; Campbell and Allen, 2008) and juvenile crust production do not always coincide on a global scale, and that a link to supercontinent cycles may in fact not exist. The reason for this is seen in the poor preservation potential of juvenile magmatic arc crust of accretionary orogens relative to continental collisional systems. This is significant as juvenile crust tends to be produced at active margins where it is also prone to destruction by subduction erosion. Granitic magmatic systems in collisional mountain belts, which later may become prolific sources of detrital zircons when eroded, are often formed by partial melting of preexisting crust. They may be volumetrically smaller than arc systems but have a better preservation potential due to their position in the interior of the evolving orogenic belts. The difference in formation and preservation potential is seen as a potential bias of the detrital zircon record towards collisional mountain belts. In contrast, non-collisional accretionary orogens should have detrital zircon age records free of this bias.

The SW Amazonia Orogenic System evolved by the episodic accretion of marginal orogenic belts to Amazonia from c. 2.3 to 0.9 Ga. From 0.9 to 0.25 Ga it was superseded by the Andean portion of the Terra Australis accretionary orogen. Recent reconsiderations of paleomagnetic data (e.g. Evans et al., 2010) together with the tectonic evolution of these orogens indicate that they reflect a c. 2 Ga long orogenic history free of major continental collisions.

A compilation of U-Pb detrital zircon ages (n= c. 5900) from Paleozoic sedimentary rocks representing the proto-Andes from Ecuador to Patagonia shows that age peaks coincide very well with the timing of assembly and dispersal of supercontinents. The coincidence with the respective record related to collisional orogenic belts indicates that the preservational bias is not necessarily as pronounced a factor in shaping this record as previously thought.

A similar compilation of Hf isotope data from proto-Andean detrital zircons (n= c. 620) shows a major divergence from the global patterns presented by Hawkesworth et al. (2009). The global data indicate peaks of juvenile crust production at the Archean-Paleoproterozoic transition and between 1.9 and 1.6 Ga. Subsequent orogenic cycles are not strongly reflected by juvenile data. This dichotomy is interpreted as due to the preferential preservation of evolved late stage orogenic crust in the rock record. In contrast, the detrital zircon Hf data from Paleozoic proto-Andean sedimentary rocks located in the the Andes from northern Peru to Patagonia reveal two important patterns, (i) production of juvenile crust occurred in the SW Amazonia Orogenic System and the proto-Andes throughout the Late Archean and Proterozoic; and (ii) a maximum seems to have been attained in the Rondonia-San Ignacio and Sunsas orogenic cycles between 1.55 and 0.9 Ga. The production of juvenile crust appears to have become a minor factor in this region at the Precambrian-Phanerozoic boundary.

References:
Campbell, I.H. & Allen, C.M., 2008, Nature Geoscience 1, 554-558.
Evans, D.A.D., 2009, Geological Society, London, Special Publication 327, 371-404.
Hawkesworth, C. et al., 2009. Science 323, 49-50.

Constraining the relative behavior of the U-Pb system and Zr in metamorphic rutile

Ellen Kooijman[1], Klaus Mezger[1,2], Jasper Berndt[1], Matthijs Smit[1]
[1]Westfälische Wilhelms-Universität Münster, Institut für Mineralogie, Münster, Germany
[2]Universität Bern, Institut für Geologie, Bern, Switzerland

Rutile (TiO_2) is a common accessory phase in metamorphic rocks and is stable over a wide range of P-T conditions, in particular at high pressures and temperatures. Because of its temperature-dependent partitioning of Zr, rutile provides a potentially reliable single-mineral thermometer (e.g. Tomkins et al., 2007). Depending on bulk-rock U content, rutile can incorporate up to 200 ppm U and can be dated with excellent analytical precision using the U-Pb system (e.g. Mezger et al., 1989). These aspects make rutile a suitable mineral for constraining the history of metamorphic rocks.

At high temperatures, the U-Pb system in rutile may (re-)equilibrate with the matrix by volume diffusion. The same may be expected for Zr and other trace elements. This complicates interpretation of results from rutile thermometry and geochronology, because Zr-in-rutile temperatures may neither represent peak conditions nor correspond to the U-Pb ages determined in the same grain. Although the diffusivities of Zr and Pb in rutile have been experimentally constrained (Cherniak, 2000; Cherniak et al., 2007), the relative behavior of these elements in natural metamorphic rutile is not well characterized. To better understand the Zr- and U-Pb systematics in rutile, we performed a combined electron microprobe (Zr) and laser ablation ICP-MS (U-Pb) study on rutile grains from slowly-cooled metapelitic rocks from the Archaean Pikwitonei Granulite Domain, Manitoba, Canada.

Laser ablation ICP-MS U-Pb dating of 35-μm spot transects across 15 rutile grains (120-280 μm) from 4 samples yielded concordant U-Pb ages with core ages of ca. 2450 Ma and decreasing ages from core to rim towards ca. 2280 Ma. The age profiles show no core plateaus, indicating that volume diffusion of Pb occurred throughout the grains. The ages were used to construct closure temperature profiles ($T_c(x)$; Dodson, 1986), representing the temperature of insignificant Pb diffusion as a function of position within the grains. The T_c estimates show a core-to-rim decrease from ca. 640 °C (depending on grain size) to an extrapolated value of ca. 490 °C. These estimates provide valuable insight into the closure behavior of the U-Pb system in rutile and allow a more effective use of U-Pb rutile dating in constraining cooling histories of metamorphic rocks.

In contrast to the U-Pb transects, Zr concentration profiles across the rutile grains show either homogeneous concentrations when present in the matrix or included in garnet, or decreasing concentrations throughout the grain from rim to rim depending on the neighboring grain. Some profiles display either a Zr decrease or increase of up to 200 ppm in the outermost 10-45 mu of grains, showing the effects of marginal volume diffusion. Variations among grains within one thin section are large (600-3400 ppm). If these concentrations are pristine, they would indicate highly variable crystallization temperatures (640-905 °C; Tomkins et al., 2007) for grains of the same mineral paragenesis, which is unlikely.

This study shows that Pb and Zr in rutile behave differently during cooling from high temperature conditions and are to variable degrees affected by volume diffusion. This decoupling indicates that U-Pb ages and Zr-in-rutile temperatures cannot be correlated directly. Our study confirms the difference between Pb- and Zr diffusion in rutile as predicted by experimental studies (Cherniak et al., 2007). Zirconium contents are likely to be pristine but may vary significantly for cogenetic minerals, possibly as a result of local Zr undersaturation. Therefore, care must be taken when applying Zr-in-rutile thermometry. In contrast, U-Pb dating of rutile is a robust method for providing reliable time constraints on various stages of cooling.

References:
Cherniak, D.J. (2000), Pb diffusion in rutile, Contributions to Mineralogy and Petrology, 139: 198-207
Cherniak, D.J., Manchester, J., and Watson, E.B. (2007), Zr and Hf diffusion in rutile, Earth and Planetary Science Letters, 261: 267-279
Dodson, M.H. (1986) Closure profiles in cooling systems, Material Science Forum, 7: 145-154
Mezger, K., Hanson, G.N. and Bohlen, S.R. (1989), High-precision U-Pb ages of metamorphic rutile: application to the cooling history of high-grade terranes, Earth and Planetary Science Letters, 96: 106-118
Tomkins, H.S., Powell, R. and Ellis, D.J. (2007), The pressure dependence of the zirconium-in-rutile thermometer, Journal of Metamorphic Geology, 25: 703-713

Evaluation of EMP-Th-U-Pb monazite ages and comparison to U-Pb SHRIMP data in the high-grade Wilson Terrane (Antarctica)

Bernhard Schulz[1], Friedhelm Henjes-Kunst[2], Ulrich Schüßler[3]
[1]TU Bergakademie Freiberg, Institute for Mineralogy, Freiberg/Sachsen, Germany
[2]Bundesanstalt für Geowissenschaften und Rohstoffe, Stilleweg 2, Hannover, Germany
[3]Universität Würzburg, Geodynamik und Geomaterialforschung, Würzburg, Germany

Zircon and monazite are widely used for U–Th–Pb dating of magmatic crystallisation and metamorphic processes in medium to high-grade rocks. Both minerals concentrate U and Th but exclude Pb when they crystallise, making them amenable to age dating. The unique and specific mineral chemistry and properties of the LREE-Th-phosphate monazite allows two different approaches for *in situ* age dating: (1) U-Pb isotopic dating by SHRIMP or LA-MC-ICPMS and (2) the Th-U-Pb EMP-CHIME dating by non-isotopic elemental analysis with an electron microprobe. Considering the common potential to date single grains and their domains *in situ*, the isotopic analyses provide data with high precision and low error at very high costs, compared to the non-isotopic EMP-CHIME method with high error upon the ages at very low costs. Further methological aspects of the contrasting methods were evaluated by analyses on garnet-biotite-gneisses (granulites, metatexites, migmatites) from the Northwestern Oates Land in the high-grade metamorphic Wilson Terrane in Northern Victorialand, Antarctica.

In a first step, monazites in grain mounts which were dated by the SHRIMP method were analysed by EMP (electron microprobe). This encloses the Madmon monazite with ~10 wt% ThO_2 and a SHRIMP age of 496±10 Ma (Schulz et al. 2007), the monazite VK1 (14.75 wt% ThO_2; 488 Ma) and the MPN monazite (2150 Ma), as reported in Henjes-Kunst et al. (2004). The Madmon monazite was also used as a standard for the calibration of Th with the EMP and its age was reproduced during all sessions at 503±11 Ma. The VK1 monazite was not suitable for EMP-CHIME dating due to its large variation in PbO. The MPN monazite was dated at 2098 ±18 Ma by EMP. As the ThO_2 contents in this monazites range from 5-7 wt% and in consequence the PbO is at 0.4-0.6 wt%, the lower ages compared to SHRIMP can not be explained by shortcomings in the Pb-EMP analysis or the YLb-on-PbMa interference correction. A considerable number of the EMP-CHIME ages range around 1600-1800 Ma and signalize a hydrothermal overprint of the MPN monazite grains. From the viewpoints of non-isotopic element analysis, the MPN and VK1 monazites which were used for adjustment and mass bias corrections of the SHRIMP have a number of unfavourable bulk compositional properties.

In a second step numerous EMP analyses were performed on sample monazites in the grain mounts. Many of these monazites display internal cauliflower-like heterogenities and internal zonal patterns with different graytones in backscattered electron imageing (BSE). This reflects a considerable variation of ThO_2 contents. A majority of EMP analyses from different monazite populations from a diatexite sample G8-57.4 (Mt Blowaway) yielded ages at 487±13 Ma, 484±10 Ma and 503±10 Ma which can be compared to the U-Pb SHRIMP monazite (493±9 Ma) and zircon (475±4 Ma) ages. In the same way the monazite populations from a metatexite sample G8-58.1 (Mt. Dalton) yielded Th-U-Pb EMP ages at 505±11 Ma, 500±9 Ma and 512±8 Ma, compared to the U-Pb SHRIMP ages of zircons (495±7 Ma composed of two populations at 500±4 Ma and 484±5 Ma) and monazites (499±10 Ma, composed of two populations at 501±5 Ma and 496±5 Ma; all SHRIMP data reported in Henjes-Kunst et al. 2004). The SHRIMP data provide indications for > 1 % common ^{206}Pb in the monazites. In the THO_2* vs PbO diagrams of the EMP analyses, in the diatexite and metatexite samples a large variation of PbO is observed, with ages ranging up to around 650 Ma. Dependent on the number of analyses and monazite grain population, these older monazites appear as a distinct group or overlap with the ~500 Ma population.

In a third step, monazites were analysed by EMP in thin sections of (cordierite-garnet)-biotite gneisses from numerous nunatak outcrops between the Pacific coast and the Daniels Range (Northern Victorialand). These monazites are mostly homogeneous in BSE images. The EMP-CHIME ages are mostly homogeneous too and range between 460 and 480 Ma. They correspond to K-Ar mica ages (Schüssler et al. 1999). The EMP-CHIME technique appears as a complementary method to the SHRIMP dating and provides a more detailed insight to the complex crystallization record of the monazites during a pre-anatectic event, partial anatexis at ~500 Ma and a prolonged cooling history within an Ordovician magmatic arc.

References:
Henjes-Kunst, F., Roland, N.W., Dunphy, J.M. & Fletcher, I.R. (2004), SHRIMP U-Pb dating of high-grade migmatites and related magmatites from Northwestern Oates Land (East Antarctica): Evidence for a single high-grade event of Ross-Orogenic age. Terra Antartica 11, 67-84.

Schulz, B., Brätz, H., Bombach, K., Krenn, E. (2007), In-situ Th-Pb dating of monazite by 266 nm laser ablation and ICP-MS with a single collector, and its control by EMP analysis: Zeitschrift für Angewandte Geologie 35, 377-392.

Schüssler, U., Bröcker, M., Henjes-Kunst, F. & Will, T. (1999), P-T-t evolution of the Wilson Terrane metamorphic basement at Oates Coast, Antarctica: Precambrian Research 93, 235-258.

S15-T05

In situ ^{238}U-^{230}Th disequilibrium dating of pyrochlore

Florian Wetzel[1,3], Axel K. Schmitt[2], Andreas Kronz[1], Gerhard Wörner[1]

[1]Georg-August-Universität Göttingen, Institute of Geochemistry, Goldschmidtstraße 1, 37077 Göttingen, Germany

[2]University of California Los Angeles, Department of Earth and Space Sciences, 595 Charles Young Drive E, Los Angeles, California 90095, USA

[3]ETH Zürich, Institute of Geochemistry and Petrology, Clausiusstraße 25, 8092 Zürich, Switzerland

We present the results of in situ ^{238}U-^{230}Th disequilibrium dating of pyrochlore [(Ca,Na,REE,Th,U)$_2$ (Nb,Ti,Ta,Zr)$_2$O$_6$(OH,F)]. This mineral is particularly useful for U-Th dating by secondary ion mass spectrometry (SIMS) because it shows high U and Th concentrations of up to 16 weight percent and Th/U ratios, which are variable over two orders of magnitude.

For our study we chose pyrochlores from cognate carbonatite fragments that were erupted from the phonolitic Laacher See volcano (Germany) about 12,900 years ago. These rocks represent the youngest known intrusive carbonatite occurrence in the world. Individual crystals were first analyzed for their U and Th isotopic composition using SIMS. The resulting ^{238}U-^{230}Th isochron yielded an internal precision of ~700 years (2σ). Afterwards, the chemical composition of pyrochlore was analyzed at the location of the SIMS spots by electron microprobe (EMP). Th/U obtained by EMP was used to correct for SIMS instrumental mass fractionation. The corrected pyrochlore isochron age is 26.1 ± 1.4 ka, including external calibration uncertainty. This age is in agreement with age constraints from zircon U-Th disequilibrium dating for the same sample that yielded an isochron age of 23 +7/-6 ka (Schmitt et al. 2010). The tightly constrained isochron and a low degree of metamictization argue for a closed U-Th system during the residence in the magma chamber carapace and during surficial weathering after the eruption 12.9 ka ago. In contrast, the same approach for pyrochlore from a Cretaceous alkali granite yielded significant disequilibrium with $(^{230}$Th$)/(^{238}$U$) = 0.90 \pm 0.04$, implying mobilization of actinides in radiation damaged pyrochlore.

Reference: Schmitt, A.K., Wetzel, F., Cooper, K.M., Zou, H. & Wörner, G. (2010), Magmatic longevity of Laacher See Volcano (Eifel, Germany) indicated by U-Th dating of intrusive carbonatites, Journal of Petrology, 51, 1053-1085

One Eclogite - Two Orogenies

Daniel Herwartz[1]*, Thorsten J. Nagel[1], Carsten Münker[2], Erik E. Scherer[3] and Nikolaus Froitzheim[1]
[1]Rheinische Friedrich-Wilhelms-Universität Bonn, Steinmann-Institut, Bonn, Germany
[2]Universität zu Köln, Institut für Geologie und Mineralogie, Köln, Germany
[3]Westfälische Wilhelms-Universität Münster, Institute for Mineralogy, Münster, Germany
*(E-mail: d.herwartz@uni-bonn.de)

Absolute dating of metamorphic rocks using radioactive decay systems is a fundamental tool in reconstructing the timing and rates of tectonic processes. Of the minerals present in metamorphic rocks, garnet is amongst the most instructive ones, providing a direct vestige of metamorphic pressure and temperature combined with age information. In rocks having a complex history, however, garnet may record more than one metamorphic episode, obscuring the geologic significance of its bulk isotopic age. We present Lu-Hf ages of two distinct garnet populations that - despite occurring in the same rock - were formed during different orogenies. An eclogite from Trescolmen (Adula Nappe, Central Alps), yielded discrete Lu-Hf ages of 37.10 ± 0.94 Ma and 336.0 ± 3.3 Ma, respectively, indicative of two distinct growth cycles. The younger cycle is attributed to the main eclogite facies (650 °C and 2 GPa) assemblage in which the garnet grew on an older generation of partially resorbed garnet. Our results confirm that subduction-related high-pressure metamorphism in the Central Alps is unambiguously Eocene in age and affected older basement that had already undergone a Paleozoic (Variscan) orogenic cycle. Although the Adula Nappe is one of the most classic and well-studied high-pressure units worldwide, its tectonometamorphic history is still vigorously debated. Rocks from the Adula Nappe have often been interpreted to represent a mélange of units with completely different metamorphic histories (Brouwer et al., 2005; Engi et al., 2001). These models asume, that mafic high pressure rocks were juxtaposed within the county rocks which lack any evidence for a high pressure history, at shallow crustal levels. However, consistent age information for large parts of the Adula Nappe, argue for subduction and exhumation of the unit as one coherent block. This interpretation is supported by the pressure gradient, which is gradually increasing from the south-western part to the northern part of the nappe (e.g. Nagel 2008). Our petrologic observations suggest that this is an entirely Alpine feature and mirrors the position of the Adula Nappe in an alpine subduction Zone. Hence the Adula Nappe underwent Alpine high-pressure metamorphism as a coherent tectonic unit and the buoyancy of intercalated felsic crustal rocks probably promoted their rapid exhumation.

Reference:
Brouwer, F.M., Burri, T., Engi, M. & Berger, A. (2005) Eclogite relics in the Central Alps: PT – evolution, Lu-Hf ages and implications for formation of tectonic mélange zones. *Schweiz. Mineral. Petrogr. Mitt.* **85**, 147-174.
Engi, M., Berger, A., & Roselle, G.T. (2001) Role of the tectonic accretion channel in collisional orogeny. *Geology* **29**, 1143-1146.
Nagel, T.J. (2008) Tertiary subduction, collision and exhumation recorded in the Adula nappe, central Alps *Geological Society, London, Special Publications* **298**, 365-392.

The first Lu-Hf garnet ages from the Eclogite Zone, Tauern Window, Eastern Alps

Silja Rexroth[1], Daniel Herwartz[1], Nikolaus Froitzheim[1], Carsten Münker[2], Thorsten Nagel[1], Sascha Sandmann[1]
[1]Rheinische Friedrich-Wilhelms-Universität Bonn, Steinmann-Institut, Bonn, Germany
[2]Universität zu Köln, Institut für Geologie und Mineralogie, Köln, Germany

The Tauern Window in the Eastern Alps exposes Penninic Units of oceanic and continental origin, including the Eclogite Zone with widespread kyanite-bearing eclogites, metamorphosed under conditions of up to 2.5 GPa and 630 °C (Hoschek, 2007). Dating of metamorphic minerals may help to link the Eclogite Zone to related units in the western Alps and thus may reveal its paleogeographic origin. A combination of geochronology with pressure and temperature estimates, can constrain timescales of tectono-metamorphic processes.

In this study we have investigated three eclogites samples from the Eclogite Zone in Frosnitztal in terms of Lu-Hf geochronology and petrology. The Eclogite Zone consists of high-pressure metasediments and intercalated eclogites and the unit is interpreted to be representative of the distal part of the former European passive continental margin. One sample (FRT5) yields a whole rock-garnet isochron of 32.8 ± 0.47 Ma with a reasonable MSWD of 1.5. This age is consistent with published Rb-Sr ages on white mica (ca. 32-28 Ma; Inger & Cliff, 1994; Glodny et al., 2005) and markedly younger than published Ar-Ar ages on phengite (45 Ma; Ratschbacher et al. 2004). Whole rock splits and garnet separates from the other two samples display some scatter in $^{176}Hf/^{177}Hf$ vs. $^{176}Lu/^{177}Hf$ space yielding an age range of ca. 50-30 Ma. The cause of this is presently unknown however the observed scatter may point towards older components in the studied samples.

Electron microprobe element mapping of individual garnet grains reveal typical prograde growth patterns with decreasing spessartine concentrations and Fe/(Fe+Mg) from core to rim. Because prograde element zoning of 2+ ions is preserved, it is reasonable to assume closed system behaviour of 3+ and 4+ ions, respectively. Hence the Lu-Hf ages most likely reflect prograde garnet growth.

We tentatively interpret the 32.8 Ma age to be representative of the alpine high pressure event for the Eclogite Zone, which is significantly younger than Eocene HP ages for various units in the western Alps (ca. 41-34 Ma), also interpreted to belong to the European margin (e.g. Dora-Maira Massif, Adula Nappe).

References:
Glodny, J., Ring, U., Kühn, A., Gleissner, P., Franz, G. (2005), Cystallization and very rapid exhumation of the youngest Alpine eclogites (Tauern Window, Eastern Alps) from Rb-Sr mineral assemblage analysis, Contrib. Mineral. Petrol. 149, 699-712
Hoschek, G. (2007) Metamorphic peak conditions of eclogites in the Tauern Window, Eastern Alps, Austria: Thermobarometry of the assemblage garnet plus omphacite plus phengite plus kyanite plus quartz, Lithos 93, 1-16.
Inger, S. & Cliff, R.A. (1994), Timing of metamorphism in the Tauern Window, Eastern Alps: Rb-Sr ages and fabric formation, Journal metamorphic Geol., 12, 695-707
Ratschbacher, L., Dingeldey, C., Miller, C., Hacker, BR., McWilliams, O. (2004), formation, subduction and exhumation of Penninic oceanic crust in the Eastern Alps: time constraints from $^{40}Ar/^{39}Ar$ geochronology, Tectonophysics 394, 123-287

Amalgamation of the Indian Dharwar Craton and the Southern Granulite Terrain: New Constraints from Lu–Hf Geochronology

Niels Noack[1], Reiner Kleinschrodt[1], Carsten Münker[1], Maria Kirchenbauer[2]
[1]Universität zu Köln, Institute for Geology and Mineralogy, Cologne, Germany
[2]Steinmann Institut, Rheinische Friedrich -Wilhelms Universität, Bonn, Germany

The amalgamation of major crustal blocks in India is still a controversial topic in models describing the framework of Gondwana assembly. A lack of systematical geochemical and geochronological surveys on structurally well-defined key sections hampers the interpretation of the regional geology and the timing of orogenic processes involved. To constrain the timing of amalgamation of the two blocks we performed Lu-Hf dating of garnet-bearing mafic granulites.

The study area Kanjamalai is located within the collisional belt between the Archean Dharwar Craton in the north and the Proterozoic Southern Granulite Terrain. Kanjamalai mountain (11.61N; 78.04E) near the town of Salem, Tamil Nadu, is a large double plunging syncline formed by a granulite-facies sequence of mafic granulites, layers of a banded-iron-formation (BIF) and migmatized metagranodiorites. The core of the Kanjamalai structure is surrounded by retrograde and intensely sheared amphibolite-facies mafic rocks associated with a regional scale shear zone. The mafic granulites occur in a primary association with BIFs, suggesting that their protoliths were formed as a former ocean floor sequence. Field observations show that the metagranodiorites intruded the association of mafic granulites and BIF. The mafic granulites suite is dominated by equilibrated, garnetiferous, coarse grained granulites with minor lensoid shaped occurrences of fine grained granulites free of garnet. The occurrence of garnet in the mafic granulites is clearly correlated with Mg# of the whole rock samples.

The sample used for isotope geochemical analysis contains cpx + grt + plag + hbl + qtz in a coarse grained foliated texture. Prevailing metamorphic conditions can be confined to pressures of ~6kbar and temperatures of ~700°C during peak granulite-facies metamorphism, corresponding to a burial depth of ~18km. Garnets are compositionally homogeneous with flat profiles for major elements. The Lu-Hf wr-grt isochron age of ca. 2.44Ga is therefore interpreted as a cooling age after closure of the Lu-Hf isotope system. Closure temperature estimates for Lu-Hf in wr-grt systems for comparable samples are ~650°C (and most certainly <700°C)(Scherer et al., 2000). Positive initial εHf values at 2.5 Ga for whole rock mafic granulites ranging from +7 to +9 indicate an already depleted mantle source for the mafic seafloor subvolcanics.

A Lu-Hf wr-grt exhumation age of 2.44Ga constrains Archean convergence and orogenic processes at the southern edge of the Dharwar Craton. Our results question earlier suggestions by Santosh et al. (2009) that mafic and ultramafic associations of the Salem area are part of the Panafrican Mozambique Ocean suture zone (550-600Ma). Gosh et al. (2004) reported Archean zircon ages of 2.53Ga from the Salem area, which constrain the onset of exhumation in this Archean orogen to roughly 100Ma after zircon growth.

References:
Ghosh, J.G., de Wit, M.J. and Zartman, R.E., (2004). Age and tectonic evolution of Neoproterozoic ductile shear zones in the Southern Granulite Terrain of India, with implications for Gondwana studies. Tectonics, 23, doi: 10.1029/2002TC001444
Santosh, M., Maruyama, S., and Sato, K., (2009). Anatomy of a cambrian suture in Gondwana: Pacific-type orogeny in southern India?, Gondwana Research, 16(2):321- 341.
Scherer, E.E., Cameron, K.L. and Blichert-Toft, J., (2000). Lu-Hf garnet geochronology: closure temperature relative to the Sm-Nd system and the effects of trace mineral inclusions, Geochimica et Cosmochimica Acta, Volume 64, Issue 19, 1 October 2000, Pages 3413-3432

Lu-Hf garnet geochronology documents Early Cretaceous and Eocene HP events in the Bulgarian Rhodopes

Maria Kirchenbaur[1,2], Silke Jahn-Awe[1], Jan Pleuger[3], Thorsten J. Nagel[1], Nikolaus Froitzheim[1], Carsten Münker[2]

[1] Steinmann-Institut, Universität Bonn, Germany; Kirchenbaur@uni-bonn.de
[2] Institut für Geologie und Mineralogie, Universität zu Köln, Germany
[3] Geological Institute, ETH Zürich, Switzerland

During the closure of the Tethyan realm, rock units of both oceanic and continental affinity were subducted at high-P conditions and subsequently incorporated in the Alpine orogen. Constraining the exact timing of these events as well as the protolith ages is crucial for reconstructing the geodynamic evolution. Especially for the eclogite-facies rocks of the Bulgarian Rhodopes little geochronological and geochemical data has been available so far to unravel the chronology of subduction, exhumation, and nappe stacking during the Alpine orogeny in the Eastern Mediterranean. The Lu-Hf isotope system has already shown to be useful to date HP mineral assemblages in other Alpine units, and therefore we applied this method to four eclogite samples from different units of the Alpine nappe stack of the Bulgarian Rhodopes: the (U)HP Kimi Complex (Upper Allochthon unit) as well as samples from the Middle Allochthon unit.

Electron microprobe analyses of the different garnet populations revealed prograde growth zoning pattern and hence, Lu-Hf ages are interpreted to date garnet growth. Estimated peak metamorphic temperatures of 600-700°C were below the closure temperature (T_C) estimated for the Lu-Hf system (e.g., Scherer et al., 2000). A somewhat younger high-T event reaching > 750°C is documented by coronae of Pl+Spl+Spr+Crn around decomposing Ky in one eclogite sample. This high-T event (1) either occurred immediately after the HP event and therefore cannot be resolved within error of the Lu-Hf age or (2) the temperature was still below T_C and did not reset the prograde garnet age. Our Lu-Hf results indicate two episodes of HP metamorphism: (1) an Early Cretaceous event in the eclogite from the Upper Allochthon unit (126.0 ± 1.7 Ma; MSWD = 3.3) and (2) Eocene metamorphism of the rocks from the Middle Allochthon unit (44.45 ± 0.78 Ma, MSWD = 1.4; 43.52 ± 0.43 Ma, MSWD = 0.19; 42.81 ± 0.48 Ma, MSWD = 0.07). Our new Lu-Hf data provide direct evidence for distinct Early Cretaceous and Eocene subduction events in the Rhodopes, in support of previous findings (U-Pb, Sm-Nd geochronology; e.g., Warwzenitz & Mposkos, 1997; Liati, 2005). Moreover, thrusting of the Middle over the Lower Allochthon unit (Pangaion-Pirin Complex) can be confined to a time span between 42 - 34 Ma.

References:
Scherer E.E., Cameron K.L., Blichert-Toft J. (2000). Lu-Hf garnet geochronology: Closure temperature relative to the Sm-Nd system and the effects of trace mineral inclusions. GCA 64 (19), pp. 3413 - 3432.
Warwzenitz N. & Mposkos E. (1997). First evidence for Lower Cretaceous HP/HT metamorphism in the Eastern Rhodope, North Aegean Region, North-East Greece. Eur. J. Mineral. 9, pp. 659 – 664.
Liati, A. (2005). Identification of repeated Alpine (ultra) high-pressure metamorphic events by U-Pb SHRIMP geochronology and REE geochemistry of zircon: The Rhodope zone of northern Greece. Contrib. Mineral. Petrol., 150, pp. 608 - 630.

The first astronomical age of a terrestrial meteorite impact: The Ries crater, SW Germany

Alexander Rocholl[1], Maria Ovtcharova[2], Urs Schaltegger[2], Jean Pohl[1], Albert Ulbig[3], Madelaine Boehme[1,4]
[1] LMU München, Department of Earth Sciences, München, Germany.
[2] Université de Genève, Section des Sciences de la Terre et de l'Environnement, Genève, Swizerland.
[3] Schlagmann Baustoffe, Zeilarn, Germany.
[4] University of Tuebingen, Institute for Geoscience, Paleontological Collection, Tübingen, Germany.

Accurate and precise dating of terrestrial impact structures is a prime intent of impact, stratigraphic, paleoclimatic, and paleontological research. Robust age estimates, however, are rare and available for only eleven of 174 confirmed impact structures (Jourdan et al. 2009). The Ries crater in SW Germany is one of the best preserved and well-studied terrestrial impact structures, yet its age is subject of discussion for over 50 years. At present, a bimodal age distribution with little overlap is apparent in published data. A long-standing „conservative" estimate of about 14.8 to 15.0 Ma (e.g., Staudacher et al. 1982; Storzer et al. 1995) was based on K-Ar, ^{39}Ar-^{40}Ar and fission track dating of impact melts (suevite glass) and tectites (moldavites). Recently, a number of ^{39}Ar-^{40}Ar studies suggested that the impact occurred some 14.3 to 14.5 Ma ago (e.g., Schwarz & Lippolt 2002; Laurenzi et al. 2003; Buchner et al. 2003 and 2010), implying that the "conservative" age estimate is too old by more than half a million years. These young ages are now frequently cited in secondary literature (e.g. Baier 2007; Stöffler et al. 2009), in spite of the fact that they pose severe problems on biostratigraphic and paleomagnetic interpretations. Most problematic is the fact that ages < 14.6 Ma are not compatible with the observed reversed magnetic field during the impact (Pohl 1977). Attemps of deducing mean ages from both the "young" and "old" age population (e.g. Jourdan et al. 2009) appear also awkward, because one of the age groups must be wrong.

Here, we deduce a highly accurate and precise age for the Ries impact by a multi-discipline approach which includes an additional dating technique, dating of material related and unrelated to the impact, geophysical evidence, and the recently established astronomical ages for the time window of interest. U-Pb single zircon ages of overlying and underlying volcanic tuffs of the Miocene bentonite series restrict the impact event to a small age-window from 15.00 ± 0.02 Ma to 14.93 ± 0.01 Ma. This age window thus confirms our recent ^{40}Ar/^{39}Ar data of the suevite impact melt of 14.89 ± 0.10 Ma (Abdul Aziz et al. 2008). Paleomagnetic evidence of a reversed Earth's magnetic field persisting during the impact together with new astronomic ages for the magnetic chrons between 15.29 and 14.17 Ma (Hüsing et al. 2010) excludes ages < 14.6 Ma and allocates the Ries event to chron C5Bn.1r. Consequently, the upper and lower limits of chron C5Bn.1r (15.000 Ma and 14.870 Ma, respectively) which are accurate to better than one per mill, constrain the Ries event at 14.94 ± 0.07 m.y. Our high-precision single grain U-Pb zircon ages in combination with the astronomical-calibrated paleomagnetic age for the first time solve the long-standing discussion on the age of the Ries impact.

References:
Abdul Aziz, H., Böhme, M., Rocholl, A., Zwing, A., Prieto, J., Wijbrans, J.R., Heissig, K., Bachtadse, V. (2008), Integrated stratigraphy and ^{40}Ar/^{39}Ar chronology of the Early to iddle Miocene Upper Freshwater Molasse in eastern Bavaria (Germany), Int. J. Earth Sci. (Geol Rundsch) 97:115–134.
Baier, J. (2007), Die Auswurfprodukte des Ries-Impakts, documenta naturae, ISBN 978-3-86544-162-1.
Buchner, E., Seyfried, H. & Bogaard, P. (2003), ^{40}Ar-^{39}Ar laser probe age determination confirms the Ries impact crater as the source of glass particles in Graupensand sediments, Int. J. Earth Sci. 92, 1-6.
Buchner, E., Schmieder, M., Schwarz, W.H., Trieloff, M., Jourdan, F., Wartho, J.-A., van Soest, M.C., Hodges, K.V. & Pösges, G. (2010), A new look at the Ries-Steinheim event, Abstract 41st Lunar Planet. Sci. Conf., 2151.
Jourdan, F., Renne, P.R., Reimold, W.U. (2009), An appraisal of the ages of terrestrial impact structures, Earth Planet. Sci. Lett. 286, 1-13.
Laurenzi, M.A., Bigazzi, G., Balestrieri, M.L. & Bou-Ka, V. (2003), ^{40}Ar-^{39}Ar laser probe dating of the Central European tectite-producing impact event, Meteor. & Planet. Sci. 38, 887-893.
Pohl, J. (1977), Paläomagnetische und gesteinsmagnetische Untersuchungen an den Kernen der Forschungsbohrung Nördlingen 1973, Geologica Bavarica 75, 329-348.
Schwarz, W.H. & Lippolt, H.J. (2002), Coeval argon-40/argon-39 ages of moldavites from the Bohemian and Lusatian strewn fields, Meteor. & Planet. Sci. 37, 1757-1763.
Staudacher, T., Jessberger, E., Dominik, B., Kirsten, T. & Schaeffer, O.A. (1982), ^{40}Ar-^{39}Ar ages of rocks and glasses from the Nördlinger Ries crater and temperature history of impact breccias, J. Geophys. Res. 51, 1-11.
Stöffler, D., Meyer, C., Reimold, W.U., Artemieva, N.A., Wünnemann, K. (2009), Ries crater and suevite revisited: Part I observations, 40th Lunar Planet. Sci. Conf., 1504.

POSTER PRESENTATIONS

Section 01

_____

CO₂ *sequestration into geological reservoirs and laboratory analogues*

P1-01

Tonmineralverlagerung bei der Injektion von CO_2 in einen salinaren Sandsteinaquifer

Kathleen Sell, Frieder Enzmann[1], Michael Kersten[1], Georg Wieber[2], Erik Spangenberg[3], Dietmar Meinel[4], Thomas Lautsch[5]

[1] Johannes Gutenberg-Universität, Institut für Geowissenschaften, Mainz, Germany, kersten@uni-mainz.de

[2] SGDN Regionalstelle Wasserwirtschaft, Montabaur, Germany

[3] Deutsches GeoForschungsZentrum, Telegrafenberg, Potsdam, Germany

[4] Bundesanstalt für Materialprüfung, Berlin, Germany

[5] Vattenfall Europe Carbon Storage Verwaltung GmbH, Cottbus, Germany

Die komplexen Wechselwirkungen zwischen Reservoirgestein, hochsalinarem Wasser und injizierten Gasgemisch sind Gegenstand einer umfangreichen Pilotstudie im Sandsteinaquifer des brandenburgischen Ketzin (www.co2sink.org). Durchströmungsexperimente an Bohrkernen dieses CO_2-Speicherstandortes wurden mit überkritischem CO_2 (+ 0,5-3,0% O_2) in einer Hochdruckapparatur für Bohrkernanalysen (FLECAS) des GFZ Potsdam durchgeführt (Kulenkampff & Spangenberg 2005). Ziel war die experimentelle Simulation der in-situ Temperatur- und Druckbedingungen bei der Injektionstiefe von 680 bis 700 m (Förster et al. 2006: $T = 40$ °C, $P_{Fluid} = 75$ bar, $P_{Con} = 150$ bar). In diesem Teilprojekt wurden Änderungen relevanter Gesteinsparameter bei den Druckversuchen wie Fluidchemismus, Porosität und Permeabilität gemessen sowie insbesondere Veränderungen der Porenmikrostruktur mit der hochauflösenden Röntgencomputertomographie (μ-XCT) untersucht.

Aus den Messungen des spezifischen elektrischen Widerstandes und des Fluidchemismus lassen sich im Rahmen der Messvarianzen keine signifikanten Fällungs- und nur relativ geringe Lösungserscheinungen während der experimentellen Durchströmungsdauer ($t \leq 250$ h) ableiten. Trotzdem hat sich die Permeabilität im Verlauf des Versuches deutlich erhöht, was die Annahme von Fluid/Gesteins-Wechselwirkungen bestätigt. Messungen der Kompressionswellengeschwindigkeit weisen auf eine heterogene Durchströmung bzw. Sättigungsverteilung der Proben hin. Die Interpretation dieser Effekte wurde erst durch den Vergleich der μ-XCT Bilder derselben Kerne vor und nach den Durchströmungsexperimenten ermöglicht. Die Sandsteinkerne aus Ketzin weisen mittlere bis hohe Tonmineralgehalte (13-36%) auf. Alle Proben zeigen nach dem Versuch eine ausgeprägt heterogene Gefügebeanspruchung, insbesondere eine deutliche Tonmineralverlagerung. Die Porosität änderte sich dadurch insgesamt zwar relativ wenig ($\leq$ 3%), die Umverteilung der Tonmineralablagerungen bewirkte aber eine inhomogene Durchströmung durch Ausbildung bevorzugter Wegsamkeiten und damit eine Änderung der Permeabilität auch ohne geochemische Lösungs-/Fällungserscheinungen.

References:

Förster, A., Norden, B., Zinck-Jørgensen, K., Frykman, P., Kulenkampff, J., Spangenberg, E., Erzinger, J., Zimmer, M., Kopp, J., Borm, G., Juhlin, C., Cosma, C. & Hurter, S. (2006), Baseline characterization of the CO2SINK geological storage site at Ketzin, Germany. – Environ. Geosci., 13, 145-161.

Kulenkampff, J. & Spangenberg, E. (2005), Physical properties of cores from the Mallik 5L-38 production research well under simulated in situ conditions using the Field Laboratory Experimental Core Analysis System (FLECAS). – In: Dalimore, S.R. & Collett, T.S. (eds.): Scientific Results from the Mallik 2002 Gas Hydrate Production Research Well Program, Mackenzie Delta, Northwest Territories, Canada. Geological Survey of Canada Bulletin 585 (CD-ROM attachment).

Development of underwater gas monitoring systems

Ingo Möller, Kai Spickenbom, Christian Seeger[1]
[1] BGR – Bundesanstalt für Geowissenschaften und Rohstoffe, Hannover, Germany

One of the major concerns related to geological storage of carbon dioxide below the seafloor or lake beds is the possibility of leakages from the reservoir and subsequent effects on the environment, which cannot completely be excluded. Underwater gas monitoring should be a required part of the establishment and secure management of sub-seabed CO_2 storage sites.

As a contribution to the EC-supported project CO_2ReMoVe, BGR's resource geochemistry section aims at the development of monitoring tools and methods for free gas emanations under water. This comprises basically two methodological steps demanding different techniques: the detection and the quantification of gas releases.

For the quantification of known underwater gas releases, a fully submersed stationary system has been constructed. Due to its relatively simple mechanical and electrical setup it is suitable for an unattended long-term monitoring even in rough marine environments. The system consists of a funnel-shaped gas collector, a sensor head and pressure housings for electronics and power supply. Since this setup is inexpensive, it can be deployed in numbers to cover larger areas. In combination with multi-channel data loggers, data transmission by acoustic modem or cable, relay stations on the seafloor or buoys etc. the infrastructure can be adapted to various environmental settings. The overall capability and robustness of the system have already been demonstrated under laboratory conditions and during extensive field tests using natural underwater gas vents in Laacher See and Lake Constanze, Germany, which serve as natural analogues to leaking storage sites.

The stationary system provides primarily point data for specific gas releases. These data are very reliable but cannot realistically be extrapolated over larger areas. To overcome these problems and to simply cover larger areas, the second approach is on mobile monitoring systems using a Micro-ROV as a carrier. The ROV (remotely operated vehicle) is equipped with an acoustic positioning system and scanning sonar for underwater navigation in low visibility water; a setup that can also be used for the localization of gas plumes (fig. 1). Other additional devices, such as tools for water and gas sampling, *in situ* gas flow measurements, and different environmental parameters like temperature and pH have been developed or adapted. Tests at the above mentioned natural analogues were very successful and promising.

Nevertheless, even by using an ROV the monitoring of large areas remains a very time consuming procedure. But it can significantly be accelerated by a preceding survey by ship-mounted acoustic methods like sidescan sonar or multibeam sonar. Rising gas bubbles leave a clear signal in sonar surveys and can be identified and localized with relatively high certainty. These methods are therefore suitable for covering large areas in a relatively short time and can be applied in defined time intervals. Once 'suspicious' areas are identified, an ROV with suitable equipment can be deployed for more detailed inspection and verification.
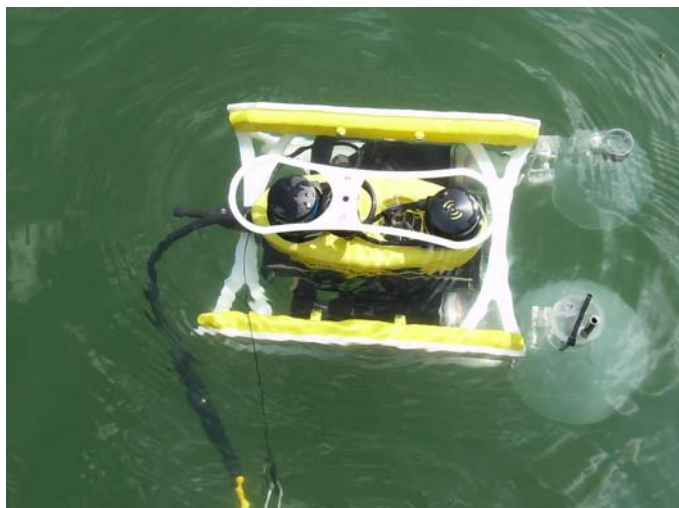
Fig. 1: Micro-ROV with gas monitoring devices in operation.

Summing up, we recommend a three-level concept for the long-term gas monitoring of offshore CO_2 storage sites. The first step is the periodical, regular use of a ship-mounted sonar system to check for indications of gas release. Secondly, if there exist anomalies suspicious to gas release, an ROV should be navigated to the site for optical verification of the first sonar information, *in situ* measurements and collecting samples for lab analysis. Finally, if leakage is confirmed by the ROV operation, a funnel-based stationary monitoring system can be installed for continuous controlling purposes.

P1-03

Construction of an autoclave system for the study of geochemical/mineralogical rock behaviour under reservoir conditions during the sequestration of CO_2: first results of the COORAL[1] project

Michael Schmidt[1], Herbert Pöllmann[1], Herwig Marbler[1], Kirsten Erickson[1], Christof Lempp[1]
[1]Martin-Luther-Universität Halle Wittenberg, Geowissenschaften, Halle/Saale, Germany

The storage of CO_2 with co-captured incidental substances in deep geological formations may affect fluid-fluid and fluid-rock interactions. These interactions may lead to mineral alterations, changes in porosity and permeability and possibly to changes in rock strength and formation stability. In order to gain knowledge about these processes, a combination of long-term geochemical/mineralogical experiments and geomechanical tests are carried out on various reservoir rocks, such as sandstones and siltstones, with supercritical CO_2 containing variable amounts of incidental substances in an autoclave system and in a triaxial pressure cell.

Aim of the described autoclave setup is to alter typical reservoir rocks under simulated *insitu* temperature and pressure conditions for both geochemical/mineralogical as well as subsequent geomechanical investigations. Therefore, a coupled autoclave system was designed and thoroughly tested. The sample size for both experiments is defined by the triaxial pressure cell requiring a cylinder of 70 x 140 mm. Two BERGHOF BR-2000 autoclaves with a volume of two litres each were used for the geochemical/mineralogical experiments. The autoclaves are equipped with PTFE liners and heating jackets. In addition to multiple valves each autoclave is equipped with a thermocouple and a pressure gauge. Stirring is possible in one of the autoclaves.

Both autoclaves are coupled through an insulated pipe loop system in order to circulate the CO_2 saturated brine. For fluid circulation a PTFE-lined magnetic pump was designed with a continuous flow rate of 50 ml/min. Pumping capacity can be adjusted to higher rates via a computer. Venting of the whole system with CO_2 or N_2 is done through valves in the pipe system which can also be used for sample extraction.

A measuring stage for pH, conductivity and redox potential for the extracted fluid is also part of the system. The three chambers of the measuring device are fed through a PTFE tube which is attached to a valve in the pipe system. Preliminary results show that after 5 minutes of continuous fluid flow stable values are recorded. Due to temperature and pressure changes of the fluid between the autoclave and the measuring chambers these obtained values for pH etc. do not represent the exact conditions of the brine within the autoclave. However, they give useful additional information in the course of experiments.

DMG, Poster, Session: CO2-Seq. in Natur und Labor

The Buntsandstein of N-Hesse and S-Thuringia as a natural analogue for CO_2-sequestration

Jens Köster[1], Ulrike Hilse[1], Dieter Pudlo[1], Jutta von der Gönna[2], Georg Nover[2], Reinhard Gaupp[1]
[1] Friedrich-Schiller-University Jena, Institute of Earth Science, Jena, Germany
[2] Rheinische Friedrich-Wilhelms-University Bonn, Steinmann Institute, Bonn, Germany

This contribution focuses on Buntsandstein deposits in N-Hesse and S-Thuringia as potential reservoirs for industrial CO_2-sequestration. Due to the proximity to the Cenozoic Central European Volcanic Province (CEVP) Buntsandstein in these areas are most likely affected by fluids containing CO_2. Natural analogues are very suitable for studying fluid –rock reactions expected during CCS projects.

The sample material originates from several shallow wells drilled in the NE-part of the Hessian Depression. The Buntsandstein in this area is a medium to very fine grained, structurally and texturally mature arkose – subarkose and exhibits typical sedimentary structures of fluvial (probably ephemeral) and lacustrine deposits.

The material was characterized with polarisation (PL) - and cathodoluminescene (CL) microscopy, XRD, XRF, directly coupled evolved gas analysis (DEGAS) and microprobe analysis. Vitrinite reflectance (VR) measurements of the underlying Kupferschiefer were performed for palaeotemperature and burial history considerations. Special emphasis was placed on differences between red (unbleached) and white (bleached) sandstones, assuming that bleaching was induced by CO_2-fluid-rock reactions. Often such alteration phenomena occur along joints and cracks, which acted as sites for preferential fluid ascent, and extent from these sites into the host rock.

The following authigenic phases could by identified by means of PL, CL and XRD (Rietveld): quartz, k-feldspar, hematite, leucoxene, calcite, dolomite, illite, chlorite/smectite, and illite/smectite. Hematite coatings of detrital clasts resulted from the infiltration of clay-sized particles under oxic conditions during early burial. Leucoxene originated from the alteration of volcanic/magmatic clasts and are more abundant in the bleached sandstones. Chlorite/smectite (probably corrensite), illite/smectite and illite (type 2M1d) evolved from smectite during continued diagenesis. Illite occurs in the form of grain rimming radial illite (IR) and illite meshwork (IM). IM is more abundant in the bleached rocks, especially as replacement of feldspars and rock fragments. In places IR growth continued into porespace, there forming thin pore-spanning fibres. Dolomite forms early diagenetic cements and late diagenetic replacements of feldspars and clay clasts. High Mg-, as well as low Mg bearing calcites reveal intensive zoning sustained by CL analysis. Central parts of zoned calcites are always enriched in Fe (0.75 -1 weight-%). The occurrence of these calcites is restricted to bleached rocks, sometimes replacing dolomite. Therefore a transfer of Fe from oxide to carbonate is likely. DEGAS measurements on adjacent bleached and unbleached sandstones within composite rocks reveal differences in the degassing behaviour of these two rock types. In the bleached part, the degassing pattern of $m/e = 1$ (H^+) displays characteristics of a second hydrogen source, except water. It correlates with $m/e = 12$ (C^+) and $m/e = 16$ (O^+, CH_4^+) pointing towards remnants of undefined hydrocarbons in the bleached area. Vitrinite reflectance of Kupferschiefer is in the order of 1.3 %, indicating burial temperatures of 140-150 °C. A similar temperature range can be assumed by Illite Crystallinity Index considerations, implying deep burial conditions with elevated temperatures for illite crystallization.

At present, investigations on the dissolution behaviour of Buntsandstein forming minerals are in progress. Here single polished feldspar and mica grains will be analysed with microprobe and SEM techniques before and after CO_2 treatment. Single feldspar crystals will also be analysed by means of atomic force microscopy (AFM) to quantify the amount of etching induced by the lab runs.

Carbonate vein geochemistry: tracer of seawater circulation during exhumation and uplift of oceanic core complexes

Wolfgang Bach[1], Niels Jöns[1], Martin Rosner[1,2], Laura Robinson[3]
[1]Geoscience Department, University of Bremen, Germany; [2]Bundesanstalt für Materialforschung und –prüfung Berlin, Germany; [3]WHOI, Woods Hole, USA

Carbonate veins are a common alteration feature of altered ocean crust (AOC). Previous studies have shown that the chemical and isotopic composition of carbonate veins can be used to gain information about the composition and physico-chemical conditions of the precipitating fluid and the age of precipitation. Due to the CO_2 uptake during its aging, the oceanic crust is an important sink for CO_2 with overall uptake rates on the order of $2 \cdot 10^{12}$ moles/yr. Most previous studies of carbonates from AOC focused mainly on volcanic sections of crust generated at intermediate and fast spreading MORs. The impact of vein carbonates in ultramafic rock on the global carbon budget, however, is unknown. The knowledge gap is critical, as about 20% of the seafloor created along slow-spreading ridges is ultramafic in composition, and ultramafic rocks are potentially important sites of CO_2 sequestration.

To reconstruct the physico-chemical conditions and timing of carbonate precipitation in ultramafic basement, we studied the chemical and isotopic composition of carbonate veins from two sites (1271 and 1274) at the Mid-Atlantic Ridge (MAR) at about 15°20'N. The combination of trace element data with Li-C-O-Sr isotope compositions and radiometric age determinations allow unique insights into the chemical and isotopic evolution of seawater within the basement and the timing of carbonate formation during sub-seafloor water-rock interactions. The data are also useful in constraining upward migration of deeply rooted hydrothermal fluids within detachment faults that expose mantle rocks at the seafloor.

Carbonate veins hosted in ultramafic basement drilled at MAR 15°20'N record two different stages of fluid-basement interaction. A first generation of carbonate veins consists of calcite and dolomite that formed syn- to postkinematically in detachment faults. These veins are hosted in talc-serpentine-chlorite schists and formed at temperatures between 90 and 170°C (oxygen isotope thermometry) and from fluids that show intense exchange of Sr and Li with the basement ($^{87}Sr/^{86}Sr = 0.7044$, $^{7}Li = 6‰$). Carbon isotopic compositions range to high ^{13}C values (9‰), indicating that methanogenesis took place within the detachment fault system. The carbonate Sr and Li isotopic composition suggest temperatures of fluid-rock interaction (>350-400°C) that are much higher than the inferred temperatures of precipitation. This discrepancy can be explained if the fluids were cooled conductively during upflow within the detachment fault. The second generation of carbonate veins are aragonite, which formed during the last 130 kyrs at low-temperatures (<15°C) within the uplifted serpentinized peridotites. Chemical and isotopic data suggest that the aragonites precipitated from cold seawater showing overall little exchange with the basement. Small but systematic down-hole variations in stable isotope and Mg/Ca ratios of aragonites indicate a distinct compositional evolution of downward migrating seawater. Oxygen isotope compositions suggest an increase in formation temperature of the veins from 2°C near the seafloor to 15°C at ~80mbsf. This increase of ~15°C in the upper 100 meters of basement sets an upper limit for the regional geothermal gradient.

Aragonite veins make up >90% of the carbonates recovered from both sites. Ages indicate episodic aragonite vein formation, some of it fairly recent (e.g., 2-12 kyrs at Site 1274). The overall aragonite vein abundance at both sites is ~0.2 wt.%, equivalent to an estimated CO_2 uptake of ~0.1 wt.%. This mass change is similar to what was proposed for uplifted gabbroic basement and young sedimented ridge flanks, but is much smaller than the CO_2 uptake estimated for old volcanic ridge flank crust (2-3 wt.% CO_2). Unless the 80-85% of basement that were not cored have dramatically higher vein abundance, it appears that the exhumed mantle took up less CO_2 than the equivalent volume of basaltic crust. This is likely due to the greater permeability of basaltic crust and to the ease at which basaltic glass weathers and releases Ca to the interacting seawater-derived solutions. Although the capacity of peridotite for sequestering CO_2 is great, the most efficient trapping mechanism invokes the formation of magnesite, which requires high activities of CO_2 and elevated temperatures. Our data suggest that low-temperature oxidative alteration of exhumed mantle is probably not a globally important sink for CO_2. This conclusion is corroborated by the general scarcity of low-temperature aragonite veins in serpentinized mantle from other drill core. All these sites are in young lithosphere, however, and the estimates of CO_2 uptake may go up if fracturing and CO_2 veining continues for tens of millions of years. This possibility can be tested by drilling in old rift mountains.

Section 02

————

Early differentiation and core formation of the terrestrial planets

Experimental study of the crystallization of the lunar magma ocean.
E. J. Tronche and W. van Westrenen [1]
Department of Petrology, Faculty of Earth and Life Sciences, VU University Amsterdam,
elodie.tronche@falw.vu.nl

The Moon likely underwent a global magma ocean stage very early in its history (Shearer et al. 2006). The crystallization of this lunar magma ocean (LMO) potentially created a series of concentric cumulate layers with different mineralogical assemblages. The crystallization of these cumulate layers is of primary importance for later events such as the formation of a plagioclase-rich crust and an overturn in the mantle, possibly leading to basaltic mare volcanism (Snyder et al. 1992). The crystallization sequence and mineralogy are dependent on the initial composition of the silicate Moon. Until 2006, it was generally believed that the lunar silicate composition was Al-rich (around 6 wt% Al_2O_3) (Shearer et al., 2006). But a recent study from Khan et al. (2006) showed that only lower Al contents can fit physical data. These authors proposed a new lunar composition, Al-poor and FeO-rich. In this study, we determined the crystallization behaviour of a magma ocean with this composition, with three main questions in mind: (1) can a thick anorthositic crust form, (2) will overturn occur in the mantle due to gravitational instability of the resulting cumulate pile, and (3) can we explain the compositions of mare basalts and other volcanic products at the lunar surface by remelting overturned cumulate piles.

We performed experiments in an end-loaded piston cylinder, at pressures from 1 to 3 GPa (which correspond to a 700 km deep magma ocean) and in a non end-loaded piston cylinder for pressures from 0.4 to 1 GPa. Temperatures varied from 1000°C to 1650°C. The oxygen fugacity in these experiments is ΔIW=-1.1. We assumed the first 50% of solidification of the magma ocean occurred as equilibrium crystallization, and the second half as fractional crystallization. We used a simple CFMAS + TiO_2 system, doped with trace elements to determine mineral-melt partition coefficients of liquidus phases.

After 50 % of crystallization under equilibrium (at approximately 1550°C), only olivine (liquidus phase) and orthopyroxene are present. Their compositions vary depending on P and T which results in compositional zonation in the cumulate layer. At lower pressures only olivine is present, while when pressure increases the orthopyroxene content increases for the same temperature. As a result, the crystals sinking at the base of the magma ocean are creating a layer that is continuously enriched in opx with depth (figure 1).
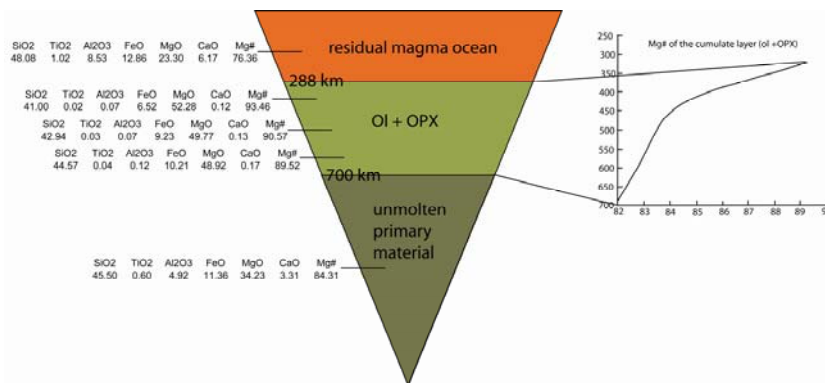
Figure 1: composition of the Moon after 50 % crystallization of the magma ocean. The graph shows the variation of the bulk Mg# in the cumulate layer.

Once half of the lunar magma ocean is solidified, the cumulate layer extends from 288 to 700 km depth. Its composition gradually varies with depth. Figure 1 gives three bulk compositions at three different depths in this layer. The remaining liquid is richer in Al and Ca than the original composition, and has the composition shown at the top left of Figure 1.

The next step (fractional crystallization) starts at the bottom of the cumulate layer (1.4 GPa) and at 1550°C, and lower temperatures. Experiments performed from 1.4, 1.2, 1 GPa and room pressure show that the next 10 % of crystallization is reached at 1500°C. It consists of only olivine (orthopyroxene appears after 15 % of crystallization). The olivine layer is 54 km thick, and has a mg# of 91. The residual LMO is getting Al, Ti and Ca enriched compared to the previous step, and is 234 km deep (up to 1.1 GPa).

Experiments are still in progress to complete the crystallization sequence of this LMO at lower pressures. Once this is completed, we will be able to establish a complete cumulate pile profile and assess the three questions mentioned above.

Reference:
Khan A. et al. (2006) EPSL 248, 579-598.
Shearer C. K. et al. (2006) in New Views of the Moon, 365-518.
Snyder et al. (1992) GCA 56, 3809-3823.

The thermal equation of state of $FeTiO_3$ ilmenite based on *in situ* X-ray diffraction at high pressures and temperatures.

E. J. Tronche[1], M. van Kan Parker[1], J. de Vries[1,2], Y. Wang[3], T. Sanehira[3], J. Li[4], B. Chen[5], L. Gao[6], S. Klemme[7], C. A. McCammon[8], and W. van Westrenen[1]

[1]Faculty of Earth and Life Sciences, VU University Amsterdam, De Boelelaan 1085, 1081 HV Amsterdam, The Netherlands.
[2]Faculty of Geosciences, Utrecht University, Budapestlaan 4, 3584 CD Utrecht, The Netherlands.
[3]Center for Advanced Radiation Sources, University of Chicago, 5640 Ellis Ave., Chicago, IL 60637, USA.
[4]Department of Geological Sciences, University of Michigan, Ann Arbor, Michigan.
[5]Division of Geological and Planetary Sciences, California Institute of Technology, Pasadena, CA 91125, USA.
[6]Department of Geology, 1301 W. Green St, Urbana-Champaign, IL 61801, USA.
[7]Institut für Mineralogie, Corrensstrasse 24, D-48149 Münster, Germany.
[8]Bayerisches Geoinstitut, Universität Bayreuth, D-95440 Bayreuth, Germany.

Ilmenite ($FeTiO_3$) plays an important role in current models of the thermal and magmatic evolution of the Moon (e.g. Shearer et al. 2006). Its crystallization toward the end of the solidification of a global lunar magma ocean resulted in a gravitationally unstable mineral stratification in the lunar mantle (Snyder et al. 1992), prompting a large-scale mantle overturn (de Vries et al. 2010). The thermal effects associated with this overturn are believed to have triggered the formation and eruption of the lunar mare basalts that cover a significant part of the lunar near-side surface (e.g. Lucey et al. 2006).

Thermo-chemical models of the internal evolution of the Moon thus require accurate knowledge of the density of ilmenite as a function of pressure (P), temperature (T) and chemical composition. Due to its limited importance for the dynamics of the interior of the Earth, the thermal equation of state of $FeTiO_3$ ilmenite has not been studied extensively. As a result, the temperature dependence of the bulk modulus, and pressure dependence of thermal expansivity are poorly constrained. In addition, the reducing conditions on the Moon lead to the absence of Fe^{3+} in lunar ilmenite, whereas in terrestrial ilmenite 15-30 % of iron is trivalent (e.g. Virgo et al. 1988). The effects of oxidation state on ilmenite's density evolution are not known.

In order to determine the thermal equation of state of reduced ilmenite, we performed *in situ* measurements of the unit-cell volume of a natural terrestrial ilmenite and a synthetic reduced ilmenite ($FeTiO_3$) at simultaneous high pressure and high temperature up to 16 GPa and 1273 K. Unit-cell volumes were determined using energy-dispersive synchrotron X-ray diffraction in a multi-anvil press. Mössbauer analyses show that the synthetic sample contained insignificant amounts of Fe^{3+} both before and after the experiment.

Results were fit to Birch-Murnaghan thermal equations of state, which reproduce the experimental data to within 0.5 and 0.7 GPa for the synthetic and natural sample, respectively (Tronche et al. 2010). At ambient conditions, the unit-cell volume of the natural sample ($V_0 = 314.75 \pm 0.23$ (1σ) Å^3) is significantly smaller than that of the synthetic sample ($V_0 = 319.12 \pm 0.26$ Å^3). The difference can be attributed to the presence of impurities and Fe^{3+} in the natural sample. The 1 bar isothermal bulk modulus K_{T0} for the reduced ilmenite is slightly larger than for the natural ilmenite (181 ± 7 GPa and 165 ± 6 GPa respectively), with pressure derivatives $K_0' = 3 \pm 1$.

Our results, combined with literature data (Wechsler and Prewitt, 1984; Bayer et al., 1972), suggest that the unit-cell volume of reduced ilmenite is significantly larger than that of oxidized ilmenite, whereas their thermoelastic parameters are similar. Our data provide more appropriate input parameters for thermo-chemical models of lunar interior evolution, in which reduced ilmenite plays a critical role.

References:
Bayer et al. (1972) X-ray study and Mossbauer spectroscopy on lunar ilmenites (Apollo 11). Earth and Planetary Science Letters, 16, 273-274.
Lucey et al. (2006) Abundance and distribution of iron on the Moon. Science 268, 1150-1153.
Shearer et al. (2006) Thermal and magmatic evolution of the Moon. Reviews in Mineralogy and Geochemistry, 60, 365-518.
Snyder et al. (1992) A chemical model for generating the sources of mare basalts: combined equilibrium and fractional crystallization of the lunar magmasphere. Geochimica et Cosmochimica Acta, 56, 3809-3823.
Tronche et al. (2010) The thermal equation of state of $FeTiO_3$ ilmenite based on *in situ* X-ray diffraction at high pressures and temperatures. Submitted to American Mineralogist.
Virgo et al. (1988) Constraints on the oxidation state of the mantle: an electrochemical and [57]Fe Mössbauer study

of mantle-derived ilmenites. Geochimica et Cosmochimica Acta, 52, 1781-1794.

de Vries et al. (2010) Formation and evolution of a lunar core from ilmenite rich magma ocean cumulates. Earth and Planetary Science Letters, 292, 139-147.

Wechsler and Prewitt (1984) Crystal structure of ilmenite ($FeTiO_3$) at high temperature and at high pressure. American Mineralogist, 69, 176-185.

Experimental study of metal-silicate partitioning during the formation of the Martian core.

C.H. Wijbrans[1], E. J. Tronche[1]and W. van Westrenen[1]
Department of Petrology, Faculty of Earth and Life Sciences, VU University Amsterdam, the Netherlands

The formation of a metallic core is the largest differentiation event in the early history of the terrestrial planets, but the processes accompanying this event are poorly constrained. Current core formation models are based on chemical equilibration of metal melts with silicate magma at the bottom of planet-wide magma oceans. These models rely on laboratory measurements of the distribution of iron-loving (siderophile) elements between molten metals and molten silicates at high pressures and temperatures. For the Earth, such experiments lead to a current estimated magma ocean depth of approximately 1800 km, providing tight constraints on Earth's temperature profile during core formation.

Unfortunately, these data cannot be directly used to constrain magma ocean depth during core formation on Mars. The Martian core is thought to be much more sulphur rich than the core of the Earth, and the effect of sulphur on element distribution at high pressure is virtually unconstrained.

Here, we performed high temperature (1600-1650°C) and high pressure (1, 2 and 3GPa) experiments in order to determine Cobalt and Nickel partitioning between silicate and metal melts, with varying content of sulphur (0, 5, 15 and 25 wt%). The silicate composition chosen was taken from Khan and Connolly (2008), and provides a best-fit to currently available geophysical data from Mars. Experiments were performed in an end-loaded piston cylinder press using graphite-lined Pt capsules.

Temperatures reached do not allow this refractory silicate composition to melt completely. Olivine and sometimes orthopyroxene were coexisting with silicate and metal melts. The sulphur-bearing metals formed two alloys, a sulphur rich and a sulphur-poor metal. Major and minor element analyses were performed with an electron microprobe (JEOL 8800 at VU University Amsterdam). Mass balance calculations show that most of our experimental charges suffered from significant Ni-loss. Because of this, Ni contents were very low and resulting errors on its partitioning behaviour are large. In addition we cannot guaranty that equilibrium was obtained for the element. Cobalt did not have this problem. The partitioning of Co between metal and silicates, or metal and melt only, does not vary significantly with sulphur content, and the coefficients for Ni are within error to each other (figure 1). Data also show that the partitioning of Co and Ni does not vary with the silicate melt composition (NBO/T).Our data agree with one previous study on Ni and Co partitioning between sulphide and silicate melt (Jana and Walker, 1999).

Figure 1: LnD$_{metal/melt}$ for Co and Ni.
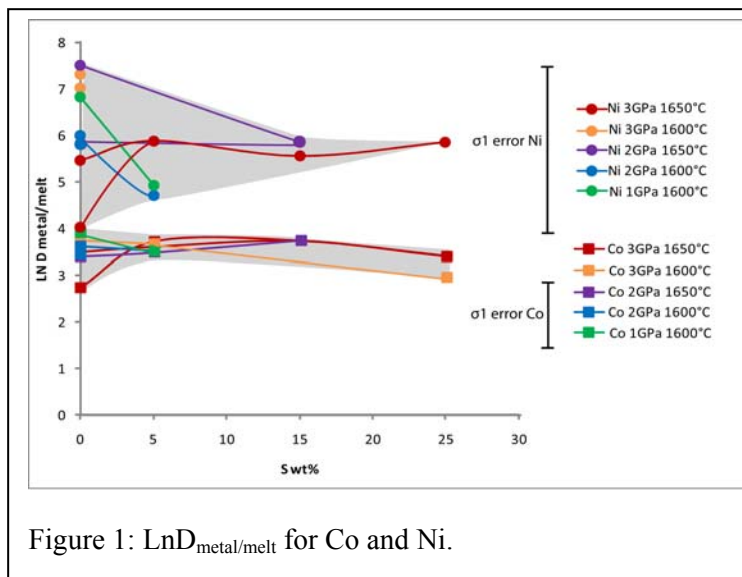
In conclusion, the partition coefficient of Co does not vary significantly with sulphur content at the conditions chosen. Nickel loss during experiment does not allow us to determine for sure if there is a trend in Ni partitioning. Experiments using denser graphite capsules are in progress to minimize Ni loss. Additional work will focus on experiments at higher temperatures and higher pressures (up to 25GPa, which correspond to the core-mantle boundary of Mars), to obtain a complete dataset of partition coefficients for these elements.

Reference:
Jana and Walker (1999) The influence of sulphur on partitioning of siderophile elements. Geochimica et Cosmochimica Acta, 61, 5255-5277.

Khan and Connolly (2008) Constraining the composition and thermal state of Mars from inversion of geophysical data. Journal of Geophysical Research, 113.

Section 03

————

Early solar system

Mineralogy of Opaque Phases in Almahata Sitta Ureilite.

Rupert Hochleitner[1], Viktor H. Hoffmann[2,3], Melanie Kaliwoda[1], Takashi Mikouchi[4]
[1]Mineralogical State Collection Munich
[2]Institute for Geosciences, University of Tuebingen
[3]Dep. Geo- and Environmental Sciences, University of Muenchen
[4]Dep. Earth and Planet. Science, University of Tokyo, Japan

Introduction

Almahata Sitta meteorite is a unique case because its parent asteroid was detected in near Earth space shortly before entering the high atmosphere and fall in North Sudan [1]. The aims of our project are investigating Almahata Sitta's (AS) magnetic signature, phase composition and mineralogy (main focus on the opaques) and getting new insights to the ureilite parent body magnetism (2008TC3 belongs to the F type asteroids). First results concerning the magnetic record of AS are found in [2,3]. The opaque mineralogy of Almahata Sitta is shown here.

Samples and methods

Quantitative chemical data of the observed opaque phases in the Almahata Sitta ureilite were obtained by electron microprobe analysis (EMPA) using a CAMECA SX100 operated at 15 keV acceleration voltage and 20 nA beam current (DEG). The observations were done on a PS of AS39 [see 2,3 for details of samples].

Mineralogy

Kamacite

According to our EMPA analyses there are several (up to five) metal phases mainly differing in the contents of Fe, Ni, Si and Co. The metal phase which builds up the large sheets between silicate grains (here named kamacite I) is composed of 90.95 wt% Fe, 4,31 wt% Ni, 3.86 wt% Si and 0.20 wt% Co. P and Cr are minor components. This kamacite is found in form of sheets depicting the olivines crystal shapes. This could be used as an argument for the derivation of this kamacite by reduction of the adjacent olivine. This is in contradiction to the low iron content (15-17 wt%) of the olivin and the rim thickness of 50 μm of reduced olivine which never could produce so much iron. Kamacite I contains remarkable Co, whereas the Co content of all other minerals in AS39 is near or below detection limit. This is a good hint that kamacite I is different from all other minerals in AS39 and thus has a different origin than the other metals and sulfides. In accordance with Gabriel and Pack [4] we suggest that the kamacite has been introduced into the polymict ureilite by the impact of a Ni-poor iron meteorite.

Troilite and Cr-rich troilite

Troilite is found in small grains in the carbon rich veins between the olivine and pyroxene individuals and in even smaller grains in the olivines. There it shows lines of tiny blebs which seem to follow ancient growth lines. The tiny troilite blebs in the olivines seem to be originating by reduction of the olivine along better potential paths as suggested by Berkley et al. [5]. Troilite phases with distinct chromium contents up to 6.8 wt. % have been identified as small grains in the carbon rich veins of Almahata Sitta.

Daubreelite

Daubreelite has been found in intergrowths with troilite embedded in the carbon rich veins. It shows a distinct Mn content up to 2.27 wt % similar to daubreelite from Neuschwanstein EL6 chondrite with 2.0 wt % [6].
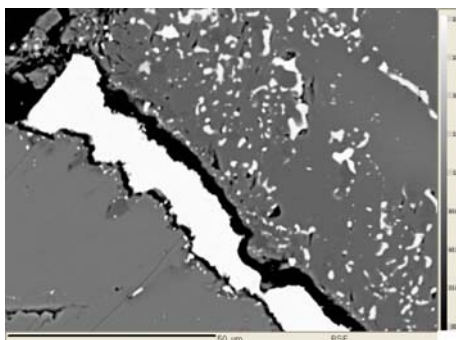
Figure: Sheet-like kamacite I, fracture filling between olivine (right) and pyroxene grains (left). The olivine grain is filled with many tiny metal blebs whereas the pyroxene is free of them. Carbon rich material in the vein is black. Backscattered image.

Reference:

[1] Jenniskens P., et al. (2009). Nature 458: 485-488.
[2] Hoffmann V., et al. (2010). 41th LPSC, #2120.
[3] Hoffmann V., et al. (2010). Meteor. Planet. Science, subm.
[4] Gabriel A.D., Pack A. (2009). 40th LPSC, # 2462.
[5] Berkley J.L., et al. (1980). Geochim. Cosmochim. Acta 44: 1569-1597.
[6] Hochleitner, R., et al. (2004). Meteor. Planet. Sciences 39: 1643-1648.

Laboratory Simulations of Circumstellar Processes in a Protoplanetary Disk: Chondrule Formation Experiments using Plasma Arcs.

Andreas Morlok[1], Yvonne C. Sutton[2] Nicholas St. J. Braithwaite[2] Monica M. Grady[1]
[1]PSSRI, The Open University, Walton Hall, Milton Keynes, MK7 6AA, UK.
[2]Department of Physics & Astronomy, The Open University, Walton Hall, Milton Keynes, MK7 6AA, UK.

Introduction: Chondrules are the dominant component in primitive meteorites. Their modal abundance is up to 80 volume% [1]. Also, they formed very early in the Solar System (~4567 Ma [2]). This makes the formation process of chondrules a very important step in the evolution of the protoplanetary disk and planets in general. Although the basic constraints about their formation are well known by experiments – most of them have been heated to 1500–1600 ºC, followed by a rapid cooling of usually between 10 to 1000 ºC/h [3], the exact process is still not known.

Most common formation scenarios proposed are formation in a protoplanetary nebular environment. The X-wind model proposes precursor dust heated by a highly active young sun [4], while the nebular shock models assume shock fronts in the protoplanetary nebula, where precursor grains are heated by collisons with gas particles [5]. Other models assume a planetary forming environment by impacts e.g. for CB chondrites [6].

In this part of our study, we try to simulate the formation of chondrules by gas-grain collisions in a nebular environment. To achieve this, we heat a precursor material (silicates, sulfides etc.) in hot plasmas created by an RF electric arc [also compare 7,8].

Techniques: A basic atmospheric pressure RF arc discharge was adapted for this work. The arc was generated between copper electrodes separated by 15 mm using a low voltage solid state switching circuit to drive a Tesla coil (natural frequency ~ 325 kHz). The gas temperature in the arc column has been determined in an earlier experiment through fitting of modeled rotational structure of emission spectra: at our typical 25W power input, the peak gas temperature is in the region of 2500 +/- 100 K.

Material (mixture of fine grained labradorite, forsterite, sulphide and metal) was dropped vertically through the arc plume. The resulting 'processed particles' were recovered, embedded in resin, polished and analyzed for their chemical composition using SEM/EDX.

Results: SEM images of particulate matter formed in the experiments show that a high abundance of spherules or 'chondrules' were produced, many in the size range 0.1-1 mm. Various phases are visible. There are compound 'chondrules' consisting of several spherules, in addition to relict grains.

EDX analysis of the polished samples shows large forsterite and labradorite grains embedded in a groundmass. While many of the former are probably relict, unmelted grains, bubbles in others indicate that these phases at least underwent melting. The chemistry of the embedded forsterite grains is unchanged compared with the starting material, but that of the feldspars shows some variations. This could indicate some mixing during melting. The groundmass shows abundant bubbles – its chemistry is a mixture of the starting materials.

Conclusions: The results of the first round of experiments were promising. The next series will focus on grains held together by organics, to simulate dust aggregates as starting materials. Following this, we will conduct experiments under low pressure conditions.

Reference:
[1] Brearley A. J. and Jones R. H. (1998) *Reviews in Mineralogy, 36,* Mineralogical Society of America.
[2] Russel, S. S. et al. (2005) ASP Conference Series 341.
[3] Zanda B. (2004) *ESPL* 224:1-24.
[4] Shu et al. (2001) *The Astrophysical Journal* 548: 1029-1050.
[5] Desch and Connolly Jr. (2002) *Meteoritics & Planetary Science* 37:183-208.
[6] Krot et al. (2005) *Nature 436*, 989-992.
[7] Hewins et al. (2000) *LPSC* XXXI, abstract #1675
[8] Guettler et al. (2008) *Icarus* 195: 5094-510.

"Cluster chondrites": Primary accretionary rocks formed by hot accretion ?

Knut Metzler
Westfälische Wilhelms-Universität Münster, Institut für Planetologie, Münster, Germany

The formation of planetesimals from a protoplanetary disk containing μm-sized dust and mm-sized chondrules is still poorly understood. In order to study this process it is important to identify remnants of primary assemblages of dust and chondrules, which escaped impact brecciation (e.g. Romstedt & Metzler, 1994; Bischoff et al., 2006) after accretion. In my view, good candidates for this are certain structures in unequilibrated ordinary chondrites (UOC´s), which are characterized by mutually indented chondrules. They have been occasionally described in the literature and are interpreted by most authors as the result of hot accretion (e.g. Hutchison & Bevan, 1983; Taylor et al., 1983; Holmen & Wood, 1986; Hutchison, 1996; Zanda, 2004). I found that these structures are restricted to a certain rock type (Figs.1,2) which occurs as clasts up to 3.5 cm in a considerable number of the investigated UOC´s (H, L, and LL). The texture of these clasts was obviously not formed by shock metamorphism since it occurs in samples from S1 (unshocked) to S4 (moderately shocked). In order to discern those clasts from other types of chondritic lithologies I propose to call them "cluster chondrites". Their main characteristics are: 1. Chondrites of low petrologic type; 2. Consisting of thousands of chondrules that indent each other, forming close-fitted textures; 3. Very few interchondrule matrix; 4. Chondrules are frequently surrounded by thin fine-grained dust mantles; 5. Most chondrules are intact; 6. Restricted chondrule size distribution. In my view these structures seem to be more than small chondrule agglomerates which formed isolated in the solar nebula. Their texture point to a large-scale agglomeration process in a hot stage ("hot accretion") and to a compression force, which led to compaction of these lithologies and the formation of their close-fitted textures. I speculate that "cluster chondrites" are fragments of former large-scale lithologies from (a certain type of) freshly accreted planetesimals, i.e. they are remnants of primary accretionary rocks.
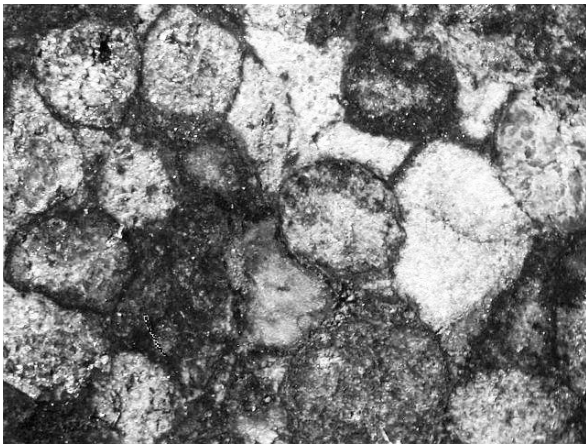
Fig.1: "Cluster chondrite" clast in an LL3.2 chondrite (cut surface; width of field is 8 mm).
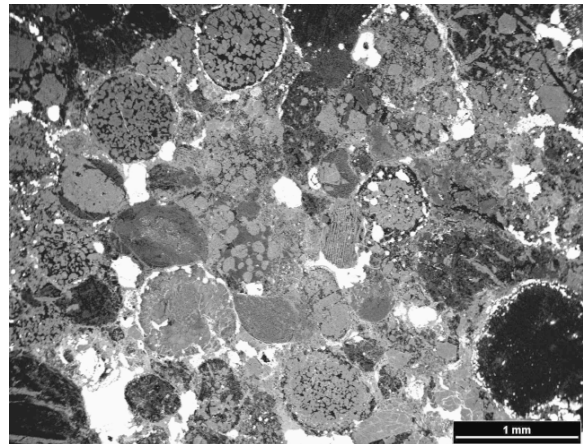
Fig. 2: "Cluster chondrite" clast in an LL3.7 chondrite (BSE image; width of field is 4.5 mm)

A study is planned to investigate those "cluster chondrites" in detail, including statistics on clast sizes, chondrule types, and chondrule size distrubutions. Petrologic and microchemical investigations will be performed to characterize the components and their intergrowths. If it turns out that "cluster chondrites" in fact accreted in a hot stage , i.e. within hours to days after chondrule formation, we would be able to study rock forming processes that occurred within a very limited time and space of the solar nebula. The proof of such a scenario would probably influence models for nebula accretion and chondrule formation.

References:
Bischoff, A., Scott, E. R. D., Metzler, K. & Goodrich, C. A. (2006), Nature and origins of meteoritic breccias, In "Meteorites and the Early Solar System II" (eds. D.S. Lauretta and H.Y. McSween Jr.), Univ. of Arizona, Tucson, 679.
Hutchison, R. & Bevan, A.W.R. (1983), Conditions and time of chondrule accretion, In "Chondrules and Their

Origins" (ed. E.A. King), Lunar and Planetary Institute, Houston, 162.

Holmen, B.A. & Wood, J.A. (1986), Chondrules that indent one another: Evidence for hot accretion ?, Meteoritics 21, 399.

Hutchison, R. (1996), Hot accretion of the ordinary chondrites; The rocks don´t lie, LPSC XXVII, 579.

Romstedt, J. & Metzler, K. (1994) Brecciation and preirradiation of unequilibrated H chondrites, Meteoritics 29, 523.

Taylor, G.J, Scott, E.R.D. & Keil, K. (1983), Cosmic setting for chondrule formation, In "Chondrules and Their Origins" (ed. E.A. King), Lunar and Planetary Institute, Houston, 262.

Zanda, B. (2004), Chondrules, Earth and Planetary Science Letters 224, 1.

Determination of erosion rate at Allchar region with cosmogenic nuclides (^{10}Be, ^{26}Al, ^{53}Mn)

M.K. Pavićević[1], P. Vermeesch[2], G. Amthauer[1], S. Niedermann[3], B. Boev[4], R. Jelenković[5], V. Pejović[6]

[1]University of Salzburg, Department of Materials Engineering and Physics, A-5020 Salzburg, Austria
[2]School of Earth Sciences, Birkbeck University of London, London WC1E 7HX, Great Britain
[3]Deutsches GeoForschungsZentrum, GFZ Telegrafenberg, D-14473 Potsdam, Germany
[4]University of Štip, Faculty of Mining and Geology, Goce Delčev 89, 92000 Štip, FYR Macedonia
[5]University of Belgrade, Faculty of Mining and Geology, Djušina 7/II, 11000 Belgrade, Serbia
[6]University of Belgrade, Faculty of Physics, Studentski Trg 12/IV, 11000 Belgrade, Serbia

Allchar is a Sb-As-Tl-Au deposit located at the north - western margin of the Kozuf Mountains in Macedonia, close to the Greek border. The mine contains the world's largest known concentration of thallium-bearing minerals, especially lorandite ($TlAsS_2$). LOREX, the acronym for LORandite EXperiment, is the only geochemical solar neutrino experiment still actively pursued. It addresses the determination of the long-term average of the solar neutrino flux, based on the neutrino-capture reaction $^{205}Tl + \nu_e \rightarrow {}^{205}Pb + e^-$ occurring in the lorandite of the Allchar mine. The final step of LOREX will be the extraction of the lorandite and the quantitative determination of the ^{205}Pb / ^{205}Tl ratio, thus providing the product of solar neutrino flux and neutrino-capture cross section, integrated over the lorandite age of $4.31 \cdot 10^6$ yr. Based on the present-day solar luminosity, it is expected that about 23 atoms of ^{205}Pb of solar neutrino origin will be found per gram of lorandite. In contrast with the production of ^{205}Pb by solar neutrinos, which is independent of depth, cosmogenic ^{205}Pb produced from fast muons of cosmic ray origin is strongly depth-dependent and very sensitive to the long-term erosion history of the field area. For erosion rate determination, we have so far applied three independent series of measurements of cosmogenic ^{26}Al, ^{10}Be and ^{53}Mn. Firstly, the ^{26}Al concentration in quartz was determined using the AMS system at VERA (**V**ienna **E**nvironmental **R**esearch **A**ccelerator). Secondly, a series of measurements of the ^{10}Be and ^{26}Al contents was performed at the AMS of PRIME Lab, Purdue University, and finally AMS measurements at the Tandem facility of the TU Munich provided the concentration of ^{53}Mn in pyrite (FeS_2). For the two ore bodies containing lorandite, we derived lower limits of the erosion rate of ~33 m/Myr at Crven Dol (NW part of Allchar deposit) and 67 m/Myr in the central part (SE part of Allchar deposit), in fair agreement with quantitative geomorphologic studies.

Section 04

_____

Environmental mineralogy and geochemistry

Geological And Geochemical Exploration For Gold Deposits In Metamorphic Rocks At Gabal Eqat Area South Eastern Desert, Egypt

Salem, M Salem
National Authority for Remote Sensing and Space Sciences, Cairo, Egypt
mail: salem_moher@yahoo.com

Geological and geochemical exploration detected gold deposits in two different geological environments at Gabal Eqat area. First, the ophioiltic environment is represented in the listwaenite ridges (iron carbonate silica) which formed later as a result of solidified residual melting from ophiolitic magma. Second environment is the alteration zones within the schistose metavolcanic rocks. The petrographical studies indicate that the study area is outcropped by serpentinites, talc carbonates and listwaenites, meta-volcano-sedimentary, and tonalite rocks. In the current search, a new base map prepared using Landsat ETM image and field verifications for the study area. And scanner electronic microscope (SEM) was used to detect the crystalline shape for both the gold and the gangue minerals in ten samples taken from the altered zone within the meatavolcanic rocks. Atomic absorption for ten samples elaborated in order to determine the gold content and mineral assemblages.

The geochemical analyses, atomic absorption method for representative samples from listwanite ridges recorded Au contents (up 3.4 g/t), Ag (up to 10 g/t), Cu (up to 2%), Pb (up to 69 ppm), Zn (up to160 ppm) and Mo (up to 180 ppm). In alteration zones the geochemical analyses recorded relatively high Au contents (up 5.1 g/t), Ag (up to 23 g/t), Cu (up to 2.4%), Pb (up to 87 ppm), Zn (up to194 ppm) and Mo (up to 200 ppm). Sulphide minerals such as pyrite, chalcopyrite and arsenopyrite are abundant in alteration zone as mineralogical-environment within metavolcanics hosting for gold. Hence, the alteration zones of the metavolcanics are promising and need more detailed exploration for Au and Ag mineralizations to evaluate their mineralogical potentiality.

Mineralogical and geochemical characterization of secondary mineral precipitations in a former uranium mining district

Franziska Schäffner[1], Matthias Händel[1], Dirk Merten[1], Kilian Pollok[2], Falko Langenhorst[2], Georg Büchel[1]
[1]Friedrich-Schiller-Universität Jena, Institute of Geosciences, Jena, Germany
[2]Universität Bayreuth, Bayerisches Geoinstitut, Bayreuth, Germany

Heavy metal contamination of large areas due to uranium mining operations poses a serious long-term environmental problem. The investigated area near Ronneburg in eastern Thuringia, Germany, was one of the former leaching heaps where low grade uranium bearing ores (uranium content < 300g/t) were leached from 1972 to 1990 using acid mine drainage (AMD; pH 2.7-2.8) and diluted sulphuric acid (10g/l). In the course of remediation efforts the former heap was removed and the site was recontoured with a cover of heterogeneous allochthonic soil material with a thickness of 10 to 80cm.

Infiltration of the leachates into the glacial sediments underneath the heap led to the current residual contamination of the soil with heavy metals like Cd, Co, Cr, Fe, Mn, Ni, Pb, Zn, rare earth elements (REE) and also radionuclides like U in spite of remediation. The formation of secondary minerals in the soils leads to an enrichment of heavy metals in certain layers. For that reason their formation and stability has a strong impact on the mobility and bioavailability of trace metals in the biogeochemical system.

At the investigated site eleven exploratory soil excavations were laid out and the enrichment horizon was sampled. The compact layer with a thickness between 5 and 15 cm is dense grey to black in color and located closely above the groundwater level in the glacial sediments. Total digestions and sequential extractions were performed to reveal the total amount of metals and to investigate how the metals are bound in the soil. The total digestions show that especially cadmium (up to 5.72 µg/g), nickel (up to 311 µg/g), cobalt (up to 133 µg/g), copper (up to 39.8 µg/g) and zinc (up to 103.6 µg/g) were enriched together with very high manganese contents (up to 48 mg/g). X-ray diffraction (XRD), microprobe analyses and transmission electron microscopy (TEM) were used to identify the manganese phases which are present as birnessite and todorokite in the enrichment horizon. The compositional data and the sequential extraction proved that the manganese oxides are mainly responsible for the retention of toxic elements in the soil. It can be attributed as a natural attenuation process which decreases bioavailable toxic element levels by the formation of secondary minerals.

Minimal invasive multiparameter monitoring of transport phenomena in column tests

Dieter Rammlmair [1], Mostafa Redwan [1,] Ismael Falcon [2]
[1]BGR, Hannover, Germany
[2]Civil Engineering School, University of A Coruña, A Coruña, Spain

During saturation, drainage , and evaporation experiments, fluids and the investigated material itself experience continuous changes of a number of physicochemical parameters. Strong gradients in ion concentration as well as changing element ratios in solution can be observed in vertical position over time as well as in subsequently extracting water from the same position by rhizons. Significant changes in fluid chemistry, pH and fluid conductivity can be observed. Since fluid and ion transport in column is capillary driven, precipitation due to super saturation of fluids in the evaporation zone is responsible for clogging pores and changing hydraulic parameters. Whilst the basal part of a column will be depleted in a number of ions, the zone of evaporation will be substantially enriched.

As fluid extraction is an impact significantly disturbing the experimental setup, non-invasive and minimal invasive methods were used while the experiment running to monitor changes in water saturation by x-ray absorption, chemical changes of the material by energy dispersive x-ray fluorescence, electrical conductivity by multi-level electrode foils, oxygen by optodes, temperature by PT100, evaporation by balance.

By combining the data achieved by these methods fluid conductivity changes can be calculated for any level of saturation (Redwan and Rammlmair, 2010 in press SSSAJ). Element transfer, zones of clogging and enrichment, progress of oxidation and temperature changes can be monitored. At the end of the experiment the final stage can be approved by destructive methods such as fluid extraction, pH, fluid conductivity and chemistry, XRF, XRD and SEM

Results show extreme variation of fluid chemistry, fluid conductivity and pH evolution in the capillary head according to water saturation and level of extraction the ion concentration can vary by a factor of > 1000 for major and trace elements such as REE. Fluids sequentially extracted show changes in chemistry related to fast fluids e.g. rich in Ca, Na , S and slow fluids enriched in e.g. Al, Si.

This experimental setup provides new insight into alteration of soils and mining residues as well as for the development of supergene ore deposits.

Mineralogical and crystallochemical characterization of the kef es Sennoun Phosphorite deposit.

Hacène Redjehimi[1], Henrik Friis[2]
[1]Laboratoire de géologie, faculté des sciences de la terre, Université Badji Mokhtar, 23000, Annaba.
[2]Department of Earth Sciences, Aarhus University, C.F. Møllers Alle´ 120, DK-8000 Aarhus C., Denmark.

The sedimentary succession of Djebel Onk is characterised by the deposition of phosphatic formations of Late Palaeocene - Early Eocene age (Upper Thanetian-Lower Ypresian). The mineralogical, textural, and crystallochemical characteristics of the different types of phosphorite sampled from Kef es Sennoun deposit were determined by X-ray diffraction, optical and Scanning Electron Microscope (SEM) equipped with energy dispersive X-ray detection system (EDAX).

X-ray diffraction studies of these phosphorites samples show that carbonate-fluorapatite (francolite) is the major phosphorite mineral, other minerals identified using the x-ray diffraction and scanning electron microscope include dolomite, calcite, pyrite, sphalerite, quartz, K- feldspar and clinoptilolite. The unit cell parameters a and c of francolite show the greatest variability and can be used as an indicator of partial substitution mainly of (CO_3^{2-} for PO_4^{3-}) and Mg and Na for Ca in the francolite structure. These unit-cell dimensions are calculated from their following respective d-spacing's: 002, 300, 202, 310, 222, 312, 213, 321, 410, 402 and 004 by least squares method using the program FullProf. These a-values of francolites range from 9.3228 to 9.33Å.

The phosphorites are generally composed of rounded-subrounded phosphate pelloids generally lacking internal structure and pseudo-oolites. Their size ranges from 50 µm to 1 mm in diameter, and they vary from cream and orange thorough shades of brown to dark brown depending on the content of organic matter and iron sulphides. Other types of phosphorite particles are coprolites, intraclasts and phosphatic bioclasts. Textural relationships observed in the scanning electron microscope (SEM) suggest that the phosphorite grains will break easily from the dolomite cement, and because of the most highly substituted francolites and the a-values are at the lower end of the francolite model, these phosphate rocks can be used directly in agriculture (direct application) because of their high solubility.

Key words: phosphorite, carbonate-fluorapatite, unit-cell, Kef es Sennoun, pseudo-oolites, pelloids, scanning electron microscopy, x-ray diffraction.

Listvenites with mercury mineralization
From Nain Ophiolite, Central Iran

Batoul Taghipour[1], Mohammad Ali Mackizadeh [2]
[1]Department of earth sciences, Faculty of sciences, Shiraz University, Shiraz, Iran, email: taghipour@shirazu.ac.ir
[2] Department of geology, Isfahan University, Isfahan, Iran, email: ma_mackizadeh@yahoo.com

Based on several field surveys, various samples were collected after detailed polarized microscope works, the selected samples were investigated by SEM. Mercury contents have been determined by NAA method.

Listvenites are hydrothermally altered rocks commonly associated with ophiolites (1). Listvenite research is of practical well as theoretical importance because listvenites host or are spatially associated world wide with Au, As, Co, Ni, and W and Hg deposits (2).

Nain ophiolite is located in Central Iran geological unit. This supra-subduction Zone-type ophiolite belongs to upper cretaceous to paleocene and outcrops with northwest-southeast trending along Nain-Baft major fault. In Nain ophiolite harzburgite and serpentinized harzburgite are the main components of ultrabasic rocks. Listvenites or carbonatized- silicified serpentine rocks are common with Nain ophiolite. They are formed because of invading of CO_2 rich fluids to serpetinites. These rocks are occurred along faults or tectonic-lithologic contacts as outstanding vein like bodies & lenses. The following critical minerals are determined in listvenites:

Quartz + Mg-Fe-Ca carbonates+ relic chromite + serpentine+ Iron Oxides + pyrites. Microcrystalline varieties of quartz replacement in listvenite are resulted in silicified parts, which are mainly characterized by jasperoide occurrence. In field outcrops these parts are dark gray to dark brown hue with patchy appearance.

Occasionally sulphide mineralization (pyrite) is closely associated with these silicified parts. SEM and geochemical data has revealed Hg mineralization with some of these pyrites. Hg minerals (native Hg & Hg-Cl-Se-S compounds?) are seen as anhedral shapes in microcrystalline quartz background, open space filling, replacement in pyrite or overgrowth on it. There is also evidence of gold association with mercury mineralized parts (3).

Reference:
1- plissart, G., Femenias, O., Maruntiu, M., Diot, H., and Demaiffe, D. (2009) The Canadian Mineralogist, vol. 47, pp. 81-105.
2- Ucurum, A. (2000) Listwaenites in Turkey: perspectives on formation and precious metal concentration with reference to occurrences in east- central Anatolia. Ofioliti 25 (1), p.15-29.
3- Noghreian, M. Haghighipoor, M.A.Mackizadeh, M.A., Taghipoor, B. and Sherafat, S. (2007) Gold Mineralization in central Iran listvenites, Research journal of university of Isfahan, vol, 25, No 3, pp. 29-38, in persian.

Colloidal retention at rough black slate surfaces

Alex Michler[1], Cornelius Fischer[1,2], Gopala K. Darbha[1], Thorsten Schäfer[3]
[1]GZG, Georg-August-Universität Göttingen, Germany,
[2]Rice University, Houston, TX 77005, USA,
[3]Inst. f. Nukleare Entsorgung, KIT, Karlsruhe, Germany

The retention of colloids plays an important role in environmental processes, because of their potential to carry contaminants in aquiferous systems. This study considers surface roughness as an important factor influencing the interaction between adsorbent and a colloidal suspension. Theoretical approaches predicted that the DLVO interaction energy between surfaces is significantly influenced by surface roughness (e.g. Bhattacharjee et al., 1998). Experimental studies showed quantitatively the importance of surface roughness for particle retention at rough mineral surfaces (e.g. Darbha et al., 2010).

This study focuses on the retention of colloids at rough black slate surfaces. Oxidative weathering of black shales is associated with the dissolution of iron sulfides, e. g. pyrite, and hence with the release of sulfuric acid. The resulting acidic conditions are responsible for the release of heavy metals like lead, cadmium or uranium from the slate. The phenomenon is commonly known as acid rock drainage (ARD) or acid mine drainage (AMD). On its way to neutralization the acidic drainage may form several iron precipitates of colloidal size, such as schwertmannite, ferrihydrite or goethite (Zänker et al., 2000). The newly formed minerals, particularly those of colloidal size, have a high potential to sorb the released heavy metals and may transport them over a far distance. The immobilization of such colloids is an important topic in the disposal of AMD and nuclear waste. Here we present a quantitative and experimental approach to investigate the relationship between micrometer to sub-micrometer surface roughness variations of black slates and the retention of particles. As an analog, well-defined polystyrene latex particles were applied. Rock surface topography as well as particle retention was quantified using three-dimensional data, collected by vertical scanning interferometry (VSI). Roughness parameters (root mean square roughness, Rq and interfacial area ratio, F) were calculated based on previous studies about roughness quantification at irregular surfaces (Fischer and Luttge, 2007). The adsorption experiments were performed as overhead dipping experiments. The dipping experiments were conducted using stirred (200, 500 rpm) and unstirred colloidal suspensions. The particle concentrations were 24×10^6 and 24×10^7 particles/mL. The particles were suspended in NaCl solutions with an ionic strength of 0.01 M. The experiments were performed around neutral pH. This resulted in negatively charged slate surfaces according to streaming potential measurements. The used polystyrene particles were of negative and neutral surface charge. Particle diameters were 428 nm, 1000 nm, and 2000 nm. With regard to the negatively charged adsorbent surface, the negatively charged particles create electrostatically unfavorable adsorption conditions whereas the neutral charged create more favorable conditions (induced electrostatic attraction).

Generally, preferred sites for adsorption at rough slate surfaces are topographic features, such as peaks and edges of mineral aggregates. Under unfavorable conditions, the amount of adsorbed particles is quite remarkable but seven times less compared to neutral charged particles. At stirring rates of 200 rpm the increased collision frequency results in an only moderate increase (approx. 1.6 times) of particle adsorption. Higher stirring rates (up to 500 rpm) do not result in an increase of particle adsorption.

Further experiments will focus on surface roughness *variations*. For this purpose adsorption experiments are planned with roughness variations in the submicrometer range. The roughness of the so far used untreated black slate surfaces ranges dominantly in the micrometer range what causes a strong filtration effect on the potential adsorbates. Furthermore, flow-through experiments in fluid cells will be performed at defined flow rates. In addition, roughness variations due to varying weathering intensities will be applied.

References:
Bhattacharjee, S., Ko, C.H. and Elimelech, M., 1998. DLVO interaction between rough surfaces. Langmuir, 14(12): 3365-3375.
Darbha, G. K., Schäfer, T.; Heberling, F.; Lüttge, A., and Fischer, C., 2010. Retention of Latex Colloids on Calcite as a Function of Surface Roughness and Topography. Langmuir, 26(7): 4743-4752.
Fischer, C. and Luttge, A., 2007. Converged surface roughness parameters - A new tool to quantify rock surface morphology and reactivity alteration. American Journal of Science, 307(7): 955-973.
Zänker, H., Richter, W., Brendler, V. and Nitsche, H., 2000. Colloid-borne uranium and other heavy metals in the water of a mine drainage gallery. Radiochimica Acta, 88(9-11): 619-624.

Impact of thermal microstructural changes of Egyptian limestones on quicklime reactivity: Mud-supported limestones

Soltan, A. M.[1], Kahl, W.-A..[2], Wendschuh, M.[3], and Hazem, M.[4]

[1]Geology Department, Faculty of Science, Ain Shams University, Cairo 11566, Egypt

[2]Institute of Geosciences, Christian-Albrechts-Univertity, Kiel 24118, Germany

[3]Crystallography Department, Faculty of Geoscience, Bremen University, Bremen 28359, Germany

[4]Chemistry Department, Faculty of Science, Ain Shams University, Cairo 11566, Egypt

The petrographic characteristics of mud-supported limestone samples representing different geographic and stratigraphic units in Egypt were examined before and after calcination at 950 °C for 0.25, 0.5, 1 and 2 hrs. The examination utilized are X-ray diffraction (XRD), X-ray fluorescence (XRF), transmitted light microscopy (TLM), scanning electron microscopy (SEM) and X-ray micro-computed tomography (μ-CT). Both the free lime content and reactivity of the produced quicklime were measured.

The quicklime produced at all the firing conditions is un-reactive, except the Chalk Series lime at 1 and 2hrs soaking, although the high content of the liberated free lime (92.81 %) in some samples. The resulted quicklime behaves as dead-burnt, however produced at mild calcination temperature (950 °C). The microstructure of the mud-supported limestones is of no significance on the resulted quicklime reactivity, where a limited preservation of the ghost fossils is recorded. The mineralogical and the chemical composition of the rocks are the main controlling variables in the degree of the quicklime crystallinity and consequently the reactivity. Samples enriched with P_2O_5 show higher crystallinity of the resulted lime associated with lowest reactivity.

Key Words: Limestone, microstructure, quicklime, reactivity

It is well known that the crystallization of $AlPO_4$ and the phase transformations between its various crystallographic forms strongly depend on the presence of chemical impurities, Flörke O.W. (1967). According to Graetsch, H.A. (2007) the hexagonal form of $AlPO_4$ tridymite ($AlPO_4$-T) is stable between 340 and 1100 °C. He applied temperature resolved XRD and DTA to monoclinic and triclinic $AlPO_4$-T samples that were prepared by heating amorphous commercial $AlPO_4$ at various temperatures up to 1100 °C for durations of one to six days. The chemical purity of that commercial precursor is not explicitly specified in the paper. The crystal structure data of the hexagonal form of $AlPO_4$-T were determined by Graetsch, H.A. (2001) from an XRD pattern collected at 320 (15) °C by heating a mixture of triclinic and monoclinic $AlPO_4$-T prior prepared by calcining the amorphous commercial precursor mentioned above at 950 °C for one day at air.

Liang R. & Nakamura T. (1985) found that the hexagonal high-temperature form of $AlPO_4$-T is stabilized to room temperature if it contains 4.5 to 7 mol % $KMgPO_4$. Samples used in that investigation were synthesized by doping $AlPO_4$ (prepared by precipitation and subsequent calcination at 800 °C) with $KMgPO_4$ (previously crystallized at 1100°C for 2 h) and heating those mixtures at 1145°C for 240 hours.

Recently, the chemically stabilized hexagonal form of $AlPO_4$-T was also found in the fly ash from an industrial sewage sludge incinerator, Peplinski B. et al. (2010). This finding was based on a large number of samples collected during a nine month product monitoring and ascertained by Rietveld analyses of the XRD data collected at room temperature. As the retention time of the ash particles in that incinerator is smaller by five orders of magnitude than the duration of the heat treatment applied by Liang R. & Nakamura T. (1985) the question arose whether there exists – under well controlled laboratory conditions – a synthesis route that allows the *fast* crystallization of the hexagonal form of $AlPO_4$-T chemically stabilized to room temperature.

During the present investigation a synthesis route was worked out that allows to produce the hexagonal form of $AlPO_4$-T chemically stabilized to room temperature whereas the (T,t) field applied during this synthesis is much closer to the conditions existing in the industrial incinerator than those reported by Liang R. & Nakamura T. (1985). Doped $AlPO_4$ samples heated at 1100 °C for 1 hour upon quenching to room temperature proved to be well-crystallized and phase-pure hexagonal $AlPO_4$-T showing nearly no sample-dependant broadening of the diffraction lines. Their diffraction patterns were well interpreted by the Rietveld method using the structure data provided by Graetsch, H.A. (2001). Samples heated at only 900 °C for 1 h upon quenching to room temperature proved to be well-crystallized and nearly phase-pure hexagonal $AlPO_4$-T showing just a moderate broadening of the XRD lines, quantitatively agreeing with the line profiles of the hexagonal $AlPO_4$-T component found in the ash from the commercial incinerator. Even samples heated at 1050 °C for only 2 min upon quenching to room temperature contained the well-crystallized hexagonal form of $AlPO_4$-T. Selected samples were characterized by XRF, ICP, SEM & EDX, DTA as well as solid state ^{27}Al and ^{31}P MAS NMR. The ^{27}Al and ^{31}P NMR-spectra of the chemically stabilized hexagonal form of $AlPO_4$-T were collected at room temperature and are significantly different from those of the monoclinic or triclinic forms of $AlPO_4$-T synthesized and analyzed for comparison.

References:
Flörke O.W. (1967), Kristallisation und Polymorphie von $AlPO_4$ und $AlPO_4$-SiO_2 – Mischkristallen,
Z. Kristallogr. **125,** 134-146.
Graetsch, H.A. (2007), High temperature phase transitions and intermediate incommensurate modulation of the tridymite form of $AlPO_4$, Z. Kristallogr. **222**, 226-233.
Graetsch, H.A. (2001), Hexagonal high-temperature form of aluminium phosphate tridymite from X-ray powder data, Acta Cryst. **C57** (2001), 665-667.
Liang R. & Nakamura T. (1985), $AlPO_4$ tridymite stabilized with $KMgPO_4$, Materials Research Bulletin (Elsevier) **20**, 1253-1256.
Peplinski, B. et al. (2010), First identification of $AlPO_4$ tridymite in a municipal sewage sludge ash, 12th European Powder Diffraction Conference, 27.-30. August 2010, Darmstadt, Germany, Book of Abstracts MS4-P03

Das Anionenaustauschverhalten von Mg-Al-LDH's der Hydrotalcit-Gruppe mit verschiedenen Kationen-Verhältnissen

Thomas Witzke[1], Luis Omar Torres-Dorante[2]
[1]Martin-Luther-Universität Halle, Institut für Geowissenschaften, Von-Seckendorff-Platz 3, 06120 Halle (Saale), thomas.witzke@geo.uni-halle.de / YARA GmbH & Co. KG / Rostock, Werkstr. 1, 18184 Poppendorf
[2]Research Centre Hanninghof, YARA International ASA, Hanninghof 35, 48249 Dülmen

Im Rahmen eines Projektes zur Untersuchung der Eignung von Layered Double Hydroxides (LDH's) der Hydrotalcit-Gruppe als Zwischenspeicher für Nitrat im Boden stellte das Austauschverhalten verschiedener Anionen einen wesentlichen Punkt dar. Das Ziel war die Entwicklung eines möglichst nitratselektiven Materials mit hoher Speicherkapazität für Nitrat sowie günstigen Austauscheigenschaften unter Bodenbedingungen. Für die Untersuchungen wurden synthetische Mg-Al-Nitrat- und -Chlorid-LDH's mit der allgemeinen Zusammensetzung $[Mg_{1-X}Al_X(OH)_2][A_X(H_2O)_n]$ (A = NO_3, Cl) mit verschiedenen Mg-Al-Verhältnissen verwendet. Für die Untersuchungen wurden Lösungen mit nur einem Anion in verschiedenen Konzentrationen sowie Multianionenlösungen zur Simulation von Bodenlösungen verwendet.

Im Unterschied zu anderen LDH's weisen die Nitrat-Verbindungen eine spezielle Eigenschaft auf. Mit wachsendem Ersatz von Mg durch Al steigt der Basisabstand c' von 8,07 Å bei Mg : Al = 6 (x = 0,14) auf 9,03 Å bei Mg : Al = 2 (x = 0,33) sehr stark an. wobei es einen steilen Anstieg um Mg : Al = 3 gibt. Die unterschiedlichen Basisabstände ließen erhebliche Auswirkungen auf den Austausch der Anionen erwarten. Die Chlorid-LDH's zeigten diesen Effekt nicht, dagegen eine schwache Verringerung des Basisabstandes mit wachsendem Ersatz von Mg durch Al.

Bei Chlorid- und Nitrat-LDHs mit Mg : Al = 5 : 1 ließen sich die Anionen komplett und wiederholt gegen Nitrat bzw. Chlorid austauschen. Der Basisabstand veränderte sich dabei nur minimal. Wurde ein Chlorid-LDH als Ausgangsmaterial verwendet, verringerte sich beim Austausch gegen Nitrat die Fehlordnung sehr deutlich, vermutlich durch die bessere strukturelle Kontrolle durch das planare Nitrat-Anionen gegenüber dem Chlorid bei der Stapelung der Hydroxid-Schichten. Carbonat erwies sich bis zu einem gewissen Grad als wiederholt austauschbar. Der Basisabstand verringerte sich dabei von etwa 8.15 Å auf etwa 8.03 Å und blieb damit deutlich über dem Wert reiner Carbonat-LDH's. Rund 40 % der Carbonat-Anionen ließen sich unter Bodenverhältnissen aus einem LDH mit Mg : Al = 5 : 1 wiederholt durch Nitrat austauschen (Witzke & Torres, 2009).

In den Versuchen mit einzelnen Anionen zeigte sich beim Sulfat eine starke Abhängigkeit vom Mg-Al-Verhältnis und damit vom Basisabstand. Bei Mg : Al = 5 : 1 wurde eine minimale Sulfatadsorption, wahrscheinlich nur an der Kristalloberfläche, festgestellt. Dabei blieb der Basisabstand konstant bei etwa 8.1 Å, zu niedrig für einen Sulfateinbau. Mit höherem Al-Gehalt ist ein verstärkter Sulfateinbau feststellen, unter Aufweitung des Schichtabstandes. Bei Mg : Al = 2 : 1 ließ sich Sulfat sehr gut einbauen, der Basisabstand blieb hier bei rund 9 Å, da er für den Sulfateinbau schon den optimalen Wert aufwies. Als sehr ungünstig für den geplanten Einsatz erwies sich hier, dass das Sulfat unter Bodenverhältnissen nicht mehr gegen Nitrat ausgetauscht werden konnte.

Bei den Versuchen mit Nitrast-LDH's und simulierten Bodenlösungen mit 150 mg N (NO_3^-), 1 mg P (HPO_4^{2-}), 200 mg Cl (Cl^-), 80 mg S (SO_4^{2-}), 10 mg C (HCO_3^-) pro Liter zeigte sich eine starke Abhängigkeit vom Basisabstand. Phosphat spielte bei diesen Versuchen keine Rolle beim Austausch. Chlorid wurde in deutlichen Mengen in dem Übergangsbereich von Mg : Al = 4 : 1 bis 2,75 : 1 eingebaut. Sulfat wurde auch hier mit steigendem Al-Gehalt besser eingebaut. Trotz des generell guten Carbonateinbaus in LDH's dominierten bei den Versuchen unter Bodenverhältnissen andere Anionen. Nur bei Mg : Al = 5 : 1 wurden ca. 35 % des Nitrats durch Carbonat ersetzt. Auch bei der Menge des insgesamt abgegebenen Nitrats zeigten sich deutliche Unterschiede. Während mit den simulierten Bodenlösungen bei Mg : Al = 5 : 1 nur etwa 40 % des Nitrats abgegeben wurden, stieg der Wert bis auf 90 % bei Mg : Al = 3 : 1 (und weist damit eine nur geringe Nitratselektivität auf), und sank dann auf 55 % bei einem Verhältnis von 2 : 1.

Die Anforderungen für den Einsatz als Zwischenspeicher für Nitrat im Boden einer guten Nitrat-Aufnahme und -Abgabe und einer möglichst geringen Carbonatselektivität erfüllte nur das LDH-Material mit Mg : Al = 5 : 1, wenn auch nicht in optimalem Umfang.

Reference:

Witzke, T. & Torres-Dorante, L. (2009): Untersuchungen zum Einsatz von LDH's der Hydrotalcit-Gruppe als Zwischenspeicher für Nitrat im Boden.- Hallesches Jahrbuch für Geowissenschaften 31, 265

Retention of colloids at mineral surfaces as a function of surface roughness

Gopala Krishna Darbha[1], Cornelius Fischer[1,2], Alex Michler[1], Thorsten Schäfer[3]
[1]GZG, Georg-August-Universität Göttingen, Department of Sedimentology/Environmental Geology, Göttingen, Germany
[2]Rice University, Houston (TX), USA
[3]Institute for nuclear waste disposal, KIT, Karlsruhe, Germany

Understanding the colloidal particle retention mechanism at fluid-solid interfaces is important to address a variety of environmental and industrial processes. Deposition of negatively charged colloids (that are ubiquitous in nature) onto rough rock and mineral surfaces under unfavorable conditions is of great importance to understand the capture of colloids in the environment. Several factors control the deposition of colloids onto surfaces, such as DLVO forces (electrostatic & van der Waals), hydrodynamic interactions, hydration forces, hydrophobic forces and steric interactions etc. (Bradford and coauthors, 2008). Although theoretical (Bhattacharjee and coauthors, 1998 and Hoek and coauthors, 2006) and experimental (Das and coauthors, 1994) investigations suggest an enhanced colloid deposition with increasing surface roughness, it is often disregarded. Specifically, at and above the pH_{PZC} (pH of point of zero charge (PZC)) where no or strong repulsive forces prevail between particle and substrate, the importance of surface roughness is increased.

Our initial experimental approach applying calcite surfaces showed a strong correlation between surface roughness (in the nanometer scale) and the efficiency of particle deposition (Darbha and coauthors, 2010). Here we expand the experimental investigations to a systematic study about colloid deposition on well-defined, surface functionalized smooth and patterned silicon surfaces. The surface pattern serves as an analog for rough mineral surfaces.

Fluid flow variations of 10^{-7} to 2×10^{-4} m/s resulted in the finding of a "critical velocity" for both smooth and patterned surfaces. Above this velocity the colloids tend to detach from the surface. This critical velocity is higher for rough vs. smooth surface, e.g., for 1 μm particles it is 10^{-4} m/s (rough) vs. 10^{-5} m/s (smooth).

The variation in colloid radius (r_c) has shown higher retention efficiency for small (size fraction: 0.3 and 0.43 μm) vs. large particles (1 and 2 μm). Our explanation is that an increase in the ratio between radius of colloids to surface pit distance and diameter results in a decrease of adhesion torque acting on colloid..

Variations in polydispersity showed that an increase in polydispersity resulted in a decrease of colloid deposition efficiency. Also, as polydispersity increases, the difference in deposition efficiency between plain vs rough surfaces decreases.

Generally, comparison of deposition behavior at smooth vs. rough surfaces showed that nano-scale surface roughness is able to increase significantly colloidal deposition and more specifically it is important under electrostatically unfavorable conditions.

We conclude that the efficiency of particle retention is increased under conditions (i) decrease in r_c/*pit density* and (ii) at lower velocities (10^{-6} to 10^{-4} m/s). We therefore interpret the results foster to implicate the applicability of roughness dependent colloid deposition at interfaces in the environment and various technical applications such as contaminant transport and filtration, drinking-water quality control, mining and nuclear waste management in the saturated zone.

Reference:
Bradford, S. A.; Torkzaban, S. (2008) Colloid transport and retention in unsaturated porous media: A review of interface-, collector-, and pore-scale processes and models. *Vadose Zone Journal,* 7, (2), 667-681.
Bhattacharjee, S.; Ko, C. H.; Elimelech, M. (1998) DLVO interaction between rough surfaces. *Langmuir***,** 14, (12), 3365-3375.
Hoek, E. M. V.; Agarwal, G. K. (2006) Extended DLVO interactions between spherical particles and rough surfaces. *Journal of Colloid and Interface Science***,** 298, (1), 50-58.
Das, S. K.; Schechter, R. S.; Sharma, M. M. (1994) The Role of Surface-Roughness and Contact Deformation on the Hydrodynamic Detachment of Particles from Surfaces. *Journal of Colloid and Interface Science***,** 164, (1), 63-77.
Darbha, G.; Schafer, T.; Herberling, F; Luttge, A.; Fischer, C. (2010) Retention of latex colloids on calcite as a function of surface roughness and topography. *Langmuir,* 26, (7), 4743-4752.

Bentorit vs. Chromettringit ?

Ivonne Haferkorn[1], David Poppitz[1], Gert Kloess[1], Michael Lux[2]

[1]Universität Leipzig, Institut für Mineralogie, Kristallographie und Materialwissenschaft, Scharnhorststr. 20, 04275 Leipzig

[2]EnviroConsult Ingenieurbüro, Meuselwitzer Str. 5, 99092 Erfurt

Ein Schadensfall im ehemaligen Industriegebiet Erfurt-Brühl, auf dem Gelände der Galvanikabteilung der Firma OPTIMA führte zu roten Chromausblühungen in einem Gebäude. Kaliumdichromat und Chrom(VI)-oxid wurden in Galvanikbädern zur Verchromung von Metallteilen eingesetzt. Durch Risse im Fundament bzw. in der Bodenplatte drang über Jahre kontinuierlich chromhaltige Lösung in das Mauerwerk ein, die ein Ettringittreiben zur Folge hatte.
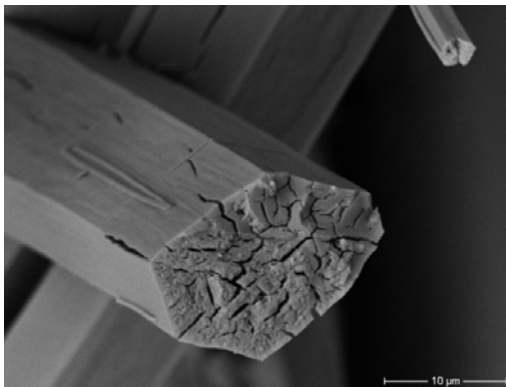
Abb. 1: SEM-Aufnahme eines chromhaltigen anthropogenen Ettringitkristalls

Es entstand die Frage, ob die gefundenen Cr-haltigen Ettringit-Kristalle strukturell der Bentoritstruktur entsprechen.

Der chromhaltige Bentorit $Ca_6(Cr,Al)_2(SO_4)_3(OH)_{12} \cdot 26H_2O$ kristallisiert in der Ettringitstruktur und bildet dihexagonal-dipyramidale Kristalle. Chrom sitzt dabei auf den Al-Plätzen.

Bentorit wurde erstmals 1980 von Gross beschrieben. Als Fundorte werden Marmor-Steinbrüche des Hatrurim-Beckens in der Negev-Wüste westlich des Toten Meeres im Süden Israels genannt.

Abb. 2: Aufnahme eines Ettringitbüschels

Es ist allgemein bekannt, dass Chrom in das Speichermineral Ettringit eingebaut werden kann (z.B. Pöllmann 2007). Der hier zu untersuchende anthropogene Chrom-Ettringit entspricht in seiner chemischen Zusammensetzung in etwa dem Bentorit.

Die an einem 72x48x5 μm^3 kleinen Einkristall durchgeführte Strukturanalyse (STOE IPDS 2T, Mo-Kα, 40h Messzeit, Auswertung mittels WinGX und SHELXL-97) wurde ergänzt durch eine chemische Nano-EDX-Analyse (HRTEM Philips CM 200). Die Strukturanalyse bestätigt das Vorliegen einer Ettringitstruktur. Zu diesem Ergebnis passen auch die in der EDX-Analyse ermittelten Elementgehalte. Der Unterschied zum Bentorit besteht darin, dass die Sulfatplätze in der Ettringitstruktur partiell durch Chromat ersetzt wurden.

Bestätigt wurde dieses Ergebnis mittels einer magnetochemischen Untersuchung, bei der Chrom-(VI) identifiziert wurde. Eine Substitution durch Chrom-(VI) ist nur auf Sulfatplätzen möglich. Die Ergebnisse der EDX-Analyse führen zu der chemischen Zusammensetzung $Ca_6Al_2((SO_4)_{1,4}(CrO_4)_{1,6})OH_{12} \cdot 26H_2O$.

Es wird gezeigt, dass anthropogen gebildeter Chrom-Ettringit strukturell nicht identisch mit dem zur Ettringitgruppe gehörenden Mineral Bentorit ist, da dass Chrom nicht, wie im Bentorit, auf dem Aluminiumplatz, sondern auf dem Sulfatplatz sitzt.

Reference:

Fleischner, M. & Cabri, L.J. (1981): New mineral names, American Mineralogist, Vol. 66, S. 637-639

Gross, S. (1980): Bentorite. A new mineral from the Hatrurim Area, west of the Dead Sea, Israel. Israel J. of Earth Sci., 29, 81–84

Pöllmann, H. (2007): Immobilisierung von Schadstoffen durch Speichermineralbildung. Shaker-Verlag

P4-12

Einfluss von Smektit und einer Illit-Smektit Wechsellagerung auf den mikrobiellen Abbau von Rohöl im Brackwasser der Ostsee

Josephin Mühlbach[1], Claudia Nickel[1], Laurence N. Warr[1], Frieder Schauer[2]

[1]Ernst-Moritz-Arndt Universität, Institut für Geographie und Geologie, Greifswald, Deutschland
[2]Ernst-Moritz-Arndt Universität, Institut für Mikrobiologie, Greifswald, Deutschland

Die Sanierung von verschmutzten Küstenbereichen durch austretendes Rohöl ist ein bekanntes Problem. In diesem Zusammenhang wurden ein reiner Smektit und eine Illit-Smektit Wechsellagerung, sowie deren Einfluss auf den mikrobiellen Abbau von Öl im Brackwasser, untersucht. Die Tone sollen im Ernstfall als Pulver auf den Ölteppich aufgebracht werden. Bisherige Arbeiten (z.B.: WARR et al. (2009) und CHAERUN & TAZAKI (2005)) beschäftigten sich mit diesen Prozessen im Meerwasser (Salzwasser). Nach der Hypothese von WARR et al. (2009) erfolgte bei der I/S-Wechsellagerung eine Calcium-Sättigung.

Für die Untersuchungen wurde ein Experiment mit 4 Proben (Probenbeschreibung siehe Tabelle) durchgeführt. Die Proben wurden kontinuierlich geschüttelt und gewogen. Der Gewichtsverlust aller Proben wurde bestimmt und ergab eine bis zu dreifach erhöhte Abbaurate bei der Zugabe von Ton. Der Ton wirkt dispersiv, vergrößert die reaktive Oberfläche und verhindert hauptsächlich das Verklumpen der schweren Kohlenwasserstoffe. Die vergrößerte Oberfläche ermöglicht den kohlenwasserstoffverwertenden Bakterien, welche durch mikrobiologische Untersuchungen nachgewiesen wurden, einen effektiveren Abbau der Rohölbestandteile. Dabei dient der Ton als zusätzliche Nährstoffquelle, die Calcium-Sättigung der I/S Wechsellagerung hatte keinen Einfluss.

Abb. 1: TEM Aufnahme der Ca gesättigten I/S Wechsellagerung mit einer Bakterie

Tabelle 1: Experimentzusammensetzung, Dauer: 9 Wochen

Probe	Zusammensetzung und Beschreibung	makroskopische Beobachtungen
1	Rohöl + Brackwasser (=Referenzprobe)	Verklumpung des Rohöls
2	Ca gesättigte Illit-Smektit Wechsellagerung (Friedland Ton) + Rohöl + Brackwasser	Schlammige Masse
3	Illit-Smektit Wechsellagerung (Friedland Ton) + Rohöl + Brackwasser	Schlammige Masse
4	Ca-Montmorillonit, US-Standard STx-1 + Rohöl + Brackwasser	Suspension

Die TEM-Aufnahmen zeigen einen direkten Kontakt zwischen Tonpartikeln und Bakterien (siehe Abbildung 1).

Vor dem Experiment zeigten die I/S Wechsellagerungen klare Kristallstrukturen. Nach dem Experiment zeigte sich nur ein undifferenziertes, aufgequollenes Erscheinungsbild. Diese Veränderung zeigte sich auch in den Röntgendiffrakometer-Analysen.

Die leicht niedrigere Abbaurate von Rohöl im Brackwasser, im Vergleich mit Meerwasser, ist der deutlich differenzierten Wasserchemie des Brackwassers geschuldet. Es konnte gezeigt werden, dass sowohl der Smektit

als auch die I/S Wechsellagerung für die Sanierung im Brackwasser in Frage kommen. In Hinsicht auf den Kosten-Nutzenfaktor wäre die Zugabe der I/S Wechsellagerung eine regionale Alternative im Falle einer Ölverschmutzung in der Ostsee.

References:

CHAERUN, S.K., TAZAKI, K. (2005): How koalinite plays an essential role in remediating oil-polluted seawater-Clay Minerals, Vol. 40, S. 481-491
WARR, L.N., et al. (2009): Clay mineral- enhanced bioremediation of marine oil pollution- Appl. Clay Sci. Vol. **46**, S. 337-345

Chemical state of chromium in extreme chromium-resistant bacteria *Leucobacter*

Juraj Majzlan[1], Gunnar Sturm[2], Jörg Göttlicher[3] and Johannes Gescher[2]
[1]Friedrich-Schiller-Universität Jena, Institute for Geosciences, Department Mineralogy, Jena, Germany
[2]Universität Freiburg, Institute for Biology II, Department Mikrobiology, Freiburg, Germany
[3]Institue for Synchrotron Radiation (ISS), Karlsruhe Institute of Technology, Karlsruhe, Germany

Chromium has become a widespread pollutant in the last decades and is the most important heavy metal pollutant in the European Union. Most cases of environmental chromium contamination result from the inadequate waste management of leather tannery, dye, car and steel industry. The toxicity of chromium results from the formation of ternary Cr-DNA adducts, ternary Cr-protein adducts, as well as an increased intracellular formation of reactive oxygen species after Cr(VI) import over the cytoplasmic membrane.

We isolated a novel *Leucobacter* strain which is capable of growing in media containing 31 g L^{-1} Cr(VI) (Sturm et al., 2010). This bacterium is so far the highest chromium-tolerant organism described. *Leucobacter chromiiresistens* forms cell aggregates in response to the chromium-induced stress. The aggregates are held together by extracellular polymeric substances that mainly consist of DNA and sugar polymers. Chromium resistance was completely lost when DNAse - an enzyme that catalyzed the hydrolysis of DNA - was added to the medium. DNAse addition did not influence the growth when no chromium was added. Furthermore, the treatment of existing aggregates with DNAse leads to a fast disintegration of the cellular network. Hence, DNA seems to be necessary for aggregate formation and either extracellular DNA itself or the formation of cell aggregates comprises an essential resistance mechanism. Beside aggregate formation, several further resistance mechanisms were already detected. The measured production of a cytoplasmic Cr(VI) reductase could be another integral factor of the chromate tolerance of *Leucobacter chromiiresistens*. Using energy-dispersive X-ray microanalyses, we could already show that *Leucobacter chromiiresistens* cells contain chromium in the cell interior as well as at the surface but we were unable to determine the oxidation state of the metal and the local structure around the chromium ions.

Using the instrumentation available at the ANKA SUL-X beamline, we have measured Cr K edge spectra of liquid suspensions and dried products thereof from the extracellular matrix, membranes, cytoplasm, and the whole cells. Some beam damage was observed, especially for the wet samples but the experiments showed conclusively that the Cr bound to the matter in our samples is exclusively or almost exclusively Cr(III). Hence, in the presence of bacteria, the initially added Cr(VI) will be reduced to Cr(III) and bound to the biological matter.

The methods used in our study provide a strong but indirect evidence that chromium binds to DNA molecules. Another piece of puzzle came from the modeling of the EXAFS spectra. Because of relatively low concentration of Cr and beam-damage effects, we processed only the spectra from the cell membranes. As expected, the first coordination shell consists of 6 oxygen atoms with a Cr-O distance of 1.987(5) Å. The second shell is more complicated but contains a light (C/N/O) atom at a distance of 3.02(4) Å and a P atom at a distance of 3.24(3) Å. The Cr-P distance corresponds to a monodentate complex of the Cr(III) octahedron with the phosphate tetrahedron. Attempts to insert a Cr atom in the second shell (to model possible Cr-oxide nanoclusters) or a sulfur atoms (binding of Cr(III) to sulfide moiety) invariably failed as they gave large negative amplitudes of the EXAFS oscillations. The shorter distance to a C/O/N atom could correspond to a carboxyl group; Arakawa et al. (2000) propose that Cr(III) binds to the N7 atom of the guanine base. Yet, when constructing a corresponding model for the EXAFS analysis, we found that such mode of binding is geometrically difficult, i.e., a close approach of octahedrally bound chromium to the N7 guanine site would probably cause excessive strain in other regions of the guanine molecule. It is possible, however, to construct a cluster of the guanine molecule, Cr(III) octahedron, and a phosphate tetrahedron, if only 5 of the Cr(III) ligands are oxygens; the sixth ligand must be the N7 atom of the guanine molecule. We will further inspect this possibility of Cr(III) local environment. The binding of Cr(III) hints, in line with other pieces of evidence, that the metal binds to the DNA molecules.

Our results are not only relevant to the binding of Cr(III) to the biological matter, likely DNA. A growing body of data shows that metals may directly bind to DNA (e.g., Ravel et al. 2009) and such complexes may find a practical industrial use. Therefore, the understanding of the metal-DNA interactions reaches beyond the specific scientific questions of this study and may lead to a development of sophisticated environmental sensors for metals (cf. Ravel et al. 2009).

References:
Arakawa, H., Ahmad, R., Naoui, M., Tajmir-Riahi, H.-A., 2000: A comparative study of calf thymus DNA binding to Cr(III) and Cr(VI) ions. *The Journal of Biological Chemistry* 275, 10150-10153.
Ravel, B., Slimmer, S.C., Meng, X., Wong, G.C.L., Lu, Y., 2009: EXAFS studies of catalytic DNA sensors for mercury contamination of water. *Radiation Physics and Chemistry* 78, S75-S79.
Sturm, G., Jacobs, J., Spröer, C., Schumann, P., Gescher, J.: *Leucobacter chromiiresistens* sp. nov., a novel chromate-resistant strain in the genus *Leucobacter*. 2010. IJSEM, *in press*.

Anthropogenic Gadolinium as Microcontaminant and Tracer in Berlin Tap Water

Serkan Kulaksız[1], Michael Bau[1,2]
[1]Earth and Space Sciences Program, Jacobs University Bremen Campus Ring 8, 28759 Bremen, Germany
[2] Integrated Environmental Studies Program, Jacobs University Bremen Campus Ring 8, 28759 Bremen, Germany

Gadolinium is a rare earth element (REE), a group of elements known to behave coherently in natural systems. Therefore, the presence of strong decoupling of a single REE from neighboring REE is likely due to anthropogenic processes. The first case of large scale single element decoupling was reported for surface waters in Berlin (Bau and Dulski, 1996) where the sheer magnitude of the decoupling ruled out natural processes as the source. The only widespread application of water-soluble Gd is as contrast agent in magnetic resonance imaging. The Gd-based contrast agents (Gd-CA) are highly stable Gd chelates and, therefore, not removed in waste water treatment plants (WWTP), but transported into surface waters with the clearwater discharge from WWTP. The presence of anthropogenic Gd in surface water can lead to contamination of groundwater, through natural and artificial bank filtration and groundwater recharge, as has been demonstrated by Knappe et al. (2005) where Gd levels in groundwater are anomalously high in those parts of Berlin where bank filtration and artificial groundwater recharge is employed.

Since drinking water will likely be in high-demand as a commodity in the future, bank filtration and groundwater recharge is expected to gain importance in the management of freshwater resources. Therefore, we investigated the extent to which tap water used as drinking water is affected by anthropogenic Gd. We found large positive Gd anomalies in tap water samples from the western districts of Berlin, indicating the presence of up to 18 ng/kg of anthropogenic Gd on top of a geogenic background of 0.54 ng/kg. In marked contrast, the amount of anthropogenic Gd in tap water from the eastern districts of Berlin is negligible to minor (maximum of 0.19 ng/kg on top of a geogenic background of 0.36 ng/kg). This strong regional difference likely results from the specific historical situation of Berlin, where before the re-unification of Germany groundwater recharge and bank filtration were necessities in isolated West Berlin, but unimportant in East Berlin. Thus, drinking water resources in the western part of Berlin are more strongly affected by anthropogenic Gd than those in the eastern part. The high anthropogenic Gd load of some tap waters in Berlin clearly shows that the Gd initially used as contrast agent is neither removed during natural nor artificial water treatment and is present in tap water consumed as drinking water, ultimately exposing millions of people to low doses of anthropogenic Gd chelates. Preliminary data for the City of London, U.K., indicate that this is not a local phenomenon and suggest that the REE distribution in tap waters used for human consumption should be monitored.

Reference:
Bau, M. and Dulski, P., 1996. Anthropogenic origin of positive gadolinium anomalies in river waters. Earth and Planetary Science Letters. 143(1-4), 245-255.
Knappe, A., Möller, P., Dulski, P. and Pekdeger, A., 2005. Positive gadolinium anomaly in surface water and ground water of the urban area Berlin, Germany. Chemie der Erde - Geochemistry. 65(2), 167-189.

From surface morphology to rates: An automated routine to evaluate converged roughness parameters of heterogeneous surfaces

Kilian Pollok, Thomas Chust, Dennis Harries
Universität Bayreuth, Bayerisches Geoinstitut, Bayreuth, Germany

Dissolution and precipitation reactions at the mineral-fluid interface constantly modify mineral surfaces. Knowledge about the evolution of surface topography and roughness is therefore of prime importance to correctly parametrize surface-controlled geochemical processes. A number of different roughness parameter is used to characterize surfaces in material science and industrial production processes. However, for natural surfaces the size of surface components is not known a priori and depend on processes (e.g. abrasion, dissolution or precipitation) as well as on structural peculiarities (e.g. steps, etch pit geometry, cleavage planes).

Converged surface roughness parameters (Fischer and Lüttge, 2007) can be used to explore how different surface components impact roughness parameters over a range of lateral scales. The convergence of roughness parameters can be identified by calculating them for recurrent section of the entire data set. A parameter is converged when it is not changing over a certain sampling length.

The calculation of the surface roughness in relation to the size of the sampling area has been automated by the newly developed program "*ROUGHNECK*" in order to minimize the bias of choosing 'representative' areas. It allows to statistically evaluate and to visualize the roughness distributions. Confocal microscopy (NanoFocus µSurf custom) was used collect 3D topographic data from a large field of view (160 x 160 µm) with a submicrometer resolution in x, y, and z.

First test objects are pyrrhotite ($Fe_{1-x}S$) surfaces which have been polished by ¼ µm diamond paste and reacted in acidic solution. The surface area ratio, $F = A_{3D}/A_{2D}$ has been evaluated for these surfaces as an example. However, other roughness parameters like the root mean square roughness, S_q, or the ten point height, S10z, can be computed as well.

The polished surface shows a convergence of the surface area ratio F between 8 and 100 µm sampling length as well as below 8 µm. The breakdown of convergence at 8 µm can be related to the average distance of polishing scratches. The F-value distribution allows a statistically robust evaluation of the converged parameters and their breakdown behaviour. For example the breakdown at 8 µm is preceded by a widening of the F-value distribution starting at about 16 µm sampling length.

Intergrown NC/4C-pyrrhotite shows a heterogeneous behaviour against chemical alteration. The 4C type appears more resistent than the NC type. After dissolution the spatial distribution of roughness parameters allows to determine the surface roughness of each structural variant as well as the bulk sample and to filter out areas which are affected by artefacts (cracks, inaccurate measured points). The latter also helps to identify relations between different roughness parameters on statistical basis. By combining the surface topography (including the intergrowth characteristics) with the roughness parameter distribution this method facilitates the estimation of rates for heterogeneous samples.

Reference:
Fischer & Lüttge (2007): Converged surface roughness parameters - a new tool to quantify rock surface morphology and reactivity alteration. American Journal of Science, 307, 955-973.

Speciation of Pb in Human Trabecular Bone and the Tidemark of Articular a Human Bone

F. Meirer[1,2], B. Pemmer[1], N. Zoeger[1] C. Streli[1], J. Goettlicher[3], R. Steininger[3], S. Mangold[3], A. Tampieri[4], S. Sprio[4], G. Pepponi[5], J. G. Hofstaetter[6,7], P. Roschger[6], K. Klaushofer[6]

[1] Atominstitut, Technische Universitaet Wien, Stationallee 2, 1020 Vienna, Austria

[2] Stanford Synchrotron Radiation Lightsource, 2575 Sand Hill Road, Menlo Park, CA 94025, USA

[3] Karlsruhe Institute of Technology, Institute for Synchrotron Radiation, Hermann-von-Helmholtz-Platz 1, D-76344 Eggenstein-Leopoldshafen, Germany

[4] Istituto di Scienza e Tecnologia dei Materiali Ceramici CNR, Faenca, Italy

[5] Fondazione Bruno Kessler – irst, Povo, Italy

[6] Ludwig Boltzmann Institute of Osteology at the Hanusch Hospital of WGKK and AUVA Trauma Centre Meidling, 4th Med. Dept., Hanusch Hospital, 1140 Vienna, Austria

[7] Department of Orthopaedic Surgery, Vienna General Hospital, Medical Univ. of Vienna, Austria

Most of the toxic trace element lead (Pb) in human beings is stored in the skeleton. Zoeger et. al. have recently shown that Pb specifically accumulates in the tidemark (TM) of human articular cartilage at much higher levels compared to trabecular bone [1,2]. However, the accumulation mechanisms as well as the chemical species of Pb at the TM, which is the border between calcified and non-calcified articular cartilage, and in trabecular bone, are not well known. It is know though that Pb is able to displace Ca^{2+} by cation exchange processes in the hydroxyapatite (HA) crystal, the main constituent of bone, suggesting that Pb is mainly built into the hydroxyapatite in bone [3, 4].

X-ray absorption spectroscopy was used to determine the chemical species of Pb in human bone. Pb L_3-edge X-ray absorption near edge structure (XANES) spectra were recorded at the TM of a human patella, on a trabecular bone and of on Pb doped synthetic hydroxyapatite standards (one with increased carbon content).

The measurements were performed at the SUL-X beamline of the synchrotron radiation source ANKA which provides a focussed beam of about 100 μm x 100 μm. Fluorescence radiation was collected with a 7 element Si(Li) detector.

The results suggest that about half of the Pb in the tidemark is incorporated in the structure of carbonated-hydroxyapatite and the rest is bound to a yet undetermined, maybe organic, compound. Although the concentration of Pb in trabecular bone is about 13-fold smaller than in the TM [1], signals were sufficient to show that Pb in trabecular bone is mostly incorporated into carbonated-hydroxyapatite.

References:
[1] Zoeger N, Roschger P, Hofstaetter JG, et al., Osteoarthritis and Cartilage, 14, 906-913 (2006).
[2] Zoeger N, Streli C, Wobrauschek P, et al., X-ray Spectrometry, 37, 3-11 (2008).
[3] Mavropoulos E, et al., Environ Sci Technol, 36(7), 1625-1629 (2002).
[4] Dowd TL, et al., Biochim Biophys Acta, 1226(2), 131-137 (1994).

Trace element distribution in stalagmite from the Dechenhöhle by micro X-ray fluorescence spectroscopy to detect environmentally significant events in the early years of industrialization

Jörg Göttlicher[1], Stephan Marks[2], Rolf Simon[1], Alexander Platte [3], Stefan Niggemann[4]
[1]Karlsruhe Institute of Technology, Institute for Synchrotron Radiation, Eggenstein-Leopoldshafen, Germany
[2]Münster, Germany
[3]Lethmate, Germany
[4]Dechenhöhle, Lethmate, Germany

We have started an investigation about the impact of a former lead and zinc smelter on karst bedrocks. First results will be presented. In this study speleothems (minerals that form mostly in caves, here $CaCO_3$: calcite/aragonite) are used to detect anthropogenic caused environmentally impacts by analyzing heavy metals that have been emitted during early years of industrialization. Data shall be correlated with measurements on tree rings like in [1].

Letmathe in the Sauerland (one of the low mountain ranges in Germany) was chosen as a suitable area to investigate the effect of industrial emissions on carstwaters because lead and zinc smelters had been in operation there from 1862 to 1925 near by a cave (Dechenhöhle). Past atmospheric pollution of Pb and Zn were found in formation of gypsum ($CaSO_4$ x 2 H_2O) at the surface of the rock formation "Pater und Nonne" about 500 m east of the former smelter and at a rock close to the cave museum [2]. The gypsum at "Pater and Nonne" contains about 1000 ppm Pb and 500 ppm Zn, the incrustations at the cave museum about 1800 ppm Pb and 1000 ppm Zn. Zn and Pb accumulation are assumed to be due to emissions of the smelter because they are located in the main wind direction. Hints for enhanced Pb levels that are not only due to the former use of lead containing fuel have been reported from analyses of deer antlers [3].

In this study, we investigate whether the emissions of mainly Pb and Zn has affected the carstwaters by analyzing stalagmites with microfocus X-ray fluorescence spectroscopy. Just about 1 km in the main wind direction east of the smelter the Dechenhöhle is located where we have taken an active stalagmite in Mai 2010. Estimated from its thickness it should be much older than 200 years, and hence, covers the period of interest and the pre-industrial background, assumed a continuous activity. Additionally, slices of beech trees that are approximately 155 to 165 years old from a location close to the cave were available for measuring their metal contents.

The young zone of the stalagmite is grey colored and has a thickness of about 10 mm (on top of the stalagmite) compared to the beige color of the inner part. Fluorescence emission profiles measured at the SUL-X and FLUO beamline of the synchrotron radiation source ANKA show that Pb and Zn incorporation in the stalagmite starts at the boundary grey/beige. Both elements are almost absent in the beige (older) part and show distinct peaks in the grey part with the highest concentrations at the boundary beige/grey. Pb and Zn are partly correlated.

Because the discovery and opening of the Dechenhöhle coincides approximately with the beginning of the smelters a second stalagmite from a part of the cave system that has not been affected from human activities shall be investigated to exclude particulate entry as source for elevated Pb and Zn contents in the speleothems. Fluorescence emission profiles from two beech trees have been measured and a few spikes of Pb have been detected. Zn contents in the trees are higher than Pb and are represented by a large number of peaks of different heights and frequencies with time.

In both types of samples (stalagmite, wood) a discrete occurrence of Pb and Zn have been found rather than a continuous elevation of metal contents during the time. Distinct peaks can be a hint that part of the atmospheric emission after precipitation might be transported directly to the underground without intermediate storage in the soil layer. But for a final explanation results shall be verified by analyzing investigating additional stalagmite and tree samples.

References:
[1] Siklosy Z., Kern Z., Demeny A., Pilet S., Leel-Ossy Sz., Lin K., Shen C-C., Szeles E. (2009) Impact of uranium mining activity on cave deposit (stalagmite) and pine trees (S-Hungary). Vol. 11, EGU2009-8239, 2009, EGU General Assembly 2009
[2] Richter D.K., Hammerschmidt E., Niggemann S. (1997) Gipskrusten an „Pater und Nonne". Speläologisches Jahrbuch – Verein für Höhlenkunde in Westfalen 1995/1996, Iserlohn 1997, 49, 49-60
[3] Kierdorf, H., Kierdorf U. (2000) Vergleichende Untersuchungen zum Bleigehalt von Rehgeweihen aus verschiedenen Regionen Nordrhein-Westfalens (Deutschland) im Zeitraum 1990-1991. Z. Jagdwiss. 46, 270-278

Remediating coastal oil spills using natural clays

Laurence N. Warr[1], Josephin Mühlbach[1], Claudia Nickel[1], Frieder Schauer[2]
[1]Ernst-Moritz-Arndt Universität, Institute for Geography and Geology, Germany
[2]Ernst-Moritz-Arndt Universität, Institute for microbiology, Germany

This contribution discusses the idea of adding volumes of clay powder to oil spills in aqueous environments in an effect to increase the rates of dispersion and bacterial digestion. It has long been known that the addition of natural clays and their constituent clay minerals increases micelle formation and hence breakup of oil.

New ideas on how to prepare the clays and add them to the spill are here presented.

Reference:
WARR, L.N., et al. (2009): Clay mineral- enhanced bioremediation of marine oil pollution- Appl. Clay Sci. Vol. 46, S. 337-345.

Section 05

_____

Experimental and theoretical petrology

New calorimetric data on feldspars: Implications for modelling the ternary mixing behaviour

Artur Benisek[1], Edgar Dachs[1], Hebert Kroll[2]
[1]Universität Salzburg, Materialforschung und Physik, Salzburg, Austria
[2]Westfälische Wilhelms-Universität Münster, Institut für Mineralogie, Münster, Germany

New calorimetric work (Benisek et al., 2009, 2010a, 2010b) on feldspars in the $NaAlSi_3O_8$ – $KAlSi_3O_8$ – $CaAl_2Si_2O_8$ system enabled the formulation of a mixing model which is based exclusively on calorimetric and volumetric data (Benisek et al., 2010c). When compared to models based on phase equilibrium experiments distinct differences are revealed. The calorimetry based model shows less solubility for both K in Ca-rich plagioclase and Ca in K-rich alkali feldspar. On the other hand, the stability field of Na-rich feldspars is broadened.

The two approaches are tested on natural feldspar assemblages from different rocks. One of them is the Klokken syenogabbro, South Greenland, which was thoroughly investigated by Parsons and Brown (1983). It contains a perthite and mesoperthite whose bulk compositions should agree with the 970°C/1kbar isotherm according to melting experiments and petrologic reasoning. The figure below compares this isotherm calculated from different mixing models. The calorimetry based model far better agrees with the petrologic expectation than do the phase equilibrium based models.
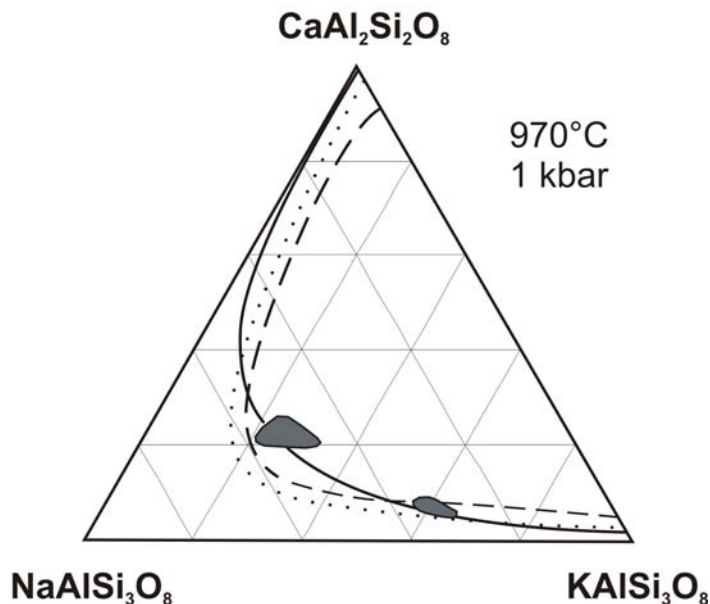
Fig. 1: Compositions of the feldspars from the Klokken syenogabbro, South Greenland (Parsons and Brown, 1983). The 970°C/1kbar isotherm of this study (*solid line*) is compared to those resulting from phase equilibrium experiments (*dashed line*: Fuhrman & Lindsley, 1988; *dotted line*: Elkins & Grove, 1990).

Reference:
Benisek A, Dachs E, Kroll H (2009) Excess heat capacity and entropy of mixing in high structural state plagioclase. American Mineral 94: 1153-1161.
Benisek A, Dachs E, Kroll H (2010a) Excess heat capacity and entropy of mixing in the high-structural state (K,Ca)-feldspar binary. Phys Chem Minerals 37: 209-218.
Benisek A, Dachs E, Kroll H (2010b) Excess heat capacity and entropy of mixing in ternary series of high structural state feldspars. Eur J Mineral DOI: 10.1127/0935-1221/2010/0022-2028.
Benisek A, Dachs E, Kroll H. (2010c) A ternary feldspar-mixing model based on calorimetric data: development and application. Contrib Min Petrol, DOI 10.1007/s00410-009-0480-8.
Fuhrman ML, Lindsley DH (1988) Ternary feldspar modeling and thermometry. Am Mineral 73: 201-215.
Elkins LT, Grove TL (1990) Ternary feldspar experiments and thermodynamic models. Am Mineral 75: 544-

559.
Parsons I, Brown WL (1983) A TEM and microprobe study of a two-perthite alkali gabbro: implications for the ternary feldspar system. Contrib Mineral Petrol 82: 1-12.

Trace element partitioning between perovskite and kimberlitic and carbonatitic melt

Christopher Beyer[1], Stephan Klemme[1], Jasper Berndt-Gerdes[1]
[1]Westfälische Wilhelms-Universität Münster, Institute for Mineralogy, Münster, Germany

The partitioning of trace elements between perovskite ($CaTiO_3$) and silicate melts of different compositions were investigated experimentally at atmospheric pressure and also at high-pressure using an end-loaded piston cylinder apparatus at temperatures between 1100 and 1200 °C, and at pressures of up to 1.4 GPa. Partition coefficients were determined for a large number of trace elements (Li, Sc, Zr, Hf, Nb, Ta, REE, Pb, Th, U) in several different bulk compositions (CaO-TiO_2-SiO_2 and CaO-TiO_2-SiO_2-Al_2O_3-MgO-K_2O-NiO-CO_2-H_2O), aiming to further our understanding of trace element signature of kimberlitic melts. Additional experiments were performed to investigate the partitioning between perovskite and carbonatite melts.

The run products were analysed with state-of-the-art 193 nm laser ablation ICPMS at Münster University. The results of the 1-atm experiments suggest that REE, Nb, Ta, and Th are compatible in Ca-perovskite whereas elements such as Si, Li, Mg, Sc, Hf and Zr are found to be incompatible. The observations confirm the notion by Corgne and Wood (2002, 2005) that Ca-perovskite favours to incorporate Th over U thus enabling perovskite to significantly fractionate Th from U.

Furthermore, we were able to approve the conclusion of Corgne and Wood (2002, 2005) that temperature and pressure have only a minor effect on the partitioning behaviour of perovskite and the content of CaO in the melt strongly affects the partitioning behaviour. First results in more complex kimberlitic and carbonatitic compositions (with H_2O and CO_2) will also be presented.

Reference:
Corgne, A. & Wood, B.J. (2002): $CaSiO_3$ and $CaTiO_3$ perovskite-melt partitioning of trace elements: Implications for gross mantle differentiation, Geophysical Research Letters, volume 29, article 1903
Corgne, A. & Wood, B.J. (2005): Trace element partitioning and substitution mechanisms in calcium perovskites, Contributions to Mineralogy and Petrology, volume 149, pp. 85-97

Towards a viscosity model for flux-rich pegmatitic melts

Bartels A.[1], Baasner A.[2], Behrens H.[1], Holtz F.[1], Schmidt B.C.[2]
[1] Institute for Mineralogy, Leibniz University of Hannover, Germany, a.bartels@mineralogie.uni-hannover.de
[2] Experimentelle und Angewandte Mineralogie, GZG, Georg-August Universität Göttingen, Germany

Measurement of transport properties of water-rich, strongly depolymerised melts is still a demanding experimental task. Such melts play an important role in volcanic eruptions as well as in formation and evolution of pegmatites. The key property governing dynamics in partially melted systems is the melt viscosity. Current models from Giordano et al. (2008) and Hui and Zhang (2007) are useful tools to predict the viscosity for a wide range of melt compositions, but are not well calibrated for melts rich in water and fluxing elements like F, Li, B and P.

To test the applicability of such models, viscosity experiments were conducted with a nominally dry to water saturated flux-rich melt representative of a melt from which a pegmatite could crystallize. The starting glass was prepared from a mixture of SiO_2, Al_2O_3, Na_2CO_3, K_2CO_3, AlF_3, Li_2CO_3, $(NH_4)H_2PO_4$ and H_3BO_3 by heating at 1400°C in a furnace at 1 atm for 40min. The resulting Li_2O, F, B_2O_3 and P_2O_5 contents were 1,68, 5,46, 2,75 and 2,46wt%, respectively. The viscosity was determined in internally heated gas pressure vessels using the falling sphere method (low viscosity range) in the temperature range 1073 - 1273 K at 200 MPa. In the low temperature range between 450 and 800 K the viscosity was determined at ambient pressure using the micropenetration technique. Including all measurements the viscosity (η) can be expressed as a function of temperature and water content according to:

$$\log \eta = -4{,}44 + (9856{,}76 - 4031{,}88 + \log(w+1{,}06))/(T - (126{,}47 - 9{,}62 + \log(w+1{,}06)))$$

where η is viscosity in Pa s, T is temperature in K, and w is water content in weight percent.

The results demonstrate that the current viscosity models are insufficiently constrained for flux-rich water bearing melts. In a second step we conducted viscosity experiments with changing F contents in the melt to determine the individual effects of this fluxing element on the transport properties of pegmatitic melts. The first results show that by increasing the F-content in the melt from 2.68 to 4.81wt%, the viscosity decreases by only ~ 0.6 log units at 1173K and water contents around 6wt%. Nevertheless more experiments needs to be done to investigate the influence of this element on melt viscosity. Additional experiments with changing Li and P contents in the melt are in progress to determine the individual effect of these elements on the transport properties of pegmatitic melts.

References:
Giordano D., Russell J.K., Dingwell D.B. (2008): Viscosity of magmatic liquids: A model, Earth and Planetary Science Letters, 271, 123-134
Hui H.J., Zhang Y.X. (2007): Toward a general viscosity equation for natural anhydrous and hydrous silicate melts, Geochimica et Cosmochimica Acta, 71, 403-416

Gladstone-Dale Relationship-Application for Moldavites

Ulrike Rantzsch[1], Gert Kloess[1], Jan-Michael Lange[2]
[1]Universität Leipzig, Institut für Mineralogie, Kristallographie and Materialwissenschaft, Deutschland
[2]Senckenberg Naturhistorische Sammlungen Dresden, Deutschland

Tektites occur in four established geographically restricted areas, the so-called strewn fields. The well known strewn fields are subdivided in several sub-strewn fields. Despite classifications of Moldavites due to geochemistry, isotopic studies, and physical properties, a Gladstone-Dale index K of moldavites has not been reported yet. The aim is to improve a statistical concept of classification with the comparison of physical and chemical properties (Kp, Kc, respectively). The value p and the empirical constant kn characterize the chemical composition whereas density D and the refractive index n characterize the physical properties of moldavites. The Gladstone-Dale relationship (1884) in the equations below will be applicable mainly for minerals with limited compositional variability:

$$K = 1 - \frac{Kp}{Kc} \qquad Kp = \frac{n-1}{D} \qquad Kc = \frac{kn \cdot p}{100}$$

Moldavite physiochemical data sets were selected from Lange (1995) and Philpotts and Pinson (1966). Gladstone-Dale ratios of physical properties and chemical composition for numerous moldavites were calculated.

For comparing Gladstone-Dale ratios an arbitrary compatibility concept (Mandarino 1979) is applied. The established concept correlates the Kp/Kc ratios with compatibility fields. Low varieties in physical properties and chemical composition revealed K values between …., which a required modified Mandarino index. The calculated K values are significant lower than in numerous mineral groups. Therefore, a best-fit modified concept of compatibility with new category groups was adapted to distinguish smallest differences.

As result it can be proposed that Moldavites can be classified using the Gladstone-Dale index. Their sub-strewn fields (Bohemia, Lusatia, Moravia) are definitely specifiable by their distinct K (Figure 1). Summarizing a distinction of the strewn- and sub-strewn fields is clearly applicable with this method.
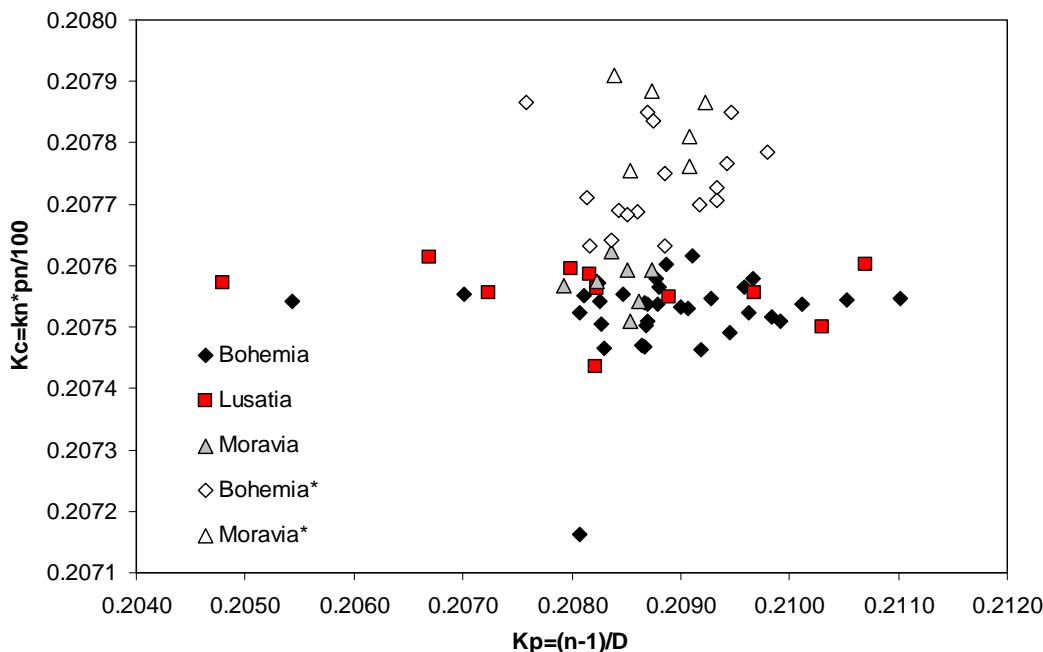
Fig. 1: Distribution of Kp versus Kc for Bohemian, Lusatian and Moravian Moldavites calculated from selected literature data (Lange 1995 and *Philpotts & Pinson 1966).

References:
Gladstone, J.H. & Dale, T.P. (1884), Researches on the refraction, dispersion and sensitiveness of liquids. Phil. Trans. R. Soc. London, 1884, 153
Lange, J.-M. (1995), Lausitzer Moldavite und ihre Fundschichten, Schriftenreihe für Geowissenschaften Halle, 3

Mandarino, J.A. (1979), The Gladstone-Dale relationship. III. Canadian Mineralogist, 1979, 17
Philpotts, J.A. & Pinson JR W.H. (1966), New data on the chemical composition and origin of moldavites. Geochimica et Cosmochemica Acta, 1966, 30

How does melt composition influence the local structural environment of trace elements in silicate melts?

Sebastian Simon[1], Max Wilke[1,] Stephan Klemme[2]
[1]Helmholtz Centre Potsdam, GFZ German Research Centre For Geosciences, Potsdam, Germany
[2]Westfälische Wilhelms-Universität Münster, Institute for Mineralogy, Münster, Germany

Trace elements are useful petrogenic indicators for understanding the formation processes of igneous rocks, and thus knowledge on their partitioning behavior during melt crystallization is essential. It is generally accepted that the partitioning of trace elements between crystals and melts is controlled by a number of parameters such as pressure, temperature, oxygen fugacity (in case of polyvalent cations) and crystal composition (e.g., [1]). So far, there are several studies that propose also a significant influence of the melt composition and thus melt structure on trace-element partitioning ([2], [3], [4], [5]) but to date there is no clear understanding of the controlling mechanism. Particularly, Prowatke and Klemme's results [5] on partitioning between melt and titanite, which varied over several orders of magnitude, suggest a strong control of the melt for the REE, Th, Nb and Ta, because the crystal composition was nearly constant. In a pioneering study, Ponader and Brown [6] find that coordination of some rare earth elements in quenched melts changes with the degree of polymerisation of the melts, which was used to explain differences in chemical partitioning. Aim of this study is to investigate the local structural environment of some selected trace elements (La, Sm, Y) in various quenched silicate-melts, for which partitioning data are available. In this contribution, we report on results of EXAFS measurements at the K-edge of La, Y and at the L-edge for Sm in quenched silicate-melts of various compositions.

Two different glass compositions were taken from [5], that varied in the ratio of aluminium over alkalis and thus ASI200 represent less peralkaline silicate melts and ASI260 strongly peralkaline silicate melts. Glasses were doped with 5000 ppm of La, Sm and Y. The EXAFS spectra were collected at beamline C at HASYLAB on powdered samples of the quenched glasses. The fluorescence signal was collected using multi-element Si(Li) and Ge solid-state detectors. The spectra were analyzed using the software Athena and Artemis by B. Ravel [7]. Amplitudes and phase shift were calculated using Feff [8] and checked on crystalline compounds (e.g. , La_2O_3, Sm_2O_3 and $Y(NO_3)_3H_2O$) with known structural parameters.

Qualitatively the measured spectra indicate differences in the local structural environment of La, Sm and Y between the two different silicate-melt compositions. In the case of La, the spectrum of ASI260 shows a considerably lower magnitude in the 1st maximum of the Fourier transform and a shift to longer distances than ASI200. For Sm, a similar difference is observed although to a smaller extent. For Y, however, ASI260 shows a marginal shift in the 1st maximum of the Fourier transform to shorter distances whereas the magnitude is smaller. Quantitative fitting of the EXAFS has been only performed for Sm, so far. The $Sm - O$ distances change from 2.33 ± 0.02 Å for ASI200 to 2.35 ± 0.01 Å for ASI260. Any differences in the distance to the nearest oxygen neighbors indicate differences in the coordination polyhedron as atomic distances and coordination are strongly related. With the new data set we expect to unravel potential differences between coordination geometries and learn about the relationship of this parameter to the partitioning behavior of the trace elements La, Sm and Y in the chosen melt model systems.

Reference:
[1] Green T. H. (1994) Chem. Geol. 117, 1-36.
[2] Watson E. B. (1976) Contrib. Mineral. Petrol. 56, 119-134.
[3] Ryerson F. J. and Hess P. C. (1978) Geochim. Cosmochim. Acta 42, 921-932.
[4] Prowatke S, Klemme S (2004) Lithos, 73 Suppl., 91
[5] Prowatke S, Klemme S (2005) Geochim. Cosmochim. Acta 69: 695-709
[6] Ponader C. W. and Brown G. E. (1989) Geochim. Cosmochim. Acta 53, 2893-2903.
[7] Ravel, B., and M. Newville (2005), J. Synch. Rad. 12, 537-541
[8] Rehr, J. J. (2000), R. M. P., 72(3), 621-654

Synthese und Stabilitätsuntersuchungen von Bütschliit und Fairchildit

Katharina Pöhler[1], Herbert Pöllmann[1]
[1]Martin-Luther-Universität Halle-Wittenberg, Institut für Mineralogie, Halle, Deutschland

Fairchildit und Bütschliit ($K_2Ca(CO_3)_2$) und die Phase A ($K_2Ca_2(CO_3)_3$) sind die Mischcarbonate des binären Systems K_2CO_3 und $CaCO_3$. Fairchildit stellt das Hochtemperaturpolymorph von Bütschliit dar und ist in einem Temperaturbereich nach COOPER et al. (1975) von 547-809°C stabil. Unterhalb von 547°C wandelt sich Fairchildit in Bütschliit um. Das dritte Doppelcarbonat $K_2Ca_2(CO_3)_3$ ist in einem Temperaturbereich von 512-810°C stabil und zersetzt sich unterhalb von 512°C in Calcit und Bütschliit.

Die Hoch-Temperatur-Synthese von Bütschliit fand nach Anlehnung an die Synthesevorschrift von PABST (1974) statt (6 Tage bei 505 ± 10°C im Kohlenstofftiegel (CO_2-Gegendruck) gesintert). Die Phasenanalyse nach 6 Tagen zeigte Bütschliit und geringe Mengen an Ausgangsphasen K_2CO_3 und $CaCO_3$, deshalb wurde das Gemisch für weitere 5 Tage 505°C ± 10°C gesintert. Nach 11 Tagen waren Fairchildit und die Phase A nachweisbar. Anschließend wurden eine röntgendiffraktometrische Heizaufnahme (bis 1000°C) sowie thermo-analytische Untersuchungen (TG, DTA, DTG bis 1000°C) durchgeführt um die Phasenbildung bzw. Umbildung der Phasen genauer zu untersuchen.

Durch die gewählten Synthesebedingungen entstand das Hochtemperaturpolymorph Fairchildit. Bei langsamer Abkühlung im Ofen bis zur RT (~2 1/2 h) wurde die Phase metastabil erhalten. Die durchgeführte Hochtemperatur-XRD zeigte die Phasenumwandlung von Fairchildit in Bütschliit bei ca. 547°C und die Rückbildung bei ca. 600°C. Thermoanalytische Untersuchungen bestätigten diese Umwandlungs-temperatur. Diese Temperatur liegt im Bereich der von COOPER et al. (1975) ermittelten (539°C). Anhand des DTA-Signals konnten die Temperaturen einiger Phasenumwandlungen im binären Phasensystem $CaCO_3$ – K_2CO_3 zugeordnet werden. Die langsame Zersetzung des Fairchildit in CaO und CO_2, sowie K_2CO_3, konnte ebenfalls nachvollzogen werden.

Reference:
COOPER, A. F., GITTINS, J., TUTTLE, O. F. (1975): The system Na_2CO_3-K_2CO_3-$CaCO_3$ at 1 kbar and its significance in carbonatite petrogenesis. American Journal of science; 275; 534-560
PABST, A. (1974): Synthesis, properties and structure of $K_2Ca(CO_3)_2$ – Buetschliite. American Mineralogist; V 59; S.353-358
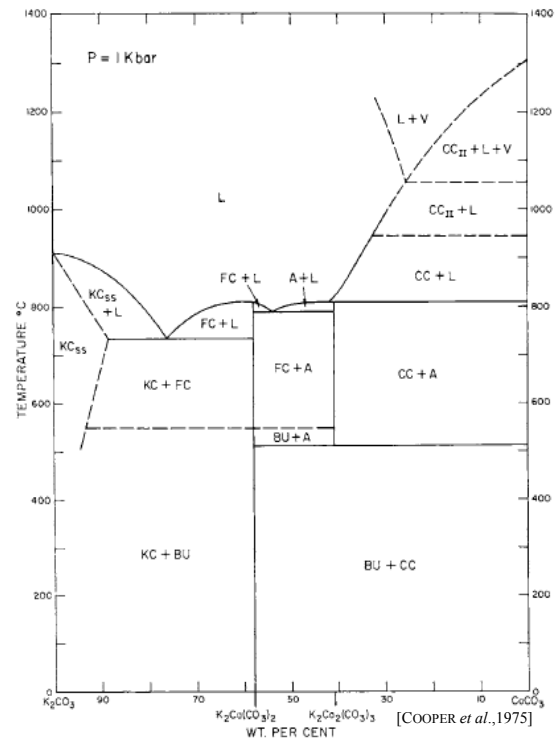
Section 06

———

Fluid-rock and fluid-mineral interaction

Carbonation of volcanic rocks induced by interaction with magmatic and hydrothermal fluids - a case study on Unzen volcano, Japan

Anna V. Simonyan[1], Stefan Dultz[2], Harald Behrens[1], Fiebig Jens[3]
[1]Institute of Mineralogy, Leibniz University of Hannover, Callinstr. 3, 30167 Hannover, Germany (simonian@mineralogie.uni-hannover.de)
[2]Institute of Soil Science, Leibniz University of Hannover, Herrenhäuser Str. 2, D-30419 Hannover
[3]Institute of Geosciences, J.W. Goethe University of Frankfurt, Altenhöferallee 1, D-60438 Frankfurt am Main

The Unzen scientific drilling project (USDP) was focused on the understanding of the mechanisms of volcanic eruptions by drilling into an active volcano shortly after eruption. The project yielded a couple of unexpected results, i.e. the temperature in the borehole was much lower than expected, and the drilling cores were highly altered with large amounts of secondary minerals such as carbonates, chlorite and pyrite, supposed to be products of reactions of discharged volcanic fluids with the host rocks. These surprising findings inspired us to use the drilling cores in combination with experimental work to identify the mechanisms of fluid-rock interaction, in particular the carbonation and decarbonation of rocks which is important for understanding the magma degassing processes, and main processes for storage of CO_2 in cavities or in porous/brecciated volcanic rocks.

Petrographic investigations of natural rocks from drilled cores with electron microprobe (WDS and EDX) and with scanning electron microscope (SEM) show that carbonates are secondary minerals substituting amphiboles during alteration of volcanic rocks in the cooling magmatic conduit. The carbonates are mostly composed of calcite with significant proportions of dolomite. Minor alteration products are clay minerals, pyrite, and quartz. The presence of clay minerals besides carbonates in the altered dacite indicates that the rock might be exposed to different weathering environments, as clay minerals usually form in long-term processes and carbonation by magmatic and hydrothermal fluids might proceed in much shorter time periods.

Secondary carbonates were analyzed for their carbon and oxygen isotopic composition using a Gas Bench II hooked up to the continuous flow inlet system of a MAT 253 gas source mass spectrometer. Carbonate was extracted from powdered silicate samples as CO2 on the addition of phosphoric acid at 72°C. Internal precision (1) typically is <0.08‰ for oxygen and <0.06‰ for carbon isotopes, respectively. The carbonate carbon isotopic composition varies between -4.7 and -6.4‰ vs VPDB and is well within the range reported for the magmatic CO_2 discharging at Unzen volcano ($^{13}C_{VPDB}$ = −3.9 to −6.4‰; Ohba et al., 2008; Shinohara et al., 2008). $^{18}O_{VSMOW}$ values of carbonates range from 6.0 to 9.1‰. These are indistinguishable from those reported for fumarolic water vapor (7.4‰ < $^{18}O_{VSMOW}$ < 10.0‰; Ohba et al., 2008) and primary volcanic rocks (6.9‰ < $^{18}O_{VSMOW}$ < 8.9‰, Ohba et al., 2008), but are different from those characteristic for the local meteoric water ($^{18}O_{VSMOW} \sim -6$‰; Mizota & Kusakabe, 1994). Our carbon and oxygen isotope data on carbonates suggest that external meteoric waters were not involved in carbonate formation reactions to any significant extent. Rather, the observed isotopic pattern is consistent with a near-quantitative reaction between magmatic CO_2 and primary silicates, where carbon from CO_2 and oxygen from silicates provide the sources for the carbonate carbon and carbonate oxygen, respectively.

The porosity and the specific surface area (SSA) of unaltered and altered rocks was investigated by N_2-absorption method and Hg-porosimetry. It was observed that altered rocks have a SSA which is more than one order of magnitude larger than that of unaltered dacite ($\sim$0.3 m^2/g) and can reach values up to 5.2 m^2/g. The typical diameter of pores in unaltered dacite is about 400 nm while pore size in altered rocks is significantly lower ($\sim$10 nm). Preliminary data show that the concentration of carbon in dome samples is about 0.08 wt% and about 1.74 wt% in altered samples. This corresponds to approximately 0.7 and 14.5 wt% carbonate, respectively. A decrease in porosity from 8.4 vol.% in the original dacite to 4.9 vol.% in the strongest altered (carbonated) sample is observed. Pore structure visualization by intrusion of the molten alloy "Wood`s metal" reveals interconnected porosity. Cracks could only be observed in the volcanic bomb. To a part pores are due to degassing. In altered samples, the progressive formation of layer silicates by mineral replacement reactions can be traced by the packing density.

Previous studies showed that the connectivity of pores is mantained mostly by narrow cracks (Watanabe et al.2008). Based on the permeability data and a modell of parallel tubes with eleptical cross-section, pore aperture is estimated to be less than 1000 nm. The low porosity of dyke samples implies that degassing from magma mostly completed and dyke samples do not provide informaton of pore structures during degasing as suggested by Watanabe et al. (2008). Our forthcoming diffusion experiments should help to answer this question.

References:

Ohba et al., 2008, JVGR, 175, 120-132. Mizota and Kusakabe, 1994. Geochem. J. 28, 387-410. Shinohara et al., 2008, JVGR, 175,133-140. Watanabe et al., 2008, JVGR, 175, 82-90.

Thermochemical sulfate reduction: An experimental study – indices of oxidation

Svenja Germerott[1,2], Christian Ostertag-Henning[2], Harald Behrens[1]
[1]Leibniz Universität Hannover, Institute for Mineralogy, Hanover, Germany
[2]Federal Institute for Geosciences and Natural Resources, Hanover, Germany

Thermochemical sulfate reduction (TSR) is commonly defined as the abiological, thermally-driven reduction of sulfate forming H_2S and CO_2 as major reaction products (Worden & Smalley, 1996). The primary reducing agents are usually hydrocarbons but inorganic compounds, e.g. ferrous iron (Alt et al., 1989), have also been proposed. The importance of TSR has been recognized by the petroleum industry since the reaction leads to the destruction of hydrocarbons and the accumulation of TSR products like CO_2 and H_2S minimizes the quality of the reservoir (Worden & Smalley, 1996). Furthermore, TSR plays a prominent role for the formation of sulfide ore deposits, such as Mississippi Valley-type deposits (Leventhal, 1990) and the Kupferschiefer mineralization (Bechtel et al., 2001). In both cases, the metal sulfide ore precipitation is initiated by H_2S and reactive sulfur intermediates that are generated during TSR (Machel, 2001). In spite of this importance, the TSR process is not well understood and the extrapolation of many experimental results to natural systems is questionable because key chemical variables, e.g. the H_2 fugacity (fH_2), were not adjusted to geologically reasonable values (Seewald, 2001).

The aim of this study was to investigate TSR in a controlled chemical system in order to elucidate fundamental mechanisms of the process. Experiments were conducted in gold capsules using C_8H_{18} (octane) as hydrocarbon and Na_2SO_4 as sulfate source, with water present in the capsules. Furthermore, the influence of elemental sulfur on the reaction rates and progress was investigated. A pyrite-pyrrhotite-magnetite (PPM) mineral assemblage was used to control the chemical environment with respect to fH_2 and fH_2S. During experiments, temperature was set to 300 respectively 350 °C and pressure to 350 bar. Duration of the experiments ranged from 24 to 336 h. After conclusion of the experiments gaseous and highly volatile organic compounds were measured using gas chromatography. In order to distinguish between pure cracking (no oxidation) and TSR (oxidation) the following indices of oxidation were used: 1) Elevated CO_2 values, 2) the average oxidation state of carbon of the products, as well as 3) elevated ketone (acetone, butanone and pentanone), 4) aromatic (benzene and toluene) and 5) organosulfur compound (thiophenes) values.

Here we present results of experiments stopped after 168 h. Those of the type PPM-H_2O-C_8H_{18} (type I) show no (300 °C) or only minor (350 °C) evidence for oxidation; while cracking is the dominant process at both temperatures. The addition of Na_2SO_4 (PPM-H_2O-C_8H_{18}-Na_2SO_4) (type II) leads to an enhanced oxidation at 350 °C only. At 300°C cracking is still the dominant process. At both temperatures the addition of Na_2SO_4 increases the total yield of the products by one order of magnitude when compared to the respective PPM-H_2O-C_8H_{18} experiments. Results of the experiments with elemental S (type III) show strongly enhanced oxidation and cracking at 300 and 350 °C. Cracking is even more pronounced at the higher temperature. First results further indicate that isomerization is promoted during TSR and hence it is suggested that the formation of radicals plays a fundamental role. Further work is underway to evaluate these findings and to quantify TSR reaction mechanisms and rates.

References:
Alt, J.C., Anderson, T.F. & Bonnell, L. (1989), The geochemistry of sulfur in a 1.3 km section of hydrothermally altered oceanic crust, DSDP Hole 504B, Geochimica et Cosmochimica Acta, 53, 1011-1023
Bechtel, A., Sun, Y., Püttmann, W., Hoernes, S. & Hoefs, J. (2001), Isotopic evidence for multi-stage base metal enrichment in the Kupferschiefer from the Sangerhausen Basin, Germany, Chemical Geology, 176, 31-49
Leventhal, J.S. (1990), Organic Matter and Thermochemical Sulfate Reduction in the Viburnum Trend, Southeast Missouri, Economic Geology, 85, 622-632
Machel, H.G. (2001), Bacterial and thermochemical sulfate reduction in diagenetic settings – old and new insights, Sedimentary Geology, 140, 143-175
Seewald, J.S. (2001), Aqueous geochemistry of low molecular weight hydrocarbons at elevated temperatures and pressures: Constraints from mineral buffered laboratory experiments, Geochimica et Cosmoschimica Acta, 65, 1641-1664
Worden, R.H. & Smalley, P.C. (1996), H_2S-producing reactions in deep carbonate gas reservoirs: Khuff Formation, Abu Dhabi, Chemical Geology, 133, 157-171

Untersuchungen zur Alteration des Pechsteins von Königssee im Triebischtal bei Meißen

Christian Selleng[1], Reinhard Kleeberg[1], Jan-Michael Lange[2], Gerhard Heide[1]
[1]TU Bergakademie Freiberg, Institut für Mineralogie, Freiberg, Germany
[2]Senckenberg Naturhistorische Sammlungen Dresden, Dresden, Germany

Pechsteine sind vulkanische Gläser mit rhyolithischem bis dazitischem Charakter und sehr hohem Wassergehalten von mehr als fünf Prozent. Die großen Vorkommen bei Meißen sind bereits seit Werners Zeiten (1749 - 1817) bekannt und beschrieben. Als Felsite werden helle, mikrokristalline bis dichte Bereiche innerhalb der Pechsteinkörper bezeichnet. Sie werden als Produkte der sogenannten "Felsitisierung" der Pechsteine angesehen.

Es wurden Proben der Lokalität Königssee mit unterschiedlichem Umwandlungsgrad untersucht. Dabei kamen Röntgenfluoreszenzanalyse (RFA), Pulver-Röntgendiffraktometrie (XRD) mit anschließender Rietveld-Analyse und Thermogravimetrie/Differentialthermoanalyse (TG/DTA) zum Einsatz.

Die Proben konnten in einer Reihe vom "frischem" Pechstein in Richtung Felsit angeordnet werden. Hierbei ändern sich verschiedenste Parameter stetig: Makroskopisch verringern sich der Glanz und die Festigkeit, während die Farbe von grün nach weiß ausbleicht. Die Gehalte der Alkalielemente Natrium und Kalium nehmen ab, die der Erdalkalielemente Calcium und Magnesium zu. Der Anteil der nicht-kristallinen Phase geht zurück und die Anteile der Zeolithe Mordenit und Klinoptilolith, sowie des Smectits und des Cristobalits steigen. Gleichzeitig vergrößert sich der Glüh- und der Trocknungsverlust.

Der dahinterstehende Prozess ist, in Übereinstimmung mit Zwahr (1997), als eine autohydrothermale Alteration zu verstehen. Die Umwandlung des Glasanteils des Pechstein in mikrokristalline Mineralphasen, vor allem Zeolithe, ist dabei mit einer Wasseraufnahme verbunden.

Reference:
Zwahr, H. (1997), Die natürlichen Umwandlungsprodukte des Pechsteins im Gebiet von Meißen. Teil 3: Mikroskopische Untersuchungen zu Veränderung des Gefüges der Gesteine, Mineralentwicklung und chemische Veränderung in den Verwitterungsprofilen auf Pechstein im Gebiet der Garsebacher und nordöstlicher des Götterfelsens gelegenen Pechsteinbrüche, FUNDGrube: Zeitschrift für Geologie, Mineralogie, Paläontologie und Bergbau, 33.3/4, S. 78-90

P6-04

Experimental carbonation of porous volcanic rocks by interaction with magmatic and hydrothermal fluids

Voges, K.[1], Simonyan, A.V.[1], Behrens, H.[1], Dultz, S.[2], Fiebig, J.[3]
[1]Institut of Mineralogy, Leibniz University of Hannover, Callinstr. 3, 30167 Hannover, Germany, (kevin.voges@online.de / simonian@mineralogie.uni-hannover.de)
[2]Institute of Soil Science, Leibniz University of Hannover, Herrenhäuser Str. 2, D-30419 Hannover
[3]Institute of Geosciences, J.W. Goethe University of Frankfurt, Altenhöferallee 1, D-60438 Frankfurt am Main

The first attempt to drill into an active volcano was made by the Unzen scientific drilling project (USDP) in the years from 1999 to 2004. The last eruption of Unzen volcano, beginning in 1990, lasted four and a half years and revealed dacitic lavas to the surface. USDP hole was drilled about 2 km into the side of Mount Unzen trying to reach the conduit of the 1990-95 eruption. The findings differed from the expectations, e.g. lower temperatures in the borehole than expected and the drilling cores were highly altered with large amounts of secondary minerals such as carbonates, chlorite and pyrite. Volcanic fluids are suggested to be the cause of these unexpected findings.

We started a series of experiments to have a closer look on the influence and mechanisms of the interaction between rock and fluids, using unaltered volcanic lavas from Mt. Unzen that are interpreted to be the precursor of the altered rocks from the drilling core. Our focus was on the carbonation and decarbonation of rocks and minerals (especially hornblende), triggered by CO_2-bearing fluids. Several experiments were performed with hornblende (Hb) crystals and powder, Hb+calcite, Hb+Ca-rich Pl, dacititic rock, dacitic rock+calcite charged with water and $Ag_2C_2O_4$ or oxalic acid into Au- and Pt-capsules. The experiments were conducted in the cold seal pressure vessels (CSPV) at the Institute of Mineralogy, Leibniz University of Hannover. Additionally, we varied the fluid composition by adding different amounts of H_2O and CO_2 to the samples in the capsules. Oxalic acid was used to generate the CO_2 ($H_2C_2O_4 + 2H_2O \rightarrow 2CO_2 + H_2 + 2H_2O$). Initial rock/fluid ratio was $0.3 - 9.5$ by weight.

In a modified test series we tried to examine the fluid composition after the experiment as well. For that reason, sample and fluid in the capsule were separated by a clip, leaving just a small way for the exchange. The idea was to analyze the precipitates on the inner wall of the fluid part of the used capsule. We applied temperatures and pressures ranging from 300 to 700°C and from 100 to 150 MPa, respectively. The annealing time of the experiments range form one to three weeks. The products were analyzed by the conventional weight-loss method and scanning electron microscopy (SEM) at the Institute of Soil Science, Leibniz University of Hannover.

First results demonstrate that carbon is indeed involved in the reaction between dacitic rock and fluid (in agreement with other experimental studies, e.g., Dufaud et al., 2009). However, individual carbon-rich phases (e.g. carbonate) were not detected in experimental products. Moreover, no measurable changes in the composition of amphiboles were observed. Additional experimental efforts (e.g., with smaller solid/fluid ratio) for the reproduction of alteration processes in natural rocks are in progress. However, it must be noted that similar experiments with olivine+H2O+oxalic acid showed abundant production of carbonates due to reaction of olivines with fluids. The reason why it is not observed up to now with amphiboles is not undersood yet. In future experiments we plan to vary systematically the experimental conditions and composition of the system to solve this problem.

References:
Dufaud et al., 2009, Chem. Geol., 265, 79-87.

Estimation of Interconnection of Melt Phase in Partial Molten Rocks based on Impedance Spectroscopy and X-Ray Diffractiontract

Georg Nover[1], Dirk Schönbohm[1], Jutta von der Gönna[1], Norbert Zisser[1]
[1]Rheinische-Friedrich-Wilhelm Universität, Steinmann Institut, Bonn, Germany

Labradorite and basalt were used to study changes in melt fraction (0.0 to 1.0) by means of electrical conductivity (IS, 1kHz up to 100 kHz) and energy-dispersive X-ray diffraction (EDX) at 0.5 GPa pressure in piston-cylinder and multi-anvil apparatus at temperatures up to 1650°C. Conductivity and activation energy of the semiconducting solid phase, of the partially molten sample and that of the melt were measured.

The activation energy of the partially molten labradorite and that of the pure melt both follow one Arrhenius law, thus excluding chemical changes in the melt to be the dominant parameter controlling bulk conductivity instead of melt fraction and interconnection.

Volume fractions (0.0-1.0) of melt present between solidus and liquidus temperatures were determined by EDX measurements. The phase diagram known for labradorite made it possible to correlate IS and EDX data so as to determine a volume fraction versus conductivity relation. This relation was compared with four geometric models of melt distribution, the cube, tube, HS$^+$ and HS$^-$ model, but none of the models fits the measured data because the models do not consider the temperature dependence of the conductivity of the solid phase and the melt. A similar finding was made for basalt.

A much better correlation was found using the differential effective medium model, which considers the shape of the inclusion and thus the distribution of the melt as well as the temperature dependence of the solid and melt conductivity. These models, however, do not consider the variation in solid phase conductivity and melt conductivity. Knowledge of these relations is essential to understand melt generation, melt segregation or rheological behavior and, ultimately to interpret geoelectric field measurements.

Reference:
Gaillard, F. and Marziano, G. (2005), Electrical conductivity of magma in the course of crystallization controlled by their residual liquid composition. J. Geophys. Res. 110, B06204. doi:10.1029/2004JB003282
Pommier, A., Gaillard, F., Pichavant, M. and Scaillet, B., (2008), Laboratory measurements of electrical conductivities of hydrous and dry Mt. Vesuvius melts under pressure. J. Geophys. Res..
doi:10.1029/2007JB005269
Ten Grotenhuis, S., Drury, M.R., Spiers, C.J. and Peach, J. (2005), Melt distribution in olivine rocks based on electrical conductivity measurements, J. Geophys. Res, Vol. 110, B12201, doi: 10.1029/2004JB003462

The Role of Segregation in Vein Formation: an Experimental Investigation

Bruce Yardley[1,2], Bernd Wunder[1], Hans-Peter Nabein[1]
[1]Helmholtz-Zentrum Potsdam Deutsches GeoForschungsZentrum, Potsdam, Germany
[2]permanent address: School of Earth and Environment, University of Leeds, Leeds, UK

Veins are only rarely absent from crystalline rocks, and in many cases can be ascribed to late-stage hydrothermal processes. What is often less clear is whether vein minerals have been introduced from an external source by fluid infiltrating along fractures or are the mobile products of hydrothermal reactions in the adjacent wall rocks, and therefore owe their origin to segregation. We have carried out experiments at 400 and 500°C and 3Kb in order to investigate the viability of segregation as a veining mechanism.

Experiments were carried out on fine grained samples of high grade hornfels, one basic, the other pelitic. Sample 330 is a fresh cordierite-biotite hornfels (courtesy of Gerhard Franz), while sample 64660 is a pyroxene hornfels formed from basalt in the inner aureole of the Cuillin gabbro, Skye (courtesy of Francine Entwistle). Cores of hornfels c.4mm in diameter and 10mm in length had a 2mm diameter hole drilled out that extended to within 2mm of the base of the cylinder to produce a hollow cylindrical vessel. Cylinders were inserted into 4mm diameter gold capsules and loaded with weighed amounts of distilled water or 3m NaCl solution before being sealed and reweighed. Runs were of 10 or 20 weeks duration.

The cylinders retained their shape throughout the experiments, although in one case the walls partially crumbled when the capsule was opened. In most cases, secondary minerals were found to have grown on the inner and outer walls of the cylinder , and sometimes also in the head space of the capsule. In one run with NaCl solution the inner wall of the basic hornfels was almost completely coated with colourless smectite crystals growing radially towards the centre of the open space, while in a 500°C run with pelite, mm-scale isolated clumps of white crystalline material (provisionally identified as quartz), were observed on the inner walls of the cylinder. Much of the walls of this sample were lined with fine-grained new mica growth, overgrown by quartz.

These experiments clearly demonstrate that mineral material can segregate into a fluid-filled cavity from the immediate wall rocks to form vein-like growths, even where there is no introduction of dissolved material from an external source. The time-scale for discernible reaction progress is short relative to even the lifetime of specific hydrothermal pathways in shallow geothermal systems. The redistribution of material that accompanied the formation of the observed cavity linings appears to reflect the nucleation sites of the product phases and the mobility of individual components.

The effect of minute amounts of water on reaction rim growth mechanisms

Bastian Joachim[1,2], Felix Prechtel[3], Emmanuel Gardés[1], Rainer Abart[4], Wilhelm Heinrich[2], Roland Stalder[3]
[1]HelmholtzZentrum Potsdam, Deutsches GeoForschungsZentrum GFZ, Sektion 3.3, Telegrafenberg, 14473 Potsdam
[2]Freie Universität Berlin, Institut für Geologische Wissenschaften, Malteserstraße 74-100, 12249 Berlin
[3]Universität Innsbruck, Fakultät für Geo- und Atmosphärenwissenschaften, Innrain 52, A-6020 Innsbruck
[4]Universität Wien, Department of Lithospheric Research, Althanstraße 14, A-1090 Wien

Rim growth experiments are a viable tool for determining the effective component mobilities in polycrystals and in polyphase aggregates. The underlying assumption is that the rim growth rate is solely determined by the diffusion of the mobile components across the growing rim, and that diffusive fluxes are restricted to the volume domain occupied by the newly growing rim, i.e. no chemical mass transfer occurs within the reactant phases. We show that this assumption need not necessarily to be hold, if water is present in the system, as additional effects may induce chemical mass transfer within the reactant phases.

We performed rim growth experiments between periclase (MgO) and wollastonite ($CaSiO_3$). Starting materials were cylindrically shaped single crystals (diameter: 2.3 mm, thickness: 1 mm) arranged as a qtz $|$ per $|$ wo sandwich. Periclase single crystals were doped with OH-defects prior to rim growth experiments. For OH-doping, single crystals of periclase were placed into a platinum capsule filled with water and brought to 1200 °C at 0.5 GPa for 25 h in an internally heated pressure vessel (IHPV). Infrared spectroscopy on pre-doped periclase shows all well-known OH-stretching vibrations and a homogeneously distributed water concentration. Preliminary calibration measurements indicate that concentrations are in the range of several hundred ppm by weight of OH.

After a rim growth experiment that was performed for 20 h at 0.5 GPa and 1200°C in an IHPV, the observed rim sequence was:

periclase (MgO) | forsterite (Mg_2SiO_4) | monticellite ($CaMgSiO_4$) | merwinite ($Ca_3MgSi_2O_8$) | åkermanite ($Ca_2MgSi_2O_7$) | wollastonite ($CaSiO_3$)

The water distribution was mapped inside the reaction products and the starting materials via IR-spectroscopy after the experiment (Fig.1) with high spatial resolution using a focal plane array (FPA) detector (Prechtel and Stalder, 2010). IR-spectra of wollastonite, quartz and the reaction products do not show structural OH-defects. Inside the periclase, water is not homogeneously distributed anymore, but a concentration maximum has been developed towards the reaction rim.
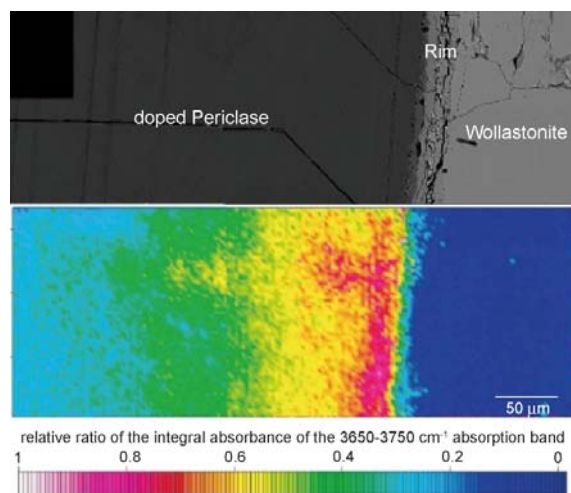
Fig.1: BSE- and Water distribution map at the periclase-wollastonite interface after the rim growth experiment.

During rim growth, OH-doped periclase is consumed and water is released. The formation of H_2O in a formerly dry system may now affect the mechanism of reaction rim growth. The released water dissociates to a certain extent to form $2H^+$ and O^{2-}. In the periclase lattice close to the reaction rim, Mg^{2+} may then be replaced by $2H^+$. Along with the remaining O^{2-}-anion, an additional mobile MgO-component is formed, which also causes reaction rim growth. The formation of this mobile MgO component results in the increase of OH-defects in the periclase lattice due to $Mg^{2+} <=> 2 H^+$ exchange, but it does not imply periclase consumption. Consequently, the MgO component needed to produce Mg-bearing phases within the reaction rim may be supplied by two different mechanisms, which are closely connected: During consumption of OH-doped periclase, MgO is mobilized and supplied for reaction rim growth. Water is released concomitantly. Presence of H_2O induces mobilization of Mg^{2+}. This results in an increase of OH-defects in the periclase lattice close to the reaction rim and supplies an additional MgO-component. As periclase consumption proceeds, these hydrogen defects are released again. It is striking that the structurally bound water released from OH-doped periclase is repartitioned into the reacting periclase.

Reference:

Prechtel F. & Stalder R. (2010) FTIR spectroscopy with a focal plane array detector: A novel tool to monitor the spatial OH-defect distribution in single crystals applied to synthetic enstatite, American Mineralogist 95, pp. 888-891.

Ammonium-bearing illite in black shales as an evident source of nitrogen-rich gas fields of CEBS

Andreas Furche, Dieter Rhede[1]
[1] Helmholtz Centre Potsdam GFZ German Research Centre for Geosciences, Potsdam, Germany

Ammonium storage in sediments, metasedimentary and metamorphic rocks is an important topic with respect to nitrogen origin in hydrocarbon gas reservoirs of the North German Basin. Ammonium is released during the decomposition of organic matter deposited in sediments and can be incorporated into the crystal lattices of feldspars, micas and clay minerals. Due to their similar ionic radii, ammonium substitutes in significant quantities for potassium in the silicate interlayer site of clay minerals during diagenesis (Williams et al., 1989). The release of ammonium from crystal structures is enabled by cation exchange reaction with KCl solution (Pöter et al., 2004), here expressed for muscovite:

$$NH_4Al_2(Si,Al)_4O_{10}(OH)_2 + K^+_{aq} \leftrightarrow KAl_2(Si,Al)_4O_{10}(OH)_2 + (NH_4)^+_{aq}$$
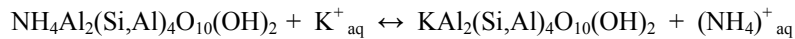
Hydrous pyrolysis experiments were performed to prove the significance of cation exchange reaction in open and closed systems ($T = 200 - 250$ °C, 0.1 mol/l $\leq c_{KCl} \leq 1.0$ mol/l, experiment duration $120 - 144$ hrs). Chemical analyses of the crushed shales before and after reaction revealed severe release of inorganically fixed ammonium (up to 16 %, depending on experimental conditions), while total organic carbon contents (TOC) are only slightly decreased with only one exception. XRD of solids showed no remarkable change in phase composition during fluid-rock interaction. Only a part of the released ammonium was found in the recovered liquids with a strongly heavier isotopic composition (3.2 ‰ $\leq \delta^{15}N \leq 7.3$ ‰) than the solids. Gas phase analyses of the vapour phases of all experiments revealed the presence of nitrogen in addition to carbon dioxide and methane. Thus, it seems to be likely, that a light nitrogen fraction is enriched in the vapour phase.

Electron probe microanalyses (EPMA) of numerous thin sections of Carboniferous shales and sandstones from various locations of the CEBS (Northeastern Germany, Lower Saxony, Northern England) were carried out using a Jeol JXA-8500F instrument equipped with 5 wavelength dispersive crystal spectrometers. One crystal spectrometer was exclusively used for the determination of nitrogen using a LDE2 analyzing crystal with $2d = 100$ Å. The detection of small amounts of light elements like nitrogen requires a careful choice of instrumental parameters (beam diameter, beam current, accelerating voltage etc.) to minimize the decomposition of the sample and migration effects. Microanalyses of all investigated shales revealed authigenic illite to be the only mineral compound with significant ammonium contents (up to 4.6 wt-% $(NH_4)_2O$) despite of the presence of potassium-bearing micas and K-feldspar. Ammonium-rich illite is always found in close vicinity to black coaly material (total organic carbon content for investigated shales TOC = $0.8 - 7.3$ %), however, it can clearly attributed to the crystalline illite phases. From our observations it seems to be likely, that ammonium is enriched at the interface illite – organic matter, from where it can be easily released by rock-fluid interaction.

References:
Pöter, B., Gottschalk, M., Heinrich, W. (2004), Experimental determination of ammonium partitioning among muscovite, K-feldspar and aqueous chloride solutions, *Lithos*, **74**, 67-90
Williams, L. B., Ferrell Jr., R. E., Chinn, E. W., Sassen, R. (1989), Fixed-ammonium in clays associated with crude oils, *Applied Geochemistry*, **4**, 605-616

The stability of the Hf isotope system in metamict zircons: hydrothermal experiments.

Christoph Lenting[1], Thorsten Geisler[1,2], Axel Gerdes[3], Ellen Kooijman[1], Erik E. Scherer[1], and Armin Zeh[4]
[1]Westfälische Wilhelms-Universität Münster, Institute for Mineralogy, Münster, Germany
[2]Universität Hamburg, Department Geoscience, Mineralogy-Petrography, Hamburg, Germany
[3]Goethe-Universität Frankfurt, Institute for Geoscience, Department of Mineralogy – Petrology and Geochemistry, Frankfurt, Germany
[4]Freie Universität Berlin, Institute for Geoscience, Berlin, Germany

The application of the Hf isotope composition of zircon as a geochemical tracer requires the closed-system preservation of Lu-Hf systematics within individual grains.. It is well known, however, that radiation-damaged zircon is prone to alteration by hydrothermal solutions, resulting in temperature-dependent recovery of the damaged structure in the altered regions that is associated with chemical changes (Geisler et al., 2003a). Here we report the results of hydrothermal experiments run at 200 °C (1080 h, autogeneous pressure), 400 °C (120 h, 1 kbar), and 600 °C (72h, 1 kbar) with a severely radiation-damaged zircon from Sri Lanka (-decay dose of $5.9 \pm 1.1 \times 10^{18}$ α-decay events/g) and a $1M$ HCl – 0.2 M HF solution containing 300 ppm of "non-natural" Hf (98.2% ^{180}Hf) and 970 ppm Yb. Although such a strongly acidic solution does not mimic natural settings, previous studies have demonstrated that the reaction mechanism involved is independent of the solutions pH from strongly acidic to mildly alkaline; the alteration kinetics is governed by the solution pH (Geisler et al., 2003a, 2003b). The major aim of this study was to investigate whether the hydrothermal alteration of radiation-damaged zircon affects its Lu-Hf systematics. Furthermore, the results of the Hf tracer experiments allowed us to distinguish between two possible alteration mechanisms. Geisler et al. (2003a) proposed that radiation-damaged zircon alters via a diffusion-reaction process, where the inward diffusion of hydrogen species catalyzes structural recovery. Such a process was accompanied by temperature-dependent losses of Zr, Si, U, REE, and radiogenic Pb, and gains of Ca, Al, and other non-formula elements that were present in solution, whereas Hf was found to be immobile (Geisler et al., 2003b). Alternatively, Putnis (2002) suggested that altered zones in radiation damaged zircon could form by an interface-coupled dissolution-reprecipitation process, where the parent or reactant radiation-damaged zircon is assumed to dissolve congruently while new zircon precipitates simultaneously along an inwardly moving reaction front. If such an interface-controlled process is operating in radiation-damaged zircon, we would expect the altered zones to have ^{180}Hf/^{177}Hf values clearly above those of natural zircon as a result of incorporation of ^{180}Hf from the experimental fluid. Because the chemical potential of ^{180}Hf in the starting zircon was greater than that of ^{180}Hf in solution, the inward diffusion of ^{180}Hf is highly unlikely. Therefore, no change in the Hf isotope composition would be expected if the process is mainly controlled by the diffusion of water species into the radiation-damaged structure.

Laser ablation inductively-coupled plasma mass spectrometry measurements of the Hf- and U-Pb isotope compositions of the experimentally altered domains revealed that the U-Pb system of such domains was severely disturbed, resulting in a discordia pointing towards the origin of the concordia diagram, but that the Hf isotope composition was unaffected. In addition, Yb enrichment was observed in the reacted zircon domains, predominantly near the zircon-solution interface. The Yb has apparently diffused into the altered domains. The new data are inconsistent with an interface-coupled dissolution-reprecipitation process, but fully support the diffusion-controlled aqueous alteration process occurring within radiation-damaged zircon that has been proposed by Geisler et al. (2003a).

References:
Geisler, T., Pidgeon, R. T., Kurtz, R., van Bronswijk, W. and Schleicher, H. (2003a), Experimental hydrothermal alteration of partially metamict zircon, American Mineralogist, Oct. 2003, 1496-1513
Geisler, T., Trachenko, K., Rios, S., Dove, M. T. and Salje, E. K. H. (2003b), Impact of self-irradiation damage on the aqueous durability of zircon (ZrSiO4): implications for its suitability as a nuclear waste form, Journal of Physics-Condensed Matter, Sep. 2003, L597-L605
Geisler, T., Zhang, M. and Salje, E. K. H. (2003), Recrystallization of almost fully amorphous zircon under hydrothermal conditions: An infrared spectroscopic study, Journal of Nuclear Materials, Aug. 2003, 280-291
Putnis, A. (2002), Mineral replacement reactions: from macroscopic observations to microscopic mechanisms, Mineralogical Magazine, Oct. 2002, 689-708

BaMn[CO$_3$]$_2$ - an analogue to dolomite: Low-temperature synthesis, compositional, structural, and spectroscopic characterization, and a its possible biogeochemical role in brackish sediments

Michael E. Böttcher[1], Patrizia Geprägs[1,2], Thomas Leipe[1], Georg Grathoff[2], Olaf Dellwig[1], Peer-Lennart Gehlken[3], Burkhard Schmidt[4], André Deutschmann[1,2], Alexander Stark[1,2], Vera Winde[1], Herta Effenberger[5] & Francisca Martinez-Ruiz[6]

[1] Geochemistry & Isotope Geochemistry Group, Marine Geology Section, Institute for Baltic Sea Research (IOW), D-18119 Warnemünde, Germany (michael.boettcher@io-warnemuende.de)

[2] Institute for Geosciences, University of Greifswald, D-17487 Greifswald, Germany

[3] Dr. Peer-Lennart Gehlken – Investigation of Raw and Residual Materials, D-37130 Gleichen-Weißenborn, Germany

[4] Experimental and Applied Mineralogy, University of Göttingen, D-37077 Göttingen, Germany

[5] Institute of Mineralogy & Crystallography, University of Vienna, A-1090 Vienna, Austria

[6] Instituto Andaluz de Ciencias de la Tierra (CSIC-UGR), Facultad de Ciencias, 18002 Granada, Spain

BaMn[CO$_3$]$_2$, a double carbonate that has been described from one metamorphic natural location (Hirowatari & Fukuoka, 1988), was only synthesized by Chang (1964) at high temperature and pressure. Its occurrence as a new mineral, however, has not been approved by IMA, so far (Jambor & Grew, 1991). We found first evidence for the possible formation of BaMn carbonates in a low-temperature natural environment from detailed SEM-EDAX and FEM investigations in anoxic brackish sediments recovered from the Landsort Deep, Baltic Sea. Samples were obtained with a multi-corer applied from research vessel P. Penck. These brackish sediments are particular rich in manganese. Dissolved sulfate was already depleted in the top 20 cm due to microbial sulfate reduction, and the water column provides biogenic barites that are dissolved in the sulfate-depleted sediments. We present a first report on the room-temperature synthesis of BaMn[CO$_3$]$_2$ from aqueous solution. The experiments are part of ongoing investigations on the low temperature (bio) geochemistry of barium in the natural barium cycle. The double carbonate, with minor co-occurrence of Ba-containing manganese(II) carbonate, was characterized by powder X-ray diffraction, SEM-EDAX, Raman and FTIR spectroscopy. Due to the similarity of tentative powder X-ray data and the spectroscopic results with BaMg[CO$_3$]$_2$ we suggest a structure similar to the mineral norsethite (Effenberger and Zemann, 1985; Chang, 1964).

The low-temperature formation of BaMn[CO$_3$]$_2$ is of particular biogeochemical interest because it is an indicator for low-sulfate suboxic depositional environments. In addition, the anhydrous double carbonate is an analogue to the mineral dolomite (CaMg[CO$_3$]$_2$), whose wide-spread occurrence in low-temperature sedimentary environments is still not fully understood. It should be noted, that significant solid-solution incorporation of divalent Mn into the crystals of precipitated witherite and Ba into the lattice of rhodochrosite were observed. This metastable SS-AS behavior requires further detailed investigation. Current research seeks to further investigate the thermodynamics and kinetics leading to the low-temperature formation of BaMn[CO$_3$]$_2$.

References:
Chang, L.L.Y. (1964) Synthesis of MBa(CO)$_3$ compounds American Mineralogist, 49, 1142.
Effenberger, E. and Zemann, J. (1985) Single crystal X-ray investigation of norsethite, BaMg(CO$_3$)$_2$: one more mineral with an aplanar carbonate group. *Z. Kristall.* **171**, 275.
Hirowatari, F., Fukuoka, M. (1988) Some problems of the studies on the manganese minerals in Japan (in Japanese). Journal Mineral. Soc. Japan, 18, 347
Jambor, J.L. and Grew, E.S. (1991) New mineral names. American Mineralogist, 76, 299

The influence of mineral replacement reactions on dissolution-precipitation creep rates.

Janneke Brouwer, Andrew Putnis
Westfälische Wilhelms-Universität Münster, Institute for Mineralogy, Münster, Germany

Dissolution − precipitation creep is a common deformation mechanism in the Earth's crust where fluids are present. The process can be described at the grain-scale by dissolution of grains at grain boundaries that are under high stress and subsequent diffusion of the dissolved ions to, and precipitation on grain boundaries that are under low stress, i.e. pore walls and grain boundaries that do not support the main principal stress.

To understand how dissolution-precipitation operates in large-scale deformation, the dependence of deformation rate on important factors as stress and grain size is investigated with theoretical models and compaction experiments (e.g. Rutter 1983, Raj 1982, de Meer&Spiers 1997). However, little is known about the effect of reaction during dissolution-precipitation creep. Since geological evidence is found that metamorphism occurs during and due to dissolution-precipitation creep (Wintsch&Yi 2002), it is important to understand how simultaneous reaction may influence dissolution-precipitation creep rates.

The simplest example of a reaction is that of a solid-solution mineral system re-equilibrating during deformation. If the re-equilibration is towards a more complete solid solution, new grain nucleation is not expected to occur. Factors that may influence the deformation rate are then limited to changes in dissolution, diffusion and precipitation rates due to the additional chemical driving force, and the increased surface area where dissolution may occur (i.e., the low stress area's where precipitation would occur if the process was only stress-driven).

We have performed compaction experiments on aggregates of KCl and KBr that react to form a solid solution during compaction. The experiments were performed using a set-up as decribed in de Meer&Spiers (1997). The results give a first insight in the importance of chemical driving forces during dissolution-precipitation creep.

References:
De Meer, S. & Spiers, C.J. (1997), Uniaxial compaction creep of wet gypsum aggregates, J. Geophys. Res., 102, No. B1, 875-891
Raj, R. (1982), Creep in polycrystalline aggregates by matter transport through a liquid phase, J. Geophys. Res. 87, 4731-4739
Rutter, E.H. (1983), Pressure solution in nature, theory and experiment, J. Geol. Soc. (Lond.) 140, 725-740
Wintsch, R.P. & Yi, K. (2002), Dissolution and replacment creep: a significant deformation mechanism in mid-crustal rocks, J. Struc. Geol., 24, 1179-1193.

Section 07

————

Functional materials, Archaeometry

The effect of Ru-doping on the phonon states of $PbZn_{1/3}Nb_{2/3}O_3$ -$PbTiO_3$ single crystals at the morphotropic phase boundary

Naëmi Waeselmann[1] Boriana Mihailova[1], Bernd Maier[1], Marin Gospodinov[2], and Ulrich Bismayer[1]
[1] Institute of Mineralogy and Petrology, University of Hamburg, Gindelallee 48, D-20146 Hamburg, Germany
[2] Institute of Solid State Physics, Bulgarian Academy of Science, Blvd. Tzarigradsko Chausse 72, 1784 Sofia, Bulgaria

Single crystals of $(1-x)Pb(Zn_{1/3}Nb_{2/3})O_3$ (PZN)-$xPbTiO_3$ (PT) show extremely strong direct and converse piezoelectric effect and are considered as one of the most promising materials for next generation electromechanical sensors and transducers (Scholz et al., 2009). Solid-solutions of (1-x)PZN-xPT with a low x-value exhibit rhombohedral symmetry, whereas those with a high x-value have a tetragonal structure.

To better understand the structural features of (1-x)PZN-xPT, we studied the temperature-induced structural transformations in pure and Ru-doped single crystals with x = 0.1, which is at the morphotropic phase boundary (MPB). On cooling, the cubic-to-rhombohedral phase transition temperature is clearly resolved by powder x-ray diffraction (XRD) and it is 475 K for pure and 450 K for Ru-doped 0.9PZN-0.1PT. However, polarized Raman spectroscopy indicates that the paraelectric matrix is still dominant down to 325 K for pure 0.9PZN-0.1PT and to 200 K for the Ru-doped compound. Synchrotron single-crystal XRD data also show that polar nanoregions persist even at 150 K.

The temperature dependences of the peak parameters (position, width, integrated intensities) clearly reveal the characteristic temperatures at which polar species nucleate and further merge in large polar clusters. At high temperatures the band near 50 cm^{-1} which arises from the Pb-localized F_{2g} mode (Lebon et al., 2001; Mihailova et al., 2008), is composed of two peaks. This indicates that on the length and time scale sensitivity of phonon spectroscopy, there is a local chemical "phase" separation between PZN- and PT- nanoregions.

Reference:
Lebon et al. (2001), Translational and orientational order in lead zinc niobate: An optical and Raman study, J. Applied Phys., 89, 7
Mihailova et al. (2008), Pressure-induced phase transition in $PbSc_{0.5}Ta_{0.5}O_3$ as model Pb-based perovskite-type relaxor ferroelectric, Phys. Rev. Lett., 101, 017602.
Scholz et al. (2009), Ferroelectric properties of ruthenium-doped lead zinc niobate-lead titanate single crystal, J. Applied Phys. 106, 074108

THE INFLUENCE OF SOME ADDITIVES ON THE HYDRATION OF CALCIUMSULPHATE HEMIHYDRATES

Pritzel Christian*, Trettin Reinhard*
Institut für Bau- und Werkstoffchemie, Universität Siegen, Germany, E-mail: Pritzel@chemie.uni-siegen.de

Gypsum is a well known mineral, which is obtained from natural resources or from technical processes. Gypsum is burned to calcium sulphate hemihydrates or anhydrite to be used in different building materials. The hemihydrate and anhydrite react with water under formation of gypsum (calcium sulphate dihydrate). The technical properties of these gypsums depend much on the morphology of the crystals which are formed during hydration[1]. This reaction, its kinetics and the reaction products' morphology can be influenced in different ways. It is possible to change the reaction temperature, to use additives or to seed crystals or different templates on which the dihydrate can grow. Some of these ways are used in contemporary technical products. All of these products imply desired influences but side effects as well. Because of this the influence of different additives on this reaction have been investigated.

To observe the hydration of gypsum by optical microscopy a special measuring cell has been invented. The cell has been built from a rubber ring which is glued on a glass slide by grease which is not soluble in water. The cell was filled with the hemihydrate, water and additive and closed by a cover glass, which was also glued with grease[2].

The observations have been carried out with an Olympus BX61 optical microscope. It is used in reflection mode in bright field. The pictures have been taken with 300 times magnification every 60 seconds one picture have been taken for about 8 hours. The results can be observed in short films and single pictures for α- and β-calciumsulphate subhydrates.

The explained measuring cell has the disadvantage that a very high water to gypsum ratio must be used. To determine the influence of this water/gypsum ratio all of the samples have been prepared with technical used ratios and the resulting morphologies were examined by scanning electron microscopy. The kinetic of the reaction was observed by heat flow calorimetry.

It could be determined that different technical used additives have a large influence on the hydration of gypsum. The influence depends on the used superplasticizer. Superplasticizer 1 (PCE1) leads to smaller, shorter gypsum crystals than the reference material without additive. The crystals have a smaller aspect ration with superplasticizer. The crystals are comparable to those which have been grown under influence of citric acids. For citric acid it is well known in literature that they occupy the fastest growing crystal surface of the dihydrate. This crystal surface could not grow anymore and the decelerating of the additive and the change in morphology could be explained [2,3].

To accelerate the reaction some alkali sulphates like potassium sulphate can be used. This sulphate influences the solubility of the hemihydrates and the dihydrate and it also changes the crystal morphology. The crystals get longer and thinner. The morphology changing character of other salts in the solution is described among others in R. Brauns "Chemische Mineralogie". A higher reaction temperature influences the crystal morphology in the same way but it is normally used nonvoluntary.

Reference:
[1] Pritzel, C., Müller, T., Trettin, R.; Tagungsbericht 17. Internationale Baustofftagung **2009,** 1, 0709.
[2] Pritzel, C., Trettin, R; 12th International Congress on the Chemistry of Cement **2007,** 00319
[3] Koslowski, T.; Dissertation, RWTH Aachen, **1983**

Nano-structured iridescent surface layers on altered bottle glass

Ralf Milke[1], Konrad Hammerschmidt[1], Nicholas Norberg[2], Richard Wirth[2]
[1]Freie Universität Berlin, Institute for Geological Sciences, Berlin, Germany
[2]Helmholtz Zentrum Potsdam, Deutsches Geoforschungszentrum, Potsdam, Germany

Iridescent glass has been found at archeological sites, where glass objects were buried in soil or sunk in the sea for several 100s or 1000s of years. This optical effect has been explained by the existence of thin chipping-off alteration layers, but no distinct mechanism for their formation has been suggested so far in the literature. We present a multi-method approach for the microstructural and microchemical characterization of iridescent alteration layers in order to get towards the identification of the critical parameters behind their generation. Apart from optical investigation the glass surface samples were studied by EMPA, TIMS, FIB-STEM, TEM, HRTEM, EELS, XRD, FTIR and Raman spectroscopy. The investigated surface layers mainly come from glass bottles dug up in Australian opal fields where they were thrown away by miners not longer than a few decades ago, but also from a sample found in the Atacama desert, Chile.

The surface layers are rich in SiO_2, and strongly depleted in Na_2O, K_2O and CaO compared to fresh bottle glass, whereas Al_2O_3 is largely retained. Isotope analyses of fresh bottle glass vs. alteration layers indicate shifts both in the Nd and Sr isotope sytematics that can only be explained by chemical exchange between a fluid and the glass surfaces. The surface layers contain about 1 wt% Cl that is absent in the fresh glass, thus indicating that the corrosion layers formed by interaction with salinar soil fluids.

The microstructure of the alteration layers was investigated by STEM and TEM methods in foils cut vertically to the surface by FIB. They consist of layers largely in the range of 120 – 200 nm thickness that mostly are very regularly spaced and that are responsible for the interference of visible light seen as iridescence. They are held together by highly porous boundary layers that are about 25 nm wide near the fresh glass surface and reach up to 100 nm before chip-off. In contrast to unweathered glass, that is unstructured on the scale of TEM bright field images, the alteration layers appear granular with single granules <10 nm. Both X-ray and electron diffraction methods indicate the absence of crystallinity in both the solid and porous layers. IR and Raman spectroscopy reveal large concentrations of hydrous species. In addition Raman spectra contain a number of bands of C-H and C-O bonds that can be traced back to organic matter derived from microorganisms or biopolymers adsorbed within the porous interlayers.

The constancy in layer thickness at each sample surface site signals a close relation to either a material-specific or a site-specific constant quality of the altered glass that leads into a chemical-mechanical feedback. The most obvious driving force for this periodic effect are volume changes (increase by hydration vs. decrease be leaching of alkali elements and others), but also structural changes (formation of granules; beginning of devitrification) might be important. At present it is not clear whether biopolymeres play a passive or active role within this process.

Another interesting finding is the enrichment of fluorine within the porous interlayers that can be mapped with EELS. Apparently the nano-sized structure has a capacity to capture adsorbable organic fluorine (from fluorinated organic compounds) similar to activated charcoal that is used in groundwater testing for environmental needs. At a given locality the fluorine concentration in the interlayers might be a measure for the relative alteration age of different glass objects, similar to relative fluorine age determination in bones.

Understanding the self-organised mechanism leading to the iridescent glass surfaces might offer the potential to control the process and to transfer the mechanism to other materials, including the option of designing and fabricating photonic metamaterials.

Decomposition reactions of magnesium sulfate hydrates and phase equilibria in the MgSO$_4$–H$_2$O and Na$^+$–Mg^{2+}–Cl$^-$–SO$_4^{2-}$–H$_2$O systems with practical implications

Michael Steiger, Kirsten Linnow, Dorothee Ehrhardt, Mandy Rohde
University of Hamburg, Department of Chemistry, Hamburg, Germany

Magnesium sulfate hydrates MgSO$_4$·nH$_2$O are important constituents in soils both on Mars and on Earth. MgSO$_4$ is also commonly found in various building materials, e.g. magnesian limestones, dolomitic sandstones and dolomitic lime mortars where it is mainly formed through deposition and oxidation of atmospheric sulfur dioxide. Due to the sensitivity of the different MgSO$_4$·nH$_2$O phases to temperature and humidity changes a better understanding of the formation and transformation of the various hydration states would provide a lot of information on the behavior of the salt. For example, the formation of magnesium sulfate hydrates implies an earlier wet and acidic environment on Mars and much could be learned about the history of water on Mars. Hydration–dehydration equilibria in the MgSO$_4$·nH$_2$O series proved also important in recent research on the use of hydration–dehydration reactions of metal salts for the thermochemical storage of energy. Finally, changes of the state of hydration and associated crystal growth in confined space is considered a major cause of damage in porous building materials.

We report new measurements of equilibrium relative humidities for stable and metastable hydration–dehydration equilibria involving several magnesium sulfates in the MgSO$_4$·nH$_2$O series. We also report a comprehensive thermodynamic treatment of the system including solution properties and experimental data from the published literature, i.e. solubilities, heat capacities and additional decomposition humidities.

While for some magnesium sulfate hydrates solubility data in the binary system MgSO$_4$–H$_2$O are sparse, there is a reasonable database of solubility measurements of these hydrates in the ternary MgCl$_2$–MgSO$_4$–H$_2$O and the quaternary reciprocal Na$^+$–Mg^{2+}–Cl$^-$–SO$_4^{2-}$–H$_2$O systems. To make these data available for the determination of solubility products, we parameterized a Pitzer ion interaction model for the calculation of activity coefficients and water activities in mixed solutions of these systems and report the ion interaction parameters for the Na$^+$–Mg^{2+}–Cl$^-$–SO$_4^{2-}$–H$_2$O system. The model predicted solubilities in the reciprocal system are in very good agreement with experimental data.

Using all available experimental data and the solution model an updated phase diagram of the MgSO$_4$–H$_2$O system covering the whole temperature range from about 170 K to 473 K is established. This treatment includes MgSO$_4$·H$_2$O (kieserite), MgSO$_4$·4H$_2$O (starkeyite), MgSO$_4$·5H$_2$O (pentahydrite), MgSO$_4$·6H$_2$O (hexahydrite), MgSO$_4$·7H$_2$O (epsomite) and MgSO$_4$·11H$_2$O (meridianiite). It is shown that only kieserite, hexahydrite, epsomite and meridianiite show fields of stable existence while starkeyite and pentahydrite are always metastable. Due to sluggish kinetics of kieserite formation, however, there is a rather extended field of metastable existence of starkeyite which makes this solid a major product in dehydration reactions. The model predicted behavior of the magnesium sulfates is in excellent agreement with observations reported in the literature. We also discuss the implications of the new phase diagram for the sulfates both on Mars and under terrestrial temperature and relative humidity conditions, e.g. in building materials and the potential use of magnesium sulfate for energy storage purposes.

The impact of SO$_2$ polluted air on dolomitic lime mortar

Anja Diekamp[1], Jürgen Konzett[1], Peter W. Mirwald[1]
[1]University of Innsbruck, Institute for Mineralogy and Petrography, Innsbruck, Austria

The impact of SO$_2$-pollution on dolomitic lime mortars from a medieval church near Bolzano, Northern Italy (St. Martin/Kampill) was studied. The samples investigated are Romanesque to Baroque mortars from the façade and intonaco-plaster from Gothic interior frescos. Their binder essentially consists of calcite [CaCO$_3$], magnesite [MgCO$_3$] and hydromagnesite [4MgCO$_3$ • Mg(OH)$_2$ • 4H$_2$O]. SO$_2$-pollution from an adjacent industrial area and a freeway caused formation of gypsum and Mg-sulfate [hexahydrite MgSO$_4$ • 6H$_2$O], the latter restricted to areas under the shades of the eaves and as efflorescence on the frescoes.

Petrographic microscope and electron microprobe analysis of thin sections indicate that the Mg-phases of the binder are less prone to sulfation than calcite. Elemental mapping on a μm-scale shows the higher solubility of Mg-sulfate compared to gypsum.

In addition Mg-sulfate efflorescence experiments were conducted at different air humidities to study the deleterious hexahydrite-epsomite phase transition by micro-Raman spectroscopy. We find that hexahydrite persists for several weeks under air humidity levels where epsomite [MgSO$_4$ • 7H$_2$O] is thermodynamically stable. Thus the hexahydrite-epsomite phase transition may under certain circumstances be much more sluggish than previously assumed. These results are important for an assessment of damages and the development of restoration strategies for sulfate-contaminated mortars.

Synthese von Schamotte-Massen aus Bauxiten und Kaolinen Griechenlands

S. Thomaidis, G. Kostakis

Technical University of Crete, Dept. of Mineral Resources Engineering, Chania, Greece

Die vorliegende Arbeit ist Vorläufer von Untersuchungen, die zum Ziel haben, aus Kombinationen verschiedener mineralischer Rohstoffe und, möglicherweise, fester Industrie-Abfallprodukte, wie z.B. aluminiumreiche Braunkohle-Flugaschen, die in Griechenland vorkommen und relativ leicht zugänglich sind, brauchbare Schamotte-Massen zu synthetisieren. Dabei soll die Breite der Felder von physikalischen Eigenschaften technischer Relevanz der Schamotte-Massen abgesteckt werden, die ohne großen Aufwand erreichbar ist.

Zu diesem Zweck wurden zunächst zwei Bauxitproben aus dem Alumina-Werk von Ag. Nikolaos (Boiotien), eine Kaolinprobe aus Chrysokefalo (Dramma, Ost-Mazedonien), zwei Kaoline von Kastriani (Milos) und Flugasche vom Lignit-Kraftwerk Achlada-Meliti (Florina, West-Mazedonien) verwendet. Die Bauxite bestanden vorwiegend aus Diaspor bzw. Gibbsit, wesentlichen Mengen von Hämatit und Goethit (und, in einer Probe, Kaolinit) und Amorphe, sowie Rutil, Anatas, $\pm$ Chlorit, $\pm$ Calcit und $\pm$ Quarz in sehr kleinen Mengen oder in Spuren. Die Kaoline von Milos enthielten, außer Kaolinit, extrem hohe Gehalte an SiO_2 (u.a. Opal, Cristoballit bzw. Tridymit und Quarz) $\pm$ Kalifeldspat in Spuren, während der Kaolin von Chrysokefalo hauptsächlich aus Kaolinit und Quarz, sowie erheblichen Mengen von Muscovit und Spuren von Kalifeldspat bestand. Die Flugasche war sehr SiO_2- und Al_2O_3-reich, bestehend hauptsächlich aus Glasphase und niedrigen Prozenten von Mullit, Quarz, Feldspat, Hercynit sowie Spuren von Anhydrit und Hämatit.

Durch Feinmahlen und Pressen von Mischungen verschiedener Zusammensetzungen wurden geeignete Prüflinge hergestellt und bei verschiedenen Temperaturen gebrannt. Anschließend wurden die Phasenzusammensetzung, die scheinbare Dichte, die Porosität und die Kaltdruckfestigkeit dieser gebrannten Massen ermittelt.

Aus den Mischungen vom Kaolinit-freien Bauxit mit den Kaolinen von Kastriani entstanden Massen, die größtenteils aus Mullit, sowie untergeordnet aus Hämatit und Tridymit und sehr kleinen Gehalten von Magnetit bestanden und bis 1500 °C stabil waren. Ihre scheinbaren Porositäten nach dem Brennen bei 1500°C waren < 1%, ihre scheinbaren Dichten variierten von 2,80 bis 2,88 g/cm^3, während sie Kaltdruckfestigkeiten von 4 bis 4.4 kN/cm^2 erreichten.

Aus den Mischungen der beiden Bauxitproben mit dem Kaolin von Chrysokefalo entstanden Massen, die größtenteils aus Mullit, sowie kleinen Mengen von Hämatit und Korund, $\pm$ Spuren von Tridymit bestanden und ebenfalls bis zu 1500 °C stabil waren. Sie zeigten Porositäten von 6 bis 10%, scheinbare Dichten von 2,4 bis 2,78 g/cm^3 und Kaltdruckfestigkeiten von 5.4 bis 8.3 kN/cm^2. Das Gelingen der Synthese von Massen aus den verwendeten Bauxit- und Kaolin-Proben, die auch bei wesentlich höheren Temperaturen stabil wären, ist, hauptsächlich wegen des hohen Gehaltes an Fe-Minerale beim Bauxit und des hohen SiO_2-Gehalte der Kaoline (und zusätzlich vom Muscovit in einem der Kaoline), dagegen nicht zu erwarten.

Verwendung nicht sortenreiner Kalksteine bei der industriellen Kalkherstellung

Martin Riedl (presenting author)[1], Thorsten Eckardt (co-author)[1], Peer Hosenthien (co-author)[2], Anatoliy Pleshakov (co-author)[2], Thomas Witzke (co-author)[1], Herbert Pöllmann (co-author)[1]
[1]Martin-Luther-Universität Halle-Wittenberg, Institut für Mineralogie, Halle.
[2]Sodawerk Staßfurt GmbH und Co. KG

Kalkstein ist ein natürlicher Rohstoff, der ungebrannt, gebrannt (Branntkalk) und gelöscht (Löschkalk) in vielen Bereichen eingesetzt wird. Ein großer Teil wird in der Bauindustrie in allen drei Verarbeitungsstufen verwendet (für Bodenverfestigung, bauchemische Erzeugnisse, Mörtel und Putze). Besonders wichtig ist gebrannter Kalk in der Eisen- und Stahlerzeugung oder für die industrielle Chemie, z.B. Zucker- oder Sodaherstellung[1,2].

Für technische Produkte werden verschiedene Anforderung an Kalke (allgemeinen Bezeichnung für CaO, $Ca(OH)_2$ bzw. CaO-MgO, $Ca(OH)_2$-$Mg(OH)_2$, nach DIN EN 459) gestellt. Löschkalk oder Kalkhydrat entsteht durch das kontrollierte Löschen (Hydratation) von Branntkalk. Unter Luftkalk versteht man nichthydraulischen Kalk, der sich mit CO_2 aus der Luft verbindet und karbonatisiert. Kalk und Luftkalk werden als Baukalk zusammengefasst[3]. Weiterhin werden Luftkalk und Kalke mit hydraulischen Eigenschaften weiter in Qualitätsstufen unterteilt. Für einen Weißkalk (Baukalk) der Klassifizierung CL90, zum Beispiel, müssen die Gehalte von CaO bei $\geq 85\%$ liegen. Durch MgO-Gehalte (Dolomit) verändern sich Verarbeitungszeiten, -eigenschaften und Festigkeiten, daher wird Dolomitkalk auch in der Norm gesondert betrachtet. Die Qualität der Kalkprodukte wird durch mergelige und tonige Anteile im Kalkstein vermindert.

Die Kalksteinvorkommen mit hohen Calcit-Gehalten (bis 100%) und wenig mineralischen Beimengungen, wie Dolomit, Quarz und Tonmineralen, sind immer schwieriger zu erschließen, daher werden zunehmend Kalksteine geringerer Qualität verwendet. Beim Brennen, die Brenntemperatur liegt zwischen 900 und 1300°C, kann es zur Schlackebildung kommen. Durch die Bildung von Sinterhäuten (Mineralneubildungen, eutektische Schmelzen, Mineralumwandlungen) um Kalkbrocken können sie sich zu Klumpen aus großen Agglomeraten zusammen-

sintern, die Kalzinierung behindern und dann den Materialdurchfluss im Brennofen stören. Diese Klumpen werden als „Bären" bezeichnet und sind nicht stabil: sie zerfallen nach kurzer Zeit. Im Querschnitt (Abbildung 1) zeigen sie deutliche Verfärbungen und zonierte Bereiche. Andere Bereiche sind deutlich blasig ausgeprägt, sie reagieren besonders schnell an der Luft unter Volumenzunahme. Auf unregelmäßigen Produktionsbedingungen und dadurch unterschiedlichen Volumenänderung deuten auch die Auffächerungen von Kalksteinschichten.

Abbildung 1: Detail aus einem angeschnittenen Schlackebären

In dem von der AiF (Arbeitsgemeinschaft industrieller Forschungsvereinigungen) gefördertem Projekt werden die beim Brennprozess entstehenden Phasen mittels XRD (qualitativ und quantitativ mittels Rietveld-Methode), Mikro-RFA und REM (mit EDAX) untersucht. Die Hydratation wird mittels Kalorimetrie charakterisiert. Für die Nachvollziehbarkeit der Reaktionen werden aus einem Tagebau über alle geologischen Einheiten Proben genommen. Da die Nebenphasen (z.B. Tone) für die Schlackebildung verantwortlich gemacht werden, werden diese separat untersucht (Anreicherung der Nebengemengteile durch selektives Lösen, Tonmineralogie).

Weiterhin werden die Produktionsproben qualitativ und quantitativ untersucht, ein Hauptaugenmerk liegt in den Nebenprodukten (Schlacke). Um die Bildung der Schlackeagglomeration nachzuvollziehen, werden die einzelnen Bereiche (Sinterhaut, Reaktionssäume, Kernbereiche und Reaktionsgrus) separiert und gesondert untersucht. Die Phasenbeziehungen werden mit den Brennbedingungen (Temperatur, Stückgröße) korreliert.

Das Ziel dieses Projektes ist es, den Kalkbrennprozess zu optimieren und die Störung durch Schlackebildung zu minimieren, sowie Kenntnisse über die mineralogischen Detailreaktionen zu gewinnen.

References:
[1]Oates, J.A.H. (1998), Lime and Limestone, WILEY-VCH-Verlag
[2]Schiele, E., Berens, L.W. (1972), Kalk. Herstellung, Eigenschaften, Verwendung, Verlag Stahleisen mbH,

Düsseldorf
[3]DIN EN 459:2008: Baukalk

Development of sulfur bearing phases in autoclaved Ultra-High Performance Concrete (UHPC)

Christian Lehmann[1], Patrick Fontana[1], Werner Österle[2], Urs Müller[1], Birgit Meng[1]
[1]Federal Institute for Materials Research and Testing (BAM), Division VII.1 Building Materials, Berlin, Germany
[2] Federal Institute for Materials Research and Testing (BAM), Division V.1 Composition and Microstructure of Engineering Materials, Berlin, Germany

The evolution of concrete technology results more and more to materials with enhanced properties such as high strength, durability and increased ecological performance. One of the more interesting aspects in the field of improving the concrete composition is Ultra-High Performance Concrete (UHPC). The exceptional strength of UHPC of 150 MPa and more as well as its increased durability is based on its dense microstructure.

It is known that thermal curing of UHPC has a strong influence on its mechanical properties (Rebentrost & Wight, 2008). The curing conditions are significantly enhanced by additional application of a water vapor saturation pressure (autoclaving), and results in an impressively increase of reaction rate. This leads to a denser micro structure and a "self-healing" of cracks, which results in strong enhanced mechanical properties (Lehmann et al, 2009). Generally the accelerated reactions allow an increased usage of secondary cementitious materials like fly ashes or blast furnace slag and therewith the simultaneous reductions of expansive components like the cement or micro silica.

One objective of our studies is the reaction of sulfur bearing mineral additions (e.g. class C fly ash) during autoclaving. Class C fly ash is a waste product from the power generation with brown coal. It is a puzzolanic material, but the high amount of sulfur is still a very problematical element in concrete technology. For example the formation of secondary sulfate phases (especially thaumasite) decreases the mechanical properties of concrete strongly. We suppose the formation of more stable sulfur-bearing phases by applying the enhanced curing conditions of autoclaving.

In the presented study the samples were cured under different conditions up to 210 °C and 16 bars of water vapor saturation pressure. The concrete samples are based on a standard mixture with cement, micro silica, quartz filler, a secondary cementitious material and quartz sand. The sulfur-containing phases were synthesized by using purely raw materials (e.g. anhydrite, portlandite, lime, quartz). To analyze the change in phase assemblage, the concentration of class C fly ash and anhydrite respectively is changed in the different tests as well as the curing conditions.

A strong change in the phase composition is visible in UHPC after autoclaving. XRD pattern of autoclaved samples show the presence of thaumasite, hydroxyl ellestadite and ternesite, dependently by the curing conditions. Analyses by SEM reveal a pseudomorphic replacement of sheets of portlandite with a crystalline sulfur-bearing calcium silicate which is identified by TEM as a mixture of ternesite and hydroxyl ellestadite. But we also detect a change in the phase composition of the calcium silicate hydrate (CSH) phases in the cement stone matrix. Because of the high amount of calcium in class C fly ash, the silicon-calcium-ratio is strongly decreased from 0.73 in samples with class F fly ash or slag, to 0.62.

It is known that a higher content of calcium in the CSH leads to lowered mechanical properties (Luke, 2000). The mechanical properties of UHPC with class C fly ash are clearly reduced, compared with samples without secondary cementitious materials (about 15% loss of compressive strength), but still around 150 MPa. Additionally tests on concrete mixtures without class C fly ash but with limestone filler show Si/Ca-ratios around 0.49 and compressive strengths of 140 MPa.

This work has shown that the usage of sulfur-rich components in concrete could be increased by applying temperatures around 200 °C and the associated water vapor saturation pressure. The moderate loss of mechanical strength by using class C fly ash is based in the lowered Si/Ca ratio of the CSH phases and less by sulfur-rich phases. Sulfur-bearing calcium silicates with a low content of water have a good potential to bind significant amounts of sulfur and prevent sulfur caused damages.

Reference:
Rebentrost, M. & Wight, G. (2008), Experiences and applications on Ultra-high Performance Concrete in Asia, In: Fehling, E. et al. (eds.): Proc. 2nd Int. Symp. on Ultra High Performance Concrete, Kassel, Germany, 5-7 Mar 2008, Schriftenreihe Baustoffe und Massivbau (10), Kassel University Press, S. 19-30.
Lehmann, C.; Müller, U.; Fontana, P.: Evolution of Phases and Micro Structure in Hydrothermally Cured Ultra-High Performance Concrete (UHPC). In: 3rd International Symposium on Nanotechnology in Construction (NICOM3), May 31- June 2, 2009, Prague, Czech Republic, pp. 287-293.

Luke, K. (2004), Phase studies of pozzolanic stabilized calcium silicate hydrates at 180 °C, Cement and Concrete Research, 34, 2004, 9, S. 1725-1732.

Section 08

_____

General and applied crystallography

Evaluation of multiple solutions in powder pattern indexing.

Rolf Heinemann[1], Diedrich Stöckelmann[1] and Herbert Kroll[1]
[1]Westfälische Wilhelms-Universität Münster, Institute for Mineralogy, Münster, Germany

Santoro et al (1980) [1] first addressed the question of equivalence when in powder pattern indexing more than one indexing solution and thus more than one reciprocal metric tensor are produced. Two metric tensors G_A^* and G_B^* are said to be equivalent when a matrix R exists such that $G_B^* = R G_A^* R^T$ (1). R is a 3×3 non-symmetric matrix consisting of rational numbers. Therefore, eq. (1) cannot be solved directly. Santoro et al (1980) [1] suggested to vary the elements of R systematically in the range (5, -5) until the equality sign in eq. (1) is fulfilled within chosen error limits.

We suggest a different procedure: First, the three shortest non-coplanar vectors that have the same Q values in both lattices A and B are identified. These vectors are taken to define a new basis common to A and B. Then, 3×3 matrices M_A and M_B are written which transform the axial systems of A and B into the new one. If the new axial system reproduces lattices A and B, then the equality $M_A G_A^* M_A^T = M_B G_B^* M_B^T$ (2) holds. Eq. (2) defines a new metric tensor common to both lattices A and B which we thus term the common metric tensor G_C^*. The coordinates of the reciprocal lattice points of A and B are transformed according to $(\eta/\kappa/\lambda)_{A,B} = (M_{A,B}^{-1})^T (h/k/l)_{A,B}$. Coincident lattice points yield $(\eta/\kappa/\lambda)_A = (\eta/\kappa/\lambda)_B$. If all lattice points coincide, lattices A and B are termed equivalent; if only a subset of points is coincident, the lattices are semi-equivalent; otherwise they are non-equivalent.

Equation (1) can be easily retrieved from equation (2): $G_B^* = M_B^{-1} M_A G_A^* M_A^T (M_B^{-1})^T = R G_A^* R^T$. Thereby we arrive at a solution to eq. (1) that avoids trial and error methods.

We take as an example two different indexing solutions A and B to $CrPO_4.6H_2O$, given by Santoro et al. (1980) [1], to demonstrate the spatial relationship of the respective reciprocal lattice points. Fig. 1 shows that lattice points A and B coincide. However, solution A only explains a subset of points.

Fig. 1 Relationship between the respective reciprocal lattice points
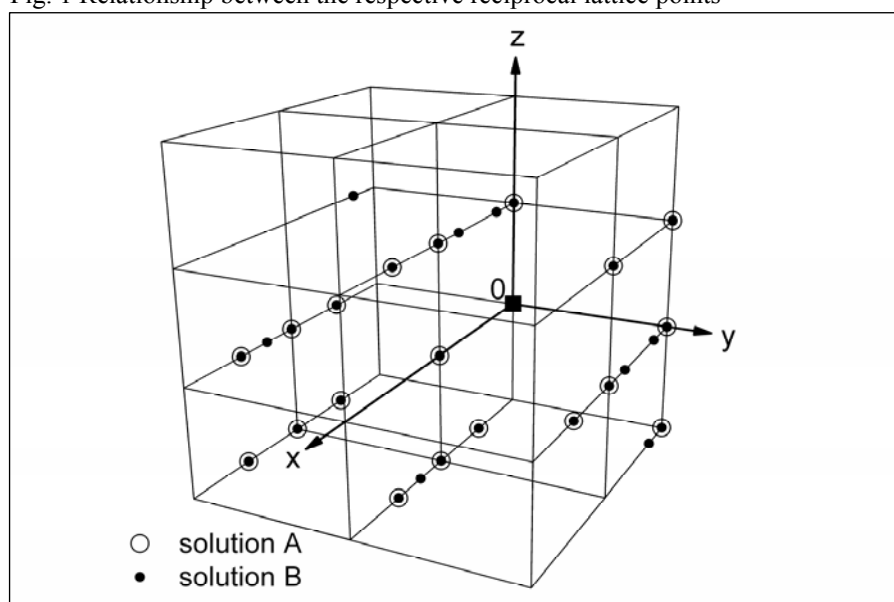
Reference:
[1] Santoro, A., Mighell, A.D., Rodgers, J.R. (1980) The Determination of the Relationship Between Derivative Lattices; Acta Crystallogr. **A36**, 796–800.

P8-02

General invariant relations as a concept for powder pattern indexing in the tradition of the Runge-de Wolff-method.

Rolf Heinemann[1], Diedrich Stöckelmann[1], Herbert Kroll[1] and Wolfgang Hoffmann[1]
[1]Westfälische Wilhelms-Universität Münster, Institute for Mineralogy, Münster, Germany

A system of 1-, 2- and 3-dimensional metrically independent relations between the squared moduli of reciprocal lattice vectors (Q values) is developed. The relations generalize and thereby resolve the earlier special Runge-de Wolff approach to indexing unknown powder patterns.

Given the background of trial-and-error-methods employed in recent automatic powder pattern indexing, we suggest an alternative route based on a generalization of the original Runge-de Wolff approach. [1], [2], [3].

For this purpose, a system of metrically invariant relations between the Q values of reciprocal lattice vectors has been developed that encompasses the earlier special relations. The invariant relations correspond to a line, a zone, a bizone, a cone and a pencil configuration. The zone configuration is particularly useful for indexing as it produces a density of information that is superior to earlier approaches. The equation reads

$$(\frac{\eta_1}{\eta_2} - \frac{\kappa_1}{\kappa_2})Q(H_1) + (\frac{\eta_2}{\eta_1} - \frac{\kappa_2}{\kappa_1})Q(H_2) - \frac{1}{\eta_1\eta_2}Q(\eta_1 H_1 + \eta_2 H_2) + \frac{1}{\kappa_1\kappa_2}Q(\kappa_1 H_1 + \kappa_2 H_2) = 0 \qquad (1)$$

where η, κ are rational coefficients.

Equation (1) combines any four lattice vectors that extend from the zero point and span a plane (Fig. 1). It is a powerful equation because systematic variation of the coefficients η and κ allows identifying among a measured set of Q values any four reciprocal lattice vectors that are *arbitrarily* distributed in a plane rather than representing a special configuration. The equation may thus be termed the general planar indexing equation and as such it is suited to become a cornerstone in an indexing procedure that in contrast to the current indexing programs would be strictly based on metrical invariants.

Figure 1: Zone configuration
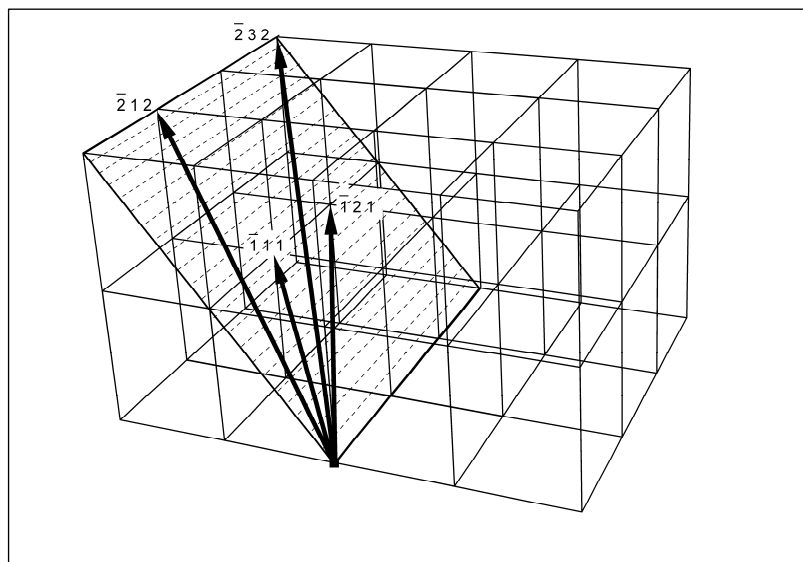
References:

[1] Runge, C. (1917) Die Bestimmung eines Kristallsystems durch Röntgenstrahlen. Phys. Zeitschr. **18**, 291-301.
[2] Wolff, P.M. de (1958) Detection of simultaneous zone relations among powder diffraction lines. Acta Crystallogr. **11**, 664-665.
[3] Wolff, P.M. de (1963) Indexing of powder diffraction patterns. Advances in X-Ray Analysis **6**, 1-17.
P8-03

Chemical mixing and Raman hard mode spectroscopy in ferroelastic lead phosphate-arsenate: local symmetry splitting and multiscaling behaviour

Ulli Bismayer[1], Ekhard Salje[2], Tobias Beirau[1], Boriana Mihailova[1], Thomas Malcherek[1]
[1]Universität Hamburg, Mineralogisch-Petrographisches Institut, Hamburg, Germany
[2]University of Cambridge, Department of Earth Sciences, Cambridge, Great Britain

The phase transition in ferroelastic $Pb_3(PO_4)_2$–$Pb_3(AsO_4)_2$ mixed crystals shows multiscaling behaviour with two relevant length and timescales. One length scale is macroscopic and shows uniform, weakly first-order phase transformations between a rhombohedral paraphase ($R\bar{3}m$) and a monoclinic ferroelastic modification ($C2/c$). The second length scale is on the level of tetrahedral complexes which show monoclinic distortions at temperatures well above the macroscopic transition point. For example, in $Pb_3(P_{0.43}As_{0.57}O_4)_2$ the AsO_4 polyhedra show static deformation up to ca. 60 K above the deformation of the PO_4 tetrahedra (Fig. 1).
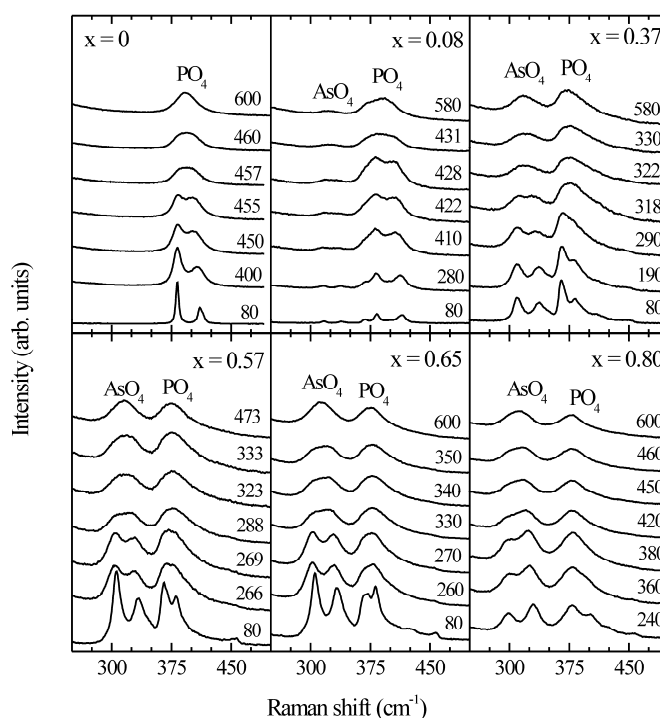
Fig. 1 Raman spectra of $Pb_3(P_{1-x}As_xO_4)_2$ in the spectral range 250-500 cm^{-1} arising from TO_4 bending modes. Temperatures [K] are indicated for each trace. The transition temperature T_c and the temperatures of the onset of splitting $T_{PO_4}^{split}$ and $T_{AsO_4}^{split}$ (bending modes) are T_c = 456, 420, 315, 265, 330 and 430 K; $T_{PO_4}^{split}$ = 456, 428, 318, 266, 260 and 360 K; and $T_{AsO_4}^{split}$ = n.a., 428, 322, 323, 340 and 450 K for x = 0, 0.08, 0.37, 0.57, 0.65 and 0.80, respectively.

The two timescales are either short compared with the time of observation, namely the dynamic reorientation of the PO_4 tetrahedral distortion, or very long (optical birefringence, X-ray diffraction). The long timescale refers then to the quasi-static distortion of the AsO_4 tetrahedra which persists at $T > T_C$. These distortions appear to be uncorrelated or only weakly correlated and their random field leads to an order/disorder contribution of the ferroelastic phase transition which remains, on a phonon timescale, essentially displacive in character.

Reference:
Salje E.K.H., Beirau T., Mihailova B., Malcherek T. & Bismayer U.(2010), J. Phys.: Condens. Matter 22, 045403.

P8-04

Recrystallization of Metamict Titanite

Tobias Beirau[1], Ulrich Bismayer[1], Carsten Paulmann[1]
[1]Universität Hamburg, Institute for Mineralogy, Crystallography and Petrography, Hamburg, Germany

The crystal structure of pure titanite with the general formula $CaTiSiO_5$ consists of corner linked TiO_6-octahedra, SiO_4-tetrahedra and sevenfold coordinated Ca^{2+} ions. Near 500 K pure titanite undergoes a phase transition from the monoclinic paraelectric high-temperature phase A2/a via an intermediate phase with average symmetry A2/a to the monoclinic antiferroelectric low-temperature phase $P2_1/a$.

In nature titanite occurs in igneous and metamorphic rocks and often incorporates various impurities like the rare-earth elements and the radiogenic elements U and Th. Through the resulting structural damage induced by α- and β-decay the titanite becomes metamict. This means over geological time scales recoil processes due to alpha radiation change the originally periodically structured material into a heterogeneous quasi-amorphous state with persisting short-range order but destroyed long-range order.

We present IR and Raman spectra as well as X-ray diffraction data of metamict and heat treated titanite from the Cardiff uranium mine in Canada. The Raman and IR modes are strongly broadened in the metamict material and became sharper on annealing. The OH-stretching mode at 3486 cm^{-1} indicates strong changes in the local environment of OH$^-$ in metamict titanite. Between 620 and 750 cm^{-1} Raman excitations appear in the metamict material, which in IR spectra result from Ti-O stretching excitations of the TiO_6 octahedra. This indicates the breakdown of the Raman selection rules and points to the breaking of the octahedral symmetry of TiO_6 polyhedra.

Reference:
Bismayer, U.; Paulmann, C.; Groat, L. & Zhang, M. (2010), Local Phenomena in metamict Titanite, Acta Phys. Pol. A, Jan. 2010, 117

Al/Si-ordering phenomena in sanidine megacrystals from quarternary volcanic fields of the Eifel

Kathrin Demtröder, Sara Dehn, Michael Gopon, Jürgen Schreuer
Ruhr-Universität Bochum, Institute of Geology, Mineralogy and Geophysics, Bochum, Germany

Sanidine megacrystals from Volkesfeld (Rieden eruptive centre, East Eifel volcanic field, Germany) are well known for their fast irreversible changes of optical properties at moderately high annealing temperatures (e.g. Zeipert and Wondratschek, 1981). Starting at about 1025 K their optic axial angle $2V$ changes rapidly with increasing temperature. This macroscopic effect has been interpreted as being associated with a corresponding change of the Al, Si order on the atomic level. However, the reason for the rapid ordering process is not yet understood. Another remarkable feature of sanidines from Volkesfeld is their high structural perfection with low concentration of dislocations indicating hydrothermal growth conditions (Widder, Wondratschek, Fehlmann and Klapper, 1994).

In order to shed light on the processes responsible for the rapid changes of the Al/Si-order, sanidine megacrystals from four different eruptive centres of the Eifel (Rockeskyller Kopf, Essinger Maar, Kerpener Maar and Rieden caldera) were studied by means of single crystal X-ray diffraction, optical techniques, IR spectroscopy and NMR spectroscopy. Sanidine crystals from Itrongay, Madagascar, served as reference standard.

The chemical composition, $Na_xK_{1-x}AlSi_3O_8$, as obtained by electron microprobe analysis, is characterised by $x \approx 0.15$ and $x \approx 0.27$ for megacrystals from the East Eifel and West Eifel volcanic field, respectively, with up to 2 at-% celsian and less than 0.02 at-% anorthite. IR spectroscopic studies revealed a characteristic H_2O absorption band at about 3500 cm^{-1}. According to mass-spectrometer coupled thermogravimetric experiments the H_2O content varies in the range 250 - 400 wt-ppm and is mainly released from the crystal between 1170 K and 1270 K. For comparison, sanidine crystals from Madagascar ($x \approx 0.05$) are almost free from water.

All investigated Eifel sanidines show irreversible optical anomalies at temperatures above 1073 K. Their optical axes angles, $2V$, change rapidly from about 30° in a plane perpendicular to (010) to about 35° within (010). According to Su et al. (1986) this corresponds to an increasing disorder of Al, Si on tetrahedral sites as indicated by the reduction of Al occupancy $2t_1$ of the T_1 site from about 0.70 to 0.58. However, tetrahedral bond distances derived from single crystal structure analyses yield $2t_1 \approx 0.58$ (Ribbe, 1969) for thermally untreated samples and only small changes after annealing. The latter findings are supported by ^{29}Si NMR-experiments. Our contradictory experimental results together with the coincidence of the temperature ranges in which the optical anomalies and the release of H_2O is observed suggest that the optical axes angle is not only influenced by the degree of Al/Si-order but also by the content of water dissolved in the crystal structure of alkali feldspars.

References:
C. Zeipert, W. Wondratschek: Ein ungewöhnliches Temperverhalten bei Sanidinen von Volkesfeld/Eifel. N. Jb. Mineral., Mh. **9** (1981) 407-415.
W. Widder, H. Wondratschek, M. Fehlmann, H. Klapper: X-ray topographic study of Eifel sanidine (Volkesfeld). Z. Kristallogr. **209** (1994) 206-209.
S.-C. Su, P. H. Ribbe, F. D. Bloss: Alkali feldspars: Structural state determined from composition and optic axial angle $2V$. Am. Min. **71** (1986) 1285-1296.
P. H. Ribbe, G. V. Gibbs: Statistical analysis and discussion of mean Al/Si-O bond distances and the aluminum content of tetrahedra in feldspars. Am. Min. **54** (1969) 85-94.

Mössbauer Study of Local Structure and Cation Distribution in $Bi_2(Fe_xM_{1-x})_4O_9$, M = Al, Ga, Mn

Weber Sven-Ulf[1], da Silva Klebson L[1], Gesing Thorsten M[2], Becker Klaus-Dieter[1]

[1] Institute of Physical and Theoretical Chemistry, Braunschweig University of Technology, Braunschweig, Germany

[2] Institute of Crystallography, University of Bremen, Bremen, Germany

In the present work, the local structure of solid solutions of type $Bi_2(Fe_xM_{1-x})_4O_9$ with M=Al, Ga, and Mn is studied by ^{57}Fe Mössbauer spectroscopy. Spectra yield quantitative information on the iron occupancy of the two structural sites in the mullite-type lattice. In the Fe-Al system, the distribution of cations is found to be almost random, whereas in the Fe-Ga system, gallium ions are found to develop a strong preference for the occupation of tetrahedral sites. Hyperfine parameters, isomer shifts and quadrupole splittings, derived from the spectra as a function of Fe concentration, e.g., provide evidence for a strong distortion of the iron sites at low iron concentrations in the Fe-Al system. In addition to measurements at room temperature, high-temperature in-situ Mössbauer spectroscopy provides information on the temperature dependence of the distribution of Fe, Al, and Ga on the two inequivalent lattice sites of the structure. In both cases, cation distributions show almost no temperature dependency, yielding site exchange energies close to zero. In the case of $Bi_2(Fe_xAl_{1-x})_4O_9$ it could be shown that this is not due to a kinetically hindered, frozen-in cation distribution but represents a real equilibrium property of the system. For the Fe-Mn system, we confirm the already known preference of iron for the pyramidal site.

P8-07

Temperature-dependent single-crystal neutron diffraction investigations of mullite-type $Bi_2Fe_4O_9$.

<u>Thorsten M. Gesing</u>[1], Gwilherm Nénert[2], Manfred Burianek[3], Manfred Mühlberg[3], Hartmut Schneider[1], Reinhard X. Fischer[1],

[1]Universität Bremen, FB05 Kristallographie, Klagenfurter Straße, 28359 Bremen, Germany
[2]Institut Laue-Langevin, 6 Rue Jules Horowitz, 38042 Grenoble Cedex 9, France.
[3]Universität Köln, Institut für Kristallographie, Zülpicher Straße 49b, 50674 Köln, Germany

Mullite has achieved outstanding importance as a material for both traditional and advanced ceramics because of its favorable thermal and mechanical properties (Fischer and Schneider, 2005). Mullite displays various Al to Si ratios referring to the solid solution $Al_{4+2x}Si_{2-2x}O_{10-x}$, with x corresponding to the number of oxygen vacancies per unit cell. Depending on the synthesis temperature and atmosphere, mullite is able to incorporate a number of transition metal cations and other foreign atoms such as Bi and Fe. In particular mullite-like $Bi_2M_4O_9$ compounds are an interesting model system for the investigation of structure-property relations (Fischer and Schneider, 2005). A great benefit in this system is the chemical variability in the occupation of the cation positions as well as the possibility to grow big single crystals of good quality (Burianek et al., 2009). All phases of the mullite-like structure family are characterized by chains of edge-sharing MO_6 octahedra placed in the $Bi_2M_4O_9$ compounds parallel to the orthorhombic **c**-axis. These octahedral chains are bridged by M_2O_7 groups of corner-sharing tetrahedra and BiO_6 groups (plus $6s^2$ lone pair electron of Bi) alternating along the **c**-axis. Every second bridging O position in these channels is vacant and could be used as an oxygen "jump" position, which could explain the ion conductivities of 0.01 Scm^{-1} observed in this material (Bloom et al., 1992). In order to investigate this mechanism behavior, high-temperature neutron diffraction experiments have been carried out. We have investigated $Bi_2Fe_4O_9$ which is particularly interesting due to the unusual short oxygen – iron interatomic distances (180.8 pm) of the double tetrahedra bridging O3 atoms and the strong anisotropic displacement parameter at room temperature derived from X-ray single-crystal investigations. This delocalization of the bridging oxygen atom is a first indication for the above mentioned "jump model" but could also be a symmetry breaking effect if O3 is not placed on the mirror plane. This mirror plane is part of the *Pbam* symmetry in which the structure was described first by Niizeki and Wachi (1968).

Single-crystal neutron diffraction data were collected at ILL Grenoble on beamline D9 using a 4-circle diffractometer equipped with a 2D detector and a furnace for sample heating. Using a crystal of 3.80 x 3.75 x 2.25 mm^3, 3308 reflections between $-8 \le h \le 8$, $-3 \le k \le 8$, $-8 \le l \le 8$ were measured at room temperature of which 243 were indexed as h,0,l (Fig. 1) and 0,k,l reflections with odd h and k, respectively, having an I/ I up to 24. Thus, they violate the reflection conditions in space group *Pbam*. Therefore, the structure was refined in the translationengleiche subgroup of index 2, $P2_12_12$. In this space group the O3 atom is displaced ($z = 0.48584(64)$) from the mirror plane present in *Pbam* ($z = \frac{1}{2}$) but still shows the biggest displacement parameter with anisotropic behavior. The same symmetry is also observed at 900 K where the "off-centering" of the O3 atom with respect to the mirror plane in the higher symmetry *Pbam* is still present as well as an anisotropic displacement towards the "jump position" which is increased at this temperature. Nevertheless, the Fe2-O3 distances having 181.4(1) pm and 180.7(1) pm at 298 K and 900 K, respectively, are still rather short compared to the expected distance of 184 pm

Fig. 1. -5 0 1 reflection in 3D(h,k,l) (Shannon, 1976).

Reference:
Bloom I., Hash M. C., Zebrowski J. P., Myles K. M., Krumpelt M.: Oxide-ion conductivity of bismuth aluminates. Solid State Ionics 53-56 (1992) 739-747.

Burianek M., Mühlberg M., Woll M., Schmücker M., Gesing Th. M., Schneider H.: Single crystal growth and characterization of mullite-type orthorhombic $Bi_2Me_4O_9$ (Me=Al^{3+}, Ga^{3+}, Fe^{3+}) Cryst. Res. Techn. 44 (2009) 1156-1162.

Fischer R. X., Schneider H.: The mullite-type family of crystal structures. In: H. Schneider and S. Komarneni (eds.): Mullite, Wiley-VCH, (2005) 1-46.

Niizeki N., Wachi M.: The crystal structure of $Bi_2Mn_4O_{10}$, $Bi_2Al_4O_9$ and $Bi_2Fe_4O_9$. Z. Kristallogr. 127 (1968) 173-187.

Shannon R. D.: Revised Effective Ionic Radii and Systematic Studies of Interatomic Distances in Halides and Chalcogenides. Acta Crystallogr. A32 (1976) 751-767.

The crystal structure of Cd$_2$Nb$_2$O$_7$: symmetry mode analysis and Monte-Carlo simulation

Thomas Malcherek
Universität Hamburg, Dpt. Geowissenschaften - Mineralogie, Hamburg, Germany

The ferroelectric properties of cadmium pyroniobate (CNO) are of fundamental interest, because of their similarity to compositionally disordered relaxor-ferroelectrics like PbMg$_{1/3}$Nb$_{2/3}$O$_3$. However, a complex sequence of phase transitions is known to occur in CNO and the exact symmetries of some of the low temperature phases have yet to be determined. Moreover, anisotropic diffuse scattering in sheets normal to $\langle 110 \rangle$ indicates local deviations from cubic symmetry in the paraphase of CNO. As has been shown by ab-initio calculations using density functional theory (Fischer et al. 2008), the phonon dispersion curve of cubic CNO, space group $Fd\bar{3}m$, exhibits instabilities throughout most of the cubic Brillouin zone, with the most pronounced instabilities located at the center and at the X-point. The largest displacements with respect to the cubic phase are observed for Nb in the calculated ground state structure.

X-ray single crystal diffraction experiments have been carried out at the F1 synchrotron beamline of Hasylab/Desy. The anisotropic diffuse X-ray scattering is confirmed and its temperature dependence below the phase transition has been followed. Structure refinement using data measured down to a temperature of 98~K (Malcherek et al. 2010) confirms the phase transition $Fd\bar{3}m$ - $Ima2$ postulated in the ab-initio calculations. Symmetry mode analysis shows that the frozen phonon mode is of T$_{2u}$-symmetry, with the transition temperature obtained as T$_c$=194K by extrapolation. As T$_{2u}$ is a non-polar mode, the transition occuring at this temperature is of the improper ferroelectric type. Below T$_c$ a significant reduction in diffuse scattering intensity is observed, accompanied by a decay of the thermal displacement parameters on one of the two Nb-positions of the *Ima2*-phase. This indicates that Nb disorder is reduced at the ferroelectric phase transition.

In order to explore the order-disorder contributions to the phase transitions in CNO, Monte Carlo simulations on the pyrochlore lattice using a 12-state modified Potts-model have been carried out. The model, mapped to individual Nb-displacements, reproduces the diffuse scattering of the cubic paraphase qualitatively correct and it exhibits a first order phase transition. Its low symmetry phase is compared to the calculated and measured low temperature structures of CNO.

References:
Fischer, M., Malcherek, T., Bismayer, U., Blaha, P. & Schwarz, K. (2008), Structure and stability of Cd$_2$Nb$_2$O$_7$ and Cd$_2$Ta$_2$O$_7$ explored by ab initio calculations, Physical Review B, 78, 014108
Malcherek, T., Bismayer, U. & Paulmann, C. (2010), The crystal structure of Cd$_2$Nb$_2$O$_7$: symmetry mode analysis of the ferroelectric phase, J. Phys.: Condens. Matter, 22, 205401

P8-09

Rietveld analysis of metal oxide nanoparticles prepared by Flame Spray Pyrolysis

Johannes Birkenstock1, Suman Pokhrel2, Lutz Mädler2
1Universität Bremen, FB5-Geowissenschaften, Kristallographie, Bremen, Germany
2Universität Bremen, IWT - Institut für Werkstofftechnik, Verfahrenstechnik, Bremen, Germany

Metal oxides as prepared by Flame Spray Pyrolysis (FSP) often exhibit exceptional material properties such as homogeneous single-crystalline nanoparticles (Pokhrel et al., 2010). In FSP combustible organic solutions with specific concentrations of metal cations are atomized and combusted in a spray. Powders are formed after the metal ions leave the droplet and react in the gas phase with subsequent growth by nucleation, coagulation, coalescence and aggregation until rapid quenching occurs. The nanoparticles can be collected as powder or on cooled substrates. This way samples of WO_3 and other simple metal oxides were prepared.

The (usually small mount of) sample was scratched off the substrate and then mounted to a "background free" sample holder made f a Si single crystal cutted oblique to any crystallographic plane so that no single crystal diffraction is observed rom the sample holder. With Cu-K_ radiation the absorption of phases like WO_3 ($\mu =$ 988 cm-1) is strong so that nly a rather thin sample (WO_3: 0.03 mm for absorption to 1/1000 of the incident intensity) is required for tandard Bragg-Brentano diffractometry.

The samples were characterized by the Rietveld method in terms of hase, structure and crystallite size analysis, applying the free Rietveld software BRASS (Birkenstock et al., 2010). The results were compared to highresolution transmission electron microscope (HR-TEM) images in terms of structural compatibility and crystal sizes. The latter were also compared to results obtained from BET (Brunauer-Emmet-Teller) analysis. The values for crystallite sizes were in reasonable agreement for all three methods. Single nanocrystals in special projections as observed with HR-TEM could be successfully matched with the structure models derived from the Rietveld refinements.

Fitting the diffraction diagrams of nanoparticles by the Rietveld method may be obstructed by nanosize effects (e.g. Müller, 2008) to the scattered intensities: Due to their small sizes the crystallite size effect extremely increases the peak widths of the reflections. Since the scattered intensity of crystals is the product $F \cdot G$ of the smoothly varying structure factor function F with the reciprocal lattice function G, for very broad reflections this product may result in non-Bragg intensity off the usual Bragg maxima. Furthermore the ratio of distorted surface volume to undistorted bulk volume of the crystals is much larger for nanocrystals possibly resulting in small shifts of the average d-spacings (and thus peak positions) and possibly some extra Non-Bragg intensity. Non-Bragg intensity cannot be fitted perfectly by Bragg reflections as used for Rietveld analyses. This effect was demonstrated with a series of samples of WO_3 consisting of nanocrystals of quite different average sizes.

Yet in cases, as we demonstrated, depending on the material a conventional Rietveld fit can even be successful for nanocrystals as small as 5 nm. Surprisingly, in such cases even structural parameters can be optimized yielding reasonable results with respect to distances and angles and with respect to thermal motion of the atoms. For these cases it must be inferred that the nanosize effects on scattering are not very pronounced.

References:
Birkenstock, J., Fischer, R. X., Messner, T. (2010), BRASS, The Bremen Rietveld Analysis and Structure Suite, www. brass.uni-bremen.de
Pokhrel, S., Birkenstock, J., Schowalter, M., Rosenauer, A., Mädler, L. (2010), Growth of Ultrafine Single Crystalline WO3 Nanoparticles Using Flame Spray Pyrolysis, Crystal Growth & Design, 10, 632-639
Müller, U. (2008), Anorganische Strukturchemie, Vieweg und Teubner, 392 p.

Neutron diffraction investigations of alkali feldspars

Susan Schorr[1], Andreas Hoser[2]
[1]Freie University Berlin, Institute of Geological Sciences, Berlin, Germany
[2]Helmholtz Zentrum Berlin für Materialien und Energie, Berlin, Germany

Feldpars are alumosilicates with the general formula AT_4O_8, where T is Al, Si and A is monovalent Na, K for the alkali feldspar series. Corner-sharing AlO_4 and SiO_4 tetrahedra are linked in an infinite three-dimensional array, charge balancing A cations with radius greater than 1.0 Å occupy large, irregular cavities in the tetrahedral framework. In the monoclinic feldspars (space group C12/m1), there are two symmetrically non-equivalent tetrahedral sites, T1 and T2. When the symmetry is lowered to triclinic, T1 and T2 split to T1o and T1m, and to T2o and T2m, respectively, enabling complete ordering (with Al in T1o) (Meneghilleno et al. 1999). A long-standing problem of alkali feldspars concerns the determination of the (Si-Al) order-disorder process. If the (Si-Al) distribution is random, the structure is said to be completely disordered (high sanidine). Nevertheless applying slow annealing, Al^{3+} is expected to migrate preferentially into the T1 sites and Si^{4+} into the T2 sites in order to satisfy local electrostatical balance considerations (low sanidine).

There are different methods to determine the (Si-Al) distribution in alkali feldspars: by means of calculations using the lattice parameter a and c (Kroll&Ribbe 1983) or using the optic axial angle $2V_x$ (Su et al. 1986) as well as directly by X-ray or neutron diffraction. But Al and Si are neighbouring elements in the periodic table, Al^{3+} and Si^{4+} have the same number of electrons and therefore, nearly similar atomic scattering factors in X-ray diffraction. Otherwise the coherent neutron scattering length of Al and Si is different. Thus structural analysis by Rietveld refinement of neutron diffraction data allows the separation of isoelectrical ions in the crystal structure like it is the case for Al^{3+} and Si^{4+}.

Two series of alkali feldspar samples were prepared for the neutron diffraction investigations:
 - natural sanidine from the Eifel (X_{Or}=0.85): untreated and heat-treated (850°C, 1050°C)
 - ion exchange between natural alkali feldspars and mixed NaCl/KCl salt/vapour: natural gem quality feldspars of close to end-member composition (sanidine from the Eifel) was exchanged with molten NaCl/KCl salt or the vapour above the molten salt at 1000°C in evacuated quartz glass tubes for 28 days, followed by a heat-treatment (925°C, 28 days).

Neutron diffraction experiments were performed on the flat-cone single crystal diffractometer (=2.39Å) and the focusing powder diffractometer (=2.45Å) at the Berlin research reactor BERII. The neutron diffraction patterns were analyzed by Rietveld refinement using the FullProf software package (Rodriguez-Carjaval 2001). The (Si-Al) distribution was obtained directly from the occupancy parameters of the tetrahedral sites (table 1 shows the results for sanidine from the Eifel as an example).

Table 1: Lattice parameter of sanidine from the Eifel ($K_{0.82}Na_{0.18}AlSi_3O_8$)

	untreated	heat-treated at 1050°C
lattice constant a / b / c [Å]	8.536(1) / 13.012(2) / 7.184(1)	8.538(1) / 13.020(2) / 7.178(1)
.	116.005 (2)°	115.982 (2)°
T1 / T2	$Si_{0.65}Al_{0.35}$ / $Si_{0.85}Al_{0.15}$	$Si_{0.71}Al_{0.27}$ / $Si_{0.79}Al_{0.23}$

The alkali feldspars resulting from the ion exchange experiments obey in dependence on the orthoclase fraction X_{Or} the monoclinic sanidine type structure ($X_{Or} \leq 0.6$) or the triclinic high albite type structure (space group $C\bar{1}$). All annealed samples of this series crystallize exclusively in the triclinic structure.

This work shows that neutron powder diffraction is a well suitable method for studying the (Si-Al) distribution in alkali feldspars.

Reference:
E. Meneghilleno, A. Alberti, G. Cruciani (1999), Order-disorder process in the tetrahedral sites of albite, American Mineralogist 84, 1144-1151
J. Rodriguez-Carvajal (2001), Recent Developments of the Program FULLPROF, Commission on Powder Diffraction (IUCr). Newsletter 26, 12-19
H. Kroll, P. H. Ribbe (1983), Lattice Parameters, Composition and Al,Si Order in Alkali Feldspars. In: Reviews

in Mineralogy Vol. 2, 2nd Edition Feldspar Mineralogy, Mineralogical Society of America
S. C. Su, P. H. Ribbe, F. D. Bloss (1986), Optical properties of single crystals in the order-disorder series low albite-high albite, American Mineralogist 71, 1384-1392

In situ HT-XRD Study Probing for an Alleged Displacive Phase Transition in Zircon

Frank Tomaschek, Peter Schmid-Beurmann
Westfälische Wilhelms-Universität Münster, Institut für Mineralogie, Münster, Germany

Information on the structural properties of zircon under high temperature conditions is still relatively scarce and partially inconclusive. Trace element distribution and solubility data, for instance, mostly determined for zircon under high temperature experimental conditions (> 900°C), is increasingly applied to aid the petrologic interpretation of the U-Pb zircon geochronometer. Extrapolation of high temperature zircon properties to geologic conditions at notably lower temperatures presently relies on the implicit assumption of a uniform structural state for the zircon phase. Yet however, there are some observations from *in situ* neutron powder diffraction (Mursic et al., 1992), and supporting PAC spectroscopic studies (Jaeger & McBride, 2007), which have been interpreted to indicate a displacive phase transition in high temperature zircon. For reasons as mentioned above, we aimed to probe for the alleged zircon phase transition.

In situ HT-XRD experiments have been performed on powdered zircon samples, using an Anton Paar HTK 1200 furnace attached to a Philips X'PERT-MDP (Cu Kα radiation). Diffraction data was collected for a large number of heating steps, along complete temperature cycles between room conditions and 1150°C. Lattice parameters were refined by Rietveld or Pattern Matching Analysis using the program FullProf.2k.

Samples investigated so far comprise: a) gem quality, colorless zircon, collected from the Mud Tank carbonatite (Harts Range, Australia), very low in trace element contents and essentially free of accumulated radiation damage; b) commercial ceramic opacifier ('Kreuzonit'), derived from industrially processed zircon sands; and c) synthetic $(Zr,Y)(Si,P)O_4$ zircon solid solutions, prepared by conventional LiMo-flux methods.

For the Mud Tank sample, lattice parameters determined at room temperature are similar to those of synthetic end member or highly crystalline, natural zircon reference materials [a_0, c_0 = 6.60533(6), 5.9804(1)]. Room temperature data of the opacifier zircon sample is characterized by a slightly expanded c_0 parameter [6.6045(4), 5.9836(5)], which commonly reflects residual expansion after near-complete annealing of previously radiation damaged natural zircon. The mean lattice parameters of the compositionally zoned flux-grown crystals [6.6161(1), 5.9809(2)] closely correspond to the increased lattice parameters predicted at about 4.5 mol.% YPO_4, by Vegard's rule for a zircon-xenotime solid solution.

Upon heating the zircon samples from room temperature to 1150°C, *in situ* lattice parameters monotonously increased with increasing temperature in such a manner that the axial ratio a/c linearly decreased. Lattice parameters determined along both limbs of the complete cycle (heating and back to room temperature) follow the same path. The slope of the axial ratio a/c is similar for all three investigated samples, and is notably constant within the explored temperature interval.

Our experiments have been cycled across the temperature of ~ 827°C, at which a previous *in situ* study (Mursic et al., 1992) observed a significant anomaly of structural properties during heating of their zircon sample. However, no anomaly in the temperature dependence of lattice parameters could be detected for the three zircon samples investigated here. Further cycled heating experiments of sample material that does show an anomaly are needed to probe for the suggested displacive phase transition in HT zircon.

References:
Jaeger, H. & McBride, S.P. (2007). Perturbed angular correlation measurement of the electric field gradient at [181]Ta in $ZrSiO_4$ and $HfSiO_4$. Hyperfine Interactions 177, 51-56.
Mursic, Z., Vogt, T. & Frey, F. (1992). High-temperature neutron powder diffraction study of $ZrSiO_4$ up to 1900 K. Acta Crystallographica B48, 584-590.

The electric field gradient in natural chrysoberyl and sinhalite

Lottermoser Werner[1], Redhammer Günther J[1], Weber Sven-Ulf[2], Tippelt Gerold[1], Litterst Fred Jochen[3], Amthauer Georg[1], Grodzicki Michael[1]

[1]Universität Salzburg, FB Materialforschung und Physik, Salzburg, Austria

[2]Technische Universität Braunschweig, Institut für Physikalische und Theoretische Chemie, Braunschweig, Germany

[3] Technische Universität Braunschweig, Institut für Physik der kondensierten Materie, Braunschweig, Germany

The electric field gradient (EFG) tensor is a central quantity when studying the relationship between structural and chemical properties in solids because it provides a most sensitive measure for the size and shape of the electric charge distribution around a given nucleus on a certain crystallographic site. Especially in case of low site symmetries the evaluation of this tensor with regard to its direction and magnitude is non-trivial but strongly correlated with other physical properties. Experimentally, the EFG is determined by Mössbauer spectroscopy yielding the quadrupole splitting ˜. Additionally, from single crystal spectra the asymmetry parameter = $(V_{XX}-V_{YY})/V_{ZZ}$, representing the rhombic distortion of the EFG-ellipsoid, can be obtained, as well as the orientation of the EFG-tensor with respect to the crystallographic axes from the intensity distribution of the Mössbauer peaks with two angle parameters and (see, e.g., Gonser 1975). Theoretically, the EFG-tensor is derived from electronic structure calculations in the local density approximation (Grodzicki 1980, 1985). This is commonly regarded as the state-of-the-art treatment of large systems, i.e. with about 100 atoms per unit cell.

This work reports on the evaluation of the EFG in two olivine-type minerals with low iron content, viz. a natural chrysoberyl (ideal formula Al_2BeO_4:Fe, 0.03 Fe ions pfu, space group Pnma, a = 9.4203(9)Å, b = 5.4871(5)Å, c = 4.4331(4)Å, Z=4) and sinhalite (ideal formula $MgAlBO_4$:Fe, 0.04 Fe ions pfu, space group Pnma a = 9.906(1)Å, b = 5.691(1)Å, c = 4.337(1)Å, Z=4). Iron in the olivine structure may be located on the two non-equivalent crystallographic sites M1 (point symmetry -1) and M2 (point symmetry m), respectively. Unlike in the isostructural alexandrite (Weber et al. 2007), there is no indication for Fe^{2+} in the chrysoberyl lattice, but the temperature-dependent Mössbauer spectra can all be reproduced by three subspectra with hyperfine parameters typical for Fe^{3+} located in chrysoberyl and hematite inclusions or clusters. In accordance with the results on alexandrite powder samples (Weber et al 2007), Fe^{3+} in chrysoberyl has strong preference for the M2 site with a minor tendency to occupy M1. Whereas the angle parameters can unequivocally be assigned to Fe^{3+} on M1, on M2 they cannot due to the large linewidth. However, the calculated angles are not contradictory to ascribing this subspectrum to M2. In addition, the calculated quadrupole splittings and asymmetry parameters are in quantitative agreement with the experimental values. An additional subspectrum is a sextet with hyperfine parameters typical for Fe^{3+} in hematite (Weber et al 2007). A superparamagnetic contribution of hematite can not be excluded.

In the Mössbauer spectra of sinhalite the doublets exhibit distinct asymmetries with regard to the direction of the incident γ-rays. Nevertheless, the spectra have been fitted with a single doublet without any restrictions using starting parameters for the quadrupole splitting and the angles between the EFG and the crystallographic axes as obtained by the electronic structure calculations for Fe^{2+} at the M2 position. Unlike in our earlier investigations (Weber et al. 2009) there is no indication for a second doublet associated with Fe^{2+} on the M1 position. The detected asymmetry in the powder spectrum has therefore to be attributed to texture. This conclusion is confirmed by the single crystal Mössbauer spectrum recorded under magic angle that yields a completely symmetric doublet. Hence, the whole iron content of sinhalite is divalent and can be located on the M2 position exclusively. This is in accordance with other experimental results, as well as the electronic structure calculations. Summarizing, even small amounts of Fe in minerals can be used as "nanoprobe" in order to derive reasonable EFG tensors leading to distinct site attributions.

References:

Gonser U (1975) From a strange effect to Mössbauer spectroscopy. In: Gonser U (ed) Topics in Applied Physics, vol 5, Mössbauer Spectroscopy. Springer, Berlin-Heidelberg-New York: 1-51.

Grodzicki M (1980) A self-consistent charge Xα method. I. Theory. J Phys B13:2683-2691.

Grodzicki M (1985) Theorie und Anwendungen der Self-Consistent-Charge-Xα Methode. Thesis of habilitation, Hamburg.

Weber SU, Grodzicki M, Lottermoser W, Redhammer GJ, Tippelt G, Ponahlo J, Amthauer G (2007) [57]Fe Mössbauer spectroscopy, X-ray single crystal diffractometry and electronic structure calculations on natural alexandrite. Phys Chem Minerals 34: 507-515.

Weber SU, Grodzicki M, Lottermoser W, Redhammer GJ, Topa D, Tippelt G, Amthauer G (2009) [57]Fe Mössbauer spectroscopy, X-ray single crystal diffractometry and electronic structure calculations on natural sinhalites. Phys Chem Minerals 36:259-269.

Section 09

––––––––

Geochemical signatures in environmental archives: Formation, preservation and application

Magnesium isotope variations in the rivers Danube, Elbe and Rhine

C. V. Ullmann[1], U. Wiechert[1], A. Meixner[2], M. Recker[1], R. L. Romer[2], H. J. Becker[1]
[1]Institut für Geologische Wissenschaften, Freie Universität Berlin, Berlin, Germany
[2]Deutsches GeoForschungsZentrum GFZ, Potsdam, Germany

The origin and sources of Mg isotopic variations in modern surface waters is little understood. Here we present a survey of the Mg isotopic composition of major rivers and their suspended sediment load in central Europe. Isotopic variations will be discussed in the context of river water composition and the predominant lithologies of their catchments.

Water samples were collected from 16 locations along three major central European rivers Danube, Elbe and Rhine in January 2010. The water from each locality was filtered through 0.45μm cellulose acetate filters and acidified with nitric acid for cation analysis. The suspended loads on the filter were dried and digested with HF-HNO_3. Major element abundances of the dissolved and the suspended load were determined on an Element-XR ICP-MS at the Freie Universität Berlin. For isotope analysis magnesium was purified on three distinct ion exchange resins AG1X8, AGW50X8 and AGW50X12. Magnesium isotope ratios were measured using a Neptune MC-ICP-MS at the Deutsches GeoForschungsZentrum in Potsdam and are reported as   values relative to DSM3.

The δ^{26}Mg of the dissolved and solid loads vary from -0.93 to -1.85 ‰ and -0.98 to 0.01 ‰, respectively. Microscopic observation provides evidence for predominantly fine grained quartz and clay minerals in solid loads. Carbonates are present in all Danubian samples, in three of four samples of the river Rhine and one sample of the Elbe close to the river mouth. Due to the lack of material exact proportions and mineralogy of the solid loads could not be investigated. The suspended magnesium loads are isotopically heavier than the dissolved magnesium in all rivers with absolute differences of 0.7 to 1.3 ‰.

The Danubian water chemistry is controlled by calcium carbonate and the Ca/Al ratio of the suspended loads are high with an average molar ratio of 1.0 reflecting the dominance of carbonate lithologies in the catchment. These samples exhibit the lowest δ^{26}Mg of -1.85 to -1.70 ‰ for dissolved loads and low δ^{26}Mg between -0.98 and -0.38 ‰ for suspended loads.

In the river Rhine, the character of the catchment changes from carbonate rich to more siliceous lithologies downstream. Accordingly the calcium is replaced by sodium as the dominant cation in the dissolved load towards the river mouth. The average Ca/Al ratio of the suspended load is not distinguishable from the river Danube. δ^{26}Mg of the dissolved and suspended load rise from -1.74 to -1.36 ‰ and -0.93 to -0.42 ‰ downstream.

The catchment of the river Elbe comprises mainly of siliceous rocks. In the dissolved loads, sodium is as abundant as calcium and molar Ca/Al ratios of the suspended loads are generally low at ~0.4. The dissolved magnesium of water samples from the river Elbe give a constant δ^{26}Mg at -1.00 ± 0.07 ‰, which is within analytical reproducibility of ± 0.08 ‰ (2 s.d.). δ^{26}Mg of the suspended loads decreases from +0.01 to -0.41 ‰.

It has been shown previously that carbonates have typically δ^{26}Mg below -2 ‰, whereas silicate rocks have δ^{26}Mg close to 0 ‰ relative to DSM3 (Tipper et al. 2006, Galy et al. 2002, Young and Galy 2004). Therefore, we speculate that the isotopic composition of the three German rivers may reflect distinct proportions of magnesium from carbonate dissolution and silicate weathering. Magnesium in the suspended load is probably mainly hosted by clay minerals and systematically heavier than magnesium of the respective dissolved load. On the basis of the data obtained during this study, a fractionation factor between solution and secondary clay minerals $\alpha_{solution-clay} < 1$ is indicated.

References:
Tipper E.T.; Galy A.; Gaillardet, J.; Bickle M.J.; Elderfield, H.; Carder E.A. (2006) The magnesium isotope budget of the modern ocean: Constraints from riverine magnesium isotope ratios. Earth Planet. Sci. Lett. 250, 241-253. Galy A.; Bar-Matthews M.; Halicz l.; O'Nions R.K. (2002) Mg isotopic composition of carbonate: insight from speleothem formation. Earth Planet. Sci. Lett. 201, 105-115. Young E.D.; Galy A. (2004) The isotope geochemistry and cosmochemistry of Mg. Rev. Min. Geochem. 55, 197-230.

Controls on calcium isotope fractionation in natural and synthetic ikaite and vaterite

Nikolaus Gussone[1], Gernot Nehrke[2], Barbara M.A. Teichert[3]
[1]Institut für Mineralogie, Universität Münster, Corrensstr. 24, 48149 Münster, Germany
[2]Alfred Wegener Institut für Polar- und Meereswissenschaften, Am Handelshafen 12, 27570 Bremerhaven, Germany
[3]Institut für Geologie und Paläontologie, Universität Münster, Corrensstr. 24, 48149 Münster, Germany

The isotopic composition of calcium (Ca) in various kinds of archives (e.g. biogenic minerals, porewaters, etc.) provides information about geological and geochemical processes as well as past environmental conditions. Paleoceanographic applications of Ca isotope ratios include reconstructions of relations in paleo-food-webs (cf. Skulan et al. 1997), reconstruction of the oceanic Ca-budget (cf. Heuser et al. 2005) and sea surface temperature (cf. Nägler et al. 2000). Shells of marine calcifiers are applied as proxy archives in most of these studies. However, complex fractionation patterns found in some of these shells, emphasise the importance of a solid understanding of Ca isotope fractionation processes during both, transport to the site of calcification and precipitation. Several studies addressed the fractionation behaviour of Ca isotopes in synthetically precipitated calcium carbonates. These studies found temperature and rate-dependent fractionation effects, which are, however, partly discrepant and Ca isotope fractionation in carbonates is presently not fully understood and its basic mechanisms are still under debate. Different models that were proposed to explain the respective observations include kinetic isotope fractionation effects (cf. Gussone et al. 2003), equilibrium fractionation (Marriott et al. 2004), disequilibrium fractionation (Lemarchand et al. 2004) and surface entrapment effects (Tang et al. 2008). In particular, the discrepant dependency of Ca isotope fractionation on precipitation rate found by Lemarchand et al. (2004) and Tang et al. (2008) are not yet understood. Research on Ca isotope fractionation so far focussed on the most abundant $CaCO_3$ polymorphs calcite and aragonite and revealed a comparable temperature dependence of about 0.015‰/°C in both and an offset between both polymorphs of approximately 0.5‰ (cf. Marriott et al. 2004, Gussone et al. 2003, 2005). In this study, we investigated the fractionation of calcium isotopes in the calcium carbonate polymorphs vaterite and ikaite. The synthetic vaterite precipitates show a smaller degree of Ca isotope fractionation than calcite or aragonite at comparable temperatures and revealed no significant temperature sensitivity between 10 and 50°C. Ikaite, the water-bearing Ca carbonate modification ($CaCO_3 \cdot 6H_2O$) was precipitated at 2°C in controlled laboratory experiments and in addition recovered from marine sediments (Zabel and Schulz 2001) and sea-ice (Diekmann et al. 2008). Synthetic and natural ikaites show similar values of Ca isotope fractionation. In general, ikaite is less depleted in heavy isotopes compared to calcite or aragonite at low temperatures. The observed offset of vaterite and ikaite to calcite or aragonite precipitated at similar temperatures is presumably mainly related to differences in precipitation rates. The respective rates however, seem to be typical for the growth of these carbonate minerals. Small differences in Ca isotope ratios of naturally formed ikaites from different locations seem to be related to different geochemical conditions in the respective sediment settings.

Reference:
Dieckmann, G. S., Nehrke, G., Papadimitriou, S., Göttlicher, J., Steininger, R., Kennedy, H., Wolf-Gladrow, D., and Thomas, D. N., 2008. Calcium carbonate as ikaite crystals in Antarctic sea ice. Geophys. Res. Lett. 35.
Gussone N., Eisenhauer A., Heuser A., Dietzel M., Bock B., Böhm F., Spero H. J., Lea D. W., Bijma J., and Nägler T. F. (2003) Model for Kinetic Effects on Calcium Isotope Fractionation (δ^{44}Ca) in Inorganic Aragonite and Cultured Planktonic Foraminifera. Geochimica et Cosmochimica Acta 67(7), 1375-1382.
Heuser A., Eisenhauer A., Böhm F., Wallmann K., Gussone N., Pearson P. N., Nägler T. F., and Dullo W.-C. (2005) Calcium Isotope ($\delta^{44/40}$Ca) Variations of Neogene Planktonic Foraminifera. Paleoceanography 20(PA2013), doi:10.1029/2004PA001048.
Marriott C. S., Henderson G. M., Belshaw N. S., and Tudhope A. W. (2004) Temperature dependence of δ^7Li, δ^{44}Ca and Li/Ca during growth of calcium carbonate. Earth and Planetary Science Letters 222, 615-624.
Nägler T. F., Eisenhauer A., Müller A., Hemleben C., and Kramers J. (2000) δ^{44}Ca- Temperature Calibration on Fossil and Cultured Globigerinoides sacculifer: New tool for reconstruction of past sea surface temperatures. Geochemistry, Geophysics, Geosystems 1, doi:10.1029/2000GC000091.
Skulan J., DePaolo D. J., and Owens T. L. (1997) Biological control of calcium isotopic abundances in the global calcium cycle. Geochim. Cosmochim. Acta 61(12), 2505-2510.
Zabel M., Schulz H.D. (2001) Importance of submarine landslides for non-steady state conditions in pore water systems – lower Zaire (Congo) deep-sea fan, Marine Geology 176, 87-99.

Primary dolomite formation – Insights from Ca-isotopes

Barbara M.A. Teichert[1], Patrick Meister[2], Charlotte Ockert[3], Nikolaus Gussone[3]

[1]Westfälische Wilhelms-Universität Münster, Institute for Geology and Paleontology, Münster, Germany

[2]Max-Planck-Institute for Microbiology, Bremen, Germany

[3] Westfälische Wilhelms-Universität Münster, Institute for Mineralogy, Münster, Germany

An apparent calcium (Ca) isotope fractionation factor of -0.5 ‰ (at 14 °C) is reported for the formation of primary, early diagenetic dolomite in the siliciclastic-dominated, organic carbon rich sediments of the Peru Margin (ODP Leg 201, Site 1229). Compared to other carbonate mineralogies, like calcite and aragonite, dolomite seems to be the least enriched in ^{40}Ca. Strontium isotopes of the dolomites and porewater (Meister et al., 2007) helped to reconstruct the original formation depth of the dolomites (between 6 and 12 m) that are now buried up to 105 m deep within the sedimentary section.

In comparison to studies on secondary, replacement dolomite (Holmden, 2009) where negligible isotopic fractionation between dolomite and dolomitizing fluid was proposed, Ca isotopes hold promise as a tool for discriminating between primary, early diagenetic and secondary, replacement dolomite formation. Calcium isotope composition of the porewater at Site 1229 shows high variability and a strong gradient from seawater-like values to a relatively light $\delta^{44/40}$Ca of 0.83 ‰SRM915a at intermediate depth (100 m). This suggests that light Ca is released from clay minerals through ion exchange with ammonium. The lower part of the profile is dominated by an upward diffusing upper Miocene brine enriched in heavy Ca isotopes.

Reference:
Holmden, C. (2009) Ca isotope study of Ordovician dolomite, limestone, and anhydrite in the Williston Basin: Implications for subsurface dolomitization and local Ca cycling. Chemical Geology 268, 180-188.
Meister, P., McKenzie, J.A., Vasconcelos, C., Bernasconi, S., Frank, M., Gutjahr, M., Schrag., D. (2007) Dolomite formation in the dynamic deep biosphere: Results from the Peru Margin. Sedimentology 54, 1007-1031.

Barium isotope fractionation in the global barium cycle: Evidence from barium minerals and precipitation experiments

Katja von Allmen[1], Michael E. Böttcher[2], Elias Samankassou[1,3], Thomas F. Nägler[4]

[1] Department of Geosciences, Chemin du Musée 6, University of Fribourg, CH-1700 Fribourg, Switzerland (katja.vonallmen@unifr.ch)

[2] Institute for Baltic Sea Research (IOW), Geochemistry & Isotope Geochemistry Group, Marine Geology Section, D-18119 Warnemünde, Germany (michael.boettcher@io-warnemuende.de)

[3] Present address: Section of Earth and Environmental Sciences, University of Geneva, Rue des Maraîchers 13, CH-1205 Geneva, Switzerland (Elias.Samankassou@unige.ch)

[4] Institute of Geological Science, Baltzerstr. 3, University of Bern, CH-3012 Bern, Switzerland (naegler@geo.unibe.ch)

In this study, we present first results from an ongoing investigation on the stable barium (Ba) isotope fractionation in the natural barium cycle. Stable Ba isotope signatures of international IAEA reference materials (synthetic barium sulfate and barium carbonate – otherwise used for stable S, C and O isotope calibration), and different terrestrial Ba gangue minerals have been analyzed as a first approach to evaluate potential discriminating processes in the global biogeochemical barium cycle. Measurements were carried out on a multi-collector ICP-MS applying a $^{135}Ba/^{130}Ba$ double spike. Data are given as per mil deviations from a laboratory Ba nitrate standard solution in the $^{137/134}Ba$ notation (external 2s stdev < 0.1 per mil).

Whereas the various synthetic solid standards and p.a. quality synthetic barium chloride show very similar isotope results close to the nitrate standard solution, the terrestrial barium gangue minerals (four barites, one norsethite $[BaMg(CO_3)_2]$) were depleted in the heavy isotope ($^{137/134}Ba$ values between 0 and -0.2 per mil). A diagenetic barite sample recovered during ODP Leg 207, gave an isotope value of -0.5 per mil. A natural barite, from an unknown Chinese locality, gave an isotope value of -0.4 per mil. Also measured high $^{34}S/^{32}S$ and $^{18}O/^{16}O$ ratios in this sample indicate that this barite has been formed under influence of microbial sulfate reduction, probably in a marine diagenetic environment. The observed natural discriminations are by far larger than the analytical uncertainty of the isotope measurements, indicating isotope discrimination in the natural barium cycle.

Precipitation experiments from aqueous barium chloride solutions at room temperature and 80°C indicate that the light Ba isotope is enriched in pure barium carbonate or barium sulfate compared to the aqueous solution. A maximum isotope fractionation of -0.3 per mil is observed, for both barium carbonate and sulfate, that seems to be influenced by precipitation rate ($BaCO_3$) and/or the aqueous speciation, but less by temperature. No significant isotope effect by the presence of 1 M NaCl upon barite formation was observed.

Ca isotope ratios of marine biogenic carbonates in response to Eocene Carbonate Accumulation Events

Katharina Rabe[1], Nikolaus Gussone[1], Barbara M.A. Teichert[2] and the IODP Expeditions 320/321 Shipboard Scientific Party
[1]Westfälische Wilhelms-Universität Münster, Institute for Mineralogy, Münster, Germany
[2]Westfälische Wilhelms-Universität Münster, Institute for Geology and Paleontology, Münster, Germany

The Cenozoic is known for its times of extreme climates and rapid climate changes. Sediment samples recovered during IODP-Expeditions 320 and 321 of the Pacific Equatorial Age Transect (PEAT) program retrieved well preserved continuous core material from the Equatorial Eastern Pacific providing an excellent archive for reconstructions of climate changes during the Cenozoic. Besides reconstruction of temperature and salinity fluctuations, a main aim of this expedition was to enhance the understanding of carbon cycling, in particular the interplay of carbonate compensation depth (CCD), $CaCO_3$-dissolution and productivity. Shipboard results revealed sharp carbonate concentration fluctuations at ~44, 41, 39, and 36 Ma, refining the carbonate accumulation events described by Lyle et al. (2005). Additional drastic changes in the carbonate chemistry are revealed by strong changes in carbonate content indicating a CCD-rise around 49 Ma, between 23-27 Ma, a Neogene CCD minimum between 17 and 18 Ma, the 'carbonate crash' interval around 10 Ma, and a newly delineated CCD minimum at about 4 Ma (Pälike et al., in press). These events reveal not only dramatic changes in the carbonate but also in the Ca budget of the ocean. The exact role of Ca in this context, is yet unclear. An ideal tool to study the changes of the Ca budget is the Ca isotopic composition of the paleo-seawater which is recorded in marine biogenic carbonates.

Here, we study the carbonate accumulation events CAE- 2 and 3 (~ 45-40 Ma), to investigate changes in the oceanic isotopic Ca budget during these times of massive carbonate accumulation, in particular to better constrain the role of Ca in terms of input, redistribution and output. Benthic foraminifer tests were handpicked from the size-fraction >63µm and thoroughly cleaned following the method described in Gussone and Filipsson (2010). Calcium isotope ratios were analysed by Thermal Ionisation mass spectrometry. $\delta^{44/40}$Ca values of the foraminifer tests range between 0.28 and 0.76 ‰ SRM915a, indicating significant variability during the carbonate accumulation events.

References:

Gussone N. and Filipsson H. L. (2010) Calcium isotope ratios in calcitic tests of benthic Foraminifers, Earth and Planetary Science Letters 290, 108-117.
Lyle M. W., Olivarez Lyle A., Backman J., and Tripati A. (2005) Biogenic sedimentation in the Eocene equatorial Pacific: the stuttering greenhouse and Eocene carbonate compensation depth, in Proc. ODP, Sci Res 199, edited by Lyle, M., Wilson, P., Janecek, T.R., and Firth, J., College Station, TX, Ocean Drilling Program: 35 pp.
Lyle, M., Pälike, H., Nishi, H., Raffi, I., Gamage, K., Klaus, A., and the IODP Expeditions 320/321 Scientific Party (2010) The Pacific Equatorial Age Transect, IODP Expeditions 320 and 321: Building a 50-Million-Year-Long Environmental Record of the Equatorial Pacific Ocean. Scientific Drilling 9, 4-15
Pälike H., Lyle M., Nishi H., Raffi I., Gamage K., Klaus A., and the Expedition 320/321 Scientists (in press) Proc. IODP, 320/321: Tokyo (Integrated Ocean Drilling Program Management International, Inc.).

Calcium isotope ratios of deepwater Ostracod-shells: a potential proxy for fluctuations of the oceanic Ca budget

Tim Greifelt[1], Nikolaus Gussone[1,2]
[1] Westfälische Wilhelms-Universität Münster, Institut für Mineralogie, Münster, Germany
[2] MARUM, Bremen, Germany

The element calcium (Ca) is abundant on Earth and involved in numerous geological as well as biological processes, including cell metabolism and global element-cycles. Isotope fractionation that is related to these processes is a basic precondition for the use of Ca isotope ratios as paleoenvironmental proxy. So far, the isotopic composition of Ca is used in paleoceanography to reconstruct relationships in ancient food-webs (Skulan et al. 1997), paleotemperature (Nägler et al. 2000) and the Ca isotopic composition of the paleo-seawater, a measure for the oceanic Ca budget (Heuser et al. 2005), an important parameter for modelling the global carbon cycle. For the latter two applications, most studies utilised microfossils composed of calcite. In order to obtain reliable Ca isotope records it is important to understand the fractionation mechanisms that occur during biomineralisation of the used microfossil tests as well as factors that might affect the direct environment of the organism, like their preferred habitat in the water column or sediment. The importance of this consideration was emphasized by complicated fractionation patterns found in some planktonic foraminifers (Gussone et al, 2009), including bimodal temperature sensitivities. In particular, for the reconstruction of the Ca isotope composition of paleo-seawater, it is important to utilize proxy-archives that exhibit only minor dependencies on environmental parameters, including temperature, salinity or carbonate chemistry.

In this study we explore the potential of Ca isotope ratios in Ostracods as temperature proxy as well as recorder for the Ca isotopic composition of paleo-seawater. Ostracods are small Crustacea that surround themselves with a shell, which is composed of two valves of calcite and organic matter, the so called carapax. Ostracods belong to the Ecydysozoa, a group of organisms that shed their shell eight times during their lifetime, making Ostracod carapaxes relative abundant in sediments. Ostracods have a predominantly epifaunal benthic habitat. Therefore, they do not migrate vertically in the water column, recording influences from different water depth and are not affected by seasonal fluctuations and short term climate variability. In addition, they do not migrate deep into the sediment and are hence not influenced by the porewater geochemistry of the sediments.

For our study we analysed the Ca isotopic composition of recent Ostracod carapaxes. The carapaxes were derived from a depth-temperature transect offshore Namibia from coretop sediment samples that were retrieved during meteor cruise M57/2 (Zabel et al. 2003). The analysed samples cover a temperature range from 1 to 18 °C. Samples were cleaned following the method applied for benthic foraminifers (Gussone and Filipsson 2010), dissolved and mixed with a Ca-double spike.

First results of two genera (*Cytherella* and *Henryhowella*) show $\delta44/40Ca$ values between 0.34 and 0.73‰. The $\delta44/40Ca$ values of the analyzed shells of *Henryhowella* sp. seem to follow an apparent temperature dependent Ca isotope fractionation pattern similar to benthic foraminifers (Gussone and Filipsson 2010). Between 3 and 15 °C the $\delta44Ca$ values show a positive correlation with the temperature (~0.029‰/°C) and below 3°C, $\delta44Ca$ values show an apparent inverse correlation which is also comparable with benthic foraminifers (Gussone and Filipsson 2010).Whereas the genera *Cytherella* sp. shows a minor temperature dependent Ca isotope fractionation in a range of 3 and 23°C with $\delta44Ca$ values between 0.5 and 0.7‰. These initial results indicate that Ca isotope ratios of Ostracod carapaxes might be suited to record fluctuations in the $\delta44/40Ca$ of paleo-seawater.

References
Gussone N., Hönisch B., Heuser A., Hemleben C., Spindler M., Eisenhauer A. (2009) A critical evaluation of calcium isotope ratios in tests of planktonic foraminifers, Geochimica et Cosmochimica Acta, 73, 7241-7255.
Gussone, N. , Filipsson, H. L., 2010. Calcium isotope ratios in Calcitic tests of benthic foraminifers, Earth and planetary science letters, 290, p. 106-117.
Heuser A., Eisenhauer A., Böhm F., Wallmann K., Gussone N., Pearson P. N., Nägler T. F., and Dullo W.-C. (2005) Calcium Isotope (20(PA2013), doi:10.1029/2004PA001048.
Nägler T. F., Eisenhauer A., Müller A., Hemleben C., and Kramers J. (2000) δ44Ca- Temperature Calibration on Fossil and Cultured Globigerinoides sacculifer: New tool for reconstruction of past sea surface temperatures. Geochemistry, Geophysics, Geosystems 1, doi:10.1029/2000GC000091.
Skulan J., DePaolo D. J., and Owens T. L. (1997) Biological control of calcium isotopic abundances in the global calcium cycle. Geochim. Cosmochim. Acta 61(12), 2505-2510.
Zabel M. and cruise participants (2003), Report and preliminary results of METEOR Cruise M 57/2, Walvis Bay - Walvis Bay, 11.02-12-03.2003. Berichte, Fachbereich Geowissenschaften, Universität Bremen, No. 220, 136p, Bremen.

Section 10

_____

Ion Microprobe characterization of geo-materials

P10-01

Li, Be, B and ^{11}B systematics in the peralkaline Ilímaussaq Intrusion (South Greenland)

Melanie Kaliwoda[1], Horst Marschall[2], Thomas Ludwig[3], Rainer Altherr[3], Gregor Markl[4]
[1]Mineralogische Staatssammlung, München, Germany
[2]University of Bristol, Department of Earth Sciences, Bristol, United Kingdom
[3]Ruprecht Karls Universität Heidelberg, Fakultät für Chemie und Geowissenschaften, Department für Mineralogie und Petrologie, Heidelberg, Germany
[4]Eberhard Karls Universität Tübingen, Institut für Geowissenschaften, Department für Petrologie, Tübingen, Germany

SIMS (secondary ion mass spectrometry) at the University of Heidelberg was used to measure all the different main and secondary minerals in the peralkaline Ilímaussaq complex (South Greenland). The aim of the measurements was to find out the behaviour of Li, Be, B within the three progressively more fractionated magmatic pulses of Ilímaussaq.

Main Li carrier in the system is Na-rich amphibole with a maximum Li content of 6000 μg/g in the foyaites and naujaites compared to the early Ca-rich amphiboles (50 μg/g) in the augite syenites. Minor phases with also high Li contents are aenigmatite (Li: 57-9000 μg/g), nepheline (60-80 μg/g) and eudyalite (300 μg/g). The highest Be contents occur in aenigmatites of late stage hydrothermal veins (500 μg/g), and somewhat lesser in nephelines (16-100 μg/g) and sodalites (15-60 μg/g). Typical B carrier of the rocks is sodalite with maximum contents of 120 μg/g. Increasing fractionation especially in the amphiboles and to some extent in the pyroxenes and eudialytes results in rising Li and Be contents, whereas sodalite displays decreasing Li and increasing Be and B contents versus increasing fractionation.

Boron isotopic compositions (expressed as δ^{11}B) were determined for sodalite, amphibole and feldspar. Boron isotope values in the cores of sodalite grains vary in a small range between −12 ‰ and −10 ‰. δ^{11}B values of amphibole and feldspar scatter around −20 ‰ and −17 ‰. In rocks from the inner part of the intrusion, but increase to higher and even positive values at the rim of the complex and in the granitic country rocks. The same is observed for δ^7Li in amphibole (Marks et al. 2007).

In conclusion we find out that, the concentration of Li, Be and B within the major rock types of the Ilímaussaq complex are mainly an effect of accumulation of minerals being compatible for the respective element. Li is mainly incorporated in Na-amphibole, whereas the major host for boron is sodalite. Thus, whole rock concentrations for Li are highest in amphibole-rich rocks and boron concentrations are highest in sodalite-rich rocks. Consequently, their whole-rock concentration does not allow for direct monitoring of magmatic differentiation processes. The intra-mineral B isotope patterns are interpreted to be influenced by kinetic isotope fractionation. On the other hand, relative differences in the diffusion of the two B isotopes through melts and fluids are probably insignificant and kinetic fractionation of B isotopes on the outcrop scale is hence considered unlikely. Fractionation of sodalite would drive the δ^{11}B of the remaining melt to lower values (by ~3 ‰ in our model). In contrast, exsolution of basic hydrous fluids would drive the δ^{11}B values in the degassed melt to more positive values (by 5 ‰ in the modelled case). The fractionation of silicates with very low mineral-melt partition coefficients for B, such as amphibole, pyroxene, feldspar, nepheline and eudialyte, would have no significant effect on δ^{11}B within the magma. In case of Ilímaussaq complex, the B concentrations and the δ^{11}B values of ortho-magmatic amphiboles throughout the three phases remain relatively constant at approximately 1 μg/g and -20 ‰, respectively. This demonstrates that the effects of sodalite fractionation, fluid exsolution and low-B silicate fractionation on B abundances and B isotopic composition of the magmas compensated each other. The high δ^{11}B values in the margin of the intrusive complex, i.e. the augite syenites and the adjacent country-rock granite is most probably influenced by entrained sea water, enriched in heavy boron (higher δ^{11}B).

Reference:
Marks, M. A. W., Rudnick, R. L., McCammon, C., Vennemann, T. & Markl, G. (2007). Arrested kinetic Li isotope fractionation at the margin of the Ilímaussaq complex, South Greenland: evidence for open system processes during final cooling of peralkaline igneous rocks. *Chemical Geology*, **246**, 207-230.

SIMS microanalysis of hydrogen and boron isotopes in hydrothermal tourmalines from the Carajás Mineral Province, Brazil

Robert B. Trumbull[1], Roberto P. Xavier[2], Michael Wiedenbeck[1]
[1] Deutches GeoForschungsZentrum GFZ, Potsdam, Germany
[2] Universidade Estadual de Campinas, Instituto de Geociências, Campinas (SP), Brazil

Tourmaline has proved valuable for the study of boron isotopic systematics in fluid-rock interaction related to hydrothermal ore formation, and still more information is potentially available from the combined study of boron and hydrogen isotope variations in tourmaline. We report here first results of a pilot B- and H-isotope study of hydrothermal tourmaline from two contrasting ore deposits in the Carajás district of Brazil, one with a marine evaporite source of fluids (Igarapé Bahia) and one where hydrothermal fluid was derived from an igneous intrusion (Breves).

The acquisition of boron isotope ratios using our Cameca ims 6f instrument is routine (e.g., Xavier et al., 2008), whereas hydrogen isotope measurements necessitate special care to minimize background hydrogen. Typical source chamber pressures are $<10^{-7}$ Pa and residual hydrogen background is further suppressed by operation at a nominal 10 kV extraction voltage with a 100 V offset. Maximum background levels for H in silicate matrices using our procedures correspond to < 5 µg/g H_2O (Rhede & Wiedenbeck, 2005). Repeated analysis of tourmaline reference materials demonstrate that $^{11}B/^{10}B$ and D/H ratios can be measured with an external reproducibility of ± 1.2 and ± 10 ‰ (1s), respectively.

The Igarapé Bahia (IB) deposit consists of breccia-hosted disseminated to massive sulfide mineralization with minor vein mineralization. The ore breccia occurs between a footwall sequence of greenschist facies mafic metavolcanics and banded iron formation and a hanging wall metaturbidite unit. Intermediate schorl-dravite tourmalines from the IB breccia have dominant 11B values from 14 to 26 ‰, indicative of a B source from non-magmatic fluids with involvement of marine evaporites or residual evaporated seawater, consistent with high Br/Cl ratios of fluid inclusions (Xavier et al., 2010). The tourmaline D values of these samples range from -89 to -69 ‰. For a mineralization temperature of 400°C estimated from quartz–magnetite 18O thermometry (Dreher et al., 2008), the corresponding fluid D values are in the range of -30 to -10‰.

The Breves disseminated and vein-hosted Cu-Au (Mo-W-Bi-Sn) deposit occurs in siliciclastic rocks in the roof zone of a Paleoproterozoic granite intrusion. Breves tourmalines are near end-member schorl, and their 11B values range from -4 to 2 ‰. These chemical and B-isotope features of Breves tourmaline are consistent with a magmatic-hydrothermal origin. The corresponding D values are -116 to -99 ‰. Mineralization temperatures at Breves are estimated at 400°C from 18O thermometry of quartz and biotite (Xavier et al., 2005). The calculated δD(fluid) is the range of -57 to -32 ‰, consistent with a magmatic-derived fluid. The Cl/Br and Na/Cl ratios of the Breves inclusion fluids strongly suggest a magmatic brine, but some contribution of non-magmatic brine (evaporite?) is not rule out by the data (Xavier et al. 2009).

Collectively, these results demonstrate the value of tourmaline B-H isotopes in constraining fluid source(s). We conclude that residual evaporative and magmatic brines were important components of the fluid regime involved in the formation of Cu-Au systems in the Carajás Mineral Province.

References:
Dreher, A.M., et al. (2008) New geologic, fluid inclusion and stable isotope studies on the controversial Igarapé Bahia Cu-Au deposit, Carajás Province, Brazil, Mineralium Deposita, 43, 161-184.
Rhede, D.& Wiedenbeck, M. (2005) SIMS Quantification of Very Low H2O Contents. SIMS XV Conference, Sept. 12-16, Manchester UK, Abstract Volume.
Xavier, R.P., et al. (2005) The Paleoproterozoic intrusion- related Breves Cu-Au-(Mo-W-Bi-Sn) deposit, Carajás Mineral Province, Northern Brazil: hydrothermal alteration, ore paragenesis and fluid evolution. I Simpósio Brasileiro de Metalogenia, May 1-4, Gramado, Abtracts CD-ROM.Xavier, R.P. et al. (2008) Tourmaline B-isotopes fingerprint marine evaporites as the source of high-salinity ore fluids in iron oxide copper-gold deposits, Carajás Mineral Province (Brazil): Geology, 36: 743-746.
Xavier, R.P. et al. (2009) Composition and Source of Salinity of Ore-bearing Fluids in Cu-Au Systems of the Carajás Mineral Province, Brazil. Society for Geology Applied to Mineral Deposits Meeting, August 17-20, Townsville, Abstract volume, 272-274.
Xavier, R.P. et al., (2010) The Iron oxide copper-gold deposits of the Carajás mineral province, Brazil: an

updated and critical review. In: Porter, T.M. (ed) Hydrothermal Iron Oxide Copper-Gold & Related Deposits: A Global Perspective: Advances in the Understanding of IPCG Deposits, v.3. PGC Publishing, Adelaide.

SIMS determined boron isotope compositions of volcanic glasses - implications for mantle heterogeneity

Marc Krienitz[1], Nicole Stroncik[1], Michael Wiedenbeck[1]
[1]Deutsches GeoForschungsZentrum GFZ, 14473 Potsdam, Germany

The boron isotopic composition of surface materials (e.g., altered oceanic crust, sediments) differs significantly from that of the Earth's mantle, meaning that boron isotopes are potentially a powerful tool for investigating material recycling processes. During this study the boron contents and isotopic compositions of submarine oceanic island basalt (OIB) and mid-ocean ridge basalt (MORB) glasses have been determined with the objectives of defining the B contents and isotope characteristics of mantle reservoirs (e.g., DMM, EM1, EM2, HIMU) and of characterizing the influence of material recycling on mantle composition.

Our preliminary SIMS data suggest that (1) the OIB type glasses are relatively enriched in B compared to MORB and (2) that EM type mantle domains (av. $\delta^{11}B$ = -3.3‰; n = 10) tend towards heavier boron isotope compositions than that observed in HIMU type glasses (av. $\delta^{11}B$ = -6.0‰; n = 4). Although these values are indistinguishable from MORB ($\delta^{11}B$ = -4.4‰; n = 2), as the total analytical uncertainty of the SIMS method is about 1.5‰ (1s), the consistent trends from EM to HIMU type glasses suggest that the mantle may be heterogeneous in terms of its boron isotopic composition.

Variations of $\delta^{11}B$ along with correlations with Sr, Nd and Pb isotopic compositions of the OIB glasses support a model that the source regions of these lavas contain recycled material. Although subduction related dehydration processes are probably highly effective mechanisms for removing boron, it seems that at least a heavy $\delta^{11}B$ component can survive subduction producing different boron isotopic compositions in deep mantle OIB source regions.

Section 11

_____

Magmatic processes

Partitioning of chlorine and sulfur between Cl-S-H$_2$O fluid and basaltic melt: implication to the magma source and redox conditions of volcanic degassing at Mt. Etna

Oliver Beermann[1], Roman E. Botcharnikov[1], Marcus Nowak[2]
[1]Leibniz Universität Hannover, Institute for Mineralogy, Hannover, Germany
[2]Eberhard Karls Universität Tübingen, Institute for Geosciences, Department Mineralogy and Geodynamics, Tübingen, Germany

Magmatic degassing of volatile-rich basaltic systems is mainly triggered by the exsolution of S/Cl-rich hydrous fluids. Variations in the S/Cl ratio of the volcanic gases are interpreted to be closely related to the eruption dynamics, e.g. at Mt. Etna (Aiuppa et al., 2004). The partitioning of S and Cl between fluid and melt is controlled by magma storage conditions and magma ascent. Thus, quantitative information on the volatile partitioning as a function of P-T-X-fO$_2$ is required for our understanding and interpretation of magma degassing processes. Therefore, we performed fluid saturated sulfur and chlorine partitioning experiments between Cl-S-H$_2$O fluid and primitive basaltic melt of Mt.Etna in internally heated Ar-pressure vessels at 1050°C, 100 to 200 MPa and ~FMQ+0.5 to FMQ+4.

At the investigated range of system composition sulfur and chlorine show a strongly non-ideal partitioning-behavior. The sulfur partitioning coefficients (Kd'S) range between ~1 and 96 ± 16 at 200 MPa and ~1 to 73 ± 12 at 100 MPa in the sulfate dominated systems (FMQ+2 to FMQ+4) and ~164 ± 16 to 236 ± 32 at 200 MPa in the sulfide dominated system (FMQ+0.5). The partitioning coefficients of chlorine (Kd'Cl) range between >0.1 and 19 ± 2 for all P and fO$_2$ investigated.

Comparison of S/Cl fluid ratios observed during passive degassing and high explosivity and the S content of melt inclusion with experimental data suggest that open system degassing at passive degassing stages (S/Cl fluid ~7) occurs at 200 MPa and ~0.3 wt.% S in the melt (Fig. 1). Decreasing S/Cl fluid ratios can only be explained by magma ascent and degassing of S-depleted melt, finally producing S/Cl fluid ratios as observed at high explosive eruption and lava fountaining. These observations are in contrast to conclusions of Keppler (2010), who proposed increasing S/Cl fluid ratios to be an indicator for pressure reduction in the magma chamber and/or magma ascent.

Our results confirm that the natural magmatic system is relatively oxidized, since natural fluid/melt compositions could not be reproduced at FMQ+0.5.
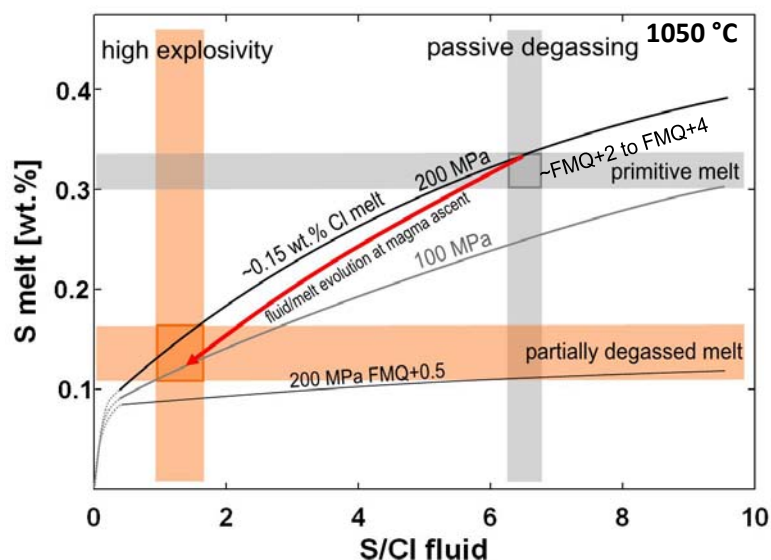
Fig.1: Evolution of fluid and melt composition during magma ascent. Natural melts contain rel. constant 0.15 wt.% Cl.

Reference:

Aiuppa, A., Federico, C., Giudice, G., Gurrieri, S., Paonita, A., Valenza, M. (2004) Earth Planet. Sci. Lett. 222, 469-483.
Keppler, H. (2010) Geochim. Cosmochim. Acta 74, 645-660.

Preliminary estimates on pre-eruptive magma conditions at the Heise volcanic field, Snake River Plain, Idaho, western USA

Torsten Bolte[1], Martin Erdmann[1], Alexander Sehlke[1], Barbara Nash[2], Renat Almeev[1] and Francois Holtz[1]
[1]Leibniz-Universität Hannover, Institute for Mineralogy, Hannover, Germany
[2]Department of Geology and Geophysics, University of Utah, Salt Lake City, USA

The Snake River Plane Yellowstone Hotspot volcanic province (SRPY) elongates from the border triangle of Oregon, Nevada and Idaho in northeast direction through the northwest of the USA to the Yellowstone plateau at the border between Wyoming and Idaho. It is widely accepted that during the last 15 Ma, North American plate moved more than 600 km in west-southwest direction over the Yellowstone hotspot and induced a bimodal (rhyolitic – basaltic) magmatism (Morgan and McIntosh, 2005). This volcanism partly produced large volume eruptions of high-silica rhyolites with ash fall tuffs and ignimbrites in a large geographic area. These well-preserved and stratigraphically good correlated outcrops provide unique information for continued studies on the magma dynamics and evolution of thermodynamic conditions in rhyolitic reservoirs prior to climatic eruptions.

There are six large eruptive centers located in the Snake River Plane along the hotspot track: Owyhee Humboldt volcanic field (15.2 – 12. Ma): Bruneau Jarbidge volcanic field (12.7 – 10.5 Ma); Twin Falls volcanic field (10.5 – 8.5 Ma); Picabo volcanic field (8.5 – 7.0 Ma); Heise volcanic field (7.0 – 3.5 Ma) and Yellowstone Plateau volcanic field (2.5 - 0Ma) (Perkins and Nash, 2002)

The major goal of our investigations is to estimate pre-eruptive-conditions of the rhyolitic magmas from several well-documented eruptive centers (Bruneau-Jarbidge, Heise and Yellowstone) and to perform a systematic analysis with providing new geochemical and experimental information on the dynamics of rhyolitic reservoirs and evolution of magma-storage conditions and magma compositions in time and space. The rhyolites from Bruneau-Jarbidge eruptive center has been thoroughly investigated by Cathey and Nash (2004) who reported high pre-eruptive temperatures and low water concentrations to explain observed mineral compositions in natural rhyolites. These conclusions are supported by the experimental determination of phase relations in two Bruneau-Jarbidge rhyolites (200 MPa, various water activities and oxygen fugacities). These experimental data can be further used to bracket the crystallization conditions for rhyolitic magmas from other eruptive centers.

In this study we present first results on mineralogical compositions, mineral thermometry as well as preliminary estimates of pre-eruptive conditions for the rhyolites from younger Heise (~6-4Ma) and Yellowstone (~2Ma) eruptive centers in comparison to older Bruneau-Jarbidge rhyolites. We investigated five rhyolitic ignimbrites and tuffs from the three representative stratigraphic units of the Heise volcanic complex as well as one rhyolitic sample from the Huckleberry Ridge Tuff, representing the initiation of the Yellowstone volcanic center. We performed petrographic descriptions and microprobe analyses of the minerals and glass shards. Temperature estimations have been obtained using pyroxene and oxide thermometry (QUILF, Anderson, 1993). Oxide thermooxybarometer was also used for estimations of redox conditions. The water activities of the natural rhyolitic melts were roughly estimated by comparing glass shard compositions with eutectic compositions and phase equilibria obtained for the ternary Qz – Ab – Or system. Our preliminary results show that the Heise and Yellowstone glasses are scattered between 500 and 100 MPa cotectic lines. The Ab/Or ratio of the natural glasses indicates that their compositions are close to eutectic or minimum compositions for very low water activities (aH$_2$O < 0.25). Pyroxene thermometry results obtained using QUILF equilibria yield pre-eruptive temperatures of 818 to 830 °C for Heise, and 905 to 925 °C for Yellowstone magmas. These temperatures are lower than those obtained for Bruneau-Jarbidge rhyolites (905 to 980 °C).

The preliminary results confirm that pre-eruptive temperatures tend to decrease with time (From BJ to Heise). Concomitantly, the glass compositions indicate that water activity tends to increase with time. The high temperatures obtained for Huckleberry Ridge Tuff pyroxenes need to be examined in detail because they may indicate that at least during the initial phase of Yellowstone temperatures were high.

References:
Anderson, D. (1993), QUILF: A Pascal program to assess equilibria among Fe-Mg-Mn-Ti oxides, pyroxenes, olivine and quartz, Computers & Geosciences, 19 (9), 1333 – 1350.

Cathey, H. & Nash, B. (2004), The Cougar Point Tuff: Implications for Thermochemical Zonation and Longevity of High Temperature, Large Volume silicic Magmas of the Miocene Yellowstone Hotspot, Journal of Petrology, 45, 27 – 58.

Holtz F., Pichavant M., Barbey P., Johannes W. (1992) Effects of H_2O on liquidus phase relations in the haplogranite system at 2 and 5 kbar. Am Mineral, 77, 1223-1241

Johannes, W. & Holtz, F. (1992), Petrogenesis and Experimental Petrology of Granitic Rocks, Minerals and Rocks, 22, 335 pp

Morgan, L.A. & McIntosh, W.C. (2005), Timing and development of the Heise volcanic field, Snake River Plain, Idaho, western USA. GSA Bulletin, 117 (3/4), 288-306.

Parat, F. & Holtz, F. (2005), Sulfur partition coefficient between apatite and rhyolite: the role of bulk S content, Contrib. Mineral petrol, 150, 643-651.

Perkins, M. & Nash, B. (2002), Explosive silicic volcanism of the Yellowstone Hotspot: The ash fall tuff record. GSA Bulletin, 114 (3), 367-381.

P11-03

Partitioning of highly siderophile elements between oxides and sulphides in anorthosites of the Mesoproterozoic Kunene Intrusive Complex, NW Namibia

Philipp Gleißner[1], Kirsten Drüppel[1], Harry Becker[2]
[1]Technische Universität Berlin, Institut für Angewandte Geowissenschaften, Berlin, Germany
[2]Freie Universität Berlin, Institut für Geologische Wissenschaften, Berlin, Germany

Highly siderophile elements (HSE) are commonly enriched in metals and sulphides. In absence of those phases their solubility and partitioning behavior in both oxides and silicates are believed to govern the geochemistry of the HSE in magmatic systems (e.g. Shirey and Walker, 1998). However, relatively few HSE data have been published for natural oxide minerals like magnetite and ilmenite. Some previous studies of natural samples indicate that magnetite is an important host of Re in mafic to silicic magmatic rocks, (e.g. Righter et al., 1998).

Ilmenite and magnetite are the dominant oxide minerals in massif-type anorthosites of the Mesoproterozoic Kunene Intrusive Complex, Namibia, and are present in major proportions in associated Fe-Ti ore deposits. The anorthosites and related rocks experienced no metamorphic overprint after their emplacement and hence allow a direct study of the igneous processes active during their formation (Drüppel et al., 2007). New highly siderophile element data of mineral separates together with bulk anorthosites and Fe-Ti ore of the Kunene Intrusive Complex shed new light on the factors controlling their fractionation in mafic magmas and during post-magmatic reequilibartion of Fe-Ti oxides.

The bulk anorthosites and Fe-Ti ore samples as well as separated magnetite, ilmenite, Al-spinel and pyrite were digested together with spike solution in quartz digestion vessels in a high-pressure asher. Osmium was separated by solvent extraction and micro-destillation followed by negative thermal ion mass spectrometry. Rhenium, Ir, Ru, Pt, Rh, Pd and Au were separated by cation exchange chromatography and measured via sector-field inductively coupled plasma mass spectromtry. In order to recover Rh and Au, a combined internal-external standardization technique modified from the method described in Fischer-Gödde et al. (2010) was used.

Oxide mineral separates from anorthosites and Fe-Ti ore display concentrations of Os, Ir and Ru in the same range like those of the corresponding bulk rocks, but are generally higher in Pt and Re. The overall abundance of Re in the bulk rocks is correlated with Fe, which in turn reflects the modal proportion of oxides and hence suggests compatibility of Re in the oxides. The abundance of highly siderophile elements in the Fe-Ti oxides has been significantly altered by redistribution during subsolidus reequilibration. In all samples magnetite displays higher Ir, Pd and Re than ilmenite, whereas ilmenite displays higher Pt and Au contents. Pyrite is a minor constituent in one leucogabbronorite sample and yields two orders of magnitude higher HSE concentrations than the associated oxides. Al-Spinel is a minor constituent of the Fe-Ti ores and displays strong enrichment in Ru and Rh. In general, the Re/Os ratios increase in the order spinel < ilmenite < magnetite < pyrite. From our data it can be concluded that Re behaved as a compatible element during fractional crystallization of Fe-Ti oxide phases like titanomagnetite. This process was presumably responsible for high Re concentrations and Re/Os ratios in the Fe-Ti ores associated with the anorthosites. Ilmenite and Al-spinel, exolved from titanomagnetite during later subsolidus reequilibration preferentially incorporated Pt and Au, and Ru and Rh, repetively.

References:
Drüppel, K., Littmann, S., Romer, R.L. & Okrusch, M. (2007). Petrology and isotope geochemistry of the Mesoproterozoic anorthosite and related rocks of the Kunene Intrusive Complex, NW Namibia. Precambrian Research 156, 1-31.
Fischer-Gödde, M., Becker, H. & Wombacher, F. (2010). Rhodium, gold and other highly siderophile element abundances in chondritic meteorites. Geochimica et Cosmochimica Acta 74, 356-379.
Righter, K., Chesley, J.T., Geist, D. & Ruiz, J. (1998). Behavior of Re during magma fractionation: an example from Volcán Alcedo, Galápagos. Journal of Petrology 39, 785-795.
Shirey, S.B. & Walker, R.J. (1998). The Re-Os isotope system in cosmochemistry and high-temperature geochemistry. Annual Review of Earth and Planetary Sciences 26, 423–500.

P11-04

Model-enhanced Geothermobarometry of mafic dikes of the Henties Bay Outjo dike swarm, Etendeka Igneous Province, Namibia

Oliver Frei[1], Axel Renno[1], Robert Trumbull[2]
[1]Technische Universität Bergakademie Freiberg, Institute of Mineralogy, Freiberg, Germany
[2]Deutsches GeoForschungsZentrum GFZ, Potsdam, Germany

The Henties Bay – Outjo dike swarm is one of the largest Mesozoic dike swarms along the western coast of southern Africa. It represents magmatic remnants of the Cretaceous opening of the South Atlantic during Gondwana breakup. At least parts of the dikes are interpreted to have functioned as feeder channels for Etendeka lavas. The dike swarm is situated in the Damara belt between the Kalahari and Congo Shield and extends about 400 km inland, more or less perpendicular to the coastline (Trumbull et al. 2004; 2007).

Although the dikes cover a complete tholeiitic differentiation trend from picritic, basaltic to andesitic and more felsic composition, the most prominent rock type is a basaltic dolerite, comprising plagioclase, clinopyroxene, olivine and Fe-Ti oxides. The texture is intergranular to subophitic. Rudimentary quenching features are visible, such as plagioclase glomerophyres. Chromian spinel occurs rarely. However, if it is present, then very abundant and often hosted in olivine crystals. In addition to an oscillatory zoned plagioclase microphenocryst generation, olivine crystals partly resemble a cumulate texture and therefore appear to be formed before the dike emplacement as well.

Comparing the olivine and whole rock Mg content clearly indicates that most of the olivines are too low in Mg to have crystallized from melts with the composition of the host rocks. In other words, the rocks are too rich in magnesium to be in equilibrium with the olivine phenocrysts, which we attribute to olivine accumulation. This has severe implications for magma classification and for geochemical or geothermometric interpretations since the whole rock compositions do not equal the melt composition. In particular, the mere Mg-rich character of the picritic samples does not qualify them as near-primary magmas. This is further supported by the plagioclase microphenocrysts, proving crustal fractionation.

To better understand the magmatic history of these samples a combination of forward and inverse modeling was used, with focus on the Mg-rich dikes. First, model melt compositions have been calculated by subtraction of olivine until equilibrium between olivine crystals and bulk composition was achieved. Since the olivine population shows a range of forsterite contents, a set of melt-olivine pairs for each sample was calculated and using these, a range of olivine-melt equilibrium temperatures were calculated. According to this, the observed olivines crystallized from magmas with up to 11.5 % MgO at temperatures from about 1000 to 1280 °C. Since olivine appears to be the liquidus phase in the rocks, the crystallization depth is less than about 30 km, or to 8 kbar (based on phase relations for dry tholeiitic basalt). Forward modeling using the COMAGMAT program (Ariskin et al., 1993) tested fractional crystallization at different pressure scenarios until the predicted mineralogy fit best the observations. These models confirm fractionation and crystallization in the upper crust. Despite the petrographic indication of olivine as the liquidus phase, the Ca-Mg variations of the magmas suggest either non- peridotitic origin or early fractionation of clinopyroxene, which is, however, not recorded in the rocks. Trace element modeling is planned to further constrain crystallization processes, especially with respect to possible involvement of clinopyroxene.

References:
Ariskin, A.A. et al. (1993) COMAGMAT: A Fortran program to model magma differentiation processes, Computers and Geosciences, 19, 1155-1170.
Trumbull, R.B., et al.(2004) Aeromagnetic mapping and reconnaissance geochemistry of the Early Cretaceous Henties Bay-Outjo mafic dike swarm, Etendeka Igneous Province, Namibia, Journal of African Earth Sciences, 40, 17-29.
Trumbull, R.B. et al., (2007). Magmatism and continental breakup at the west margin of southern Africa: A geochemical comparison of dolerite dikes from NW Namibia and the Western Cape, South African Journal of Geology, 110, 477-502.

TEM-analyses of nanocrystals in obsidian

Jens Kirste[1], Nora Schulze[1], Gerald Wagner,[1] Gert Kloess[1]
[1]University of Leipzig, Institute for Mineralogy, Cristallography and Material Science, Leipzig, Germany

TEM-analyses of nanocrystals in obsidians lead to a number of unexpected results. Using a Philips CM 200 HRTEM we combined bright field (BF) and dark field (DF)-imaging, Nano-EDX and SAED (Selected Area Electron Diffraction).
We found:

1) The average chemical compositions determined by TEM-EDX on the one hand and XRF on the other hand show a perfect match.
2) According to susceptibility the predominating mineral phases are hematite nanocrystals and magnetite microrcrystals. But in some cases the measurements showed exceptional compositions like wuestite or Al-bearing hematite. Additionally we found a phase of so far unknown structure and composition in the obsidian.
3) Contrary to the expected process of devitrification we observed evidences for decrystallisation, especially at albite-like feldspars and hematites. The process of decrystallisation is accompanied with a decolourization of the red-brown obsidian.

The process of decrystallization is displayed amongst others by the dissolution of hematite (Fig. 1). For a better illustration the chemical composition of the measured hematite is given in Table 1.

Fig.1: TEM-image of an affected crystal of hematite in a glassy matrix of obsidian from Büyük Yayla
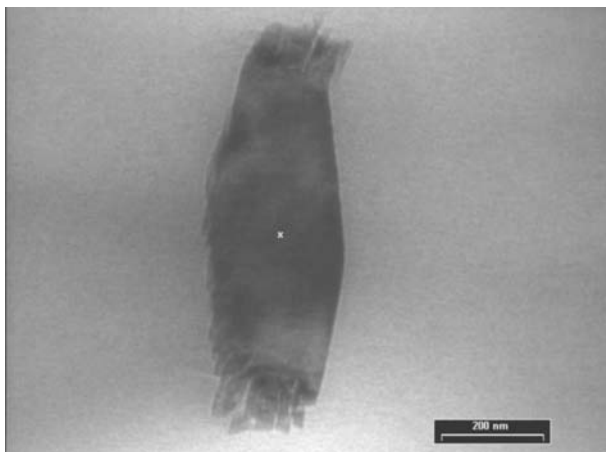
Table 1: Chemical composition of hematite (Al-bearing)

Element	wt-%	at-%
O	30.01	59.40
Al	1.20	1.40
Si	0.60	0.70
Mn	0.90	0.50
Fe	67.20	38.00

Additionally one can observe crystals of wuestite in the vitreous matrix. The EDX-measurements processed by HRTEM are supported by the comparison of the measured and calculated diffraction patterns. Determined patterns are given in Fig. 2.

Fig.2: TEM-image of wuestite with diffraction patterns, viewing direction [111]
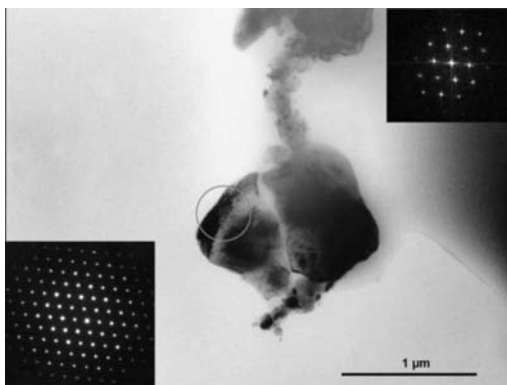
Table 2: Chemical composition of wuestite in point 1 & 2

Element	wt-%	at-%
	Point 1	
O	23.70	51.20
Mg	1.10	1.60
Al	0.40	0.60
Si	0.50	0.60
Mn	1.10	0.70
Fe	73.20	45.40
	Point 2	
O	23.40	50.80
Mg	1.10	1.50
Al	0.50	0.60
Si	0.40	0.40
Mn	0.90	0.60
Fe	73.80	46.00

Supercritical H$_2$O-SiO$_2$ fluid studied by ab initio molecular dynamics

Georg Spiekermann[1,2], Sandro Jahn[1]
[1]GFZ German Research Centre for Geosciences, Telegrafenberg, 14473 Potsdam, Germany
[2]spiek@gfz-potsdam.de

Fluids in high-grade metamorphism or wet partial melting above subducted slabs could possibly be in supercritical state where a distinction between (hydrous) fluid and silicate melt is no longer possible. As recently confirmed by Newton and Manning (2008), for SiO$_2$-H$_2$O there is complete miscibility of silicate melt and hydrous fluid beyond 1 GPa and 1080 °C. This being established for the simplified analogue system of hydrous rhyolite melt, the *P-T*-conditions of the upper critical end point may vary quite strongly on changing melt compositions towards geologically more relevant systems, see e. g. Stalder et al. (2000) or Mysen (2009).

We are interested in the molecular structure and dynamics of hydrous silicate melt and their changes with increasing *P-T*-conditions across and above the immiscibility region. Since experimental approaches require in situ measurements and are technically very challenging, we employ molecular modelling to address this issue.

There are several experimental studies on the speciation of SiO$_2$ in H$_2$O fluid at high *P* and *T*. At low SiO$_2$ concentrations several studies predict Si(OH)$_4$-monomers and corner-sharing dimers to be the most abundant speciation. Already at a around 20mol% SiO$_2$ (45wt% SiO$_2$) there is a steep increase of polymerization (Newton & Manning 2008) to larger polymers. At further rise in SiO$_2$-content a network is formed. Earlier molecular dynamics studies focussed on either silicate speciation in water (Doltsinis et al. 2007) or hydrous silicate melt with 3.8wt% H$_2$O (Pöhlmann et al. 2004) and 8.25wt% H$_2$O (Karki & Stixrude 2010).

We focus here on an intermediate composition with 23wt% (50mol%) H$_2$O and study a system of 32 H$_2$O and 32 SiO$_2$ molecules as a function of pressure up to about 5.5 GPa and temperature between 2400 K and 3000 K. These high temperatures are a concession to today's computing power. At our level of precision it allows only a time span of dozens of picoseconds to be modelled. The molecular dynamics has to be fast enough to reach equilibration in such a short time span. We need to use extrapolation for lower temperatures.

In nature this intermediate composition is restricted to very narrow conditions by both the shape of the wet solidus and the excess amount of silicate in natural systems. But its intermediate character enforces maximal interaction between H$_2$O and the hydroxylated SiO$_2$ loose network and is therefore suitable for studying the exchange dynamics between these two subsystems. We find the structure of the single-phase fluid to be dominated by hydroxyl groups in coexistence with some free H$_2$O molecules. The number of H$_2$O molecules increases upon cooling of the system. The polymerization of the SiO$_2$ network consequently increases and is at all conditions found to consist of mainly Q^2 and Q^3 species. Q^1 and Q^4 species are observed in minor amounts.

References:
Doltsinis, N. L., Burchard, M., Maresch, W. V., Boese, A. D. & Fockenberg, T. (2007), Ab initio molecular dynamics study of dissolved SiO$_2$ in supercritical water, Journal of Theoretical and Computational Chemistry 6, 49-62
Karki, B. B. & Stixrude, L. (2010), First-principles study of enhancement of transport properties of silica melt by water, Physical Review Letters 104, 215901
Mysen, B. O. (2009), Solution mechanisms of silicate in aqueous fluid and H$_2$O in coexisting silicate melts determined in-situ at high pressure and high temperature, Geochimica et Cosmochimica Acta 73, 5748-5763
Newton, R. C. & Manning, C. E. (2007), Thermodynamics of SiO$_2$-H$_2$O fluid near the upper critical end point from quartz solubility measurements at 10 kbar, Earth and Planetary Science Letters 274, 241-249
Pöhlmann, M., Benoit, M. & Kob, W. (2004), First-principles molecular-dynamics simulations of a hydrous silica melt: Structural properties and hydrogen diffusion mechanism, Physical Review B 70, 184209
Stalder, R., Ulmer, P., Thompson, A. B. & Günther, D. (2000), Experimental approach to constrain second critical end points in fluid/silicate systems: Near-solidus fluids and melts in the system albite-H$_2$O, American Mineralogist 85, 68-77

Section 12

———————

Metamorphic processes

P12-01

Formation of Spinel-cordierite-plagioclase symplectites replacing andalusite in metapelitic of the Alvand aureole, Iran

Adel Saki

Department of Geology, Shahid Chamran University of Ahvaz, Iran

Spinel-cordierite-plagioclase symplectites partially replacing andalusite occur in the metapelitic migmatite rocks of Alvand aureole within Sanandaj-Sirjan metamorphic belt, Hamadan, Iran. The presence of melt shows that corona development occurred under partial melting conditions. Spinel is predicted to grow with cordierite at around 700 °C. Exhaustion of the available SiO_2 and ∕ or separation of sillimanite/Andalusite from SiO_2-rich matrix domains by cordierite resulted in the formation of localized low-silica activity domains and thus triggered the growth of spinel in the rime of andalusite, therefore suggests the reaction Sil/And + Bt = Crd + Sp l+ Kfs + melt, as the most reaction for the development of coronas in the metapelitic of Alvand aureole. The P–T diagram and inferred paths do not account for the decompression history of the terrane. The breakdown of garnet to plagioclase + sillimanite, dehydration melting and the formation of spinel-plagioclase symplectite could occur during decompression or heating; these textures are limited to the contact aureole in the studied area, so heating is perhaps the more likely explanation for formation of the symplectites in the metapelitic of Alvand aureole.

The microstructural and thermobarometric(Major element compositions of biotite, garnet, spinel, plagioclase, cordirite and ilminite in selected sample were determined by wavelength-dispersive spectrometry using a Cameca SX100 microprobe) study of this work enabled us to make some conclusions regarding the spinel-cordierite-plagioclase symplectites replacing andalusite in the Hamadan pelites in the Alvand aureole:

1. The presence of melt shows that spinel-cordierite-plagioclase symplectites replacing andalusite development occurred under partial melting conditions.
2. Estimates of the temperature (700 ºC) and pressure (~2-4 kbar) for the peak metamorphism show that it has occurred under LP/HT condition, the geothermal gradient obtained for the peak metamorphism is 58 °C km-1, which is in the upper range of contact aureole values.
3. The presence of melt shows that corona development occurred under partial melting conditions.
4. Reaction Sil/And + Bt = Crd + Sp l+ Kfs + melt, is the most reaction for the development of coronas in the metapelitic of Alvand aureole.
5. The P–T diagram and inferred paths do not account for the decompression history of the terrane, so breakdown of garnet to plagioclase + sillimanite, dehydration melting and the formation of spinel-plagioclase symplectite are limited to the contact aureole, therefore heating is perhaps the more likely explanation for formation of the symplectites in the metapelitic of Alvand aureole.

Growth and breakdown of corundum in layered mafic complexes of the Palghat Cauvery Shear Zone, South India

Michael M. Raith[2], Pulak Sengupta[1], Beate Spiering[2], C. Srikantappa[3]
[1]Department of Geological Sciences, Jadavpur University, Kolkata 700 032, India
[2]Steinmann Institut, Universität Bonn, 53115 Bonn, Germany
[3]Department of Geology, Manasagangotri, University of Mysore, Mysore 570 006, India

Corundum-bearing layers of late-Archaean mafic-anorthositic complexes of the Palghat Cauvery Shear Zone, southern India preserve evidence of a polyphase metamorphic evolution: an early-Paleoproterozoic HP-metamorphic stage and hydrous alteration stages related to Neo-Proterozoic reworking of the area.

At the two localities studied (Manavadi and Ayyarmalai), corundum-bearing layers are likely to have formed from infiltration-driven HP-metamorphism of a precursor 'troctolitic' mineralogy with stabilization of the coarse-grained assemblage pargasite (Prg_1: X_{Mg}=0.64, $Al^{[4]}$ 2.0-1.78, X_K^A~0.2) + anorthite (Pl_1: An_{90}) + corundum (Crn_1: <0.15 wt% Cr_2O_3). The tabular corundum crystals, up to 3 cm in diameter, commonly overgrow the granoblastic Pl_1+Prg_1 fabric in random orientation, but locally also occur in parallel alignment to the foliation, indicating either a syn-kinematic development of the Prg_1+Pl_1+Crn_1 assemblage or a phase of post-growth deformation followed by chemical and textural equilibration at static conditions in the *P-T* stability field of the assemblage. From pseudosection modelling we infer Crn_1 to have formed through completion of the reaction Spl + Pl + Fluid → Prg_1 + Crn_1 at ca. 750-800°C and >10 kbar. A conspicuous feature of the rocks is the partial to complete replacement of porphyroblastic corundum by composite coronae of spinel (Spl_2: X_{Mg}=0.50-0.70; next to Crn_1) and anorthite (Pl_2: An_{97-99}; next to Prg_1) which suggest that the pair Crn_1–Prg_1 became unstable by the reaction Prg_1 + Crn_1 → Spl_2 + Pl_2 + Fluid.

During the hydrous alteration stage(s) the Crn_1-Spl_2-Pl_2 domains developed diverse reaction textures, either through reaction with residual fluids or, more likely, related to fluid-infiltration from nearby late-Neoproterozoic granite intrusions, that document: (1) Formation of högbomite (Hgb), commonly by topotactic replacement of spinel [$(0001)^{Hgb}$//$(111)^{Spl}$], and accompanied by development of magnetite (Mt) on Crn_1. Hgb is strongly zoned, with Ti-content decreasing and X_{Mg} ($Mg/(Mg+Fe^{2+})$) increasing from the Mt-Crn_1 interfaces (~7.8 wt% TiO_2, X_{Mg}~0.55) towards spinel (~3.0 wt% TiO_2, X_{Mg}~0.70). Hgb lamellae progressing along $(111)^{Spl}$ into spinel are lowest in Ti (0.8-0.5 wt% TiO_2, X_{Mg}~0.88). (2) Decomposition of Hgb to fine graphic intergrowths of magnetite (Mt_2) and rutile. (3) Partial replacement of Spl_1 by intergrown corundum (Crn_2) and magnetite (Mt_2). (4) Partial resorption of Crn_1 by margarite. (5) Replacement of Pl_2 proceeding from Spl_2 interfaces by domains of clinozoisite (X_{Fe3+}=0.09-0.15) + margarite + chlorite (X_{Mg}~0.86) ± relict anorthite that are rimmed by an aggregate of muscovite + chlorite (X_{Mg}~0.45) + clinozoisite (X_{Fe3+}=0.15).

Interpreting the reaction textures in *P(T)*- $_{H2O}$ and isothermal-isobaric $_{H2O}$- $_{O2}$ diagrams it is suggested that: (1) the retrograde reactions 1-5 set in at 8 ± 1 kbar, 700 ± 50°C and progressed further to lower *P-T* conditions; (2) Composition of the substrate minerals and strong gradients of chemical potentials of O_2 and H_2O were instrumental in the formation and breakdown of Hgb in millimetre size domains. These findings, in agreement with Sengupta et al. (2009) and Raith et al. (2010), do not support ultra-high temperature conditions of Pan-African metamorphism in the PCSZ as has been suggested in recent studies (e.g. Tsunogae et al., 2008).

References:
Raith, M.M., Sengupta, P., Kooijman, E., Upadhyay, D. & Srikantappa C. (2010). Corundum–leucosome-bearing aluminous gneiss from Ayyarmalai, Southern Granulite Terrain, India: A textbook example of vapor phase-absent muscovite-melting in silica-undersaturated aluminous rocks. American Mineralogist, in press.
Sengupta, P., Dutta, U., Bhui, U.K. & Mukhopadhyay, D. (2009). Genesis of wollastonite- and grandite-rich skarns in a suite of marble-calc-silicate rocks from Sittampundi, Tamil Nadu: constraints on the *P-T*–fluid regime in parts of the Pan-African mobile belt of South India. Mineralogy and Petrology, 95, 179–200.
Tsunogae, T., Santosh, M., Ohyama, H. & Sato, K. (2008). High-pressure and ultrahigh temperature meta-morphism at Komateri, northern Madurai Block, southern India. Journal of Asian Earth Sciences, 33, 395–413.

Origin of the ophiolite-related Al-(Mg) metamorphites – case study of sapphirine and corundum amphibolites from the Central Dinaridic Ophiolite Zone (CDOB, NE Bosnia and Herzegovina)

Branimir Šegvić[1], Rainer Altherr[2]
[1]Darmstadt University of Technology, Institute of Applied Geosciences, Technical Petrology, Darmstadt, Germany, *bsegvic@geo.tu-darmstadt.de*
[2]Heidelberg University, Institute of Earth Sciences, Heidelberg, Germany

Two rare amphibolite parageneses consisting of Am, Pl, Spr, and Spl (paragenesis 1), and Am, Pl, Crn, and Spl (paragenesis 2) were reported within the suite of metamorphic sole rocks that are associated to the Krivaja-Konjuh ophiolite complex (KKOC) in NE Bosnia and Herzegovina. It is the biggest Tethyan ophiolite complex of the CDOB, hosting diverse metamorphic rocks from greenschist to granulite and eclogite facies. These rocks are found in forms of separated zones of up to 10 km long and several hundred metres in width (Operta, 2004; Šegvić, 2010). The sapphirine and corundum rich amphibolites present a small portion of the KKOC metamorphites, dominated by the porphyroblastic Grt-Di and Grt-Di-Hy amphibolites as well as Di-Hbl and Pl-Grt-Di gneisses. In this study, we put an accent to the protolith ambiguities and an amphibolite formation mechanism, since the occurrence of sapphirine and corundum amphibolites is relatively rare, often being explained by a material exchange of the Al-rich rocks and ultrabasic rocks (e.g. Nicollet, 1986).

Sapphirine amphibolite is featured by granoblastic to poikiloblastic, partly preserved relict ophitic texture, defined by coarse-grained amphibole (~0.25 mm). Often, blasts of Cr-spinel are rimmed with a corona composed of sapphirine and Al-rich spinel. Corundum amphibolite is characterised by medium-size amphibole and corundum blasts (~0.15 mm), defining the rock's granoblastic to porphyroblastic texture. Textural characteristics, primarily marked by coarse euhedral pargasite crystalloblasts devoid of subgrain development and tapered mechanical twinning of basic plagioclase (~81.3 An) are usually considered to indicate the high temperature metamorphic conditions.

The TAS diagram classifies the analysed rocks as basalts implying their tholeiitic affinity. They are silica-undersaturated (~40 wt%), rich in Al_2O_3 (~17-27 wt%) and MgO (>10 wt%), and low in TiO_2 (0.06-0.09 wt%). Generally, their REE normalisation patterns are MORB-like, having significantly lower compositional levels (0.4-2 x chondrite). Elevated Mg# (~87), high abundances of incompatible trace elements (35-153 ppm Ni, 30-63 ppm Co, 41-57 ppm V), low abundances of high field strength elements (HFSE), coupled with low light rare earth elements concentration (LILE) suggest that the protolith of the analysed metamorphites must have been an igneous cumulate, most probably of troctolitic origin rather than crystallised from the 'normal' tholeiitic melts. Phase chemistry characteristics, like high Al_2O_3 and K_2O contents in amphibole (~17 and 0.69 wt%), corroborate an extreme heat influx having affected the protolith.

Geothermobarometric calculations (sapphirine-spinel and amphibole-plagioclase pairs) provided peak metamorphic conditions of 0.90-1.10 GPa and ~880 °C. A *P-T-t* clockwise path is inferred. Comparing the petrological implications with the actual geotectonic models of the Dinaric Tethyan oceanic evolution in the Jurassic/Cretaceous period, the analysed metamorphic rocks are considered to represent a pile of a meta-cumulate sequence that experienced a HT-MP metamorphism as a metamorphic sole associated to near-ridge thrusting processes. As well, there are strong indications suggesting that during metamorphosis some of the mantle material was assimilated. It is evidenced in the preservation of igneous Cr-spinel in sapphirine and amphibole, along with a formation of calcite 'blebs' in amphibole. A sapphirine blastosis is linked to spinel destabilization induced by a change of chemical potentials.

References:
Nicollet, C (1986), Saphirine et staurotide riche en magnésium et chrome dans les amphibolites et anorthosites ŕ corindon du Vohibory Sud, Madagascar, Bull.Minéral. 109, 599-612
Operta, M. (2004), Mineraloške i petrografske karakteristike amfibolita iz okolice Vareša, PhD thesis, Tuzla University (Bosnia and Herzegovina), 243 p
Šegvić, B. (2010), Petrologic and geochemical characteristics of the Krivaja-Konjuh ophiolite complex (NE Bosnia) - petrogenesis and regional geodynamic implications, PhD thesis, Heidelberg University, 301 p

Mineralogisch-erzpetrographische Untersuchung der goethitischen Eisenerze von Trypa-Arolithi, Rethymno (Kreta)

G. Alevizos
Technical University of Crete, Mineral Resources Engineering Dept., Chania, Greece

Eisenerzvorkommen befinden sich in vielen Regionen West-Kretas, einige von denen wurden zuzeiten abgebaut. Sie treten innerhalb der Phyllit-Quarzit-Serie (PQS) auf, die als eine der tektonischen Einheiten der Phyllit-Decke Kretas betrachtet wird. Die PQS wird der unteren Teildecke der Phyllit-Decke Kretas zugeordnet, die zwischen der Plattenkalk-Serie im Liegenden und Tripolitza-Serie im Hangenden eingeschaltet ist. Die PQS enthält meist Phyllite und Quarzite, sowie Metakonglomerate, Marmore, Kalkphyllite und Metabasalte. Die Serie ist durch eine hochmarine Conodontenfauna gekennzeichnet, die eine stratigraphische Reichweite von Oberkarbon bis Untertrias nachweist.

Das untersuchte Vorkommen von Trypa liegt 30 km süd-westlich von Rethymno in der Nähe des Ortes Arolithi. Das Eisenerz, meist poröser Goethit, kommt in Form von Linsen in einer Kontaktzone zwischen Phylliten und Quarziten der Hochdruck/Tieftemperatur metamorphen PQS vor. Die mineralogische Bestandteile sowie die Gefüge der Eisenerze wurden mittels Erzmikroskopie, SEM und Röntgendiffraktometrie ermittelt. Zur Bestimmung des Chemismus der einzelnen Proben wurde die RFA angewendet.

Innerhalb der Kontaktzone sind die Phyllite und Quarzite intensiv zerrüttet und brecciert. Diese Gesteine sind stark von Goethit imprägniert und werden durch eine gelbe bis rötliche Farbe charakterisiert. Der Goethit ist pulverig und porös tritt aber auch in Form von harten Krusten auf. Der Stoffbestand der Eisenerze setzt sich überwiegend aus Goethit und Quarz zusammen. Untergeordnet treten Hämatit, Chlorit, Muskovit, Paragonit und seltener Pyrit, Kryptomelan und Rutil auf. Die Quarzkristalle sind allotriomorph ausgebildet und durch tektonische Vorgänge kataklastisch zerteilt. Kompakte Goethitvererzung epigenetischen Ursprungs entwickelt sich zwischen den Quarzkörnern und verdrängt das Bindemittel des Quarzits, oft in zwei verschiedenen Entwicklungsphasen. Goethit erscheint auch als strahlige kolloidale Ausfällung in Spalten und Hohlräumen und bildet oft rhythmisch, konzentrisch-schalige Texturen. Hämatit spielt in den Eisenerzen eine untergeordnete Rolle und ist meist sekundär durch Dehydratation des Goethits entstanden. Vereinzelt wurden kleine Pyritkristalle beobachtet, die zum Teil in Form von Pseudomorphosen nach Goethit vorliegen.

Anhand des erzmikroskopischen Befunds geht hervor, dass die Eisenvererzung der Wirtgesteine in zwei Stadien stattgefunden hat. Die Verdrängungen des schon vererzten Bindemittels sowie der vorhandenen Quarzkörner des Quarzits werden von eisenreichen Lösungen einer zweiten Generation hervorgerufen, die das Gestein durch massive Vereisenung umgestalten. Die goethitische Eisenerze werden mit einer Eisensulfidmineralisation geringen Ausmaßes, die unmittelbar am Ort Arolithi auftritt, genetisch verknüpft. Dies gibt Anlass zur Vermutung, dass der Abbau der Eisensulfide eine sekundäre Eisenmobilisation bewirkt hat, die den Quarzit deszendent durchsetzt.

Traces of free gold and silver within ferruginous stockworks of the Phyllite-Quartzite-Unit of West Crete, Greece.

Th. Markopoulos, E. Manutsoglu, G. Alevizos, E. Repouskou.
Technical University of Crete, Department of Mineral Resources Engineering, Chania, Greece

The island of Crete is located north of the Hellenic trench. The geological framework consists largely of nappes of contrasting lithologies and metamorphism that were stacked southwards during an Oligocene to early Miocene N-S compression. Most of the whole nappe stack of continental Greece is recognized in Crete. The Plattenkalk Unit represents the lowermost known tectonic unit beneath the nappe pile of Crete. Their formation has been involved in the tectonometamorphic process during the Oligocene-Miocene. The overlying Phyllite-Quarzite Nappe has been divided into four subunits by Dornsiepen & Manutsoglu (1994): Tyros Group, Variscan, Phyllite-Quarzite Group and Gypsum-Rauhwacke-Formation. The lithological monotonous Phyllite-Quartzite-Unit, the first definitely allochthonous unit of the island, is dominant in western Crete and contains primarily phyllites and quartzites as well as metaconglomerates, marbles, metabasalts and metatuffs.

Ferruginous stocworks occur in the Phyllite-Quartzite-Unit within cataclastic shear zones of diverse thickness varying from a couple of mm up to 50 cm, especially in contacts between quartzites, phyllites and marbles (Markopoulos et al, 2005). Samples of ferruginous materials from the Karanos area, located roughly 20 Km SW of the City of Chania, have been collected for mineralogical, chemical and petrological investigations, using reflected light microscopy, scanning electron microscopy, X-ray diffraction (XRD) and X-ray fluorescence analyses (XRF).

At least two different iron oxides and iron hydroxides generations have been recognized as result of deformations and tectonic stresses. Goethite, hematite, quartz, talc and muscovite, in varying proportions, dominate these ferruginous materials. Diaspore, calcite, lepidocrocite, pyrite and feldspar are accessory mineral phases. The manganese minerals cryptomelane and lithiophorite occur in minor amounts. Gold and silver have been detected via scanning electron microscope on hematitic and goethitic rich samples. Au and Ag appear in free forms of rounded particles about 1 µm in size.

The presence of Au and Ag particles in free form within ferruginous materials was detected for the first time in Crete. The presence of Au and Ag in the ferruginous stockwork formations in western Crete can be explained by the action of hydrothermal fluids. These hydrothermal fluids are connected with the volcanic activity during Perm-Triassic, which formed basalts, tuffs and sulfide deposits in western Crete. The simultaneous appearance of Au and Ag within the stockwork structures of the ferruginous materials will become the focus of further research.

References:
Dornsiepen, U. F.& Manutsoglu, E. (1994), Zur Gliederung der Phyllit-Decke Kretas und des Peloponnes. Z. dt. Geol. Ges. 145, S. 286-304.
Markopoulos, Th., Alevizos, G., Manutsoglu, E., Repouskou, E., (2005), Mineralogische und erzmikroskopische Untersuchung eisenvererzter Breccien aus der Karanouregion, West-Kreta, Griechenland. -Ber. Deutsch. Mineral. Ges., Beih. z. Eur. J. Mineral. Vol. 17, p. 86.

Mineralogical examination and mineral processing of the bauxitic Ni-laterite from Parhari area in Vermion (N.W. Greece)

F. Stathogianni, G. Alevizos
Technical University of Crete, Mineral Resources Engineering Dept., Chania, Greece

Notable occurrences of Ni-lateritic ore exist in the broader area of West Vermion and they are a subject of research by the LARCO Company, aiming at their future exploitation. The geological structure of Vermion is associated with units of the Pelagonian and Almopian geotectonic zones. These units include a series of metamorphic rocks of Triassic-Jurassic age, ophiolites, transgressed carbonate rocks of Middle Cretaceous - Lower Santonian age and flysch of Santonian age, which are located at the east margin of the Pelagonian zone. They are tectonically covered by ultrabasic and carbonate rocks of the Almopian zone. The Ni-lateritic ore formation is connected with the lateritization of ophiolites during Lower Jurassic-Upper Cretaceous. The bauxitic Ni-laterites develop on serpentinized peridotites and are located at Parhari area.

The aim of the present study is the mineralogical examination and the potential of mineral processing of the bauxitic Ni-lateritic ore deposit from Parhari area by physical methods. The ore consists mainly of hematite, gibbsite, diaspore, chromite, quartz, chlorite (clinochlore) and secondly of Ni-chlorite and illite. Hematite occurs in fine-crystalline form gradually replacing the matrix around grains. Also, it occurs in a compact form as the main component of peloids and ooids, the majority of which have undergone partial leaching of the hematitic component, due to alteration. In addition, clastic grains of chromite and quartz are scattered in the matrix, which consists of chlorite (clinochlore), Ni-chlorite, gibbsite, diaspore and partially of illite. The structure of the ore is generally allotriomorphic inequigranular and the texture is oolitic-pisolitic.

The physical methods for the mineral processing include heavy liquid and magnetic separation. Heavy liquid separation of the fraction (-8+4 mm) is satisfactory, as the highest amount of nickel is distributed to the sinks. The concentration of Ni in the (-4+1 mm) fraction is not satisfactory. Magnetic separation of the fraction (-8+4 mm) is satisfactory and nickel is distributed mainly to the concentrates. However there is also a small loss to the tailings, due to the incomplete liberation of nickel minerals. Along with the grain size decrease, the Ni-bearing phases are concentrated in the (-4+1 mm) fraction. The fraction (-1+0,250 mm) gave also satisfactory results concerning the mineral separation. Nickel is distributed mainly to the concentrates and reaches up to 0,70 %. However, a small amount of nickel is concentrated in the tailings, due to the incomplete liberation of nickel silicates even in small size fractions.

Generally, the separation was satisfactory for both mineral processes (heavy liquid and magnetic separation). On the other hand, the concentrates taken from the beneficiation did not yield satisfactory results, because the nickel content is lower than 1%. This is related to the ore textural characteristics and was predicted from the size fraction microscopic examination.

Deformation und Metamorphose in der Stora Le-Marstrand Formation Tjuvkil, Lökeberg (nördlich von Göteborg, SW Schweden)

Andy Allenberg[1], Christin Bieligk[2]
[1]Martin Luther Universität Halle-Wittenberg, Institute of Geosciences, Halle, Germany,
andy.allenberg@student.uni-halle.de
[2]Martin Luther Universität Halle-Wittenberg, Institute of Geosciences, Halle, Germany,
christin.bieligk@student.uni-halle.de

1. Einleitung
1.1 Regionale Geologie
Schweden ist Teil des Baltischen Schildes, dessen Entstehung auf progressives Krustenwachstum im Zeitraum zwischen 3,5 und 1,5 Ga zurückzuführen ist. Archaische und präkambrische Einheiten bilden dem zufolge die Basis des Baltischen Schildes. In diesem Zeitraum kam es zur Akkretion mehrerer Terranes aus südwestlicher Richtung. Dieser Vorgang wurde begleitet von Subduktionsprozessen sowie von drei dominanten orogenen Phasen. Dies ermöglicht die Untergliederung des Baltischen Schildes in verschiedene Provinzen.

1.2 Geologie des Untersuchungsgebietes
Das Untersuchungsgebiet ist Teil der Sveconorwegischen Provinz, welche zu den Großeinheiten Süd-Schwedens zählt. Durch die Akkretion mehrerer kleinerer Terranes aus westlicher Richtung kann diese Provinz in verschiedene N-S streichende Formationen unterteilt werden. Die Untersuchungen fanden in der Stora Le-Marstrand Formation statt. Diese erstreckt sich von den Inseln im Süden Göteborgs bis nördlich von Oslo in den Östfold-Marstrand Belt und ist vorwiegend durch das Auftreten von Metasedimenten gekennzeichnet. Das Alter dieser Gesteine liegt zwischen 1,66 und 1,58 Ga (BINGEN et al., 2001). Die Gesteine der Stora Le-Marstrand Formation sind mit mafischen Vulkaniten assoziiert und werden von intermediären bis felsischen intrusiven Körpern unterschiedlichen Alters durchschlagen.

2. Beobachtungen
Charakteristisch für diese Region ist das Auftreten der unterschiedlichen Lithologien in Form eines Scheibenbaus, hervorgerufen durch Scherprozesse, die mit orogenen Deformationsphasen in Verbindung gebracht werden können. Die Geländebeobachtungen sowie die Auswertung von Dünnschliffen belegen prograde als auch retrograde Entwicklungsphasen.

Die kartierten Einheiten zeigen im gesamten Gelände eine ausgeprägte Foliation, die in dieser Region dem Hauptdeformationsereignis zugeordnet werden kann. Die Gesteinskomplexe weisen lokal stark migmatisierte Bereiche auf, deren Neosomlagen parallel zur Hauptfoliation ausgebildet sind. Sie bestehen überwiegend aus Quarz und Feldspat. Eine weitere Deformationsphase wird hauptsächlich durch Bewegungs- und Streckungslineare repräsentiert. Diese wird im Gelände ebenso durch Krenulation sowie durch die Ausbildung ptygmatischer Falten wiedergegeben.

In den angefertigten Dünnschliffen konnten reliktische Granate, zwei unterschiedliche Generationen von Biotit, sowie poikilitisch überprägende Pyroxene erkannt werden. Außerdem konnten rekristallisierte Quarze, Pseudomorphosen von Biotit zu Chlorit sowie die Serizitisierung von Plagioklasen beobachtet werden. Weiterhin traten Alterationserscheinungen von Olivin zu Krysotil und Pyroxen zu Amphibol auf.

3. Schlussfolgerungen
Anhand der Mineralparagenesen und Geländebeobachtungen, können drei metamorphe Faziesfelder ermittelt werden. Die zum Teil ausgeprägte Migmatisierung setzt eine höhergradige amphibolitfazielle Metamorphose voraus. Die poikilitisch überprägenden Pyroxene sind jedoch schon Anzeichen für die Bedingungen der unteren Granulitfazies, sodass ein Regime von 650 °C-750°C und 6-7 kbar angenommen werden kann. Das Auftreten einer zweiten Biotitgeneration, spricht für eine weitere prograde Metamorphose im amphibolitfaziellen Bereich.

Die Alterationserscheinungen wie Chloritisierung, Serizitisierung und Serpentinisierung sind Anzeiger der retrograden Metamorphose im Grünschieferbereich zwischen 350 °C-450 °C und 3-4 kbar. Auf Grund dieser Mineralumwandlungen kann mit hoher Wahrscheinlichkeit von der Anwesenheit fluider Phasen während der metamorphen Prozesse ausgegangen werden. Die Ergebnisse lassen darauf schließen, dass das Untersuchungsgebiet mehreren aufeinander folgenden tektonometamorphen Ereignissen unterlag. Eine genaue Aussage über die Anzahl der Deformationen ist in diesem Zusammenhang nicht zu treffen, da viele Strukturen durchaus früh- bzw. spätgenetisch während nur einer Phase der metamorphen Überprägung entstanden sein können.

Referenzen:

BINGEN B., BIRKLAND A., NORDGULEN O. & SIGMOND E. (2001): Correlation of supracrustal sequences and origin of terranes in the Sveconorwegian orogen of SW Scandinavia: SIM data on zirkon in clastic metasediments. - Precambrian Res.,108, S. 293-318.

EMP-monazite dating and geothermobarometry in micaschists of the Austroalpine Oetztal-Stubai basement (Erlanger Hütte, Umhausen, Tyrol, Austria)

Sören Rode[1], Bernhard Schulz[1]
[1]Institute of Mineralogy, Economic Geology and Petrology, Technische Universität Bergakademie Freiberg, Germany

The Austroalpine Oetztal-Stubai basement is one of the polymetamorphic crystalline complexes of the Eastern Alps. Ordovician-Silurian, Variscan (Devonian-Carboniferous) and Early-Alpine (Cretaceous) metamorphic events have been reported by Thöny et al. 2008 from various parts of the complex. Within such a frame, the age dating of distinct metamorphic events is a difficult task. The *in situ* Th-U-Pb chemical dating of monazite by electron microprobe (EMP-CHIME method) has proven its potential to resolve several thermal events in a polymetamorphic terrain (Montel et al. 1996). This method is applied here to micaschists in combination with geothermobarometry of garnet-bearing assemblages.

To the west of Umhausen and around Erlanger Hütte in the central part of the Oetztal-Stubai basement the predominant meta-psammopelitic series are interlayered by several W-E trending hornblende gneiss and felsic orthogneiss units. Monazite appears as an accessory phase in garnet bearing micaschists of Ca-poor bulk compositions within meta-psammopelites. The anhedral monazite grains occur commonly as inclusions in biotite and reach a size of 120 µm. They mostly display homogeneous gray-tone in BSE images. The grains were analysed along profiles composed of several points following the procedure described in Schulz et al. (2007). No larger age variations were detected and the weighted means from 4 studied samples from the Umhausen region are at 317±5 Ma. Four samples from the Sellrain and Central Oetztal regions nearby display also uniform ages around 314±7 Ma.

Metapelite garnet zonations are preserved and can be classified into 3 distinct trends in grossular-pyrope-spessartine coordinates. The porphyroblasts display only small rims with increase of Mn as a sign of retrogression. All garnets are dominated by almandine (55 - 85 wt.%). Grossular takes in core areas up to 20 wt.%; pyrope increases in general from 5 wt.% in the core to 15 wt.% in the garnet rim. The compositions of coexistent plagioclase and biotite, enclosed in garnet or aligned along successive foliation generations, have also been determined. All analysed plagioclases are oligoclases with homogeneous, poorly zoned crystals with An_{10-13}. Biotite in the main foliation as well as inclusions in garnet show variable composition (X_{Mg} 0,30 - 0,43). P-T-conditions and P-T-paths were estimated by using geothermobarometry with cation-exchange and net transfer reactions. Since all micaschists contain kyanite or sillimanite, the geothermometer of Bhattacharya et al. (1992) combined with the geobarometer of Holland & Powell (1990) was used. From one sample a prograde metamorphic evolution with maximum pressure of 11,8 kbar at maximal 680 °C was determined. Other samples recorded P-T-conditions of 9 - 11 kbar at 500 - 600 °C. The maximal pressures were passed along increasing temperatures. Temperatures increased up to 700 °C during decompression toward 5 kbar. This indicates an evolution at the border of the muscovite stability field. As the garnets display microstructures of syntectonic crystallisation, the P-T-paths can be considered as successive stages of a progressive and continuous syn-deformational metamorphism.

The variations of the Y_2O_3 in monazite show no correlation or grouping with the overall range of Carboniferous ages. This provides no hints to a massive garnet breakdown during the metamorphism, and it appears likely that garnet was present when monazite crystallised. Uniform and unimodal distribution of the monazite ages gives no indications to a pre-Variscan, Permian or an Early Alpine (Cretaceous) events in the Umhausen area, as it has been described from other parts of the Oetztal-Stubai basement. In consequence one can conclude to a Variscan age of the dominant amphibolite-facies P-T evolution. Possibly, pre-Variscan metamorphic events have been completely extinguished. The temperatures during Permian or Early Alpine metamorphic overprints probably were too low to allow monazite crystallisation.

References:
Bhattacharya, A., Mohanty, L., Majl, A., Sen, S.K. & Raith, M. (1992), Non-ideal mixing in the phlogopite-annite binary: constraints from experimental data on Fe-Mg partitioning and a reformulation of the garnet-biotite geothermometer. Contrib. Mineral. Petrol. 111, 87-93.

Holland, T. J. B. & Powell, R. (1990), An enlarged and updated internally consistent thermodynamic dataset with uncertainties and correlations: the system K_2O-Na_2O-CaO-MgO-MnO-FeO-Fe_2O_3-Al_2O_3-TiO_2-SiO_2-C-H_2-O_2. J. of Metamorphic Geology 8, 89-124.

Montel, J.-M., Foret, S., Veschambre, M., Nicollet, C. & Provost, A. (1996), Electron microprobe dating of monazite. Chem. Geol. 131. 37-53.

Schulz, B., Brätz, H., Bombach, K., Krenn, E. (2007), In-situ Th-Pb dating of monazite by 266 nm laser ablation and ICP-MS with a single collector, and its control by EMP analysis: Zeitschrift für Angewandte Geologie 35, 377-392.

Thöny, W.F., Tropper, P., Schennach, F., Krenn, E., Finger, F., Kaindl, R., Bernhard, F., Hoinkes, G. (2008), The metamorphic evolution of migmatites from the Ötztal Complex (Tyrol, Austria) and constraints on the timing of the pre-Variscan high-T event in the Eastern Alps. Swiss J. Geosci. 101. Supplement 1, 111-126.

Metamorphic evolution of phyllites from the Sierra Cabrera, SE Spain

Andreas Hertwig, Kirsten Drüppel, Gerhard Franz

Technische Universität Berlin, Institut für Angewandte Geowissenschaften, Berlin, Germany,

andreas.hertwig@alumni.tu-berlin.de

The Sierra Cabrera forms the easternmost range of the internal zone of the WSW-ENE trending Betic Cordillera in southeastern Spain and exposes Palaeozoic-Mesozoic basement rocks that record prograde metamorphism related to the Alpine orogeny (e.g. Weijermars, 1991). Towards the south, the Sierra Cabrera is bordered by andesites of the Miocene Cabo de Gata volcanic province which are unconformably overlain by undeformed sedimentary rocks of the Nijar basin in the south. According to Puga et al. (2002) the alpine metamorphism in this area is characterized by Cretaceous-Palaeocene subduction of oceanic crust and continental margins, Eocene-Oligocene continental collision and nappe transport followed by Miocene to Quaternary crustal extension and uplift.

The Sierra Cabrera mainly comprises phyllites, interlayered with quartzites, lenses of minor greenschists, marbles and overlain by massive marble. The phyllites can be divided into several discrete, WSW-ENE trending subzones, displaying characteristic greenschist to amphibolite facies mineral parageneses like Grt-Msc, Grt-Chl, St-Ctd, and St-Bt whereas greenschists are characterized by a Grt-Chl-Ctd assemblage. At the direct contact to the hornblende-bearing andesites up to centimeter-sized andalusite blasts occur in the phyllites, partly displaying characteristic snowball structures. The observed mineral reaction history, combined with conventional geothermometry and calculated P–T-x phase diagrams in the Na_2O-CaO-K_2O-FeO-MgO-Al_2O_3-SiO_2-H_2O system of the Grt-St-Msc phyllites containing late andalusite, point to a clockwise retrograde P–T path, documenting subsequent stages of an almost isothermal decompression. Maximum P-T conditions of 6-10 kbar/500-550°C are estimated from the composition of relics of early garnet. Within error, these values are in agreement with P-T conditions calculated for the Grt-Chl-Ctd-Msc assemblage of associated greenschists (9-10 kbar, 450-500°C) and Grt-Chl-Msc phyllites (6-8 kbar, 480-520°C). Subsequent decompression to 3-5 kbar at 520-550°C is recorded by staurolite formation in the Grt-St-Msc phyllites. Late andalusite in these samples is stable at P < 3 kbar and temperatures of 520-650°C.

The retrograde near-isothermal decompression path (10 to <3 kbar at c. 500 ± 50°C) recorded by the basement rocks of the Sierra Cabrera is in agreement with published P-T data from the neighboring Sierra Alhamilla (Augier et al., 2005) and suggests fast exhumation on a regional scale. The late formation of andalusite is apparently linked to the bordering andesites and subvolcanic equivalents, suggesting that the magmas intruded during the end-stages of the exhumation of the Sierra Cabrera, causing a contact-thermal overprint and minor syn-emplacement ductile deformation of the bordering phyllites.

References:

Augier, R. (2005), Exhumation, doming and slap retreat in the Betic Cordillera (SE Spain): in situ Ar-40/Ar-39 ages and P-T-d-t paths for the Nevado-Filabride complex, Journal of Metamorphic Geology, 23(5), 357-381

Puga, R. , De Frederico, A. & Nieto, J. (2002), Tectonostratigraphic subdivision and petrological characterisation of the deepest complexes of the Betic zone: a review, Geodinamica Acta, 15(1), 23-43

Weijermars, R. (1991), Geology and tectonics of the Betic Zone, SE Spain, Earth-Science Reviews, 31(3-4), 153-236

P12-10

Metamorphose unterschiedlicher Intrusionen im westlichen Teil der Stora Le-Marstrand Formation auf Tjörn (SW-Schweden)

Nadine Liebetrau[1]
[1]Martin Luther Unisversität Halle-Wittenberg, Institute of Geosciences, Halle, Deutschland, nadine.liebetrau@student.uni-halle.de

1.Einleitung
1. 1. Geologischer Rahmen
Das Baltische Schild weist nach GAÁL & GORBATSCHEV (1987) eine gleichmäßige geochronologische Zonierung, mit einer Verjüngung von Nordosten nach Südwesten, auf. Diese Zonierung reflektiert die Entstehung der kontinentalen Kruste des Baltischen Schildes während drei aufeinanderfolgenden Haupt-Orogenen Phasen zwischen 2.9 Ga bis1,5 Ga. Dieses progressive Krustenwachstum ist auf die Akkretion mehrerer Terranes aus südwestlicher Richtung zurückzuführen. Aufgrund dessen ist eine Untergliederung des Präkambriums des Baltischen Schildes in 3 Domänen gegeben.

1.2.Geologie des Untersuchungsgebietes
Das Bearbeitungsgebiet befindet sich auf der Insel Tjörn im Südwesten von Schweden, welches einen Teil der Südwestskandinavische Gneiss-Provinz (Sveconorwegische Provinz) darstellt. Nach KINCK et al. (1993) wurde diese in einem Zeitraum von 1,75-1,5 Ga (Gothische Orogenese) an den Westrand der Svekofennischen Provinz akkretiert. Das untersuchte Areal ist der Stora Le-Marstrand Formation, eines der drei suprakrustalen Einheiten des Idefjorden Terranes, zuzuordnen. Nach ÅHÄLL & CONNELLY (2008) besteht dieses hauptsächlich aus unterschiedlich stark deformierten Metasedimenten und Intrusivgesteinen, in die eine Vielzahl von voluminösen Granitoiden intrudiert sind, welche u. a. Gegenstand der Untersuchungen sind.

2. Ergebnisse
In den angefertigten Dünnschliffen wurden Mikrotexturen wie Myrmektie dokumentiert. Weiterhin wurden poikilitische Granate, rekristallisierte Quarze, sericitisierte sowie saussuritisierte Feldspäte und das Auftreten von Epidot, Allanit, Chlorit, Muskovit und Amphibolen beobachtet. Pseudomorphosen von Biotit zu Chlorit sowie die poikilitische Überwachsung von Pyroxen nach Hornblende konnten ebenso dokumentiert werden. Bei den Biotiten konnten weiterhin zwei verschiedene Generationen nachgewiesen werden.

3. Schlussfolgerungen
Die Ergebnisse der Geländedaten sowie der Mineralparagenesen zeigen, dass alle Lithologien prograd und retrograd mehrere metamorphe Faziesfelder durchlaufen haben. So belegen die Ausbildung von Chlorit und Epidot eine grünschieferfazielle Überprägung bei Temperaturen zw. 350°C - 460 °C und 4 - 6 kbar. Die Bildung der Amphibole, Granate, Muskovite, der zwei Biotitgenerationen sowie der lokal auftretenden Migmatisierung setzt eine amphibolitfazielle bis höher amphibolitfazielle Überprägung zwischen 600°C – 650 °C und 6 – 7 kbar voraus. Eine untere granulithfazielle Überprägung konnte anhand der poikilitischen Überwachsung von Pyroxen nach Amphibol belegt werden, wobei hierfür ein Regime bei ca. 700°C und 6 – 7 kbar angenommen werden kann. Myrmekite belegen nach OKRUSCH & MATTHES (2005) eine retrograde Abbaureaktion, welche im hochmetamorphen Regime einzuordnen ist.

Referenzen:
ÅHÄLL, K.-I. & CONNELLY, J. N. (2008): Long-term convergence along SW fennoscandia: 330 m.y. of proterozoic crustal growth. Prec. Res. 161, 452–474.
GAÁL, G. & GORBATSCHEV , R. (1987): An Outline of the Precambrian Evolution of the Baltic Shield. Precambrian Research 35, 15-52.
KINCK, J. J., HUSEBYE, E. S. & LARSSON, F. R. (1993): The Moho depth distribution in Fennoscandia and the regional tectonic evolution from Archean to Permiam times. Prec. Res. 64, 23-51.
OKRUSCH, M. & MATTHES, S. (2005): Mineralogie – Eine Einführung in die spezielle Mineralogie, Petrologie und Lagerstättenkunde: 526 S., Springer-Verlag Berlin Heidelberg.

P12-11

Deformation fabrics of aragonite under high pressure and temperature

Florian Heidelbach[1], Nico Walte[1]
[1]Universität Bayreuth, Bayerisches Geoinstitut, Bayreuth, Germany

Aragonite ($CaCO_3$) is the orthorhombic high pressure modification of trigonal calcite and is formed in carbonaceous sedimentary sequences that undergo deep subduction. Structurally similar to calcite it is likely one of the weaker components in the subducting slab and thus accommodating large strains during the subduction process. Little is known about the deformation microstructures and textures of aragonite. The aragonite-calcite transformation is a reconstructive phase transition such that aragonite is rarely preserved in exhumed subducted terranes. However, aragonite deformation fabrics may be inherited in the calcite microstructures in exhumed crustal carbonates and therefore contain information about the deformation path of subducting continental slabs.

In this study we investigate the deformation fabrics of aragonite and how they may still be detectable after the back-transformation to calcite. Therefore we deformed aggregates of aragonite plastically at 3 GPa and 800°C in the D-Dia multianvil press in order to produce deformation fabrics that may be similar to those in natural aragonite mylonites. We performed experiments in different deformation geometries (axial compression, simple shear) and analyzed the fabrics with SEM-EBSD. The starting material was produced by pressurizing (3 GPa) and heating (800°C) Carrara marble for up to five days in Piston cylinder press. The long run duration were needed to produce a sufficiently large grain size (~10 m) in the starting material.

The deformation experiments were carried with strain rates of 10^{-4} sec^{-1} (axial compression) and 10^{-5} sec^{-1} (simple shear) and reached strains of 30% (axial compression) and 2 (in simple shear) sufficient to produce a characteristic fabric. All samples showed grain shape preferred orientation and crystallographic preferred orientations (CPO) indicative of dislocation creep. Twinning on (011) was also abundant in all the samples. Crystallographic preferred orientations display an alignment of (100), (001) and (101) in the compression plane/shear plane making them likely to be intracrystalline slip planes. The (100) plane, which shows the strongest alignment corresponds structurally to the basal plane of calcite. The [010] direction is aligned perpendicular to the compression direction and parallel to the shear direction respectively indicating that **b** (as shortest lattice repeat) may serve as a Burgers vector in intracrystalline slip. Invoking a shear mechanism during the phase transition (Gillet et al. 1987) the **b** direction corresponds to the **a** direction of the calcite structure. Potentially inherited fabrics in calcite can be constructed from these orientation data and compared with those from naturally exhumed carbonatitic mylonites.

Reference:
Gillet et al. (1987): The calcite-aragonite transition: mechanisms and microstructures induced by the transformation stresses and strain. *Bulletin de la Minéralogie*, **110**, 481-496.

Petrology and EMP monazite dating of the host rock sequence to the polymetallic Salt River deposit near Pofadder, Bushmanland Terrane, South Africa

Th. Dittrich[1], J. Gutzmer[1] and B. Schulz[1].

[1] Institut für Mineralogie, TU Bergakademie Freiberg, Brennhausgasse 14, 09596 Freiberg, Germany; Thomas.Dittrich@student.tu-freiberg.de

The stratabound Salt River base metal deposit and related prospects de_ne a narrow E-W oriented trend in the SE portion of the Bushmanland Terrane of the Mesoproterozoic Namaqualand Metamorphic Province (Joubert, 1971), in the Northern Cape Province, South Africa. It is hosted by the Geelvloer sequence that is part of the Kouboom Subgroup of the Bushmanland Group (McClung et al., 2007). The Bushmanland Group was a_ected by polyphase deformation and high grade metamorphism during the Namquan Orogeny (Clifford et al., 2004). The purpose of this investigation was threefold, namely (i) the quanti_cation of PT conditions during metamoprhism of the Geelvloer formation and the Salt Ricer deposit, (ii) assessing the e_ects of high-grade metamorphism on the mineralogy of hydrothermal altered (chloritized, sericitized) footwall rocks to the Salt River deposit, and (iii) date the age of metamorphism by electron microprobe-based chemical dating of monazite.

The host rock sequence to the deposit comprises three general rock types and hydrothermal altered (Mg-metasomatism) equivalents of those. The petrological studies revolved that the host rock succession was subjected to typical MP/MT Barrovian regional metamorphism. The metamorphism was dated at 1146 _ 6.4 Ma by the EMP-Th-U-Pb monazite method and developed under prograde metamorphic conditions from upper greenschist-facies (482_/2.9 kbar) to upper amphibolite-facies (700_/7 kbar) as was reconstructed by amphibole geothermobarometry. Monazite geochronology also revolved a second metamorphic event that a_ected the succession at 1035 _ 11 Ma. This is likely related to the intrusions of the Spektakel, Koperberg or Wortel Suites that intruded into the Bushmanland Terrane during the Klondikean event of the Namaquan Orogeny (Clifford et al., 2004). This was immediately followed by exhumation at 971 _ 6 Ma, accompanied by small scale decompressional intracrustal melts causing intrusions of pegmatites, retrograde mineral reactions and renewed growth of monazite. The late retrograde metamorphism is expressed by intense sericitization of plagioclase, chloritization of biotite and probably pinitization of cordierite.

References:
T.N. Cli_ord, E.S. Barton, R.A. Stern, and J.C. Duchesne. U-Pb Zircon Calendar for Namaquan (Grenville) Crustal Events in the Granulite-facies Terrane of the O'okiep Copper
District of South Africa. J. Petrology, 45(4):669_691, 2004.
P. Joubert. The regional tectonism of the gneisses of part of Namaqualand. Precambrian Research Unit Bulletin, University of Cape Town, Cape Town, 10:220pp, 1971.
C.R. McClung, N. Norman, and M. Welthagen. Geology of the Salt River volcanogenic massive sulphide (VMS) deposit, South Africa. In C. J. Andrew, editor, Digging Deeper, volume 2 of 9th biennial meeting of the Society for Geology Applied to Mineral Deposits,
Dublin, Ireland, Aug. 20-23, 2007, page 307p. Irish Association for Economic Geology,
Dublin, Ireland (IRL), 2007.

Stapelung unterschiedlicher metamorpher Einheiten im Fjällfjäll-Duplex (nördliche Kaledoniden, Schweden)

D. Budach[1], K. Dietz-Laursonn[2]
[1]Martin Luther University Halle-Wittenberg, Institute for Geosciences, Halle, Germany
[2]Martin Luther University Halle-Wittenberg, Institute for Geosciences, Halle, Germany

1 Einleitung

In der zentralen Region der östlichen Kaledoniden, Västerbotten, sind Allochthone Einheiten in einem tektonischen Fenster aufgeschlossen. Das Arbeitsgebiet befindet sich innerhalb einer solchen Struktur, dem nördlichen Teil des Fjällfjäll-Fensters. Eine detaillierte Kartierung zeigt aufgebaut durch die Mittleren und Oberen Allochthonen Decken einen intensiv verschuppten Duplex. Im südlichen Fjällfjäll-Fenster wurde durch Degen (1997) zusätzlich eine interne Verschuppung des Mittleren Allochthons bestätigt. Im Gegensatz zum nördlichen Gebiet, kartiert durch die Autoren selbst, sind beide Deckeneinheiten an der Verschuppung beteiligt. Weiterhin kann das Obere Allochthon in zwei Sub-Decken, der Seve- und Köli- Decke, gegliedert werden. Der Rand des Fjällfjäll-Fensters ist ausschließlich durch Gesteine der Köli-Decke aufgebaut. Der Kern des Duplex**es** ist durch eine Stapelung aller drei Einheiten aufgebaut (Mittlere Allochthon, Seve- und Köli-Decke), welche durch die unterschiedliche metamorphe Überprägung deutlich getrennt werden können.

2 Ergebnisse

Die Ergebnisse zeigen, dass alle lithologischen Einheiten eine regionalmetamorphe Überprägung erfahren haben. Die verschiedenen metamorphen Grade des Deckenkomplexes erlauben eine genaue Unterscheidung der individuellen Einheiten. Die lithologische Zusammensetzung des Mittleren Allochthons besteht hauptsächlich aus klastischem Material, wohingegen im Kontaktbereich zum Oberen Allochthon stark mylonitisierte Gesteine auftreten. Die Mineralparagenesen dieser Einheit lassen auf eine grünschiefermetamorphe Überprägung mit ungefähren p-T-Bedingungen von 450°C und 4 kbar schließen. Eine jüngere, niedriggradigere grünschieferfazielle Überprägung konnte ebenfalls während der Dünnschliffanalysen erkannt werden. Die mylonitisierten Gesteine wurden während des Transportprozesses bei der Überschiebung des Oberen Allochthons gebildet. Niedriggradigere metamorphe Anzeichen konnten auf Grund der Mylonitisierung nicht mehr festgestellt werden.

Das überlagernde Obere Allochthon ist in zwei Sub-Decken, der Seve- und Köli-Decke gegliedert. Beide Einheiten können auf Grund der höheren metamorphen Grade eindeutig vom Mittleren Allochthon unterschieden werden. Die Seve-Einheit besteht aus mafischen und ultramafischen Gesteinen. Die Mineralparagenesen deuten auf eine mittlere bis hochgradige amphibolitfazielle Überprägung hin. Die metamorphen Bedingungen werden mit 600-650°C und 5,5 kbar angenommen. Dünnschliffe aus der Seve-Decke zeigen granulitfazielle Relikte, welche auf deutlich höhere metamorphe Bedingungen von über 700°C und 6,5 kbar schließen lassen. Die Köli-Einheit ist hauptsächlich durch verschiedene Schiefer vertreten. Die Mineralparagenesen dieser Gesteine zeigen eine höhere grünschiefer- bis untere amphibolitfazielle metamorphe Überprägung an. Die p-T-Bedingungen dieser Einheit können mit 500-550°C und 5 kbar angenommen werden. Beide, die Seve- und Köli-Decke, zeigen eine zweite, jüngere grünschieferfazielle Überprägung.

Die gezeigten metamorphen Ergebnisse in Kombination mit der Lagerung der einzelnen Einheiten lassen auf eine Stapelung der verschiedenen Allochthonen Einheiten schließen. Der im Gelände erarbeitete tektonische Stapelbau zeigt eine deutliche Verschuppung der oben genannten metamorphen Einheiten, die den Kern des nördlichen Fjällfjäll-Duplex repräsentieren. Dabei kann eine inverse Abfolge, von niedriggradig metamorph überprägten Einheiten an der Basis zu höhergradig metamorphen Folgen am Top des gesamten Komplexes nachgewiesen werden. Dieses charakteristische Merkmal des Deckenstapels lässt die Veränderung der metamorphen Grade der Decken erkennen und zeigt die Zusammensetzung und Mächtigkeit des paläozoischen Orogenen Keils sowie den Prozess der Schließung des Iapetus-Ozeans.

Referenzen:
Degen, T. J. (1997), Deformation and metamorphism in the area between Borgafjäll und Børgefjäll in the northern Caledonides of Scandinavia (Jämtland/Västerbotten), Hallesches Jahrbuch für Geowissenschaften, B/2: 100.

Replacement processes in crystalline rocks

Timm John[1], Andrew Putnis[1]
[1]Westfälische Wilhelms-Universität Münster, Institute for Mineralogy, Münster, Germany

A substantial question in metamorphism is what is the mechanism that dominates the conversion of one mineral assemblage to another in response to a change in the ambient physical and/or chemical conditions. Petrological, microstructural, and isotopic data indicate that aqueous fluids must be involved even in the reequilibration of large-scale systems. Fluid-mineral reactions take place by dissolution - precipitation processes, but converting one solid rock to another requires pervasive, either dominantly advective or diffusive fluid-mediated transport through the entire rock. The generation of reaction-induced porosity and the spatial and temporal coupling of dissolution and precipitation can account for fluid and element transport through rocks and the replacement of one mineral assemblage by another.

To determine the mechanism of metamorphic reactions we refer to examples of interfaces and reaction textures which contain both the "before" (precursor) and "after" mineral assemblages - case studies where the process of conversion is frozen in. We will illustrate some aspects of the role of fluids in metamorphic reactions and discuss how reactive fluids can pervasively infiltrate a rock. The examples we will use are focussed on crystalline rocks and include reactions from the lower continental crust, the subducting oceanic crust, and the continental upper crust to show that except at very high-temperature conditions, essentially the same mechanisms are responsible for converting rocks to thermodynamically more stable mineral assemblages for given Pressure-Temperature-fluid composition (P-T-X) conditions.

Fluid-induced processes: metasomatism and metamorphism

Andrew Putnis[1], Håkon Austrheim[2]
[1]Westfälische Wilhelms-Universität Münster, Institute for Mineralogy, Münster, Germany
[2]Physics of Geological Processes, University of Oslo, Norway

Metamorphism and metasomatism both involve the reequilibration of mineral assemblages due to changes in pressure, temperature and/or chemical environment. Both processes involve material transport but on different length scales, so every metamorphic reaction is metasomatic on a local scale. Fluids provide a transport mechanism which is orders of magnitude faster than solid state diffusion and induce reequilibration through dissolution of parent phases and reprecipitation of products. Chemical weathering (kaolinitisation and serpentinisation), and albitisation are used as examples to describe the coupling between dissolution and precipitation. Albitisation of feldspars in nature and in experiments is a pseudomorphic replacement which generates porosity in the albite. Porosity generation associated with interface-coupled dissolution-precipitation allows rapid material transport and together with fluid induced fracturing, is the mechanism of pervasive fluid flow through reacting crystals. Examples of metamorphic reactions in granulite-eclogite rocks illustrate the role of fluids in inducing chemical changes along fluid pathways. Microstructural criteria for a metamorphic event (i.e. change in P,T) are critically reviewed by describing the corona formed by reaction between kyanite and garnet, as well as partial replacement textures. We conclude that both corona structures and partial replacement textures are equally indicative of a metasomatic reaction (driven by a fluid-induced compositional change) as they may be of a metamorphic reaction driven by a change in P and/or T. This raises the question of the extent to which fluids play not only a catalytic role, but also a thermodynamic role in determining the course of a metamorphic reaction.

Reference:
Putnis, A. & Austrheim, H. (2010) Fluid-induced processes: metasomatism and metamorphism. Geofluids 10, 254-269.

Tourmaline as a tracer for metasomatic alteration processes in the Bamble area, southern Norway

Rebecca Bast[1], Erik E. Scherer[1], Klaus Mezger[2], Thomas Ludwig[3], Horst Marschall[4], Håkon Austrheim[5]
[1]Westfälische Wilhelms-Universität Münster, Institut für Mineralogie, Münster, Germany[2]Universität Bern, Institut für Geologie, Bern, Switzerland
[3]Universität Heidelberg, Institut für Geowissenschaften, Heidelberg, Germany
[4]University of Bristol, Department of Earth Sciences, Bristol, United Kingdom
[5]University of Oslo, Physics of Geological Processes, Oslo, Norway

The Bamble sector, southern Norway, comprises strongly altered metagabbro and metasediments that have undergone Na-metasomatism during a late stage of the Sveconorwegian orogeny (~1.05 Ga). The infiltration of a highly saline brine along veins led to penetrative scapolitization and albitization on a regional scale and the deposition of Fe-Ti-oxides. Tourmaline crystals associated with secondary minerals such as marialitic scapolite or albite and with ores were studied to determine the source of the hydrothermal fluid.

All tourmaline samples are schörl-dravite solid solutions with minor feruvite, uvite, and foitite components as determined by electron microprobe analysis (EMPA). Some crystals display a homogenous major element distribution, but others show zoning in their Fe, Ti, and Ca abundances. This chemical zoning is parallel to the crystal faces in some crystals, and is patchy in others. Two subhedral tourmaline crystals are crosscut by Fe-poor tourmaline veins, indicating that there were at least two episodes of tourmaline growth.

Boron isotope measurements at high spatial resolution were carried out by secondary ion mass spectrometry (SIMS) on a modified Cameca ims 3f at the Institut für Geowissenschaften at the Universität Heidelberg. (See Marschall et al., 2009 for analytical methods.) The B isotope compositions are relatively homogeneous (1-2 ‰ variation) within tourmaline crystals of a single generation, even in the presence of major element zoning. However, different generations of tourmaline show significant B isotope variations of 5-6 ‰ that correlate with Fe contents, which may be the result of an evolving fluid composition during metasomatism. On the regional scale, variations in $\delta^{11}B$ are even larger, ranging from -5 to +25 ‰ relative to SRM-951, suggesting that B-bearing fluids of different origins were involved in the tourmaline formation. Heavy B is suggestive of a seawater-derived fluid as generated by either 1) dehydration of altered oceanic crust during subduction (Marschall et al., 2006) or 2) mobilization of marine evaporates during metamorphism (Palmer & Swihart, 2002). This ore-forming fluid was probably mixed to varying extents with a crustal-derived component having a typical $\delta^{11}B$ of ca. -10 ‰ relative to SRM-951.

References:
Marschall, H.R., Ludwig, T., Altherr, R., Kalt, A. & Tonarini, S. (2006), Syros metasomatic tourmaline: evidence for very high- $\delta^{11}B$ fluids in subduction zones, J. Petrol. 47, 1915-1942.
Marschall, H.R., Meyer, C., Wunder, B., Ludwig, T. & Heinrich, W. (2009), Experimental boron isotope fractionation between tourmaline and fluid: confirmation from in situ analyses by secondary ion mass spectrometry and from Rayleigh fractionation modeling, Contrib. Mineral. Petrol. 158, 675-681.
Palmer, M.R, & Swihart, G.H. (2002), Boron isotope geochemistry: an overview, In: Grew, E.S. (2002), Boron: Mineralogy, Petrology and Geochemistry, Rev. Mineral. 33, 709–744.

Section 13

_____

Subduction zone processes

P13-01

Nitrogen mobility during fluid-rock interaction in subduction zones
Ralf Halama[1], Gray E. Bebout[2], Horst R. Marschall[3]
[1]SFB 574 and Institute of Geosciences, Christian-Albrechts-Universität Kiel, Kiel, Germany
[2]Earth and Environmental Sciences Department, Lehigh University, Bethlehem, Pennsylvania, USA
[3]Department of Earth Sciences, University of Bristol, Bristol, UK

Nitrogen (N) isotopes have shown great potential as geochemical tracers of crustal and volatile recycling, in part because of the large differences in the N isotope compositions of the various terrestrial reservoirs. Since N abundance in the lithosphere is largely tied to its fixation by organic processes in sedimentary environments, N is a sensitive tracer of sediment-derived fluids, and combinations of N isotope data with other geochemical tracers can yield information regarding the scales and extents of fluid-rock interaction and metasomatic processes in subduction zones (Bebout, 1997).

High-pressure metamorphosed rocks are commonly exhumed in subduction mélanges, where various lithologies are metamorphosed together. They represent a natural laboratory to study the effects of fluid-induced metasomatism during subduction zone metamorphism. During subduction, N, as NH^{4+} in phengite, can be retained in sediments and oceanic crust to depths approaching those beneath arcs (Busigny et al., 2003; Halama et al., 2010). However, preferential loss of N to a fluid phase with increasing metamorphic grade and metasomatic effects in eclogites have also been observed, suggesting mobility of N under certain circumstances. In this study, we focus on two detailed sampling profiles across lithologic contacts to elucidate the behavior on N and its isotopes during fluid-rock interaction in the subduction zone.

The first sampling profile was taken from the Les Essarts high-pressure unit in the Southern Armorican Massif (France), which is interpreted as a tectonic mélange. The profile stretches from an approximately 1 km thick eclogite lens via retrogressed eclogite and amphibolite into surrounding metasedimentary gneisses. Nitrogen concentrations increase from the eclogites towards the country rock gneisses, and N shows a positive correlation with fluid-mobile elements K, Ba and Li. ^{15}N values are somewhat scattered for the pristine eclogites (0.9-4.5), but the retrogressed eclogites and the amphibolites fall into the range of the gneisses (2.9-5.8). These features suggest an influx of metasedimentary-derived N from the gneisses into the eclogite lens, possibly aided by transport of N via amphibole veins that occur in the eclogites. Some inhomogeneities, inherited from the precursor, appear to have been preserved in the inner part of the eclogite lens.

The second profile is a reaction zone on a meter scale at the contact of metasedimentary glaucophane schist and serpentinite from the subduction mélange of Syros (Greece), representing a contact between subducting oceanic crustal rocks and the mantle above the slab. Two dominant processes operating at this contact have been identified: Diffusion of chemical components driven by compositional contrast and flux of hydrous fluids along the contact, which depleted (LILE, SiO_2) or enriched (B, LREE) certain elements in various zones (Miller et al., 2009). For nitrogen, there is a clear positive correlation of N contents with ^{15}N values, interpreted to reflect N addition from the blueschist to the hybrid rocks of the reaction zone and the serpentinites.

Our results show that N can be mobilized in subduction-related fluids and N-bearing fluids can interact with the various lithologies present in subduction mélanges. N is predominantly derived from metasedimentary sources, but N elemental and isotopic characteristics of precursor rocks can be preserved in rocks not affected by the fluid influx.

References:
Bebout, G.E. (1997), Nitrogen isotope tracers of high-temperature fluid-rock interactions: Case study of the Catalina Schist, California. Earth Planet. Sci. Lett. 151:77-90.
Busigny, V., Cartigny, P., Philippot, P., Ader, M. & Javoy, M. (2003), Massive recycling of nitrogen and other fluid-mobile elements (K, Rb, Cs, H) in a cold slab environment: evidence from HP to UHP oceanic metasediments of the Schistes Lustrés nappe (western Alps, Europe). Earth Planet. Sci. Lett. 215:27-42.
Halama, R., Bebout, G.E., John, T. & Schenk, V. (2010), Nitrogen recycling in subducted oceanic lithosphere: The record in high- and ultrahigh-pressure metabasaltic rocks. Geochim. Cosmochim. Acta 74:1636-1652.
Miller, D.P., Marschall, H.R. & Schumacher, J.C. (2009), Metasomatic formation and petrology of blueschist-facies hybrid rocks from Syros (Greece): Implications for reactions at the slab-mantle interface. Lithos 107:53-67.

Experimental simulation of mantle wedge metasomatism

Tina Block[1], Bernd Wunder[2]
[1] Friedrich-Schiller-Universität Jena, Institute for Geosciences, Department Mineralogy, Jena, Germany
[2] German Research Centre for Geosciences GFZ Potsdam, Telegrafenberg, Potsdam, Germany

The main goal of this experimental study was to simulate metasomatic processes within the mantle wedge triggered by fluids expelled from the subducting oceanic slab. Simplified model assemblages of slab and mantle material were placed at the bottom and top of a 1 cm long gold capsule, respectively. Synthetic lawsonite, $CaAl_2Si_2O_7(OH)_2*H_2O$, was chosen as slab material, synthetic Fe-free forsterite and enstatite (mixed in the weight proportion 3:1) represented the simplified mantle wedge. 5 wt.% of additional water was given to the solid starting material. The experiment was performed in a piston-cylinder press at 2.0 GPa in such a way, that a temperature gradient of about 50 K occurred between the lawsonite (600°C) and the mantle assemblage (650°C). Run duration was 4 days. At these conditions lawsonite dehydrated to zoisite + kyanite + quartz + water. Through the thermal gradient the fluid ascended through a perforated Au-foil (to avoid direct chemical contact) and reacted with the overlying mantle assemblage.

After the experiment, the capsule was cut vertically. A polished sample was prepared for optical investigations, EMP analyses and for high resolution Al, Si, Mg, Ca element maps. For TEM analyses a FIB foil was cut from the "slab-mantle" contact region.

The run product consisted of zoisite, kyanite and quartz in the low-temperature part of the capsule and of a mixture of enstatite and forsterite in the upper part of the capsule. At the contact region we observe newly formed hydrous phases talc, brucite and chlorite. No reasonable EMP analyses could be performed because the newly formed phases were too fine-grained. Chlorite forms an about 30 m thick seem at the contact to the former lawsonite material. In nature talc + brucite are associated with serpentine at the slab-mantle interface and should promote aseismic behaviour.
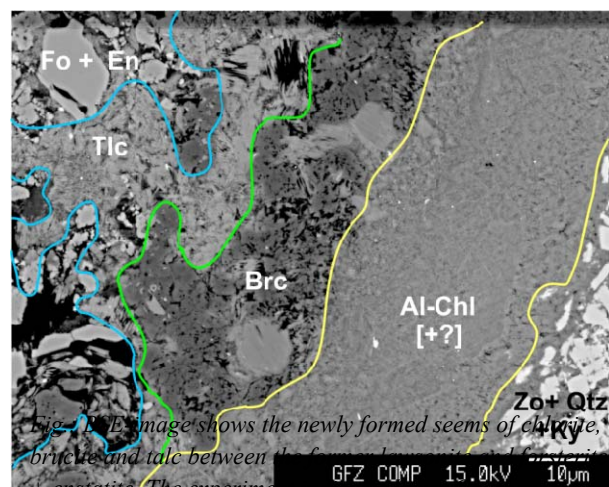
Fig. 1: BSE-image shows the newly formed seems of chlorite, brucite and talc between the former lawsonite and forsterite + enstatite. The experiment indicates lower Ca- than Al-mobility. Interestingly, we find no indication of serpentinization of the mantle wedge, even often proposed in literature. Formation of talc at the slab-mantle interface is expected when SiO_2-rich fluids infiltrate periodotites,

Experimental studies on trace element mobility in subduction zone fluids

Sven Wortelkamp[1], Stephan Klemme[1], Jasper Berndt[1]
[1]Westfälische Wilhelms-Universität Münster, Institute for Mineralogy, Münster, Germany

Our understanding of fluid transport processes in subduction zones is rather limited. Whilst mid-ocean-ridge basalts show a depletion of incompatible elements, such as Ba, Rb or Th, island-arc basalts display a relative enrichment of these elements, whilst the high field strength elements are depleted. Recent experimental results at very high pressures (corresponding to some 120-180 km depths) showed strong effects of pressure and temperature on the composition of the fluid phase liberated from the subducting slab (Kessel et al, 2005). The aim of our study is to evaluate the influence of fluid composition and residual mineralogy on trace element signature of HP-HT fluids at moderate pressures between 5 and 20 kbar.

The experiments were conducted in an end-loaded piston-cylinder apparatus at Münster University. The starting material consists of synthetic mixture of average altered mid-ocean-ridge basalt (MORB) composition doped with 27 trace elements. We use a 200 ppm Cs standard solution as an internal standard for the measurements by LA-ICP-MS.

This study also presents a modified method to study trace element composition of high-temperature highpressure fluids with LA-ICP-MS (Laser Ablation- Inductively Coupled Plasma- Mass Spectrometry). We employ diamond aggregates in our experiments to capture fluids (Kessel et al, 2005), which are equilibrated with a residual mineral assemblage of basaltic bulk composition. After quenching of the experiments, the capsule was frozen, then sectioned and placed in a home-built freezing stage, designed to fit a 193 nm New Wave Laser system, to ensure constant temperature during the whole duration of the analysis.

Reference:

Kessel, R, Schmidt, MW, Ulmer, P, Pettke, T (2005): Trace element signature of subduction-zone fluids, melts and supercritical liquids at 120–180 km depth. Nature, 437, 724-727

Lawsonite and its pseudomorphs in blueschists on Syros (Cyclades, Greece) – indicators for close-to-peak metamorphic strain distribution

Mark Keiter[1] & Chris Ballhaus[2]
[1]Institut für Mineralogie, Westfälische Wilhelms-Universität Münster
[2]Steinmann-Institut für Geologie, Mineralogie, Paläontologie, Universität Bonn

The morphologies of pseudomorphs after Lws provide relative temporal constraints on the relationship between strain, Lws growth, and Lws-out reaction along the prograde and close-to-peak metamorphic path in blueschist- to eclogite facies rocks of Syros, Greece. Deformed pseudomorphs stretched to s-parallel Czo-Chl-Phen-Qtz stringers result if the host rocks continued to recrystallize dynamically to near peak temperature in the Gln-Czo field. Undeformed pseudomorphs require a P-T path that was already static when it crossed from the Gln-Lws to the Gln-Czo subfacies of the blueschist stability field. Skeletal Lws may even imply near-static conditions as early as low-pressure stabilization of Gln-Lws parageneses. Several explanations for the variable Lws pseudomorph morphologies are possible:

(1) the width of the temperature window between the Gln-Lws out reaction and endmember stability varied as a result of variable bulk compositions and/or H_2O/CO_2 ratios of a coexisting fluid phase;

(2) temperature was heterogeneously distributed at given pressure, such that outcrops with static pseudomorphs experienced deformation at generally lower temperature than outcrops with dynamically recrystallized pseudomorphs; or

(3) strain was heterogeneously distributed during the prograde and close-to-peak deformation events.

The third alternative is best supported by field relations. Mechanically, the metabasite occurrences on Syros are often extremely heterogeneous. In a tectonic mélange with undeformed metagabbro and eclogite macro-boudins juxtaposed and embedded in a ductile schist matrix, it is highly likely that during prograde deformation, strain was distributed heterogeneously. During tectonic transport in the mélange, ductile lithologies may occasionally end up structurally isolated in pressure shadows of static metabasite complexes, with the consequence that they experience further prograde and even early retrograde evolution under static conditions. Such an environment would also favor local, small-scale extensions and emplacement of static high-pressure veins. Only by local structural isolation, blueschist outcrops with strained pseudomorphs occuring next to blueschists in which the pseudomorphs after Lws are undeformed seem reasonable.

High-field strength elements complexes in aqueous fluids of subduction zones

Julien Dubrail[1], Max Wilke[1], Christian Schmidt[1], Karen Appel[2] and Sakura Pascarelli[3]

[1] Helmholtzzentrum Potsdam Deutsches GeoForschungsZentrum (GFZ), Potsdam, Germany

[2] DESY, ein Forschungszentrum der Helmholtzgemeinschaft, Hamburg, Germany

[3] European Synchrotron Radiation Facility, Grenoble, France

The mobilization of certain elements within subduction zones has important implications regarding the evolution of the crust and the mantle and the formation of magmas. One example of this mobilization is the characteristic depletion of high-field strength elements (HFSE, e.g., Nb, Ta, Hf, Zr, Ti, V) relative to large ion lithophile elements (LILE, e.g., Rb, Sr, Cs, Ba, Th, U) in arc-related magmas. The origin of the enhanced mobility of the HFSE within subduction zones remains uncertain. This depletion of the HFSE in arc magmas has been recently attributed to the stability of HFSE-bearing minerals, which is closely related to the ability of fluids to incorporate HFSE. A mechanism for efficient transport of HFSE by fluids is suggested by formation of complexes with, most likely, sodium-aluminosilicates in the hydrous fluids released from subducted slabs [1-2]. The determination of the HFSE complexes and their relation to temperature, pressure and chemical composition is crucial for the understanding of geochemical processes such as magma evolution, subduction-zone metasomatism and element cycling. However, there is only fragmentary knowledge on the complexation of the HFSE in aqueous silicate-bearing fluids at the P-T conditions of the lower crust and the upper mantle.

Using in-situ techniques, information has been obtained on the Hf concentration in aqueous fluids containing $Na_2Si_3O_7$ (NS3) or $Na_2Si_3O_7 + 5$ wt% Al_2O_3 (NS3Al5) or in NaOH and HCl solutions. Fluids were equilibrated with hafnon in hydrothermal diamond-anvil cells at temperatures up to 750 °C and pressures up to ~1 GPa and analysed using synchrotron radiation micro-XRF and XAFS at ID 24, ESRF.
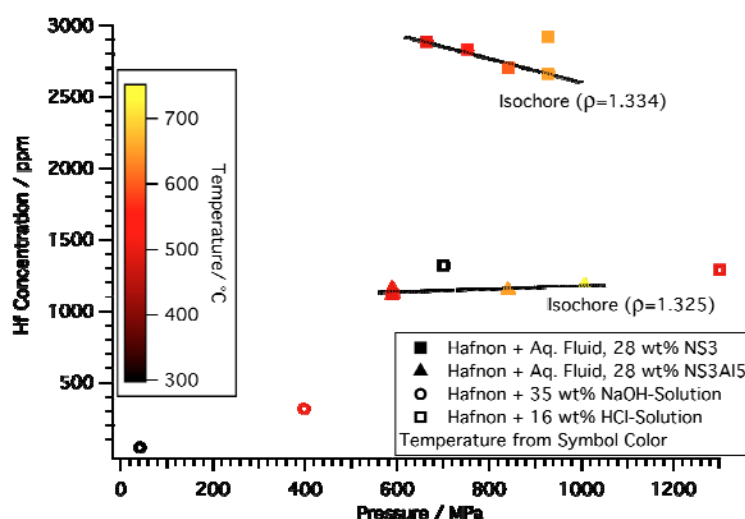
The Hf concentrations in the fluid are highest with dissolved NS3 and decrease by addition of alumina. Hafnium concentrations in these fluids are similar or higher than for NaOH and HCl solutions (see Figure), which points to the formation of (Hf)-O complexes involving Na and/or Si. This signifies the importance of silicate components in fluid for transport of Hf and other HFSE. To further determine the nature of the complexes formed by HFSE in aqueous fluids and to get better insight into their formation mechanisms, we performed dispersive XAFS measurements at the Hf-L_3 edge. To extract structural data from the experimental spectra, theoretical ab-initio EXAFS and XANES spectra using the FEFF8.4 code were calculated. A model based on an HfO_6 octahedron at R(Hf-O)=2.07 Å (equal to that of Zr in peralkaline $Na_{3.3}AlSiO_{17}$ glass [3]) reproduced the experimental Hf-L_3 XANES spectrum well. Fitting of the EXAFS region also indicates a regular HfO_6 octahedron first coordination-shell. Preliminary results from simulations of the XANES spectra with the FEFF code were coupled to a refined analysis using the MXAN XANES fitting procedure [4]. The theoretical XANES spectrum was refined to fit the data by changing the relevant geometrical parameters of the site around the absorbing atom. Best fit structural parameters (bond distances and angles) allow to determine the geometry of the polyhedra formed around Hf in the fluids.

References:

[1] Manning, C. E. (2004), Earth Planet. Sci. Lett. 223, 1-16

[2] Manning, C.E. et al. (2008), Earth Planet. Sci. Lett. 272, 730-737
[4] Farges, F. et al. (1991) , Geochim Cosmochim Acta 55, 1563-1574
[3] Benfatto, M., et al. (2001), J. Synchrotron Radiat. 8, 267-269

Gain and loss of fluid-mobile elements in subduction zones: an experimental approach

A. Mutter, A. Holzheid
University of Kiel, Institute of Geoscience, Kiel, Germany

The knowledge of partitioning behaviour of trace elements (LILE, REE and HFSE) between mineral assemblages of the subducting slab and fluids released from the slab is essential to quantify the fluxes of fluids in the entire subduction zone (Zack and John, 2007). Models of subduction zone dynamics (Poli and Schmidt, 2002) suggest that slab related fluids released into the mantle are not only derived from a single source, but most likely represent a mixture of fluids formed by dehydration of sedimentary rocks, altered oceanic crust and/or serpentinized mantle. However, the majority of former experimental studies to determine solid-fluid partitioning behaviour of trace elements used simplified chemical compositions of solid and fluid phases as starting materials (e.g., Spandler et al., 2007, Kessel et al., 2005). The experimental approach of this present study is not only to use natural and synthetic analogues of the different lithological components of the subducting slab as solid starting materials but also to investigate the evolution, and thus the changes of the composition, of the solid starting materials as well as the fluids. Synthetic analogues of these evolved compositions of the solid and fluid phases are used in subsequent experiments with modified pressure and temperature conditions. This present study is therefore a dynamic approach to investigate the continuous changes of trace element partitioning behaviour between the solid and fluid phases steadily moving down along the subducting slab.

At first the focus was to quantify the release of trace elements during the early stages of the subduction processes. Experiments in cold seal pressure vessels (CSPV) were performed. As solid starting materials three natural samples, two basalts and a gabbro, as well as a synthetic silicate glass were used. The natural samples are from ODP Leg 206 and Site 1256D (IODP expeditions 309 and 312), see Teagle et al. (2006) for more details. The synthetic glass is of gabbroic composition. Pure water was used as leaching agent. Powdered solid starting materials (250 and 500 mg) were placed together with the water (1 g) in Au capsules (width/length: 46 / 100 – both in mm). The temperature and pressure was held at 400°C and 4 kbar. Run durations were either 7 days or 14 days. Both, the fluid and the residual silicate phases, were recovered after terminating the experiments. The fluid phases were analysed with ICP-MS and ICP-OES techniques (inorganic geochemistry lab, University Kiel). The residual silicate phases are powders. Small glass spheres (fusion whole-rock glasses) were manufactured from the solid residue using the technique described by Fedorowich et al. (1993). The major and minor element contents of these glass spheres were than analysed by electron microprobe (EMP lab, University Kiel) and the trace element concentrations were measured by LA-HR-ICP mass spectrometry (Institute of Mineralogy, University Münster). Comparison of the bulk composition of the individual silicate starting materials (natural and synthetic samples) and their corresponding post-run silicate charges as well as the post-run fluid chemistries reflect only a minor mobility of trace elements at pressure and temperature conditions comparable to the upper part of the subduction slab. The present focus is on the element mobility at slightly higher temperatures and pressures (500°C, 7 kbar), corresponding to a depth of ~21 km in the subduction zone. These experiments were performed in internally heated pressure vessels (IHPV; experimental lab of Department 3.3, GFZ Potsdam). Both, the silicate and the leaching agent, compositions remained identical compared to the CSPV experiments. Preliminary results indicate smaller solid-fluid partition coefficients, implying a slight change in trace element (REE) mobility at higher pressure and temperatures.

Following the above mentioned dynamic approach, additional CSPV experiments will be performed. The solid starting material will remain identical, while the composition of the modified starting fluid will mimic the composition of the post-run fluid phase of the IHPV experiments. Furthermore, piston-cylinder and multi-anvil experiments will be performed to simulate further (high temperature / high pressure) subduction processes. Synthetic silicates identical in composition to the post-run silicates of the IHPV-experiments will be used as silicate starting materials in these piston-cylinder and multi-anvil experiments.

Reference:
Zack, T. & John, T. (2007), An evaluation of reactive fluid flow and trace-element mobility in subducting slabs, Chemical Geology, 239, 199.
Spandler, C., Mavrogenes, J. & Hermann, J. (2007), Experimental constrains on element mobility from subducted sediments using high-P synthetic fluid/melt inclusions, Chemical Geology, 239, 228.
Kessel, R., Ulmer, P. & Pettke, T. (2005), Trace element signature of subduction-zone fluids, melts and supercritical liquids at 120-180 km depth, Nature, 437, 724.
Poli, S. & Schmidt, M.W. (2002), Petrology of subducted slabs, Annual Review of Earth and Planetary Science, 30.207.

Teagle, D.A.H. Akt, J.C., Umino, S., Miyashita, S., Banerjee, N.R., Wilson, D.S. & the Expedition 309/312 Scientists (2006), Proceedings IODP 309/312, 1

Fedorowich, J.S, Richards, J.P, JAIN, J.C, Kerrich, R., Fan, J. (1993), A rapid method for REE and trace-element analysis using laser sampling ICP-MS on direct fusion whole-rock glasses. Chemical Geology 106, 229.

Section 14

_____

Time constraints on geological processes

Time scales for vertically moving axial magma chambers at fast-spreading ocean ridges and involved magmatic reactions: Insights from IODP Site 1256

C. Kirchner [1], J. Koepke [1], H. Behrens [1]
[1]Institut fuer Mineralogie, Leibniz Universitaet Hannover, Callinstr. 3, 30167 Hannover, Germany
(c.kirchner@mineralogie.uni-hannover.de)

It is well accepted that AMCs ("axial magma chamber") under fast spreading ocean ridges located at the boundary between lower and upper crust are dynamic systems with the potential to move up and down. Nevertheless, the time scales of these vertical movements are poorly constrained up to now with very rough estimations, varying between 10 and 10000 years.

This project focuses on a close investigation on the gabbro/sheeted dike transition, which is part of a reference profile of the upper oceanic crust recently drilled by IODP multi-cruise mission „Superfast Spreading Crust" (Site 1256, equatorial East Pacific Rise). Of substantial interest is a specific horizon defined as CBL ("conductive boundary layer"), separating the AMC and the hydrothermally altered dikes. The ascent of the AMC leads to the formation of "granoblastic dikes" due to an intense metamorphic overprint under granulite-facies conditions [Koepke et al. 2008].

In order to quantify the vertical oscillations of the AMC described above, we plan to apply tools of diffusion profile modeling to relictic, zoned plagioclase and clinopyroxene phenocrysts within the granoblastic dikes, which were metamorphosed by the thermal imprint of the AMC (~1200°C) in a high position. Provided that the zoning patterns in the crystals studied are due to temperature-induced diffusion processes, the conditions of metamorphic overprint (temperature, volatile fugacities), and diffusion coefficients are known, the detailed analysis and modeling of the concentration profiles allows us a quantification of the residence time of the heat source (AMC) in a high position and hence, temporal information about the vertical fluctuations of the AMC can be constrained.

At this stage of the project, we are collecting a high number of concentration profiles with respect to CaAl-NaSi diffusion (An-Ab content and selected trace elements) in several relictic plagioclases with electron microprobe.

The measured An-profiles show the typical shape of diffusion profiles resulting from the exchange between plagioclase and matrix as presented in Figure 1. The profiles were fitted using the diffusion equation [Crank, 1975] assuming constant diffusivity and an initially homogenous plagioclase (r^2=0.999). First estimations yield time scales of 50000 years for the development of the concentration profiles.

Provided that the examined dike diverges with a maximum rate of 11 cm/a away from the spreading center, the calculated values of residence time of the AMC in a high position are obviously too high because after these times the corresponding dike would have left the on-axis environment where AMC's reside exclusively. Due to this unexpected result, we identified that the initial profile shapes in samples unaffected by the thermal imprint have to defined more precisely, which were based on approximations so far.

Moreover, many of the measured profiles up to now exhibit irregularities most likely caused by alteration reactions or inclusions and cannot be used for our modeling approach. Thus, a statistical approach is necessary to collect a high number of diffusion profiles in order to develop a final numerical model.

In addition to the diffusion modeling, an experimental subproject has just started, which aims on the simulation of melt/rock interactions occurring during the up-ward burning of the AMC into the previously altered sheeted-dike complex. With these experiments we attempt to extent our knowledge on the underlying magmatic reactions under fast spreading ocean ridges, regarding processes like stoping, assimilation and contamination.
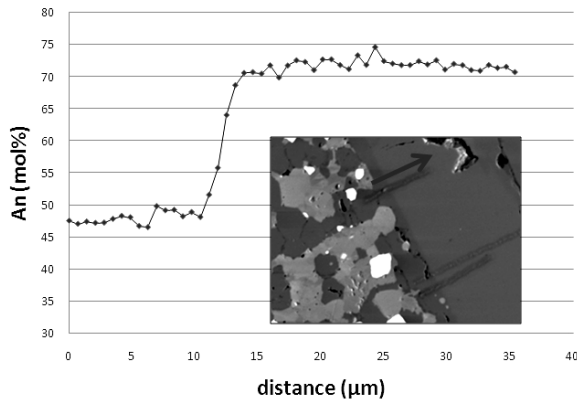
Figure 1. Backscattered electron image showing a relictic plagioclase with idiomorphic shape (medium grey) surrounded by plagioclase of the granoblastic matrix (dark grey) within a typical granoblastic dike drilled at Site 1256D (sample number **312-1256D-203-1-10-14**) The arrow marks the direction where the concentration profile was measured with the electron microprobe. The light grey and withish phases are hornblende, pyroxene, and oxides of the granoblastic matrix (including products of secondary alteration).

References:

Crank, J. (1975), The Mathematics of Diffusion, 414 pp., Oxford Univ. Press, Oxford, U. K.

Koepke et al. (2008), Petrography of the dike-gabbro transition at IODP Site 1256 (equatorial Pacific): The evolution of the granoblastic dikes, Geochem. Geophys. Geosyst., 9, Q07O09, doi:10.1029/2008GC001939.

HP metamorphism in the Sistan Suture Zone, eastern Iran: New insights from Rb-Sr data

Stephanie Theunissen[1], Michael Bröcker[1], Gholamreza Fotoohi Rad[2]
[1]Westfälische Wilhelms-Universität Münster, Institut für Mineralogie, Münster, Germany
[2]University of Birjand, Department of Mining Engineering, Faculty of Engineering, Birjand, Iran

The Sistan Suture Zone (SSZ) in eastern Iran documents convergence between the Central Iranian and Afghan microcontinents and the associated closure of a north-facing arm of the Neotethys (Fotoohi Rad et al., 2005). The SSZ (500 x 100 km^2) represents a well-preserved subduction zone complex and includes a tectonic mélange consisting of meta-ophiolitic rocks within a matrix of chlorite-talc schists, mica schists and greenschists. Large slabs of ultramafic rocks and meta-gabbros only experienced low-grade metamorphism, but some smaller metabasic blocks (< 200 m) record HP/LT or epidote amphibolite facies P-T conditions. Radiolaria in pelagic cherts from the mélange reveal that the Sistan ocean existed already in Early Cretaceous time (Aptian to Albian; Babazadeh & De Wever, 2004), but the closure history is yet poorly understood. Unravelling of the petrological and geochronological information that is stored in the mélange rocks plays a key role for refinement of existing geodynamic models.

P-T conditions recorded by different HP blocks vary considerably. For the eclogite and blueschist-facies stages, pressures of ca. 1.5-2.4 GPa and temperatures of ca. 450-650 °C were estimated, whereas studies on epidote amphibolite facies rocks indicate pressure conditions of ca. 0.5-0.7 GPa and temperatures of ca. 520-590 °C (Fotoohi Rad et al., 2009). Previously published Ar-Ar white mica and barroisite data for an eclogite, a blueschist and two epidote amphibolites indicate apparent ages of ca. 125 Ma, which were interpreted as cooling ages (Fotoohi Rad et al., 2009). However, due to the potential importance of excess Ar in HP and UHP rocks, the geological significance of these dates needs to be corroborated by other chronometric methods. For this purpose, we use a multimethod geochronological approach (Rb-Sr, Sm-Nd, Lu-Hf, U-Pb) on samples from the Ratuk Complex, collected near the locations Gazik, Gurchang and Sulabest. First Rb-Sr results (internal mineral isochrons comprising several grain size fractions of white mica, ± epidote, ± omphacite, ± glaucophane) indicate substantially younger ages than the Ar-Ar data and show a regional consistent age pattern (86.1 ± 1.0 Ma, 86.6 ± 0.6 Ma, 84.3 ± 4.7 Ma, 84.7 ± 0.7 Ma, 85.7 ± 0.7 Ma). This observation is consistent with assuming variable amounts of extraneous argon in the white mica, and suggests that the Ar-Ar data do not provide reliable ages. The Rb-Sr ages correspond with expectations from field observations and biostratigraphic data and document subduction of the Sistan ocean in Late Cretaceous time. The results obtained so far underline the necessity to apply several geochronometers for unravelling the age information of HP rocks. Sm-Nd and Lu-Hf dating (work in progress) will help to further constrain the time of HP metamorphism.

Due to incomplete overprinting, white mica dates of multiply metamorphosed rocks are often difficult to interpret. Hence only texturally well-constrained, newly formed phases are here used to determine the age of the greenschist- to amphibolite-facies episode. For an incompletely overprinted eclogite collected near Sulabest, it was possible to date both the HP and the greenschist facies stages on the same sample. Phengite and omphacite provided a Rb-Sr age of 85.7 ± 0.7 Ma. The lower pressure overprint is indicated by the occurrence of epidote, biotite and plagioclase in small domains that formed due to breakdown of garnet, omphacite and phengite. Rb–Sr dating of the retrograde mineral assemblage provided an apparent age of 78.3 ± 0.8 Ma, placing constraints on the time of cooling below ca. 300–350 °C.

References:
Fotoohi Rad, G.R., Droop, G.T.R., Amini, S. & Moazzen, M. (2005), Eclogites and blueschists of the Sistan Suture Zone, eastern Iran: A comparison of P-T histories from a subduction mélange, Lithos, 84, 1–24.
Fotoohi Rad, G.R., Droop, G.T.R. & Burgess, R. (2009), Early Cretaceous exhumation of high-pressure metamorphic rocks of the Sistan Suture Zone, eastern Iran, Geological Journal, 44, 104–116.
Babazadeh, S.A. & De Wever, P. (2004), Early Cretaceous radiolarian assemblages from radiolarites in the Sistan Suture (eastern Iran), Geodiversitas, 26, 185–206.

The bearing of composition on the rheology of tektites from the Australasian strewn field: limiting factors of the tektite production process

Kai-Uwe Hess[1]; Rupert Hochleitner [2]; Karl Thomas Fehr [1]; Gabriele Giuli[3], Fabio Arzilli[3]; Andrea Fortunati[3], Donald B. Dingwell[1]
[1] Department of Earth Sciences, Ludwig-Maximilians-Universität, München, Germany
[2] Mineralogiche Staatssammlung München, München, Germany
[3] Dipt. di Scienze della Terra, Universita' di Camerino, 62032 Camerino, Italy

Tektites are natural impact-generated glasses that are found in four distinct strewn fields on Earth (North America, Central Europe, Ivory Coast and Australia/Asia). The Australasian strewn field is by far the largest one, covering approximately 1/3 of the Earth's surface and ranging from Tibet to Australia. Tektites from the Australasian strewn field are commonly up to a few centimetres in size. Their chemical and isotopic composition closely resembles those of upper continental crustal rocks. Studies have demonstrated that they were formed during hypervelocity impacts on Earth, but still numerous open questions regarding the formation process exist.

During the course of this study Australasian tektites from six localities (Tibet, Guangdong, Hainan, Thailand, Philippines and Australia) were investigated with respect to various key structural melt properties suspected to control the rheology of the super-cooled melt during tektite formation. The composition of all samples was analysed by EMPA and the ferric/ferrous iron ratio both by Moessbauer spectroscopy and wet chemical analysis. The glass transition temperature and the viscosity were determined by calorimetric and dilatometric methods (advanced dilatometry and micro-penetration).

First preliminary results on selected samples (between 10 and 20 mm in diameter, high in silica content) show (a) a good correlation between the SiO_2 content and calorimetric glass transition temperatures (approx. 770 to 810 °C) and (b) an increase in viscosity at a fixed temperature in the glass transition regime. The ratios of total alkali/alumina and total alkaline earth/alumina (on a molar basis) exert an additional, though minor control on the rheological properties. In contrast, the iron and titanium contents seem to have no or very minor control. Note, that the iron is highly reduced in all samples (the Fe^{3+}/Fe^{2+} ratio $\sim$ 0.1).

For a few selected tektites, geospeedometric profiles across the samples have been performed. The first and unexpected results reveal apparently homogenous and moderate cooling rates throughout the sample, approximately in the order of degrees per minute during the last stage of formation.

Lu-Hf garnet geochronology applied to dating the high-pressure metamorphic event of the Maksyutov Complex, Southern Urals

Nicole S. Bender[1], Erik E. Scherer[1], Ralf Hetzel[2]

[1]Westfälische Wilhelms-Universität Münster, Institute for Mineralogy, Münster, Germany

[2]Westfälische Wilhelms-Universität Münster, Institut für Geologie und Paläontologie, Münster, Germany

The Southern Urals are a well-preserved example of an arc-continent collision zone. They contain a crustal unit that was subducted and metamorphosed at eclogite-facies conditions (~550°C and ~2 GPa; Hetzel et al. 1998). Although different isotopic systems have been used to date the high-pressure metamorphism, the exact age remains ambiguous: Published ^{40}Ar-^{39}Ar data on phengite, U-Pb data on rutile, and Rb-Sr and Sm-Nd mineral data span from 370 to 400 Ma (Hetzel & Romer, 2000).

Garnet generally has high Lu/Hf and is therefore a useful mineral for dating metamorphic events (e.g., Duchêne et al., 1997). When dating garnet, the Lu-Hf system can provide important advantages over the Sm-Nd system, namely: 1) a higher closure temperature, 2) relative insensitivity of ages to ubiquitous REE-rich inclusions, and 3) the effects of inherited Hf-rich mineral inclusions on ages can be greatly reduced by using a selective digestion method (e.g., Scherer et al., 2000, Lagos et al., 2006). In this study, we use the Lu-Hf system to date garnet and omphacite growth and hence the age of eclogitization during high-pressure metamorphism of the Maksyutov Complex.

Two eclogite samples, 95R39 and 95R45, of the high-pressure unit of the Maksyutov Complex (from the type locality of Shubino) were analyzed for their Lu-Hf systematics using multi-collector inductively coupled mass spectrometry. Both samples have the mineral assemblage garnet + omphacite + rutile + white mica ± zoisite ± titanite ± blue amphibole. Garnet porphyroblasts of sample 95R45 show a bimodal size distribution (ca. 2-3 mm, and ca. 4-5 mm). Isochrons were defined by garnet, whole rock, omphacite, and rutile. Garnet data points comprise both single-grain analyses of large porphyroblasts and multi-grain analyses of the smaller porphyroblasts. Element maps obtained by electron microprobe analysis of the garnets provide constraints on garnet growth history and, together with the new Lu-Hf ages, provide information on the PTt-path of the high-pressure unit of the Maksyutov Complex.

A 5-point isochron from sample 95R39, defined by the whole rock, rutile, omphacite, and two garnet aliquots, yields an age of 378.4±6.4 Ma with a MSWD of 0.48. A 5-point isochron from sample 95R45, also defined by the whole rock, rutile and two garnet aliquots, yields an age of 382.2±2.2 Ma with a MSWD of 1.09. A 2-point isochron for sample 95R45 defined by a large garnet porphyroblast and omphacite yields an age of 382.3±3.9 Ma, and the same omphacite aliquot regressed with the aliquot of small garnet porphyroblasts yields an age of 382.3±4.7 Ma. That the ages of the large and small garnets are identical argues against the presence of significantly older cores being present in the large garnet porphyroblasts. A 10-point isochron defined by all aliquots of both samples yields an age of 382.0±2.0 Ma. All obtained ages overlap within their errors.

As the temperature during high-pressure metamorphism and the subsequent exhumation of the Maksyutov Complex did not exceed 600°C (Hetzel et al. 1998), the Lu-Hf system has most likely remained closed during pro- and retrograde metamorphism. Furthermore, the electron microprobe element maps for small and large garnet porphyroblasts from both samples are characterized by bell-shaped Mn distributions suggestive of original growth zoning. We interpret the Lu-Hf ages, which agree with published ^{40}Ar-^{39}Ar data on phengite and U-Pb data on rutile, to date garnet growth in the presence of omphacite and rutile and thus the eclogitization of the Maksyutov Complex at 382.0±2.0 Ma.

References:

Duchêne, S., Blichert-Toft, J., Luais, B., Télouk, P., Lardeaux, J.-M., Albarède, F. (1997), The Lu-Hf dating of garnets and the ages of the Alpine high-pressure metamorphism, Nature, 387, June 1997, 586 – 589

Hetzel, R., Echtler, H. P., Seifert, W., Schulte, B. A., Ivanov, K. S. (1998), Subduction- and exhumation related fabrics in the Paleozoic high-pressure-low-temperature Maksyutov Complex, Antingan area, Southern Urals, Russia, GSA Bulletin, July 1998, 110, 7, 916 – 930

Hetzel, R. & Romer, R. L. (2000), A moderate exhumation rate for the high-pressure Maksyutov Complex, southern Urals, Russia, Geological Journal, 35, 327 – 344

Lagos, M., E. E. Scherer, Tomaschek, F., Münker, C., Keiter, M., Berndt, J., Ballhaus, C. (2007), High precision Lu-Hf geochronology of eocene eclogite-facies rocks from Syros, Cyclades, Greece, Chemical Geology, 243, 16 – 35

Scherer, E. E., Cameron, K. L., Blichert-Toft, J. (2000), Lu-Hf garnet geochronology: Closure temperature relative tot he Sm-Nd system and the effects of trace mineral inclusions, Geochimica et Cosmochimica Acta, 64, 19, 341 - 3432

Section 15

_____

Mineralogy of the deep earth

High resolution seismic investigation of upper mantle discontinuities

Stephan Lessing[1], Christine Thomas[1] and Sebastian Rost[2]
[1] Westfälische Wilhelms-Universität Münster, Institut für Geophysik, Münster, Germany (stephan.lessing@uni-muenster.de)
[2] The University of Leeds, School of Earth and Environment, Institute of Geophysics and Tectonics, Leeds, United Kingdom

In recent years numerous seismic experiments have investigated the depth and topography of upper mantle discontinuities in different tectonic settings. The investigation of upper mantle discontinuities and the transition zone have provided valuable constraints on the thermal, chemical and dynamic state of the Earth's mantle. One method very frequently employed to study the upper mantle is the receiver function analysis of converted phases at the discontinuities. The regions which can be studied with this method are close to the receivers and thus limited by the station distribution.

More remote upper mantle regions (e.g. oceanic regions) can be studied by investigating precursor phases to PP and SS which are caused by underside reflections of P or S at the discontinuities. The arrival time of the underside reflections can be used to measure the depth of transition zone at the midpoint between source and receiver. In this study we investigate the upper mantle discontinuities using high resolution array methods to improve vertical and lateral resolution of the seismic structures.

We are focusing on the behaviour of upper mantle discontinuities, examining their topography, sharpness, density and velocity contrasts in a subduction region. Several source-receiver combinations are used to sample these regions with underside reflections using data from international data centres (e.g. IRIS, GEOFON etc.) and earthquakes in the Northwest to Southwest Pacific. Using broadband data we can filter with various bandpass filters to determine the dominant frequency of the precursor phases. The precursors are analysed in terms of frequency content, polarity, amplitude and waveform as well as in arrival time. The sharpness of discontinuities helps to determine the depth interval of phase transitions and the results will then be compared with synthetic seismograms using full waveform modelling to verify the interpretation. Beside the 410 and the 660 km discontinuity, we investigate the possible existence and properties of other discontinuities e.g. at 520 km depth.

The results of this study will provide further information and further constraints with regard to mineral physics and the state of the Earth's mantle.

AUTHOR INDEX